
AIR QUALITY - MODELS AND APPLICATIONS

Edited by **Dragana Popović**

INTECHWEB.ORG

Air Quality - Models and Applications

Edited by Dragana Popović

Published by InTech

Janeza Trdine 9, 51000 Rijeka, Croatia

Copyright © 2011 InTech

All chapters are Open Access articles distributed under the Creative Commons Non Commercial Share Alike Attribution 3.0 license, which permits to copy, distribute, transmit, and adapt the work in any medium, so long as the original work is properly cited. After this work has been published by InTech, authors have the right to republish it, in whole or part, in any publication of which they are the author, and to make other personal use of the work. Any republication, referencing or personal use of the work must explicitly identify the original source.

Statements and opinions expressed in the chapters are these of the individual contributors and not necessarily those of the editors or publisher. No responsibility is accepted for the accuracy of information contained in the published articles. The publisher assumes no responsibility for any damage or injury to persons or property arising out of the use of any materials, instructions, methods or ideas contained in the book.

Publishing Process Manager Natalia Reinic

Technical Editor Teodora Smiljanic

Cover Designer Jan Hyrat

Image Copyright MADDRAT, 2010. Used under license from Shutterstock.com

First published June, 2011

Printed in Croatia

A free online edition of this book is available at www.intechopen.com
Additional hard copies can be obtained from orders@intechweb.org

Air Quality - Models and Applications, Edited by Dragana Popović

p. cm.

ISBN 978-953-307-307-1

INTECH OPEN ACCESS
PUBLISHER

INTECH open

free online editions of InTech
Books and Journals can be found at
www.intechopen.com

Contents

Preface IX

Part 1 Mathematical Models and Computing Techniques 1

- Chapter 1 **Advances in Airborne Pollution Forecasting Using Soft Computing Techniques 3**
Aceves-Fernandez Marco Antonio, Sotomayor-Olmedo Artemio, Gorrostieta-Hurtado Efren, Pedraza-Ortega Jesus Carlos, Ramos-Arreguin Juan Manuel, Canchola-Magdaleno Sandra and Vargas-Soto Emilio
- Chapter 2 **Urban Air Pollution Modeling 15**
Anjali Srivastava and B. Padma S. Rao
- Chapter 3 **Artificial Neural Network Models for Prediction of Ozone Concentrations in Guadalajara, Mexico 35**
Ignacio García, José G. Rodríguez and Yenisse M. Tenorio
- Chapter 4 **Meandering Dispersion Model Applied to Air Pollution 53**
Gervásio A. Degrazia, Andréa U. Timm, Virnei S. Moreira and Débora R. Roberti
- Chapter 5 **Bioaerosol Emissions: A Stochastic Approach 67**
Sandra M. Godoy, Alejandro S. M. Santa Cruz and Nicolás J. Scenna
- Chapter 6 **Particle Dispersion Within a Deep Open Cast Coal Mine 81**
Sumanth Chinthala and Mukesh Khare
- ### **Part 2 Air Pollution Models and Application 99**
- Chapter 7 **Mathematical Modeling of Air Pollutants: An Application to Indian Urban City 101**
P. Goyal and Anikender Kumar

- Chapter 8 **A Gibbs Sampling Algorithm to Estimate the Occurrence of Ozone Exceedances in Mexico City** 131
Eliane R. Rodrigues, Jorge A. Achcar and Julián Jara-Ettinger
- Part 3 Measuring Methodologies in Air Pollution Monitoring and Control** 151
- Chapter 9 **Optical Measurements of Atmospheric Aerosols in Air Quality Monitoring** 153
Jolanta Kuśmierczyk-Michulec
- Chapter 10 **A Mobile Measuring Methodology to Determine Near Surface Carbon Dioxide within Urban Areas** 173
Sascha Henninger
- Part 4 Urban Air Pollution: Case Studies** 195
- Chapter 11 **Impacts of Photoexcited NO₂ Chemistry and Heterogeneous Reactions on Concentrations of O₃ and NO_y in Beijing, Tianjin and Hebei Province of China** 197
Junling An, Ying Li, Feng Wang and Pinhua Xie
- Chapter 12 **Analyzing Black Cloud Dynamics over Cairo, Nile Delta Region and Alexandria using Aerosols and Water Vapor Data** 211
Hesham M. El-Askary, Anup K. Prasad, George Kallos, Mohamed El-Raey and Menas Kafatos
- Chapter 13 **Spatial Variation, Sources and Emission Rates of Volatile Organic Compounds Over the Northeastern U.S.** 233
Rachel S. Russo, Marguerite L. White, Yong Zhou, Karl B. Haase, Jesse L. Ambrose, Leanna Conway, Elizabeth Mentis, Robert Talbot, and Barkley C. Sive
- Chapter 14 **Evaluation of an Emission Inventory and Air Pollution in the Metropolitan Area of Buenos Aires** 261
Laura E. Venegas, Nicolás A. Mazzeo and Andrea L. Pineda Rojas
- Chapter 15 **Variation of Greenhouse Gases in Urban Areas-Case Study: CO₂, CO and CH₄ in Three Romanian Cities** 289
Iovanca Haiduc and Mihail Simion Beldean-Galea

Part 5 Urban Air Pollution: Health Effects 319

- Chapter 16 **Assessment of Environmental Exposure to Benzene: Traditional and New Biomarkers of Internal Dose 321**
Piero Lovreglio, Maria Nicolà D'Errico, Silvia Fustinoni, Ignazio Drago, Anna Barbieri, Laura Sabatini, Mariella Carrieri, Pietro Apostoli, Leonardo Soleo
- Chapter 17 **The Influence of Air Pollutants on the Acute Respiratory Diseases in Children in the Urban Area of Guadalajara 341**
Ramírez-Sánchez HU, Meulenert-Peña AR, García-Guadalupe ME, García-Concepción FO, Alcalá-Gutiérrez J and Ulloa-Godínez HH

Preface

Air pollution has been a major transboundary problem and a matter of global concern for decades. High concentrations of different air pollutants may be particularly harmful to residents of major city areas, where numerous anthropogenic activities (primarily heavy traffic, domestic and public heating, and various industrial activities), strongly influence the quality of air. Consequently, air quality monitoring programs become a part of urban areas monitoring network and strict air quality standards in urban areas were in the focus of interest of environmental pollution studies in the last decade of the 20th century. Although there are many books on the subject, the one in front of you will hopefully fulfill some of the gaps in the area of air quality monitoring and modeling, and be of help to graduate students, professionals and researchers. The authors, all of them experts in their field, have been invited by the publisher, and also some recommendations have been given to them mainly concerning technical details of the text, the views and statements they express in the book is their own responsibility.

The book is divided in five different sections.

The first section discusses mathematical models and computing techniques used in air pollution monitoring and forecasting. The chapter by Aceves-Fernandez Marco Antonio et al., presents and compares the advantages and disadvantages of some airborne pollution forecasting methods using soft computing techniques, that include neuro-fuzzy inference methods, fuzzy clustering techniques and support vector machines, while the chapter on urban air pollution modeling, by Anjali Srivastava and B. Padma S. Rao, is a general overview of the air quality modeling that provides a useful support to decision making processes incorporating environmental policies and management process. The chapter focuses on urban air models, physical, mathematical and statistical, on local to regional scale. An interesting approach is presented in the next chapter on artificial neural network (ANN) models for prediction of ozone concentrations, by Ignacio García et al.. The authors consider to the great flexibility, efficiency and accuracy of the models that, since having a large number of features similar to those of the brain, are capable to learn and thus perform tasks based on training or initial experience. The model is applied to the study of tropospheric ozone, as the main component of photochemical smog, in the Metropolitan Zone of Guadalajara, Mexico.

In the chapter presenting a meandering dispersion model applied to air pollution by Gervásio A. Degrazia et al., the authors discuss the turbulence parameterization technique that can be employed in Lagrangian stochastic dispersion models to describe the air pollution dispersion in the low wind velocity stable conditions, using two classical approaches to obtain the turbulent velocity variances and the decorrelation time scales: Taylor statistical diffusion theory based on the observed turbulent velocity spectra, and the Hanna (1982) approach based on analyses of field experiments, theoretical considerations and second-order closure model.

Also, in this section Sandra Godoy and the co-workers in their chapter deal with the stochastic approach to the mechanisms of bio aerosols dispersion is atmospheric transport, as a phenomenon that cause serious social, health and economic consequences. Finally, the chapter on particle dispersion within a deep open cast coal mine, by Sumanth Chinthala & Mukesh Khare, presents a comprehensive overview of the dispersion mechanisms in the deep open pit coal mines considering the topographic, thermal and meteorological factors.

The second section presents two chapters on air pollution models and application. First chapter on Mathematical modeling of air pollutants: An application to Indian urban city, by P. Goyal and Anikender Kumar, formulates and uses the statistical and Eulerian analytical models for prediction of concentrations of air pollutants released from different sources and different boundary conditions. The model is applied to the city of Delhi, the capital of India, and is validated by the observed data of concentration of respirable suspended particulate matter in air. In the second chapter in this section, the authors Eliane R. Rodrigues et al., apply Gibbs sampling algorithm to estimate the occurrence of ozone exceeding events in Mexico City.

The third section of the book contains two chapters on measuring methodologies in air pollution monitoring and control. The first one, by Jolanta Kuśmierczyk-Michulec, presents an optical method for measuring atmospheric aerosols. The chapter is an overview of various efforts tending toward finding a relationship between atmospheric optical thickness and particulate matter, and discussing possibilities of using the Angstrom coefficient in air quality estimation. The second chapter, by Sasha Henninger, presents the advantages of a mobile measuring methodology to determine near surface carbon dioxide in urban areas.

Five chapters in the section four are dealing with experimental data on urban air pollution. The first one, by Junling An et al., discusses the impacts of photoexcited NO_2 chemistry and heterogeneous reactions on concentrations of O_3 and NO_2 in Beijing, Tianjin and Hebei Province of China, using WRF-CHEM model. The second one, by Hesham El-Askary et al., analyses the phenomena of the *Black Cloud* pollution event over Cairo, Nile Delta Region and Alexandria, Egypt, using aerosols and water vapor data, and the main sources of air pollution in the region, including heavy traffic, industrial, residential, commercial and mixed emissions or biomass burning. In the chapter on Spatial Variation, Sources, and Emission Rates of Volatile Organic Com-

pounds over the Northeastern U.S., the authors Rachel S. Russo et al., study the chemical and physical mechanisms influencing the atmospheric composition over New England, applying the University of New Hampshire's AIRMAP program, that was developed to conduct continuous measurements of important trace gases, meteorological parameters and volatile organic compounds. The chapter four in this section is an evaluation of emission inventory and air pollution in the central area of Buenos Aires, presented by Laura E. Venegas et al. The chapter is a summary of the development and results of a high spatial and temporal resolution version of the emission inventory of carbon monoxide and nitrogen oxides in this area, including area source emissions (motor vehicles, aircrafts, residential heating systems, commercial combustion and small industries), estimated by an urban atmospheric dispersion model (DAUMOD).

Finally, Iovanca Haiduc and Mihail S. Beldean-Galea, in the chapter on Variation of Greenhouse Gases in Urban Areas, present the results of a case study of CO₂, CH₄ and CO variations during one year, as well as the ¹³CO₂ and ¹³CH₄ isotopic composition in three selected cities from Romania, in order to identify the influence of biogenic and anthropogenic sources to the budget of the greenhouse gases.

The final section of the book deals of the health effects and contains only two chapters. The first one, titled Assessment of Environmental Exposure to Benzene: Traditional and New Biomarkers of Internal Dose, by Piero Lovreglio et al., is aimed to assess the significance and limits of t,t-MA, SPMA and urinary benzene for biological monitoring of subjects with non occupational exposure to very low concentrations of benzene, as well as to study the influence of the different sources of environmental exposure on these biomarkers. The second one, on the influence of air pollutants on the acute respiratory diseases in children living in the urban area of Guadalajara, by Ramirez Sanchez et al., presents the epidemiological evidence that the exposure to atmospheric contaminants, even at low levels, is associated with an increase in respiratory diseases in small children.

However, besides the efforts of the authors of the individual chapters, the book is primarily the result of the hard work of the editing and technical team of the publisher, as the accomplishment of its goal to present a highly professional and informative text in air pollution and quality research.

Prof Dragana Popovic
Department of Physics and Biophysics,
Faculty of Veterinary Medicine, University of Belgrade,
Serbia

Part 1

Mathematical Models and Computing Techniques

Advances in Airborne Pollution Forecasting Using Soft Computing Techniques

Aceves-Fernandez Marco Antonio, Sotomayor-Olmedo Artemio,
Gorrostieta-Hurtado Efren, Pedraza-Ortega Jesus Carlos, Ramos-Arreguín
Juan Manuel, Canchola-Magdaleno Sandra and Vargas-Soto Emilio
*Facultad de Informática, Universidad Autónoma de Querétaro,
México*

1. Introduction

There are many investigations reported in the scientific literature about Particulate Matter (PM) 2.5 and PM10 in urban and suburban environments [Vega *et al* 2002, Querol *et al* 2004, Fuller *et al* 2004].

In this contribution, the information acquired from PM_x monitoring systems is used to accurately forecast particle concentration using diverse soft computing techniques.

A number of works have been published in the area of airborne particulates forecasting. For example, Chelani[*et al* 2001] trained hidden layer neural networks for CO forecasting at India. Caselli [*et al* 2009] used a feedforward neural network to predict PM10 concentration. Other works such as Kurt's [*et al* 2010] have constructed a neural networks model using many input variables (e.g. wind, temperature, pressure, day of the week, Date, concentration, etc) making the model too complex and inaccurate.

However, not many scientific literature discuss a number of robust forecasting methods using soft computing techniques. These techniques include neuro-fuzzy inference methods, fuzzy clustering techniques and support vector machines. Each one of these algorithms is discussed separately and the results discussed. Furthermore, a comparison of all methods is made to emphasize their advantages as well as their disadvantages.

2. Fuzzy inference methods

Fuzzy inference systems (FIS) are also known as fuzzy rule-based systems. This is a major unit of a fuzzy logic system. The decision-making is an important part in the entire system. The FIS formulates suitable rules and based upon the rules the decision is made. This is mainly based on the concepts of the fuzzy set theory, fuzzy IF-THEN rules, and fuzzy reasoning. FIS uses "IF - THEN" statements, and the connectors present in the rule statement are "OR" or "AND" to make the necessary decision rules.

Fuzzy inference system consists of a fuzzification interface, a rule base, a database, a decision-making unit, and finally a defuzzification interface as described in Chang(*et al* 2006). A FIS with five functional block described in Fig.1.

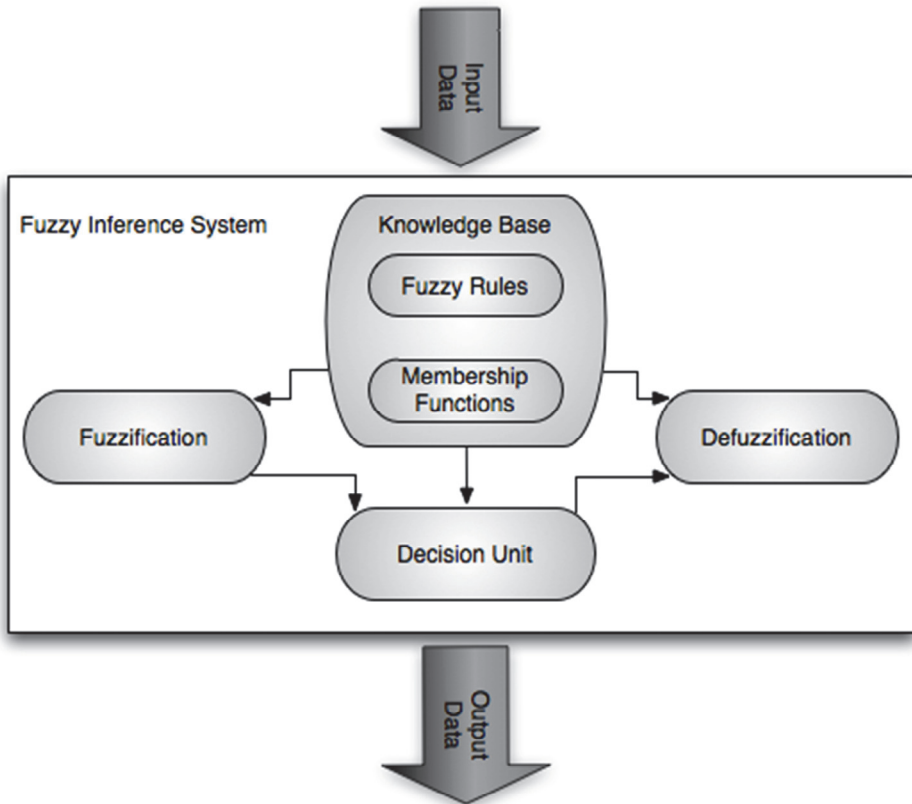


Fig. 1. Fuzzy Inference System

The function of each block is as follows:

- A rule base containing a number of fuzzy IF-THEN rules;
- A database which defines the membership functions of the fuzzy sets used in the fuzzy rules;
- A decision-making unit which performs the inference operations on the rules;
- A fuzzification interface which transforms the crisp inputs into degrees of match with linguistic values; and
- A defuzzification interface which transforms the fuzzy results of the inference into a crisp output.

The working of FIS is as follows. The inputs are converted in to fuzzy by using fuzzification method. After fuzzification the rule base is formed. The rule base and the database are jointly referred to as the knowledge base.

Defuzzification is used to convert fuzzy value to the real world value which is the output.

The steps of fuzzy reasoning (inference operations upon fuzzy IF-THEN rules) performed by FISs are:

- Compare the input variables with the membership functions on the antecedent part to obtain the membership values of each linguistic label. (this step is often called fuzzification.)
- Combine (through a specific t-norm operator, usually multiplication or min) the membership values on the premise part to get firing strength (weight) of each rule.
- Generate the qualified consequents (either fuzzy or crisp) or each rule depending on the firing strength.
- Aggregate the qualified consequents to produce a crisp output. (This step is called defuzzification.)

A typical fuzzy rule in a fuzzy model has the format shown in equation 1

$$\text{IF } x \text{ is } A \text{ and } y \text{ is } B \text{ THEN } z = f(x, y) \quad (1)$$

where AB are fuzzy sets in the antecedent; $Z = f(x, y)$ is a function in the consequent. Usually $f(x, y)$ is a polynomial in the input variables x and y , of the output of the system within the fuzzy region specified by the antecedent of the rule.

A typical rule in a FIS model has the form (Sugeno et al 1988): IF Input 1 = x AND Input 2 = y , THEN Output is $z = ax + by + c$.

Furthermore, the final output of the system is the weighted average of all rule outputs, computed as

$$\text{FinalOutput} = \frac{\sum_{i=1}^N w_i z_i}{\sum_{i=1}^N w_i} \quad (2)$$

3. Fuzzy clustering techniques

There are a number of fuzzy clustering techniques available. In this work, two fuzzy clustering methods have been chosen: fuzzy c-means clustering and fuzzy clustering subtractive algorithms. These methods are proven to be the most reliable fuzzy clustering methods as well as better forecasters in terms of absolute error according to some authors [Sin, Gomez, Chiu].

Since 1985 when the fuzzy model methodology suggested by Takagi-Sugeno [Takagi *et al* 1985, Sugeno *et al* 1988], as well known as the TSK model, has been widely applied on theoretical analysis, control applications and fuzzy modelling.

Fuzzy system needs the precedent and consequence to express the logical connection between the input output datasets that are used as a basis to produce the desired system behavior [Sin *et al* 1993].

3.1 Fuzzy clustering means (FCM)

Fuzzy C-Means clustering (FCM) is an iterative optimization algorithm that minimizes the cost function given by:

$$J = \sum_{k=1}^n \sum_{i=1}^c \mu_{ik}^m \|x_k - v_i\|^2 \quad (3)$$

Where n is the number of data points, c is the number of clusters, x_k is the k th data point, v_i is the i th cluster center μ_{ik} is the degree of membership of the k th data in the i th cluster, and m is a constant greater than 1 (typically $m=2$) [Aceves *et al* 2011]. The degree of membership μ_{ik} is defined by:

$$\mu_{ik} = \frac{1}{\sum_{j=1}^c \left(\frac{\|x_k - v_i\|}{\|x_k - v_j\|} \right)^{2/(m-1)}} \quad (4)$$

Starting with a desired number of clusters c and an initial guess for each cluster center v_i , $i = 1, 2, 3, \dots, c$, FCM will converge to a solution for v_i that represents either a local minimum or a saddle point cost function [Bezdek *et al* 1985]. The FCM method utilizes fuzzy partitioning such that each point can belong to several clusters with membership values between 0 and 1. FCM include predefined parameters such as the weighting exponent m and the number of clusters c .

3.2 Fuzzy clustering subtractive

The subtractive clustering method assumes each data point is a potential cluster center and calculates a measure of the likelihood that each data point would define the cluster center, based on the density of surrounding data points. Consider m dimensions of n data point (x_1, x_2, \dots, x_n) and each data point is potential cluster center, the density function D_i of data point at x_i is given by:

$$D_i = \sum_{j=1}^n e^{-\left(\frac{\|x_i - x_j\|^2}{(r_a/2)^2} \right)} \quad (5)$$

where r_a is a positive number. The data point with the highest potential is surrounded by more data points. A radius defines a neighbour area, then the data points, which exceed r_a , have no influence on the density of data point.

After calculating the density function of each data point is possible to select the data point with the highest potential and find the first cluster center. Assuming that X_{c1} is selected and D_{c1} is its density, the density of each data point can be amended by:

$$D_i = D_i - D_{c1} e^{-\left(-\frac{\|x_i - x_{c1}\|^2}{(r_b/2)^2} \right)} \quad (6)$$

The density function of data point which is close to the first cluster center is reduced. Therefore, these data points cannot become the next cluster center. r_b defines an neighbour area where the density function of data point is reduced. Usually constant $r_b > r_a$. In order to avoid the overlapping of cluster centers near to other(s) is given by [Yager *et al* 1994]:

$$r_b = \eta \cdot r_a \quad (7)$$

4. Support vector machines

The support vector machines (SVM) theory, was developed by Vapnik in 1995, and is applied in many machine-learning applications such as object classification, time series prediction, regression analysis and pattern recognition. Support vector machines (SVM) are based on the principle of structured risk minimization (SRM) [Vapnik *et al* 1995, 1997].

In the analysis using SVM, the main idea is to map the original data x into a feature space F with higher dimensionality via non-linear mapping function ϕ , which is generally unknown, and then carry on linear regression in the feature space [Vapnik 1995]. Thus, the regression

approximation addresses a problem of estimating function based on a given data set, which is produced from the ϕ function. SVM method approximates the function by:

$$y = \sum_{i=1}^m w_i \phi_i(x) + b = w\phi(x) + b \quad (8)$$

where $w = [w_1, \dots, w_m]$ represent the weights vector, b is defined as the bias coefficients and $\phi(x) = [\phi_1(x), \dots, \phi_m(x)]$ the basis function vector.

The learning task is transformed to the weights of the network at minimum. The error function is defined through the ε -insensitive loss function, $L_\varepsilon(d, y(x))$ and is given by:

$$L_\varepsilon(d, y(x)) = \begin{cases} |d - y(x)| - \varepsilon & |d - y(x)| \geq \varepsilon \\ 0 & \text{others} \end{cases} \quad (9)$$

The solution of the so defined optimization problem is solved by the introduction of the Lagrange multipliers α_i , α_i^* (where $i=1,2,\dots,k$) responsible for the functional constraints defined in Eq. 9. The minimization of the Lagrange function has been changed to the dual problem [Vapnik *et al* 1997]:

$$\begin{aligned} \phi(\alpha, \alpha^*) = & \left[\sum_{i=1}^k d_i (\alpha_i - \alpha_i^*) - \varepsilon \sum_{i=1}^k (\alpha_i - \alpha_i^*) \right. \\ & \left. - \frac{1}{2} \sum_{i=1}^k \sum_{j=1}^k (\alpha_i, \alpha_i^*) (\alpha_j, \alpha_j^*) K(x_i, x_j) \right] \end{aligned} \quad (10)$$

With constraints:

$$\begin{aligned} \sum_{i=1}^k (\alpha_i, \alpha_i^*) &= 0, \\ 0 \leq \alpha_i \leq C, 0 \leq \alpha_i^* &\leq C \end{aligned} \quad (11)$$

Where C is a regularized constant that determines the trade-off between the training risk and the model uniformity.

According to the nature of quadratic programming, only those data corresponding to non-zero $\alpha_i - \alpha_i^*$ pairs can be referred to support vectors (nsv). In Eq. 10 $K(x_i, x_j) = \phi(x_i)^* \phi(x_j)$ is the inner product kernel which satisfy Mercer's condition [Osuna *et al* 1997] that is required for the generation of kernel functions given by:

$$K(x_i, x_j) = \langle \phi(x_i), \phi(x_j) \rangle \quad (12)$$

Thus, the support vectors associates with the desired outputs $y(x)$ and with the input training data x can be defined by:

$$y(x) = \sum_{i=1}^{N_{sv}} (\alpha_i, \alpha_i^*) K(x, x_i) + b \quad (13)$$

Where x_i are learning vectors. This leads to a SVM architecture (Fig. 2) [Vapnik 1997, Cristianini *et al* 2000].

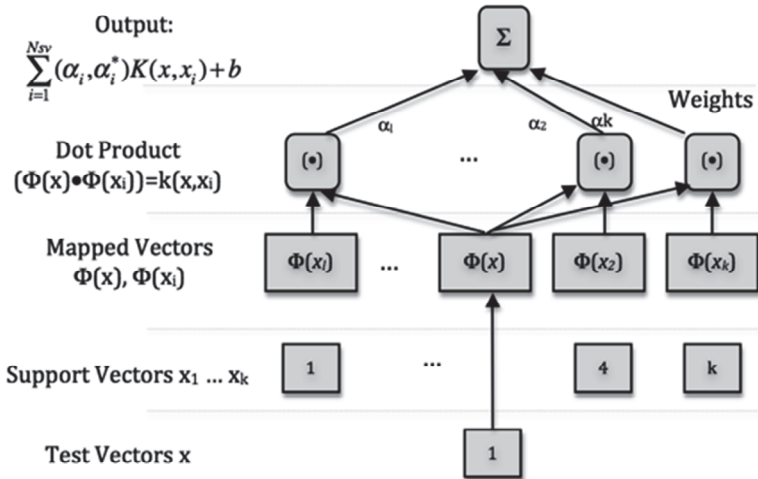


Fig. 2. Support Vector Machine Architecture.

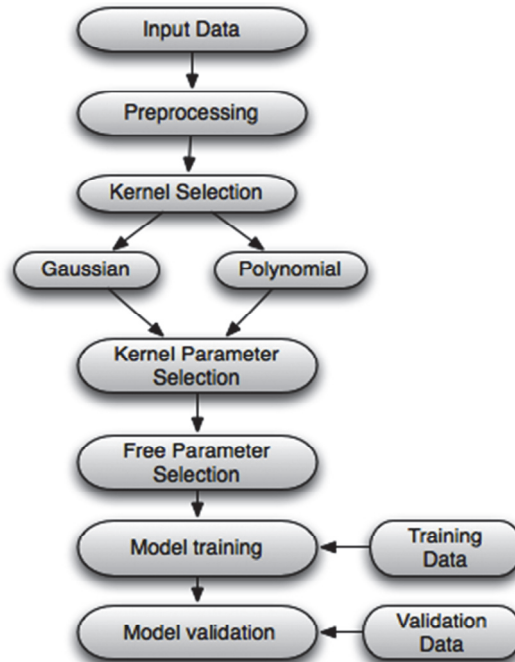


Fig. 3. Support Vector Machine Methodology.

The methodology used for the design, training and testing of SVM is proposed as follows based in a review of Vapnik, Osowski [et al 2007] and Sapankevych[et al 2009]

- Preprocess the input data and select the most relevant features, scale the data in the range $[-1, 1]$, and check for possible outliers.
- Select an appropriate kernel function that determines the hypothesis space of the decision and regression function.
- Select the parameters of the kernel function the variances of the Gaussian kernels.
- Choose the penalty factor C and the desired accuracy by defining the ε -insensitive loss function.
- Validate the model obtained on some previously, during the training, unseen test data, and if not pleased iterate between steps (c) (or, eventually b) and (e).

5. Discussion of results

Simulations were performed using fuzzy clustering algorithms using the equations [3-7], in this case study, the datasets at Mexico City in 2007 were chosen to construct the fuzzy model. Likewise, the data of 2008 and 2009 from the same geographic zone in each case were used to training and validating the data, respectively. The result of the fuzzy clustering model was compared then to the real data of Northwest Mexico in 2010.

The results obtained show an average least mean square error of 11.636 using Fuzzy Clustering Means, whilst FCS shows an average least mean square error of 10.59. Table 1 shows a list of the experiments carried out. An example of these results is shown in figure 4 for FCM and figure 5 shows the estimation made using FCS at Northwest Mexico City.

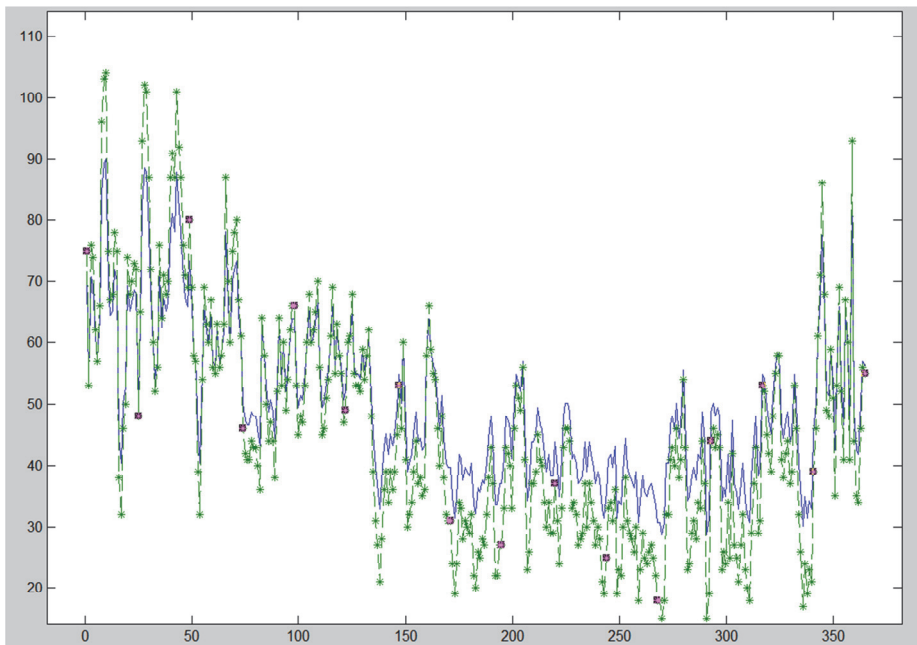


Fig. 4. Fuzzy Clustering Means (FCM) Results at Northwest Mexico City. Raw Data VS. Fuzzy Model

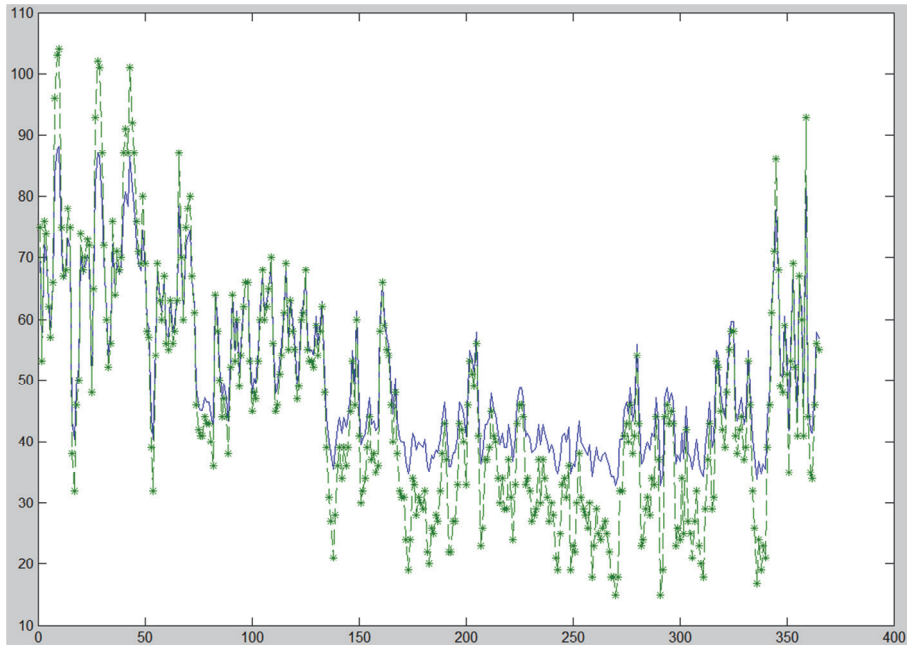


Fig. 5. Fuzzy Clustering Subtractive (FCS) Results at Northwest Mexico City. Raw Data VS. Fuzzy Model

In figures 4 and 5, the raw data (shown in blue solid line) and the constructed fuzzy model (in dashed-starred green line) shown that the trained model is approximated to the raw data with an average least mean square error of 8.7%, implying that a fuzzy model can be accurately constructed using this technique.

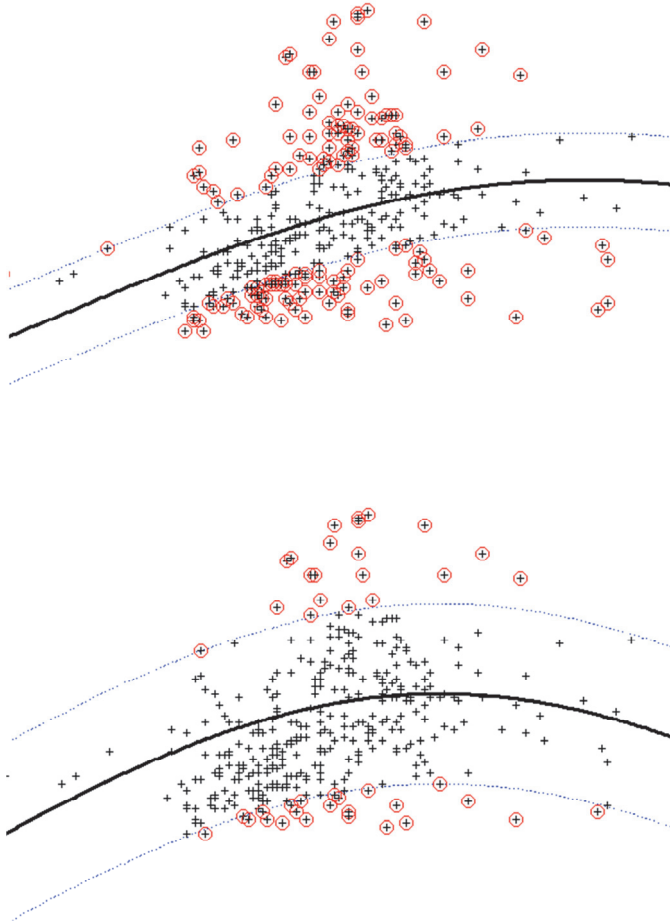
Site	LMSE using FCM	LMSE using FCS
Northwest	10.1917	7.4807
Northeast	13.6282	13.7374
Center	18.5757	15.1409
Southwest	5.0411	7.4953
Southeast	10.7428	9.1188

Table 1. List of the experiments carried out using FCM and FCS.

In table 1 is shown that the best prediction in terms of error percentage is given at southwest for both fuzzy clustering means and fuzzy clustering subtractive, whilst the less estimation is given at the city center. This may be due to the high variations in terms of PM10 particles making it more difficult to predict. However, more research is needed to confirm this.

Furthermore, detailed simulations were carried out using Support Vector Machines following the proposed methodology shown in figure 3. These simulations were carried out

using the same dataset as the fuzzy clustering technique. In this case, values 2σ was chosen, and an ϵ of 11 and 13 were chosen since it was demonstrated to give better results in previous contributions (Sotomayor *et al* 2010, Sotomayor *et al* 2011). Figure 6 shows the results of the model using support vector machines with a Gaussian kernel, whilst figure 7 shows the results using the same datasets, with polynomial kernel

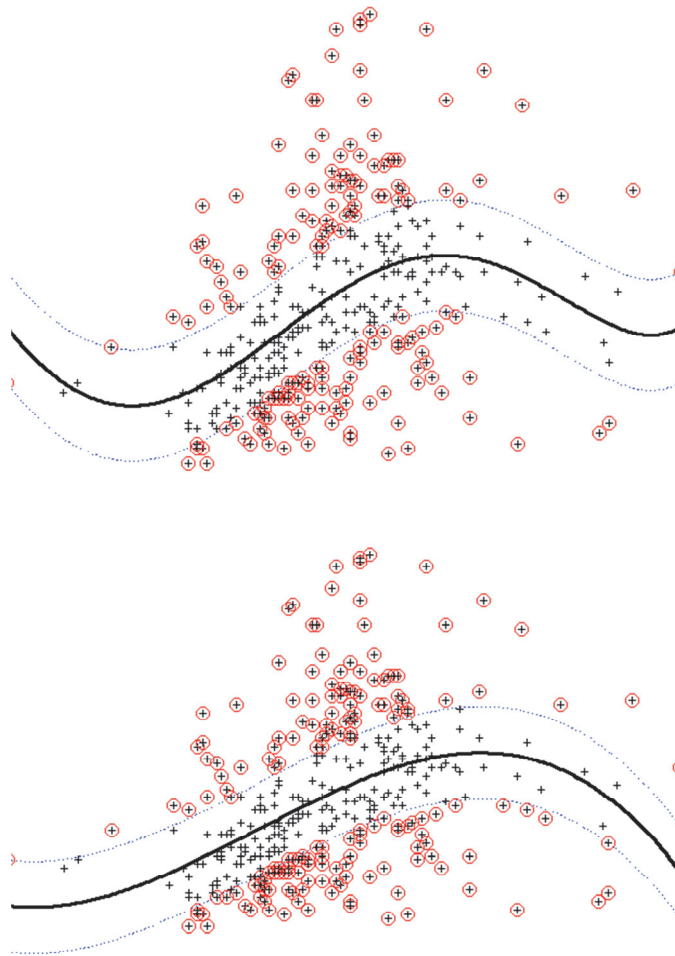


- a) SVM Estimated with free parameters of $\epsilon = 13$ and $\sigma = 2$
- b) SVM Estimated with free parameters of $\epsilon = 11$ and $\sigma = 2$

Fig. 6. SVM Results at Northwest Mexico City using Gaussian Kernel.

Figure 6 indicates a summary of the results with the Support vector machine (in red circles), the raw data (black cross) and the behavior of the data (solid black line). These results show that for Gaussian Kernel (fig 6) gives 11.8 error using the same LMSE Algorithm than the

fuzzy model with an epsilon of 13 giving a total number of support vector machines of 157. In the case of figure 5b, using the Gaussian kernel, it was also used the same σ and an epsilon of 11. For this figure, the support vector shows an improvement by having an LMSE of 8.7.



- a) SVM Estimated with free parameters of $\epsilon = 13$ and $\sigma = 2$
- b) SVM Estimated with free parameters of $\epsilon = 11$ and $\sigma = 2$

Fig. 7. SVM Results at Northwest Mexico City using Polynomial Kernel.

For figure 7a, the estimation gives an error of 9.8 using an σ of 2 and an epsilon of 11 using 177 support vector machines. Likewise, figure 7b also shows the estimation using a third degree polynomial kernel with an ϵ of 13. In this case, a 10.1 LMSE is shown by having 183 support vector machines.

6. Conclusions and further work

An assessment in the performance of both fuzzy systems generated using Fuzzy Clustering Subtractive and Fuzzy C-Means was made taking in account the number or membership functions, rules, and Least Mean Square Error for PM10 particles. As a case study, Estimations were made at Northwest Mexico City in 2010, giving consistent results.

In case of SVMs, it can be concluded that for this case study an ϵ of 11 gives a better estimation than an ϵ of 13 for the Gaussian kernel. In general, the Gaussian kernel gives better results in terms of estimation than its corresponding polynomial kernel. In general terms, fuzzy clustering gives a better estimation than Gaussian and polynomial kernels, although in-depth studies are needed to corroborate these results for other scenarios.

For future work, more SVM kernels can be implemented and comparison can be made to find out which kernels give better estimation. Also, SVMs can be implemented along with other techniques such as wavelet transform to improve the performance of these algorithms

7. References

- Aceves-Fernández M.A., Sotomayor-Olmedo A., Gorrostieta-Hurtado E., Pedraza-Ortega J.C., Tovar-Arriaga S., Ramos-Arreguin J.M., Performance Assessment of Fuzzy Clustering Models Applied to Urban Airborne Pollution, *CONIELECOMP 2011, 21th International Conference on Electrical Communications*, pp. 212-216 (2011).
- Bezdek, J. C., "Pattern Recognition with Fuzzy Objective Function Algorithms", *Plenum Press, NY*, 1981.
- Caselli M. & Trizio L. & de Gennaro G. & Ielpo P., "A Simple Feedforward Neural Network for the PM10 Forecasting: Comparison with a Radial Basis Function Network and a Multivariate Linear Regression Model", *Water Air Soil Pollut* (2009) 201:365-377
- Chang Wook A., "Advances in Evolutionary Algorithms: Theory, Design and Practice", Springer, ISSN: 1860-949X, 2006.
- Chelani A.B.; Hasan M. Z., "Forecasting nitrogen dioxide concentration in ambient air using artificial Neural networks", *International Journal of Environmental Studies*, 2001, Vol. 58, pp. 487-499
- Chiu S, "Fuzzy model identification based on cluster estimation", *Journal of Intelligent and Fuzzy Systems*; September 1994, 2, pp. 267-78.
- Cristianini, N., Shawe-Taylor, J., An introduction to Support Vector Machines and other kernel-based learning methods, Cambridge University Press, Cambridge, UK (2000)
- Fuller G W and Green D., "The impact of local fugitive PM10 from building works land road works on the assessment of the European Union Limit Value", *Atmospheric Environment* 2004, 38, pp. 4493-5002.
- Gomez, A. F., M. Delgado, and M. A. Vila, "About the Use of Fuzzy Clustering Techniques for Fuzzy Model Identification", *Fuzzy Set and System.*, 1999, pp. 179-188.
- Kurt Atakan, Oktay Ayse Betül, "Forecasting air pollutant indicator levels with geographic models 3 days in advance using neural networks", *Expert Systems with Applications*, 37 (2010) 7986-7992.
- Osowski S. and Garanty K., "Forecasting of the daily meteorological pollution using wavelets and support vector machine," *Engineering Applications of Artificial Intelligence*, vol. 20, no. 6, pp. 745-755, September 2007.

- Osuna, E., R. Freund, F. Girosi.: Support vector machines: Training and applications. AI Memo 1602, Massachusetts Institute of Technology, Cambridge, MA 44. (1997).
- Querol X, Alastvey A, Ruiz C.R., Avtinano B, Hausson H.C., Harrison R.M, Buringh E, Ten Brink H.M, Lutz M, Bruckmann P, Straehl P and Schnerflev J., "Speciation and origin of PM10 and PM 2.5 in selected European cities", *Atmospheric Environment*. 2004, 38, pp. 6547 - 6555.
- Sapankevych I. and Sankar R., "Time series prediction using support vector machines: A survey," *Computational Intelligence Magazine*, IEEE, vol. 4, no. 2, pp. 24-38, 2009.
- Schölkopf B.: Smola A. J.: and Burges C.: Advances in Kernel Methods -Support Vector Learning. Cambridge, M.A.: MIT Press. 1999.
- Sin, S. K., and De Figueiredo, "Fuzzy System Designing Through Fuzzy Clustering and Optimal preDefuzzification", *Proc. IEEE International Conference on Fuzzy Systems*. 1993 2, 190-195.
- Sotomayor-Olmedo A., Aceves-Fernandez M.A., Gorrostieta-Hurtado E., Pedraza-Ortega J.C., Ramos-Arreguin J.M., Vargas-Soto J.E., Tovar-Arriaga S., "Modeling Trends of Airborne Particulate Matter by using Support Vector Machines", *7th International Conference on Electrical and Electronics Engineering Research (CIIIEE 2010)*, November 10-12 2010, Aguascalientes, Ags. Mexico, ISBN: 978-607-95060-3-2
- Sotomayor-Olmedo A., Aceves-Fernandez M.A., Gorrostieta-Hurtado E., Pedraza-Ortega J.C., Vargas-Soto J.E., Ramos-Arreguin J.M., Villaseñor-Carillo U., "Evaluating Trends of Airborne Contaminants by using Support Vector Regression Techniques", *CONIELECOMP 2011, 21th International Conference on Electrical Communications*, pp. 137-141 (2011).
- Sugeno, M., and G. T. Kang. "Structure Identification of Fuzzy Model", *Fuzzy Sets and Systems*. 1988, 28, pp. 15-33.
- Takagi, T., and M. Sugeno, "Fuzzy Identification of Systems and its Application to Modeling and Control", *IEEE Trans. Systems Man and Cybernetics*. 1985 -15, pp. 116-132.
- Vapnik, V.: The Nature of Statical Learning Theory. Springer-Verlang, New York. 1995.
- Vapnik, V., Golowich, S., Smola A.: Support method for function approximation regression estimation, and signal processing. *Advance in Neural Information Processing System 9*. MIT Press, Cambridge, MA. 1997.
- Vega E, Reyes E Sanchez G, Ortiz E, Ruiz M, Chow J, Watson J and Edgerton S, "Basic Statistics of PM2.5 and PM10 in the atmosphere of Mexico City", *The science of the total environment* 2002, 287, pp. 167-176.
- Yager, R. and D. Filev, "Generation of Fuzzy Rules by Mountain Clustering", *Journal of Intelligent & Fuzzy Systems*, 1994, 2, pp. 209- 219.

Urban Air Pollution Modeling

Anjali Srivastava and B. Padma S. Rao
*National Environmental Engineering Research Institute,
Kolkata Zonal Centre
India*

1. Introduction

All life form on this planet depends on clean air. Air quality not only affects human health but also components of environment such as water, soil, and forests, which are the vital resources for human development.

Urbanization is a process of relative growth in a country's urban population accompanied by an even faster increase in the economic, political, and cultural importance of cities relative to rural areas. Urbanization is the integral part of economic development. It brings in its wake number of challenges like increase in population of urban settlement, high population density, increase in industrial activities (medium and small scale within the urban limits and large scale in the vicinity), high rise buildings and increased vehicular movement. All these activities contribute to air pollution. The shape of a city and the land use distribution determine the location of emission sources and the pattern of urban traffic, affecting urban air quality (World Bank Reports 2002). The dispersion and distribution of air pollutants and thus the major factor affecting urban air quality are geographical setting, climatological and meteorological factors, city planning and design and human activities.

Cities in the developing countries are characterized by old city and new development. The old cities have higher population density, narrow lanes and fortified structures.

In order to ensure clean air in urban settlements urban planning and urban air quality management play an important role. New legislations, public awareness, growth of urban areas, increases in power consumption and traffic pose continuous challenges to urban air quality management. UNEP (2005) has identified niche areas Urban planning need to primarily focus on as:

- Promotion of efficient provision of urban infrastructure and allocation of land use, thereby contributing to economic growth,
- managing spatial extension while minimizing infrastructure costs,
- improving and maintaining the quality of the urban environment and
- Prerecording the natural environment immediately outside the urban area.

Air quality modelling provides a useful support to decision making processes incorporating environmental policies and management process. They generate information that can be used in the decision making process. The main objectives of models are: to integrate observations, to predict the response of the system to the future changes, to make provision for future development without compromising with quality

2. Urban air quality

The urban air is a complex mixture of toxic gases and particulates, the major source is combustion of fossil fuels. Emissions from fossil fuel combustion are reactive and govern local atmospheric chemistry. Urban air pollution thus in turn affect global troposphere chemistry and climate (e.g. tropospheric O₃ and NO_x budgets, radiative forcing by O₃ and aerosols). Sources of air pollutants in urban area, their effect and area of concern are summarized in Table 1.

Source	Pollutants	Effects	Area of concern
Large number of vehicles	Particulate matters (PM ₁₀ , PM _{2.5}), Lead (Pb), Sulphur dioxide (SO ₂), Oxides of nitrogen (NO _x), Ozone (O ₃), Hydro carbons (HCs), Carbon monoxide (CO), Hydrogen fluoride (HF), Heavy metals (e.g. Pb, Hg, Cd etc.)	Human Health (acute and chronic)	Local, Regional and Global
Use of diesel powered vehicle in large number			
Use of obsolete vehicles in large number			
Large number of motor cycles/three wheelers (2 stroke and three stroke)		Ecosystem (acute and chronic)	Local, Regional and Global
Unpaved and/or poorly maintained street			
Open burning		Greenhouse gas emission	Global
Inadequate infrastructure			
Low quality of fuel/fuel adulteration			
Little emission control & technology in industry			
Presence of industries (e.g. ceramic, brick works, agrochemical factory)			
Waste incineration		Stratospheric ozone depletion	Global
Limited dry deposition of pollutants		Long-range transport	Global

Table 1. Urban sources of air pollutants, their effect and area of concern.

Urban air pollution involves physical and chemical process ranging over a wide scale of time and space. The urban scale modeling systems should consider variations of local scale

effects, for example, the influence of buildings and obstacles, downwash phenomena and plume rise, together with chemical transformation and deposition. Atmospheric boundary layer, over 10 to 30 km distances, governs the dispersion of pollutants from near ground level sources. Vehicular emissions are one the major pollution source in urban areas. Ultrafine particles are formed at the tailpipe due to mixing process between exhaust gas and the atmosphere. Processes at urban scale provide momentum sink, heat and pollutant source thereby influencing the larger regional scale (up to 200 km). Typical domain lengths for different scale models is given in table 2.

Model	Typical Domain Scale	Typical resolution	Motion Example
Micro scale	200x200x100m	5m	Molecular diffusion, Molecular viscosity
Mesoscale (urban)	100x100x5km	2km	Eddies, small plumes, car exhaust, cumulus clouds
Regional	1000x1000x10km	36km	Gravity waves, thunderstorms, tornados, cloud clusters, local winds, urban air pollution
Synoptic (continental)	3000x3000x20km	80 km	High and low pressure system, weather fronts, tropical storms, Hurricanes Antarctic ozone hole,
Global	65000x65000x20km	4° x 5°	Global wind speed, rossby (planetary) waves stratospheric ozone reduction Global worming

Table 2. Typical domain length for different scale model

Piringer et al., 2007, have demonstrated that atmospheric flow and microclimate are influenced by urban features, and they enhance atmospheric turbulence, and modify turbulent transport, dispersion, and deposition of atmospheric pollutants. Any urban scale modeling systems should consider effects of the various local scales, for example, the influence of buildings and obstacles, downwash phenomena and plume rise, chemical transformation and deposition. The modelling systems also require information on emissions from various sources including urban mobile pollution sources. Simple dispersion air quality pollution transport models and complex numerical simulation model require wind, turbulence profiles, surface heat flux and mixing height as inputs. In urban areas mixing height is mainly influenced by the structure heights and construction materials, in terms of heat flux. Oke (1987, 1988, 1994), Tennekes (1973), Garrat (1978, 1980), Raupach et al (1980) and Rotach (1993, 1995) divided the Atmospheric Boundary Layer within the urban structures into four sub layers (Figure 1).

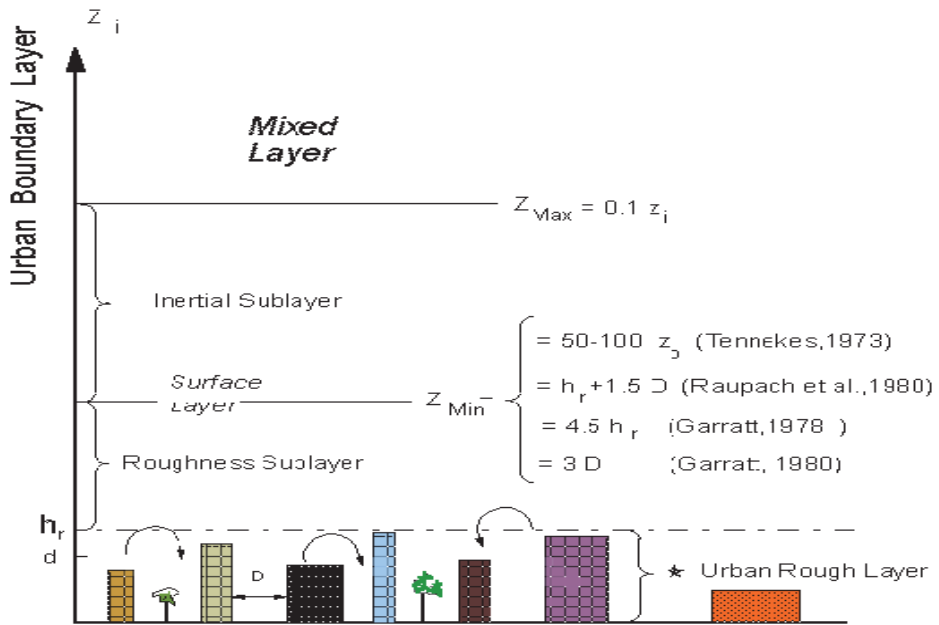


Fig. 1. Boundary-layer structure over a rough urban built-up area. A daytime situation is displayed where Z_i denotes the mixed layer height. Modified after Oke (1988) and Rotach (1993).

In urban establishments anthropogenic activities take place between the top of highest building and the ground. People also live in this area. The layer of atmosphere in this volume is termed as Urban Canopy. The thermal exchanges and presence of structures in urban canopy modify the air flows significantly and this makes the atmospheric circulations in urban canopy highly complex. The heterogeneity of urban canopies poses a challenge for air quality modeling in urban areas. The importance of various parameters in different models for urban atmosphere study is given in Table 3. Figure 2 shows the flow and scale lengths within an urban boundary layer, UBL.

Parameter	Air Quality	Urban Climatology	Urban Planning
Wind speed	Very important	Important	Very Important
Wind Direction	Very important	Important	Very Important
Temperature Humidity	Important	Extremely important	Very Important
Pollutant Concentration	Extremely important	Very important	Very important
Turbulent Fluxes	Very important	Very important	Very important

Table 3. Ranking of parameters in different applications for urban air environment

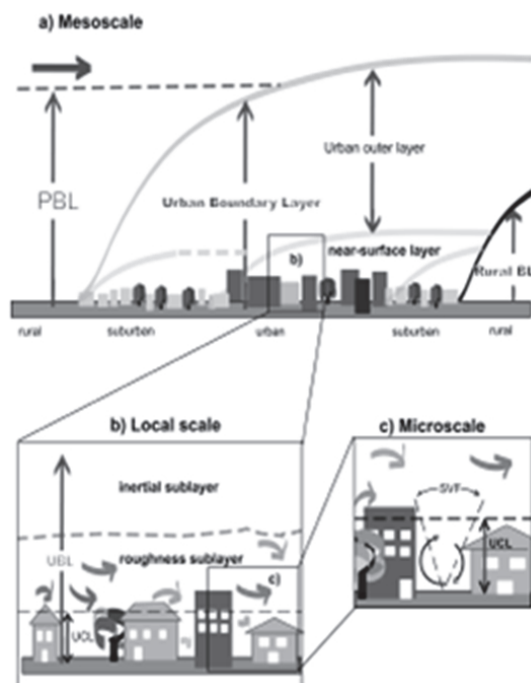


Fig. 2. Schematic diagram showing processes, flow and scale lengths within an urban boundary layer, UBL. This is set in the context of the planetary boundary layer, PBL, the urban canopy layer, UCL, and the sky view factor, SVF, a measure of the degree to which the sky is obscured by surrounding buildings at a given point which characterises the geometry of the urban canopy. Ref. Meteorology applied to urban pollution problems-Final report COST Action 715. Dementra Ltd Publishers

Vehicles are one of the important pollution sources in urban areas. Maximum exposure to local public is from this source and thus they form important receptor group. Pollutant dispersion of vehicular pollution is at street scale and is the smallest scale in urban environment. Hosker (1985) showed that flows in street canyon are like recirculating eddy driven by the wind flow at the top with a shear layer which separates the above canyon flows from those within it. In deep street canyons the primary vortex does not extend to the ground but a weak contra rotating vortex is formed near the ground and is relatively shallow (Figure 3). Pavageau et al (2001) demonstrated that wind directions which are not normal to the street axis cause variations in the flow. The real geometry of the street canyon and the mean flow and turbulence generated by vehicles within the canyon also affect the recirculating flow.

Concentrations of pollutants at a receptor are governed by advection, dispersion and deposition. Air pollutants can be divided into two main categories namely conventional air pollutants and Hazardous Air Pollutants (HAPs). Conventional air pollutants include particulate matters, sulphur dioxide, nitrogen dioxide, carbon monoxide, particles, lead and the secondary pollutant ozone. HAPs include Volatile Organic Compounds, toxic metals

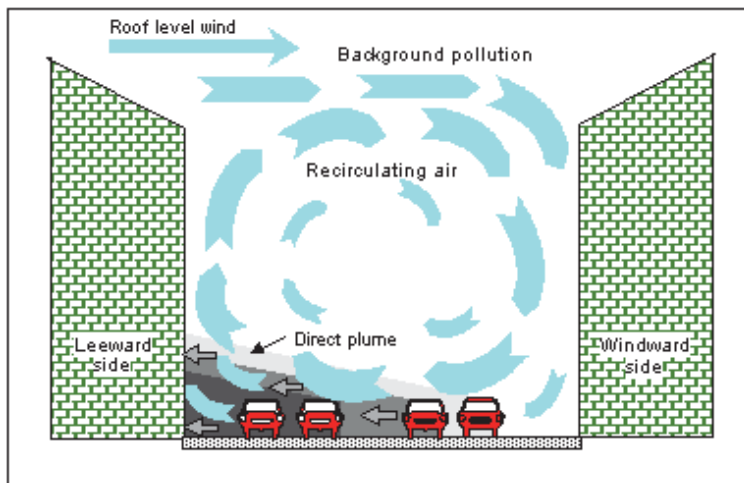


Fig. 3. Air flow pattern in a Street Canyon

and biological agents of many types. All pollutants are not emitted in significant quantities. Secondary pollutants like some VOCs, carbonyls and ozone are formed due to chemical transformation in air. These reactions are often photochemical.

The important components of air quality modelling are thus,

- Knowledge of sources and emissions
- Transport, diffusion and parametrisation
- Chemical transformations
- Removal process
- Meteorology

Understanding contribution from various sources to air quality is the key for effective management of the air quality. Air quality models offer a useful tool in comprehending these issues. These models evaluate the relationship between air pollutant emissions and their resulting concentration in the ambient air. Commonly used air quality models are: 1) Conceptual Models 2) Emission Models 3) Meteorological Models, 4) Chemical Models, 5) Source Oriented Models and 6) Receptor Models.

3. Air quality model classification

Air quality models cover either separately or together atmospheric phenomena at various temporal and spatial scales. Urban air models generally focus from local (micro- tens of meters to tens of kilometers) to regional (meso) scale. Models can be broadly divided into two types namely physical and mathematical.

Physical models involve reproducing urban area in the wind tunnel. Scale reduction in the replica and producing scaling down actual flows of atmospheric motion result in limited utility of such models. Moreover these are economically undesirable.

Mathematical models use either use statistics to analyse the available data or mathematical representation of all the process of concern. The second type of mathematical models is constrained by the ability to represent physical and chemical processes in equations without assumptions.

Statistical models are simple but they do not explicitly describe causal relationships and they cannot be extrapolated beyond limits of data used in their derivation. Thus dependence on past data becomes their major weakness. These cannot be used for planning as they cannot predict effect of changes in emissions.

3.1 Eulerian and Lagrangian models

Eulerian approach has been used to predict air pollutant concentrations in urban areas. The space domain (geographical area or air volume), are divided into "small" squares (two-dimensional) or volumes (three-dimensional), i.e. grid cells. Thus Eulerian models are sometimes called "grid models". Equidistant grids are normally used in air pollution modeling. Then the spatial derivatives involved in the system of Partial Differential Equations are discretized on the grid chosen. The transport, diffusion, transformation, and deposition of pollutant emissions in each cell are described by a set of mathematical expressions in a fixed coordinate system. Chemical transformations can also be included. Long range transport, air quality over entire air shed, that is, large scale simulations are mostly done using Eulerian models. Reynolds (1973), Shir and Shieh (1974) applied Eulerian model for ozone and for SO₂ concentration simulation in urban areas, and Egan (1976) and Carmichael (1979) for regional scale sulfur. Holmes and Morawska (2006) used Eulerian model to calculate the transport and dispersion over long distances. The modeling studies by Reynolds (1973) on the Los Angeles basin formed the basis of the, the well-known Urban Air shed Model-UAM. Examples of Eulerian models are CALGRID model and ARIA Regional model or the Danish Eulerian Hemispheric Model (DEHM).

Lagrangian Model approach is based on calculation of wind trajectories and on the transportation of air parcels along these trajectories. In the source oriented models the trajectories are calculated forward in time from the release of a pollutant-containing air parcel by a source (forward trajectories from a fixed source) until it reaches a receptor site. And in receptor oriented models the trajectories are calculated backward in time from the arrival of an air parcel at a receptor of interest (backward trajectories from a fixed receptor). Numerical treatment of both backward and forward trajectories is the same. The choice of use of either method depends on specific case. As the air parcel moves it receives the emissions from ground sources, chemical transformations, dry and wet depositions take place. If the models provide average time-varying concentration estimates along the box trajectory then Lagrangian box models have been used for photochemical modeling. The major shortcoming of the approach is the assumption that wind speed and direction are constant throughout the Physical Boundary Layer. As compared to the Eulerian box models the Lagrangian box models can save computational cost as they perform computations of chemical and photochemical reactions on a smaller number of moving cells instead of at each fixed grid cell of Eulerian models. Versions of EMEP (European Monitoring and Evaluation Programme) are examples of Lagrangian models. These models assume pollutants to be evenly distributed within the boundary layer and simplified exchange within the troposphere is considered.

3.2 Box models

Box models are based on the conservation of mass. The receptor is considered as a box into which pollutants are emitted and undergo chemical and physical processes. Input to the model is simple meteorology. Emissions and the movement of pollutants in and out of the

box is allowed. The air mass is considered as well mixed and concentrations to be uniform throughout. Advantage of the box model is simple meteorology input and detailed chemical reaction schemes, detailed aerosol dynamics treatment. However, following inputs of the initial conditions a box model simulates the formation of pollutants within the box without providing any information on the local concentrations of the pollutants. Box models are not suitable to model the particle concentrations within a local environment, as it does not provide any information on the local concentrations, where concentrations and particle dynamics are highly influenced by local changes to the wind field and emissions.

3.3 Receptor models

Receptor modeling approach is the apportionment of the contribution of each source, or group of sources, to the measured concentrations without considering the dispersion pattern of the pollutants. The starting point of Receptor models is the observed ambient concentrations at receptors and it aims to apportion the observed concentrations among various source types based on the known source profile (i.e. chemical fractions) of source emissions. Mathematically, the receptor model can be generally expressed in terms of the contribution from 'n' independent sources to 'p' chemical species in 'm' samples as follows:

$$C_{ik} = \sum_{j=1}^n a_{ij} f_{jk} \quad (1)$$

Where C_{ik} is the measured concentration of the k^{th} species in the i^{th} sample, a_{ij} is the concentration from the j^{th} source contributing to the i^{th} sample, and f_{jk} is the k^{th} species fraction from the j^{th} source. Receptor models can be grouped into Chemical mass balance (CMB), Principal Component Analysis (PCA) or Factor analysis, and Multiple Linear Regression Analysis (MLR) and multivariate receptor models.

The Chemical Mass Balance (CMB) Receptor Model used by Friedlander, 1973 uses the chemical and physical characteristics of gases and particulate at source receptor to both identify the presence of and to quantify source contributions of pollutants measured at the receptor. Hopke (1973, 1985) christened this approach as receptor modelling. The CMB model obtains a least square solution to a set of linear equation, expressing each receptor concentration of a chemical species as a linear sum product of source profile species and source contributions. The output to the model consists of the amount contributed by each source type to each chemical species. The model calculates the contribution from each source and uncertainties of those values. CMB model applied to the VOC emissions in the city of Delhi and Mumbai (Figure 4) shows that emissions from petrol pumps and vehicles at traffic intersection dominate.

PCA and MLR are statistical models and both PMF and UNMIX are advanced multivariate receptor models that determine the number of sources and their chemical compositions and contributions without source profiles. The data in PMF are weighted by the inverse of the measurement errors for each observation. Factors in PMF are constrained to be nonnegative. PMF incorporates error estimates of the data to solve matrix factorization as a constrained, weighted least-squares problem (Miller et al., 2002; Paatero, 2004).

Geometrical approach is used in UNMIX to identify contributing sources. If the data consist of 'm' observations of 'p' species, then the data can be plotted in a p-dimensional data space, where the coordinates of a data point are the observed concentrations of the species during a

sampling period. If n sources exist, the data space can be reduced to a $(n-1)$ dimensional space. An assumption that for each source, some data points termed as edge points exist for which the contribution of the source is not present or small compared to the other sources.

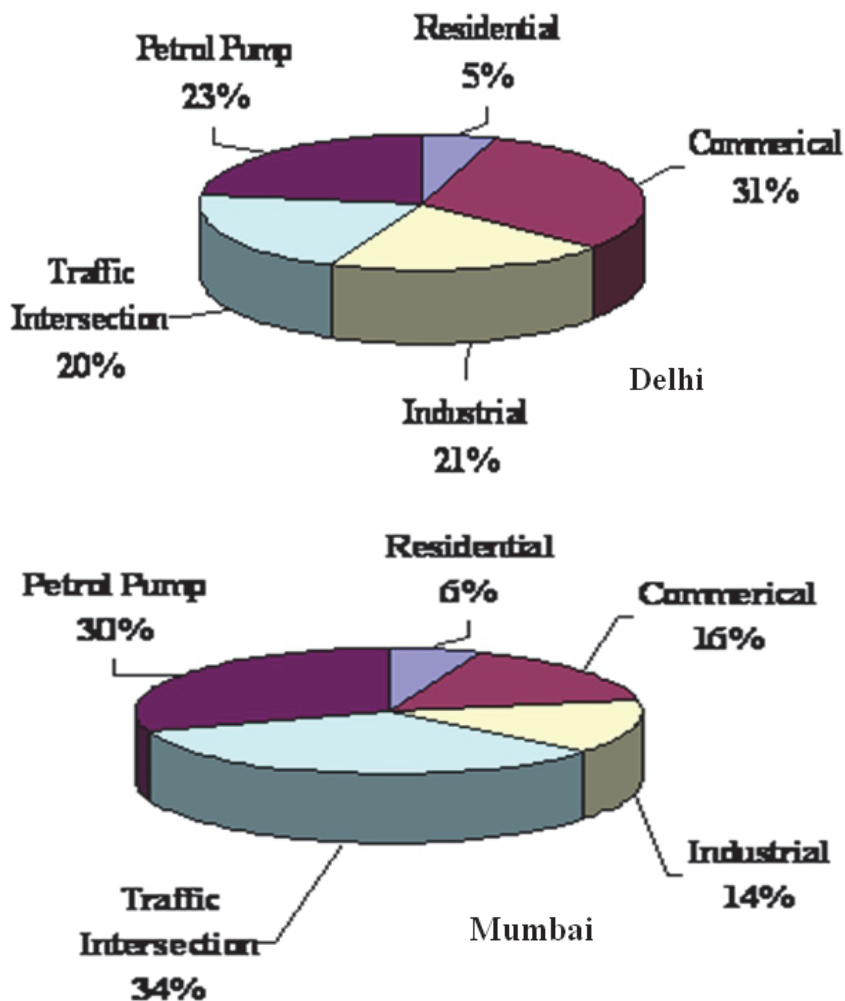


Fig. 4. Category wise Contribution to Total VOCs at Mumbai and Delhi based on CMB results(Ref: Anjali Srivastava 2004, 2005)

UNMIX algorithm identifies these points and fits a hyperplane through them; this hyperplane is called an edge. If n sources exist, then the intersection of $n-1$ of these edges defines a point that has only one contributing source. Thus, this point gives the source composition. In this way, compositions of the n sources are determined which are used to calculate the source contributions (Henry, 2003).

3.4 Computational fluid dynamic models

Resolving the Navier-Stokes equation using finite difference and finite volume methods in three dimensions provides a solution to conservation of mass and momentum. Computational fluid dynamic (CFD) models use this approach to analyse flows in urban areas. In numerous situation of planning and assessment and for the near-sources region, obstacle-resolved modeling approaches are required. Large Eddy Simulations (LES) models explicitly resolve the largest eddies, and parameterize the effect of the sub grid features. Reynolds Averaged Navier Stokes (RANS) models parameterize all the turbulence, and resolve only the mean motions. CFD (large eddy simulation [LES] or Reynolds-averaged Navier-Stokes [RANS]) model can be used to explicitly resolve the urban infrastructure. Galmarini et al., 2008 and Martilli and Santiago,2008, used CFD models to estimate spatial averages required for Urban Canopy Parameters. Using CFD models good agreement in overall wind flow was reported by field Gidhagen et al. (2004). They also reported large differences in velocities and turbulence levels for identical inputs.

3.5 The Gaussian steady-state dispersion model

The Gaussian Plume Model is one of the earliest models still widely used to calculate the maximum ground level impact of plumes and the distance of maximum impact from the source. These models are extensively used to assess the impacts of existing and proposed sources of air pollution on local and urban air quality. An advantage of Gaussian modeling systems is that they can treat a large number of emission sources, dispersion situations, and a receptor grid network, which is sufficiently dense spatially (of the order of tens of meters). Figure 5 shows a buoyant Gaussian air pollutant dispersion plume. The width of the plume is determined by σ_y and σ_z , which are defined by stability classes (Pasquill 1961; Gifford Jr. 1976)

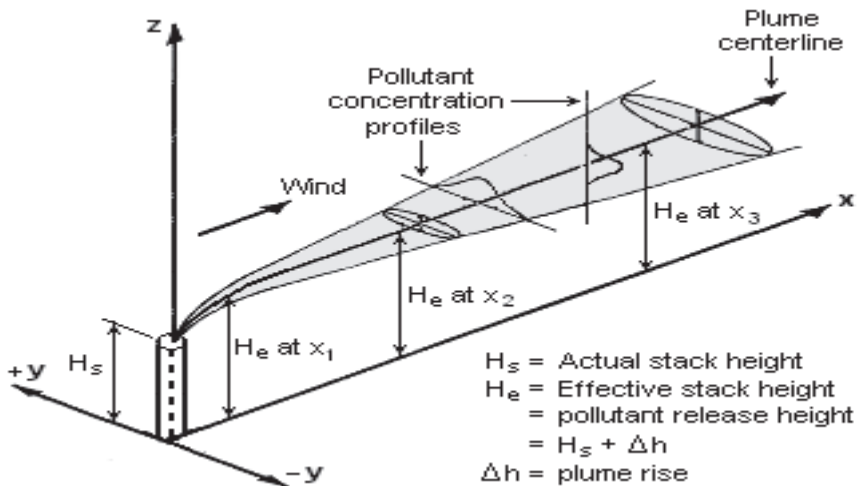


Fig. 5. A buoyant Gaussian air pollutant dispersion plume
 The assumptions of basic Gaussian diffusion equations are:

- that atmospheric stability and all other meteorological parameters are uniform and constant throughout the layer into which the pollutants are discharged, and in particular that wind speed and direction are uniform and constant in the domain;
- that turbulent diffusion is a random activity and therefore the dilution of the pollutant can be described in both horizontal and vertical directions by the Gaussian or normal distribution;
- that the pollutant is released at a height above the ground that is given by the physical stack height and the rise of the plume due to its momentum and buoyancy (together forming the effective stack height);
- that the degree of dilution is inversely proportional to the wind speed;
- that pollutant material reaching the ground level is reflected back into the atmosphere;
- that the pollutant is conservative, i.e., not undergoing any chemical reactions, transformation or decay.

The spatial dynamics of pollution dispersion is described by the following type of equation in a Gaussian model:

$$C(x, y, z; He) = \frac{Q}{2\pi u \sigma_y \sigma_z} \cdot \left[\exp\left(-\frac{y^2}{2\sigma_y^2}\right) \cdot \left\{ \exp\left(-\frac{(z-He)^2}{2\sigma_z^2}\right) + \exp\left(-\frac{(z+He)^2}{2\sigma_z^2}\right) \right\} \right] \quad (2)$$

Where

$C(x, y, z)$: pollutant concentration at. point (x, y, z) ;

U : wind speed (in the x "downwind" direction, m/s)

Σ : represents the standard deviation of the concentration in the x and y direction, i.e., in the wind direction and cross-wind, in meters;

Q : is the emission strength (g/s)

He : is the effective stack height, see below.

From the above equation, the concentration in any point (x, y, z) in the model domain, from a constant emission rate source, in steady state can be calculated.

Plume rise equations have been developed by Briggs (1975). The effective stack height (physical stack height plus plume rise) depends on exit velocity of gas, stack diameter, average ambient velocity, stack gas temperature and stability of atmosphere

$$H_e = H + \Delta H, \Delta H = 1.4Q_H^{1/4} \left(\frac{d\theta}{dz}\right)^{-3/8}, Q_H = \rho Q C_p (T_G - 15) / 3600 \quad (3)$$

Where

H : height of stack

T_G : Temperature of exit gas

Q : Volume of exit gas

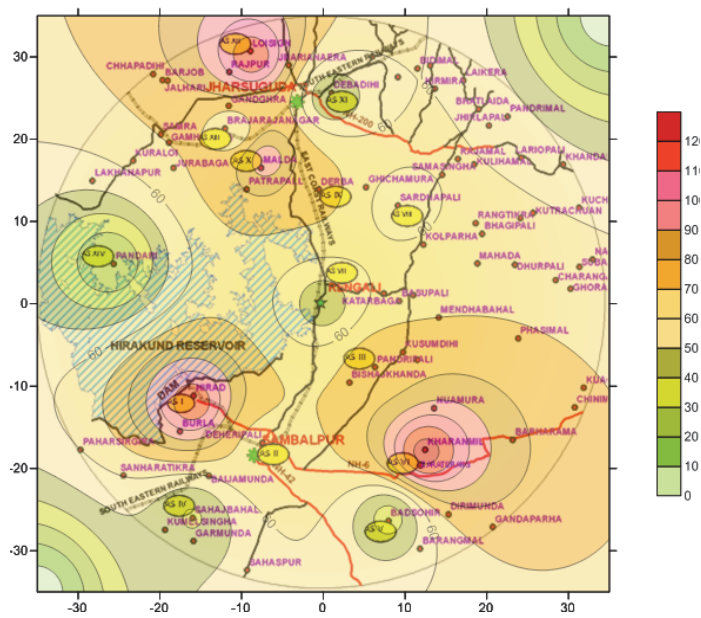
$d\theta/dz$: Temperature Gradient

ρ : Density of exit gas

C_p : Specific heat at constant pressure

Some major air pollution dispersion models in current use

- ADMS 3: Developed in the United Kingdom (www.cerc.co.uk)
- AERMOD: Developed in the United States , (www.epa.gov/scram001/dispersion_prefrec.htm)
- AUSPLUME: Developed in Australia, (<http://www.epa.vic.gov.au/air/epa>)
- CALPUFF: Developed in the United States , (www.src.com/calpuff/calpuff1.htm)
- DISPERSION2: Developed in Sweden , (www.smhi.se/foretag/m/dispersion_eng.htm)
- ISC3: Developed in the United States, (www.epa.gov/ttn/scram/dispersion_alt.htm)
- LADM: Developed in Australia, (Physick, W.L,et al, 1994)
- NAME: Developed in the United Kingdom, (www.metoffice.gov.uk/research/modelling-systems/dispersion-model)
- MERCURE: Developed in France, (www.edf.com)
- RIMPUFF: Developed in Denmark, (<http://www.risoe.dtu.dk>)



AQI of ambient air	Description of air quality
Below 20	Excellent
Between 20 and 39	Good
Between 40 and 59	Fair
Between 60 and 79	Poor
Between 80 and 99	Bad
Beyond 100	Dangerous

Fig. 6. Air Quality Index of an Industrial Area: Orissa, India

8 regional air quality modeling leading to setting up of air quality index for an industrial area in India is given in Fig 2. This study has resulted in estimating the air assimilative capacity of the region and delineating developmental plans accordingly

3.6 Urban pollution and climate integrated modeling

Integrated air quality modelling systems are tools that help in understanding impacts from aerosols and gas-phase compounds emitted from urban sources on the urban, regional, and global climate. Piringer et al., 2007 have demonstrated that urban features essentially influence atmospheric flow and microclimate, strongly enhance atmospheric turbulence, and modify turbulent transport, dispersion, and deposition of atmospheric pollutants. Numerical weather prediction (NWP) models with increased resolution helps to visualize a more realistic reproduction of urban air flows and air pollution processes.

Integrated models thus link urban air pollution, tropospheric chemistry, and climate. Integration time required is ≥ 10 years for tropospheric chemistry studies in order to consider CH_4 and O_3 simulation and aerosol forcing assessment. Tropospheric chemistry and climate interaction studies extend the integration time to ≥ 100 years.

Urban air quality and population exposure in the context of global to regional to urban transport and climate change is proposed to be assessed by integrating urbanized NWP and Atmospheric Chemistry (ACT) models (Baklanov et al., 2008; Korsholm et al., 2008). A. A. Baklanov and R. B. Nuterman (2009) suggested a multi-scale modelling system which comprised of downscaling from regional to city-scale with the Environment -High Resolution Limited Area Model (Enviro-HIRLAM) and to micro-scale with the obstacle-resolved Microscale Model for Urban Environment (M2UE). Meteorology governs the transport and transformations of anthropogenic and biogenic pollutants, drives urban air quality and emergency preparedness models; meteorological and pollution components have complex and combined effects on human health (e.g., hot spots, heat stresses); and pollutants, especially urban aerosols, influence climate forcing and meteorological events (precipitation, thunderstorms, etc.), thus this approach is closer to real life scenario. Examples of integrated models are Enviro-HIRLAM: Baklanov and Korsholm, 2007, WRF-Chem: Grell et al., 2005; EMS-FUMAPEX: Forecasting Urban Meteorology, Air Pollution and Population Exposure; CFD (large eddy simulation [LES] or Reynolds-averaged Navier-Stokes [RANS]) models: Galmarini et al., 2008 and Martilli and Santiago., 2008; MIT Integrated Global System Model Version 2 (IGSM2): A.P. Sokolov, C.A. Schlosser, S. Dutkiewicz, S. Paltsev, D.W. Kicklighter, H.D. Jacoby, R.G. Prinn, C.E. Forest, J. Reilly, C. Wang, B. Felzer, M.C. Sarofim, J. Scott, P.H. Stone, J.M. Melillo and J. Cohen., 2005; US EPA and NCAR communities for MM5 (Dupont et al., 2004; Bornstein et al., 2006; Taha et al., 2008), WRF models (Chen et al., 2006); THOR - an Integrated Air Pollution Forecasting and Scenario Management System: National Environmental Research Institute (NERI), Denmark.

The outline of overall methodology of FUMAPEX and MIT interactive chemistry model is shown in Figure 6 and 7. Schematic of couplings between atmospheric model and the land model components of the MIT IGSM2 is given in Figure 8.

Need of integrated models

All of these models have uncertainties associated with them. Chemical transport models, such as Gaussian plume models and gridded photochemical models, begin with pollutant emissions estimates and meteorological observations and use chemical and physical principles to predict ambient pollutant concentrations. Since these models require temporally and spatially resolved data and can be computationally intensive, they can only be used for well-characterized regions and over select time periods. Eulerian grid models are not suitable to assess individual source impacts, unless the emissions from the individual source are a significant fraction of the domain total emissions. This limitation

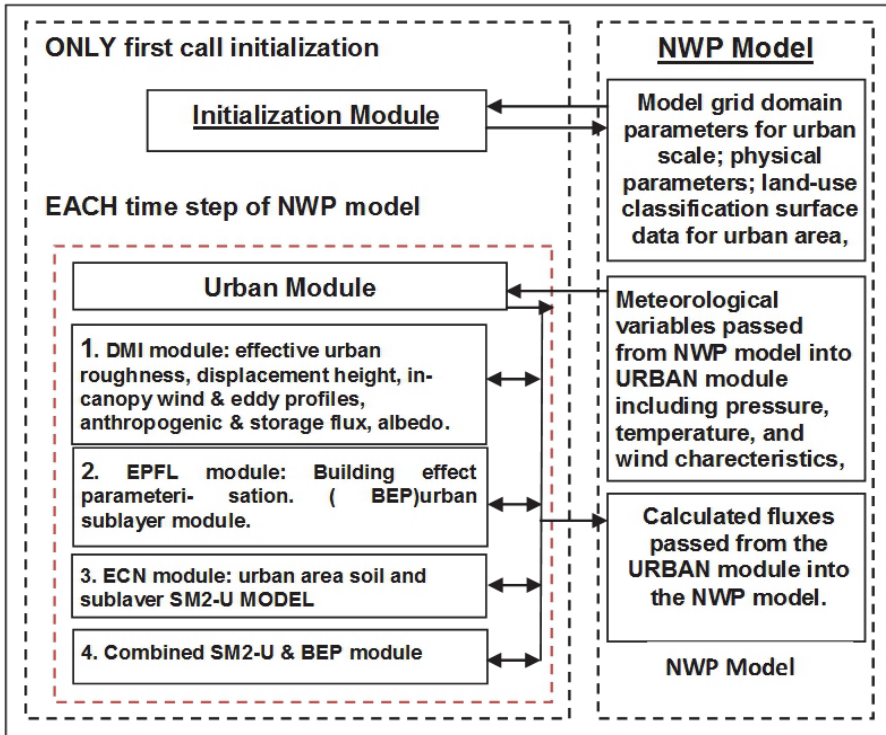


Fig. 7. General scheme of the FUMAPEX urban module for NWP models.

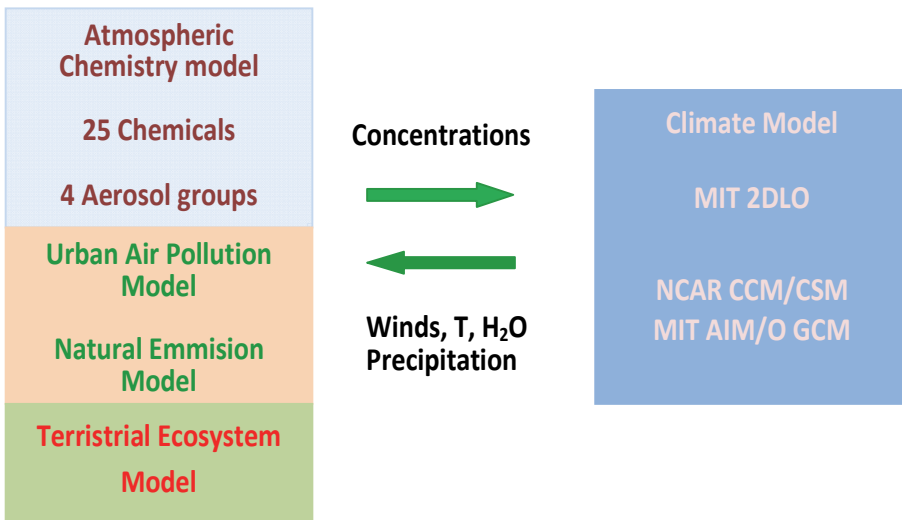


Fig. 8. Overall Scheme MIT Interactive Chemistry-Climate Model

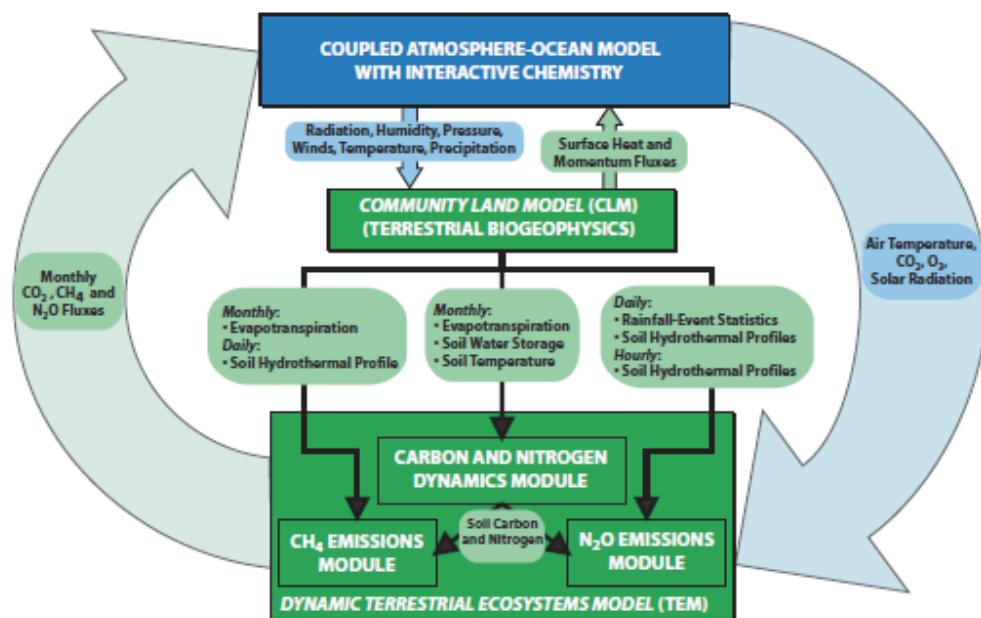


Fig. 9. Schematic of coupling between the atmospheric model (which also includes linkages to the air chemistry and ocean models) and the land model components of the IGSM2, also shown are the linkages between the biogeophysical (CLM) and biogeochemical (TEM) subcomponents. All green shaded boxes indicate fluxes/storage that are explicitly calculated/tracked by this Global Land System (GLS). The blue shaded boxes indicate those quantities that are calculated by the atmospheric model of the IGSM2.

arises from the assumption that emissions are uniformly mixed within the grid cell, and thus do not properly address the initial growth and dispersion of the pollutants. Lagrangian plume and puff models account for chemical processes by simple linear transformations in time. These models can track individual source impacts, thus enabling user to outline source specific air pollution control strategies. Considerable differences are observed when concentrations are compared in time and space because of uncertainties in the characterization of the direction of transport that are of the order of the actual plume width. The observed and simulated concentrations for fixed receptors, give estimates of maximum concentration values within a factor of two or three of those observed. These differences are an order of magnitude larger than those observed for estimates of secondary pollutants. Both Eulerian and Lagrangian, models are not suitable to handle inert pollutants and secondary pollutants whose concentrations depend on reaction rates and are photochemical in nature.

Receptor models, such as Positive Matrix Factorization and Chemical Mass Balance (CMB), source apportionment addresses the problem by statistical inference of source contributions to total pollution from observations of ambient air chemical composition. Mass balance methods of source apportionment use linear models with chemical composition vectors of sources as covariates. Knowledge of meteorological variables is not required but may be

used to refine the analysis. Knowledge of emission sources is useful for the interpretation of results from statistical-based receptor models and is required by receptor models that use a mass balance approach. Less data and computational resource requirement by Receptor models as compared to chemical transport models, make them more convenient tool for evaluation of ambient pollutant concentrations and pollutant emission inventory. However, their utility for reactive air pollutants is uncertain and questionable. The disadvantage of CMB model arises from its assumptions. such as constant compositions of source emissions over the period of ambient and source sampling; linear additive and unreactive chemical species; identification of all sources contributing to the receptor and knowledge of their emission profile, linearly independent emission profiles.

The urban air quality models requires

- Good net work ambient air concentrations of pollutants of concern: Geography of the urban area, constructed clusters, road network, location of buildings etc play a major role in dispersion of pollutants. Thus to understand the ambient status of pollutants it is necessary to have sufficient number of monitoring locations to cover the urban sprawl of concern.
- Micro meteorology data: The wind patterns, temperature, humidity alter in urban areas according to anthropogenic activity and architecture
- Building details: To account for the effect of anthropogenic architecture falling in path of plume, its geometry is required to be known.
- Knowledge of all sources: All sources and their emission profiles are required to be known to plan for further development in urban area and control of pollutant emission
- Atmospheric Chemistry: All transformations of emitted chemical species, their reaction rates pathways must be known to account for observed concentration of pollutants.
- Healthy Impacts: Models need to incorporate health effect of pollutants

None of the models available can handle all the requirements of urban air quality management. Each one focuses on one aspect and thus coupling of different models are required.

4. Further issues to be addressed

COST an intergovernmental framework for European Cooperation in Science and Technology, Europe, addressed issues related to urban air quality models in its action programmes. Cost 728 focussed on enhancing mesoscale meteorological Modeling capabilities for air pollution and Dispersion applications under larger programme of urbanization of meteorological and air quality models. The issues identified for improvements to the state of urbanization of models can be summarized as

- Systematic evaluation of urban land surface schemes
- Increasing the range of variables observed to ensure as complete a range of evaluation as possible
- evaluation over a broad spectrum of conditions (meteorological, morphological, geographical setting, etc.
- Testbeds and observatories with different objectives and dataset richness.
- A deeper understanding of urban PBL dynamics i.e development of long-term urban test beds in a variety of geographic regions (e.g., inland, coastal, complex terrain) and in

many climate regimes, with a variety of urban core types (e.g., deep versus shallow, homogeneous versus heterogeneous).

- A framework to address conceptual issue of evaluation of model prediction of the flow within the canopy
- User friendly and multifaceted urban databases and enabling technology
- Developing core capabilities for advancing urban modeling and boundary layer research
- An open database to address issues of availability and sources of high-resolution data sets easily to all with mechanism for its maintenance, upgrading, updating, and archiving.
- www.unep.org/urban_environment/pdfs/handbook.pdf

5. References

- Baklanov, A., and U. Korsholm, 2007: On-line integrated meteorological and chemical transport modelling: advantages and prospective. In: Preprints ITM 2007: 29th NATO/SPS International Technical Meeting on Air Pollution. Modelling and its Application, 24-28.09.2007, University of Aveiro, Portugal, pp. 21-34.
- Baklanov, A., Korsholm, U., Mahura, A., Petersen, C., and Gross, A.: ENVIRO-HIRLAM: on-line coupled modelling of urban meteorology and air pollution, *Adv. Sci. Res.*, pp. 2, 41-46, 2008.
- Baklanov A. A. and Nuterman. R. B., Multi-scale atmospheric environment modeling for urban areas, *Advances in Science and Research*, 3, 53-57, 2009
- Bornstein, R., R. Balmori, H. Taha, D. Byun, B. Cheng, J. Nielsen-Gammon, S. Burian, S. Stetson, M. Estes, D. Nowak, and P. Smith, 2006: Modeling the effects of land-use land cover modifications on the urban heat island phenomena in Houston, Texas. SJSU Final Report to Houston Advanced Research Center for Project No. R-04-0055, pp. 127.
- Briggs, G. A. (1975). Plume Rise Predictions. Lectures on Air Pollution and Environmental Impact Analysis. D. A. Haugen. Boston, MA, American Meteorology Society: pp.59-111.
- Carmichael, G.R., and Peters, L.K., 1979, Numerical simulation of the regional transport of SO₂ and sulfate in the eastern United States, *Proc. 4 th Symp. on turbulence, diffusion and air pollution*, AMS 337.
- Chen, F., M. Tewari, H. Kusaka and T. L. Warner, 2006: Current status of urban modeling in the community Weather Research and Forecast (WRF) model. Sixth AMS Symposium on the Urban Environment, Atlanta GA, January 2006.
- Dupont, S., T.L. Otte, and J.K.S. Ching, 2004: Simulation of meteorological fields within and above urban and rural canopies with a mesoscale model (MM5) *Boundary-Layer Meteor.*, 2004, 113:111-158.
- Egan, B.A., Rao, K.S., and Bass, A., 1976, A three dimensional advective-diffusive model for long-range sulfate transport and transformation 7 th ITM, 697, Airlie House.
- Friedlander, S.K. (1973). Chemical element balances and identification of air pollution sources, *Environmental Science and Technology* 7, 235-240
- Galmarini, S., J.-F. Vinuesa, and A. Martilli, 2008: Relating small-scale emission and concentration variability in air quality models, Chapter 1.2, URBANIZATION OF

- METEOROLOGICAL AND AIR QUALITY MODELS, COST Action 728, 15 May 2008, <http://www.cost728.org>
- Garratt, J. R. (1978): Transfer Characteristics for a Heterogeneous Surface of Large Aerodynamic Roughness. *Quart. J. R. Meteorol. Soc.*, 104: pp.491-502.
- Garratt J.R. (1980) Surface influence upon vertical profiles in the nocturnal boundary layer *Boundary-Layer Meteorology* Volume 26, Number 1, pp. 69-80, DOI: 10.1007/BF00164331
- Garratt J.R. 1994. Review: the atmospheric boundary layer, *Earth-Science Reviews*, 37, pp.89-134.
- Gidhagen, L., C. Johansson, J. Langner and G. Olivares. (2004). "*Simulation of NO_x and ultrafine particles in a street canyon in Stockholm, Sweden.*" *Atmospheric Environment* 38(14): 2029-2044.
- Gifford Jr., F. A. (1976). "*Consequences of Effluent Releases.*" *Nuclear Safety* 17(1): 68-86.
- Grell, G. A., S. E. Peckham, R. Schmitz, S. A. McKeen, G. Frost, W. C. Skamarock, and B. Eder, 2005: Fully coupled "online" chemistry within the WRF model, *Atmos. Environ.*, 39(37), 6957-6975.
- Henry, R.C., 2003. Multivariate receptor modeling by N-dimensional edge detection. *Chemometrics and Intelligent Laboratory Systems* pp.65, 179-189.
- Holmes, N. S., L. Morawska, et al. (2005). "*Spatial distribution of submicrometre particles and CO in an urban microscale environment.*" *Atmospheric Environment* 39(22): 3977-3988.
- Holmes, N. S., Morawska, L. (2006) A review of dispersion modelling and its application to the dispersion of particles: An overview of different dispersion models available. *Atmospheric Environment*, pp. 40, 5902-5928.
- Hopke, P.K. (1985). *Receptor Modeling in Environmental Chemistry*, Wiley, New York.
- Hopke, P.K., ed. (1991). *Receptor Modeling for Air Quality Management*, Elsevier, Amsterdam.
- Hosker, G. L. 1985 *Clin. Phys. Physiol. Meas.* 6 131 A uni-directional urethral force gauge
- Pavageau, M., Rafailidis, S. and Schatzmann, M. (2001) '*A comprehensive experimental databank for the verification of urban car emission dispersion models*', *International Journal of Environment and Pollution*, 15, pp. 417-425
- Jacoby, H.D., Prinn, R.G., Forest, C.E., Reilly, J., Wang, C., Felzer, B., Sarofim, M.C., Scott, J., Stone, P.H., Melillo J.M. and Cohen, J., Report No. 124, July 2005
- Korsholm, U. S., Baklanov, A., Gross, A., and Sørensen, J. H.: On the importance of the meteorological coupling interval in dispersion modeling during ETEX-1, *Atmos. Environ.*, doi:10.1016/j.atmosenv.2008.11.017, 2008.
- Martilli, A., and J.L. Santiago, 2008: How to use computational fluid dynamics models for urban canopy parameterizations. Chapter 2.1, URBANIZATION OF METEOROLOGICAL AND AIR QUALITY MODELS, COST Action 728, 15 May 2008, <http://www.cost728.org>
- Miller, S.L., Anderson, M.J., Daly, E.P., Milford, J.B., 2002. Source apportionment of exposures to volatile organic compounds. I. Evaluation of receptor models using simulated exposure data. *Atmospheric Environment* pp. 36, 3629-3641.
- Mumovic, D., Crowther, J., Stevanovic, Z. (2006). Integrated Air Quality Modelling for a Designated Air Quality Management Area in Glasgow, *Building and Environment*, 41(12): 1703-1712. doi:10.1016/j.buildenv.2005.07.006
- Mumovic, D., Crowther, J. (2006). Assessing Urban Air Quality using Microscale CFD Modeling, PHOENICS CFD Newsletter Spring 2006, 10-10

- Oke, T. R., 1988: "The urban energy balance," Progress in Physical Geography, vol.12, pp. 471-508.
- Paatero, P., 2004. User's Guide for Positive Matrix Factorization Programs PMF2 and PMF3, Part 1: Tutorial. University of Helsinki, Finland.
- Pasquill, F. (1961). "The Estimation of the Dispersion of Windborne Material." Meteorology Magazine 90(1063): pp. 33-40.
- Pavageau, M., Rafailidis, S. and Schatzmann, M. (2001) 'A comprehensive experimental databank for the verification of urban car emission dispersion models', International Journal of Environment and Pollution, 15, 417-425
- Physick. W.L., Noonan. J.A., MacGregor, J.L. (1994). LADM: a Lagrangian Atmospheric Dispersion Model [Monograph], CSIRO Division of Atmospheric Research technical paper.
- Piringer M., Petz E., Groehn I., Schauburger G. (2007) A sensitivity study of separation distances calculated with the Austrian Odour Dispersion Model (AODM), Atmospheric Environment, pp.41, 725-1735.
- Raupach, M.R., Thom, A.S., and Edwards, I.: 1980, "A Wind Tunnel Study of Turbulent Flow Close to Regularly Arrayed Rough Surfaces", *Boundary-Layer Meteorol.* 18, 373-397.
- Reynolds, S., Roth, P., and Seinfeld, J., 1973, *Mathematical modeling of photochemical air pollution* *Atm.Env* 7.
- Rotach, M. W.: 1993, Turbulence close to a rough urban surface, Part II: *Variances and gradients*, *Boundary Layer Meteorol.*, pp. 66, 75-92,
- Rotach M W (1995) 'Profiles of turbulence statistics in and above an urban street canyon', *Atmospheric Environment*, Vol 29, pp. 1473-1486
- Shir, C.C. and L.J. Shieh, 1974, A generalized urban air pollution model and its application to the study of SO₂-distribution in the St. Louis Metropolitan area, *J. Appl. Met.* 19, 185-204.
- 2002: South Asia Urban Air Quality Management Briefing. Note No. 4., What Do We Know About Air Pollution? – India Case Study, <http://www.worldbank.org/sarurbanair>
- 2002: South Asia Urban Air Quality Management Briefing Note No. 5., Impact of Traffic Management, <http://www.worldbank.org/sarurbanair>.
- Srivastava, Anjali ; Sengupta B., Dutta S.A., 'Source apportionment of ambient VOCs in Delhi City Science of The Total Environment', Volume 343, Issues 1-3, 1 May 2005, pp.207-220
- Srivastava, Anjali ; 'Source apportionment of ambient VOCS in Mumbai city Atmospheric Environment', Volume 38, Issuey39, December2004, pp. 6829-6843
- Stanners, D., Bourdeau, P. (Eds.), 1995. Europe's Environment: The Dobris Assessment, European Environment Agency. Office for Publications of the European Communities, Luxemburg.
- Sokolov, A.P., C.A. Schlosser, S. Dutkiewicz, S. Paltsev, D.W. Kicklighter, 2005 :The MIT Integrated Global System Model (IGSM), Version 2: Model Description and Baseline Evaluation,
- Taha, H., 2008: Sensitivity of the urbanized MM5 (uMM5) to perturbations in surface properties in Houston Texas. *Boundary-Layer Meteorology*, pp. 127: 193-218
- Tennekes, H., 1973. *A model for the dynamics of the inversion above a convective boundary layer.* *Journal of Atmospheric Science* 30, pp.550-567

THOR - an Integrated Air Pollution Forecasting and Scenario Management System. Available at thor.dmu.dk National Environmental Research Institute (NERI), Denmark

Urban Environment Management, Tool book United Nations Environment Programme, United Nations Human Settlements Programme. Available at www.unep.org/urban_environment/pdfs/handbook.pdf

Artificial Neural Network Models for Prediction of Ozone Concentrations in Guadalajara, Mexico

Ignacio García¹, José G. Rodríguez² and Yenisse M. Tenorio²

¹*Centro Mexicano para la Producción Más Limpia (IPN), Departamento de Posgrado, Barrio La Laguna, Col. Ticomán, Delegación Gustavo A. Madero,*

²*Escuela Superior de Ingeniería y Arquitectura (IPN-ESIA Zacatenco), Sección de Investigación y Posgrado, U. Prof. "Adolfo López Mateos", Zacatenco, Del. Gustavo A. Madero, México,*

1. Introduction

Advances in mathematical models to describe the formation, emission, transport and disappearance of air pollutants have led to a greater understanding of the dynamics of these pollutants. However, the more complex the model, the more information is required for their application to have sufficient certainty that the results will have technical or scientific value (Russell & Dennis, 2000). These deterministic models require much information that is not always possible to obtain; the data available have not always resulted in successful outcomes upon application of the model (Roth, 1999), or the cost of obtaining reliable data can be prohibitive (Pun & Louis, 2000).

There are other methods requiring less information that can be used to study air pollution in some areas. These methods generally make use of statistical techniques such as regression or other data-fitting methods using numerical techniques to establish the respective relationships between the various physicochemical parameters and variable of interest based on routinely-measured historical data.

The main objectives of these methods include investigating and assessing trends in air quality, making environmental forecasts and increasing scientific understanding of the mechanisms that govern air quality (Thompson et al., 2001).

Among the techniques being examined to relate air quality in a given area to measured physical and chemical parameters, the three that have been used most often are i) multivariate regression (Hubbard & Cobourne, 1998, Comrie & Diem, 1999, Davis & Speakman, 1999; Draxler, 2000, Gardner & Dorling, 2000), ii) artificial neural networks (ANN) (Perez & Reyes, 2006; Brunelli et al., 2006; Thomas & Jacko, 2007; Grivas & Chaloulakou, 2005; Gardner & Dorling, 1999), and iii) time series and spectral analysis (Raga & Moyné, 1996, Chen et al., 1998; Milanchus et al., 1998, Salcedo et al., 1999, Sebald et al., 2000).

Artificial neural networks have greater flexibility, efficiency and accuracy, since they have a large number of features similar to those of the brain; i.e., they are capable of learning from experience, of generalizing from previous cases to new cases, and of abstracting essential features from inputs containing irrelevant information; they use adaptive learning, one of

the most attractive features of ANN, as well as the ability to learn to perform tasks based on training or initial experience. ANN do not need an algorithm to solve a problem because they can generate their own distribution of the weights of the links through learning and are easily inserted into the existing technology. Because of these characteristics, ANN generally has low computational requirements and their construction is less complex.

The pollutant of interest in this study is tropospheric ozone, as it is the main component of a type of air pollution known as smog or photochemical smog. According to the National Ecology Institute (NEI), the Metropolitan Zone of Guadalajara, Mexico (GMA) is in second place in Mexico in exceeding the NOM-020-SSA1-1993 Mexican air pollution standard. Tropospheric ozone is one of the five major pollutants with harmful effects on human health, causing respiratory problems and ailments such as headaches, and eye irritation as well as affecting vegetation, metals and construction materials, dyes and pigments.

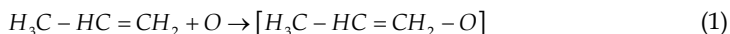
1.1 Tropospheric ozone formation

Photochemical smog is formed through a photochemical process from a combination of gases in the troposphere, such as nitrogen oxides (NO_x , i.e., NO and NO_2), volatile organic compounds (VOCs) and carbon monoxide (CO), as has been documented (Seinfeld, 1978; Boubel, 1994 & Godish, 1991, as cited scientist in Comrie, 1997).

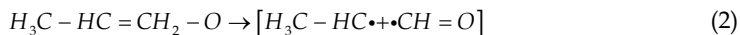
The sequence of events begins in the early hours of the morning when a heavy emission of hydrocarbons (HC) and nitrogen monoxide (NO) is produced at the start of human activity in large cities (heaters are turned on, and traffic density increases). Nitric oxide (NO) is oxidized to nitrogen dioxide (NO_2), increasing the concentration of the latter in the atmosphere. Higher concentrations of NO_2 together with increasing solar radiation as the morning wears on starts the photolytic NO_2 cycle, generating atomic oxygen which, as it is transformed into ozone, leads to an increase in the concentration of oxygen and hydrocarbon free radicals. These, when combined with significant amounts of NO, cause NO in the atmosphere to decrease.

This impedes completion of the photolytic cycle, rapidly increasing the ozone (O_3) concentration (Comrie, 1997).

These relationships can be expressed conceptually; the polluted urban atmosphere contains approximately one hundred different hydrocarbons, olefins being the most reactive. The result of the atomic oxygen attack on the olefin produces two free radicals. In the case of propylene, the first stage of the reaction is the addition of oxygen to the double bond to give a reactive complex (1)



which can break up in two different ways (reactions 2 and 3)



The more likely reaction is (2), since it implies less regrouping of the activated complex than (H). $\text{CHO}\cdot$ and $\text{CH}_3\text{CO}\cdot$ radicals quickly form formaldehyde and acetaldehyde, respectively. Reactions (2) and (3) are the initial stages of a chain process





The chain reaction enables rapid oxidation of NO to NO₂ by alkoxy radicals (RO•) and peroxyacyl (RO₂•) without the intervention of atomic oxygen and O₃, which provides some explanation for the changes observed in the concentration of gaseous pollutants during the day. When atmospheric concentrations of hydrocarbons increase because of motor vehicle activity, the photolytic cycle of NO₂ is disturbed and NO is oxidized to NO₂ by the chain reaction involving the hydrocarbon radical (equations 2-8). As a result, the constant low O₃ concentration found in the photolytic cycle of NO₂ grows, and ozone is not consumed in the oxidation of NO to NO₂ (Seinfeld, 1978).

As the morning advances, solar radiation promotes the formation of photochemical oxidants, increasing their concentration in the atmosphere. When concentrations of precursors (NO_x and HC) in the atmosphere are lowered, the formation of oxidants stops and their concentrations decrease as the day progresses. Hence, photochemical pollution in cities builds up mainly in the mornings.

Due to industrial development in the GMA in recent years, there has been an urban-green-industrial zone imbalance, leading to the generation of various kinds of pollutants that alter the quality of the environment and exceed the assimilative capacity of the ecosystem.

Given this situation, it is vital to have a mathematical model that correctly predicts ozone concentrations at any given time, as this will help determine preventive measures and/or corrective actions to prevent exposure to high ozone concentrations. These models are able to relate air quality to certain other specific parameters of the air shed, such as emission levels and weather conditions.

2. Data sources

From an analysis of reports from 2002–2005, it was determined that the highest ozone concentrations were in the southern area of the GMA, so specific data for meteorological and chemical variables were obtained from the Miravalle weather station, located in the south. These are shown in Table 1.

Station \ Year	2002	2003	2004	2005
Las Águilas	0.169	0.165	0.164	0.131
Atemajac	0.152	0.185	0.165	0.144
Centro	0.166	0.171	0.157	0.137
L. Dorada	0.225	0.195	0.197	0.215
Miravalle	0.232	0.225	0.226	0.154
Tlaquepaque	0.142	0.149	0.138	0.109
Vallarta	0.171	0.217	0.175	0.096

Table 1. Peak ozone concentrations (ppm) for the years 2002, 2003, 2004 and 2005 (Semades, 2005)

2.1 Meteorological and chemical variables

Meteorological data for the period April 1999 to June 2005 were obtained from the Mexican National Weather Service (MNWS). These data consist of averages over time intervals ranging from 0 to 23 hrs.

The meteorological variables are Wind Direction (average and maximum average) (degrees), wind speed (average and maximum average) (km/h) Average Temperature ($^{\circ}\text{C}$), Relative Humidity (%). Barometric Pressure (mbar), Precipitation (mm) and Solar Radiation (W/m^2). The data were obtained from the Chapala station, which belongs to the Automatic Monitoring Stations (AMS) system.

Data on the following chemical variables were provided by the National Ecology Institute (NEI) for the Miravalle station; Ozone, Nitrogen Oxides— NO_x and NO_2 , as shown in Figure 1.



Fig. 1. Distribution of GMA Atmospheric Monitoring Automatic Network (Semarnat & INE, 2009).

3. Selection of meteorological and chemical variables

Meteorological and chemical variables used to carry out ground-level ozone forecasts were selected based on existing knowledge from the scientific literature and an analysis of correlations between different variables, and on availability of data from monitoring stations.

3.1 Analysis of meteorological variables

3.1.1 Wind speed

Atmospheric movements of the air (i.e. winds) are responsible for the spread of high concentrations of pollutants (in this case the O_3 and its precursors) through the atmosphere, but this may or not occur quickly, because if the winds are calm, i.e., the wind speed is low and the topography traps the air mass, pollutants can not disperse. More pollutants continue to accumulate and their concentration can reach very high levels. In contrast, if wind speeds are high, the pollutants tend to disperse quickly (Melas et al., 2000).

3.1.2 Temperature

This variable has shown a strong correlation with the concentration of ozone. The basic reasoning is that photochemical reaction rates are sensitive to temperature, so that increasing the temperature in the troposphere stimulates a series of interlinked reactions that contribute to ozone formation. (Garcia, 2003)

3.1.3 Relative humidity

Water vapor is one of the most basic components of the atmosphere. Its amount can be quite variable. It is important because it is one of the atmospheric elements which most absorbs solar radiation, preventing it from interacting with the primary pollutants and forming secondary pollutants such as ozone (Ayllón, 1996).

3.1.4 Precipitation

This process is one of the main ways that pollutants are removed from the atmosphere, but as a result, pollutants removed from the air then contaminate the earth's surface, which in some cases results in their becoming even more active due to their effects on surface water, plants and materials (acid rain) (Melas et al., 2000).

3.1.5 Pressure

The relationship between temperature and pressure is that the vertical motion of air is determined by vertical variation in temperature in the troposphere; temperature decreases at a rate of 0.64 °C per 100 m of altitude. Thus, the earth's surface warms the air parcel next to it, and this hot air expands, becoming less dense than the cooler air above it. The warm air rises and cool air takes its place to then be heated in turn, making contact with the surface, and subsequently also rises. This creates air currents (vertical mixing) that contribute to the dispersion of pollutants (Rodríguez & Tenorio, 2006).

3.1.6 Solar radiation

This is the factor that has the greatest effect on photochemical reactions, i.e., it is involved in the formation and destruction of the various compounds involved in the increase of tropospheric ozone (Melas et al., 2000).

Photochemical dissociation in the atmosphere can be considered as a two-step process. The dissociation energy of a photon by a molecule causes it to be in an excited state, and the excited product disassociates into new products that can be highly reactive, generating photochemical smog (Wark & Warner, 2000), as explained in Section 1.1.

3.2 Analysis of chemical variables

Many pollutants are highly persistent, and it is generally accepted that the probability of pollution episodes is increased if the previous day's pollution levels were higher than normal.

In this study, the previous day's maximum O₃ and NO_x are used as chemical input variables (Melas et al., 2000).

3.2.1 Previous day's ozone

Even when the tropospheric ozone photolytic cycle is considered to be in equilibrium (generation and degradation of ozone in equilibrium with NO_x), when hydrocarbons are involved (equations 2–8) the ozone generated is not consumed in the oxidation of NO to NO₂ (Seinfeld, 1978). There is ozone remaining from the previous day, which should be

input to the structure of the neural network model as an initial ozone concentration on the day of interest.

3.2.2 Oxides of nitrogen

These variables are the main precursors to ozone formation. Oxides that are present in the atmosphere in significant quantities are nitrogen monoxide and nitrogen dioxide ($\text{NO}_x = \text{NO} + \text{NO}_2$); approximately 90% of them are destroyed by photolysis in the formation of ozone (Wark & Warner, 2000).

These variables experience higher photolytic breakdown between 11 a.m. and 3 p.m.; i.e., when there is a higher incidence of light, after which time the levels start to gradually rise. Thus the concentrations which remain following the photolytic period participate as raw material for the formation of ozone the next day. Therefore, the maximum concentration between 3 p.m. and 11 p.m. on the previous day is used as the input variable (Seinfeld, 1978).

3.3 Statistical analysis

In addition to the analysis described in 2.1 and 2.2, the selection of variables was based on 1) individual regressions between the variable of interest (maximum ozone) and the various parameters (temperature, humidity, etc.), selecting only those with correlation coefficients (r) 0.3 and greater (Garcia, 2003); and 2) the t -ratio (t), used to obtain the degree of importance of each of the variables with respect to the dependent variable, namely ozone (see Table 2).

This analysis indicates that the higher the absolute value of t , the more necessary the variable (Miller et al., 1992) in the ANN model. All values of meteorological variables correspond to the day in question, so if models are to be used in real time, the values for that day are required. The values of the chemical variables correspond to the day previous to the day of interest.

Variable \ Year	1999	2000	2001	2002	2003	2004
Constant	-2.344	-0.242	-10.033	-0.591	-1.295	-0.795
Wind speed	-0.049	-0.365	1.859	-0.719	-2.617	-3.490
Temperature	7.847	4.637	2.519	10.951	7.031	5.036
Humidity	1.340	1.583	-3.777	-0.437	-5.512	-3.978
Pressure	2.261	0.197	10.228	0.499	1.358	0.806
Precipitation	-0.071	-0.905	.635	-1.721	-1.692	-1.092
Solar radiation	-2.959	-0.778	3.132	-2.973	-2.699	0.316
NO_2 previous day	0.243	-0.875	1.293	0.105	1.213	3.654
NO_x previous day	-1.143	1.223	-0.950	-0.296	0.842	-0.152

Table 2. t -ratio values by variable and year.

With the results shown in Table 2, the database used had daily maximum temperature values (°C) Solar Radiation (W/m^2), nitrogen dioxide (NO_2) on the previous day and oxides of nitrogen (NO_x) on the previous day, the latter two measured from 3 p.m. to 11 p.m.; and daily average values of wind speed (km/h), humidity (%) pressure (mbar) and precipitation (mm).

4. Artificial neural networks

The artificial neural network employed was a multilayer backpropagation network, which has been used successfully in several studies (Garcia & Shigidi, 2005, Kuo et al., 2003, Helle et al., 2001; Yesilnacar et al., 2007; Yetilmezsoy & Demirel, 2007).

The important feature of this network is its ability to self-adapt the weights of neurons in intermediate layers to learn the relationship between a set of patterns given as examples and their corresponding outputs, so that after having been trained, it can apply the same relationship to new input vectors and produce appropriate outputs from inputs that the system has never seen before, a feature known as the generalizability of an ANN (Mehrotra et al., 1997).

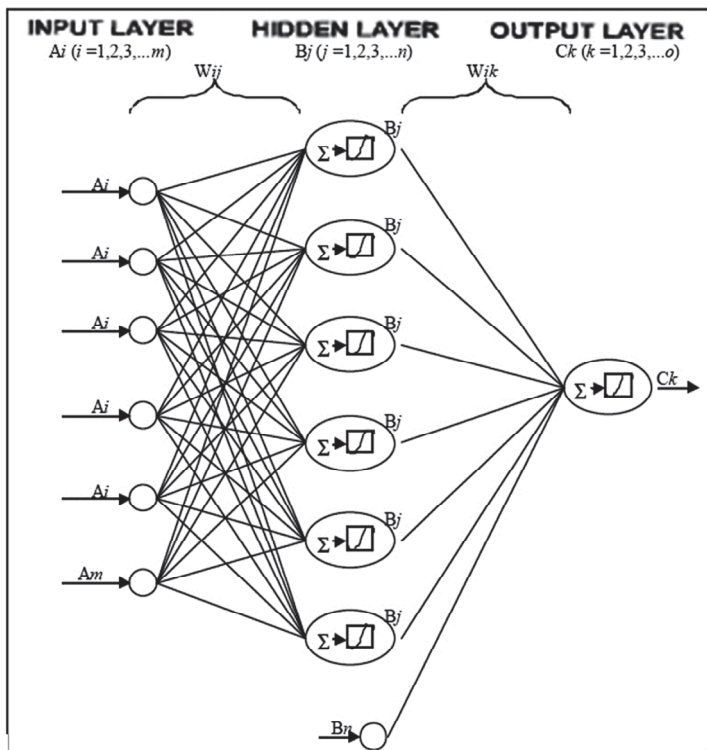


Fig. 2. Schematic example of an $m \times n \times o$ artificial neural network, showing a multilayer perceptron with a $4 \times 6 \times 1$ structure (additional shaded circles indicate bias nodes), which each contain an activation function (Σ) and a nonlinear transfer function (Comrie, 1997).

This type of network consists of three layers. There is an input layer A_i with m neurons, an output layer C_k with o neurons and at least one hidden layer B_j with n internal neurons. Each neuron in a layer (except the input layer) receives inputs from all neurons of the previous layer and sends its output to all neurons of the next layer (except the output layer), as shown in Figure 2 (Comrie, 1997).

The learning algorithm involves a forward propagation step in which the input pattern is presented to the network and propagated through the layers until it reaches the output layer, followed by a backward propagation step in which errors are passed from the output layer back to all the neurons in the intermediate layer and then back to the input layer, adjusting the synaptic weights so that the system converges (Gurney, 2003). In this way the network learns to recognize different features of the input patterns (Freeman et al., 1993, Lek et al., 2000). The important point is that each iteration of the ANN decreases the error between the actual data and forecast values.

To develop the ANN, we used the MATLAB version 7.4.0.287 computer program (R2007a), specifically the Neural Network Toolbox toolkit (Wang et al., 2006, Yetilmezsoy & Demirel et al., 2008, Garcia et al., 2008).

4.1 Parameters used to build artificial neural network models

The training algorithm selected for use in the ANN models was the Levenberg-Marquardt algorithm, because it achieves rapid convergence (TRAINLM) (Beale et al., 2010, Yetilmezsoy & Demirel et al., 2008 Yesilnacar et al., 2007, Wang et al., 2006) with a learning rate of 0.001. It is worth noting that when the learning rate increases or decreases, the performance of the models are neither improved nor impeded, so the 0.001 value was maintained. The ANN models were trained with 10,000 iterations on the training data (Comrie, 1997; Guardani et al., 1999).

To evaluate the results of the ANN models, three performance features were considered; the mean square error (MSE), mean squared error with regularization (MSEREG) and the error sum of squares (SSE). In the hidden layer, a log-sigmoidal function (*LOGSIG*) was used, and in the output layer, the transfer function was linear (*PURELINE*).

4.2 Number of hidden layers and hidden layer neurons

ANN models generally have acceptable performance with three layers; input, hidden and output (Del Brio & Sanz, 2001, Yetilmezsoy & Demirel et al., 2008, Helle et al., 2001). Deciding the number of neurons in the hidden layer is usually not so obvious, so the decision was based on the rules suggested by Goethals et al., (2007). The number of hidden neurons is based on the number of input variables (N_i) and output nodes (N_o) as shown in Table 3.

$2/3 * N_i$	$2/3 * (9) = 6$
$0.75 * N_i$	$0.75 * (9) = 6.75 \approx 7$
$0.5 * (N_i + N_o)$	$0.5 * (9 + 1) = 5$
$2 * N_i + 1$	$(2 * (9)) + 1 = 19$
$2 * N_i$	$2 * (9) = 18$

Table 3. Rules suggesting the number of hidden neurons based on the number of input (N_i) and/or output (N_o) nodes Goethals et al., (2007).

With these rules, and various studies predicting tropospheric ozone (Comrie, 1997; Guardani et al., 1999; Hooyberghs et al., 2005; Jiang et al., 2004; McKendry et al., 2002; Melas et al., 2000, David & Speakman, 1999, Hubbard & Cobourn, 2001), four arrays were created for training and testing the ANN models, each with a different number of neurons in the hidden layer as shown in Table 4. This is because there is no rule for the optimal number of neurons in the hidden layer (Yetilmezsoy and Demirel et al., 2008, Helle et al., 2001). In each problem, different arrangements should be tried for organizing the internal representation, selecting the one that gives the best results according to the stated objectives.

5. Development of artificial neural network models

Four different ANN structures were created; $9 \times 6 \times 1$ (nine input signals, six nodes in the transfer layer and one node in the output layer) (R-6); $9 \times 10 \times 1$ (R-10), $9 \times 12 \times 1$ (nine input signals, twelve nodes in the transfer layer and one node in the output layer) (R-12) and $9 \times 15 \times 1$ (R-15).

In training, the three performance criteria mentioned above were used; mean square error (MSE), mean squared error with regularization (MSEREG) and error sum of squares (SSE).

As a source of data for the training process, a database was used which contained daily maximum temperature values ($^{\circ}\text{C}$), Solar Radiation (W/m^2), nitrogen dioxide (NO_2) on the previous day, and nitrogen oxides (NO_x) on the previous day; the latter two for the period 3 p.m. to 11 p.m., and daily average values of Wind Speed (km/h), Humidity (%) Pressure (mbar) and Precipitation (mm) for the period 1999–2004. The database contained 2065 validated data for each variable.

5.1 Training of ANN models

The models were trained on 1990–2004 data. Real and predicted O_3 values were classified into three concentration ranges according to the NOM-020-SSA1-1993 standard, quantifying the number of data falling within each range (percentage of correct answers) in order to estimate the performance of each model.

This was done under the assumption that it would be very difficult to try to get specific concentrations from models. The concentration ranges were: low <0.06 ppm, intermediate $0.06\text{--}0.11$ ppm and high >0.11 ppm, the latter corresponding to the maximum allowable range of the rule.

The number of observed values and estimated values in each of these ranges were counted to find how many times the model made a correct estimate.

In order to refine the 12 trained models, an analysis based on the correlation coefficient (r) was carried out. A linear regression was performed between real ozone and estimated ozone as shown in Table 4. Based on the results, the models with 12 and 15 neurons in the hidden layer were chosen, as they had the best correlation between the calculated and actual data, in both cases using MSE to evaluate performance.

No. of neurons in hidden layer	Performance criterion		
	MSE	MSEREG	SSE
6	0.740	0.664	0.744
10	0.735	0.688	0.752
12	0.753	0.722	0.743
15	0.744	0.735	0.739

Table 4. Correlation coefficients of the ANN with each performance criterion.

Figure 3 and 4 shows correlation plots of the networks with 12 and 15 neurons in the hidden layer, respectively, during the training phase using 1999–2004 data. The dispersion of clouds of points is very similar in the two cases, corresponding to correlation coefficients close to each other.

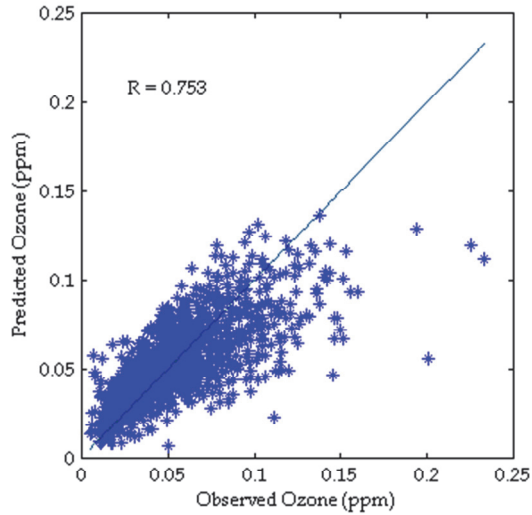


Fig. 3. Scatterplot of the predicted vs. observed ozone concentrations (ppm) for the model with 12 neurons in the hidden layer in the training phase for the years 1999–2004.

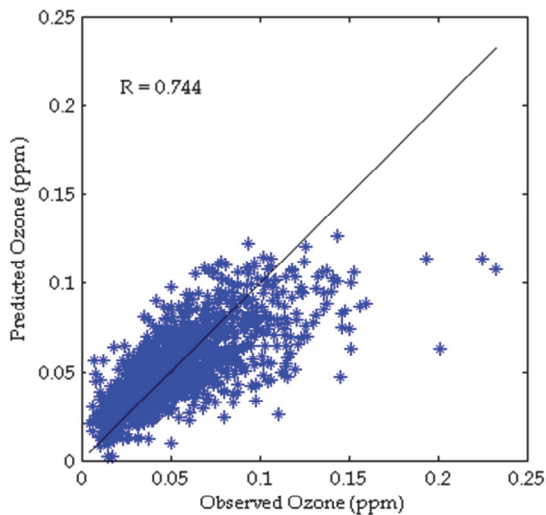


Fig. 4. As in Figure 3, but for the model with 15 neurons in the hidden layer.

5.2 Performance of ANN models

Once training was completed, performance was evaluated with 2005 data. This second database has 173 validated values for each parameter under the same conditions as the training database, containing daily data from January to June 2005.

Table 5 shows the number and percentage of times that correct concentrations were obtained by the networks with respect to the observed values, where R-12 and R-15 refer to networks with 12 and 15 neurons in the hidden layer respectively.

	Low (<0.06 ppm)	Medium (0.06-0.11 ppm)	High (>0.11 ppm)
Total days	79	77	17
R-12	41 (52%)	33 (43%)	0 (0%)
R-15	50 (63%)	48 (62%)	2 (12%)

Table 5. Number and percentage of correct estimated O3 values with respect to observed values, at the performance stage.

Figure 5 shows the ANN regression models corresponding to 12 neurons in the hidden layer (R-12), and Figure 6 shows the ANN model with 15 neurons in the hidden layer (R-15), both models with data from January to June 2005.

Figure 5 shows the regression with the R-12 network, with a regression coefficient of 0.575, and Figure 6 shows the correlation of the network with 15 neurons and a regression coefficient of 0.545.

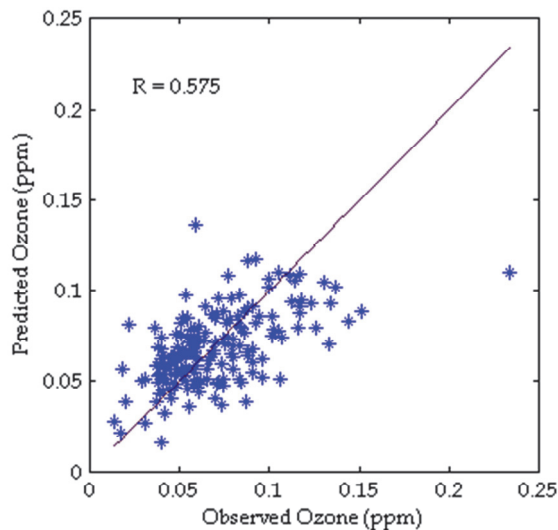


Fig. 5. Scatterplot of the predicted concentrations with observed ozone concentrations for the model with 12 neurons in the hidden layer in the test phase for the year 2005.

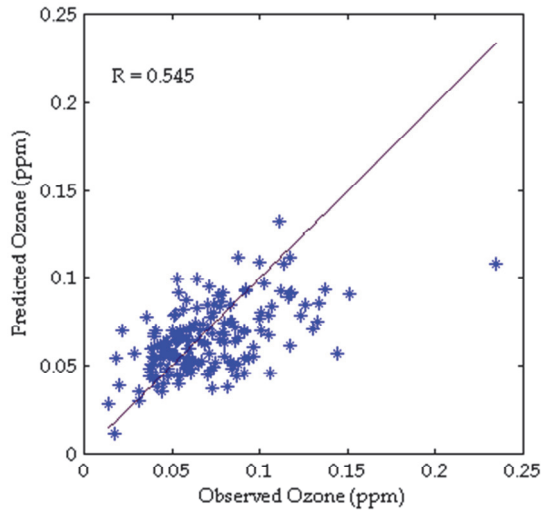


Fig. 6. As in Figure 5, but for the model with 15 neurons in the hidden layer.

The performance of the two networks is very similar. However, it is clear that it is difficult for both models to detect ozone concentrations exceeding the standard, which is important for this study.

In order to remedy the estimation problem in the high concentration range, it was decided to scale the value estimated by the network. Thus, the final estimated value of ozone (O_3) is calculated as

$$\hat{O}_3 = \alpha \hat{O}_3 \quad (9)$$

where α is the scaling factor and O_3 is the ozone concentration (ppm) estimated by the neural network model. The value of α was obtained by an incremental search of values that when the equation was applied, reached the number of times that the observed concentration standard for each year was exceeded, without knowing (until then) if the times when estimated concentration exceeded the standard also corresponded to the days when this actually occurred. This process yielded an average value of α for both models of 1.21. Thus ozone values estimated by each network were multiplied by 1.21, giving the results in Table 3, which shows that efficiency is lost in the lower range at the expense of a gain in the intermediate and high ranges (which are of greatest interest).

	Low (<0.06 ppm)	Intermediate (0.06-0.11 ppm)	High (>0.11 ppm)
Total days	79	77	17
R-12 ($\alpha=1.21$)	18 (23%)	57 (74%)	11 (65%)
R-15 ($\alpha=1.21$)	23 (29%)	57 (74%)	8 (47%)

Table 6. Number and percentage of correct O_3 values estimated by different networks using the scaling.

Table 6 shows that the overall performance of the networks is 50%, and 64% for the detection of elevated ozone concentrations with R-12, and 47% with R-15. It may be noted that using 12 neurons in the hidden layer fails to detect a greater number of days in the high range. With the results, it was decided to work with the model with 12 neurons in the hidden layer; this model was selected in the present study for predicting tropospheric ozone concentrations in the metropolitan area of Guadalajara, Jalisco. Figure 7 shows a comparison with the previously selected model without the scaling factor. As can be seen graphically, the model shows a good trend in the low and intermediate range of tropospheric ozone concentrations but a poor performance for the higher concentrations.

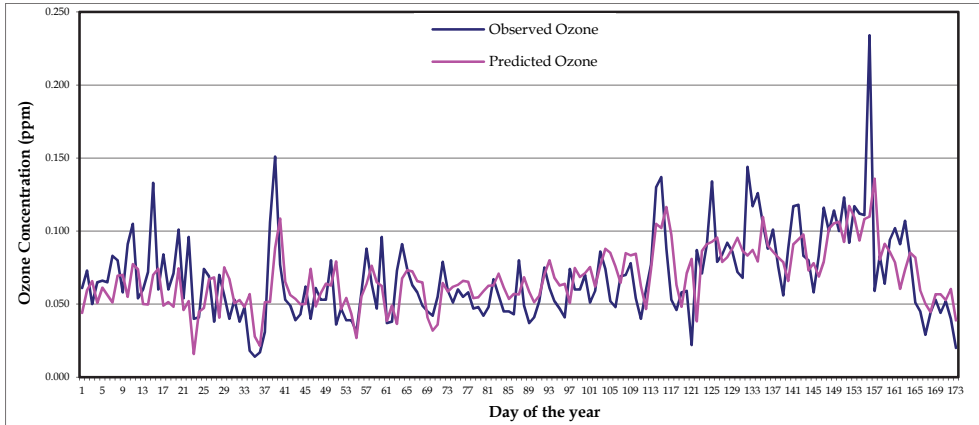


Fig. 7. Comparison of predicted concentrations Vs. observed concentrations of ozone from ANN model with 12 neurons in the hidden layer for 2005 without the scaling factor.

In Figure 8 a scaling factor of 1.216 has been applied. Although accuracy is lost in the low range of concentrations, performance in the midrange is improved from 43% to 74%, that is, by 31 percentage points.

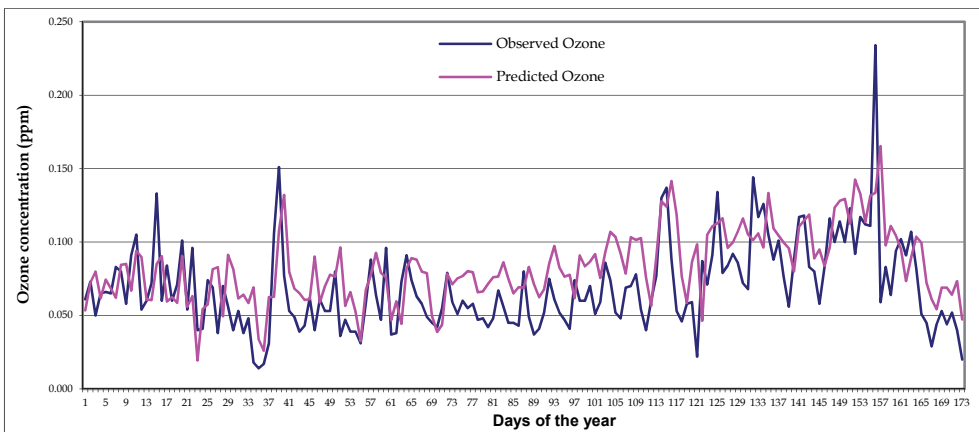


Fig. 8. As in Figure 7, but with the scaling factor.

In the high range, it is clear that after the unscaled model did not detect any concentrations, after applying the scaling factor, efficiency was improved by 65%, i.e., it predicted 11 of the 17 days that exceeded the concentration of 0.11 ppm.

6. Conclusions

With the results obtained by the model and selected variables, it was concluded that in the GMA, the most important meteorological variables for significantly reducing the tropospheric O₃ concentration are wind speed, which can disperse ozone precursors or ozone itself, decreasing the concentration of the pollutant; and rainfall, as this will wash out the atmosphere thereby lowering the concentration of ozone, as well as the concentrations of precursors and other pollutants (it can be observed that the morning after a day with rainfall tends to be clear in the early hours).

The chemical variables that are important in increasing ozone concentration are maximum temperature, maximum solar radiation, O₃ on the previous day, and oxides of nitrogen (NO_x and NO₂) (Gomez et al., 2006) because they are involved directly in the photochemical cycle of ozone formation (Wark & Warner, 2005).

The important variables related to nitrogen oxides (NO₂ and NO_x) are maximum values, since these elements are directly involved in the photolytic cycle and influence the formation of ozone. They are measured from 3 p.m. to 11 p.m. because ozone formation takes place between 11 a.m. and 3 p.m., so there is no consumption of these two pollutants and accumulations of these oxides in the afternoon will serve as raw material for the next day.

Along with the physical and chemical meteorological variables involved in increasing or decreasing O₃ concentrations, the characteristics of the basin of the Jalisco Basin are also important. It is located 1583 meters above sea level, surrounded by the Sierra Madre Occidental, plateaus and the Neovolcanic Belt, and with industrial parks to the NW, SE, and SW. The Sierra Madre Occidental is formed by the Los Huicholes, Los Guajolotes and San Isidro mountains, the Gordo hill and the Tequila volcano. The Neo-Volcanic or Transversal Volcanic Belt includes the Cacoma, Manantlán Tapalpa and Lalo mountains, among others. Other notable peaks are El Tigre and Garcia, Cerro Viejo, the Tequila Volcano and to the south, the Nevado de Colima mountain and Colima Volcana, which create a particular basin structure and formation and dispersal patterns of specific pollutants that directly affect the GMA in terms of the model performance.

The ANN models perform acceptably for predicting ozone in the lower and intermediate range, however the aim of this study was to predict high levels of ozone, so it was necessary to use the scaling factor so that the models would be able to predict concentrations in the high range. This scaling factor was obtained in training the models by matching observed and predicted days that exceeded the standard. Using the scaling factor, the model obtained can predict maximum O₃ concentrations in ppm with an overall efficiency of approximately 50%, and 65% for the detection of high concentrations.

These models were trained on data from the period between 1999 and 2004 in the Guadalajara Metropolitan Area (GMA) and their performance was evaluated using data from the period from January to June 2005 with data from the SMN and INE. The performance of the two models was assessed and compared by comparing forecast and actual ozone concentrations in three ranges (called percent of correct answers) related to the NOM-020-SSA1-1993 standard, low ($C_{O_3} < 0.060$ ppm), intermediate ($0.060 \leq C_{O_3} \leq 0.110$

ppm) and high ($C_{O_3} > 0.110$ ppm), with high concentrations considered to be values that exceeded the standard.

The general characteristics of the selected ANN model for forecasting of O_3 are: 9 independent variables (3 chemical and 6 weather). The structural arrangement of the network was $9 \times 12 \times 1$ (input \times hidden \times output); transfer functions were sigmoidal in the hidden layer and linear in the output layer, the training function was TRAINLM; the performance criterion was mean square error (MSE) and the scaling factor was 1.21.

This model is able to predict 22% of concentrations lower than 0.060 ppm, i.e. it predicted 17 of 79 days for this range; a 74% success rate in the intermediate range of concentrations from 0.060 to 0.110 ppm, i.e. 57 days of the 77 days recorded; and 65% success for concentrations greater than 0.110 ppm, i.e. 11 of the 17 days recorded for the 2005 period.

The overall efficiency of the model for the period January to June 2005 was 49.13% with the scaling factor and 54.34% without the factor.

The models obtained employed the meteorological variables maximum temperature and solar radiation, and average values of wind speed, barometric pressure, rainfall, relative humidity for each day of interest, and maximum values of the chemical variables ozone, NO_x and NO_2 on the previous day (measured from 3 p.m. to 11 p.m.).

Finally, the models generated are easy to implement, have only moderate technological requirements and simple, easily understood structures, giving them minimal operating costs. These models can be used to help alert the community at times when the air quality is undesirable, so that precautionary measures can be taken to safeguard the health of the population.

7. References

- Ayllón, M. T. (Second edition). (2003). *Elementos de meteorología y climatología*. Trillas, ISBN 968-24-6725-X, México.
- Beale, M. H.; Hagan, M. T. & Demuth, H. B. (Version 7). (2010). *Neural Network Toolbox 7, User's Guide*, The MathWorks, Inc., ISBN 0-9717321-0-8, Natick, Massachusetts, USA.
- Brunelli, U.; Piazza, U. & Pignato, L. (2007). Two-days ahead prediction of daily maximum concentrations of SO_2 , O_3 , PM_{10} , NO_2 , CO in the urban area of Palermo, Italy. *Atmospheric Environment*, Vol. 41, No. 14 (May 2007), pp. 2967–2995, doi: 10.1016/j.atmosenv.2006.12.013
- Chen, J.-L.; Islam, S. & Biswas, P. (1998). Nonlinear dynamics of hourly ozone concentrations: nonparametric short term prediction, *Atmospheric Environment*, Vol. 32, No. 11 (June 1998), pp. 1839–1848, doi: 10.1016/S1352-2310(97)00399-3
- Cobourn, W. G. & Hubbard, M.C. (1999). An enhanced ozone forecasting model using air mass trajectory analysis, *Atmospheric Environment*, Vol. 33, No. 28 (December 1999), pp. 4663–4674, doi: 10.1016/S1352-2310(99)00240-X
- Comrie, A. (1997). Comparing neural networks and regression models for ozone forecasting, *Air & Waste Manage. Assoc.*, Vol. 47, (June 1997), pp. 653 – 663, ISSN 1047– 3289.
- Comrie, A.C. & Diem, J.E. (1999). Climatology and forecast modeling of ambient carbon monoxide in Phoenix, Arizona, *Atmospheric Environment*, Vol. 33, No. 30, (October 1999), pp. 5023–5036, doi: 10.1016/S1352-2310(99)00314-3
- Davis, J.M. & Speckman, P. (1999). A model for predicting maximum and 8 h average ozone in Houston, *Atmospheric Environment*, Vol. 33, No. 16, (July 1999), pp. 2487–2500 *begin_of_the_skype_highlighting*, doi: 10.1016/S1352-2310(98)00320-

3end_of_the_skype_highlighting

- Del Brío, B. M. & Sanz, A. (3ª Edición). (2006). *Redes Neuronales y Sistemas Borrosos*, Ra-Ma Editorial, ISBN 978-84-7897-743-7, Spain.
- Draxler, R. R. (2000). Meteorological factors of ozone predictability at Houston, Texas, *Journal of the Air & Waste Management Association*, Vol. 50, No. 2, (February 2000), pp. 259-271, PMID: 10680356
- Freeman, J. A. & Skapura, D. M. (1993). *Redes Neuronales: algoritmos, aplicaciones y técnica de programación*. Díaz de Santos, ISBN 9780201601152, Spain.
- García, I. (2003). *Aplicación de modelos semi-empíricos para el análisis y pronóstico de la calidad del aire en el Área Metropolitana de Monterrey, N.L.*, Master's thesis, ITESM, Monterrey, México.
- García, I.; Marbán, A.; Tenorio, Y. M. & Rodríguez, J. G. (2008). Pronóstico de la Concentración de Ozono en Guadalajara-México usando Redes Neuronales Artificiales, *Información Tecnológica*, Vol. 9, No. 3, (Junio 2010), pp. 89-96, doi: 10.1612/inf.tecnol.3925it.07
- García, L. A. & Shigidi, A. (2006). Using neural networks for parameter estimation in ground water, *Journal of Hydrology*, Vol. 318, No. 1-4, (March 2006), pp. 215-231. doi: 10.1016/j.jhydrol.2005.05.028
- Gardner, M. W. & Dorling, S. R. (1998). Artificial neural networks (the multilayer perceptron) - a review of applications in the Atmospheric Sciences, *Atmospheric Environment*, Vol. 32, No. 14-15, (August 1998), pp. 2627-2636, doi: 10.1016/S1352-2310(97)00447-0
- Gardner, M.W. & Dorling, S. R. (2000). Statistical surface ozone models: an improved methodology to account for nonlinear behaviour, *Atmospheric Environment*, Vol. 34, No. 1, (January 2000), pp. 21-34, doi: 10.1016/S1352-2310(99)00359-3
- Goethals, P. L. M.; Dedecker, A. P.; Gabriels, W.; Lek, S. & De Pauw, N. (2007). Applications of artificial neural networks predicting macroinvertebrates in freshwaters, *Aquatic Ecology*, Vol. 41, No. 3 (May 2007), pp. 41, 491-508, doi: 10.1007/s10452-007-9093-3
- Gómez, J; Martín, J.D.; Soria, E.; Vila, J.; Carrasco, J. & Valle, S. (2006). Neural networks for analysing the relevance of input variables in the prediction of tropospheric ozone concentration, *Atmospheric Environment*, Vol. 40, No. 32, (October 2006), pp. 6173-6180, doi: 10.1016/j.atmosenv.2006.04.067
- Grivas, G. & Chaloulakou, A. (2006). Artificial neural network models for prediction of PM₁₀ hourly concentrations, in the Greater Area of Athens, Greece, *Atmospheric Environment*, Vol. 40, No. 7 (March 2006), pp. 12161229. doi: 10.1016/j.atmosenv.2005.10.036
- Guardani, R.; Nascimento C.; Guardani, M.; Martins, M. & Romano, J. (1999). Study of atmospheric ozone formation by means of a neural network-based model, *Air & Waste Manage. Assoc.*, Vol. 49, (March 1999), pp. 316323, ISSN 1047 - 3289.
- Gurney, K. (1997). *An Introduction to Neural Networks*, University College London Press, ISBN 1-85728-503-4, London.
- Helle, H. B.; Bhaatt, A. & Ursin, B. (2001). Porosity and permeability prediction from wireline logs using artificial neural networks: a North Sea case study, *Geophysical Prospecting*, Vol. 49, No. 4 (December 2001), pp. 431-444. doi: 10.1046/j.1365-2478.2001.00271.x
- Hooyberghs, J; Mensink, C.; Dumont, G.; Fierens, F. & Bresseur, O. (2005). A neural network forecast for daily average PM₁₀ concentrations in Belgium, *Atmospheric Environment*, Vol. 39, (January 2005), pp. 3279-3289, doi: 10-1016/j.atmosenv.2005.01.050.

- Hubbard, M. & Cobourn, W. G. (1998). Development of a regression model to forecast ground-level ozone concentration in Louisville, KY, *Atmospheric Environment*, Vol. 32, No. 14-15, (August 1998), pp. 2637-2647, doi: 10.1016/S1352-2310(07)00444-5
- Jiang, D.; Zhang, Y.; Hu, X.; Zeng, Y.; Tan, J. & Shao, D. (2004). Progress in developing an ANN model for air pollution index forecast, *Atmospheric Environment*, Vol. 38, (October 2003), pp. 7055-7064, doi: 10-1016/j.atmosenv.2003.10.066.
- Kuo, Y.; Chen-Wuing, L. & Lin, K. (2004). Evaluation of the ability of an artificial neural network model to assess the variation of groundwater quality in an area of blackfoot disease in Taiwan, *Water Research*, Vol. 38, No. 1 (January 2004), pp. 148-158. doi: 10.1016/j.watres.2003.09.026
- Lek, S. & Guégan, J. F. (2000). *Artificial Neural Networks: application to ecology and evolution*, Springer, ISBN 3540669213, Michigan.
- McKendry, I. (2002). Evaluation of artificial neural networks for fine particulate pollution (PM10 and PM2.5) forecasting, *Air & Waste Manage. Assoc.*, Vol. 52, (September 2002), pp. 1096-1101, ISSN 1047-3289.
- Melas, D.; Kioutsioukis I. & Ziomas I. (2000). Neural network model for predicting peak photochemical pollutant levels, *Air & Waste Manage. Assoc.*, Vol. 50, (April 2000), pp. 495-501, ISSN 1047-3289.
- Mehrotra, K.; Mohan, C. K. & Ranka, S. (Second printing) (2000). *Elements of Artificial Neural Networks*, MIT Press, Cambridge MA.
- Milanchus, M.L.; Rao, T. & Zurbenko, I. G. (1998). Evaluating the effectiveness of ozone management efforts in the presence of meteorological variability, *Journal of the Air & Waste Management Association*, Vol. 48, No. 3, (1998), pp. 201-215, ISSN 1096-2247.
- Miller, I.R.; Freund, J. E. & Jonson. R. (4th edition). (2004). *Probabilidad y Estadística para Ingenieros*, Reverté Ediciones, Spain.
- Secretaria de Salud, (2000). Norma Oficial Mexicana NOM-020-SSA1-1993, Salud ambiental. Criterio para evaluar el valor límite permisible para la concentración de ozono (O₃) de la calidad del aire ambiental, Mexico
- Pérez P.; Trier, A. & Reyes, J. (2000). Prediction of PM_{2.5} concentrations several hours in advance using neural networks in Santiago, Chile, *Atmospheric Environment*, Vol. 34, No. 8 (February 2000), pp. 1189-1196, doi: 10.1016/S1352-2310(99)00316-7.
- Perez P. & Reyes, J. (2006); An integrated neural network model for PM10 forecasting, *Atmospheric Environment*. Vol. 40, (January 2006), pp. 2845-2851, doi: 10.1016/j.atmosenv.2006.01.010.
- Pun, B. K.; Louis, J. F.; Pai, P; Seigneur, C.; Altshuler, S. & Franco, G. (2000). Ozone formation in California's San Joaquin Valley: A critical assessment of modeling and data needs, *Journal of the Air & Waste Management Association*, Vol. 50, No. 6, (2000), pp. 961 - 971, ISSN 1096-2247.
- Raga, G. B. & Le Moyne, L. (1999). On the nature of air pollution dynamics in Mexico City - I. Nonlinear analysis, *Atmospheric Environment*, Vol. 30, No. 23, (February 1999), pp. 3987-3993, doi: 10.1016/1352-2310(96)00122-7
- Rodríguez, J. G. & Tenorio, Y. M. (2006). *Desarrollo de modelos pronóstico para la calidad del aire en la Zona Metropolitana de Guadalajara, Jalisco*, Bachelor's thesis, ESQIE-IPN, Mexico.
- Roth, P. M. (1999). A qualitative approach to evaluating the anticipated reliability of a photochemical air quality simulation model for a selected application, *Journal of the Air & Waste Management Association*, Vol. 49, No. 9, (1999), pp. 1050-1059, ISSN 1096-2247.

- Russell, A. & Dennis, R. (2000). NARSTO critical review of photochemical models and modeling, *Atmospheric Environment*, Vol. 34, No. 12-14, (March 2000), pp. 2283-2324, doi: 10.1016/S1352-2310(99)00468-9
- Salcedo, R. L. R.; Alvim, M. C. M.; Alves, C. A. & Martins, F. G. (1999). Time-series analysis of air pollution data, *Atmospheric Environment*, Vol. 33, No. 15, (July 1999), pp. 2361-2372, doi: 10.1016/S1352-2310(99)80001-6
- Thomas, S. & Jacko, R. B. (2007). Model for forecasting expressway fine particulate matter and carbon monoxide concentration: Application of regression and neural network model, *Air & Waste Management Association*, Vol. 57, No. 4 (April 2007), pp. 480-488, ISSN 1096-2247.
- Sebal, L.; Treffeisen, R; Reimery, E. & Hies, T. (2000). Spectral analysis of air pollutants. Part 2: Ozone time series, *Atmospheric Environment*, Vol. 34, No. 21, (June 2000), pp. 3503-3509, doi: 10.1016/S1352-2310(00)00147-3
- Seinfeld, J. (1978). Contaminación atmosférica. Fundamentos físicos y químicos, *Instituto de Estudios de Administración Local*, ISBN 8470882139, Madrid.
- Secretaría de Medio Ambiente para el Desarrollo Sustentable Jalisco. (2006). *Informe de calidad del aire, evaluación: 2001-2005*, Semades, Retrieved from <<http://www.jalisco.gob.mx/wps/wcm/connect/813336004dbe3344a756ef5160bedb77/ReporteAire2006.pdf?MOD=AJPERES&CACHEID=813336004dbe3344a756ef5160bedb77>>
- Secretaría de Medio Ambiente y Recursos Naturales & Instituto Nacional de Ecología (2003). *Segundo almanaque de datos y tendencias de la calidad del aire en seis ciudades mexicanas*, Semarnat & INE, ISBN 968 817 614 177, Mexico.
- Thomas, S. & Robert, B. J. (2007). Model for forecasting expressway fine particulate matter and carbon monoxide concentration: Application of regression and neural network model, *Air & Waste Management Association*. Vol. 57, No. 4, (2007), pp. 480-488, ISSN 1096-2247.
- Thompson, M. L.; Reynolds, J.; Cox, L. H.M; Guttorp, P. & Sampson, P. D. (2001). A review of statistical methods for the meteorological adjustment of tropospheric ozone, *Atmospheric Environment*, Vol. 35, No. 3, (November 2000), pp. 617-630, doi: 10.1016/S1352-2310(00)00261-2
- Wang, M. X.; Liu, G. D.; Wu, W. L.; Bao, Y. H. & Liu, W. N. (2006). Prediction of agriculture derived groundwater nitrate distribution in North China Plain with GIS-based BPNN, *Environmental Geology*, Vol. 50, No. 5, (April 2006), pp. 637-644, doi: 10.1007/s00254-006-0237-x
- Wark, K. & Warner, C. F. (2004). *Contaminación del aire: Origen y control*, Limusa - Wiley, ISBN 9789681819545, Mexico.
- Yesilnacar, M. I.; Sahinkaya, E.; Naz, M & Ozkaya, B.; Naz M. & Bestamin O. (2007). Neural network prediction of nitrate in groundwater of Harran Plain, Turkey, *Environmental Geology*, Vol. 56, No. 1 (November 2007), pp. 19-25 doi: 10.1007/s00254-007-1136-5
- Yetilmezsoy, K. & Demirel, S. (2008). Artificial neural networks (ANN) approach for modeling of Pb (II) adsorption from aqueous solution by Antep pistachio (*Pistacia Vera L.*) Shells, *Journal of Hazardous Materials*. Vol. 153, No. 3, (May 2008), pp. 1288-1300. Doi: 10.1016/j.jhazmat.2007.09.092

Meandering Dispersion Model Applied to Air Pollution

Gervásio A. Degrazia, Andréa U. Timm, Virnei S. Moreira, Débora R. Roberti
Universidade Federal de Santa Maria/UFSM
Brazil

1. Introduction

Generally in stable conditions, during situations of low wind speed ($\bar{u} \leq 1 - 2 \text{ms}^{-1}$), low-frequency horizontal wind oscillations (meandering) are observed in a nocturnal Planetary Boundary Layer (PBL). The study of low wind speed conditions is of interest, partly because the simulation of airborne pollutant dispersion in these conditions is rather difficult. In fact, most of the existing regulatory dispersion models become unreliable as \bar{u} approaches zero, so that their application is generally limited to ($\bar{u} > 2 \text{ms}^{-1}$). The meandering movements are clearly distinct from those associated to a full developed turbulence, which are responsible for the pollutants dispersion in a PBL. Even when the stability reduces the vertical dispersion and the instantaneous plume may be thin, meandering disperses the plume over a rather wide angular sector. As a consequence, any air pollution operational dispersion model to be reliable must take into account the transport effect provoked by the meandering.

Transport phenomenon in turbulence, including the diffusion of passive scalars and the dispersion of pollutants in the PBL, are controlled by the advection processes associated with the action of stochastic velocity fluctuations in time and space. As a consequence, a Lagrangian description following the movement of infinitesimal fluid particles, as they are carried by the velocity turbulent fluctuations, is conceptually correct and from practical point of view useful for describing turbulent transport (Yeung, 2002).

Lagrangian stochastic particle models are powerful computational tools for the investigation of the atmospheric dispersion process (Rodean, 1996). In these models, the fluid particle displacements are produced by stochastic velocities and the movement evolution of a particle can be considered a Markov process (Wang, 1945), in which past and future are statistically independent when the present is known. This method is based on Langevin equation, which is derived from the hypothesis that the velocity is given by the combination between a deterministic and a stochastic term (Chandrasekhar, 1943). Each fluid particle moves taking into account the transport due to the mean wind velocity and the turbulent fluctuations of the wind velocity components. From the spatial distribution of the particles it is possible to determine the pollutant concentrations. The implementation of the Lagrangian stochastic dispersion model in air pollution problems permits to take into account complex situations such as turbulent flows generated above inhomogeneous topography (different terrains) (Carvalho et al., 2002), in non-stationary situations associated with the evolutionary transition

periods of the PBL (sunset transition period) and low wind speed conditions which for many places in the world occur for a substantial percentage of time (Oetl et al., 2001). Concerning this last complexity, it is important to note that in low wind velocity situations, particularly during stable conditions, the turbulent dispersion in the PBL is poorly described. As a consequence, the occurrence of low wind speed is generally considered the most critical situation associated with the air pollution dispersion problem.

The aim of this chapter is to report a turbulence parameterization that can be employed in Lagrangian stochastic dispersion models to describe the air pollution dispersion in the situation of low wind velocity stable conditions. This specific parameterization employs an observational value for the meandering period and turbulent velocity variances and decorrelation time scales varying with height for a stable boundary layer. Therefore, are used two classical approaches to obtain the turbulent velocity variances and the decorrelation time scales. The first turbulence approach used in this study was derived by Degrazia et al. (2000) utilizing Taylor statistical diffusion theory while the second one was developed by Hanna (1982). Degrazia et al. (2000) turbulence approach is based on the observed turbulent velocity spectra while Hanna (1982) approach is based on analyses of field experiments, theoretical considerations and second-order closure model.

An additional aim is to incorporate this new parameterization for the meandering dispersion phenomenon in a numerical Lagrangian stochastic particle model to simulate the dispersion of air pollution in a low wind velocity stable boundary layer. The Lagrangian particle model employed in the present investigation is constituted by a system of two coupled Langevin equations describing the meandering dispersion associated to the lateral and longitudinal components of the wind velocity fluctuations. This dispersion model is based on the so-called Thomson simplest solution and can be applied to more general case of inhomogeneous turbulence. The horizontal coupling, occurring between the lateral and longitudinal velocity components, reproduces the meandering enhanced air pollution transport.

Finally, the observed concentration data employed in the comparison with the coupled Langevin equations model, incorporating Degrazia et al. (2000) and Hanna (1982) approaches, were obtained from the low wind speed experiment performed in a stable boundary layer from the series of field observations conducted at the Idaho National Engineering Laboratory - INEL.

2. The SCLE dispersion model

Simulating the dispersion of contaminants in low wind speed stable conditions is a difficult physical task. In such situations, the airborne contaminants are dispersed over rather wide angular sectors and therefore it is no longer possible to establish a definite mean wind direction since low-frequency horizontal wind oscillations start to dominate and diffusion of contaminants in the PBL becomes controlled by these degrees of freedom, characterized by low frequencies (large characteristic time associated with the meandering period). The horizontal meandering of a flow occurs when the wind speed presents a threshold low value and the low-frequency horizontal wind oscillations generate autocorrelation functions of the horizontal wind components showing a looping behavior evidenced by the presence of accentuated negative lobes (Anfossi et al., 2005; Oetl et al., 2005). This oscillatory character associated with the meandering phenomenon and consequently the presence of large negative lobes in the observed autocorrelation functions were recently explained as an

intrinsic property of atmospheric flows occurring in weak horizontal turbulent momentum flux conditions (Goulart et al., 2007).

The low wind speed autocorrelation functions of the horizontal wind components displaying an oscillation behavior and the presence of large negative lobes can be very well fitted by the following relationship

$$R(\tau) = e^{-p\tau} \cos(q\tau) \quad (1)$$

where

$$p = \frac{1}{(m^2 + 1)T_{Lu,v}} \quad (2)$$

and

$$q = \frac{m}{(m^2 + 1)T_{Lu,v}}. \quad (3)$$

The functional form as given by the Eqs. (1), (2) and (3) is composed of the product of the classical exponential function (representing the autocorrelation function for a fully developed turbulence) by the cosine function (describes the meandering phenomenon associated with the observed low frequency horizontal wind oscillations) (Frenkiel, 1953). The Frenkiel function (Eq. (1)) is a hybrid formula described in terms of $T_{Lu,v}$, the local horizontal Lagrangian time scale for a fully developed turbulence, and m , the loop parameter which controls the meandering oscillation frequency associated with the horizontal wind. It is worth noting that large m values characterize the dominant presence of the meandering phenomenon in comparison with the fully developed turbulence.

Anfossi et al. (2006) proposed a system of two coupled Langevin equations (SCLE) to describe the contaminants dispersion in meandering conditions. Therefore, the following system of equations describes the dispersion in low wind speed conditions

$$du = \{-p(u - \bar{u}) - q(v - \bar{v})\} dt + \sqrt{2pdt}\sigma_u\zeta_u \quad (4)$$

and

$$dv = \{q(u - \bar{u}) - p(v - \bar{v})\} dt + \sqrt{2pdt}\sigma_v\zeta_v \quad (5)$$

where u and v are the horizontal components of the wind velocity fluctuations, ζ_u and ζ_v are random Gaussian variables having zero mean and unit variance, σ_u and σ_v are standard deviations of the horizontal wind components. It is important to note that Eqs. (4) and (5) are valid assuming horizontal homogeneous conditions (Anfossi et al., 2006).

For the vertical component of the velocity fluctuation w we solve the Langevin equation according to the usual LAMBDA model (Anfossi et al., 2006; Thomson, 1987)

$$dw = a_i(z, w) + b_0(z)dW_j \quad (6)$$

where dW_j is the incremental Gaussian Wiener process (with zero mean and variance dt), $b_0(z) = \sqrt{2\sigma_w^2/T_{Lw}}$ (σ_w^2 is the vertical turbulent velocity variance and T_{Lw} is the vertical local Lagrangian time scale) and $a_i(z, w)$ is computed by solving the Fokker-Planck equation associated with Eqs. (4) and (5) using a PDF of Gram-Chalier type truncated to the third-order (Ferrero & Anfossi, 1998).

The position of each particle, at each time step, is obtained by the numerical integration of Eqs. (4) and (5) and (6) and the following equation:

$$dx_i = u_i dt, \quad (7)$$

where $i = 1, 2, 3$, x_i is the position vector of each particle, u_i is its corresponding Lagrangian velocity vector. Therefore, to describe the diffusion of passive scalars in the PBL the Langevin equation is integrated according to the rules of the Ito calculus (Gardiner, 1997), which was developed to get solutions of the stochastic differential equations.

3. Turbulence parameterization for modeling meandering effects in the stable PBL

The fundamental parameters to reproduce meandering transport effects, employing the Eqs. (4) and (5), are the quantities m , $\sigma_{u,v}$ and $T_{Lu,v}$ which define the Eqs. (1), (2), (3), (4) and (5). In this section the values of these physical parameters will be computed.

In PBL turbulent dispersion models the selection of an adequate parameterization plays a fundamental role to evaluate the contaminants concentration in the atmosphere. Thusly, the efficiency of each approach to reproduce correctly the contaminants concentration field depends on the manner turbulent parameters are related to physical properties of the PBL. In the specific case of parameterization of the enhanced horizontal diffusion of passive scalars, controlled by the meandering phenomenon, the variables p and q need to be introduced into Eqs. (4) and (5). Analyzing the Eqs. (1), (2) and (3) we can define the following meandering period (Anfossi et al., 2005).

$$T_* = \frac{2\pi(m^2 + 1)T_{Lu,v}}{m}, \quad (8)$$

from which can be obtained a relation for m given by (Carvalho et al., 2006)

$$m = \frac{T_* + \sqrt{T_*^2 - 16\pi^2 T_{Lu,v}^2}}{4\pi T_{Lu,v}} \quad (9)$$

As seen in Eq. (9), this formula for the loop parameter, defines m as a quantity that can be estimated from the meandering period T_* and of the local horizontal time scale associated with a fully developed turbulence $T_{Lu,v}$. On the other hand, analyzing Eq. (9) it is possible to notice that the presence of large values for the local turbulent time scales impede the increasing of m and consequently the meandering reinforced transport tends to vanish in the PBL. Time series of sonic anemometer wind speeds were analyzed by Anfossi et al. (2005). These observational data suggest that the mean magnitude of the meandering period is of the order of $T_* \cong 2000s$.

3.1 Turbulence parameterization derived by Degrazia et al. (2000) and Hanna (1982)

It is possible to relate turbulent parameters (wind velocity standard deviations $\sigma_{u,v,w}$ and Lagrangian decorrelation time scales $T_{Lu,v,w}$) to spectral distribution of turbulent kinetic energy (TKE). Following this approach, Degrazia et al. (2000) developed expressions for the wind velocity variances and Lagrangian decorrelation time scales. The velocity variances were obtained directly from the integration of the turbulence velocity spectra (Caughey & Palmer, 1979). On the other hand, the Lagrangian decorrelation time scales were derived

from the peak wavelength of the turbulent velocity spectra (Caughey, 1982). Therefore, the turbulent velocity variances ($\sigma_{u,v,w}$) and the local turbulent time scales ($T_{Lu,v,w}$) for a stable boundary layer are given respectively by the following expression (Degrazia et al., 2000)

$$\sigma_{u,v,w}^2 = \frac{2.32c_{u,v,w}\phi_\epsilon^{2/3}u_*^2}{[(f_m^*)_{u,v,w}^s]^{2/3}} \quad (10)$$

and

$$T_{Lu,v,w} = \frac{z}{\sqrt{c_{u,v,w}}} \left\{ \frac{0.059}{[(f_m^*)_{u,v,w}^s]^{2/3} (\phi_\epsilon^s)^{1/3} u_*} \right\} \quad (11)$$

where z is the height above the surface, $c_{u,v,w} = \alpha_{u,v,w}\alpha_u(2\pi k)^{-2/3}$ with $k = 0.4$ (von Karman constant), $\alpha_u = 0.5 \pm 0.05$ and $\alpha_{u,v,w} = 1, 4/3, 4/3$, respectively (Champagne et al., 1977; Sorbjan, 1989). For a shear-dominated stable PBL the adimensional dissipation rate $\phi_\epsilon^s = \epsilon_s k z / u_*^3$ can be written as $\phi_\epsilon^s = 1.25(1 + 3.7z/\Lambda)$ where Λ is the local Obukhov length given by $\Lambda = L(1 - z/h)^{(1.5\alpha_1 - \alpha_2)}$, with h being the height of the turbulent stable PBL and L is the surface Obukhov length. Furthermore, for a shear-dominated stable PBL, the local friction velocity is defined by $u_* = (u_*)_0(1 - z/h)^{\alpha_1/2}$, where $(u_*)_0$ is the surface friction velocity and $\alpha_1 = 1.5$ and $\alpha_2 = 1.0$ (Nieuwstadt, 1984). Finally, the reduced frequency of the stable horizontal spectral peaks is provided by the following relation $(f_m^*)_{u,v,w}^s = (f_m)_{(u,v,w)s}^n(1 + 3.7z/\Lambda)$ where $(f_m)_{us}^n = 0.045$, $(f_m)_{vs}^n = 0.16$ and $(f_m)_{ws}^n = 0.33$ are the frequencies of the spectral peaks in the surface for neutral conditions (Olesen et al., 1984; Sorbjan, 1989).

Based on analyses of field experiments (Hanna, 1981; 1968; Kaimal, 1976), theoretical considerations (Irwin, 1979; Panofsky et al., 1977) and second-order closure models (Wyngaard et al., 1974), Hanna (1982) proposed the following turbulence parameterization for the turbulent velocity variances ($\sigma_{u,v,w}$) and the local turbulent time scales ($T_{Lu,v,w}$):

$$\frac{\sigma_u}{(u_*)_0} = 2 \left(1 - \frac{z}{h}\right) \quad (12)$$

and

$$\frac{\sigma_w}{(u_*)_0} = \frac{\sigma_v}{(u_*)_0} = 1.3 \left(1 - \frac{z}{h}\right), \quad (13)$$

$$T_{Lu} = 0.15 \frac{h}{\sigma_u} \left(\frac{z}{h}\right)^{0.5}, \quad (14)$$

$$T_{Lv} = 0.07 \frac{h}{\sigma_v} \left(\frac{z}{h}\right)^{0.5} \quad (15)$$

and

$$T_{Lw} = 0.10 \frac{h}{\sigma_w} \left(\frac{z}{h}\right)^{0.8} \quad (16)$$

From Eqs. (10) and (11), it can be seen that the turbulent velocity variances and the local Lagrangian time scales associated with the fully developed turbulence in the shear-dominated stable turbulent flow in PBL are formulated in terms of a similarity theory and expressed by

three fundamental parameters associated with the turbulence in a PBL; the friction velocity, the adimensional dissipation rate and the reduced frequency of the horizontal spectral peaks. On the other hand, Eqs. (12), (13), (14), (15) and (16) are expressed in terms of a similarity theory and described by two fundamental scales, the friction velocity (u_*) and the height of the turbulent stable PBL.

Therefore, using Eq. (9), with $T_* \cong 2000s$ and $T_{Lu,v}$ given by the Eqs. (11), (14) and (15), the low-frequency horizontal wind oscillation effects can be parameterized and introduced into Eqs. (4) and (5) to simulate the observed dispersion of passive scalars, caused by the meandering transport in the stable PBL.

4. Meandering dispersion simulation

The results of the proposed model are compared with the concentration data collected under stable conditions in low wind speeds over flat terrain at the Idaho Engineering Laboratory (INEL). These observed results have been published in a U.S. National Oceanic and Atmospheric Administration (NOAA) report (Sagendorf & Dickson, 1974). Because of wind direction large variability associated with the meandering phenomenon, a full 360° sampling grid was implemented. Arcs were laid out at radii of 100, 200 and 400 m from the emission point source. Samplers were placed at intervals of 6° on each arc for a total of 180 sampling locations. The receptor height was 0.76 m. The tracer SF₆ was released at a height of 1.5 m. The 1 h average concentrations were determined by means of an electron capture gas chromatography. Wind speeds measured at levels 2, 4, 8, 16, 32 and 61 m were used to calculate the coefficient for the exponential wind vertical profile. According to Brusasca et al. (1992) and Sharan & Yadav (1998) the roughness length used was $z_0 = 0.005m$. The Monin-Obukhov length L and the friction velocity u_* were not available for the INEL experiment but can be roughly estimated by different formulations. Then, L may be calculated from an empirical formulation suggested by Zannetti (1990) and the stable turbulent PBL height h was determined according to expression derived by Zilitinchevick (1972).

INEL observed concentrations, $\chi_m(m^{-2})$, were normalized according to the following relation (Sagendorf & Dickson, 1974)

$$\chi_m = C_m \frac{U_4}{Q}, \quad (17)$$

where C_m is the dimensional concentration expressed in gm^{-3} , U_4 is the mean wind speed at 4 m and Q is tracer emission rate (gs^{-1}). Consequently, predicted concentrations are for the INEL experiments expressed in (m^{-2}).

For the simulations, the turbulent flow field is considered as inhomogeneous in the vertical direction and the transport is performed by the longitudinal component of the mean wind velocity. In the simulations the horizontal domain was determined according to sampler distances and the vertical domain was set equal to the observed PBL height h . The emission point source was localized at the domain centre. The time step was maintained constant and equal to $\Delta t = 0.5s$ during the simulations. The magnitude of this time step is of the order of the time scales of Kolmogorov's turbulent energy spectrum inertial subrange. Furthermore, this value of Δt performs the following inequality $\Delta t \ll T_L$. This condition ensures that the turbulent velocities can be considered a Markov process (Rodean, 1996). For each simulation, the number of particles released was 10^6 . In the case of the INEL experiments, the cells of

concentration at ground-level have a vertical dimension of $\Delta z = 3m$ (Anfossi et al., 2006). On the other hand, the horizontal dimensions were computed from the following relation

$$\Delta x = \Delta y = \frac{2\pi r}{N_{ang}}, \quad (18)$$

where r is the arc radius and $N_{ang} = 60$ is the number of samplers per arc. This way of computing the cell size covers all the compass at the three radii without significant overlapping. From these criteria results $dx = 10.47m$, $dy = 20.93m$ and $dz = 41.87m$ for the three arcs respectively. The simulated concentrations were obtained by counting the number of particles in volumes generated from the vertical and horizontal dimensions above presented.

5. Results and discussion

The performance of the SCLE model, employing the meandering parameterization for u and v components as given by the Eqs. (9), (10), (11), (12), (13), (14) and (15) is shown in Figures 1 to 6 and in Table 1. Figs. 1 and 2 show some typical simulation results obtained with the SCLE model employing Degrazia et al. (2000) turbulence parameterization. On the other hand, Figs. 3 and 4 show these same results reproduced with the SCLE model utilizing Hanna (1982) turbulence approach. Figs. 1 and 3 refer to experiment 8, which is characterized by a plume that spreads horizontally over a wide angular sector (one having the widest horizontal plume spread), meaning that the tracer is collected at all angles. The results of the simulations show that the SCLE model containing (Degrazia et al., 2000) and Hanna (1982) turbulence parameterization is able to reproduce the dispersion of the contaminants plume over all the 360° . Concerning to the environmental effects of air contaminants released in the PBL, the estimation of the location in which the maximum concentration occurs is a fundamental data. Regarding this information, the maximum concentration for experiment 8 at 400 m is approximately well reproduced by the SCLE model using Degrazia et al. (2000) and Hanna (1982) parameterization. Observing Figs. 2 and 4, we can see that the SCLE model with the Degrazia et al. (2000) and Hanna (1982) turbulence approach simulates fairly well the observed maximum concentrations for experiment 6 at 100, 200 and 400 m.

In addition, to obtain a global evaluation about of the quality of the simulations that were made using the meandering parameterization, the following statistical indices have been computed at each arc, for the ten INEL experiments: $conc_{max}$, $top5$ and S_y . $Conc_{max}$ (m^{-2}) is the maximum ground-level concentration, $top5$ (m^{-2}) refers to the mean of the 5 highest measured and computed ground-level concentration and $S_y = \sqrt{\frac{\sum_{i=1}^N (\vartheta_i - \bar{\vartheta})^2}{\sum_{i=1}^N \chi_i}}$, where ϑ_i are the sampler angles and $\bar{\vartheta}$ their average value (weighted with the concentrations). Considering the INEL experiments, the Figs. 5 and 6 show the results of these statistical indices ($conc_{max}$, $top5$ and S_y) obtained from the Eqs. (4) and (5) employing the meandering parameterization and respectively Degrazia et al. (2000) and Hanna (1982) turbulence approach. Figs. 5 (a,b and c) (Degrazia et al. (2000) turbulence approach) and Figs. 6 (a,b and c) (Hanna (1982) turbulence approach) show respectively the scatter diagram between observed and predicted $conc_{max}$, $top5$ and S_y values. Observing these figures it is possible to notice that there is a certain data spread, however this scattering is not sufficient to avoid a reasonable alignment in relation to the straight of perfect agreement.

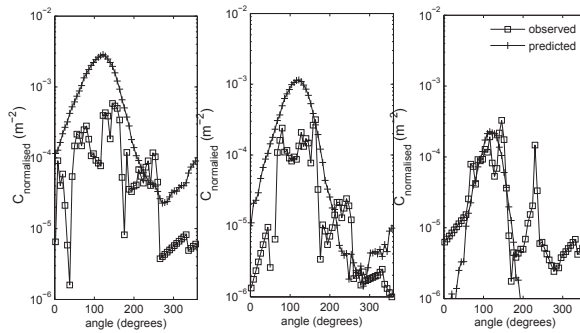


Fig. 1. Normalized ground level concentration (m^{-2}) for experiment 8 at 100, 200 and 400 m as a function of the sampler angles for (Degrazia et al., 2000) turbulence parameterization. Open squares indicate observed concentrations and crosses indicate simulated concentrations.

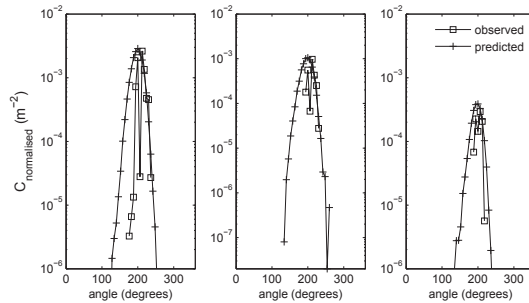


Fig. 2. As Fig. 1 but for experiment 6.

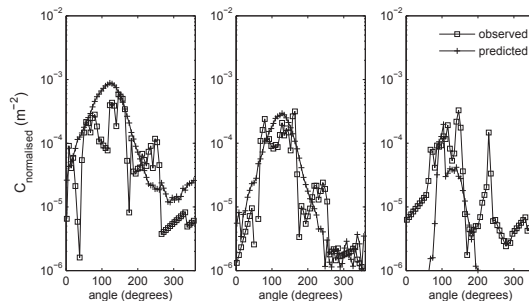


Fig. 3. Normalized ground level concentration (m^{-2}) for experiment 8 at 100, 200 and 400 m as a function of the sampler angles for Hanna (1982) turbulence parameterization. Open squares indicate observed concentrations and crosses indicate simulated concentrations.

Table 1 shows the results of the statistical analysis made with observed and predicted values of peak concentration ($n = 30$). Furthermore, this Table presents a comparison between SCLE

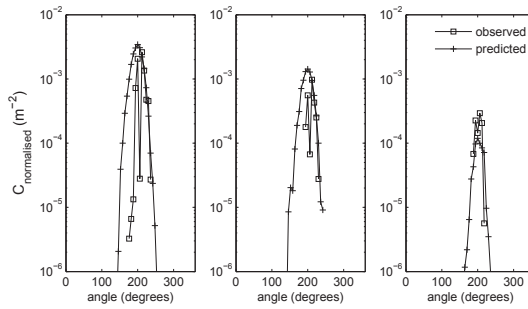


Fig. 4. As Fig. 3 but for experiment 6.

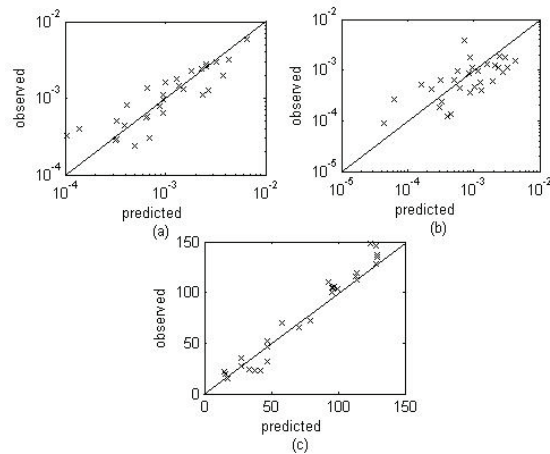


Fig. 5. Plot of (a) $conc_{max}$, (b) $top5$ and (c) S_y calculated with SCLE model utilizing the Degrazia et al. (2000) turbulence parameterization. X-axis shows predicted values whereas observed values are on the Y-axis.

model employing the parameterization (Eqs. (9), (11), (14) and (15)) and other three models (Oettl et al., 2001; Sagendorf & Dickson, 1974; Sharan & Yadav, 1998).

The statistical indices are suggested by Hanna (1989):

$$NMSE = \frac{(\overline{C_o} - \overline{C_p})^2}{\overline{C_o} \overline{C_p}} \text{ (Normalized Mean Square Error)}$$

$$FB = \frac{(\overline{C_o} - \overline{C_p})}{(0.5(\overline{C_o} + \overline{C_p}))} \text{ (Fractional Bias)}$$

$$FS = \frac{2(\sigma_o - \sigma_p)}{(\sigma_o + \sigma_p)} \text{ (Fractional Standard Deviation)}$$

$$R = \frac{(\overline{C_o} - \overline{C_o})(\overline{C_p} - \overline{C_p})}{\sigma_o \sigma_p} \text{ (Correlation Coefficient)}$$

$$FA2 = 0.5 \leq C_o / C_p \leq 2 \text{ (Factor 2)}$$

where C is the analyzed quantity (concentration) and the subscripts "o" and "p" represent the observed and the predicted values, respectively. The overbars in statistical indices indicate averages. The statistical index FB indicates if the predicted quantity underestimates or overestimates the observed one. The statistical index NMSE represents the quadratic error of the predicted quantity in relation to the observed one. The statistical index FS indicates the measure of the comparison between predicted and observed plume spreading. The statistical

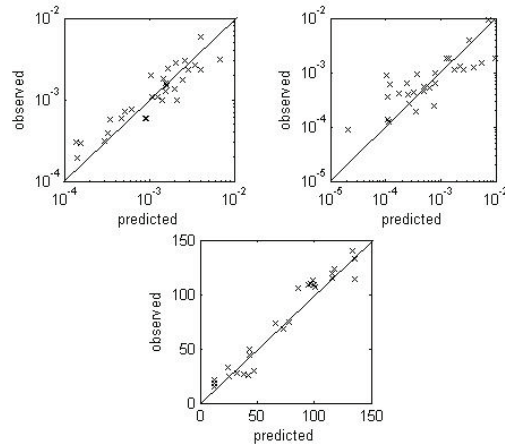


Fig. 6. Plot of (a) concmax, (b) top5 and (c) S_y calculated with SCLE model utilizing the Hanna (1982) turbulence parameterization. X-axis shows predicted values whereas observed values are on the Y-axis.

index FA2 provides the fraction of data for which $0.5 \leq C_o/C_p \leq 2$. As nearest zero are the NMSE, FB and FS and as nearest one are the R and FA2, better are the results.

Analyzing the results shown in Table 1, it is possible to infer that the SCLE model employing the meandering parameterization developed in this study reproduces well the experimental data in stable meandering conditions. Furthermore, the SCLE model with these meandering enhanced dispersion parameterizations presents results comparable or even better than ones obtained by other models. Therefore, the proposed parameterizations for the meandering phenomenon reported in the present analysis generate magnitudes of the statistical indices that are within acceptable ranges, with NMSE, FB and FS values relatively near to zero and R and FA2 relatively near to 1.

	NMSE	R	FA2	FB	FS
SCLE model Degrazia et al. (2000)	0.19	0.88	0.89	-0.054	-0.21
SCLE model Hanna (1982)	0.35	0.78	0.90	-0.038	-0.22
Sagendorf and Dickson (1974)	0.60	0.42	0.80	0.06	-
Sharan and Yadav (1998)	0.53	0.55	0.60	-0.02	-
Oettl et al. (2001)	0.21	0.86	0.87	-0.13	-

Table 1. Statistical evaluation considering other for the INEL experiment.

6. Conclusions

The investigation deals with contaminants dispersion associated with the low wind speed cases. In low wind velocity conditions in the stable PBL, the meandering horizontal of the wind is a physical mechanism that dominates the horizontal spread of contaminants. This means that as the average wind speed decreases, large horizontal low frequency oscillations start to control the flow field, surpassing both the transport and the small-scale diffusion

generated by the fully developed turbulence. Therefore, based on meandering phenomenon observational evidences and Degrazia et al. (2000) and Hanna (1982) turbulence approach, which allows to calculate local (at distinct-heights) horizontal Lagrangian time scales, parameterizations for the reinforced meandering diffusion were derived and presented.

The parameters p and q (Eqs. 2 and 3) are important quantities describing the meandering phenomenon. They are defined in terms of m , which controls the magnitude of negative lobes in the meandering observed autocorrelation functions, and of the local horizontal time scales $T_{Lu,v}$ for a fully developed turbulence. Therefore, Eq. (9) is a formulation for the meandering parameterization that is described in terms of the meandering period T_* and of the time scales $T_{Lu,v}$. Concerning to the T_* , an observed representative mean value of the meandering period of the order of $T_* = 2000s$, obtained from a large number of experimental data, was employed in this study. This phenomenological choice for the value of T_* allows that the present approach can be applied to meandering distinct cases. On the other hand, the parameterization of $T_{Lu,v}$ was obtained from Degrazia et al. (2000) and Hanna (1982) turbulence descriptions. Thusly, the equations that provide $T_{Lu,v}$ (Eqs. 11, 14 and 15) are expressed in terms of a similarity theory describing the shear dominated stable turbulence.

The meandering parameterizations above discussed were evaluated and tested through the comparison with observational data and other different meandering dispersion models. The results generated by the simulations using the two coupled Langevin equations (SCLE), employing the new parameterizations, agree well with the experimental data, pointing that the present approaches reproduce the contaminants meandering spread process adequately in low wind speed stable conditions.

Finally, considering the good agreement between the results of the proposed model with the experimental ones, the new parameterizations for the meandering phenomenon employed in the SCLE are found to be suitable to simulate meandering enhanced dispersion of contaminants in a low wind speed stable PBL.

7. Acknowledgement

The authors acknowledge the financial support provided by CAPES (Coordenação de Aperfeiçoamento de Pessoal de Nível Superior) and CNPq (Conselho Nacional de Desenvolvimento Científico e Tecnológico).

8. References

- Anfossi, D.; Alessandrini, S.; Trini Castelli, S.; Ferrero, E.; Oetl, D. & Degrazia, G. (2006). Tracer dispersion simulation in low wind speed conditions with a new 2D Langevin equation system, *Atmospheric Environment*, Vol. 40, pp. 7234-7245.
- Anfossi, D.; Oetl, D.; Degrazia, G. & Goulart, A. (2005). An analysis of sonic anemometer observations in low wind speed conditions, *Boundary-Layer Meteorology*, Vol. 114, pp. 179-203.
- Brusasca, G.; Tinarelli, G. & Anfossi, D. (1992). Particle model simulation of diffusion in low wind speed stable conditions, *Atmospheric Environment*, Vol. 26A, pp. 707-723.
- Carvalho, J.C.; Degrazia, G.A.; Vilhena, M.T.; Magalhães, S.G.; Goulart, A.; Anfossi, D.; Acevedo, O.C. & Moraes, O.L.L. (2006). Parameterization of meandering phenomenon in a stable atmospheric boundary layer, *Physica A*, Vol. 368, pp. 247-256.

- Caughey, S.J. (1982). Observed characteristics of the atmospheric boundary layer. In: Nieuwstadt, F.T.M., van Dop, H. (Eds.), *Atmospheric Turbulence and Air Pollution Modelling*, Reidel, pp. 107-158, Dordrecht.
- Caughey, S.J. & Palmer, S.G. (1979). Some aspects of turbulence structure thought the depth of the convective boundary layer, *Quarterly Journal of the Royal Meteorological Society*, Vol. 105, pp. 811-827.
- Chandrasekhar, S. (1943). Stochastic Problems in Physics and Astronomy, *Review of Modern Physics*, Vol. 15, pp.1-89.
- Champagne, F.H.; Friehe, J.C.; La Rue, J.C. & Wyngaard, J.C. (1977). Flux measurements, flux estimation techniques, and fine-scale turbulence measurements in the unstable surface layer over land, *Journal of Atmospheric Science*, Vol. 34, pp. 515-530.
- Carvalho, J.C.; Anfossi, D.; Castelli, S.T. & Degrazia, G.A. (2002). Application of a model system for the study of transport and diffusion in complex terrain to the TRACT experiment, *Atmospheric Environment*, Vol. 36, pp. 1147-1161.
- Cirillo, M.C. & Poli, A.A. (1992). An intercomparison of semiempirical diffusion models under low wind speed, stable conditions, *Atmospheric Environment*, Vol. 26A, pp. 765-774.
- Csanady, G.T. (1992). Turbulent diffusion in the environment, *Geophysics and Astrophysics Monographs*, Reidel, 248pp, Boston.
- Degrazia, G.A.; Anfossi, D.; Carvalho, J.C.; Mangia, C.; Tirabassi, T. & Campos Velho, H.F. (2000). Turbulence parameterization for PBL dispersion models in all stability conditions, *Atmospheric Environment*, Vol. 34, pp. 3575-3583.
- Dosio, A.; Guerau de Arellano, J.V. & Holtslag, A.A.M. (2005). Relating Eulerian e Lagrangian statistics for the turbulent dispersion in the Atmospheric Convective Boundary Layer, *Journal of the Atmospheric Sciences*, Vol. 62, No. 4, pp. 1175-1191.
- Ferrero, E. & Anfossi, D. (1998). Comparison of FDPs, closure schemes and turbulence parameterizations in Lagrangian stochastic models, *International Journal of Environment and Pollution*, Vol. 9, pp. 384-410.
- Frenkiel, F.N. (1953). Turbulent diffusion: mean concentration distribution in a flow field of homogeneous turbulence, *Advances in Applied Mechanics*, Vol. 3, pp. 61-107.
- Gardiner, C.W. (1997). *Handbook of stochastic methods*, Springer, 442pp, Berlin.
- Goulart, A.; Degrazia, G.A.; Acevedo, O.C. & Anfossi, D. (2007). Theoretical considerations of meandering winds in simplified conditions, *Boundary-Layer Meteorology*, Vol. 125, pp. 279-287.
- Hanna, S.R. (1989). Confidence limits for air quality model evaluations, as estimated by Bootstrap and Jackknife Resampling Methods, *Atmospheric Environment*, Vol. 23, pp. 1385-1398.
- Hanna, S.R. (1982). Applications in air pollution modelling, In: *Atmospheric Turbulence and Air Pollution Modelling*, Nieuwstadt, F.T.M., van Dop, H., Reidel, page numbers (275-310), Dordrecht.
- Hanna, S.R. (1981). Lagrangian and Eulerian time-scale relations in the daytime boundary layer, *Journal of Applied Meteorology*, Vol. 20, pp. 242-249.
- Hanna, S.R. (1968). A method of estimating vertical eddy transport in the planetary boundary layer using characteristics of the vertical velocity spectrum, *Journal of the Atmospheric Sciences*, Vol. 25, pp. 1026-1033.

- Irwin, J.S. (1979). Estimating plume dispersion - a recommended generalized scheme. Preprints fourth symposium on turbulence, diffusion and air pollution, *American Meteorological Society*, 45 Beacon Street, Boston, Mass. 02108, pp. 62-69.
- Kaimal, J.C. (1976). Turbulence structure in the convective boundary layer, *Journal of Atmospheric Science*, Vol. 33, pp. 2152-2169.
- Nieuwstadt, F.T.M. (1984). The turbulent structure of the stable, Nocturnal Boundary Layer, *Journal of the Atmospheric Sciences*, Vol. 41, No. 14, pp. 2202-2216.
- Oettl, D.; Almbauer, R.A. & Sturm, P.J. (2001). A new method to estimate diffusion in stable, low-wind conditions, *Journal of Applied Meteorology*, Vol. 40, pp. 259-268.
- Oettl, D.; Goulart, A.; Degrazia, G.A. & Anfossi, D. (2005). A new hypothesis on meandering atmospheric flows in low wind speed conditions, *Atmospheric Environment*, Vol. 39, pp. 1739-1748.
- Olesen, H.R.; Larsen, S.E. & Hojstrup, D. (1984). A new hypothesis on meandering atmospheric flows in low wind speed conditions, *Atmospheric Environment*, Vol. 39, pp. 1739-1748.
- Panofsky, H.A.; Tennekes, H.; Lenschow, D.H. & Wyngaard, J.C. (1977). The characteristics of turbulent velocity components in the surface layer under convective conditions, *Boundary-Layer Meteorology*, Vol. 11, pp. 355-361.
- Rodean, H.C. (1996). *Stochastic Lagrangian Models of Turbulence Diffusion*, American Meteorological Society, 84pp, Boston.
- Sagendorf, J.F. & Dickson, C.R. (1974). *Diffusion under low wind speed, inversion conditions*, NOAA Technical Memorandum ERL ARL-52, 89pp.
- Sharan, M. & Yadav, K. (1998). Simulation of diffusion experiments under light wind, stable conditions by a variable k-theory model, *Atmospheric Environment*, Vol. 32, pp. 3481-3492.
- Sharan, M.; Yadav, K. & Sing, M.P. (1995). Comparison of sigma schemes for estimation of air pollutant dispersion in low winds, *Atmospheric Environment*, Vol. 29, pp. 2051-2059.
- Sorbjan, Z. (1989). *Structure of the Atmospheric Boundary Layer*, Prentice-Hall, Englewood Cliffs, NJ, 317pp.
- Thomson, D.J. (1987). Criteria for the selection of stochastic models of particle trajectories in turbulent flows, *Journal of Fluids Mechanics*, Vol. 180, pp. 529-556.
- Wang, M.C. (1945). Influence of magnetic field on the Brownian motion of charged particle, *Journal of the Physical Society of Japan*, Vol. 28, pp. 559-564.
- Wilson, J.D. & Sanford, B.L. (1996). Review of Lagrangian stochastic models for trajectories in turbulent atmosphere, *Boundary-Layer Meteorology*, Vol. 78, pp. 191-210.
- Wilson, R.B.; Start, G.E.; Dickson, C.R. & Ricks, N.R. (1976). *Diffusion under low wind speed conditions near Oak Ridge, Tennessee*, NOAA Technical Memorandum ERL ARL-61, 83pp.
- Wyngaard, J.C.; Coté, O.R. & Rao, K.S. (1974). Modelling of the atmospheric boundary layer *Advances in Geophysics*, Academic Press, Vol. 18A, pp. 193-212, New York.
- Yeung, P.K. (2002). Lagrangian investigations of turbulence, *Annual Review of Fluid Mechanics*, Vol. 34, pp. 115-142.
- Zannetti, P. (1990). *Air Pollution Modeling. Theories, Computational Methods and Available Software*, Kluwer Academic Publisher, 444pp, New York.

Zilitinchevick, S.S. (1972). On the determination of the height of the Ekman boundary layer, *Boundary-Layer Meteorology*, Vol. 3, pp. 141-145.

Bioaerosol Emissions: A Stochastic Approach

Sandra M. Godoy, Alejandro S. M. Santa Cruz and Nicolás J. Scenna
CAIMI – Centro de Aplicaciones Informáticas y Modelado en Ingeniería
Universidad Tecnológica Nacional - Facultad Regional Rosario
Argentina

1. Introduction

Several studies have shown that one of the main and uncontrollable mechanisms of bioaerosols dispersion is atmospheric transport (Casal et al., 1995; Daggupaty & Sellers, 1990; Donaldson et al., 2001; Lighthart & Frish, 1976; Lighthart & Kirilenko, 1998; Pillai & Ricke, 2002). This phenomenon can cause serious social and economic consequences, so the prediction of affected zones is very important for controlling epidemics and for avoiding economic losses.

Atmospheric micro-organism dispersion can come from natural origin as well as agricultural and industrial activities. Activities associated to waste treatment plants (liquid or solid), waste processing sites, compost plants, landfill, etc., can produce aerosols containing bacteria, viruses, fungi and odours (Buttner & Stetzenbach, 1991; Crawford & Jones, 1979; Pascual et al., 2003; Ranalli et al., 2000). They can cause serious health upsets on workers and people neighbouring these sites. As several studies about biologic risk evaluation have shown, the exposure to low levels of fine particles over an extended period of time greatly affects human health (Ackermann-Liebrich et al., 1999; Ebel et al., 2000; Lippmann, 2007; U.S. EPA, 2004). Particles with diameter between 2.5 and 10 μm can enter the lungs, however, those with diameter less than or equal to 2.5 can reach the alveolus and enter directly into the bloodstream, causing consequences like light discomfort, allergic reactions, sinusitis, pulmonary infection and aggravate asthma.

Bioaerosol size particles can vary from 0.1 μm or less for viruses, to approximately 1 μm for simple bacteria; even though, in some cases, can be formed conglomeration of about 50 μm in diameter (Eduard, 2003; Wickman, 1994).

In other hand, several authors have remarked the importance of studying the propagation mechanism of animal epidemics like foot-and-mouth disease (FMD), one of the most important animal diseases (Casal et al., 1995-1997; Donaldson & Alexandersen, 2002; Donaldson et al., 2001; Thompson et al., 2002).

It is well known that bioaerosol multiplication and survival as well as downwind levels concentrations strongly depend on meteorological conditions like wind intensity, wind direction, temperature, humidity, and atmospheric stability, which are uncertain and specific of the place under study.

Airborne virus concentrations in FMD epidemic cases (Hampshire & Worcestershire - 1997) as well as micro-organism dispersion in rubbish dump, transference sites and municipal wastewater treatment plants, have been estimated using Gaussian models (Garner &

Beckett, 2005a; Gloster et al., 2010; Karra & Katsivela, 2007; Mikkelsen et al., 2003; Pascual et al., 2003; Sorensen et al., 2000). In many works algorithms developed for consequences analysis (gas diffusion) have been modified and used for bioaerosols diffusion simulations (Casal et al., 1995; Garner et al., 2005b; Holmes & Morawska, 2006; Sorensen et al., 2000).

Consequently, it is very important for managers to provide useful information about those activities that can potentially generate bioaerosols, considering the meteorological influence in the prediction of impacted areas.

So, in this chapter a methodology that takes into account the stochastic behaviour of atmospheric variables, which was successfully used for toxic gas release risk assessment, is adapted for the analysis of micro-organism spread.

Bacteria and fungi concentration distribution from a waste water treatment plant and the foot-and-mouth disease spread from an infected farm, are presented as study cases from this point of view, in a specific region of Argentina.

2. Dispersion models

2.1 Virus

The Gaussian model is recognized to be appropriate to estimate aerosols concentration consisting of particles of less than about 20 μm in diameter, released from a continuous point source (Sellers & Parker, 1969). In this size ranges, particles have the same behaviour as the gas which drags it, and the effect of atmospheric turbulence is more important than the gravitational deposition.

Also, considering the low virus concentration emitted from the source, it is accepted that the exhaled air has the same density as air does.

So, the basic equation of the Gaussian plume for a continuous emission placed at a height (h), following a two-dimension dispersion model is used. Reflection and thermal inversion are not considered. On the other hand, the chemical formation or aerosol dynamics (nucleation, coagulation, condensation, etc.) to evaluate particle processes occurring within the plumes are not modelled. Also, it is supposed that emission takes place on open plain areas not including the effect of obstacles such as mountains, trees or buildings which can cause a plume deviation, turbulence and dilution of the particle concentration.

So, according to these assumptions, the more important input parameters affecting pollutants dispersion are temperature, wind velocity, stability class, mixing height, horizontal and vertical dispersion parameters as well as seasonal variation. Frequency distributions of wind velocity, wind direction and stability class are included in the input files. Mixing height is computed as a function of the other meteorological parameters. The average concentration (given as $\text{ID}_{50}^1/\text{m}^3$) at each point is given by means of the following equation:

$$\bar{C} = \frac{Q}{2\pi u\sigma_y\sigma_z} \exp\left[-\left(\frac{y^2}{2\sigma_y^2} + \frac{(z-h)^2}{2\sigma_z^2}\right)\right] \quad (1)$$

Where

\bar{C} = Average infection dose at point x, y, z ($\text{ID}_{50}/\text{m}^3$)

¹ ID_{50} (Infectious Dose 50%): the dose of a pathogen that will infect 50% of the population.

Q = Emission rate (ID_{50}/s)

h = Emission source height (m)

σ_y, σ_z = Dispersion coefficients (m)

x = Downwind distance from the source (m).

u = Wind speed (m/s).

The FMD emission rate is calculated considering a certain flow rate of exhaled air containing a given concentration of virus which depends on the different virus strain, species and the date and period of time of the infection (Casal et al., 1995; Donaldson et al., 2002; Kitching et al., 2005).

2.2 Bacteria

It is accepted that simple bacteria size range vary between $0.2 \mu m$ y $10 \mu m$ (Wickman, 1994) and for fungi spore between $4 \mu m$ y $20 \mu m$. It is accepted that under this conditions, downwind concentration can be modelled through a Gaussian model, introducing a lethality factor or micro-organism death rate, to consider the bacteria viability.

Some works present experimental measurement of this factor (Lighthart & Frisch, 1976; Pascual et al., 2003; Santos Burgoa et al., 1992). Although the environmental conditions under micro-organism which are exposed in the "real world" are different from lab conditions (due to the atmospheric dynamic), these values are a good approximation of the lethality factors. So, atmospheric bacteria and fungi dispersion, for a point source and fixed meteorological conditions can be evaluated by means of the following equation:

$$\bar{C} = \frac{Q}{2 \pi u \sigma_y \sigma_z} \exp\left(-\frac{fx}{u}\right) \exp\left[-\left(\frac{y^2}{2\sigma_y^2} + \frac{(z-h)^2}{2\sigma_z^2}\right)\right] \quad (2)$$

\bar{C} = Average concentration at point x, y, z (CFU^2/m^3)

Q = Emission rate (CFU/s)

h, σ_y, σ_z, u and x have the same meaning as in equation (1)

f = Lethality or death rate factor (s^{-1}).

For fungi particles, due to their major size, it must be considered particle deposition effects introducing the Stokes settling velocity (W_p), according to the following expression:

$$\bar{C} = \frac{Q}{2 \pi u \sigma_y \sigma_z} \exp\left(-\frac{fx}{u}\right) \exp\left[-\left(\frac{y^2}{2\sigma_y^2} + \frac{\left(z-h-\frac{w_p x}{u}\right)^2}{2\sigma_z^2}\right)\right] \quad (3)$$

When considering a background bioaerosol concentration, C_b , the total bioaerosol concentration C_B can be obtained as:

$$C_B = \bar{C} + C_b \quad (4)$$

² CFU (Colony-forming unit): the number of viable bacterial cells in a sample per ml.

3. Stochastic concentration levels and impact distances calculation methodology

3.1 Concentration distribution calculation

As previously stated, a Gaussian-type dispersion model is used to carry out simulations considering bioaerosol emission rate, release concentration and ground roughness as deterministic inputs. In addition, some atmospheric parameters within the model are considered by frequency distributions using a Monte Carlo strategy. In this way, a number of random scenarios are generated.

For fungi dispersion, the settling velocity is calculated as function of the scenario characteristics (particle diameter ranges, Reynolds number, spreading coefficients, etc.)

The proposed methodology is based on a simple representation of emitters and receptors (a squared grid) according to Godoy et al., 2007, 2010 and Scenna & Santa Cruz, 2005.

Every potential receptor is supposed to be placed in the geometrical centre of each grid square represented by the (X_j, Y_k) coordinates. Considering random scenarios, the expected micro-organism concentration at ground-level is calculated at every grid point (or receptor) applying the appropriate dispersion model (Eq. (1) to (3)). As a result, the approximation to the output concentration distribution or the critical concentrations levels (those exceeding the lethal/infectious threshold), are computed at each given grid point according to the input data distributions and the assumed specified (seasonal, annual, or other) time horizon. According to Eq. (4), a background concentration level (given by either a distribution or a single value) can be used if it is available.

Then, a map concentration identifying bioaerosol levels and critical areas (with potential health problems) can be plotted. Representative concentration values at each receptor $R_{jk}(X_j, Y_k)$ can be computed by taking the 90-percentile value of the concentration distribution.

Finally, using the same strategy, area sources are modelled as multiple point sources.

Summarizing, Fig. 1 shows the general implemented computational strategy which can be concise in the flowchart and presents the three basic modules the computational package STRRAP (Godoy et al., 2007, 2010; Scenna & Santa Cruz, 2005) has:

1. The pre-processor
2. The processor
3. The post-processor

The pre-processor module is in charge of the input file generation for the dispersion model. It reads the emission data included within a pattern file (micro-organism characteristics, emission rates, meteorological data, etc.) and then generates the random variable values. That is, it writes a file to be used by the processor or calculus module. After the time horizon (a season or the whole year) and the day or night condition are fixed, the values of the random variables (wind direction, wind velocity and atmospheric stability) are determined. Then, the processor module (using the appropriate dispersion model) computes the downwind bioaerosol concentration according to each trial previously defined by the pre-processor module.

The post-processor module stores and manages all trial results in the database and displays graphic results (for example, bioaerosol concentration and frequency maps, as well as affected zones).

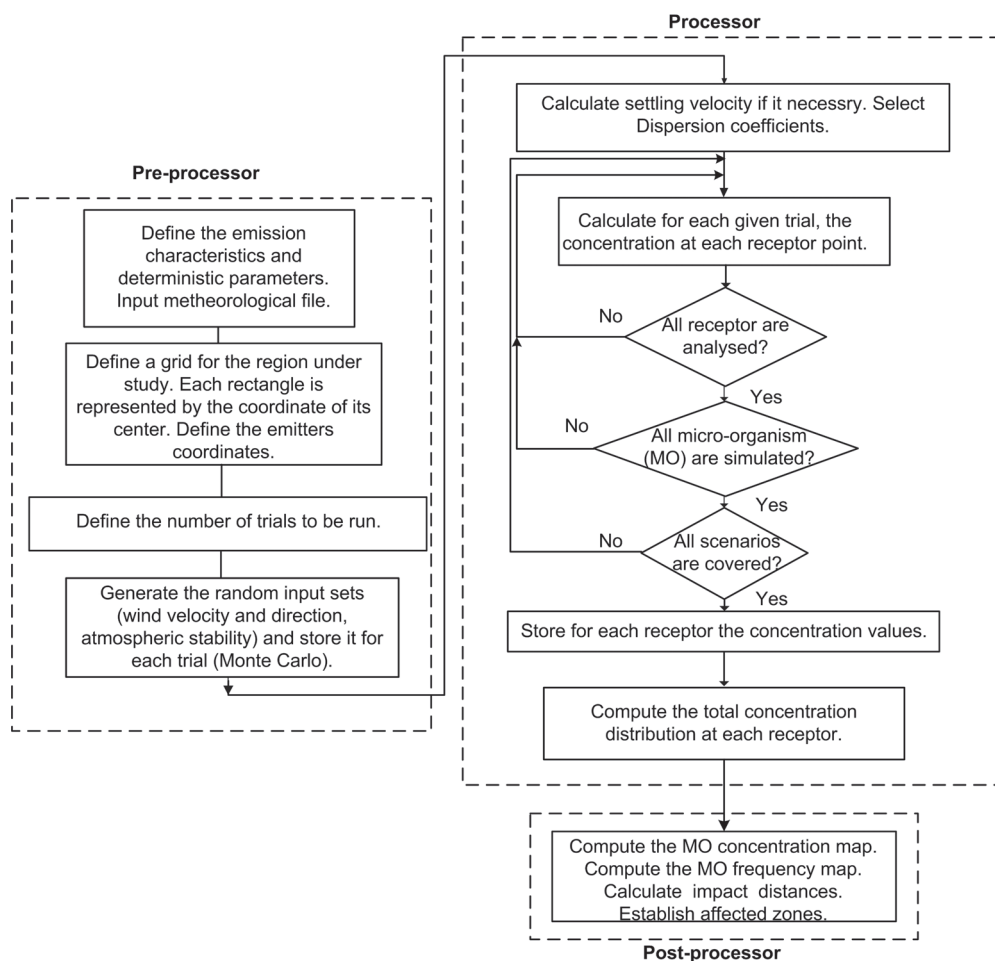


Fig. 1. System Calculus Steps

3.2 Statistically weighted impact distance definition

Considering the concentration distributions at each defined receptor point as explained in Section 3.1, and the micro-organism unhealthy concentration levels, we can determine the zones around the source where these critical concentrations levels are exceeded. For receptors where the limit concentration is exceeded, the distance between each affected receptor and the emission point/s can be computed. As a result, a distance frequency distribution is achieved.

In this way, we can calculate a statistically weighted impact distance (RI) by taking, for example, the maximum, or the 90 percentile as representative impact distance values. The unhealthy or critical area is defined here as a circle of radius RI (see Fig. 2). In fact, every receptor placed at a distance longer than RI can practically be considered as not affected.

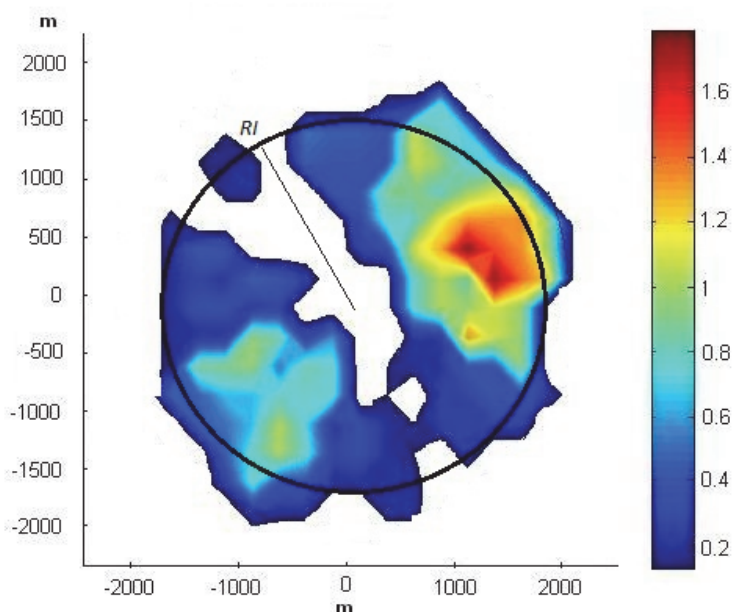


Fig. 2. Impact distance definition

4. Study cases

4.1 Bacteria, coliform and fungi dispersion

Different stages in effluent treatment plants are important bioaerosols sources (Cannon, 1983; Kenline & Scarpino 1972; Napolitano & Rowe, 1966); particularly, the aeration chambers at municipal waste water treatment plants (Brandi et al., 2000). So, bioaerosol emission from a sewage treatment plant near the city of Rosario is presented as a study case. The major potential pathogen micro-organism to study here are bacteria, total fungi, total coliforms, enterococcus and staphylococcus. Sometimes, gram-negative bacteria are studied. It is known that bioaerosols are subjected to certain conditions which can inhibit their biological activity (solar radiation, humidity, etc.), but some of them can survive in the unfavourable environmental conditions (Jones & Harrison, 2007; Karra & Katsivela, 2007; Korzeniewska et al., 2009). Mean temperature, pressure and humidity for the region under study are included in the input files. Indeed, wind velocity; wind direction and stability class distributions must be provided for this zone. Data collected over the last ten years are used in this work to obtain the histograms for each stochastic parameter. So, probability density functions which take into account the variability of the local meteorological conditions are used. As the local relative humidity is always higher than 75% in the selected time horizon, it is assumed a high bacteria survival. Also it is accepted that fungi are resistant to very low relative humidity. So, it is adopted a mean death rate factor of 5×10^{-5} micro-organism/s for all species (Barth, E., 2006; Brandi et al., 2000; Karra & Katsivela, 2007; Santos Burgoa et al., 1992). Although this is a very important factor in the downwind bioaerosol level concentration determination, there is a great uncertainty on experimental

data due to the lack of exhaustive studies considering different species and environmental parameters (Lighthart & Frisch, 1976; Lighthart et al. 1995).

Emission flowrates are taken from literature (Karra & Katsivela, 2007). Currently there are some uncertainties in this parameter but it is important to note that some expressions were exposed to reduce it (Swan et al., 2003). Background concentration for Salmonella, Coliforms and Aspergillus fumigatus are taken from Barth, 2006. The adopted density (Kg/m³) and particle diameter (µm) (Deacon et al., 2009) for fungi settling velocity calculation are shown in figure 5.

Here the health criteria values suggested by NIOSH, 1994 are adopted as shown in Table 1.

Micro-organism	Flowrate (CFU /s)	Background Conc. (CFU /m ³)	Health criteria (CFU /m ³)
Total Bacteria	1.9 10 ⁶	10	10 ³
Total Coliforms	2.0 10 ⁶	5	10 ³
Fungi	2,5 10 ⁶	2,1	10 ³

Table 1. Simulation Parameters

Figures 3 to 5 summarize all input parameters to the model, according to the software input windows.

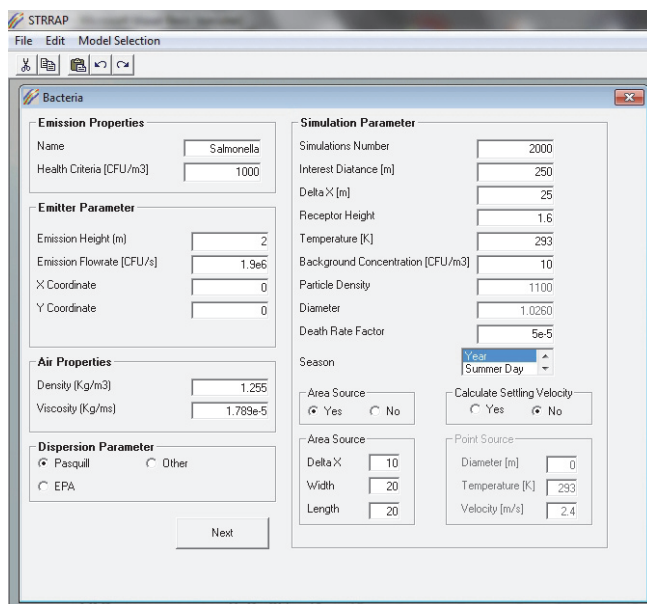


Fig. 3. Simulation parameters (Bacteria)

The screenshot shows the STRRAP software interface for configuring simulation parameters for Bacteria. The window title is "STRRAP" and the menu bar includes "File", "Edit", and "Model Selection". The main content area is titled "Bacteria" and contains several sections:

- Emission Properties:** Name: Total Coliform; Health Criteria [CFU/m³]: 1000.
- Emission Parameter:** Emission Height [m]: 2; Emission Flowrate [CFU/s]: 2.0e6; X Coordinate: 0; Y Coordinate: 0.
- Air Properties:** Density [Kg/m³]: 1.255; Viscosity [Kg/ms]: 1.789e-5.
- Dispersion Parameter:** Radio buttons for Pasquill (selected), Other, and EPA.
- Simulation Parameter:**
 - Simulations Number: 2000
 - Interest Distance [m]: 50
 - Delta X [m]: 5
 - Receptor Height: 1.6
 - Temperature [K]: 293
 - Background Concentration [CFU/m³]: 5
 - Particle Density: 1100
 - Diameter: 1.0260
 - Death Rate Factor: 5e-5
 - Season: Year (selected), Summer Day
 - Area Source: Yes, No
 - Calculate Settling Velocity: Yes, No
 - Area Source (sub-section): Delta X: 2.5, Width: 10, Length: 10
 - Point Source (sub-section): Diameter [m]: 0, Temperature [K]: 293, Velocity [m/s]: 2.4

A "Next" button is located at the bottom center of the window.

Fig. 4. Simulation parameters (Total Coliforms)

The screenshot shows the STRRAP software interface for configuring simulation parameters for Fungi. The window title is "STRRAP" and the menu bar includes "File", "Edit", and "Model Selection". The main content area is titled "Fungi" and contains several sections:

- Emission Properties:** Name: Aspergillus Fumi; Health Criteria [CFU/m³]: 1000.
- Emission Parameter:** Emission Height [m]: 2; Emission Flowrate [CFU/s]: 2.5e6; X Coordinate: 0; Y Coordinate: 0.
- Air Properties:** Density [Kg/m³]: 1.255; Viscosity [Kg/ms]: 1.789e-5.
- Dispersion Parameter:** Radio buttons for Pasquill (selected), Other, and EPA.
- Simulation Parameter:**
 - Simulations Number: 2000
 - Interest Distance [m]: 250
 - Delta X [m]: 25
 - Receptor Height: 1.6
 - Temperature [K]: 293
 - Background Concentration [CFU/m³]: 2.1
 - Particle Density: 1100
 - Diameter: 1.0260
 - Death Rate Factor: 5e-5
 - Season: Year (selected), Summer Day
 - Area Source: Yes, No
 - Calculate Settling Velocity: Yes, No
 - Area Source (sub-section): Delta X: 10, Width: 20, Length: 20
 - Point Source (sub-section): Diameter [m]: 0, Temperature [K]: 293, Velocity [m/s]: 2.4

A "Next" button is located at the bottom center of the window.

Fig. 5. Simulation parameters (Fungi)

After all simulations are performed (Monte Carlo method), assuming open plain areas, bioaerosol concentration distributions are obtained. Figures 6 to 8 show the estimated

colony-forming unit (CFU) maps of the evaluated species and their corresponding impact distances (RI). These were computed taking the 90 percentile of distance distributions as was explained in Section 3.2.

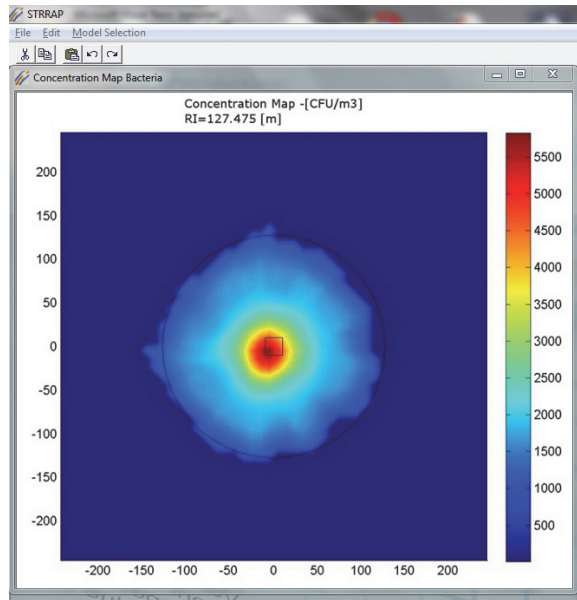


Fig. 6. Concentration map and impact distance (RI) for Bacteria

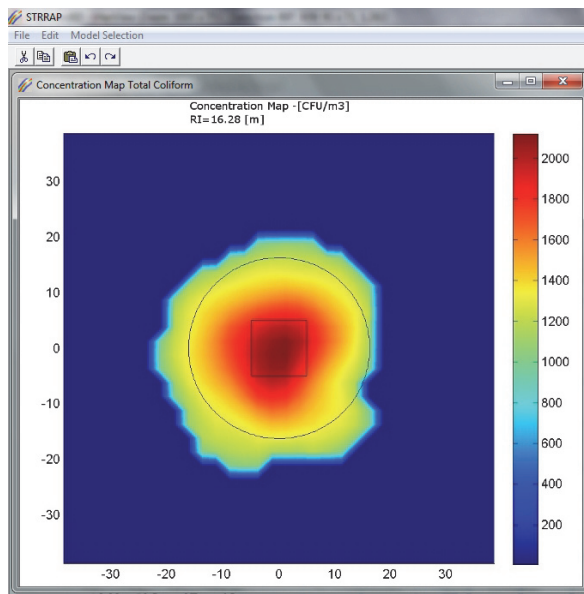


Fig. 7. Concentration map and impact distance (RI) for Total Coliforms

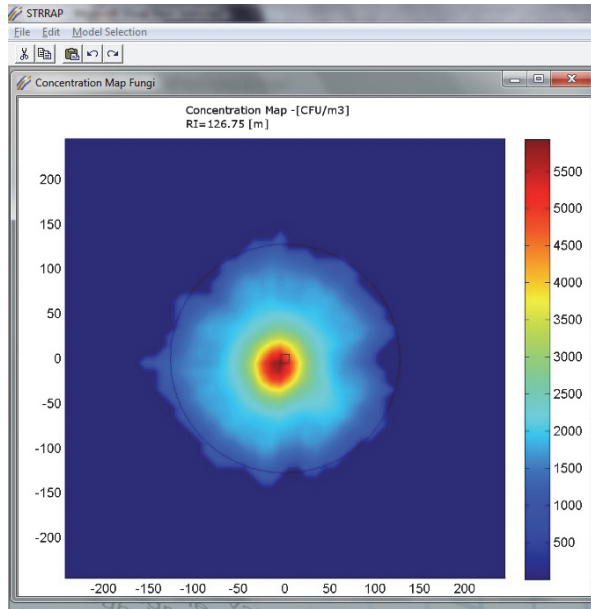


Fig. 8. Concentration map and impact distance (RI) for Fungi

For bacteria, every receptor placed at a distance longer than 127.475 m can practically be considered as not affected. For coliforms and fungi, the receptors in a radius of 16.28 m and 126.75 m, respectively, could be seriously affected.

4.2 Virus dispersion

In this section we consider a hypothetical infected farm placed near Rosario city. The number of animals at the source, the virus strain and species affected have significant effect on the distance that virus can travel and still be infectious. Here it is supposed that there are 50 infected pigs with the FMD C Noville strain (Sorensen et al., 2000). The emission flowrate of FMD is calculated considering certain exhaled air flow by each infected animal with a given virus concentration while infection occurs. The adopted infectious units and respiratory rates for common farm animal are taken from literature as summarized in Table 2.

Here we define the impact zones considering the critical infection dose, which is capable to cause the infection on half of the sheep population of a neighbouring farm, because it is well known that sheep are the more vulnerable species (Kitching, 2005; Donaldson, 2002).

Source	Flow of infectious units (ID_{50}/min)	Respiratory rate (lt/min)
Pig	4×10^3	25
Cattle	85	100
Sheep	66	10

Table 2. Emission rate of FMD virus for common farm animals (Taken from Casal et al., 1995)

Table 3 shows the rest of simulation parameters required to define the model input files completely

Emission flowrate (ID ₅₀ /s)	3,333
Min. Concentration required to cause infection in sheep (ID ₅₀ /m ³)	6x10 ⁻²
Number of simulation	2,000

Table 3. Simulation Parameters

After all simulations are performed (Monte Carlo method), virus concentration distributions around the infection source are computed as explained in previous Sections, considering critical concentration. So, the calculated impact distance value (90-percentile) is 3,005.2 m.

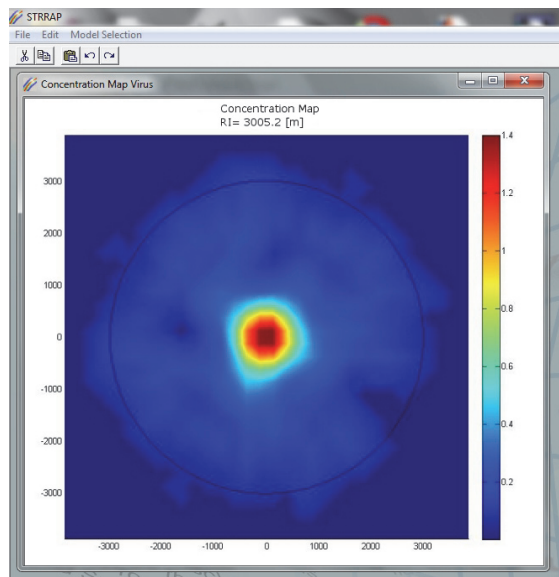


Fig. 9. Concentration map and impact distance (RI) for FMD

5. Conclusion

A methodology to compute stochastic air micro-organism concentration and impact distances due to bioaerosols emission from different sources is presented. The emission of bacteria and fungi at a sewage treatment plant, and an outbreak of FMD virus at a hypothetical infected farm are studied. The model considers variability of meteorological conditions. If micro-organism death rate factor as a function of temperature and relative humidity were available, it would be included in the different scenarios generation. In both cases map concentration and impact distances are obtained.

It is important to note that uncertainty was found in some data reported in the literature, such as the excretion rate, the infectious dose of different species and death rate factor, critical for an accurate prediction.

Furthermore, it must be remarked that only atmospheric transport mechanism were considered. Other complex physicochemical mechanism involved can affect the estimations significantly. Also, in FMD virus spread the movement of animals, people and articles may increase the infected area determined by this methodology.

Despite of the fact that bioaerosols threshold levels are a complex topic and nowadays is under discussion, it is very important to develop tools capable of predicting stochastic bioaerosol level dispersion and to determine the affected zones, with the aim of avoiding environmental and health population risks.

6. Acknowledgment

The authors thank to Universidad Tecnológica Nacional, CONICET and Agencia Nacional de Promoción Científica y Tecnológica for their financial support to carry out this work. Thanks are also given to Fabricio Todeschini for helping in the simulations and the programming tasks.

7. References

- Ackermann-Liebrich, U., Leuenberger, P., Schwartz, J., Schindler, C., Monn, C. & Bolognini, G. (1997). Lung function and long term exposure to air pollutants in Switzerland. *American Journal of Respiratory and Critical Care Medicine*, Vol. 155, pp. 122-129.
- Barth, E. (2006). *Evaluation of Bioaerosol Components, Generation Factors, and Airborne Transport Associated with Lime Treatment of Lead-Contaminated Sediment for Beneficial Use Purposes*, Thesis Ph.D. in Environmental and Occupational Hygiene, Available from http://rave.ohiolink.edu/etdc/view?acc_num=ucin1155653589
- Brandi, G., Sisti, M. & Amagliani, G. (2000). Evaluation of the environmental impact of microbial aerosols generated by wastewater treatment plants utilizing different aeration systems, *Applied microbiology*, Vol. 88, pp. 845-852
- Buttner, M.P. & Stetzenbach, L.D. (1991). Evaluation of four aerobiological sampling methods for the retrieval of aerosolized *Pseudomonas syringae*, *Applied and Environmental Microbiology*, Vol. 57, pp. 1268-1270
- Cannon, R.E. (1983). Aerosol release of cyanophages and coliforms from activated sludge basis, *Water Pollution Control Federation*, Vol. 55, pp. 1070-1074
- Casal, Joaquim., Planas-Cuchí, E., Moreso, J. & Casal Jordi. (1995). Forecasting virus atmospherical dispersion. Studies with food-and-mouth disease, *Hazardous Materials*, Vol. 43, pp. 229-244
- Casal J., Moreso JM, Planas-Cuchi E. & Casal J. (1997). Simulated airborne spread of Aujeszky's disease and foot-and-mouth disease, *Veterinary Record*; Vol. 140, pp. 672-676
- Crawford, G.V. & Jones, P.H. (1979). Sampling and differentiation techniques for airborne organisms emitted from wastewater, *Water Research*, Vol. 13, pp. 393-399
- Daggupaty, S. M. & Sellers, R. F. (1990). Airborne spread of food-and-mouth disease in Saskatchewan, Canadá, 1951-1952, *Canadian Journal of Veterinary Research*, Vol. 54, pp. 465-468
- Deacon, L.J., Pankhurst, L.J., Drewa, G.H., Hayes, E.T., Jackson, S. , Longhurst, P.J., Longhurst, J.W.S. , Liu, J., Pollard, S.J.T. & S.F. Tyrrel. (2009). Particle size distribution of airborne *Aspergillus fumigatus* spores emitted from compost using membrane filtration, *Atmospheric Environment*, Vol. 43, pp. 5698-5701
- Donaldson, A. I., Alexandersen, S. A., Sorensen & J. H., Mikkelsen, T. (2001). Relative risks of the uncontrollable (airborne) spread of FMD by different species, *Veterinary Record*, Vol. 148, No. 19, pp. 602-604

- Donaldson, A.I. & Alexandersen S. (2002). Predicting the spread of foot and mouth disease by airborne virus, *Revue Scientifique et Technique de l' Office International des Epizooties*; Vol. 21, No. 3, pp. 569-575
- Ebelt, S.T., Petkau, A.J., Vedal, S., Fisher, T.V. & Brauer, M. (2000). Exposure of chronic obstructive pulmonary disease patients to particulate matter: relationships between personal and ambient air concentrations, *Air & Waste Management Association*, Vol. 50, pp. 1081-1094
- Eduard, W. (2003). The Performance of Culture-Based Methods and Microscopy for Quantification of Noninfectious Airborne Microorganisms in Epidemiological Studies of Highly Contaminated Work Environments, *American Industrial Hygiene Association Journal*, Vol.64, pp. 684-689
- Garner, M. & Beckett, S. (2005a). Modelling the spread of foot-and-mouth disease in Australia, *Australian Veterinary Journal*, Vol. 83, pp. 30-38
- Garner, M.G., Hess, G.D. & Yang, X. (2005b). An integrated modelling approach to assess the risk of wind-borne spread of foot-and-mouth disease virus from infected premises, *Environmental Modelling and Assessment*, Vol. 11, pp. 195-207
- Gloster, J., Blackall, R. M., Seller, R. F. & Donaldson A. I. (1981). Forecasting the airborne spread of foot-and-mouth disease, *Veterinary Record*, Vol. 108, pp. 370-374
- Gloster, J., Jones, A., Redington, A., Burgin, L., Sorensen, J., Turner, R., Dilon, M., Hullinger, P., Simpson, M., Astrup, P., Garner, G., Stewart, P., D'Amours, R., Sellers, R. & Paton D. (2010). Airborne spread of food-and-mouth disease - Model Intercomparison, *The Veterinary Journal*, Vol. 183, No.3, pp. 278-286
- Godoy, S. M., Santa Cruz, A. S. M. & Scenna, N.J. (2007). STRRAP SYSTEM - A Software for Hazardous Materials Risk Assessment and Safe Distances Calculation, *Reliability Engineering and System Safety*, Vol. 92, No. 7, pp. 847-857, ISSN: 0951-8320
- Godoy, S. M. (2010). *Cálculo del Riesgo Asociado a la Dispersión de Contaminantes en la Atmósfera Considerando Incertidumbre Estocástica* (1° Ed.), Universidad Tecnológica Nacional-Rectorado, ISBN 978-950-42-0132-8, Buenos Aires, Argentina
- Holmes, N. & Morawska, L. (2006). A review of dispersion modelling and its application to the dispersion of particles: An overview of different dispersion models available, *Atmospheric Environment*, Vol. 40, No. 30, pp. 5902-5928
- Jones, A. & Harrison A. (2007). *The Effects of Meteorological Factors on Atmospheric Bioaerosol Concentrations - A Review*, School of Geography, Earth and Environmental Science. The University of Birmingham Edgbaston, Birmingham B15 2TT
- Karra, S. & Katsivela, E. (2007). Microorganisms in bioaerosol emissions from wastewater treatment plants during summer at a Mediterranean site, *Water Research*, Vol. 41, pp. 1355-1365
- Kenline, P.A. & Scarpino, P.V. (1972). Bacterial air pollution from sewage treatment plants, *American Industrial Hygiene Association Journal*, Vol. 33, pp. 346-352
- Kitching, R.P., Hutber, A.M, Thrusfield, M.V. (2005). A review of foot-and-mouth disease with special consideration for the clinical and epidemiological factors relevant to predictive modelling of the disease, *The Veterinary Journal*, Vol. 169, N° 2, (March 2005), pp. 197-209
- Korzeniewska, E., Z. Filipkowskaa, A. Gotkowska-Płachtaa, W. Janczukowiczb, B. Dixonc & M. Czulowskaa. (2009). Determination of emitted airborne microorganisms from a BIO-PAK wastewater treatment plant, *Journal of Water Research*, Vol. 43, No. 11, pp. 2841-2851

- Lighthart, B. & Frisch A.S. (1976). Estimation of Viable Airborne Microbes Downwind from a Point Source, *Applied and Environmental Microbiology*, Vol. 31. N° 5, 700-704
- Lighthart, B. & Kirilenki A. (1998). Simulation of Summer-Timer Diurnal Bacterial Dynamics in the Atmospheric Surface Layer, *Atmospheric Environment*, Vol. 32. N° 14/15, pp. 2491-2496
- Lippmann, M. (2007). Health effects of airborne particulate matter, *The New England Journal of Medicine*, 357(23):2395-2397
- Mikkelsen, T., Alexandersen, S., Astrup, P., Donaldson, A.I., Dunkerley, F.N., Gloster, J., Champion, H., Sorensen, J.H. & Thykier-Nielsen, S. (2003). Investigation of airborne foot-and-mouth disease virus transmission during low wind conditions in the early phase of the UK 2001 epidemic, *Atmospheric Chemistry Physical Discussions*, Vol. 3, pp. 677-703
- Napolitano, P.J. & Rowe, D.R. (1966). Microbial content of air near sewage treatment plants, *Water Sewage Works*, Vol. 113, pp. 480 - 483
- NIOSH. 1994a. Preventing Organic Dust Toxic Syndrome. NIOSH Pub. No. 94-102, Cincinnati, OH
- Pascual, L., Perez-Luz, S., Adela Yanez, M., Santamaria, A., Gibert, K., Salgot, M., Apraiz, D. & Catalan, V. (2003). Bioaerosol emission from wastewater treatment plants, *Aerobiologia*, Vol. 19, pp. 261-270
- Pillai, S.D. & Ricke, S.C. (2002). Bioaerosols from municipal and animal wastes: background and contemporary issues, *Canadian Journal of Microbiology*, Vol. 48, pp. 681-696
- Ranalli, G., Principi, P. & Sorlini, C. (2000). Bacterial aerosol emission from wastewater treatment plants: culture methods and biomolecular tools, *Aerobiologia*, Vol. 16, pp. 39-46.
- Santos Burgoa, C., Rojas Bracho, L., Barrera Romero, N., Ongay Delhumeau, E. & Escamilla Cejudo, J. A. (1992). Método para Estimar el Riesgo Poblacional Atribuible a una Estación de Transferencia de Desechos Sólidos Municipales, *Salud Pública de México*, Vol. 34, N° 5
- Scenna N.J. & Santa Cruz A. (2005). Road Risk Analysis due to the Transportation of Chlorine in Rosario city, *Reliability Engineering and System Safety*, Vol. 90, pp. 83 - 90
- Sellers, R.F. & Parker, J. (1969). Airborne excretion of foot-and-mouth disease virus, *Journal of Hygiene*, Vol. 67, pp. 671-677
- Sorensen, J.H., Mackay, D.K.J, Jensen, C.O & Donaldson, A.L. (2000). An integrated model to predict the atmospheric spread of foot-and-mouth disease virus, *Epidemiology and Infection*, Vol. 124, pp. 577-590
- Swan, J., Kelsey, A. & Crook. B. (2003). Occupational and Environmental Exposure to Bioaerosols from Compost and Potential Health Effects - A Critical Review of Published Data, In: *Health and Safety Executive Books*, Research Report No. 130, Nortamptonshire, England.
- Thompson, D., Muriel, P., Russell, D., Osborne, P., Bromley, A., Rowland, M., Creigh-Tyte, S. & Brown, C. (2002). Economic costs of the foot-and-mouth disease outbreak in the United Kingdom in 2001, *Revue Scientifique et Technique de l'Office International des Epizooties*, Vol. 21, pp. 675-687
- U.S. EPA. Environmental Protection Agency. (2004). Air quality criteria for particulate matter. Washington, DC: EPA 600/P-99/002aF-bF
- Wickman, H. (1994). *Deposition, Adhesion, and Release of Bioaerosols*. *Atmospheric Microbial Aerosols*, B. Lighthart and A. Mohr, eds., Chapman and Hall Publishing Co., New York

Particle Dispersion Within a Deep Open Cast Coal Mine

Sumanth Chinthala and Mukesh Khare
*Indian Institute of Technology Delhi
India*

1. Introduction

Dust generation and its dispersion has been the major concern in ambient air quality in deep cavities such as open cast mines. Major mining activities in deep open pit coal mines range from exploration to the processing of end product that primarily contribute particulate matter (PM), dominantly PM_{10} leading to the problem of air pollution and related health hazards (Falk and Jurgelski, 1979; Pless-Mulloli et al, 2000). As a result, the simulation of dispersion characteristics within the deep open pit coal mines becomes essential to analyze the complex wind flow patterns that significantly affect the dispersion of PM_{10} . The dispersion equations developed within the deep pit boundary provide a reasonable accurate estimate of PM_{10} dispersion within the near field region of the deep open pit coal mines (Silvester et al, 2009). The fundamental equations of continuity and momentum describe the in pit dispersion mechanisms within the atmospheric boundary layer (ABL). In addition, the meteorological conditions within the deep open pit coal mine are significantly affected by temperature (stability) and roughness conditions which ultimately generate complex dispersion phenomenon including separation of atmospheric boundary layer, recirculation, resuspension and settling of PM_{10} (Bitkolov, 1969; Grainger and Merony, 1993). However, the in-field measurements of PM_{10} within the deep open pit coal mines are constrained by safety regulations, complex geometry of the pit, uncontrolled wind flows and different operation types that make it extremely difficult to carry out monitoring of the PM_{10} conventionally (Roy et al, 2011). Further, the simulation of dispersion characteristics using the fundamental governing equations may require modifications to incorporate the in pit microclimatic effects on the flow regimes (Markov et al, 1978; Aloyan et al, 1982). Therefore, it is essential to analyze and evaluate microclimatic parameters including the wind turbulence and shear in order to simulate the dispersion of PM_{10} (Turner, 1994). This chapter presents a comprehensive description of the dispersion mechanisms in the deep open pit coal mines considering the topographic, thermal and meteorological factors.

2. Dispersion mechanism in deep open pit coal mine

Dispersion mechanisms consist of *diffusion* and *advection* processes. The atmospheric motions *transport* and *diffuse* the pollutants that are released from sources. Richardson (1926)

has investigated the dispersion characteristics by using tracers. The fundamental scaling and power laws have been studied by Taylor (1921) and Roberts (1923). The temporal and spatial scales of motion serve to disperse pollutants in the atmosphere by mixing and thus lowering the ambient pollutant concentrations (Turner, 1994). Mikkelsen (2003) and Hanna et al (1982) have discussed various aspects of dispersion and associated parameters that are primarily influenced by source dimensions, buoyancy and momentum of the release, roughness and surrounding topography, atmospheric stability and large scale differential heating. In case of PM₁₀ its dispersion is additionally affected by inertial and dynamic forces acting on the particulates acting on them. Open cast coal mining involves various operations e.g overburden removal, drilling, blasting, mineral loading, haulage and unloading that generate particulates due to various mechanisms. It has been observed that out of total particulates generated, the PM₁₀ constitute one-third to half (Ghose & Majee, 2007; Trivedi et al, 2009). The operations and their contribution to the generation of the particulates have been listed in table 1.

Operation	% of particulates generated
Overburden removal	7%
Top soil removal	1%
Coal processing	72%
Coal extraction	3%
Wind erosion	17%

Table 1. Contribution of operations to the particulate generation (Ghose & Majee, 1998)

3. Flow dynamics in deep open pit coal mines

The flow in the deep pit coal mine is a special case of a deep cavity flow where shear stresses are dominant (Tani et al, 1961; Chang, 1970). It depends significantly upon the state of the boundary layer ahead of the cavity, pressure and forces due to the flow. Sometimes, vortices are formed in the cavities due to the deflection of part of the separated boundary layer. Cavities are generally classified according to their length to depth (L/D) and length to width (L/W) ratios, respectively. A cavity is deep, if $L/D < 1$; and shallow, if $L/D > 1$; two dimensional if $L/W < 1$; and three dimensional if $L/W > 1$ (Larcheveque et al, 2003). The cavity flows are further classified into *open type* ($L/D < 10$) and *closed type* ($L/D > 13$) according to the *aspect ratio*. In the closed type cavity, the shear layer generated at the leading edge collides with the cavity floor. The layer is reflected from the floor forming the expansion waves and the flow escapes the trailing edge. Therefore, two small separate zones are formed in the cavity. In the open type cavity, the free stream shear layer is reattached to the trailing edge and divides the flow into internal and external flow (Woo et al, 2008). Table 2 describes different types of cavities and their characteristics.

Sl no	Property /parameter	Shallow	Intermediate	Deep
1	Recompression layer	Not Investigated	Not Investigated	Decreases with increased L/D ratio
2	Boundary layer and its influence	Not Investigated	Not Investigated	Bridges the cavity and has little influence over the cavity flow parameters
3	Redevelopment length	Redevelopment is small	Redevelopment is maximum	Redevelopment is small
4	Variation of coefficient of pressure	Low	Maximum	Low
5	Boundary layer thickening	More	Less	More
6	Free shear layer flow	Less strongly distributed	More strongly distributed	Less strongly distributed
7	Drag Coefficient	High	Medium	Low
8	Flow type	unsteady	Not Investigated	Dead/laminar
9	Flow reattachment	Occurs on the floor of the cavity	Not Investigated	Occurs on the rear shoulder of the cavity
10	Reynolds number	Large	Medium	Small
11	Velocity	Large	Medium	Small
12	Skin friction	Large	Medium	Small
13	Base pressure	First decreases and then increases	Not Investigated	Constant in the middle and slightly irregular in the front and rear portions
14	Three dimensionality of shear layer flow	Slightly	Strongly	Slightly

Table 2. Types of cavities and their characteristics (Chowdhary, 1977)

3.1 The cavity regions

The cavity region contains different zones where the boundary layer undergoes various changes (Figure 1). The *Upstream zone* comprises the developing boundary layer zone which is upstream of the front corner of the notch with a finite approaching boundary layer. *Expansion zone* is a small zone just downstream of the separation corner where the pressure falls to the base pressure level. In this zone, the inner 10-15% of the approaching boundary layer adjusts rapidly to expansion at the separation corner and forms a new viscous sublayer slightly below the separation corner. *Mixing zone* is in the initial part of the free shear layer. The flow is similar to a separated jet type wake and lies between the isoenergetic free stream flow and the dividing stream line. This intermediate buffer zone acts as a coupling between the outer free stream flow and the inner dissipative flow and brings about the transport of mass and momentum from the former to the latter. The pressure is nearly constant in this zone. This region is associated with large velocity gradients and substantial viscous activity. After the constant pressure mixing region, the shear layer negotiates the pressure rise which continues up to the reattachment point where a part of the shear layer gets reversed and forms a recirculating cavity flow. The recirculating cavity flow lies between the separation point and the reattachment point, having a low Reynolds number and a constant static pressure. This zone is called as *compression zone*. This recirculating cavity flow has also been termed as separation wake. After the reattachment point, the shear layer negotiates the further pressure rise which continues upto the free stream value. This is called as the *recompression zone*. The flow in the ramp corner as well as in the recompression zone is assumed to be isentropic and invicid. Further, the recompression zone entrains an unsteady vertical flow, which is known as the *recompression wake*. After the recompression region the flow forms a new uniform stream with a *redeveloping zone* which becomes fully developed at some distance downstream. Various factors affecting the flow dynamics in the case of deep open pit coal mines have been discussed in subsequent sections.

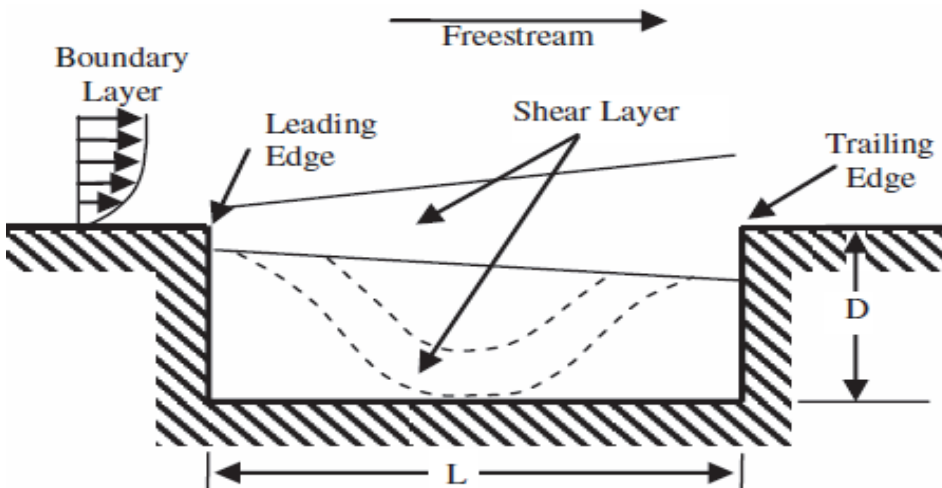


Fig. 1. Cavity flow field operating in open configuration (solid line) and closed configuration (dotted line). Source: Lazar et al, 2008

3.1.1 Topographic factors

The open pit coal mine topography is mostly rugged and uneven. In general, it is a few kilometers wide and more than 50 m deep. In the case of deep open pits, the depth may be as high as 300-400 meters. The complexity arises due to the presence of overburden dumps, construction of access roads and blasting activities. The topography affects the dispersion of pollutants due to changes in the mean flow (Castro & Apsley, 1997). It also affects the trajectory of the wind that channels and confine the plume dispersion and also causes flow re-circulations within the pit (Shi et al, 2000; Appleton et al, 2006).

3.1.1.1 Slopes & benches

Slopes facilitate an easy penetration of the wind because the shape of the pit guides the wind flow (Grainger & Merony, 1993; Peng & Lu, 1995). Besides, the slopes play a major role in the reduction of the size of the primary eddies (Mcquain et al, 1994). The presence of slopes also result in increase in the wind speed (Figure 2). Additionally, the faces and elevation of the benches cause the local deflection of the plume affecting the direction of the dispersion (Figure 3). Moreover, the presence of corners enable the particulate matter to get confined to a particular region within the deep open pit till they reach a particular height where the effect of topography gets diminished and plume expansion is observed. This is called the *venturi effect* (Appleton et al, 2006). The sloping terrain may result in *katabatic* and *anabatic* flows (i.e drainage of air down or uphill sides in response to changing vertical temperature profiles). Further, the terrain elevation may either restrict or exacerbate aerial dispersion when the lower boundary layer heights confine the particulate plume closer to the terrain surface.

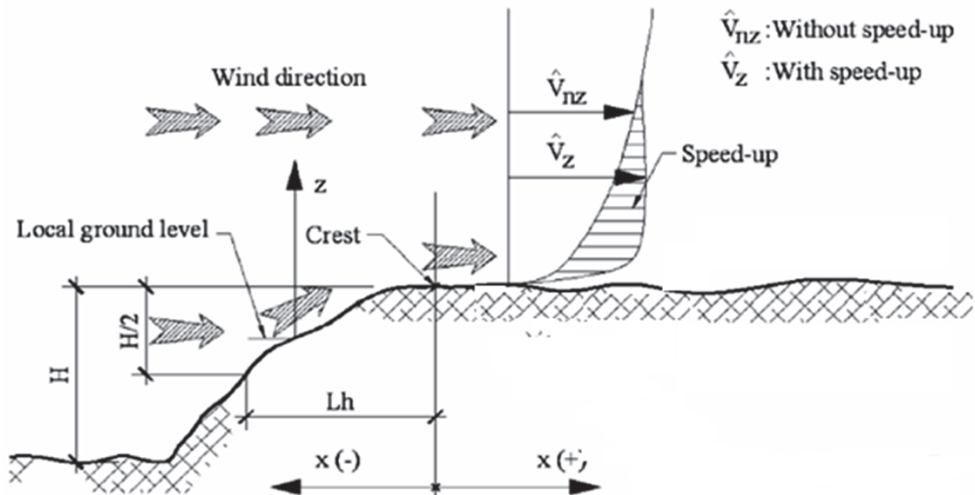


Fig. 2. Wind speed due to the presence of slopes (Ngo and Lechford, 2008)

3.1.1.2 The depth of the open pit coal mine

When the depth of a mining pit is increased, an open air space with characteristic properties under extreme physical conditions is created (Baklonov, 1986). Under such conditions, the

depth of the open pit affects the penetration angle α , which is defined as the angle of the shear interface line defining the boundary between the penetration of the external ABL velocity profile and the induced leeward in pit recirculation zone (Figure 4). Further, the depth has a significant effect on the air flow patterns within the mine. In case of shallow pits, air flow expands gradually, without any gap in mine area. There is a little compression of flow line on outlet area due-to action of flow inertia. In case of medium depth mines, fluid vortex has shape of flattened ellipse whose height and width differ significantly.

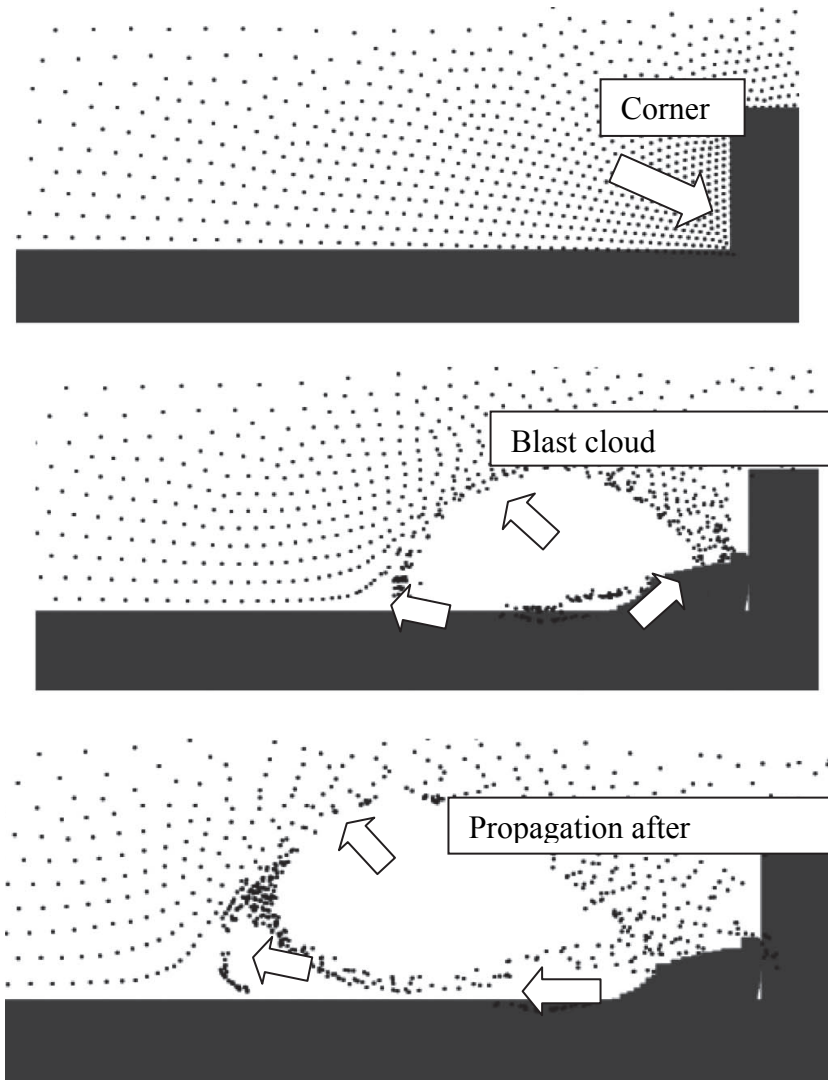


Fig. 3. Effect of local deflection on the dispersion of particulate plume (Appleton et al, 2006)

The viscous forces, pressure gradients and turbulence friction act as driving mechanisms (Figure 5). Close to leeward side, there is detached point area of thickened boundary layer. In windward side zone, there is flow connection point zone, near which part of flow turns back in detached vortex zone and part moves up and toward exit from zone (Markov et al, 1978). Moreover, for the same incoming airflow and the same slope angle, the mechanical forcing and turbulence increase with increase in the depth, which will result in or strengthen the reverse airflow and the recirculation (Shi et al, 2000).

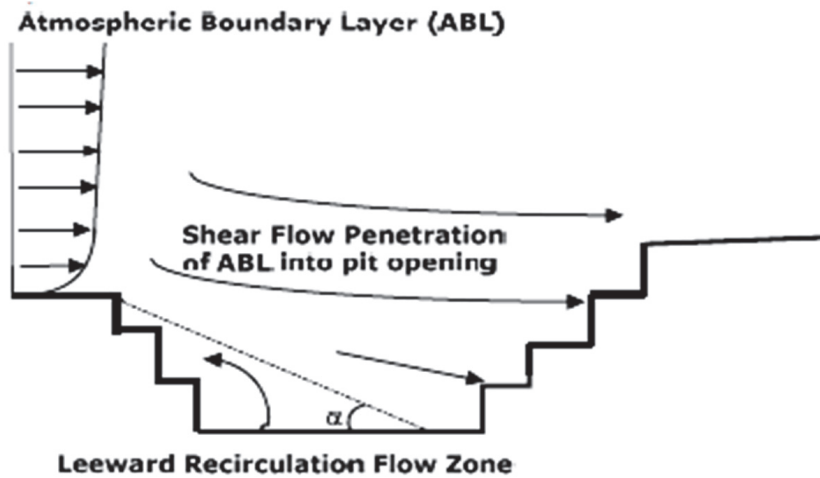


Fig. 4. Penetration angle α in deep open pit mines (Peng and Lu, 1995)

3.1.1.3 Width and breadth of deep open pit coal mine

The width and breadth of the coal mine affects the rate of cooling in the mine, which is defined in terms of terrain *amplification factor* (*TAF*) (Equation 1).

$$TAF = 3W_1B_1 / [W_1B_1 + W_2B_2 + (W_1B_1W_2B_2)^{1/2}] \quad (1)$$

where W_1 , width of the mine at the top,
 B_1 , breadth of the mine at the top,
 W_2 , width of the mine at the bottom and
 B_2 , breadth of the mine at the bottom.

3.1.1.4 Aspect ratio

The *aspect ratio* decides whether the air outside the pit intrudes into the pit or not. Recirculation zones are formed based on the aspect ratio of the pit (Figure 6). The formation of the secondary vortex has been observed as the aspect ratio increases. It is due to the fact that the penetration of the external boundary layer in to the cavity acts as a driving force for the formation of the secondary vortex.

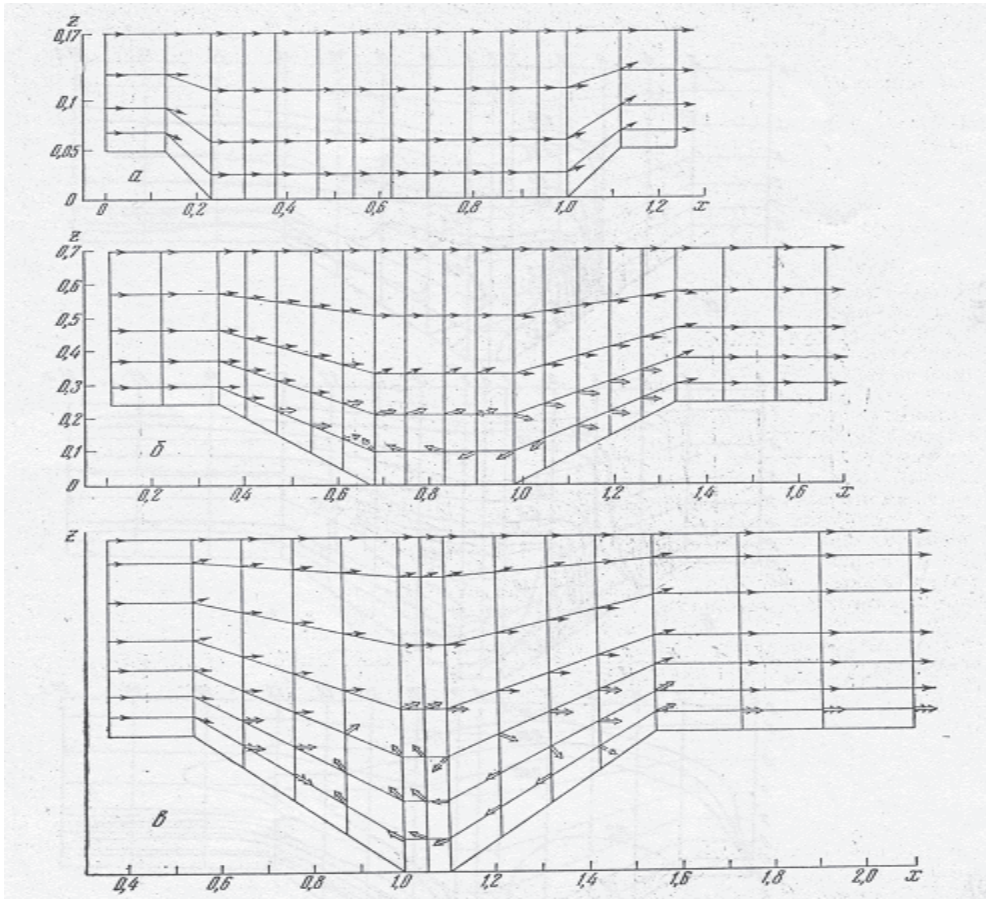


Fig. 5. Vector fields of speed of steady-state flow processes in the deep open pit mines (Markov et al, 1978).

3.1.1.5 Effect of overburden dumps

Baklonov and Regina (1998) has investigated the effect of overburden dumps on dispersion and observed that the velocity increases as the wind passes through the dump from bottom to the top. Further, if the dump is located at the upwind side, it alters the wind flow and turbulence characteristics from those measured at the nearest meteorological station. The rough terrain changes the wind speed directions and turbulence characteristics and enhance mixing in the air stream (Kirchgessner et al, 1993). Huertas (2009) has observed the effect of deposition by altering the area of dumps which shows that the retention of particulates is dependent on the volume and the area of the overburden.

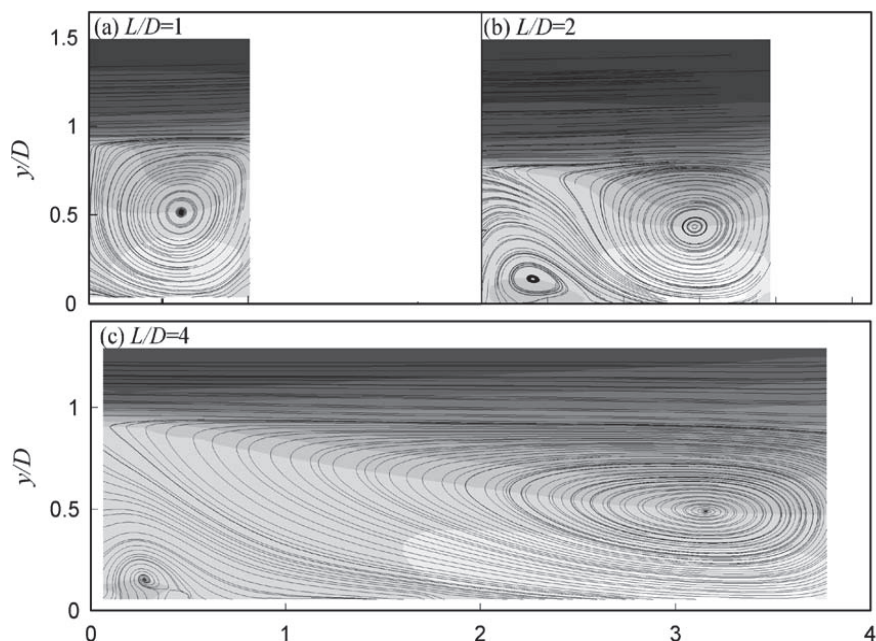


Fig. 6. Effect of aspect ratio on the flow (Kang & Sung, 2009)

3.1.2 Meteorological effects

3.1.2.1 Wind speed & direction

It is observed that the wind speed is positively correlated and reduced to three fourth after entering into the pit (USEPA, 1985). The higher wind speeds attribute to the lesser deposition fluxes and lesser concentrations of particulates due to the elongation of the particle plumes generated inside the pit. Further, higher wind speeds cause an elongation of particulate plume and a reduction in the airborne concentration and deposition flux gradients observed near source (Appleton et al, 2006). The wind direction inside and outside the pit are not positively co- related. The wind direction displaces the air to a particular direction, thus causing thermal inhomogeneities within the open pit mine. The standard deviations of vertical and horizontal wind directions enable the prediction of the deviation of the wind from its original direction. It has been found that the wind direction changes by an angle of 60° with respect to the direction at the surface (USEPA, 1985).

3.1.2.2 Stability

The stability affects the flow in the mine by influencing the vertical motion. It is observed that stable atmosphere suppresses the vertical motion of the pollutants resulting into deposition of pollutants. However, for unstable and neutral conditions, the escape fraction of the particulates has been found to be more. Under the effect of stratification, the flows in a pit are expected to be similar to the night time flows occurring in the mountains due to the accumulation of cold air and nocturnal cooling (Grainger & Merony, 1993). Further, the inversion depth and strength tend to be stronger than those found over valleys or flat terrain

(Maki et al, 1986). Grainger & Merony (1993) have observed that inversion effects are more predominant in pits rather than on flat terrains. The occurrence of the inversion in the pit depends upon the Froude number (Fr), which is independent of the pit geometry. Further, it has been found that the coal pit dispersion under stably-stratified conditions is dominated by the buoyancy-inertia forces (Equation 2).

$$Fr = U_h \left[\frac{gh(\theta_h - \theta_0)}{\theta} \right]^{-1/2} \quad (2)$$

where,

θ_h , is the air temperature at the ridge top

θ_0 , is the air temperature at the valley floor

If $Fr > 1.6$, then inversion is swept away;

If $1.3 < Fr < 1.6$, the air in the basin is coupled to the air above the basin;

and if $Fr < 1.3$, the air is totally decoupled

Further, the dispersion is dependent on the pasquill stability classes (Table 3).

Stability class	Effects on dispersion in the coal mines
A	(2), (3), (4)
B	(2), (3), (4)
C	(2), (4)
D	(2)
E	(1), (2), (3), (5)
F	(1), (3), (5)
G	(1), (3), (5)

Table 3. Factors affecting dispersion for different stability classes

Where,

1. Aids dispersion if terrain is flat and restricts dispersion if the terrain is rising
2. Impact by particulate deposition
3. Impact by airborne particulates
4. Higher values of Surface heat flux aids dispersion due to the generation of upward air currents
5. Lower values of surface heat flux restricts aerial dispersion

3.1.3 Thermal effects

The combined action of the mechanical shear of the ABL across the surface opening and the thermal buoyancy forces produce the air flow by the differential heating in the pit surface (Silvester et al, 2009). Solar energy controls the physical processes of the atmosphere through the mediation of the surface. Open pit mining modifies the ground surface material composition, structure, cover, morphology, colour which affects the meteorological processes and also affects the partitioning of the incoming solar radiation into sensible and latent heat fluxes which affects the amount of solar radiation that is scattered back to the space. The airspace of a mine pit tends to warm up rapidly when insolation is intense, while

cold air tends to accumulate in it when insolation is low or missing (Loska, 2007). More over the solar radiation has different effects during different seasons, which affects the total amount of air heated in the open pit mine (Figure 7). Further, the solar radiation influences many physical processes. The physical processes and their interactions form chains of interactions, which are highly dependent on the type of the terrains and surrounding conditions, like radiation (Figure 8).

3.1.3.1 Thermal inhomogenities

Due to the combined effect of nonuniform horizontal temperature field and the wind direction, thermal inhomogenities are created in the deep open pit. With an active influx of solar radiation, the effect of thermal forces is manifested not only as the component of the resulting wind velocity, but also affects the stability within the deep open pit. The inhomogenities can be classified into four types

1. With increasing depth, the air temperature rises by a value greater than the adiabatic temperature gradient
2. The air temperature increases with depth
3. The air temperature remains constant with depth
4. The air temperature decreases with depth

Thus two main types of stratification exist within the deep open pit space: unstable (1st type) and stable (2nd, 3rd, and 4th types), which may be present in single form or as combinations (Bitkolov, 1969).

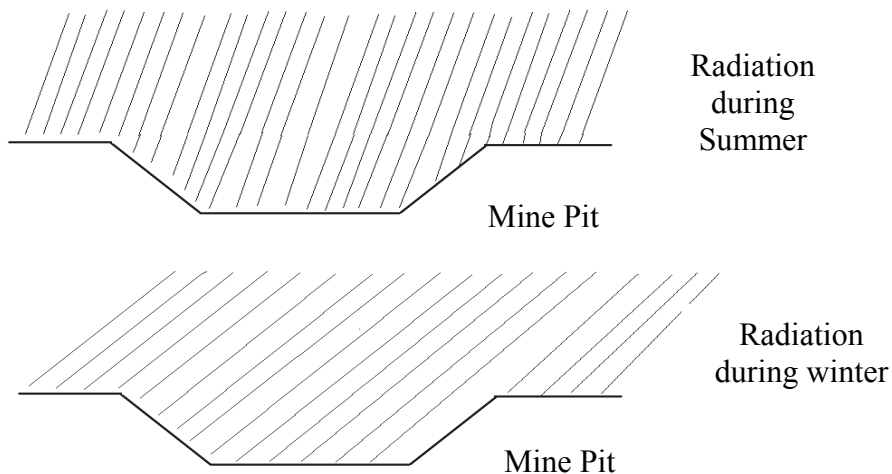


Fig. 7. Effect of solar radiation during winter and summer in the mine pit

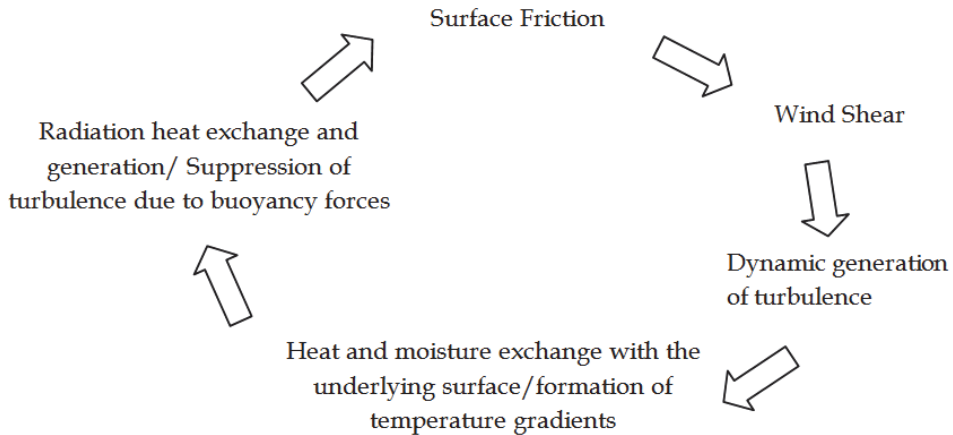


Fig. 8. Chains of interactions of physical processes (Zilitinkevich, 1990)

4. Modelling the flow in open pit coal mines

Dispersion uses mathematical equations describing the atmosphere along with chemical and physical processes to estimate and predict concentrations at various locations. Dispersion models for predicting particulate concentrations have been discussed by Mikkelsen (2003), Reed (2005) and Holmes & Morwska (2006). The conventional models of dispersion for the plane terrain retain flow stationarity and horizontal uniformity hypothesis. As a result, they are no longer valid when the open pit terrain complexity produces mesoscale and local scale circulations. Most of the conventional models employ the hydrostatic approximation which neglects the vertical acceleration versus the pressure gradient and the gravitational terms. This implies that the vertical scale of motion is smaller than the horizontal scale. This applicability of the hydrostatic approximation depends not only on the geometry of the wind, but also on the vertical stability. Hence the non-hydrostatic multiscale approach is preferred. Penenko & Aloyan (1976) have proposed a three-dimensional non stationary model for mesoscale boundary layer of atmosphere. The model includes the effects of horizontal gradients of potential temperatures, stratification parameters and vertical and horizontal turbulence factors. Later, a two dimensional model has been proposed by improving this model to allow considering substantial two-dimensional effects of flow in the deep open pit coal mines having complex geometry (Markov et al, 1978). Further, Aloyan et al (1982) have used a fictitious region method in which the equations are generated in a rectangular cartesian coordinate system. The model has helped in simulation of the winds in a quarry under various thermal conditions (stable, unstable and equilibrium stratifications) and investigating the effects of the external wind on the temperature inversion. The model describes the flow in deep open pit coal mines and helps analyzing influence of their geometric parameters by detailed consideration of characteristics of impurity sources. Later, these mathematical models describing the dynamics of the atmosphere in the deep open pits have been combined with the system for calculating the thermal and radiational balance on the surface (Baklonov, 1984). Baklonov (1986) has also

established a thermodynamic model for the deep open pit ventilation systems. The model simulates the diurnal changes that take place during the differential solar heating of the surface during the day and the release of this energy during the evening. Further, Baklanov (1995) has presented the results of a series of numerical modeling case studies that consider the pollutant dispersion within naturally ventilated deep open pits, for a range of different external wind speeds and directions, internal thermal stratifications, recirculation flow regimes and the interaction of local open pit thermal circulations with the external atmospheric flow field. In a later study, a high-resolution, non-hydrostatic and three dimensional PBL model for characterizing the flow in the open mine has been developed by Shi et al (2000). The classical 2-D Navier-Stokes equation and a 0-D bond-graph model have been used to investigate the flow dynamics of the mines by discussing the interconnections, nonlinearities and turbulence. The 0-D model efficiently provides for a fast and representative global model for the mine ventilation problem (Witrant et al, 2008). Table 4 summarizes the various studies conducted on open pit mines.

4.1 The model and its features

The governing equations which serve the basis of modeling the deep open pit mines have been described (Markov et al, 1978). Equations 3-6 include non stationary hydrodynamic equations of Navier-Stokes, continuity equation for incompressible fluid and equation for carryover of impurity concentration in plane cartesian system of coordinates.

$$\frac{\partial u}{\partial x} + \frac{\partial w}{\partial z} = 0 \quad (3)$$

$$\frac{\partial u}{\partial t} + u \frac{\partial u}{\partial x} + w \frac{\partial u}{\partial z} = -\frac{\partial p}{\partial x} + \frac{1}{Re_r} \left[\frac{\partial}{\partial x} \left(k \frac{\partial u}{\partial x} \right) + \frac{\partial}{\partial z} \left(k \frac{\partial u}{\partial z} \right) \right] \quad (4)$$

$$\frac{\partial w}{\partial t} + u \frac{\partial w}{\partial x} + w \frac{\partial w}{\partial z} = -\frac{\partial p}{\partial z} + \frac{1}{Re_r} \left[\frac{\partial}{\partial x} \left(k \frac{\partial w}{\partial x} \right) + \frac{\partial}{\partial z} \left(k \frac{\partial w}{\partial z} \right) \right] \quad (5)$$

$$\frac{\partial c}{\partial t} + u \frac{\partial c}{\partial x} + w \frac{\partial c}{\partial z} = \frac{1}{Pr_d Re_r} \left[\frac{\partial}{\partial x} \left(k \frac{\partial c}{\partial x} \right) + \frac{\partial}{\partial z} \left(k \frac{\partial c}{\partial z} \right) \right] \quad (6)$$

where,

u, w - projection of velocity vectors on horizontal and vertical directions (m/sec);

p - deviation of pressure from hydrostatic (Kpa);

c - specific volumetric concentration of impurities (g/m^3);

k - turbulent kinematic viscosity factor ($kg/m/s$);

L_B - characteristic longitudinal dimension of upper section of the mine(m);

$Re_T = L_B u_\infty / k_\infty$, Reynold's turbulence number;

$Pr_d = k/k_e$, Prandtl's diffusion number, which characterizes ratio between turbulence viscosity factor k and diffusion factor k_e .

For the values $L_B/u_\infty, u_\infty, \rho_\infty u_\infty^2$ and k_∞ , the subscript ∞ characterizes the parameters of incident flow.

This model overcomes the limitations of the single dimensional models, which does not allow considering substantial two-dimensional effects of flow in open pit coal mines having

complex geometry of surface. This approach helps in solving wide range of problems concerning natural air exchange. The model describes dispersion in deep open coal mines and helps analyzing influence of their geometric parameters on natural air exchange, by considering pollutant characteristics. Thus, the model with sufficient practical accuracy describes the natural ventilation process and can be useful for calculation of flows in deep open pit coal mines.

4.2 The model limitations

The present model has no provision for considering the effects of settling of the particles. Moreover, it does not consider: stability (temperature effect)/ buoyancy effects that govern the dispersion of PM within the mine boundary. The model can be modified to incorporate the effects of the buoyancy interms of the temperature difference (Equation 5). Due to the temperature difference existing between the two vertical layers of the atmosphere within the mine, the buoyant force may rise the particle vertically (Grainger & Merony, 1993). Moreover, the temperature equation (Equation 6) can be modified to incorporate the effect of the vertical temperature gradient and the existing temperature gradient. These limitations are presently being addressed as Ph.D problem in Civil Engineering Department at IIT Delhi (Chinthala, 2010).

AQ model/ Technique	Type	Reference
3-D Non Hydrostatic Model	Numerical	Gresho et al (1976)
Non Stationary N-S model	Numerical	Markov et al (1978)
3-D Non Stationary Model	Numerical	Aloyan et al (1982)
Cole and Fabrick	Box model	Cole & Fabrick (1984)
2-D Hydrostatic Model	Numerical	Herwehe (1984)
ISC3	Gaussian	USEPA(1995c)
Wind Tunnel	Physical	Peng & Lu (1995)
K-ε hydrodynamic model	Numerical	Fomin (1996)
Wind Tunnel	Physical	Shi et al (2000)
Wind Tunnel	Physical	Grainger & Merony (2003)
Fabrick	Gaussian	Reed (2005)
Gelekin	Gaussian	Reed (2005)
Herwere	Eulerian	Reed (2005)
Kalgoorlie	Unknown	Reed (2005)
PerieraSoares&Branquinho	Gaussian	Reed (2005)
Winges	Gaussian	Reed (2005)
2-D Non Hydrostatic model	Numerical	Kharytonov et al (2005)
ADMS	Gaussian	Appleton et al (2006)
RANS	Numerical	Bodnor et al (2008)
CFD	Numerical	Silvester et al (2009)
k-ε model	Numerical	Kakosimos et al (2011)

Table 4. Modelling studies on open pit mines

5. Conclusions

Simulating the dispersion in deep open pit coal mines is an effective tool to give advanced warning of potential emission problems and providing the basis for future planning applications. The meteorological conditions within an open pit coal mine are significantly affected by temperature (stability) and roughness conditions that generate complex fluid flows phenomenon e.g. separation of atmospheric boundary layer, recirculation, resuspension and settling of particulates. The complex geometry, uncontrolled wind flows and different operations taken place within the deep open pit coal mines, makes it extremely difficult to measure the particulates. Therefore, an appropriate mathematical model is needed which may predict the complex processes in the near field regions of the deep open pit coal mines effectively. The fundamental understanding of the microclimate that is created in the deep open pit mine due to influence of the external ABL and the contributions of the mechanical and thermal forces present, can be achieved by developing a dynamic numerical based inverse hill model to investigate the complex wind flows and dispersion mechanisms.

6. References

- Aloyan, A.E., Baklonov, A.A., and Penenko, V.V. (1982). Application of fictitious domain method in numerical simulation problems of open cast mine ventilation, *Meteorologiya i gidrologiya*, Vol., 7, pp. 42-49.
- Appleton, T., Kingman, S., Lowndes, I., and Silvester, S. (2006). The development of a strategy for the simulation of fugitive dust emissions from in-pit quarrying activities: a UK case study, *International Journal of Mining, Reclamation and Environment*, Vol., 20 (1), pp. 57-82.
- Baklanov, A.A. (1984). A Method For Evaluating The Energy Characteristics Of The Air In An Open Pit Mine, *Fiziko-Tekhnicheskie Problemy Razrabotki Poleznykh Iskopaemykh*, No. 1, pp. 73-78.
- Baklonov, A. (1986). A method for evaluating the energy characteristics of the air in an open pit mine, *Journal of Mining Science*, 22,1, pp.66-70.
- Baklanov, A. (1995). Numerical of atmosphere processes in mountain cirques and open pits, *Proceedings of International Conference on Air Pollution*, pp. 231-238, Greece, Porto Carras.
- Baklonov, A. and Rigina, O. (1998). Environmental of dusting from the mining and concentration sites in the kola peninsula, North west Russia, Proceedings in IUAPPA-NACA, Vol 1, 4F-3, The XI world clear air and environment congress, South Africa, 14-18 september, 1998, Durban.
- Bitkolov, N.Z (1969). Wind and Temperature of quarry atmospheres. *Fiziko-Tekhnicheskie Problemy Razrabotki Poleznykh Iskopaemykh*, No. 5, September-October, pp. 66-73.
- Bodnor, T., Benes, L. and Kozel, K. (2008). Numerical simulation of flow and pollution dispersion in the area of opencast coal mine, *American Institute of Physics, Conference Proceedings*, 1048, pp.100-103.
- Castro, I.P and Apsley, D.D. (1997). Flow and dispersion over topography: A comparison between numerical and laboratory data for two dimensional flows, *Atmospheric Environment*, Vol., 31, 6, pp. 839-850.
- Chang, P.K. (1970). Separation of flow, Pergamon Press, Oxford, London.

- Chinthala, S. (2010). Near field Simulation of PM₁₀ Dispersion in deep open pit coal mines. *Unpublished report*, IIT Delhi.
- Chowdhary, K.K. (1977). An experimental and theoretical investigation of turbulent seperated reattached and redeveloped flows with transverse rectangular cavities. Phd thesis, Indian Institute of Technology Delhi, New Delhi.
- Cole, C., and Fabrick, A. (1984). Surface mine pit retention. *Journal of the Air Pollution Control Association*, Vol., 34, 6, pp.674-675.
- Fomin, A.A. (1996). Modeling of a natural convection in an open pit, *Izvestiya Rossiiskoi Akademii Nauk, Mekhanika Zhidkosti i Gaza*, Vol., 4, pp.12-20.
- Falk, L.H and Jurgelski, W. Jr (1979). Health effects of coal miing and combustion: Carcinogens and cofactors. *Environmental Health Perspective*, 33, pp 203-226.
- Ghose, M. K. and Majee, S. R. (1998). Assessment of dust generation due to opencast coal mining - an Indian case study, *Environmental Monitoring and. Assesment. Vol.*, 61, pp.255-263.
- Ghose, M.K., and Majee, S.R. (2007). Characteristics of Hazardous Airborne Dust Around an Indian Surface Coal Mining Area, *Environmental Monitoring and Assessment*, Vol., 130, pp.17-25.
- Grainger, C. and Meroney, R.N. (1993). Dispersion in an open-cut coal mine in stably stratified flow. *Boundary-Layer Meteorology*, Vol., 63, pp.117-140.
- Gresho, P.M., Lee, R.L. and Sani, R.L. (1976). Modelling the planetary boundary layer using the galerkin finite element model, Third Symposium on Atmospheric turbulence diffusion and Air quality, Raleigh, NC, October 26-29, 1976.
- Hanna, S. R., Briggs, G.A., and Hosker, R. F. (1982). Handbook on Atmospheric Diffusion Technical Information Center, U.S. Department of Energy DOE/TIC 11223.
- Herwehe, J.A. (1984). Numerical Modelling of Turbulent Difussion of fugitive dust from an idealized open pit mine, Masters thesis, Iowa state university, Ames, Iowa.
- Holmes, N.S. and Morawska, L. (2006). A review of dispersion and its application to the dispersion of particles: An overview of different dispersion models available, *Atmospheric Environment*, Vol., 40, pp.5902-5928.
- Huertas (2009). Dispersion and deposition of particulate material in areas open pit mining using CFD. *Eighth National Congress of Science and Technology of Coal and Alternative Fuels*, November 12-13.
- Kakosimos, K.E., Assael, M.J., Lioumbas, JS and Spiridis, A.S (2011). Atmospheric dispersion of the Zugitive particulate matter from overburden dumps with numerical and integral models, *Atmospheric Pollution Research*, Vol., 2, pp.24-33.
- Kang, W and Sung, H.J. (2009). Large scale structures of turbulent flows over an open cavity, *Journal of Fluids and Structures*, Vol., 25, pp.1318-1333.
- Kharytonov, M., Zberovsky, A., Drizhenko, A. and Babiy, A. (2005). Air pollution assessment inside and around iron ore quarries, in I. Farago et al. (eds.), *Advances in Air Pollution Modeling for Environmental Security*, pp.263-274.
- Kirchgessner, D.A., Piccot, S.D and Chadha, A. (1993). Estimation of methane emissions from a surface coal mine using open-path FTIR spectroscopy and modeling techniques, *Chemosphere*, Vol., 26, 1-4, pp.23-44.
- Larcheveque, L., Sagaut, P., Mary, I., Labbe, O and Comte, P. (2003). Large-eddy simulation of a compressible flow past a deep cavity, *Physics of Fluids*, Vol., 15, 1, pp.193-210.

- Lazar, E., Elliott, G., and Glumac, N. (2008). Control of the shear layer above a supersonic cavity using energy deposition, *AIAA Journal*, Vol., 46, pp. 2987-2997.
- Loska, G. (2007). Variations in microclimate modified by open-cast mining: case studies from Hungary, *Gogr.Fis. Dinan.Quat*, Vol., 30, pp 215-218.
- Markov, V.A., Potashnik, E.L. and Rivkind, V.Y. (1978). Two dimensional mathematical model of natural ventilation processes in opencast mines, *Atmosphere and Ocean physics*, Vol., 14-5.
- Mcquain, W.D., Calvin, I., Ribbens, I.C., Wang, Y and Watson, L.T. (1994). Steady viscous flow in a trapezoidal cavity, *Computers Fluid*, Vol., 23, No. 4, pp. 613-626.
- Mikkelsen, T. (2003). Dispersion of pollutant in the atmosphere, *Position paper*, Atmospheric physics division, Denmark.
- Merony, R.N. and Grainger, C. (1992). Night time flow and dispersion over large basins or mining pits, symposium on measurement and modeling of environmental flows, *ASME winter annual meeting*, Anaheim, California, November, pp. 8-13.
- Maki, M., Harimaya, T and Kikuchi, K. (1986). Heat budget studies on nocturnal cooling in a basin, *Journal of Meteorological society of Japan*, 64, 5, 727-740.
- Ngo, T and Letchford, C. (2008). A Comparison of topographic effects on gust wind speed. *Journal of Wind Engineering and Industrial Aerodynamics*, 96, pp. 2273-2293.
- Penenko, V.V. and Aloyan, A.E. (1976). Numeric method for calculating fields of meteorological elements in atmosphere boundary layer, *Meteorology and Hydrology*, 6, pp.11-26.
- Peng, X. and Lu, G. (1995). Physical of natural wind and its guide in a large open pit, *Journal of Wind Engineering and Industrial Aerodynamics*, 54/55, pp. 473-481.
- Reed, W. (2005) Significant Dust Dispersion Models for Mining Operations, Tech.Rep. IC 9478. NIOSH, Pittsburgh, PA, USA.
- Richardson, L.F. (1926). Atmospheric diffusion shown on a distance neighbour graph, *Proc. R. Soc. Lond., Ser. A*, 110, pp. 709-737.
- Roberts, O.F.T. (1923). The theoretical scattering of smoke in a turbulent atmosphere, *Proc. R. Soc. (A)*, 104, pp. 640-654.
- Roy, S., Adhikari, G.R., Renaldy, T.A and Jha, A.K. (2011). Development of multiple regression and neural network models for assessment of blasting dust at a large surface coal mine. *Journal of Environmental science and Technology*, 4(3), pp 284-301.
- Shi, Y., Feng, X., Wei, F., and Jiang, W., (2000). Three-dimensional non-hydrostatic numerical simulation for the PBL of an open-pit mine, *Boundary-Layer Meteorology*, 94, pp. 197-224.
- Silvester, S.A., Lowndes, I.S., Hargreaves, D. M. (2009). A computational study of particulate emissions from an open pit quarry under neutral atmospheric conditions, *Atmospheric Environment*, Volume 43, Issue 40, December 2009, pp. 6415-6424.
- Taylor, G.I. (1921). Diffusion by continuous movements, *London Mathematical Society*, 20, pp.196-211.
- Trivedi, R., Chakraborty, M. K., and Tewary, B. K., (2009). Dust deposition using fugitive dust model at an opencast coal project of western coalfields limited, India, *Journal of Scientific and Industrial Research*, Vol., 68, pp.71-78.
- Turner D. B. (1994). Workbook of atmospheric dispersion estimates. li.S. Environmental Protection Agency, AP-26, Warren Spring Laboratory, National survey of smoke and sulphur dioxide, Instruction manual.

- USEPA (1976). Evaluation of Fugitive dust emission from mining, 68-02-1321.
- USEPA (1980). The Environmental Impact of Coal Transfer and Terminal Operations, 600/S7-80-169.
- USEPA (1985). Dispersion of Airborne particulates in surface mines, 450/4-85-001.
- USEPA (1995c). User's guide for the industrial source complex (ISC3) dispersion models. Vol. II. Description of model algorithms. Research Triangle Park, NC: U.S. Environmental Protection Agency, Office of Air Quality Planning and Standards, Emissions, Monitoring, and Analysis Division, EPA publication No. EPA-454/B-95-003b.
- Witrant, E., Johansson, K. and the HynX team, (2008). Air flow in deep wells: Application to mining ventilation, *IEEE Conference on Automation Science and Engineering (CASE)*, USA, August 23-26, Washington DC.

Part 2

Air Pollution Models and Application

Mathematical Modeling of Air Pollutants: An Application to Indian Urban City

P. Goyal and Anikender Kumar
*Centre for Atmospheric Sciences,
Indian Institute of Technology Delhi
India*

1. Introduction

Continuous development and increase of population in the urban areas, a series of problems related to environment such as deforestation, release of toxic materials, solid waste disposals, air pollution and many more, have attracted attention much greater than ever before. The problem of air pollution in cities has become so severe that there is a need for timely information about changes in the pollution level. The air pollution dispersion is a complex problem. It covers the pollutant transport and diffusion in the atmosphere. The pollutant dispersion in the atmosphere depends on pollutant features, meteorological, emission and terrain conditions. Physical and mathematical models are developed to describe the air pollution dispersion. Physical models are small scale representations of the atmospheric flow carried out in wind tunnels. Mathematical models are divided in to statistical and deterministic models. Statistical models are based on analysis of past monitoring air quality data. Deterministic models are based on a mathematical description of physical and chemical processes taking place in the atmosphere. These models are based on mathematical equations, express conservation laws of mass, momentum and energy. Both the models are discussed in this chapter.

Statistical models are also divided into linear and non-linear models. Several studies based on the statistical models have been carried out in different regions to identify local meteorological conditions, most strongly associated with air pollutants concentration to forecast the air quality (McCollister & Willson, 1975; Aron & Aron, 1978; Lin, 1982; Aron, 1984; Katsoulis, 1988; Robeson & Steyn, 1990). Many of the previous studies (Sanchez et. al., 1990; Mantis et al., 1992; Milionis & Davies, 1994) analyzed the meteorological conditions associated with high pollutant concentration. These studies usually produced qualitative or semi quantitative results and shed light on the relation between the meteorological conditions and pollutant concentrations. Shi & Harrison, 1997 developed a linear regression model for the prediction of NO_x and NO_2 in London. A linear regression model was used by Cogliani, 2001 for air pollution forecast in cities by an air pollution index highly correlated with meteorological variables. Since the relation between air pollutants and meteorological variables is not linear, some non-linear models i.e., Neural Network can also be used to forecast the pollutant concentrations (Bozner et al., 1993; Comrie, 1997).

The deterministic models are divided in to Eulerian, Lagrangian and Gaussian models. In this chapter we discuss only the Eulerian analytical models. The atmospheric diffusion

equation (Seinfeld, 1986) has long been used to describe the dispersion of airborne pollutants in a turbulent atmosphere. The use of analytical solutions of this equation was the first and remains the convenient way for modeling the air pollution problems (Demuth, 1978). Air dispersion models based on analytical solutions possess several advantages over numerical models as all the influencing parameters are explicitly expressed in a mathematically closed form. Analytical models are also useful in examining the accuracy and performance of numerical models. In practice, most of the estimates of dispersion are based on the Gaussian plume model, which assumes the constant wind speed and turbulent eddies with height. Hinrichsen (1986) compared a non-Gaussian model, in which wind speed and turbulence, are not constant with height and observed that non-Gaussian model agreed better than Gaussian model with the observed data.

Several efforts have also been made for the development of non-Gaussian models of point and line sources, since observational studies show that the wind speed and eddy diffusivity vary with vertical height above the ground (Stull, 1988). Analytical solutions of the advection diffusion equation, with wind speed and vertical eddy diffusivity both as power function of vertical height, bounded by Atmospheric Boundary Layer (ABL) are well known for point and line sources (Seinfeld, 1986; Lin & Hildemann, 1996). Taylor's (1921) analysis and statistical theory suggest that the eddy diffusivity depends on the downwind distance from the source (Arya, 1995). The advection diffusion equation has also solved analytically with wind speed as function of height and eddy diffusivity as a function of downwind distance from the source (Sharan & Modani, 2006). Thus in general, the eddy diffusivity should be a function of both vertical as well as downwind distance (Mooney & Wilson, 1993). Recently (Sharan & Kumar, 2009) formulate the advection diffusion equation considering the wind speed as a function of vertical height and eddy diffusivity as a function of both vertical height and downwind distance applicable only for point source release in reflecting boundary condition. However, Dirichlet (total absorption), Neumann (total reflection) and mixed boundary conditions are also appropriate for calculating the actual ground-level concentration of air pollutants. In addition to these, the few studies have been made for analytical solution of the advection diffusion equation for area sources. Park & Baik (2008) have solved the advection diffusion equation analytically for finite area source with wind speed and vertical eddy diffusivity as power function of vertical height in unbounded region

The objective of this chapter is to formulate and use the statistical (linear and non-linear) and Eulerian analytical models for prediction/forecast of air pollutants released from point, line and area sources. The analytical models are developed by using four different set of boundary conditions. The model with reflecting boundary condition is used for urban city Delhi, the capital of India and is validated by the observed values of concentration of Respirable Suspended Particulate Matter (RSPM).

2. Mathematical models

2.1 Statistical models

The main role of statistical models is to analyze past monitored air quality data. They are divided into linear and non-linear models. Linear Models as Multiple Linear Regression (MLR) can be used to make a linear empirical relationship between air pollutants and meteorological variables. The methodology of MLR is explained briefly in next section.

2.1.1 Multiple Linear Regression (MLR) models

A forecast/prediction of air pollutants can be made through regression equation in which unknown variable can be expressed as a function of certain number of known variables. There is one dependent variable to be predicted in relation to the two or more independent variables. The general form of MLR can be expressed as

$$Y = b_1 + b_2 X_2 + \dots + b_k X_k + e \tag{1}$$

where Y is dependent variable, X_2, X_3, \dots, X_k are independent variables, b_1, b_2, \dots, b_k are linear regression parameters and e is an estimated error term, which is obtained from independent random sampling from the normal distribution with mean zero and constant variance. The purpose of regression modeling is to estimate the b_1, b_2, \dots, b_k , which can be made using minimum square error technique.

The (Eq. (1)) can also be written as

$$Y = X b + e \tag{2}$$

where $Y = \begin{bmatrix} Y_1 \\ Y_2 \\ \vdots \\ Y_n \end{bmatrix}$, $X = \begin{bmatrix} 1 X_{21} X_{31} \dots X_{k1} \\ \dots & & & \dots \\ 1 X_{2n} X_{3n} \dots X_{kn} \end{bmatrix}$, $b = \begin{bmatrix} b_1 \\ b_2 \\ \vdots \\ b_k \end{bmatrix}$ and $e = \begin{bmatrix} e_1 \\ e_2 \\ \vdots \\ e_n \end{bmatrix}$

Here Y is an $n \times 1$, X is an $n \times k$, b is a $k \times 1$ and e is an $n \times 1$ matrix. The solution of above equation can be obtained as $b = (X'X)^{-1} (X'Y)$ using minimum square error technique. Further the F-test has been performed to determine whether a relationship exists between the dependent variables and regressors. The t-test is also performed in order to determine the potential value of each of the regressors' variables in the regression model. The resulting model can be used to predict future values.

If the relationship between air pollutants and meteorological variables is not linear, non-linear models like Artificial Neural Network can be used for treating the non-linear relationship. The model's characteristics are described in next section.

2.1.2 Artificial Neural Network

The Artificial Neural Network (ANN) represents an alternative methodology to conventional statistical modeling because of their computational efficiency and generalization ability. ANN models are mathematical models inspired by the biological neurons. The use of ANN as mentioned in the literature is an effective alternative to more traditional statistical techniques for forecasting time series. ANN can be trained to approximate virtually any smooth, measurable and highly nonlinear functions between input and output and requires no prior knowledge to the nature of this relationship (Gardner & Dorling, 1998) and can also be trained to generalize, when presented with new and unseen data. ANNs are made up of interconnected processing elements called neurons or nodes that are arranged in the layers. These layers include an input layer, one or more hidden layers and an output layer which are connected to each neuron of the next layer by the weights. The number of hidden layer is selected based upon the problem complexity. The number of neuron in the input and output layer is problem specific. The information

transfer is allowed only to the next consecutive layer. Each node of the hidden layer receives incoming signals from the nodes of the input layer. Each input value is weighted and based on its relative importance before entering the hidden layer. The total input signal NET is calculated as

$$\text{NET} = \sum_i W_i X_i \quad (3)$$

The total incoming signal is then passed through a non-linear transfer function F to produce the outgoing signal F (NET) of the node.

$$F(\text{NET}) = \frac{1}{1 + e^{-\text{NET}}} \quad (4)$$

The output signal of a hidden node is finally passed to the nodes of the next layer (hidden or output), where a similar procedure takes place. There are several transfer functions available such as pure linear, hyperbolic tangent, sigmoid etc. Transfer function plays a key role in training process of neural network because the ANN produce different results sensitive to its transfer function (Wassermann, 1989). The process of optimizing the connection weights is known as training or learning of ANN. This is equivalent to the parameter estimation phase in the conventional statistical models. Iterative techniques are used to get the best values for connection weights by minimizing the performance function i.e. error between model output and the provided target values. The trained network is then used for the forecasting/prediction purpose. ANN has the capability to recognize the patterns in the time series data presented to it and is thus useful in many types of pattern recognition problems.

2.2 Deterministic models

Deterministic models are based on a mathematical description of physical and chemical processes taking place in the atmosphere. These models are divided into different categories on the basis of source characteristics as point, line and area sources or on the basis of topography of the region as flat or complex terrain. These models can also be classified on the basis of size of the field they are describing:

- Short distance (distance from source less than 30-50 km)
- Mesoscale models (concentration fields of the order of hundreds of kms)
- Continental or planetary circulation models

Finally, models can also be classified on the basis of the time resolution of the concentration produced:

- Episodic models (temporal resolution of less than an hour)
- Short-time models (temporal resolutions grater than or equal to an hour and less than or equal to 24h)
- Climatologically models (with resolution grater than 24h, generally seasonal or annual) (Tirabassi, 2010).

These models are divided into three categories according to different approaches as Eulerian, Lagrangian and Gaussian. Eulerian approach is based on a fixed spatial-temporal grid. The basic equation used in Eulerian air pollution dispersion models is derived from the equation of the pollutant molecular diffusion:

$$\frac{\partial C}{\partial t} = -\mathbf{U} \cdot \nabla C + D \nabla^2 C + S \quad (5)$$

where: C- concentration of pollutant in the atmospheric air,

\mathbf{U} - wind speed vector of the components u, v, w,

D- Molecular diffusion coefficient,

S- Represents the sources and sinks of pollutant in the atmosphere i.e. its emission, removal from the atmosphere by dry and wet deposition, chemical reactions,

∇ - Gradient operator,

∇^2 - Laplacian.

Eq. (5) has been modified for the turbulent flow in the atmosphere. Modifications include the averaging procedure and closure procedure. The wind speed is expressed as the sum of two components, mean and turbulent: $\mathbf{U} = \bar{\mathbf{U}} + \mathbf{U}'$ and the same can be made for C as $C = \bar{C} + C'$ in (Eq. (5)) and hypothesizing a wind with divergence nil:

$$\frac{\partial \bar{C}}{\partial t} = -\bar{\mathbf{U}} \cdot \nabla \bar{C} - \nabla \cdot \overline{C' \mathbf{U}'} + D \nabla^2 \bar{C} + \bar{S} \quad (6)$$

where $\overline{C' \mathbf{U}'}$ is turbulent concentration flux.

The simplest closure method of (Eq. (6)) is a local first order closure in which K-theory is used. Assuming that turbulent concentration flux is proportional to the gradient of the average concentration, the following relation is obtained as:

$$\overline{C' \mathbf{U}'} = -K \nabla \bar{C} \quad (7)$$

where K (3x3) is turbulent diffusion coefficient.

When K tensor is diagonal, molecular diffusion is negligible and $C(x, y, z, t)$ represents the concentration of a non-reactive pollutant ($\bar{S}=S$). Thus, the (Eq. (6)) can be written as

$$\frac{\partial \bar{C}}{\partial t} = -\bar{\mathbf{U}} \cdot \nabla \bar{C} + \nabla \cdot K \nabla \bar{C} + S \quad (8)$$

Eq. (8) can be solved for C analytically or numerically if input data for \mathbf{U} , K and S are provided with initial and boundary conditions. Exact solution can be obtained by analytical methods, while numerical methods give the only approximate solutions. In this section we will discuss only the Eulerian analytical models.

2.2.1 Eulerian analytical solutions of the advection diffusion equation for point source in different atmospheric boundary conditions

Analytical solutions of the above equation are of fundamental importance in understanding and describing physical phenomena. The deterministic models for the dispersion of pollutants in atmosphere, based on the advection diffusion equation and K-theory as (Eq. (8)), can be written as:

$$\frac{\partial C}{\partial t} + u \frac{\partial C}{\partial x} + v \frac{\partial C}{\partial y} + w \frac{\partial C}{\partial z} = \frac{\partial}{\partial x} \left(K_x \frac{\partial C}{\partial x} \right) + \frac{\partial}{\partial y} \left(K_y \frac{\partial C}{\partial y} \right) + \frac{\partial}{\partial z} \left(K_z \frac{\partial C}{\partial z} \right) + S, \quad (9)$$

where K_x , K_y and K_z are the eddy diffusivities along x , y and z directions respectively. The following assumptions are made in solution of Eq. (9):

- Steady-state condition is considered (i.e., $\frac{\partial C}{\partial t} = 0$).
- The vertical velocity component (w) is neglected in comparison to horizontal velocity components (u and v).
- x -axis is oriented in the direction of mean wind (i.e., $u=U$, $v=0$).
- Downwind diffusion is neglected in comparison to transport due to mean wind

$$\text{i.e., } \left| U \left(\frac{\partial C}{\partial x} \right) \right| \gg \left| \left(\frac{\partial}{\partial x} \right) \left(K_x \left(\frac{\partial C}{\partial x} \right) \right) \right|.$$

Applications of these assumptions in (Eq. (9)), leads the steady state advection-diffusion equation for dispersion of a non reactive contaminate released from continuous source as (Seinfeld, 1986):

$$U \frac{\partial C}{\partial x} = \frac{\partial}{\partial y} \left(K_y \frac{\partial C}{\partial y} \right) + \frac{\partial}{\partial z} \left(K_z \frac{\partial C}{\partial z} \right), \quad (10)$$

where x , y , and z are coordinates in the along-wind, cross wind and vertical directions respectively. C is the mean concentration of pollutants and U is the mean wind speed in downwind direction. K_y and K_z are eddy diffusivities of pollutants in the crosswind and vertical directions respectively.

Eq.(10) is solved with the following boundary conditions, in which, h is the top of the inversion/mixed layer:

Dirchlet Boundary Condition (total absorption)

$$C(x,y,z)=0 \quad \text{at } z=0$$

$$C(x,y,z)=0 \quad \text{at } z=h \quad (11.a)$$

Neumann Boundary Condition (total reflection)

$$K_z \frac{\partial C(x,y,z)}{\partial z} = 0 \quad \text{at } z=0$$

$$K_z \frac{\partial C(x,y,z)}{\partial z} = 0 \quad \text{at } z=h \quad (11. b)$$

Mixed (type-I) Boundary Condition

$$K_z \frac{\partial C(x,y,z)}{\partial z} = 0 \quad \text{at } z=0$$

$$C(x,y,z)=0 \quad \text{at } z=h \quad (11. c)$$

Mixed (type-II) Boundary Condition

$$C(x,y,z)=0 \quad \text{at } z=0$$

$$K_z \frac{\partial C(x,y,z)}{\partial z} = 0 \text{ at } z=h \quad (11. d)$$

The pollutant decays in cross wind direction:

$$C(x, y, z) \rightarrow 0 \text{ as } y \rightarrow \pm\infty \quad (12)$$

The pollutant is released from an elevated point source of strength Q_p located at the point $(0, y_s, z_s)$,

$$U C(0, y, z) = Q_p \delta(y - y_s) \delta(z - z_s), \quad (13)$$

where δ is the Dirac delta function.

The transport of contaminant emitted from a source primarily depends on the wind speed U . The formulations of the commonly used dispersion models in air quality studies assume wind speed to be constant. However, it is well known that wind speed increases with height in the lower part of the atmospheric boundary layer (Arya, 1999). The height dependent wind speed can be expressed as

$$U(z) = az^\alpha, a = U(z_r)z_r^{-\alpha}, \quad (14)$$

where $U(z_r)$ is the wind speed at reference height z_r and α depends on atmospheric stability.

In formulation of dispersion models, K_z is parameterized as a function of height z only (Lin & Hildemann, 1996; Park & Baik, 2008). However, based on the Taylor's analysis and statistical theory, it is revealed that the eddy diffusivity depends on the downwind distance x (Arya, 1995). Thus, the eddy diffusivity can be a function of x and z both (Mooney & Wilson, 1993; Sharan & Kumar, 2009). The modified form of $K_z(x, z)$ is given as:

$$K_z(x, z) = K'_z(z)f(x), \quad (15)$$

where $K'_z(z)$ is the form of eddy diffusivity depending on z and $f(x)$ is assumed to be function of x . $K'_z(z)$ is parameterized as a power law profile in z :

$$K'_z(z) = bz^\beta, b = K'_z(z_r)z_r^{-\beta}, \quad (16)$$

where $K'_z(z_r)$ is the value of K'_z at height $z = z_r$ and β depends on atmospheric stability.

Using Taylor's hypothesis, the lateral eddy diffusivity can be represented by (Huang, 1979; Brown et al., 1997)

$$K_y(x, z) = \frac{1}{2} U(z) \frac{d\sigma_y^2(x)}{dx}, \quad (17)$$

where σ_y is the standard deviation of concentration distribution in the crosswind direction.

Based on the analysis of Prairie Grass and some other historical tracer experiments of atmospheric dispersion, Irwin et al., 2007 concluded that the ground level crosswind concentration profile of dispersing plume on average is well characterized as having a Gaussian shape, which is well predicted by all atmospheric transport and diffusion models, regardless of their sophistication. Thus, by assuming the Gaussian concentration

distribution in crosswind direction (Huang, 1979; Irwin et al., 2007), the steady state concentration of a pollutant released from point source in a three dimensional domain can be described as

$$C(x, y, z) = C(x, z) \frac{\exp(-y^2/2\sigma_y^2)}{\sqrt{2\pi}\sigma_y}, \quad (18)$$

where $C(x, z)$ is the crosswind integrated concentration.

The mathematical formulation of $C(x,z)$ is obtained by substituting the wind profile (Eq. (14)), diffusivity profile (Eq. (15)) and boundary conditions (Eqs. (11-13)) in the advection-diffusion equation (Eq. (10)) as:

$$\frac{1}{f(x)} \frac{\partial C}{\partial x} = \frac{b}{a} z^{-\alpha} \frac{\partial}{\partial z} \left(z^\beta \frac{\partial C}{\partial z} \right), \quad (19)$$

provided $f(x) \neq 0, \forall x \in (0, \infty)$.

By using the separation of variables technique, the solution of the (Eq. (19)) is assumed in the form:

$$C(x,z) = X(x) Z(z), \quad (20)$$

which transforms the (Eq. (19)) into two following ordinary differential equations by taking $-\lambda^2$ as the separation constant:

$$\frac{dX}{dx} + f(x)\lambda^2 X = 0 \quad (21)$$

$$\frac{d}{dz} \left(z^\beta \frac{dZ}{dz} \right) + \lambda^2 \left(\frac{a}{b} \right) z^\alpha Z = 0 \quad (22)$$

Eq. (21) has the solution:

$$X(x) = A \exp\left(-\lambda^2 \int_0^x f(s) ds\right), \quad (23)$$

where A is an arbitrary constant.

The solution of Eq. (22) is obtained in different boundary conditions as follows:

i. Eq. (22), along with the following boundary condition corresponding to Eq. (11.a):

$$Z = 0 \quad \text{at } z = 0, h \quad (24)$$

represents a Sturm-Liouville eigen value problem.

The solution of (Eq. (22)) with boundary condition (Eq. (24)) is zero for $\lambda=0$.

For a non-zero value of λ , the transformation of the variables

$$t = z \left(\frac{\alpha - \beta + 2}{2} \right) \quad (25)$$

and

$$Z(z) = z^{\left(\frac{1-\beta}{2}\right)} G(t) \tag{26}$$

in (Eq. (22)) leads to:

$$t^2 \frac{d^2G}{dt^2} + t \frac{dG}{dt} + (k^2t^2 - \mu^2)G = 0, \tag{27}$$

where

$$k = \frac{\sqrt{a/b} \lambda}{(\alpha - \beta + 2)/2} \text{ and } \mu = \frac{(1 - \beta)}{(\alpha - \beta + 2)} \tag{28}$$

Eq. (27) is the Bessel's equation, whose solution can be given as:

$$G(t) = B_1 J_\mu(kt) + B_2 J_{-\mu}(kt), \tag{29}$$

where J_μ and $J_{-\mu}$ are the Bessel's functions of first kind of order μ and $-\mu$ respectively. From (Eqs. (25), (26) and (29)), we have

$$Z(z) = z^{\frac{1-\beta}{2}} \left\{ B_1 J_\mu \left(kz \frac{\alpha-\beta+2}{2} \right) + B_2 J_{-\mu} \left(kz \frac{\alpha-\beta+2}{2} \right) \right\} \tag{30}$$

Application of the boundary condition (Eq. (24)) at $z = 0$ in (Eq. (30)) yields $B_2 = 0$ and the condition at $z = h$ (Eq. (24)) gives rise:

$$J_\mu \left(kh \frac{\alpha-\beta+2}{2} \right) = 0 \tag{31}$$

The corresponding eigen functions are:

$$Z_n(z) = z^{\frac{1-\beta}{2}} J_\mu \left(k_n z \frac{\alpha-\beta+2}{2} \right), \quad n = 1, 2, 3 \tag{32}$$

The general solution of (Eq. (19)) is obtained by using (Eqs. (23), (31) and (32)) as:

$$C(x, z) = z^{\frac{1-\beta}{2}} \sum_{n=1}^{\infty} A_n J_\mu \left(k_n z^{(\alpha-\beta+2)/2} \right) \exp \left(-\frac{b(\alpha-\beta+2)^2 k_n^2}{4a} \int_0^x f(s) ds \right), \tag{33}$$

where A_1, A_2, \dots, A_n are the unknown coefficients. The (Eq. (33)) represents the concentration distribution C through the Fourier-Bessel series (Abramowitz & Stegun, 1972) corresponding to a set of eigen functions Z_n .

Estimation of the coefficients A_n 's for crosswind integrated concentration: The source at $x = 0$, Eq. (13) gives:

$$az^\alpha \left[z^{\frac{1-\beta}{2}} \sum_{n=1}^{\infty} A_n J_\mu \left(k_n z^{(\alpha-\beta+2)/2} \right) \right] = Q_p \delta(z - z_s) \tag{34}$$

The coefficients A_n 's are estimated using the orthogonal property of eigen functions (Abramowitz & Stegun, 1972).

Multiplying (Eq. (34)) by $z^{(1-\beta)/2} J_\mu(k_m z^{(\alpha-\beta+2)/2})$ for $m \geq 1$, and integrating it with respect to z from 0 to h , we get:

$$A_n = Q_p \frac{\alpha - \beta + 2}{a h^{\alpha - \beta + 2}} \frac{(z_s)^{\frac{1-\beta}{2}} J_\mu(k_n z_s^{(\alpha-\beta+2)/2})}{J_{\mu+1}^2(k_n h^{(\alpha-\beta+2)/2})} \quad (35)$$

Substituting the expression for A_n 's for $n \geq 1$ in (Eq. (33)), the final solution is obtained as:

$$C(x, z) = Q_p \left[\frac{\alpha - \beta + 2}{a h^{\alpha - \beta + 2}} (z z_s)^{(1-\beta)/2} \sum_{n=1}^{\infty} \frac{J_\mu[Y_n(z/h)^{(\alpha-\beta+2)/2}] J_\mu[Y_n(z_s/h)^{(\alpha-\beta+2)/2}]}{J_{\mu+1}^2(Y_n)} \right. \\ \left. \times \exp\left(-\frac{b(\alpha - \beta + 2)^2 Y_n^2}{4 a h^{\alpha - \beta + 2}} \int_0^x f(s) ds\right) \right], \quad (36)$$

in which Y_n is given as:

$$J_\mu(Y_n) = 0. \quad (37)$$

ii. The solution of Eq. (22) for crosswind integrated concentration by substituting the wind profile (Eq. (14)) and diffusivity profile (Eq. (15)) in (Eq. (10)) for Neumann boundary condition (Eq. (11.b)) is obtained from earlier study by Sharan & Kumar (2009) as:

$$C(x, z) = Q_p \left[\frac{\alpha + 1}{a h^{\alpha + 1}} + \frac{\alpha - \beta + 2}{a h^{\alpha - \beta + 2}} (z z_s)^{(1-\beta)/2} \times \sum_{n=1}^{\infty} \frac{J_{-\mu}[Y_n(z/h)^{(\alpha-\beta+2)/2}] J_{-\mu}[Y_n(z_s/h)^{(\alpha-\beta+2)/2}]}{J_{-\mu}^2(Y_n)} \right. \\ \left. \times \exp\left(-\frac{b(\alpha - \beta + 2)^2 Y_n^2}{4 a h^{\alpha - \beta + 2}} \int_0^x f(s) ds\right) \right], \quad (38)$$

in which Y_n is given as:

$$J_{-\mu+1}(Y_n) = 0. \quad (39)$$

iii. The (Eq. (22)), along with the following boundary conditions corresponding to (Eq. (11.c)):

$$b z^\beta \frac{dZ}{dz} = 0 \text{ at } z = 0 \quad \text{and} \quad Z = 0 \text{ at } z = h \quad (40)$$

The solution of (Eq. (22)) with boundary condition (Eq. (40)) is zero for $\lambda = 0$.

For a non-zero value of λ , the boundary condition (Eq. (40)) at $z = 0$ in (Eq. (30)) yields $B_1 = 0$ and the condition at $z = h$ (Eq. (40)) gives rise:

$$J_{-\mu} \left(k h \frac{\alpha-\beta+2}{2} \right) = 0 \tag{41}$$

The corresponding eigen functions are:

$$Z_n(z) = z^{\frac{1-\beta}{2}} J_{-\mu} \left(k_n z^{\frac{\alpha-\beta+2}{2}} \right), \quad n = 1, 2, 3, \tag{42}$$

The general solution of (Eq. (19)) is obtained by using (Eqs. (23), (41) and (42)) as:

$$C(x, z) = z^{\frac{1-\beta}{2}} \sum_{n=1}^{\infty} A_n J_{-\mu} \left(k_n z^{(\alpha-\beta+2)/2} \right) \exp \left(-\frac{b(\alpha-\beta+2)^2 k_n^2}{4a} \int_0^x f(s) ds \right), \tag{43}$$

where A_1, A_2, \dots are the unknown coefficients.

The (Eq. (43)) represents the concentration distribution C as the Fourier-Bessel series (Abramowitz & Stegun, 1972) corresponding to a set of eigen functions Z_n .

Estimation of the coefficients A_n 's for crosswind integrated concentration

The source condition at $x = 0$ (Eq. (13)), gives:

$$az^\alpha \left[z^{\frac{1-\beta}{2}} \sum_{n=1}^{\infty} A_n J_{-\mu} \left(k_n z^{(\alpha-\beta+2)/2} \right) \right] = Q_p \delta(z - z_s) \tag{44}$$

The coefficients A_n 's are estimated using the orthogonal property of eigen functions (Abramowitz & Stegun, 1972).

Multiplying (Eq. (44)) by $z^{(1-\beta)/2} J_{-\mu} \left(k_m z^{(\alpha-\beta+2)/2} \right)$, $m \geq 1$, and integrating it with respect to z from 0 to h , we get:

$$A_n = Q_p \frac{\alpha-\beta+2}{ah^{\alpha-\beta+2}} \frac{(z_s)^{\frac{1-\beta}{2}} J_{-\mu} \left(k_n z_s^{(\alpha-\beta+2)/2} \right)}{J_{-\mu+1}^2 \left(k_n h^{(\alpha-\beta+2)/2} \right)} \tag{45}$$

Substituting the expression for A_n 's, $n \geq 1$ into (Eq. (45)), the final solution of an elevated point source at crosswind is obtained as:

$$C(x, z) = Q_p \left[\frac{\alpha-\beta+2}{ah^{\alpha-\beta+2}} (zz_s)^{(1-\beta)/2} \sum_{n=1}^{\infty} \frac{J_{-\mu} \left[Y_n(z/h)^{(\alpha-\beta+2)/2} \right] J_{-\mu} \left[Y_n(z_s/h)^{(\alpha-\beta+2)/2} \right]}{J_{-\mu+1}^2(Y_n)} \right. \\ \left. \times \exp \left(-\frac{b(\alpha-\beta+2)^2 Y_n^2}{4ah^{\alpha-\beta+2}} \int_0^x f(s) ds \right) \right], \tag{46}$$

in which Y_n is given as:

$$J_{-\mu}(Y_n) = 0. \tag{47}$$

iv. The (Eq. (22)), along with the following boundary conditions corresponding to (Eq. (11.d)):

$$Z = 0 \text{ at } z = 0 \text{ and } bz^\beta \frac{dZ}{dz} = 0 \text{ at } z=h \tag{48}$$

The solution of (Eq. (22)) with (Eq. (48)) is zero for $\lambda = 0$.

For a non-zero value of λ , the boundary condition (Eq. (48)) at $z = 0$ in (Eq. (30)) yields $B_2 = 0$ and the condition at $z = h$ (Eq. (48)) gives rise:

$$J_{\mu-1} \left(kh \frac{\alpha-\beta+2}{2} \right) = 0 \tag{49}$$

The corresponding eigen functions are:

$$Z_n(z) = z^{\frac{1-\beta}{2}} J_\mu \left(k_n z^{\frac{\alpha-\beta+2}{2}} \right), \quad n = 1, 2, 3, \tag{50}$$

The general solution of (Eq. (19)) is obtained by using (Eqs. (22), (49) and (50)) as:

$$C(x, z) = z^{\frac{1-\beta}{2}} \sum_{n=1}^{\infty} A_n J_\mu \left(k_n z^{(\alpha-\beta+2)/2} \right) \exp \left(-\frac{b(\alpha-\beta+2)^2 k_n^2}{4a} \int_0^x f(s) ds \right), \tag{51}$$

where A_1, A_2, \dots are the unknown coefficients. The Eq. (51) represents the concentration distribution C as the Fourier-Bessel series (Abramowitz & Stegun, 1972) corresponding to a set of eigen functions Z_n .

Estimation of the coefficients A_n 's for crosswind integrated concentration

The source condition at $x = 0$ (Eq. (13)), gives:

$$az^\alpha \left[z^{\frac{1-\beta}{2}} \sum_{n=1}^{\infty} A_n J_\mu \left(k_n z^{(\alpha-\beta+2)/2} \right) \right] = Q_p \delta(z - z_s) \tag{52}$$

The coefficients A_n 's are estimated using the orthogonal property of eigen functions (Abramowitz & Stegun, 1972).

Multiplying (Eq. (52)) by $z^{(1-\beta)/2} J_\mu \left(k_m z^{(\alpha-\beta+2)/2} \right)$, $m \geq 1$, and integrating it with respect to z from 0 to h , we get:

$$A_n = Q_p \frac{\alpha - \beta + 2}{ah^{\alpha-\beta+2}} \frac{(z_s)^{\frac{1-\beta}{2}} J_\mu \left(k_n z_s^{(\alpha-\beta+2)/2} \right)}{J_\mu^2 \left(k_n h^{(\alpha-\beta+2)/2} \right)} \tag{53}$$

Substituting the expression for A_n 's, $n \geq 1$ into (Eq. (51)), the final solution of an elevated point source at crosswind is obtained as:

$$C(x, z) = Q_p \left[\frac{\alpha - \beta + 2}{ah^{\alpha - \beta + 2}} (zz_s)^{(1-\beta)/2} \sum_{n=1}^{\infty} \frac{J_{\mu} \left[Y_n(z/h)^{(\alpha - \beta + 2)/2} \right] J_{\mu} \left[Y_n(z_s/h)^{(\alpha - \beta + 2)/2} \right]}{J_{\mu}^2(Y_n)} \right. \\ \left. \times \exp \left(- \frac{b(\alpha - \beta + 2)^2 Y_n^2}{4ah^{\alpha - \beta + 2}} \int_0^x f(s) ds \right) \right], \tag{54}$$

in which Y_n is given as:

$$J_{\mu-1}(Y_n) = 0. \tag{55}$$

2.2.2 Point source models

The steady state three dimensional solution of a point source can be obtained from (Eq. (18)) and $f(x)$, which is expressed as a linear function of downwind distance, i.e., $f(x) = \gamma \bar{U}x$ (Sharan & Modani, 2006), in different boundary conditions:

i. The solution in Dirichlet Boundary condition is given as

$$C(x, y, z) = \frac{Q_p}{\sqrt{2\pi\sigma_y}} \left[\frac{\alpha - \beta + 2}{ah^{\alpha - \beta + 2}} (zz_s)^{(1-\beta)/2} \times \sum_{n=1}^{\infty} \frac{J_{\mu} [Y_n(z/h)^{(\alpha - \beta + 2)/2}] J_{\mu} [Y_n(z_s/h)^{(\alpha - \beta + 2)/2}]}{J_{\mu+1}^2(Y_n)} \right. \\ \left. \times \exp \left(- \frac{b\gamma \bar{U} (x-x_s)^2 (\alpha - \beta + 2)^2 Y_n^2}{8ah^{\alpha - \beta + 2}} \right) \right] \times \exp \left[- \frac{(y - y_s)^2}{2\sigma_y^2} \right], \tag{56}$$

where $\mu = (1 - \beta) / (\alpha - \beta + 2)$, J_{μ} is the Bessel function of order μ and Y_n 's are obtained from the equation:

$$J_{\mu}(Y_n) = 0 \tag{57}$$

ii. The solution in Neumann Boundary condition is given as

$$C(x, y, z) = \frac{Q_p}{\sqrt{2\pi\sigma_y}} \left[\frac{\alpha + 1}{ah^{\alpha + 1}} + \frac{\alpha - \beta + 2}{ah^{\alpha - \beta + 2}} (zz_s)^{(1-\beta)/2} \times \sum_{n=1}^{\infty} \frac{J_{-\mu} [Y_n(z/h)^{(\alpha - \beta + 2)/2}] J_{-\mu} [Y_n(z_s/h)^{(\alpha - \beta + 2)/2}]}{J_{-\mu}^2(Y_n)} \right. \\ \left. \times \exp \left(- \frac{b\gamma \bar{U} (x-x_s)^2 (\alpha - \beta + 2)^2 Y_n^2}{8ah^{\alpha - \beta + 2}} \right) \right] \times \exp \left[- \frac{(y - y_s)^2}{2\sigma_y^2} \right], \tag{58}$$

where $\mu = (1 - \beta) / (\alpha - \beta + 2)$, $J_{-\mu}$ is the Bessel function of order is $-\mu$ and Y_n 's are obtained from the equation:

$$J_{-\mu+1}(Y_n) = 0 \tag{59}$$

iii. The solution in Mixed (type-I) Boundary condition is given as

$$C(x, y, z) = \frac{Q_p}{\sqrt{2\pi}\sigma_y} \left[\frac{\alpha - \beta + 2}{ah^{\alpha - \beta + 2}} (zz_s)^{(1-\beta)/2} \times \sum_{n=1}^{\infty} \frac{J_{-\mu}[Y_n(z/h)^{(\alpha-\beta+2)/2}] J_{-\mu}[Y_n(z_s/h)^{(\alpha-\beta+2)/2}]}{J_{-\mu+1}^2(Y_n)} \right. \\ \left. \times \exp\left(-\frac{b\gamma\bar{U}(x-x_s)^2(\alpha-\beta+2)^2 Y_n^2}{8ah^{\alpha-\beta+2}}\right) \right] \times \exp\left[-\frac{(y-y_s)^2}{2\sigma_y^2}\right], \quad (60)$$

where $\mu = (1 - \beta) / (\alpha - \beta + 2)$, $J_{-\mu}$ is the Bessel function of order $-\mu$ and Y_n 's are obtained from the equation:

$$J_{-\mu}(Y_n) = 0 \quad (61)$$

iv. The solution in Mixed (type-II) Boundary condition is given as

$$C(x, y, z) = \frac{Q_p}{\sqrt{2\pi}\sigma_y} \left[\frac{\alpha - \beta + 2}{ah^{\alpha - \beta + 2}} (zz_s)^{(1-\beta)/2} \times \sum_{n=1}^{\infty} \frac{J_{\mu}[Y_n(z/h)^{(\alpha-\beta+2)/2}] J_{\mu}[Y_n(z_s/h)^{(\alpha-\beta+2)/2}]}{J_{\mu}^2(Y_n)} \right. \\ \left. \times \exp\left(-\frac{b\gamma\bar{U}(x-x_s)^2(\alpha-\beta+2)^2 Y_n^2}{8ah^{\alpha-\beta+2}}\right) \right] \times \exp\left[-\frac{(y-y_s)^2}{2\sigma_y^2}\right], \quad (62)$$

where $\mu = (1 - \beta) / (\alpha - \beta + 2)$, J_{μ} is the Bessel function of order μ and Y_n 's are obtained from the equation:

$$J_{\mu-1}(Y_n) = 0 \quad (63)$$

2.2.3 Correspondence between present solutions to the earlier solutions

In present solution, wind speed is a function of z and vertical eddy diffusivity is considered a function of x and z as $K_z(x, z) = bz^{\beta} f(x)$. If $f(x)$ is equal to 1.0, the solutions of Eqs. (56), (58), (60) and (62) are become same as the solutions obtained by Lin & Hildemann (1996). When wind speed is power law function of z and vertical eddy diffusivity is function of x only, i.e. $K_z(x, z) = f(x) = K(x)$ (for $\beta = 0$ and $b = 1.0$), the expression for the two dimensional concentration i.e., Eq. (38) is same as solution by Sharan & Modani (2006).

2.2.4 Line source models

A line source can be considered as a superposition of point sources. The solution for finite line source can be obtained by integrating point source solution from $y_s = y_1$ to y_2 with unit source strength Q_{ℓ} with the same Y_n 's as in point source in different boundary conditions:

i. The solution in Dirichlet Boundary condition is given as

$$C(x, y, z) = \frac{Q_{\ell}}{2} \left[\frac{\alpha - \beta + 2}{ah^{\alpha - \beta + 2}} (zz_s)^{(1-\beta)/2} \times \sum_{n=1}^{\infty} \frac{J_{\mu}[Y_n(z/h)^{(\alpha-\beta+2)/2}] J_{\mu}[Y_n(z_s/h)^{(\alpha-\beta+2)/2}]}{J_{\mu+1}^2(Y_n)} \right. \\ \left. \times \exp\left(-\frac{b\gamma\bar{U}(x-x_s)^2(\alpha-\beta+2)^2 Y_n^2}{8ah^{\alpha-\beta+2}}\right) \right] \times \left[\operatorname{erf}\left(\frac{y-y_1}{\sqrt{2}\sigma_y}\right) - \operatorname{erf}\left(\frac{y-y_2}{\sqrt{2}\sigma_y}\right) \right] \quad (64)$$

ii. The solution in Neumann Boundary condition is given as

$$C(x,y,z)=\frac{Q_\ell}{2}\left[\frac{\alpha+1}{ah^{\alpha+1}}+\frac{\alpha-\beta+2}{ah^{\alpha-\beta+2}}(zz_s)^{(1-\beta)/2}\times\sum_{n=1}^{\infty}\frac{J_{-\mu}[Y_n(z/h)^{(\alpha-\beta+2)/2}]J_{-\mu}[Y_n(z_s/h)^{(\alpha-\beta+2)/2}]}{J_{-\mu}^2(Y_n)}\right. \\ \left.\times\exp\left(-\frac{b\gamma\bar{U}(x-x_s)^2(\alpha-\beta+2)^2Y_n^2}{8ah^{\alpha-\beta+2}}\right)\right]\times\left[\operatorname{erf}\left(\frac{y-y_1}{\sqrt{2}\sigma_y}\right)-\operatorname{erf}\left(\frac{y-y_2}{\sqrt{2}\sigma_y}\right)\right] \tag{65}$$

iii. The solution in Mixed (type-I) Boundary condition is given as

$$C(x,y,z)=\frac{Q_\ell}{2}\left[\frac{\alpha-\beta+2}{ah^{\alpha-\beta+2}}(zz_s)^{(1-\beta)/2}\times\sum_{n=1}^{\infty}\frac{J_{-\mu}[Y_n(z/h)^{(\alpha-\beta+2)/2}]J_{-\mu}[Y_n(z_s/h)^{(\alpha-\beta+2)/2}]}{J_{-\mu+1}^2(Y_n)}\right. \\ \left.\times\exp\left(-\frac{b\gamma\bar{U}(x-x_s)^2(\alpha-\beta+2)^2Y_n^2}{8ah^{\alpha-\beta+2}}\right)\right]\times\left[\operatorname{erf}\left(\frac{y-y_1}{\sqrt{2}\sigma_y}\right)-\operatorname{erf}\left(\frac{y-y_2}{\sqrt{2}\sigma_y}\right)\right] \tag{66}$$

iv. The solution in Mixed (type-II) Boundary condition is given as

$$C(x,y,z)=\frac{Q_\ell}{2}\left[\frac{\alpha-\beta+2}{ah^{\alpha-\beta+2}}(zz_s)^{(1-\beta)/2}\times\sum_{n=1}^{\infty}\frac{J_{\mu}[Y_n(z/h)^{(\alpha-\beta+2)/2}]J_{\mu}[Y_n(z_s/h)^{(\alpha-\beta+2)/2}]}{J_{\mu}^2(Y_n)}\right. \\ \left.\times\exp\left(-\frac{b\gamma\bar{U}(x-x_s)^2(\alpha-\beta+2)^2Y_n^2}{8ah^{\alpha-\beta+2}}\right)\right]\times\left[\operatorname{erf}\left(\frac{y-y_1}{\sqrt{2}\sigma_y}\right)-\operatorname{erf}\left(\frac{y-y_2}{\sqrt{2}\sigma_y}\right)\right], \tag{67}$$

where erf is the error function defined by

$$\operatorname{erf}(a)=\frac{2}{\sqrt{\pi}}\int_0^a e^{-t^2} dt$$

The solution of an infinite line source of source strength Q_ℓ can be obtained by integrating point source along the crosswind direction $y_s = -\infty$ to ∞ , which is different than the finite line source formulation, since $\int_{-\infty}^{\infty} \frac{\exp(-(y-y_s)^2/2\sigma_y^2)}{\sqrt{2\pi}\sigma_y} dy_s = 1$.

2.2.5 Area source models

The concentration of air pollutants due to a finite area source at (x, y, z) is calculated as a superposition of finite line sources extending from x_1 to x_2 in x direction is obtained as

$$C(x,y,z)=\int_{x_1}^{x_2} C(x-x_s,y,z)dx_s, \tag{68}$$

where $C(x-x_s, y, z)$ is equivalent to the finite line source as obtained in section 2.2.4. However, the source strength Q_ℓ is replaced by Q_a in (Eqs. 64, 65, 66 and 67) with same Y_n 's as in point source.

For an infinite area source with uniform strength Q_a , the solution is obtained as:

$$C(x,z)=\int_{x_1}^{x_2} C(x-x_s,z)dx_s, \tag{69}$$

where $C(x-x_s, z)$ is equivalent to the crosswind integrated concentration. However, the source term Q_p is replaced by Q_a in (Eqs. 36, 38, 46 and 54) with same γ_n 's as in point source.

Eqs. 68 and 69 are the solutions for finite and infinite area sources and can be solved numerically.

If wind speed and vertical eddy diffusivity are considered as function of z , i.e. $K_z(x, z) = bz^\beta$ ($f(x) = 1.0$) with unbounded region ($h \rightarrow \infty$) and ground level source ($z_s \rightarrow 0$) in (Eq. (68)), the expression obtained for the concentration is same as in Park & Baik, 2008.

3. Case study of Delhi

A case study of Delhi has been attempted through the application of two different categories namely statistical and analytical models to fulfill the objective of the chapter.

3.1 Application of statistical models

First of all the daily Air quality index (AQI) as a comprehensive assessment of air quality concentration of criteria pollutants namely Respirable Suspended Particulate Matter (RSPM), Sulphur dioxide (SO₂), Nitrogen dioxide (NO₂) and Suspended Particulate Matter (SPM) has been calculated at ITO (a busiest traffic intersection) for a period of seven years (2000-2006), monitored continuously by Central Pollution Control Board (CPCB). A method of US Environmental Protection Agency (USEPA) has been used for estimating the AQI, in which the sub-index and breakpoint pollutant concentrations depend on Indian National Ambient Air Quality Standard (NAAQS). There are primarily two steps involved in formulating an AQI: first the formation of sub-indices of each pollutant, second the aggregation (breakpoints) of sub indices. The Breakpoint concentration of each pollutant, used in calculation of AQI, is based on Indian NAAQS and results of epidemiological studies indicating the risk of adverse health effects of specific pollutants. It has been noticed that different breakpoint concentrations and different air quality standards has been reported in literature (Environmental Protection Agency, 1999). In India, to reflect the status of air quality and its effects on human health, the range of index values has been designated as "Good (0-100)", "Moderate (101-200)", "Poor (201-300)", "Very Poor (301-400)" and "Severe (401-500)" (Nagendra et al. (2007)) as shown in Table 1.

The formula (EPA, (1999)) used to calculate AQI for four criteria pollutants RSPM, SO₂, NO₂ and SPM from 2000-2006 is given below:

$$I_p = \left[\frac{(I_{Hi} - I_{Lo})}{(BP_{Hi} - BP_{Lo})} \right] (C_p - BP_{Lo}) + I_{Lo}, \quad (70)$$

where I_p = the AQI for pollutant 'p',

C_p = actual ambient concentration of the pollutant 'p',

BP_{Hi} = the breakpoint in Table 1 that is greater than or equal to C_p ,

BP_{Lo} = the breakpoint in Table 1 that is less than or equal to C_p ,

I_{Hi} = the subindex value corresponding to BP_{Hi} ,

I_{Lo} = the sub index value corresponding to BP_{Lo} .

SI.No.	Index values	Descriptor	SO ₂ (24-h avg.)	NO ₂ (24-h avg.)	RSPM (24-h avg.)	SPM (24-h avg.)
1	0-100	Good ^a	0-80	0-80	0-100	0-200
2	101-200	Moderate ^b	81-367	81-180	101-150	201-260
3	201-300	Poor ^c	368-786	181-564	151-350	261-400
4	301-400	Very Poor ^d	787-1572	565-1272	351-420	401-800
5	401-500	Severe ^e	>1572	>1272	>420	>800

All the values of SO₂, NO₂, RSPM and SPM are in $\mu\text{g}/\text{m}^3$.

^a Good: Air quality is acceptable; however, for some pollutants there may be a moderate health concern for a very small number of people.

^b Moderate: Members of sensitive groups may experience health effects.

^c Poor: Members of sensitive groups may experience more serious health effects.

^d Very poor: Triggers health alter, everyone may experience more serious health effects.

^e Severe: Triggers health warnings of emergency conditions.

Table 1. Propose sub-index and breakpoint pollutant concentration for Indian-AQI.

The overall AQI is now determined on the basis of the AQI for above pollutant 'p' and highest among them is declared as the overall AQI for that day.

The above estimated daily AQI along with meteorological variables like daily maximum temperature (t_{max}), minimum temperature (t_{min}), daily temperature range (difference between daily maximum and minimum temperature, t_{range}), average temperature (t_{avg}), wind speed (wsp), wind direction index (wdi), relative humidity (rh), vapor pressure (vp), station level pressure (slp), rainfall (rf), sunshine hours (ssh), cloud cover (cc), visibility (v) and radiation (rd), monitored at Safdarjung airport by Indian Meteorological Department (IMD), Delhi, have been used in statistical models to forecast daily AQI one day in advance. This study has been carried out for four different seasons namely summer (March, April, May), monsoon (June, July, August), post monsoon (September, October, November) and winter (December, January, February). The location ITO has been chosen in the present study due to various reasons: (i.) a busiest traffic intersection, (ii.) air pollutants concentration of RSPM, SO₂, NO₂ and SPM is monitored continuously and (iii.) the meteorological station Safdarjung airport is within 10 km radius. These models include previous day's AQI and meteorological variables as input and yield daily forecasting of AQI. The input and output is normalized between -1 to +1 using the minimum and maximum of the time series before any preprocessing. Forecast of daily AQI in Delhi has been obtained by two models MLR and ANN independently. The performance of both the models has been assessed with respect to the statistical parameters.

3.1.1 AQI by MLR model

The following MLR equations for different seasons are resulted through training of AQI and meteorological data of 2000-2005 using SPSS software for summer, monsoon, post monsoon and winter respectively:

$$[AQI] = 0.0478 + 0.504 \times [AQI_{d-1}] - 0.079 \times [rh] + 0.126 \times [t_{max}] - 0.068 \times [cc] \quad (71)$$

$$[AQI] = 0.181 + 0.599 \times [AQI_{d-1}] - 0.282 \times [rh] - 0.128 \times [v] - 0.155 \times [t_{min}] \quad (72)$$

$$[AQI] = -0.324 + 0.537 \times [AQI_{d-1}] + 0.573x [slp] - 0.112x [vp] + 0.070 \times [ssh] - 0.135 \times [v] + 0.066 \times [t_{max}] \quad (73)$$

$$[AQI] = 0.171 + 0.503 \times [AQI_{d-1}] - 0.191x [v] - 0.115 \times [cc] - 0.169x [wsp] - 0.157 \times [rh] + 0.151 \times [rf] \quad (74)$$

The previous day's AQI is the common variable in all four equations. The above equations have also been used to forecast the daily AQI of 2000-2005 for all four seasons, which have been compared with the observed AQI, used as trained data of the corresponding seasons during 2000-2005 and are shown graphically Figs.1 (a), (b) (c) and (d).

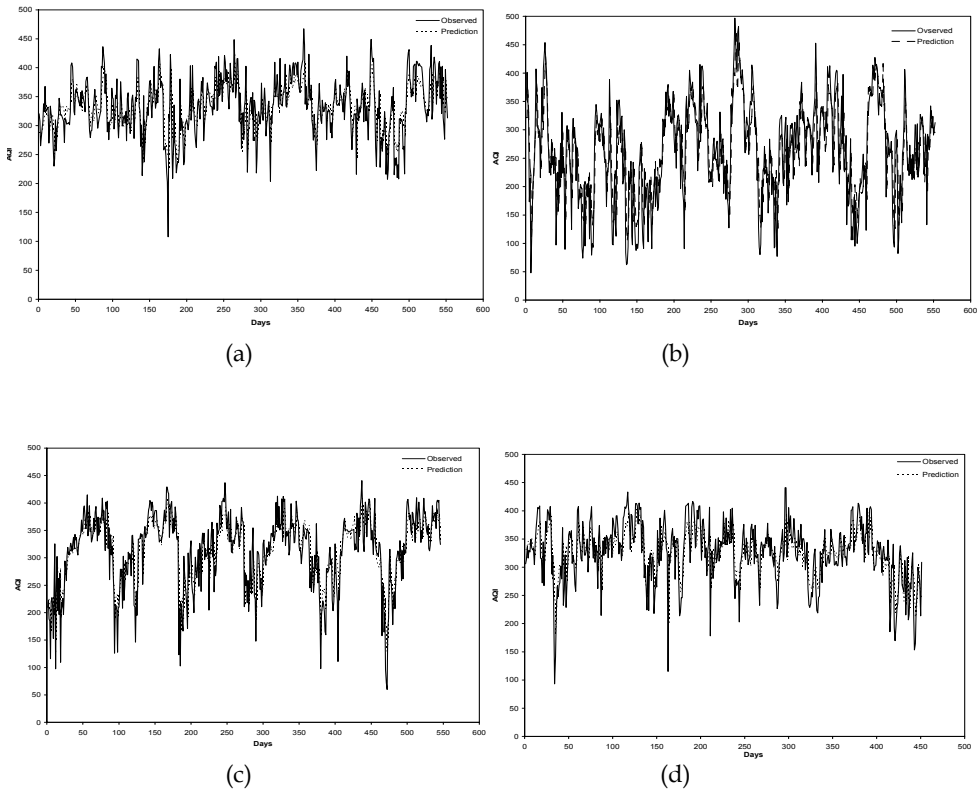


Fig. 1. Comparison of observed and MLR model predicted values of daily AQI in (a) Summer, (b) Monsoon, (c) Post Monsoon and (d) Winter seasons during the years 2000-2005.

The Fig. 1 reflects that the trained values of AQI are matching well with observed values (calculated directly from formulation Eq. (70)). The same set of Eqs. (71-74) have been used for forecasting the daily AQI in all four seasons of the year 2006 which have been shown graphically in Figs. 2 (a), (b), (c) and (d) for summer, monsoon, post monsoon and winter seasons respectively. The observed values of AQI of year 2006 for each season have also been plotted in the Fig. 2 in order to validate the forecasted values of AQI.

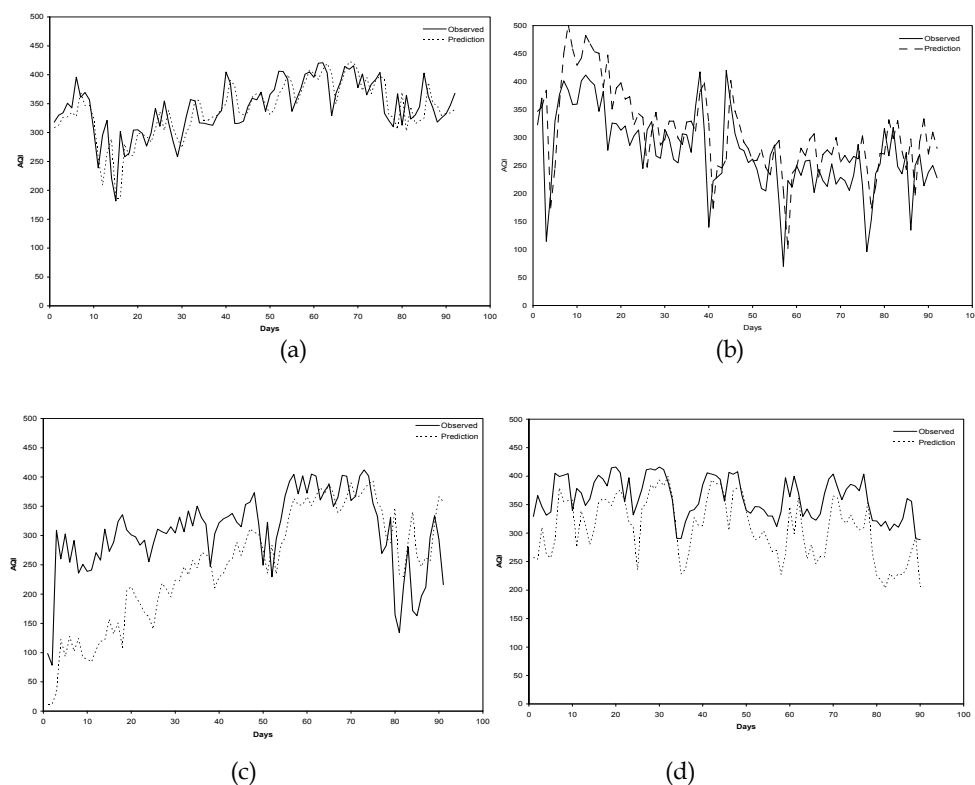


Fig. 2. Comparison of observed and model's predicted values of daily AQI in (a) Summer, (b) Monsoon, (c) Post Monsoon and (d) Winter seasons during the year 2006.

The quantitative analysis of comparison of forecasted and observed values of AQI has been made through statistical parameters, which are summarized in Table 2. The NMSE and coefficient of determination (R^2) are found as (0.0094, 0.5718) in summer season which are followed by (0.0369, 0.5247) in winter; (0.0629, 0.3913) in monsoon and (0.1287, 0.3021) in post monsoon seasons, showing good performance of the model as the ideal values of NMSE and R^2 are 0 and 1 respectively. The values of R^2 in four different seasons reflect that the model's forecasted and observed AQI could be correlated explained by the selected input variables as approximately 57% in summer, 52% in winter, 39% in monsoon and 30% in post monsoon seasons. However, the fractional bias shows the under-prediction in all the seasons except Monsoon.

S.N.	Season	2006			
		RMSE	NMSE	coefficient of determination	Fractional Bias
1	Summer	33.13	0.0094	0.5718	0.0126
2	Monsoon	72.99	0.0629	0.3913	-0.1246
3	Post Monsoon	99.18	0.1287	0.3021	0.1972
4	Winter	64.39	0.0369	0.5247	0.1573

Table 2. Comparison of MLR model predicted and observed values in years 2000-2005 and year 2006.

3.1.2 AQI by ANN model

The ANN model for different seasons is developed through training of AQI and meteorological data of 2000-2005 using MATLAB. The weights of a network are iteratively modified to minimize the total mean squared error between the desired target and actual output values. The above model has also been trained using observed daily AQI (same values as in MLR) of 2000-2005 for all four seasons. The comparison of observed and trained AQI has been shown graphically in Figs.3 (a), (b) (c) and (d).

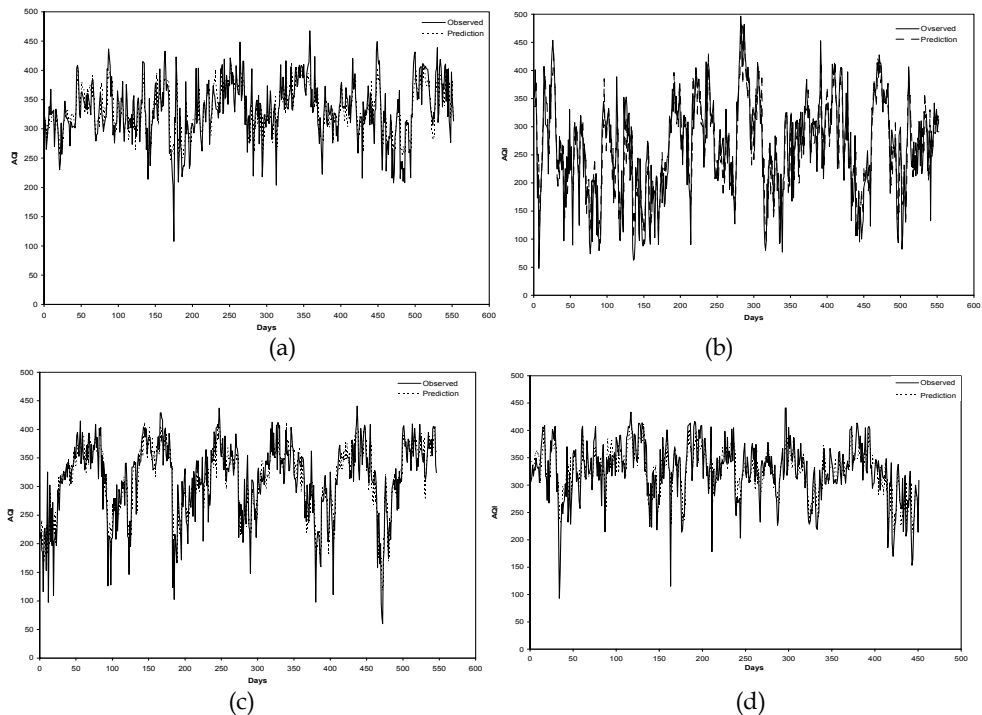


Fig. 3. Comparison of observed and ANN model predicted values of daily AQI in (a) Summer, (b) Monsoon, (c) Post Monsoon and (d) Winter seasons during the years 2000-2005.

The Fig. 3 reflects that the trained values of AQI are showing the same trend as observed values. The same trained architectures have been used for forecasting the daily AQI in all four seasons of the year 2006, which have been shown graphically in Figs. 4 (a), (b), (c) and (d) for summer, monsoon, post monsoon and winter seasons respectively. The observed values of AQI of year 2006 for each season have also been plotted in the Fig. 4 in order to validate the forecasted values of AQI.

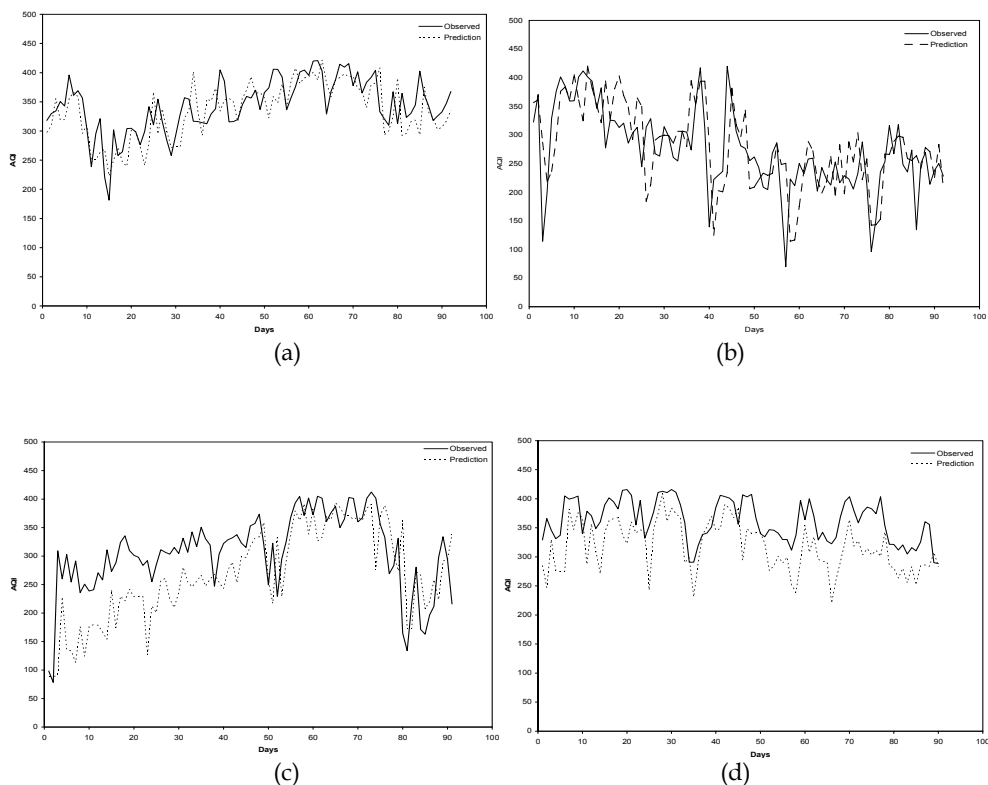


Fig. 4. Comparison of observed and ANN model forecasted values of daily AQI in (a) Summer, (b) Monsoon, (c) Post Monsoon and (d) Winter seasons during the year 2006.

The comparison of forecasted and observed values of AQI has been made through statistical parameters in Table 3, which reveals that the NMSE and coefficient of determination (R^2) are found as (0.0118, 0.4976) in summer season which are followed by (0.0277, 0.3986) in winter; (0.0540, 0.3619) in monsoon and (0.0718, 0.3816) in post monsoon seasons, showing good performance of the model as the ideal values of NMSE and R^2 are 0 and 1 respectively. The values of R^2 in four different seasons reflect that the model's forecasted and observed AQI could be correlated explained by the selected input variables as approximately 50% in summer, 40% in winter, 38% in post monsoon and 36% in monsoon seasons. However, the fractional bias shows the under-prediction in all the seasons except Monsoon.

S.N.	Season	2006			
		RMSE	NMSE	Coefficient of determination	Fractional Bias
1	Summer	36.88	0.0118	0.4976	0.0269
2	Monsoon	64.27	0.0540	0.3619	-0.0224
3	Post Monsoon	76.44	0.0718	0.3816	0.1355
4	Winter	56.52	0.0277	0.3986	0.1330

Table 3. Comparison of ANN model predicted and observed values in years 2000-2005 and year 2006

3.1.3 Comparison of MLR and ANN models

On the basis of above exercise, it can be seen that ANN model is giving better results than MLR model with respect to RMSE and NMSE as shown in Tables 2 and 3, although, the R² is showing almost same values in both the models throughout all four seasons.

3.2 Application of analytical models

The above discussed analytical model with Neumann boundary condition is applied to simulate the hourly concentration of RSPM in the month of January (representative of winter season) 2008 due to point, line and area sources. The most important parameters of the models are emission inventory and meteorological variables, which are pre-process according to the model's requirement.

A gridded emission inventory of RSPM has been developed over an area of 26 km x 30 km of Delhi. The total area has been divided into 195 square grids of size 2 km x 2 km. Emission of RSPM has been estimated in each grid due to all anthropogenic sources viz., domestic, industries, power plants and vehicles for the year 2008 using the primary and secondary data. The emission of RSPM from domestic sector has been calculated on the basis of fuel consumption data and the emission factor of the corresponding fuel. The emission estimation from industrial sources has been made by using the data obtained from concerned agencies / department. The emission of RSPM from power plants has been calculated on the basis of information given by Delhi Pollution Control Committee (DPCC). However, estimation of vehicular emission in each grid are made by using the following mathematical formulation, based on total number of registered vehicles, emission factors, vehicle kilometer traveled (VKT) of each type of vehicle, different type of roads:

$$E_i = N_i \times e_{fi} \times VKT_i \quad (75)$$

where N_i is the number of vehicle of i^{th} category, E_i is the emission of pollutant by vehicle of i^{th} category (g/day), e_{fi} is emission factor of i^{th} category vehicle for the pollutant (g/km-vehicle). VKT_i is vehicle kilometer travel per day for i^{th} category vehicle (km/day).

Further, the total emission of pollutant has been calculated by summing the emissions from each category of vehicles:

$$E = \sum_i E_i \quad (76)$$

The emissions of RSPM due to vehicular sources in Delhi for the year 2008 have been apportioned into each grid w. r. t. to the road lengths.

The gridded emission inventory shows the spatial distribution of emissions of RSPM due to all types of sources (domestic, industries, power plants and vehicles) in Fig. 5. The emission from domestic sources has been distributed uniformly in all the grids and the emission from industries and traffic intersections have been apportioned according to their locations. The emissions of RSPM due to three power plants namely Indraprastha, Badarpur and Rajghat are superimposed in the grids as per their locations. It has been found that vehicles are the major source, contributing 57% of RSPM among all the estimated sources, which is followed by power plants 29% of total RSPM. While the contributions of domestic and other industrial sources are 8% and 6% respectively. The Fig.5 reflects that grids, in which power plants are located in addition to traffic intersections and industries, have higher values of emissions compared to others. This emission inventory is used as input to the model.

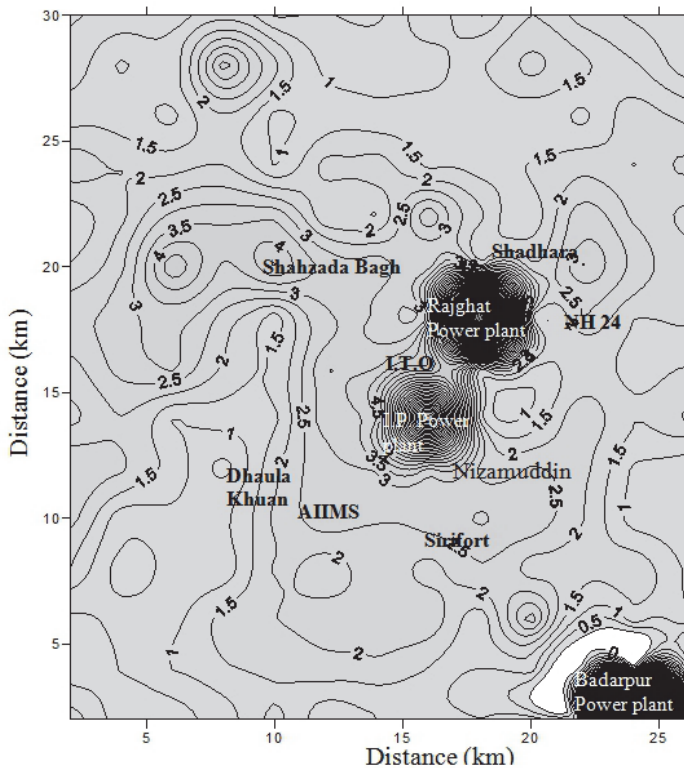


Fig. 5. Emission inventory of RSPM (g/s) over Delhi from all sources (point, line and area).

From an atmospheric pollution perspective, the most important season in Delhi is the winter lasting from December to February. This period is dominating by cold, dry air and ground based inversion with low wind conditions ($<1 \text{ ms}^{-1}$), which increase the concentration of pollutants (Anfossi et al., 1990). For practical reasons, the January month of 2008 is used in this case study. The hourly meteorological data, measured at Safdarjung Airport from India

Meteorological Department (IMD) is used as second input file to the models. There are some traditional methods, which are used to determination, the stability classes to produce the input in the model. The some traditional methods based on (i.) the wind velocity, sun radiation intensity and cloud cover; (ii.) measurement of the wind direction fluctuations; (iii.) the vertical temperature gradient; (iv.) the Richardson number can used to determination, the stability classes.

Day		Night			
Incoming Solar Radiation		Cloud Cover			
Surface wind speed at 10m (m/s)	Strong	Moderate		Mostly Overcast	Mostly Clear
		Slight			
<2	A	A-B	B	E	F
2-3	A-B	B	C	E	F
3-5	B	B-C	C	D	E
5-6	C	C-D	D	D	D
>6	C	D	D	D	D

Source: D.B. Turner. Workbook of Atmospheric Dispersion Estimate. USEPA 999-AP-26. U.S.

Environmental Protection Agency, Washington, D.C, 1969.

Note: A, strongly unstable; B, unstable; C, weakly unstable; D, neutral; E, weakly stable and F, stable.

Table 4. Stability Classification based on wind velocity, sun radiation intensity and cloud cover.

Stability Class	Stability class of Pasquill	σ_θ (in degree)	Vertical Temperature Gradient ($^{\circ}\text{C}/\text{m } 10^{-2}$)	Richardson Number at 2 m
Very unstable	A	25.0	<-1.9	-0.9
Moderately unstable	B	20.0	-1.9 to -1.7	-0.5
Slightly unstable	C	15.0	-1.7 to -1.5	-0.15
Neutral	D	10.0	-1.5 to -0.5	0
Slightly stable	E	5.0	-0.5 to 1.5	0.4
Moderately stable	F	2.5	1.5 to 4.0	0.8

Source: Zannetti, P., Air Pollution Modelling, Computational Mechanics Publications, Southampton, U.K. and Van Nostrand Reinhold, New York, 1990.

Note: σ_θ is the standard deviation of horizontal wind direction.

Table 5. Classification of Atmospheric Stability based on wind direction fluctuations, vertical temperature gradient and the Richardson number.

In this study atmospheric stability is measured on the basis of surface wind speed, cloud cover and solar insolation (strong, moderate, slight). These stability are classified according to Pasquill's stability classes of A, B, C, D, E and F, which range from extremely unstable to extremely stable as given by Turner (1969). The dispersion parameters have also been calculated based on the stability parameters as discussed in section 2.

In the above solutions discussed in section 2, the exponent α has relationship with Pasquill's Stability Classes (Hanna et al., 1982) and $\beta=1-\alpha$ is based on the Schmidt's conjugate law.

Pasquill's Stability Classes	A	B	C	D	E	F
α for Urban	0.15	0.15	0.20	0.25	0.40	0.60

Table 6. Approximate Correspondence between Pasquill's Stability Classes and alpha (α) (Hanna, 1982).

In these formulations $f(x)$ is expressed as a linear function of downwind distance as $f(x) = \gamma \bar{U}x$. In this function \bar{U} is average velocity and γ is turbulence parameter. This turbulence parameter γ is parameterized as the square of turbulent intensity using Taylor statistical theory of diffusion $\gamma = \left(\frac{\sigma_w}{\bar{U}}\right)^2$ (Arya, 1995; 1999). Turbulent intensity can be expressed as $\left(\frac{\sigma_w}{\bar{U}}\right) = \tan(\sigma_\phi)$, where σ_ϕ is the standard deviation of vertical wind direction in radians. For small σ_ϕ , the turbulent intensity which is also depends on atmospheric stability is approximated as (Arya, 1999): $\left(\frac{\sigma_w}{\bar{U}}\right) = \sigma_\phi$.

Pasquill's Stability Classes	A	B	C	D	E	F
σ_ϕ	≥ 11.5	10.0-11.5	7.8-10.0	5.0-7.8	2.4-5.0	< 2.4

Table 7. Approximate Correspondence between Pasquill's Stability Classes and Turbulence parameters σ_ϕ (Arya, 1999).

In the above solutions, standard deviation of concentration distribution in crosswind direction is represented by a power of downwind distance $\sigma_y = Rx^r$ (Seinfeld, 1986). These R and r are constants as depending on the atmospheric stability.

Source	Coefficient	Stability Class					
		A	B	C	D	E	F
(Turner, 1969; Martin, 1976)	R	0.443	0.324	0.216	0.141	0.105	0.071
	r	0.894	0.894	0.894	0.894	0.894	0.894

Table 8. Approximate Correspondence between Pasquill's Stability Classes and Gaussian plume dispersion parameters (Seinfeld, 1986).

The 24 hourly averaged ground level concentration of RSPM from point, line and area sources for Jan 2008 has been obtained by using the emission inventory and meteorological data as input parameters to the models. The power plants are considered as the point sources. Most of the analytical methods for predicting the concentration from stack need the plume rise height (Δh) of stack (power plants). There are numerous methods for calculating the plume rise height; in this study it has been calculated, given by Carpenter et al., 1970:

$$\Delta h = \frac{114G(I)^{1/3}}{u}, \quad (77)$$

where $I = gV_s d^2(T_s - T_a) / 4T_a$, m^4s^{-3} ; $G = 1.58 - 41.4 \left(\frac{\Delta\theta}{\Delta z} \right)$, dimensionless; $\left(\frac{\Delta\theta}{\Delta z} \right)$ = potential temperature gradient, $^{\circ}K/m$; the constant 114 in this equation has unit of $m^2/3$; V_s is the stack gas exit velocity, in m/s ; d is the stack exit diameter in m ; u is the speed at the stack exit in m/s ; T_s is the stack gas temperature; T_a is the environmental temperature and g is the gravitational acceleration, m/s^2 . This method is especially useful because the potential temperature gradient factor is used for adjusting the different stability conditions.

The spatial distribution of RSPM concentration obtained from models (Eqs. (58), (64) and (68)) with background concentration $40 \mu g/m^3$ for Delhi (Kansal et al., 2011) is shown in Fig. 2 in the form of isopleths, which indicates the hot spots of RSPM ranging from 300-800 $\mu g/m^3$ at different locations namely I.T.O., Nizamuddin, Badarpur power station, I.P. powers station, Rajghat power station, AIIMS, Sirifort and Dhaula Khuan, which are major traffic intersections or power plants. This figure also shows the higher concentration near the Shahzada Bagh, which has maximum number of industries.

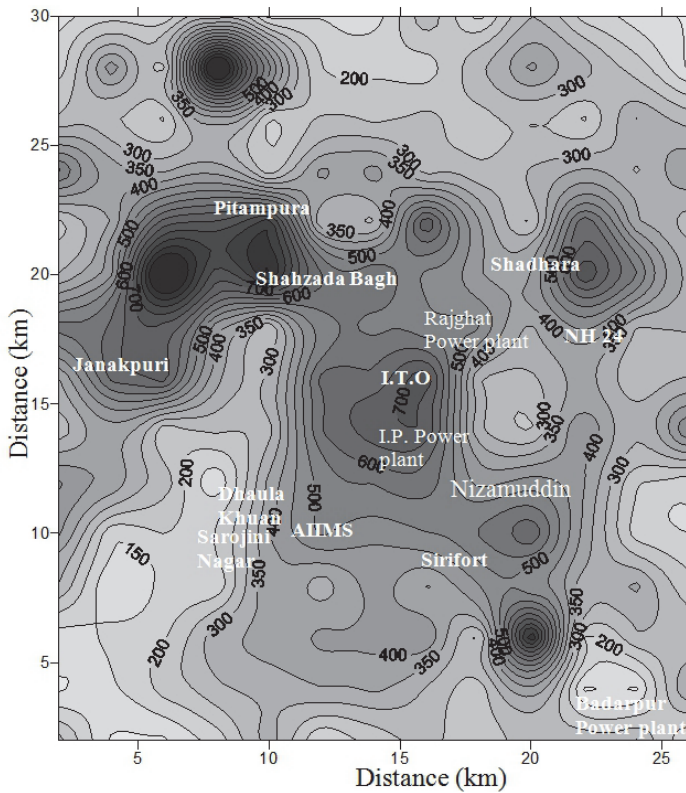


Fig. 6. 24 hourly averaged concentration of RSPM ($\mu g/m^3$) due to all types of sources in Jan 2008.

The concentrations of RSPM, cumulative sum of concentrations due to point, line and area sources, is evaluated against observed concentrations obtained from CPCB and NEERI, at different locations, as shown in Table 9.

Location	Observed ($\mu\text{g}/\text{m}^3$)	Model predicted ($\mu\text{g}/\text{m}^3$)	National Ambient Air Quality Standard ($\mu\text{g}/\text{m}^3$)
Pitampura	353.00	411.30	100.00
Sirifort	374.00	449.45	100.00
Janakpuri	279.00	345.49	100.00
Shahzada Bagh	478.74	603.01	100.00
Sarojini Nagar	363.77	401.28	100.00

Table 9. Comparison of 24 hourly averaged predicted and observed concentration of RSPM at different locations in Delhi in Jan 2008.

The table 9 shows that the models predictions are higher than observed as well as NAAQS. However, these values are well within a factor of two of observed values, which satisfies the criteria of Chang and Hanna (1982) for assessing the performance of the model with conclusion that the models are performing satisfactory.

4. Conclusion

In the present study, the statistical (linear and non-linear) and analytical dispersion models of air pollutants released from point, line and area sources are discussed. Air quality index has been forecasted using MLR and ANN models. Performance of both the modes has been compared and observed that ANN model is doing better than MLR.

The analytical models are formulated by considering the wind speed as a power law profile of vertical height above the ground and vertical eddy diffusivity as an explicit function of downwind distance and vertical height in different boundary conditions. A case study of Delhi has been made for predict 24 hourly concentration of RSPM through the application models with Neumann boundary condition in the month of Jan 2008. The input parameters namely emission inventory and meteorological variables are pre-processed as per the requirement of the model. The different types of primary and secondary sources of RSPM due to vehicular, domestic, industries and power plants have been used in emission inventory for year 2008. Some traditional methods for determining the meteorological field are also discussed in this chapter, which are used as an input to these analytical models. The analytical models are evaluated with observed concentration at different locations in Delhi obtained from CPCB and NEERI, which show that the concentration levels obtained from the models are always high in comparison to the observed values and NAAQS. However, the models are performing satisfactory. Although the present models have the limitation as the longitudinal diffusion is neglected in comparison to the advection and are not considering the wind directions at different vertical heights. These models can be used for other Indian urban cities.

5. Appendix A

The statistical measures, which have been used for statistical evaluation of the performance of models has been given by Chang & Hanna (2004) as follows:

5.1 Coefficient of correlation (R)

Coefficient of correlation (R) is relative measure of the association between the observed and predicted values. It can vary from 0 (which indicates no correlation to ± 1 (which indicates perfect correlation). A value of R close to 1.0 implies good agreement between the observed and predicted values i.e. good model performance.

$$R = \frac{(\overline{C_o - \bar{C}_o})(\overline{C_p - \bar{C}_p})}{\sigma_{C_p} \sigma_{C_o}}$$

5.2 Coefficient of determination (R²)

Coefficient of determination (R²), which is the square of coefficient of correlation, determines the proportion of variance that can be explained by the model.

5.3 Root Mean Square Error (RMSE)

RMSE, is a measure of the differences between values predicted by a model and the observed values and is expressed as follows:

$$RMSE = \sqrt{\overline{(C_o - C_p)^2}}$$

5.4 Normalized Mean Square Error (NMSE)

NMSE, as a measure of performance, emphasizes the scatter in the entire data set and is defined as follows:

$$NMSE = \frac{\overline{(C_o - C_p)^2}}{\bar{C}_o \cdot \bar{C}_p}$$

The normalization by $\bar{C}_o \cdot \bar{C}_p$ ensures that NMSE will not be biased towards models that over predict or under predict. Ideal value for NMSE is zero. Smaller values of NMSE denote better model performance.

5.5 Fractional Bias (FB)

It is a performance measure known as the normalized or fractional bias of the mean concentrations:

$$FB = \frac{(\bar{C}_o - \bar{C}_p)}{0.5(\bar{C}_o + \bar{C}_p)},$$

where:

C_p : model predictions,

C_o : observations,

Overbar ($\bar{}$): average over the dataset, and

σ_C : standard deviation over the data set.

6. References

- Abramowitz, M. & Stegun, I.A. (1972). Handbook of Mathematical Functions with Formulas, Graphs and Mathematical Tables. 9th printing. Dover Publications, New York.
- Anfossi, D.; Brisasca, G. & Tinarelli, G. (1990). Simulation of atmospheric diffusion in low wind speed meandering conditions by a Monte Carlo dispersion model. *IL Nuovo Climento*. 13 C, 995-1006.
- Aron, R. & Aron, I. M. (1978). Statistical forecasting models: I. Carbon monoxide concentrations in the Los Angeles basin. *Journal of Air Pollution Control Association* 28, 681-684.
- Aron, R. (1984). Models for estimating current and future sulphur dioxide concentrations in Taipei. *Bulletin of Geophysics* 25, 47-52.
- Arya, S.P. (1995). Modeling and parameterization of near source diffusion in weak winds. *Journal of Applied Meteorology*, 34, 1112-1122.
- Arya, S.P. (1999). *Air Pollution Meteorology and Dispersion*. Oxford University Press, New York.
- Boznar, M.; Lesjak, M. & Mlakar, P. (1993). A neural network-based method for short-term predictions of ambient SO₂ concentrations in highly polluted industrial areas of complex terrain. *Atmospheric Environment B27(2)*, 221-230.
- Brown, M.J.; Arya, S.P. & Snyder, W.H. (1997). Plume descriptors derived from a non-Gaussian concentration model. *Atmospheric Environment* 31, 183-189.
- Carpenter, S.B.; Montgomery, T.; Leavitt, J.M.; Colbaugh, W.C. & Thomas, F.W. (1970). Principal plume dispersion models, TVA power plants. 63rd Annual Meeting, Air Pollution Control Association, June 1970.
- Chang, J.C. & Hanna, S.R. (2004). Air quality model performance evaluation. *Meteorology and Atmospheric Physics*, 87, 167-196.
- Cogliani, E. (2001). Air pollution forecast in cities by an air pollution index highly correlated with metrological variables. *Atmospheric Environment* 35, 2871-2877.
- Comrie, A. C. (1997). Comparing neural networks and regression models for ozone forecasting. *Journal of air and waste management association* 47, 653-663.
- Demuth, C.I. (1978). A contribution to the analytical steady solution of the diffusion equation for line sources. *Atmospheric Environment*, 12, 1255-1258.
- EPA (1999). Air quality index Reporting Final Rule 1999-Federal Register, Part III, CFR Part 58.
- Gardner, M. W. & Dorling (1999). Neural network modelling and prediction of hourly NO_x and NO₂ concentrations in urban air in London. *Atmospheric Environment* 33, 709-719.
- Hanna, S.R.; Briggs, G.A. & Hosker, R.P. Jr. (1982). Handbook on Atmospheric Diffusion. Atmospheric Turbulence and Diffusion Laboratory National Oceanic and Atmospheric Administration.
- Hinrichsen K. (1986). Comparison of four analytical dispersion models for near-surface releases above a grass surface. *Atmospheric Environment* 20, 29-40.
- Huang, C.H. (1979). A theory of dispersion in turbulent shear flow. *Atmospheric Environment*, 13, 453-463.
- Irwin, J. S.; Petersen, W. B. & Howard, S. C. (2007). Probabilistic characterization of atmospheric transport and diffusion. *Journal of Applied Meteorology*, 46, 980-993.
- Kansal, A.; Khare, M. & Sharma, C.S. (2011). Air quality modelling study to analyse the impact of the World Bank emission guidelines for thermal power plants in Delhi. *Atmospheric Pollution Research*, 2 (2011), 99-105.
- Katsoulis, B. D. (1988). Some meteorological aspects of air pollution in Athens, Greece. *Meteorology and Atmospheric Physics*, 39, 203-212.

- Lin, G. Y. (1982). Oxidant prediction by discriminant analysis in the South coast air basin of California. *Atmospheric Environment*, 16, 135-143.
- Lin, J.S. & Hildemann, L.M. (1996). Analytical solutions of the atmospheric diffusion equation with multiple sources and height-dependent wind speed and eddy diffusivity. *Atmospheric Environment*, 30, 239-254.
- Mantis, H. T.; Repapis, C. C.; Zerefos, C. S. & Ziomas, J. C. (1992). Assessment of the potential for photochemical air pollution in Athens: a comparison of emissions and air pollutant levels in Athens with those in Los Angeles. *Journal of Applied Meteorology*, 31, 1467-1476.
- Martin, D.O. (1976). Comment on the change of concentration standard deviation with distance. *Journal of Air Pollution Control Association*, 26, 145-146.
- McCollister, G. M. & Wilson, K. R. (1975). Linear stochastic models for forecasting daily maxima and hourly concentrations of air pollutants. *Atmospheric Environment*, 9, 417-423.
- Milionis, A. E. & Davies, T. D. (1994). Regression and stochastic models for air pollution I. review, comments and suggestions. *Atmospheric Environment*, 28 (17), 2801-2810.
- Mooney, C.J. & Wilson, J.D. (1993). Disagreements between gradient-diffusion and Lagrangian stochastic dispersion models, even for surface near the ground. *Boundary Layer Meteorology*, 64, 291-296.
- Park, Y.S. & Baik, J.J. (2008). Analytical solution of the advection-diffusion equation for a ground-level finite area source. *Atmospheric Environment*, 42, 9063-9069.
- Robeson, S. M. & Steyn, D. G. (1990). Evaluation and comparison of statistical forecast models for daily maximum ozone concentrations. *Atmospheric Environment*, 24B, 303-312.
- Sanchez, M. L.; Pascual, D.; Ramos, C. & Perez, I. (1990). Forecasting particulate pollutant concentrations in a city from meteorological variables and regional weather patterns. *Atmospheric Environment*, 24A (6), 1509-1519.
- Seinfeld, J.H. (1986). *Atmospheric Chemistry and Physics of Air Pollution*. Wiley-Interscience, New York.
- Sharan, M. & Kumar P. (2009). An analytical model for crosswind integrated concentration released from a continuous source in a finite atmospheric boundary layer. *Atmospheric Environment*, 43, 2268-2277.
- Sharan, M. & Modani, M. (2006). A two-dimensional analytical model for the dispersion of air-pollutants in the atmosphere with a capping inversion. *Atmospheric Environment*, 40, 3479-3489.
- Shi, J. P. & Harrison, R. M. (1997). Regression Modelling of Hourly NO_x and NO₂ concentrations in urban air in London. *Atmospheric Environment*, 31(24), 4081-4097.
- Shiva Nagendra, S. M.; Venugopal, K. & Jones, S. L. (2007). Assesment of air quality near traffic intersections in Bangalore city using air quality index. *Transportation Research Part D*, 12, 167-176.
- Stull, R.B. (1988). *An Introduction to Boundary Layer Meteorology*. Kluwer Academic, p. 666.
- Taylor, G.I. (1921). Diffusion by continuous movements. *Proc. London Math. Soc. Ser 2*
- Tirabassi, T. (2010). Mathematical air pollution models: Eulerian models, in *Air pollution and turbulence modeling and application*, D. Moreira and M. Vilhena, pp. (131-155), CRC press, 978-1-4398-1144-3, New York.
- Turner, D.B. (1969). *Workbook of Atmospheric Diffusion Estimates*. USEPA 999-AP-26. U.S. Environmental Protection Agency, Washington, D.C.
- Wassermann, P. D. (1989). *Neural Computing Theory and Practice*. New York Van Nostrand Reinhold, 196-212.
- Zannetti, P. (1990). *Air Pollution Modelling*, Computational Mechanics Publications, Southampton, U.K. and Van Nostrand Reinhold, New York.

A Gibbs Sampling Algorithm to Estimate the Occurrence of Ozone Exceedances in Mexico City

Eliane R. Rodrigues¹, Jorge A. Achcar² and Julián Jara-Ettinger³

¹*Instituto de Matemáticas, Universidad Nacional Autónoma de México*

²*Faculdade de Medicina de Ribeirão Preto, Universidade de São Paulo*

³*Facultad de Ciencias Físico-Matemáticas, Universidad Michoacana*

^{1,3}*Mexico*

²*Brazil*

1. Introduction

Inhabitants of many cities around the world suffer the effects of high levels of ozone air pollution. When the ozone concentration stays above the threshold of 0.11 parts per million (0.11ppm) for a period of one hour or more, a very sensitive part of the population (e.g. elderly and newborn) in that environment may experience serious health deterioration (Bell et al., 2004, 2005, 2007; Gauderman et al., 2004; Loomis et al., 1996; O'Neill et al., 2004; WHO, 2006). Therefore, being able to predict when exceedances of the 0.11ppm threshold (or any threshold above this value) may occur is a very important issue.

Depending on the country, different thresholds may be considered to declare environmental alerts. The US Environmental Protection Agency (US-EPA) has established as its standard that the three-year average of the fourth highest daily maximum 8-hour average ozone concentration measured at each monitor within an area over each year must not exceed 0.075ppm (see EPA, 2008). In the case of Mexico, the standard is 0.11ppm and an individual should not be exposed, on average, for a period of an hour or more (NOM, 2002). In Mexico City when the ozone concentration surpasses the threshold 0.2ppm an emergency alert is issued and measures are taken to prevent population exposure to the pollutant (see <http://www.sma.df.gob.mx>).

It is possible to find in the literature a large number of works focussing on the study of the behaviour of air pollutants in general. Among the ones related to ozone air pollution we may quote, Horowitz (1980), Roberts (1979a, 1979b), Smith (1989) considering extreme value theory; Flaum et al. (1996), Gouveia & Fletcher (2000), Kumar et al. (2010), Lanfredi & Macchiato (1997) and Pan & Chen (2008) using time series analysis; Álvarez et al. (2005) and Austin & Tran (1999) considering Markov chain models; Achcar et al. (2008b, 2009a, 2009b) using stochastic volatility models; and Huerta & Sansó (2005) with an analysis of the behaviour the maximum measurements of ozone with an application to the data from Mexico City. Davis (2008) and Zavala et al. (2009) present studies that analyse the impact on air quality of the driving restriction imposed in Mexico City.

When the aim is to estimate the number of times that a given environmental standard is surpassed, Raftery (1989) and Smith (1989) use time homogeneous Poisson processes to model

this event. Aiming to overcome the time homogeneity hypothesis, Achcar et al. (2008a, 2010, 2011) consider non-homogeneous Poisson processes. However, one shortcoming of those works is that they estimate the parameters involved in the model using the Gibbs sampling algorithm internally implemented in the software WinBugs. One particular problem that occurred when using the data set from the monitoring network of Mexico City was that the software was very slow and sometimes, convergence of the algorithm could not be achieved unless very informative prior distributions were used. In the present work we keep the assumption of a non-homogeneous Poisson process. However, the estimation of the parameters of the intensity function of this Poisson process is made using a combination of Gibbs sampling and Metropolis-Hasting type algorithms implemented using the R software. The algorithm produces very fast running time (with rare exceptions) even with non informative prior distributions. We are going to apply the theoretical part of this work to the ozone data provided by the monitoring network of the Metropolitan Area of Mexico City. The Metropolitan Area is divided into five regions or sections corresponding to the Northeast (NE), Northwest (NW), Centre (CE), Southeast (SE) and Southwest (SW) and the ozone monitoring stations are placed throughout the city (see Álvarez et al., 2005; Achcar et al., 2008a and <http://www.sma.df.gob.mx>). We are going to analyse the data for each region separately. Even though the threshold to emit an environmental alert in Mexico City is 0.2ppm, we are going to consider the threshold 0.17ppm in order to see how the frequency of environmental alerts is affected if 0.17ppm were the new threshold for declaring that type emergency.

This work is organised as follows. In Section 2, the basic assumptions of the Poisson models are presented. Section 3 describes the Bayesian formulation used. In Section 4, the Gibbs sampling and the Metropolis-Hastings algorithms used to estimate the parameters of the intensity functions of the Poisson models are described as well as the methodology used to select the best model fitting the data considered. An application to the case of ozone measurements in Mexico City is given in Section 5. Finally, in Section 6 some comments about the results obtained are presented. The codes of the R programmes used to estimate the parameters of the models are given in an Appendix before the list of references.

Remark. In here the notation $X \sim F$ is used to indicate that the random variable X has distribution function F .

2. Some non-homogeneous Poisson models

There are several works that use non-homogeneous Poisson model to study problems in a wide variety of research areas (see for example Achcar, 2001; Achcar et al., 1998; Ramírez-Cid & Achcar, 1999; Wilson & Costello, 2005, among others). As in Achcar et al. (2008a, 2010, 2011), in here, non-homogeneous Poisson processes are used as models to estimate the probability that an ozone measurement surpasses a given threshold a certain number of times in a time interval of interest. However, in here we focus mainly in the behaviour of the mean of the Poisson process. The description of the models considered here are given as follows.

Let $N_t \geq 0$ record the number of times that a given threshold for a given pollutant is surpassed in the time interval $[0, t)$, $t \geq 0$. We assume that $N = \{N_t : t \geq 0\}$ follows a Poisson process which is non-homogeneous in time and with rate function $\lambda(t) > 0$, $t \geq 0$. Therefore, at time t , the random variable N_t has Poisson distribution with rate function $\lambda(t)$ and mean function

$$m(t) = \int_0^t \lambda(s) ds, \text{ i.e., for } k = 0, 1, \dots \text{ and } s, t \geq 0,$$

$$P(N_{t+s} - N_t = k) = \frac{[m(t+s) - m(t)]^k}{k!} \exp(-[m(t+s) - m(t)]). \tag{1}$$

The function $\lambda(t), t \geq 0$, will depend on some parameters that need to be estimated. Once those parameters are estimated, the resulting form for $\lambda(t)$ may be substituted in (1) and the corresponding probabilities may be calculated. Additionally, since the rate function is related to the rate at which a surpassing occurs, we are able to obtain information on that as well.

There are several forms that $\lambda(t), t \geq 0$, may assume. Based on the information provided by previous works, we are going to consider three forms for the rate function. They are given by the Weibull (W), Musa-Okumoto (MO) (Musa & Okumoto, 1984), and a generalised form of the Goel-Okumoto (GGO) (Goel & Okumoto, 1978) models, i.e.,

$$\lambda^{(W)}(t) = (\alpha/\sigma) (t/\sigma)^{\alpha-1}, \tag{2}$$

$$\lambda^{(MO)}(t) = \beta/(t + \alpha), \tag{3}$$

$$\lambda^{(GGO)}(t) = \alpha\beta\gamma t^{\gamma-1} e^{-\beta t^\gamma}, \tag{4}$$

respectively. Hence, the vectors of parameters to be estimated are $\theta = (\alpha, \sigma), (\alpha, \beta) \in \mathbb{R}_+^2$, in (2) and (3), respectively, and is $\theta = (\alpha, \beta, \gamma) \in \mathbb{R}_+^3$ in (4).

The problem is reduced to estimating the vector of parameters that produces the behaviour of $\lambda(t), t \geq 0$ that more adequately fits the situation presented by the ozone measurements of the Mexico City monitoring network. In order to do so, a Bayesian approach will be used.

Remark. Note that, even though the rate functions (2), (3) and (4) have been considered in past works, the interest here is to analyse the fitting for more recent data. That is justified by the fact that the year 2000 was the point in time where the last of a series of important measures to control pollution emission were taken by the environmental authorities in Mexico City. Previous preliminary analysis shows that the behaviour of the daily maximum ozone measurements have changed.

3. A Bayesian formulation of the model

In this section a Bayesian formulation of the model is presented in which the likelihood function follows a Poisson model with rate function that is time dependent. The aim is to estimate the parameters describing this rate function. Therefore, assume that there are $K \geq 1$ days in which a given threshold is surpassed by the daily maximum ozone measurement. Let d_1, d_2, \dots, d_K be those days and denote by $\mathbf{D} = \{d_1, d_2, \dots, d_K\}$ the set of observed data. There is a natural relationship among posterior and prior distributions and the likelihood function of the model which is given by

$$P(\theta | \mathbf{D}) \propto L(\mathbf{D} | \theta) P(\theta) \tag{5}$$

where $P(\theta | \mathbf{D})$ and $P(\theta)$ are the posterior and the prior distributions of the vector of parameters θ , respectively, and $L(\mathbf{D} | \theta)$ is the likelihood function of the model. The components of (5) are given as follows.

1. **The likelihood function.** Since a non-homogeneous Poisson model has been assumed, we have that the likelihood function will take the form (see for instance Cox & Lewis, 1966; Lawless, 1986)

$$L(\mathbf{D} | \theta) = \left[\prod_{i=1}^K \lambda(d_i) \right] \exp(-m(d_K)), \quad (6)$$

where θ is the vector of parameters. The likelihood function takes different forms depending on the expression for the rate function $\lambda(t)$, $t \geq 0$. Hence, taking that into account we have the following.

In the case of the Weibull function given by (2), we have that $m^{(W)}(t) = (t/\sigma)^\alpha$, and therefore,

$$L^{(W)}(\mathbf{D} | \alpha, \sigma) \propto \left(\frac{\alpha}{\sigma^\alpha}\right)^K \left(\prod_{i=1}^K d_i^{\alpha-1}\right) \exp[-(d_K/\sigma)^\alpha]. \quad (7)$$

When considering the Musa-Okumoto function given by (3), we have that $m^{(MO)}(t) = \beta \log(1 + t/\alpha)$, and then,

$$L^{(MO)}(\mathbf{D} | \alpha, \beta) \propto \beta^K \left(\prod_{i=1}^K \frac{1}{d_i + \alpha}\right) \exp[-\beta \log(1 + d_K/\alpha)]. \quad (8)$$

In the case of the generalised Goel-Okumoto function given by (4), we have that the mean is $m^{(GGO)}(t) = \alpha [1 - \exp(-\beta t^\gamma)]$, and therefore,

$$L^{(GGO)}(\mathbf{D} | \alpha, \beta, \gamma) \propto (\alpha\beta\gamma)^K \left(\prod_{i=1}^K d_i^{\gamma-1}\right) \exp\left(-\beta \sum_{i=1}^K d_i^\gamma\right) \exp\left[-\alpha \left(1 - e^{-\beta d_K^\gamma}\right)\right]. \quad (9)$$

2. **The prior distributions.** Assuming prior independence among the parameters of each model considered we have the following prior distributions. In the case of the Weibull intensity (2), in a first instance we consider for all regions and parameters, uniform prior distributions defined on appropriate intervals. In a second instance, we take Beta(a_1, b_1) and Gamma(a_2, b_2) prior distributions for α and σ , respectively. (In here, we are denoting by Beta(a, b) and Gamma(c, d) the Beta and Gamma distributions with means $a/(a+b)$ and c/d , respectively, and variances $ab/[(a+b)^2(a+b+1)]$ and c/d^2 , respectively.) When considering the intensity function (3) we take uniform prior distributions, with appropriate hyperparameters, for all parameters and regions. In the case of the intensity function (4) we assume that α and β have uniform prior distributions (with appropriate hyperparameters) for all regions. In the case of the parameter γ we have $\gamma \sim \text{Gamma}(a_3, b_3)$ for all regions. The hyperparameters a_i and b_i , for $i = 1, 2, 3$ are considered to be known and will be specified later. They will be such that either we have non-informative prior distributions or using prior information of experts we have informative prior distributions for the parameters of each model.

3. **The posterior distributions.** The posterior distributions for the models considered here have the following forms. In the case of the Weibull intensity (2), we have that

$$P(\alpha, \sigma | \mathbf{D}) \propto \alpha^{a_1+K-1} (1-\alpha)^{b_1-1} \sigma^{a_2-\alpha K-1} e^{-b_2\sigma} \left[\prod_{i=1}^K d_i^{\alpha-1} \right] \exp[-(d_K/\sigma)^\alpha]. \tag{10}$$

Remark. In the case of uniform prior distributions for α and σ , we have that $P(\alpha, \sigma | \mathbf{D}) \propto (\alpha/\sigma^\alpha)^K \left[\prod_{i=1}^K d_i^{\alpha-1} \right] \exp[-(d_K/\sigma)^\alpha]$.

When considering $\lambda(t)$ given by (3), we have that,

$$P(\alpha, \beta | \mathbf{D}) \propto \beta^K \left(\prod_{i=1}^K \frac{1}{d_i + \alpha} \right) \exp\left(-\beta \log\left[1 + \frac{d_K}{\alpha}\right]\right). \tag{11}$$

In the case of $\lambda(t)$ given by (4) we have that

$$P(\alpha, \beta, \gamma | \mathbf{D}) \propto (\beta \alpha)^K \gamma^{K+a_3-1} e^{-\gamma b_3} \exp\left[-\alpha \left(1 - e^{\beta d_K^\gamma}\right)\right] \exp\left[-\beta \left(\sum_{i=1}^K d_i^\gamma\right)\right] \left[\prod_{i=1}^K d_i^{\gamma-1}\right]. \tag{12}$$

4. Conditional marginal posterior distributions, a Gibbs sampling and a Metropolis-Hasting algorithm

In order to simulate values from the joint posterior distribution in each model, we use a combination of Gibbs and Metropolis-Hastings type algorithm (see Metropolis et al., 1953; Hastings, 1970; Gelfand & Smith, 1990). The estimation of the parameters in each model will be made through a sample obtained from their complete marginal conditional posterior distribution using a Metropolis-Hasting algorithm. The values obtained are used in the next step of the Gibbs sampling. The complete marginal conditional posterior distributions in each model are given as follows.

1. In the case of the Weibull intensity (2) and complete posterior distribution given by (10), we have that

$$P(\alpha | \sigma, \mathbf{D}) \propto \psi_1(\alpha, \sigma) \alpha^{a_1-1} (1-\alpha)^{b_1-1}$$

$$P(\sigma | \alpha, \mathbf{D}) \propto \psi_2(\alpha, \sigma) \sigma^{a_2-1} e^{-b_2\sigma},$$

where

$$\psi_1(\alpha, \sigma) = \exp\left[K \log(\alpha) - K\alpha \log(\sigma) + (\alpha - 1) \sum_{i=1}^K \log(d_i) - \left(\frac{d_K}{\sigma}\right)^\alpha\right],$$

$$\psi_2(\alpha, \sigma) = \exp\left[-K\alpha \log(\sigma) - \left(\frac{d_K}{\sigma}\right)^\alpha\right].$$

Remark. In the case of uniform prior distribution for α and σ we have that $P(\alpha | \sigma, \mathbf{D}) \propto \psi_1(\alpha, \sigma)$ and $P(\sigma | \alpha, \mathbf{D}) \propto \psi_2(\alpha, \sigma)$.

2. When considering the intensity function given by (3) we have that

$$\begin{aligned} P(\alpha | \beta, \mathbf{D}) &\propto \psi_3(\alpha, \beta), \\ P(\beta | \alpha, \mathbf{D}) &\propto \psi_4(\alpha, \beta), \end{aligned}$$

where

$$\begin{aligned} \psi_3(\alpha, \beta) &= \exp \left[- \sum_{i=1}^K \log(d_i + \alpha) - \beta \log \left(1 + \frac{d_K}{\alpha} \right) \right], \\ \psi_4(\alpha, \beta) &= \exp \left[K \log(\beta) - \beta \log \left(1 + \frac{d_K}{\alpha} \right) \right], \end{aligned}$$

i.e., conditioned on α and \mathbf{D} , $\beta \sim \text{Gamma}(K, \log(1 + d_K/\alpha))$

3. In the case of the intensity function (4) we have

$$\begin{aligned} P(\alpha | \beta, \gamma, \mathbf{D}) &\propto \psi_5(\alpha, \beta, \gamma), \\ P(\beta | \alpha, \gamma, \mathbf{D}) &\propto \psi_6(\alpha, \beta, \gamma), \\ P(\gamma | \alpha, \beta, \mathbf{D}) &\propto \psi_7(\alpha, \beta, \gamma) \gamma^{\alpha_3-1} e^{-b_3 \gamma}, \end{aligned}$$

where

$$\begin{aligned} \psi_5(\alpha, \beta, \gamma) &= \exp \left[K \log(\alpha) - \alpha \left(1 - e^{-\beta d_K^\gamma} \right) \right], \\ \psi_6(\alpha, \beta, \gamma) &= \exp \left[K \log(\beta) + \alpha e^{-\beta d_K^\gamma} - \beta \sum_{i=1}^K d_i^\gamma \right], \\ \psi_7(\alpha, \beta, \gamma) &= \exp \left[K \log(\gamma) + \alpha e^{-\beta d_K^\gamma} - \beta \sum_{i=1}^K d_i^\gamma + (\gamma - 1) \sum_{i=1}^K \log(d_i) \right]. \end{aligned}$$

Note that from the forms of most of the marginal conditional distributions obtained here it is not straightforward to obtain sampled values of the parameters directly from them. Hence, we are going to obtain a sample by using a Metropolis-Hastings algorithm.

We sample the proposed values for the parameters using their respective prior distributions. Therefore, if $\boldsymbol{\theta} = (\theta_1, \theta_2, \dots, \theta_n)$ is the vector of parameters in the present step of the algorithm, then the acceptance probability in the Metropolis-Hastings algorithm is given by

$$q(\theta_j, \theta'_j) = \min \left\{ 1, \frac{\psi_l(\theta'_j, \boldsymbol{\theta}_{(-j)})}{\psi_l(\theta_j, \boldsymbol{\theta}_{(-j)})} \right\}, \quad j = 1, 2, \dots, n, \quad (13)$$

where $\boldsymbol{\theta}' = (\theta'_1, \theta'_2, \dots, \theta'_n)$ is the proposed vector where each coordinate was sampled using its prior distribution, $\boldsymbol{\theta}_{(-j)}$ is the vector $\boldsymbol{\theta}$ without its j th coordinate and ψ_l is the appropriate ψ function that appears in the expression for the marginal conditional distributions.

In order to select the model that best explains the behaviour of the data considered here, we use the plots of the Monte Carlo estimates for $m(t)$ based on the simulated samples versus t and the accumulated number of occurrences up to t versus time. If the curves are similar,

we have an indication of a good fit of the proposed model to the data. We also consider a Bayesian discrimination method. Hence, from Raftery (1996) we have that the marginal likelihood function of the whole data set \mathbf{D} for Model $l, l = 1, 2, \dots, J$ is given by

$$V_l = \int L(\mathbf{D} | \theta^{[l]}) P(\theta^{[l]}) d\theta^{[l]} \tag{14}$$

where $\theta^{[l]}$ is the vector of parameters for Model l and $P(\theta^{[l]})$ is the joint prior distribution for $\theta^{[l]}$. The Bayes factor criterion prefers Model i to Model j if $V_j/V_i < 1$. A Monte Carlo estimate for the marginal likelihood V_l is given by

$$\hat{V}_l = \frac{1}{M} \sum_{i=1}^M L(\mathbf{D} | \theta^{[l,i]}) \tag{15}$$

where M is the size of the simulated Gibbs sample and $\theta^{[l,i]}, i = 1, 2, \dots, M$ is the sample obtained when considering the Model $l, l = 1, 2, \dots, J$.

5. An application to the ozone measurements in Mexico City

In this section we apply the results described in earlier sections to the case of daily maximum ozone measurements from the monitoring network of the Metropolitan Area of Mexico City. The data used in the analysis (obtained from <http://www.sma.df.gob.mx/simat/>) corresponds to seven years (from 01 January 2003 to 31 December 2009) of the daily maximum measurements in each region. The measurements are obtained minute by minute and the averaged hourly result is reported at each station. The daily maximum measurement for a given region is the maximum over all the maximum averaged values recorded hourly during a 24-hour period by each station placed in the region. The seven-year average measurements in regions NE, NW, CE, SE and SW are 0.085, 0.097, 0.098, 0.101 and 0.112, respectively, with standard deviation 0.028, 0.036, 0.036, 0.033 and 0.039. We also have that the threshold 0.17ppm was surpassed 13, 78, 53, 40 and 143 days in regions NE, NW, CE, SE and SW, respectively.

The computational details of the implementation of the computer programme of the algorithm used to estimate the parameters are given as follows. When considering the Weibull rate function, we have used three different initial values for the algorithm generating the values of α and σ . Those initial values were based on the results given by Achcar et al. (2008a) for each specific region. Hence, we have taken one value near the left extreme of the 95% credible interval for the mean, another near the right extreme and the mean itself. In the case of the rate functions (3) and (4) similar procedure was considered.

Regarding the hyperparameters of the prior distributions when considering the Weibull rate function we have the following. In the case of the first stage of the sampling procedure (i.e., uniform prior distributions for α and σ), we have that in all regions the parameter α has a $U(0,1)$ prior distribution. The parameter σ has a $U(0,10)$ prior distribution when using data from region CE and a $U(0,100)$ prior distribution for the remaining regions. In the case of non uniform prior distributions, the value of the hyperparameters may vary from region to region. In the case of the parameter α we have that the Beta distribution has hyperparameters $a_1 = 3/25$ and $b_1 = 2/25$ in the case of regions NW, SE and SW, and is $Beta(1/8, 1/8)$ and $Beta(7/200, 3/200)$ in the case of regions CE and NE, respectively. When considering the

parameter σ we have that the prior distributions are Gamma(3249/640, 57/640), Gamma(3/2, 1/2), Gamma(9/4, 3/4), Gamma(1.69, 0.13) and Gamma(49/20, 7/20) for regions NE, NW, CE, SE and SW, respectively.

Remark. Observe that taking either $\alpha \sim U(0,1)$ or α with a Beta distribution, we have that $\lambda^{(W)}(t)$ is a decreasing intensity function.

In almost all cases and regions we consider a burn-in period of 30000 steps. The exceptions are the cases of Weibull rate function with α having a Beta prior distribution and regions CE, NE and SW, and the case of GGO rate function and region SW where we have a burn-in period of 130000 steps. In all cases a sample of size 10500 was used to estimate the parameters of the models. The burn-in period was determined by trace plot analysis as well as by using the Gelman-Rubin test (see Gelman & Rubin, 1992).

Remark. In the case of GGO rate function and region SW, the sampling procedure were as follows, for each iteration producing a value of β we had 20 iterations for α and σ . Hence, we have 20 iterations for α , and the last generated value is used to generate a β . This generated β is used to generate σ and again we have 20 iterations for σ and the 20th generated value is used to generate α , and so on. This artifice was necessary to obtain convergence of the Gibbs and Metropolis-Hastings algorithms.

The estimated mean, standard deviation (indicated by SD) and the 95% credible interval in the case of Weibull rate function are given in Table 1.

Weibull		Mean		SD		95% credible interval	
		uni	no-uni	uni	no-uni	uni	no-uni
NE	α	0.7	0.891	0.11	0.14	(0.476, 0.917)	(0.575, 1)
	σ	3.47	91.05	2.37	33.404	(0.7635, 9.652)	(28.909, 152.84)
NW	α	0.6	0.62	0.063	0.054	(0.543, 0.792)	(0.526, 0.726)
	σ	3.47	2.48	2.37	1.524	(0.763, 9.561)	(0.642, 5.884)
CE	α	0.58	0.56	0.063	0.052	(0.462, 0.699)	(0.471, 0.674)
	σ	3.075	2.49	2.136	1.502	(0.432, 8.492)	(0.524, 6.228)
SW	α	0.62	0.61	0.013	0.029	(0.591, 0.642)	(0.569, 0.675)
	σ	0.785	0.84	0.087	0.31	(0.626, 0.962)	(0.387, 1.541)
SE	α	0.69	0.65	0.093	0.075	(0.525, 0.884)	(0.517, 0.811)
	σ	13.83	10.07	10	6.373	(2.129, 39.865)	(1.984, 25.831)

Table 1. Posterior mean, standard deviation (indicated by SD) and 95% credible interval of the parameters α and σ when the Weibull rate function is considered.

In the case of the MOP model, we have that α and β will have U(0,700) and U(1,2500) prior distributions, respectively, in all regions.

Remark. Note that in the case of the parameters β its marginal conditional posterior distribution depends on the values of K and d_K which may vary from region to region. Hence, we have that $K = 13, 78, 53, 40$ and 143 , and $d_K = 1927, 2258, 2283, 2282$ and 2431 for regions NE, NW, CE, SE and SW, respectively. Table 2 gives the estimated quantities of interest.

When the GGO rate function is taken into account, we have for all regions that the parameters β and γ have U(0.000001,0.001) and Gamma(0.5,1.5) prior distributions, respectively. In the case of the parameter α we have that for regions NE, NW, CE and SE, its prior distribution is U(300,2000). In the case of region SW we have α with U(0,3000) prior distribution. A summary of the estimated quantities of interest is given in Table 3.

The value of the Bayes factor for each model and region are given in Table 4.

We may see from Table 4 that the best model according to the Bayes factor criterion in each region is the one using the Weibull rate function. In the case of regions NE and CE the model

MO		Mean	SD	95% credible interval
NE	α	199.178	356.8562	(0, 1115)
	β	2.981576	5.195376	(0, 16.09559)
NW	α	96.21955	167.9046	(0, 536.9866)
	β	10.90067	17.844407	(0, 49.76161)
CE	α	209.7355	102.5246	(73.91646, 476.3019)
	β	21.49208	4.840937	(13.94708, 32.71157)
SW	α	507.8983	109.1856	(292.9967, 687.4573)
	β	81.2965	10.885889	(60.82191, 102.7176)
SE	α	379.7262	148.8562	(134.278, 672.9357)
	β	20.83115	4.98808	(12.37612, 31.46646)

Table 2. Posterior mean, standard deviation (indicated by SD) and 95% credible interval of the parameters α and β when the MO rate function is considered.

GGO		Mean	SD	95% credible interval
NE	α	1024	483.15	(330.65, 1938.55)
	β	3.946E-04	0.0003	(2.33E-5, 0.000947)
	γ	0.522	0.126	(0.321, 0.8165)
NW	α	1200	454.73	(389.173, 1957.981)
	β	0.00064	0.00022	(0.000212, 0.0009803)
	γ	0.624	0.0624	(0.5173, 0.7563)
CE	α	1309	424.0873	(486.984, 1964.205)
	β	0.00067	0.00020	(0.000265, 0.000985)
	γ	0.5451	0.0573	(0.449, 0.671)
SW	α	710	450.32	(0.6246, 0.8995)
	β	0.000724	0.000193	(0.000179, 0.000999)
	γ	0.77	0.0758	(0.583, 0.9612)
SE	α	1059	480.94	(332.122, 1942.537)
	β	0.00052	0.0025	(0.000118, 0.000969)
	γ	0.592	0.076	(0.4511, 0.7464)

Table 3. Posterior mean, standard deviation (indicated by SD) and 95% credible interval of the parameters α , β and γ when the GGO rate function is considered.

	Weibull		MO	GGO
	uni	no-uni		
NE	3.499E-16	2.0712E-19	3.564126E-39	9.08166E-35
NW	1.684E-44	6.8451E-35	1.996936E-146	7.3953E-144
CE	8.2569E-26	5.6684E-29	2.673235E-108	1.52702E-104
SE	2.6252E-29	1.00755E-28	4.4002195E-89	4.7143E-86
SW	2.7104E-69	7.1844E-57	4.037815E-250	7.8386E-233

Table 4. Bayes factor for each model and region considered.

assuming uniform prior distribution for α and σ is the one with larger Bayes factor. In the case of the other regions the version where α has a Beta prior distribution is the one with larger Bayes factor.

Another way of verifying the fitting of a model to the data, is to perform graphical analysis. Hence, in Figure 1 we have the plots of the observed and estimated means for each of the

regions and rate functions considered here. The plain solid line represents the accumulated observed mean. The lines with \blacksquare , \blacklozenge , \blacktriangle and \blacktriangledown , correspond to the accumulated estimate means for models GGO, MO, Weibull where α has a uniform prior and Weibull where α has a Beta prior, respectively

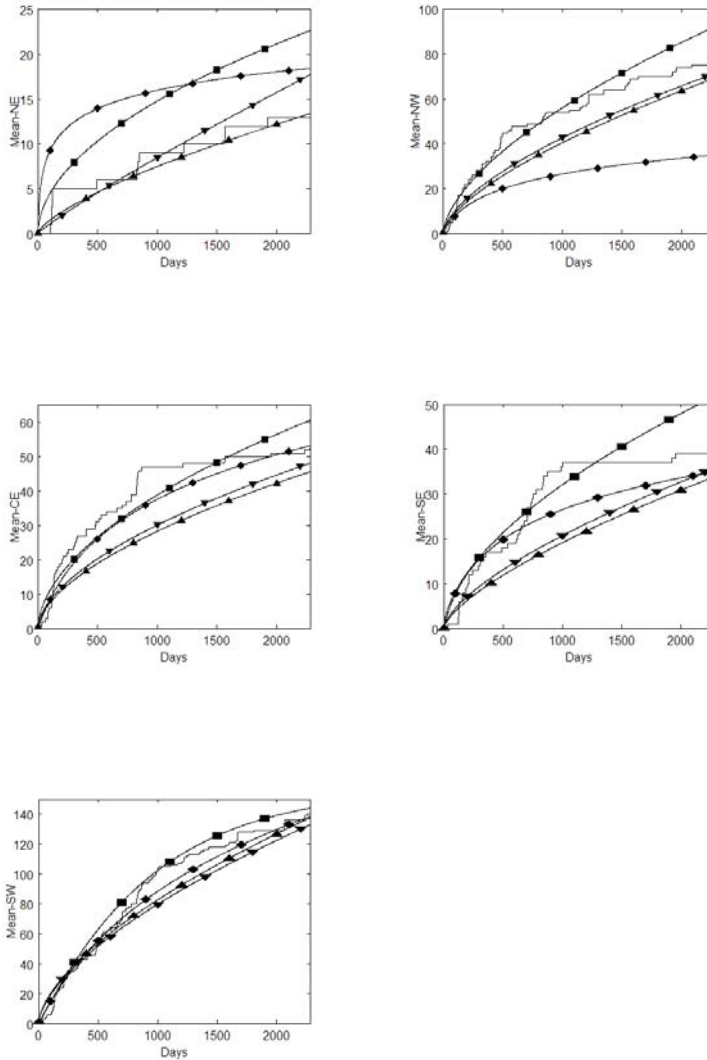


Fig. 1. Accumulated observed and estimated means for all models and all regions. Solid plain line represents the accumulated observed mean. Lines with \blacksquare , \blacklozenge , \blacktriangle and \blacktriangledown , correspond to the accumulated estimate means for models GGO, MO, Weibull where α has a uniform prior and Weibull where α has a Beta prior, respectively.

It is possible to see from Figure 1 that the model that best fit the data varies according to the region. We have that for region NE the estimated mean obtained by using the Weibull

rate function with α uniformly distributed is the one that best fit the observed mean. In the case of region NW, we have that the GGO model is the most adequate to represent the behaviour of the observed mean. However, we may notice that towards the end of the observational period the estimated Weibull mean function (either formulation) also provides a good approximation. When we look at the observed mean in region CE, we have that the GGO model fits quite well the observed mean until approximately the year 2007 and then it starts to drift away from it. However, the estimated mean using the MO model gives a good approximation from the year 2007 on. The case of region SE is similar to that of region CE. However, the fitting of the estimated mean function using the GGO model ends earlier (around 2006) and the fitting using the MO model is not as good as in the case of region CE. When we consider region SW, we have that the estimated mean function using any of the models provides a very good approximation for the observed mean. The best approximation is the one given by the GGO model though.

6. Conclusion

In this work we have considered a Gibbs sampling algorithm to estimate the parameters of a rate function of a non-homogeneous Poisson process. The methodology was applied to some models used to study the behaviour of ozone measurements from the monitoring network of Mexico City. Two criteria were used to select the model that best adjusts to the observed data. One of them was graphical analysis and the other was the Bayes factor.

Looking at Table 3 we have that the Weibull rate function is the one producing the largest Bayes factor and therefore, under this criterion, that is the model that should be considered. However, when looking at Figure 1, we have that depending on the region of the city considered, we might have a better adjustment of the estimated and observed mean number of exceedances if other rate function were considered.

We have that the Weibull rate function has the best graphical adjustment only when region NE is considered. In the other regions we have that the best graphical adjustment either is when using the GGO rate function or when using the MO (see Figure 1, regions NW, CE and SW). There are situations where the GGO rate function adjusts well until a given point in time and afterwards some of the other rate functions considered are the ones that give the best graphical fitting (see Figure 1, regions CE and SE).

Looking at Figure 1, we have that perhaps in the case of regions NW, CE and SE one could consider the GGO model with the presence of change-points. Another option is to consider two different parametric forms for the rate function of the Poisson process. One of them explaining the behaviour of the data up to a point in time and another explaining the behaviour afterwards.

When comparing the results obtained here with previous works, we have the following. Taking into account the study performed using measurements from 01 January 1998 to 31 December 2004, in all regions the selected model (using the Bayes information criterion and the deviance information criterion) is when the Weibull rate function is used (see Achcar et al., 2008a). In terms of graphical adjustment, in most of the cases, results were similar to the ones obtained here using the 2003-2009 data. However, when considering regions CE and SE, the fitting of the Weibull rate function is better when using the 1998-2004 data. The values of the parameters α and σ of the Weibull rate function are very different with the exception of regions NW and SW, where the parameters α are very similar, but the parameter σ presents significant differences.

In Achcar et al. (2010), we have that the GGO and MO rate function were used when considering measurements also taken from 01 January 1998 to 31 December 2004. In that case the regional splitting of the city was not taken into account, but the ozone measurements were the overall measurements for the Metropolitan Area of Mexico City. In that work, the presence of a change-point was assumed and we have that the model selected using the deviance information criterion to represent the behaviour of the ozone measurements was the GGO with the presence of a change-point. In terms of graphical fitting we have that the GGO model with a change-point also provides the best fit. When considering the 2003-2009 data and the regional division of the city, we have that not always the GGO model is the one providing the best graphical fitting. Additionally, when using other criteria for selecting the models, the GGO may not be the selected model either, as we can see from Figure 1. In the cases where the GGO rate function is selected as providing the best graphical fitting, we have that, when compared to the results obtained using the 1998-2004 data, the values of the parameters α and β are similar except in the case of region SW. However, the parameter γ presents very different behaviour (see Achcar et al., 2010).

As we can see from Figure 1, sometimes the MO rate function may be used to explain the behaviour of the data in the last years of the period 2003-2009. This rate function was also considered for the overall measurements during the period 1998-2004. The graphical fitting was much worse than the fitting obtained when using the 2003-2009 data.

We would like to recall that around the year 2000 was implemented the last of the major environmental measures taken by the environmental authorities in Mexico. We also have that from that year on, the daily maximum ozone concentration presents a decreasing tendency. The change in behaviour is captured by the models presented here, where different graphical fittings and values of parameters are detected when considering the 1998-2004 and 2003-2009 data sets.

An advantage of using the algorithm and consequently the programme presented here is that it may be modified by the user to adapt to each particular case studied. Each step of the algorithm and programme can be monitored and therefore, if there is any problem with the model considered, one can detect precisely where the problem is. Even though in some cases the burn-in period of the algorithm is larger than in previous cases, the overall running time is smaller than when considering some other software packages as the ones used by Achcar et al. (2008a, 2010, 2011).

7. Acknowledgements

The authors thanks Guadalupe Tzintzun of the Instituto Nacional de Ecología of the Ministry of Environment of Mexico for providing the data from the monitoring network. This work is funded by the PAPIIT research project IN104110-3 of the DGAPA-UNAM, Mexico.

8. Appendix

In this Appendix we provide the R code of the Gibbs and Metropolis-Hastings algorithms for each rate function considered in this work.

1. Weibull rate function

In here we have the code for the case where the Weibull rate function is considered.

```
w<-function(zona,cant_iteraciones,alfa_inicial,
```

```

        sigma_inicial,a1,b1,a2,b2){
# creates the Markov chain and store the initial state
alfa<-vector("numeric",cant_iteraciones)
sigma<-vector("numeric",cant_iteraciones)
alfa[1]<-alfa_inicial
sigma[1]<-sigma_inicial
# upload the vector with the observed data
datos_observados<-scan(file = zona, what = double(0), nmax = -1,
  sep = " ", quote = "", dec = ".",
  skip = 0, nlines = 0, na.strings = "NA",
  flush = FALSE, fill = FALSE, strip.white = FALSE,
  quiet = FALSE, blank.lines.skip = TRUE, multi.line = TRUE,
  comment.char = "", allowEscapes = TRUE)
for(i in 2:cant_iteraciones){
# obtain the proposed value from the Beta and Gamma prior
# distributions
alfa_propuesta<-rbeta(1,a1,b1)
sigma_propuesta<-rgamma(1,a2,b2)
# leave sigma fixed and check if the proposed
# value for alpha is accepted
aceptacion<-min(1,aceptar_alfa(sigma[i-1],alfa[i-1],
  alfa_propuesta,datos_observados))
a<-runif(1)
if(a<aceptacion)
  alfa[i]=alfa_propuesta # accepted
else
  alfa[i]=alfa[i-1] #not accepted
# leave alpha fixed and check if the proposed value
# for sigma is accepted
aceptacion<-min(1,aceptar_sigma(tail(datos_observados,1),
  length(datos_observados),alfa[i],
  sigma[i-1],sigma_propuesta))
a<-runif(1)
if(a<aceptacion)
  sigma[i]=sigma_propuesta #accepted
else
  sigma[i]=sigma[i-1] # not accepted
}
}
aceptar_alfa<-function(sigma_actual,alfa_actual,
  alfa_propuesta,datos_observados){
n<-length(datos_observados)
dn<-tail(datos_observados,1)
logsum<-0
for(k in 1:n){
  logsum<-logsum+log(datos_observados[k])
}
}

```

```

term<-n*log(alfa_propuesta/alfa_actual)+n*log(sigma_actual)
      *(alfa_actual-alfa_propuesta)+logsum
      *(alfa_propuesta-alfa_actual)
      +(dn/sigma_actual)^(alfa_actual)
      -(dn/sigma_actual)^(alfa_propuesta)
exp(term)
}
aceptar_sigma<-function(dn,n,alfa_actual,sigma_actual,
                        sigma_propuesta){
  term<-n*alfa_actual*log(sigma_actual/sigma_propuesta)
      +(dn/sigma_actual)^(alfa_actual)
      -(dn/sigma_propuesta)^(alfa_actual)
exp(term)
}

```

2. GGO rate function

In this subsection of the Appendix we have the code for the Gibbs and Metropolis-Hastings algorithms when we take the GGO rate function.

```

ggo<-function(zona,cant_iteraciones,alfa_inicial,
             beta_inicial,gamma_inicial,a5,b5,
             a6,b6,a7,b7){
  # create Markov chain and store initial values
  alfa<-vector("numeric",cant_iteraciones)
  beta<-vector("numeric",cant_iteraciones)
  gamma<-vector("numeric",cant_iteraciones)
  alfa[1]<-alfa_inicial
  beta[1]<-beta_inicial
  gamma[1]<-gamma_inicial
  # upload the vector with the observed data
  datos_observados<-scan(file = zona, what = double(0), nmax = -1,
    sep = " ", quote = "", dec = ".",
    skip = 0, nlines = 0, na.strings = "NA",
    flush = FALSE, fill = FALSE, strip.white = FALSE,
    quiet = FALSE, blank.lines.skip = TRUE, multi.line = TRUE,
    comment.char = "", allowEscapes = TRUE)
  logsum<-0
  for(i in 1:length(datos_observados)){
    logsum<-logsum+log(datos_observados[i])
  }
  for(i in 2:cant_iteraciones){
    # obtain the proposed value from the uniform and Gamma prior
    # distributions
    alfa_propuesto<-runif(1,a5,b5)
    beta_propuesto<-runif(1,a6,b6)
    gamma_propuesto<-rgamma(1,a7,b7)
  }
}

```

```

# leave the parameters beta and gamma fixed and check if the
# proposed value for alpha is accepted
aceptacion<-min(1,aceptar_alfa(beta[i-1],alfa[i-1],
                             alfa_propuesto,datos_observados,gamma[i-1]))
a<-runif(1)
if(a<aceptacion)
  alfa[i]=alfa_propuesto # accepted
else
  alfa[i]=alfa[i-1] # not accepted
# leave the parameters alpha and gamma fixed and check if the
# proposed value for beta is accepted
aceptacion<-min(1,aceptar_beta(tail(datos_observados,1),
                              length(datos_observados),alfa[i],
                              beta[i-1],beta_propuesto,
                              datos_observados,gamma[i-1]))
a<-runif(1)
if(a<aceptacion)
  beta[i]=beta_propuesto # accepted
else
  beta[i]=beta[i-1] # not accepted
# leave teh parameters alpha and beta fixed and check if the proposed
# values for gamma is accepted
aceptacion<-min(1,aceptar_gamma(datos_observados,logsum,
                                gamma_propuesto,gamma[i-1],beta[i-1],alfa[i-1]))
a<-runif(1)
if(a<aceptacion)
  gamma[i]=gamma_propuesto # accepted
else
  gamma[i]=gamma[i-1] # not accepted
}
}
aceptar_alfa<-function(beta_actual,alfa_actual,
                      alfa_propuesto,datos_observados,
                      gamma_actual){
n<-length(datos_observados)
dn<-tail(datos_observados,1)
res<-(alfa_propuesto/alfa_actual)^n
      *exp((alfa_actual-alfa_propuesto)
      *(1-exp(-beta_actual*dn^gamma_actual)))
}
aceptar_beta<-function(dn,n,alfa_actual,beta_actual,
                      beta_propuesto,datos_observados,
                      gamma_actual){
disum<-0
for(i in 1:n){
  disum<-disum+datos_observados[i]^gamma_actual
}
}

```

```

term<-disum*(beta_actual-beta_propuesto)
      +alfa_actual*(exp(-beta_propuesto*dn^gamma_actual)
      -exp(-beta_actual*dn^gamma_actual))
res<-((beta_propuesto/beta_actual)^n)*exp(term)
res
}
aceptar_gamma<-function(datos_observados,logsum,
                        gamma_propuesto,gamma_actual,
                        beta_actual,alfa_actual){
n<-length(datos_observados)
dn<-tail(datos_observados,1)
expsum<-0
for(i in 1:n){
  expsum<-expsum+(datos_observados[i]^gamma_actual
                  -datos_observados[i]^gamma_propuesto)
}
term<-logsum*(gamma_propuesto-gamma_actual)
      +beta_actual*expsum+alfa_actual
      *(exp(-beta_actual*dn^gamma_propuesto)
      -exp(-beta_actual*dn^gamma_actual))
result<-((gamma_propuesto/gamma_actual)^n)*exp(term)
result
}

```

3. MO rate function

In here we present the R code of the Gibbs and Metropolis-Hastings algorithms when the MO rate function is used.

```

mo<-function(zona,cant_iteraciones,alfa_inicial,
            beta_inicial,a3,b3,a4,b4){
  # creates the Markov chain and store the initial state
  alfa<-vector("numeric",cant_iteraciones)
  beta<-vector("numeric",cant_iteraciones)
  alfa[1]<-alfa_inicial
  beta[1]<-beta_inicial
  # upload the vector with the observed data
  datos_observados<-scan(file = zona, what = double(0), nmax = -1,
    sep = " ", quote = "", dec = ".",
    skip = 0, nlines = 0, na.strings = "NA",
    flush = FALSE, fill = FALSE, strip.white = FALSE,
    quiet = FALSE, blank.lines.skip = TRUE, multi.line = TRUE,
    comment.char = "", allowEscapes = TRUE)
  n<-length(datos_observados)
  dn<-tail(datos_observados,1)
  for(i in 2:cant_iteraciones){
    # obtain a proposed value for alpha from its Gamma prior distribution
    # and check is the value is accepted

```

```

    alfa_propuesta<-rgamma(1,a3,b3)
    aceptacion<-aceptar_alfa(beta[i-1],alfa[i-1],alfa_propuesta,
                             datos_observados)

    a<-runif(1)
    if(a<aceptacion)
        alfa[i]=alfa_propuesta # accepted
    else
        alfa[i]=alfa[i-1] # not accepted
        # obtain a random sample for the parameter beta using its Gamma
        # posterior distribution
        beta[i]<-rgamma(1,n+1,log(1+(dn/alfa[i])))
    }
}
aceptar_alfa<-function(current_beta,alfa_actual,alfa_propuesta,
                       datos_observados){
    # obtain the cardinality of the observed data sets and obtain
    # the last value of the set
    n<-length(datos_observados)
    dn<-tail(datos_observados,1)
    # calculate the sum of log(di)
    logsum<-0
    for(i in 1:n){
        logsum<-logsum+log((datos_observados[i]+alfa_actual)
                           /(datos_observados[i]+alfa_propuesta))
    }
    term<-logsum+current_beta*log((alfa_actual*(alfa_propuesta+dn)
                                   /(alfa_propuesta*(alfa_actual+dn)))
    exp(term)
}

```

9. References

- Achcar, J.A. (2001). Bayesian analysis for software reliability data, *Advances in Reliability Handbook of Statistics* Vol. 20: 733-748.
- Achcar, J.A., Dey, D.K. & Niverthy, M. (1998). A Bayesian approach using nonhomogeneous Poisson process for software reliability models, in: S.K. Basu & S. Mukhopadhyay (eds.), *Frontiers in Reliability. Series on Quality, Reliability and Engeneering Statistics* Vol. 4, Calcutta University, India, pp. 1-18.
- Achcar, J.A., Fernández-Bremauntz, A.A., Rodrigues, E.R. & Tzintzun, G. (2008a). Estimating the number of ozone peaks in Mexico City using a non-homogeneous Poisson model, *Environmetrics* Vol. 19: 469-485. (<http://www.interscience.wiley.com>, DOI: 10.1002/env.890)
- Achcar, J.A., Zozolotto, H.C. & Rodrigues, E.R. (2008b). Bivariate volatility models applied to air pollution data, *Rev. Bras. Biom.* Vol. 26: 67-81.
- Achcar, J.A., Zozolotto, H.C. & Rodrigues, E.R. (2009a). Bivariate stochastic volatility models applied to Mexico City ozone pollution data, in G.C. Romano & A.G. Conti (eds.), *Air Quality in the 21st Century*, Nova Publishers, New York, pp. 241-267.

- Achcar, J.A., Rodrigues, E.R. & Tzintzun, G. (2009b). Using stochastic volatility models to analyse weekly ozone averages in Mexico City, *Environmental and Ecological Statistics*, (DOI:10.1007/s10651-010-0132-1).
- Achcar, J.A., Rodrigues, E.R., Paulino, C.D. & Soares, P. (2010). Non-homogeneous Poisson processes with a change-point: an application to ozone exceedances in Mexico City, *Environmental and Ecological Statistics* Vol. 17: 521-541. (DOI: 10.1007/s10651-009-0114-3)
- Achcar, J.A., Rodrigues, E.R. & Tzintzun, G. (2011). Using non-homogeneous Poisson models with multiple change-points to estimate the number of ozone exceedances in Mexico City, *Environmetrics* Vol. 22: 1-12. (<http://www.interscience.wiley.com>, DOI: 10.002/env.1029)
- Álvarez, L.J., Fernández-Bremauntz, A.A., Rodrigues, E.R. & Tzintzun, G. (2005). Maximum a posteriori estimation of the daily ozone peaks in Mexico City, *Journal of Agricultural, Biological, and Environmental Statistics* Vol. 10: 276-290.
- Austin, J. & Tran, H. (1999). A characterization of the weekday-weekend behavior of ambient ozone concentrations in California, in *Air Pollution VII*, WIT Press, Ashurst Lodge, Ashurst, Southampton, UK, pp. 645-661.
- Bell, M.L., McDermonntt, A., Zeger, S.L., Samet, J.M. & Dominici, F. (2004). Ozone and short-term mortality in 95 US urban communities, 1987-2000, *Journal of the American Medical Society* Vol. 292: 2372-2378.
- Bell, M.L., Peng, R. & Dominici, F. (2005). The exposure-response curve for ozone and risk of mortality and the adequacy of current ozone regulations, *Environmental Health Perspectives* Vol. 114: 532-536.
- Bell, M.L., Goldberg, R., Rogrefe, C., Kinney, P.L., Knowlton, K., Lynn, B., Rosenthal, J., Rosenzwei, C. & Patz, J.A. (2007). Climate change, ambient ozone, and health in 50 US cities, *Climate Change* Vol. 82: 61-76.
- Cox, D.R. & Lewis, P.A. (1966). *Statistical analysis of series events*, Methuen, UK.
- Davis, L.W. (2008). The effect of driving restrictions on air quality in Mexico City, *Journal of Political Economy* Vol. 116: 39-81.
- EPA (US Environmental Protection Agency) (2008). *National Ambient Air Quality Standards*. Available at <http://www.epa.gov/air/criteria.html>.
- Flaum, J.B., Rao, S.T. & Zurbenko, I.G. (1996). Moderating influence of meteorological conditions on ambient ozone concentrations, *Journal of the Air and Waste Management Association* Vol. 46: 33-46.
- Gauderman, W.J., Avol, E., Gililand, F., Vora, H., Thomas, D., Berhane, K., McConnel, R., Kuenzli, N., Lurmmman, F., Rappaport, E., Margolis, H., Bates, D. & Peter, J. (2004). The effects of air pollution on lung development from 10 to 18 years of age, *The New England Journal of Medicine* 351: 1057-1067.
- Gelfand, A.E. & Smith, A.F.M. (1990). Sampling-based approaches to calculating marginal densities, *Journal of the American Statistical Association* Vol. 85: 398-409.
- Gelman, A. & Rubin, D.B. (1992). Inference from iterative simulation using multiple sequences, *Statistical Sciences* Vol. 7: 457-511.
- Goel, A.L. & Okumoto, K. (1978). An analysis of recurrent software failures on a real-time control system, *Proceedings of ACM Conference*, Washington-DC, USA, pp. 496-500.
- Gouveia, N. & Fletcher, T. (2000). Time series analysis of air pollution and mortality: effects by cause, age and socio-economics status, *Journal of Epidemiology and Community Health* Vol. 54: 750-755.

- Hastings, W.K. (1970). Monte Carlo sampling methods using Markov chains and their applications, *Biometrika* Vol. 57: 97-109.
- Horowitz, J. (1980). Extreme values from a nonstationary stochastic process: an application to air quality analysis, *Technometrics* Vol. 22: 469-482.
- Huerta, G. & Sansó, B. (2005). Time-varying models for extreme values, *Technical Report 2005-4*, Department of Applied Mathematics and Statistics. University of California, USA.
- Kumar, U., Prakash, A. & Jain, V.K. (2010). A multivariate time series approach to study the interdependence among O₃, NO_x and VOCs in ambient urban atmosphere. *Environmental Modelling and Assessment*, (DOI: 10.1007/s10666-008-9167-1).
- Lanfredi, M. & Macchiato, M. (1997). Searching for low dimensionality in air pollution time series, *Europhysics Letters* Vol. 40: 589-594.
- Lawless, J. F. (1982). *Statistical models and methods for lifetime data*, John Wiley & Sons, USA.
- Loomis, D., Borja-Arbuto, V.H., Bangdiwala, S.I. & Shy, C.M. (1996). Ozone exposure and daily mortality in Mexico City: a time series analysis, *Health Effects Institute Research Report* Vol. 75: 1-46.
- Metropolis, N., Rosenbluth, A., Rosenbluth, M., Teller, A. & Teller, E. (1953). Equations of state calculations by fast computing machine, *J. Chem. Phys.* Vol. 21: 1087-1091.
- Musa, J.D. & Okumoto, K. (1984). A logarithmic Poisson execution time model for software reliability measurement, *Proceedings of Seventh International Conference on Software Engineering*, Orlando, USA, pp. 230-238.
- NOM (2002). Modificación a la Norma Oficial Mexicana NOM-020-SSA1-1993, *Diario Oficial de la Federación*, 30 October 2002, Mexico. (In Spanish.)
- O'Neill, M.R., Loomis, D. & Borja-Aburto, V.H. (2004). Ozone, area social conditions and mortality in Mexico City, *Environmental Research* Vol. 94: 234-242.
- Pan, J.-N. & Chen, S.-T. (2008). Monitoring long-memory air quality data using ARFIMA model, *Environmetrics* Vol. 19: 209-219.
- Raftery, A.E. (1989). Are ozone exceedance rate decreasing?, Comment of the paper "Extreme value analysis of environmental time series: an application to trend detection in ground-level ozone" by R. L. Smith, *Statistical Sciences* Vol. 4: 378-381.
- Raftery, A.E. (1996). Hypothesis testing and model selection, in W. Gilks, S. Richardson & D.J. Spiegelhalter (eds.), *Markov chain Monte Carlo in practice*, Chapman and Hall, UK, pp. 163-187.
- Ramírez-Cid, J.E. & Achcar, J.A. (1999). Bayesian inference for nonhomogeneous Poisson processes in software reliability models assuming non monotonic intensity functions, *Computational Statistics and Data Analysis* Vol. 32: 147-159.
- Roberts, E.M. (1979a). Review of statistics of extreme values with applications to air quality data. Part I. Review, *Journal of the Air Pollution Control Association* Vol. 29: 632-637.
- Roberts, E.M. (1979b). Review of statistics of extreme values with applications to air quality data. Part II. Applications, *Journal of the Air Pollution Control Association* Vol. 29: 733-740.
- Smith, R.L. (1989). Extreme value analysis of environmental time series: an application to trend detection in ground-level ozone, *Statistical Sciences* Vol. 4: 367-393.
- Wilson, S.P. & Costello, M.J. (2005). Predicting future discoveries of European marine species using non-homogeneous renewal processes, *Journal of the Royal Statistical Society Series C* Vol. 54: 425-442.

- WHO (World Health Organization) (2006). *Air Quality Guidelines - 2005. Particulate matter, ozone, nitrogen dioxide and sulfur dioxide*, World Health Organization Regional Office for Europe, EU.
- Zavala, M., Herndon, S.C., Wood, E.C., Onasch, T.B., Knighton, W.B., Marr, L.C., Kolb, C.E. & Molina, L.T. (2009). Evaluation of mobile emissions contributions to Mexico City's emissions inventory using on road and cross-road emission measurements and ambient data, *Atmos. Chem. Phys.* Vol. 9: 6305-6317.

Part 3

Measuring Methodologies in Air Pollution Monitoring and Control

Optical Measurements of Atmospheric Aerosols in Air Quality Monitoring

Jolanta Kuśmierczyk-Michulec
*Institute of Oceanology, Polish Academy of Sciences
Poland*

1. Introduction

Human activities are changing the composition of Earth's atmosphere, and thus influence the air quality. In that respect, one of the most important elements of the atmosphere are aerosols. They play a fundamental role in physical and chemical processes affecting both air quality and regional and global climate. Aerosols affect the Earth's radiative balance both in the cloud-free and the cloudy atmosphere. These so-called direct and indirect aerosol effects which depend on the chemical and physical aerosol properties still represent an uncertain factor in estimates about climate change.

The direct effect of aerosols is related with scattering and absorption of solar radiation, and as a consequence, reduction of the amount of radiation reaching the surface (e.g. IPCC 2001). In case of indirect effects, we distinguish the first and the second one. Aerosols act as cloud condensation nuclei (CCN), modifying the optical and radiative properties of clouds, e.g. albedo. This is known as the first indirect effect (Twomey, 1977). The second indirect effect is related to the shift in the cloud droplet spectrum resulting from the nucleation. It is seen by a decrease in precipitation and an increase in cloud lifetime (e.g. Charlson et al., 1992).

The best parameters that quantify the direct aerosol effect are the aerosol extinction, linked also to atmospheric visibility, and the aerosol optical thickness. The aerosol extinction reveals how aerosols attenuate the solar radiation in relation to a given distance (e.g. per km); the aerosol optical thickness is the extinction integrated over a whole column of atmosphere (usually in the vertical from the surface to the top of the atmosphere). Aerosol extinction can be derived from in-situ measurements (aerosol counters, impactors) or from path-integrated measurements (transmissometer); aerosol optical thickness is usually obtained from sun photometer measurements.

Nowadays, in the era of AERONET, information about the aerosol optical thickness (AOT) is available online for nearly 400 sites in the world; only in Europe the number of AERONET station is more than 80. Hence, more and more researchers try to find a relationship between the aerosol optical thickness (AOT) and PM_{10} (particulate matter with an aerodynamic diameter of less than 10 μm) in order to use it as an indicator of air quality. It should be emphasized that the aerosol optical thickness values represent vertical column-integrated properties whereas the PM_{10} data are the "surface" data. This kind of comparison is justified in the well-mixed boundary layer. Therefore not always both parameters are well correlated. Nevertheless, such a relationship between (AOT) and PM_{10} would be useful in air quality monitoring.

The variation of the extinction coefficient with wavelength can be presented as a power law function with a constant (related to the power factor) known as the Ångström coefficient.

When the particle size distribution is dominated by small particles, usually associated with pollution, the Ångström coefficients are high; in clear conditions they are usually low. Long residence time of air masses over land and in particular the passage over large urban areas cause high concentrations of fine particles and thus high values of the Ångström coefficients. The opposite effect can be observed over water. The longer the time that the air masses spent over water the more evident is a change in the aerosol size distribution caused by the deposition of continental aerosols. As a result of this process the measured Ångström coefficient values become much smaller. Therefore this parameter is a good tracer for the concentration of aerosols originated over land e.g. black carbon (Kuśmierczyk-Michulec et al., 2007; Kuśmierczyk-Michulec & Van Eijk, 2007).

This chapter will give an overview of various efforts tending toward finding a relationship between AOT and PM₁₀. Moreover, it will discuss possibility of using the Ångström coefficient in air quality estimation. The aerosol optical thickness and the Ångström coefficient are routinely monitored by AERONET sun photometers, or can be estimated using satellite data, therefore their application in air quality monitoring would be of great value.

2. Methodology

This section presents definitions of the main parameters usually used by various authors in the AOT-PM formulas.

2.1 Aerosol size distribution and related optical parameters: extinction, aerosol optical thickness and Ångström coefficient

The aerosol size distribution can be represented by the number size distribution $N(r)$, the volume size distribution $V(r)$, or by the mass size distribution $m(r)$. In each case the lognormal function is used and details are presented e.g. by Seinfeld and Pandis (1998).

The aerosol number size distribution for a given aerosol type can be presented by the following equation, where r is the particle radius, r_n is the median radius, σ is the standard deviation and N_n is particle concentration:

$$\frac{dN(r)}{d \ln r} = \frac{N_n}{\sigma\sqrt{2\pi}} \exp\left\{-\frac{(\ln r - \ln r_n)^2}{2\sigma^2}\right\} \quad (1)$$

From the number size distribution can be derived directly an effective radius R_{eff} (in μm):

$$R_{\text{eff}} = \frac{\int r^3 \frac{dN(r)}{d \ln r} d \ln r}{\int r^2 \frac{dN(r)}{d \ln r} d \ln r} \quad (2)$$

The effective radius is a very useful parameter in characterization of the aerosol mixtures. Assuming that particles are spherical the following relation can be used to calculate the mass concentration PM at the surface in ($\mu\text{g}/\text{m}^3$):

$$PM = \frac{4}{3}\pi\rho \int_{r_{\min}}^{r_{\max}} r^3 \frac{dN(r)}{d \ln r} d \ln r \quad (3)$$

where ρ is the aerosol mass density in (g/cm^3).

The spectral optical coefficient, called the extinction coefficient $ext(\lambda)$ (in km^{-1}) can be calculated from the number size distribution:

$$ext(\lambda) = \pi \int_{r_{\min}}^{r_{\max}} r^2 Q_{ext} \frac{dN(r)}{d \ln r} d \ln r \quad (4)$$

where λ is wavelength, r is radius and Q_{ex} is the extinction efficiency factor, being a function of the complex index of refraction (Mie, 1908). The coefficient Q_{ex} can be calculated according to algorithm published by Bohren and Huffman (1983). The size-distribution integrated extinction efficiency $\langle Q_{ext} \rangle$ is defined as (Hansen & Travis, 1974):

$$\langle Q_{ext} \rangle = \frac{\int r^2 Q_{ext} \frac{dN(r)}{d \ln r} d \ln r}{\int r^2 \frac{dN(r)}{d \ln r} d \ln r} \quad (5)$$

The extinction coefficient integrated over the whole column of atmosphere is a dimensionless parameter and it is called the aerosol optical thickness (AOT):

$$AOT(\lambda) = \int_{H_{\min}}^{H_{\max}} ext(\lambda, h) dh \approx \int_{H_{\min}}^{H_{\max}} ext(\lambda) f(h) dh \quad (6)$$

where $f(h)$ represents the vertical distribution of aerosols, h is the altitude in km, H_{\min} and H_{\max} are the lower and the upper altitude, respectively, at which a given aerosol type can be found. Variation of the extinction coefficient with the wavelength can be presented in the form of a power law function (Ångström, 1929):

$$ext(\lambda) = \gamma_c \lambda^{-\alpha} \quad (7)$$

The same type of relation is also valid for the aerosol optical thickness,

$$AOT(\lambda) = \gamma_\tau \lambda^{-\alpha} \quad (8)$$

where γ_c and γ_τ are constant and α is the Ångström coefficient (also known as Ångström exponent or Ångström parameter). Usually, this parameter is determined in the spectral range from 440 nm to 870 nm.

From the set of equations 2-6 the following relation between PM and AOT can be derived:

$$PM = \xi \times AOT(\lambda) \quad (9)$$

where coefficient ξ is defined as:

$$\xi = \frac{4\rho R_{eff}}{3 \langle Q_{ext} \rangle H} \quad (10)$$

and the vertical distribution H is given by:

$$H = \int_{H_{\min}}^{H_{\max}} f(h)dh \quad (11)$$

2.2 Visual range (VR) and air pollution index (API)

Some authors looking for the best correlation between the particulate matter (PM) and optical parameters take into account not only the standard parameters like AOT or aerosol extinction but also other parameters like visual range (e.g. Bäumer et al., 2008; Jung et al., 2009) or air pollution index (e.g. Xia et al., 2006; Lasserre et al., 2008). Because of that reason it is worth to present definitions of the above parameters.

According to the empirical formula by Koschmieder (1925) the total atmospheric extinction coefficient at 550 nm is inversely proportional to horizontal visibility, known also as visual range (VR) in (km):

$$VR = \frac{-\ln(0.02)}{ext(550)} \quad (12)$$

Air Pollution Index (API) is a number used by government agencies to characterize the quality of the air at a given location. For example in China, the estimates of API are provided by the State Environmental Protection Agency (SEPA), (http://www.sepa.gov.cn/english/air_s.php3). The API level in China is based on the level of 5 atmospheric pollutants, namely sulfur dioxide (SO₂), nitrogen dioxide (NO₂), suspended particulates (PM₁₀), carbon monoxide (CO), and ozone (O₃) measured at the monitoring stations throughout each city. An API daily value gives information about the most concentrated pollutant of the day. Some authors (e.g. Lasserre et al. 2008) used API index to determine the PM₁₀ concentration. However in such a case the exact chemical composition is not known.

3. Experimental

The overview of the main experimental techniques used to measure the particulate matter (PM) and optical properties like AOT and aerosol extinction are shortly presented in the subsequent subsections. Since the aim of this paper is to give an overview of different approaches leading to a relationships between PM and AOT, it is worth to mention as well various experimental techniques. None of them is perfect. In consequence the method of measurements can have an effect on such a relationship.

3.1 Aerosol optical thickness (AOT) measurements

3.1.1 Sun photometer measurements

The spectral aerosol optical thickness and derived aerosol properties are routinely available from AERONET network (Holben et al., 2001). The measurements are made with CIMEL sun photometers. The instruments measure the direct solar radiation, from which the spectral values of the aerosol optical thickness can be derived. Most of the instruments in this network have the following channels: 440 nm, 670 nm, 870 nm and 1020 nm; some of them have more channels and thus can give more detailed spectral information. In addition, the sky radiance in aerosol channels in the azimuth plane (the almucantar technique) and in the principal plane is measured. The technical details of the instrument are described in the

Cimel Sun Photometer Manual. These data are used in the AERONET standard procedures to retrieve information on columnar aerosol characteristics such as the aerosol optical thickness, Ångström coefficient and size information. Data processing, cloud-screening algorithm, and inversion techniques are described by Holben et al. (1998, 2001), Eck et al. (1999), Smirnov et al. (2000), Dubovik and King (2000), and Dubovik et al. (2000).

3.1.2 Multi-Filter Shadow-band Radiometer (MFSR) measurements

The spectral aerosol optical thickness data can be also obtained from the measurements using the multi-filter shadow-band radiometer. The instrument measures simultaneously the total sky irradiance and the diffuse sky irradiance. These measurements allow estimation of the direct solar beam irradiance at the central wavelengths in each channel, and then, the aerosol optical thickness spectral values (e.g. Harrison and Michalsky, 1994; Olszewski et al., 1995). Similarly to sun-photometer measurements, the high quality MFSR measurements can be performed only for cloud-free days. This method of measurements of AOT was reported for example by Vaughan et al. (2001) or Alexandrov et al. (2005).

3.1.3 Satellite retrievals of the aerosol optical thickness

Satellites are best suited to determine the spatial distribution of aerosols over large areas during extended time periods, needed to evaluate their effects. Satellite observations since more than 25 years provide the aerosol index (AI) from the Total Ozone Mapping Spectrometer (TOMS) (Herman et al., 1997) and, over the oceans, the aerosol optical thickness (AOT) from the Advanced Very High Resolution Radiometer (AVHRR). Instruments become more and more sophisticated, reaching the compromise between spatial and spectral resolution, i.e., the Moderate Resolution Imaging Spectrometer (MODIS) (Kaufman and Tanré, 1996).

The accuracy of the aerosol optical thickness derived from the satellite data depends on the quality of data (e.g. radiometric calibration) but also on the algorithm used for conversion of satellite data to the AOT data. Since the retrieving process of AOT is performed only during daytime and for cloud-free pixels, the important step is the proper cloud mask. The smaller is a pixel size the more efficient is the process of removing cloudy pixels. Usually, instruments used for aerosol retrieval are designed for this purpose, such as Along Track Scanning Radiometer 2 (ATSR-2) or MODIS, and have small pixel sizes. Use of instruments with high spectral resolution but with a large pixel size, like for a example Global Ozone Monitoring Experiment (GOME) or Scanning Absorption Spectrometer for Atmospheric Chartography (SCIAMACHY) results in a very low probability of clear sky pixels which limits the usefulness of such instruments for aerosol retrieval (e.g. Kuśmierczyk-Michulec and De Leeuw, 2005).

It is worth to notice that the AOT retrieved from satellite data is the end product of a very complex data processing which involves many assumptions and may be a source of many uncertainties. The total radiance received by a sensor at the top of the atmosphere (TOA) contains contributions from aerosols, molecules, and the surface. Instead of radiance, it is often more convenient to use reflectance, i.e. a dimensionless function, defining the ratio of the measured radiance to the solar flux at the top of the atmosphere. In both representations the molecular contribution is assumed to be well known.

The main issue is the separation of the aerosol and surface contributions to the total reflectance. The high underestimation in the surface reflectance (e.g. over bright surface),

results in a large overestimation of the retrieved aerosol optical thickness. Similarly, the overestimation in the surface reflectance values may lead to underestimation of the AOT values, producing even the negative AOT values.

Thus, the proper surface correction is crucial. Over land the surface contribution to the TOA reflectance in the spectral range between 380 nm and 670 nm is not higher than 60% (except in the case of snow) (Kuśmierczyk-Michulec and De Leeuw, 2005). This contribution increases with wavelength reaching a value of around 80% at 770 nm. These numbers are based on the analysis of the surface reflectances taken from the GOME surface reflectance database (Koelemeijer et al., 2003). Over water, the proper surface correction is also important, especially in the UV and the visible part of spectrum. In that range the contribution of the water-leaving reflectance to the TOA reflectance is the most significant, around 60%, depending on the type of water and atmosphere. This contribution decreases with the wavelength, reaching at 670 nm around 1–8%. For Case I waters (Morel, 1988), i.e., mainly oceanic waters which optical properties are determined by phytoplankton and their immediate derivatives, the contribution at 670 nm will be almost negligible, because the water-leaving reflectance is close to zero. For Case II waters (Morel, 1988), i.e., all coastal waters which optical properties are also determined by the presence of sediments or dissolved yellow substances, this contribution can be much higher.

To account for the surface contribution different approaches, depending on instruments, can be used. For example, in case of MODIS instrument, the surface reflectivity at visible wavelengths is obtained by assuming a constant ratio between surface reflectivity at 2100 nm and that at 470 and 660 nm (eg. Chu et al., 2003; Remer et al., 2005). For MERIS data Retalis & Sifakis (2010) suggested using the differential textural analysis (DTA) algorithm which quantifies the contrast reduction as local “textural degradation” by comparing “a pollution image” and a “reference image”, representing a day with the lowest level of aerosol concentration. For the aerosol retrieval with GOME data (Kuśmierczyk-Michulec and De Leeuw, 2005), the surface reflectance databases can be used (Koelemeijer et al., 2003) or combined approach using two instruments: GOME and ATSR-2 (Holzer-Popp et al., 2002).

The accuracy of the retrieved aerosol optical thickness values is tested by comparison with collocated sun photometer measurements e.g. available from the AERONET stations. In this way a bias between retrieved and measured AOT values can be found. It is especially important in case both AOT from ground measurements and satellite retrievals are used as a one dataset.

3.2 Aerosol extinction measurements

To measure the aerosol extinction, several methods can be used. Wang et al. (2010) reported the aerosol extinction measurements carried out by a visibility meter. According to the empirical formula by Koschmieder (1925) the total atmospheric extinction coefficient at 550 nm is inversely proportional to horizontal visibility. Hence, the aerosol extinction coefficient at 550 nm can be derived after removal the molecular contribution from the total atmospheric extinction coefficient.

Jung et al. (2009) used the transmissometer system, consisting of a transmitter and a receiver, to measure the atmospheric transmission over a long-path at a given wavelength. Using the exponential relationship between the transmittance and extinction, and removing the molecular contribution, the aerosol extinction can be determined (e.g. Kuśmierczyk-Michulec et al., 2008).

3.3 PM₁₀ measurements

The most frequently used techniques to measure PM₁₀ (particulate matter with an aerodynamic diameter of less than 10 μm) data are presented below. Some of these methods were used to determine PM_{2.5} (particulate matter with an aerodynamic diameter of less than 2.5 μm) or even PM_{1.0} (particulate matter with an aerodynamic diameter of less than 1 μm).

3.3.1 Beta – absorption technique

The beta-absorption technique is used for example in The Netherlands (e.g. Kuśmierczyk-Michulec et al., 2007). The PM₁₀ (particulate matter with an aerodynamic diameter of less than 10 μm) and black carbon concentrations are measured by the Dutch National Air Quality Network (LML) operated by RIVM (<http://www.rivm.nl/milieukwaliteit/lucht/>). Black carbon (particles mostly smaller than 2.5 μm) is available as daily values and PM₁₀ is available on an hourly basis.

RIVM's National Air Quality Monitoring Network in the Netherlands performs continuous PM measurements i.e. PM₁₀ and PM_{2.5}, using an FAG-type β-dust monitor (Van Elzakker, 2000). The sampling air is heated (to 50 °C) in order to remove water from aerosol particles (Buringh and Opperhuizen, 2002). The drawback of the heating is a removal of semi-volatile compounds e.g. ammonium nitrate which leads to the losses in PM measurements. The correction methods for a systematic underestimation by the sampling equipment are described by Hammingh (2001) and discussed in detail by Buringh and Opperhuizen (2002). The amount of black carbon is estimated based on the PM measurements using the so-called light-reflectance method (Buringh and Opperhuizen, 2002).

3.3.2 Tapered element oscillating microbalance (TEOM) technique

The tapered oscillating microbalance technique was used for example in Beijing (e.g. Xia et al., 2006; Wang et al., 2010), in Amazonia (Artaxo et al., 2002), in the South-Eastern France (e.g. Péré et al., 2009), in the North France and Belgium (Pelletier et al., 2007) or in Italy (Barnaba et al., 2010). Similarly to beta-absorption technique, the sampled air is heated before collecting the aerosols on a filter, to avoid humidification of the filter. In consequence of heating, a loss of semi-volatile compounds can occur. Using this method of measurements, an underestimation can exist on PM₁₀ values due to the volatilization of ammonium nitrate or semi-volatile organic species during the conditioning procedure at 50 °C (e.g. Allen et al., 1997). The uncertainty of PM₁₀ measurements using TEOM, reported by authors, is ± 10%.

3.3.3 Aerosol spectrometer measurements

The aerosol spectrometer determines the concentration of aerosols by quantifying the scattering caused by the passage of particles of various sizes through a light beam produced by a laser diode. This technique was used for example in Beijing (e.g. Jung et al., 2009) to measure PM₁₀, PM_{2.5} and PM_{1.0} mass concentrations. The PM concentrations were measured under dry condition (RH<40%) by diluting the sample air with dry clean air.

4. Influence of relative humidity (RH) on aerosol optical properties and particulate matter (PM)

When the ambient relative humidity is changing the hygroscopic atmospheric aerosols undergo processes of phase transformation, droplet growth, and evaporation. The phase

transformation from a solid particle to a saline droplet usually occurs spontaneously when the ambient relative humidity reaches a level called the deliquescence humidity. Its value is specific to the chemical composition of the aerosol particle (e.g. Orr et al., 1958; Tang, 1976). The relative humidity influences the size of hygroscopic particles, the effective radius of an aerosol mixture, their density and finally the aerosol scattering properties. In consequence, values of the particulate matter (PM), the aerosol extinction, the aerosol optical thickness (AOT) and the Ångström coefficient are modified. Similar effect can be observed when the aerosol composition changes (e.g. Kuśmierczyk-Michulec, 2009).

The main aerosol components affected by a change in the relative humidity are sea-salts (SSA, i.e. NaCl) and anthropogenic salts e.g. ammonium nitrate (NH_4NO_3) and ammonium sulphate ($(\text{NH}_4)_2\text{SO}_4$). It should be mentioned that another aerosol component on which the relative humidity could have an influence is organic carbon (OC). In contrast to black carbon (BC) which is considered to be insoluble (e.g. Kanakidou et al., 2005), about 40% of organic carbon (OC) is soluble (Rulleau, 2000, personal communication; IPCC, 2007). However, there is still a lack of detailed description of the interactions among organic and inorganic aerosol compounds and water (e.g. Kanakidou et al., 2005). The interest in the hygroscopic properties of OC relevant to atmospheric applications started within the last few years only and the data are still rather scarce. Hence, considering all associated uncertainties, the common assumption is that OC is not hygroscopic.

The relative humidity modify the optical properties not only the hygroscopic aerosol mixtures but also mixtures containing some contribution of non-hygroscopic aerosols like for example organic carbon or black carbon (e.g. Kuśmierczyk-Michulec, 2009). Due to the wetting process the hygroscopic particles grow, modifying the effective radius of an aerosol mixture and finally the values of aerosol extinction or the aerosol optical thickness. This effect is substantial especially when $\text{RH} > 90\%$; at $\text{RH} = 98\%$ an increase in AOT value may be up to 6 times its value at $\text{RH} = 80\%$ (Kuśmierczyk-Michulec, 2009). This effect is observed at different wavelengths, but for higher RH, the increase in AOT values is more evident at 412 nm than at 865 nm. As a consequence of such a non-uniform increase, the Ångström coefficient also becomes a function of RH.

The observed variations in the Ångström coefficient values can be explained by changes in the effective radius of a mixture. These changes can be caused by relative humidity, as well as, by aerosol composition. For example, an increased contribution of small aerosol particles causes that the effective radius decreases and the Ångström coefficient increases. However, increase or decrease in relative humidity does not exert such a change in the Ångström coefficient like the one caused by modification in the composition of an aerosol mixture (Kuśmierczyk-Michulec, 2009).

A change from dry to wet radius, and from dry to wet density depends on the aerosol component, and more precisely on the type of salt. The general formulas proposed by some authors like for example Gong et al. (1997) are practical but not so accurate like formulas for different salts based on the laboratory work and suggested by Tang (1996) and Tang and Munkelwitz (1994). In case of known aerosol composition it is better to use the formulas suggested by the latter authors.

5. Relationships between optical parameters and particular matter

5.1 Linear and non-linear models: overview

In the past years a number of studies have explored the possibility of using optical parameters for evaluation air quality and estimation the particular matter (PM)

concentration. Most of these studies focused on finding a linear relationship between AOT data obtained from ground-based sun photometers and PM_{10} measurements (e.g. Chu et al., 2003; Xia et al., 2006; Kuśmierczyk-Michulec et al., 2007; Péré et al., 2009; Wang et al., 2010; Barnaba et al., 2010) or $PM_{2.5}$ (e.g. Jung et al., 2009; Wang et al., 2010). To improve the AOT-PM relationship some authors have investigated the possibility of using non-linear models (e.g. Pelletier et al., 2007; Liu et al., 2005; Vidot et al., 2007). Jung et al. (2009) have found that non-linear models between visual range and PM concentrations (PM_{10} , $PM_{2.5}$, $PM_{1.0}$) give very high correlation coefficients (cf. Table 1).

Similarly to the ground-based AOT, also a possibility of using satellite-derived AOT has been explored. For that purpose mostly MODIS data has been used (e.g. Wang & Christopher, 2003; Engle-Cox et al., 2004; Li et al., 2005a, 2005b; Koelemijer et al., 2006; Barnaba et al., 2010), but also MERIS data (e.g. Retalis & Sifakis, 2010), SeaWiFS data (e.g. Vidot et al., 2007; Fischer et al., 2009) and MISR data (e.g. Liu et al., 2005). Since the aerosol retrieval is quite complex thus the AOTs derived from satellite are less accurate than ground-based AOT, and hence a weaker correlation between AOT-PM (c.f. Table 1).

AOT represents the column integrated value while PM is measured at ground level, thus the correlation between them may depend on the vertical distribution of aerosols. In case a boundary layer is well-mixed, the column integrated value should be a good indicator of a surface observation and vice versa. Otherwise, the vertical distribution of aerosols should be taken into account. Another factor having an influence on the AOT-PM relationship is the relative humidity. While PM represents dry aerosols, the AOT measurements are taken at ambient conditions. In case the hygroscopic aerosols are present, an increase or decrease in RH causes changes in their sizes, volume and density, and eventually in the aerosol optical thickness values. Changes in RH may also explain sometimes observed seasonal changes in the AOT values (e.g. Kuśmierczyk-Michulec & Rozwadowska, 1999) which may lead to observed seasonal variations between AOT-PM relationships (e.g. Xia et al. 2006). In winter the air is much drier than in summer, so in winter RH should have lower impact. On the other hand, the altitude of the mixing layer is lower in winter; thus for a given AOT the PM value is expected to be larger in winter than in summer.

Thus, estimation of PM concentrations from AOT may lead to significant errors. To reduce the uncertainties, some authors (e.g. Koelemijer et al., 2006; Li et al., 2005a) have suggested scaling of the AOT values by dividing them by the boundary layer height and the hygroscopic growing factor describing the increase of the aerosol extinction cross-section with relative humidity. The positive result of this approach was reported by e.g. Koelemijer et al. (2006). Similar improvements were noted by Wang et al. (2010). To improve the correlation between the aerosol optical thickness and the particulate matter, the authors applied the vertical-and-RH correcting method to the measurements in Beijing. The authors found that the correlation coefficients between AOT and PM_{10} and between AOT and $PM_{2.5}$ have increased from 0.52 to 0.65 and from 0.48 to 0.62 respectively. Analogous effect was achieved by Barnaba et al. (2010). To get information about aerosol vertical profiles, the authors used the lidar measurements to calculate the monthly AOT weighing functions as the ratio between the lidar-derived monthly median aerosol extinction profiles and the associated AOT. These monthly vertical scaling factors allowed for conversion the AOT values into the surface aerosol extinction values. Next, after applying the RH-correction, the dry aerosol extinction values were compared with the dry PM values leading to the significant increase correlation coefficient (cf. Table 1). The potential of this method was demonstrated for the data from the Po Valley (Italy).

Source	Study area	Model description	Optical parameters	R ²
Kuśmierczyk-Michulec et al., (2002)	The Baltic Sea	Non-linear models: α & BC/TPM α & OC/TPM α & SSA/TPM	Angstrom coefficient (α)	0.84 0.88 0.91
Chu et al. (2003)	Ispra (Italy)	Linear model between AOT & PM10: PM10=55 x AOT +8	Ground based AOT	0.82
Wang & Christopher (2003)	Alabama (USA)	Linear model between AOT & PM2.5	AOT retrieved from MODIS 10 km	0.49
Engle-Cox et al. (2004)	USA	Linear model between AOT & PM2.5	AOT retrieved from MODIS 10 km	0.40
Li et al. (2005a)	Beijing (China)	Linear model between AOT & PM10 (API)	AOT retrieved from MODIS (corrected)10 km	0.29
Li et al. (2005b)	Hong Kong (China)	Linear model between AOT & PM10	AOT retrieved from MODIS 1km	0.50
Liu et al. (2005)	Eastern USA	Non-linear model between AOT & PM2.5	AOT retrieved from MISR	0.48
Xia et al. (2006)	Beijing (China)	Linear model between AOT & PM10: summer/autumn/ winter/spring	Ground based AOT at 440 nm	0.77 0.70 0.61 0.37
Koelemijer et al. (2006)	Europe	Linear models between AOT & PM10 AOT & PM2.5	AOT at 550 nm retrieved from MODIS (corrected)10 km	0.46 0.59
Vidot et al. (2007)	Western Europe	Non linear models: AOT & PM10 AOT & PM2.5	AOT retrieved from SeaWiFS	0.43 0.61
Pelletier et al. (2007)	Lille (France)	Non linear model between AOT & PM10; Semi parametric approach (Principal Component Analysis)	Ground based AOT at 440, 670 & 870 nm	0.76
Kuśmierczyk-Michulec et al., (2007)	The Hague (The Netherlands)	Linear model between AOT & PM10 Non-linear models α & BC/PM10: 1) PM<50 μ g/m ³ 2) 50 μ g/m ³ ≤PM<200 g/m ³	Ground based AOT at 555 nm Angstrom coefficient (α)	0.59 0.83 0.84
Péré et al. (2009)	South-Eastern France	Linear model between AOT & PM10: PM10=54 x AOT +13	Ground based AOT at 440 nm	0.69
Jung et al. (2009)	Beijing (China)	Non-linear models: VR & PM1 VR & PM2.5 VR & PM10 Linear models between AOT & PM2.5	Visual range (VR) based on aerosol extinction at 550 nm Ground based AOT at 550 nm	0.93 0.93 0.81 0.70 0.44

Source	Study area	Model description	Optical parameters	R ²
Fischer et al. (2009)	The Taklaman & Gobi Deserts/ The U.S. Pacific Northwest	Linear models between AOT & PM _{2.5} AOT & PM ₁₀	AOT at 550nm retrieved from SeaWiFS, selected for $\alpha \leq 0.7$	0.48 0.50
Barnaba et al. (2010)	The Po Valley (Italy)	Linear models between AOT & PM ₁₀ AOT (corrected) & PM ₁₀ AOT & PM ₁₀ AOT (corrected) & PM ₁₀	Ground based AOT at 500 nm AOT at 550nm retrieved from MODIS, 50 km	0.66 0.94 0.32 0.35
Wang et al. (2010)	Beijing (China)	Linear models between AOT & PM ₁₀ PM ₁₀ =96.96 x AOT + 22.67 ext & PM ₁₀ AOT & PM _{2.5} PM _{2.5} =19.58 x AOT + 8.52 ext & PM _{2.5}	Ground based AOT at 550 nm Aerosol extinction (ext) at 550 nm	0.52 0.77 0.48 0.66
Retalis & Sifakis (2010)	Athens (Greece)	Linear model between AOT & PM ₁₀ : PM ₁₀ =195.7 x AOT + 14.5	AOT at 560 nm retrieved from MERIS	0.83

R²- squared correlation coefficient, TPM- total particulate matter, SSA - sea salts

Table 1. Models associating optical parameters with particular matter concentrations in some of the previous studies.

5.2 Use of the Ångström coefficient in air quality estimation

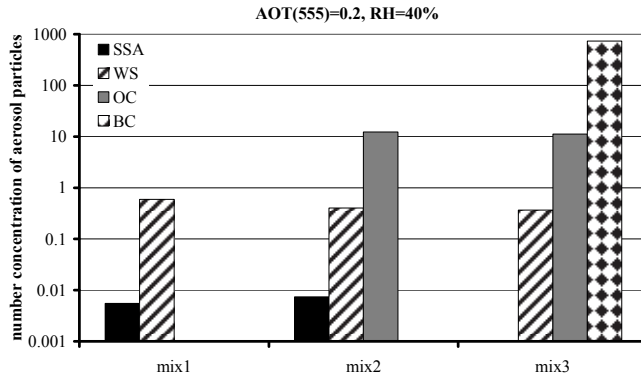
5.2.1 Importance of the spectral measurements

Measurements at one single wavelength will not supply accurate information about the aerosol mixture. Figure 1 shows that one single measurement of the aerosol optical thickness at one wavelength, e.g. $\lambda=555$ nm, will not provide unique information about an aerosol type. The condition that $AOT(555) = 0.2$ at $RH=40\%$ was satisfied by three different mixtures (Figure 1A). Mixture 1 (mix1) consists of 40% of WS (NH_4HSO_4 , $r_n=0.112$, $\sigma=0.58$), and 60% of SSA (NaCl, $r_n=0.5$, $\sigma=0.56$). Mixture 2 (mix2) consists of 20% of WS, 20% of OC (Organic Carbon, $r_n=0.06$, $\sigma=0.3$) and 60% of SSA. Mixture 3 (mix3) consists of 40% of WS, 40% of OC and 20% of BC (Black Carbon, $r_n=0.0118$, $\sigma=0.3$). In consequence, depending on the type of aerosol mixture, different PM values can be obtained. For example at $RH=40\%$, a mixture 2 would lead to approximately 1.4 times higher mass than mixture 1. Accordingly, a mixture 3 would produce approximately 0.6 times lower mass than mixture 1. The reason is that mixture 3 contains a large amount of fine particles of BC, which results in much smaller total mass.

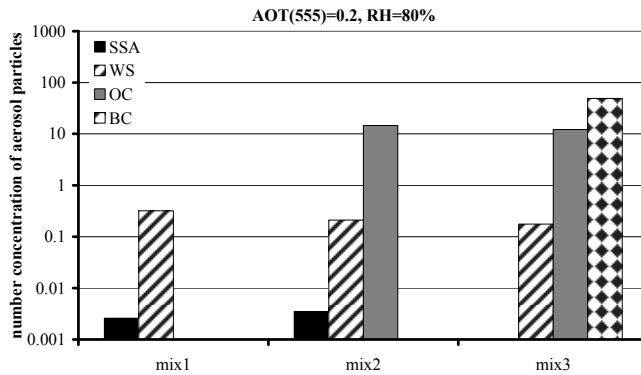
The similar situation is demonstrated in Figure 1B, but for $RH=80\%$. Three different mixtures satisfy the condition that $AOT(555) = 0.2$ at $RH=80\%$. Figure 1C shows that a distinction among mixtures is possible using the Ångström coefficient as an additional parameter. In each case the same composition of aerosol mixtures were used. The effect of

humidity was taken into account by using the formulas proposed by Tang (1976, 1996) and Tang & Munkelwitz (1994).

A)



B)



C)

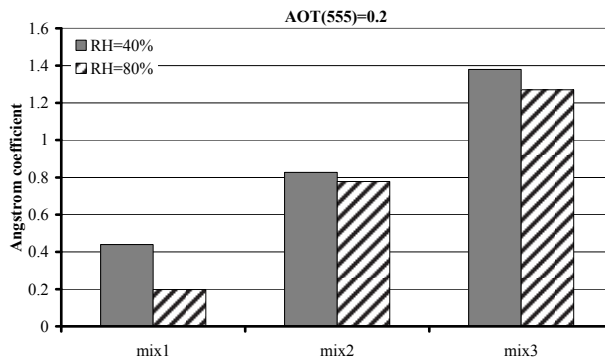


Fig. 1. Three different aerosol mixtures giving as a final result $AOT(555)=0.2$. The composition of mixtures is as follows: mix1: 40% of WS, 60 % of SSA; mix2: 20% of WS, 20% of OC, 60% of SSA; mix3: 40% of WS, 40% of OC, 20% of BC. A) & B) Number concentration of aerosol particles in each mixtures estimated for $RH=40\%$ and $RH=80\%$, respectively. C) The Ångström coefficient as a function of aerosol mixture and relative humidity.

5.2.2 Ambiguity of the proposed formulas

Table 1 gives an overview of various linear and non-linear formulas, developed for different geographical locations and based on measurements taken under different ambient conditions. Some formulas forecast the amount of PM on the basis of dry AOT values; other use AOT values defined at ambient conditions. The AOT is a function of wavelength. Table 1 demonstrates that usually a wavelength for which AOT was determined depends on the type of instrument used for measurements. Hence, the variety of spectral bands: 440 nm (eg. Péré et al. 2009), 550 nm (e.g. Jung et al. 2009), 555 nm (Kuśmierczyk-Michulec et. al. 2007), 500 nm (Barnaba et al., 2010) or 560 nm (Retalis & Sifakis, 2010). Because of that reason a direct comparison is often not straightforward. In addition, most of the formulas presented in Table 1 do not inform about chemical composition. However, it should be emphasized that the AOT-PM relationship depends on the chemical composition of the atmospheric aerosol mixture.

In general transition from AOT at one wavelength to AOT at another wavelength can be done using the Ångström coefficient (see eq. 8). In case the chemical composition is not known and the spectral measurements are not available, the Ångström coefficient can not be determined. In such a case, a direct comparison between amounts of PM in various locations may lead to ambiguity.

Let's assume that AOT at 550 nm is 0.2. Depending on the aerosol type, the Ångström coefficients will vary, from very low, even negative ones corresponding to e.g. desert dust, to very high values, typical for the industrial aerosol type. The higher is the Ångström coefficient the more significant is the contribution of fine particles usually related to the presence of black carbon or anthropogenic salts (e.g. Kuśmierczyk-Michulec, 2009). To compare PM values based on AOT at 550 nm with PM values determined using AOT at 440 nm, application of equation (8) is necessary. To illustrate this problem the formula of Péré et al. (2009) was selected as one of those which use AOT at 440 nm. Figure 2 shows possible changes in PM values caused only by the fact that the Ångström coefficient is not known. Figure 2 demonstrates that lack of information about the Ångström coefficient value may lead to large uncertainties in PM estimation. A difference between the extreme cases (i.e. $\alpha = -0.5$ and $\alpha = 2$) is about $8 \mu\text{g}/\text{m}^3$.

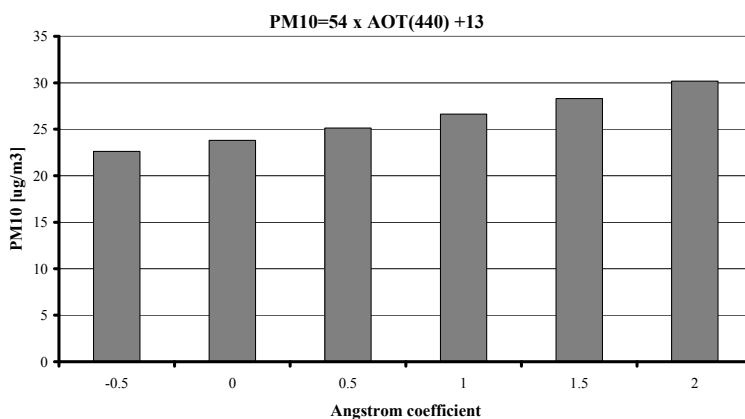


Fig. 2. Influence of the aerosol type, defined by the different Ångström coefficient values on the estimation of PM₁₀ values. The simulations are based on the formula proposed by Péré et al. (2009) for the South-Eastern France.

Another aspect that should be mentioned is a seasonal character of a data sample which is used to derive AOT-PM relationship. In winter time the amount of PM is usually much higher than in summer time, hence possible variations between various formulas. Because of that reason one formula derived for summer data will give different results than a formulae based on the winter data. Figure 3 illustrates such a situation. The amount of PM₁₀ for the Netherlands depends on season, or more precisely whether a formula was obtained for winter data or other seasons. It is interesting to notice that PM₁₀ for France, estimated on the basis of formula obtained for summer data, gives comparable values as the “summer” formula for the Netherlands.

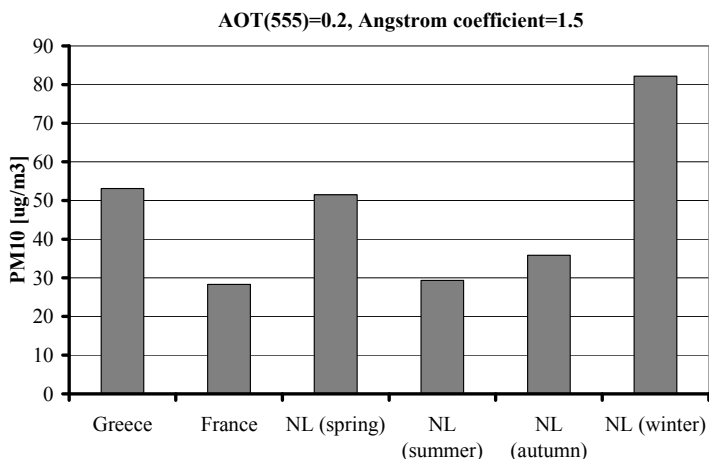


Fig. 3. Estimation of PM₁₀ for three locations in Europe, for the same AOT. The simulations are based on the following formulas: Greece (Retalis & Sifakis, 2010), France (Péré et al., 2009) and The Netherlands (Kuśmierczyk-Michulec et al., 2007).

5.2.3 Application of the Ångström coefficient

When aerosol measurements are made at a land, it can be expected that they represent a mixture which composition depends on the aerosol sources and the air mass history. The large influence will have the type of aerosol emitted by nearby sources, e.g. factories. In general, the main aerosol components of natural atmospheric mixtures include sea-salts (SSA), black carbon (BC), organic carbon (OC), dust-like particles (DL), and anthropogenic salts like ammonium hydrogen sulphate (NH₄HSO₄), ammonium nitrate (NH₄NO₃) and ammonium sulphate ((NH₄)₂SO₄), which belong to a large group of water-soluble particles (WS). Each of these aerosol components is characterized by its own optical and physical properties like for example refractive index or aerosol size distribution (e.g. McClatchey et al., 1984). The optical properties of the aerosol mixture can be represented by the aerosol extinction or by the aerosol optical thickness. Both parameters can be modelled using the external mixing approach. The resultant aerosol optical thickness (or aerosol extinction) is obtained as the corresponding weighted averages of the extinction coefficients using the volume percentages (e.g. McClatchey et al., 1984; Hess et al., 1998). The influence of aerosol composition on aerosol optical thickness and the Ångström coefficient at various relative humidity conditions is discussed by Kuśmierczyk-Michulec (2009).

Since the aerosol optical thickness represents the integrated effect, measurements of AOT at one single wavelength will not supply accurate information about the aerosol mixture (see sections 5.2.1 & 5.2.2). If spectral measurements are available they provide an additional parameter, the Ångström coefficient. This parameter can help to indicate the probable aerosol type which can be useful information (Kuśmierczyk-Michulec, 2009). The Ångström coefficient is far less sensitive to variation in RH than AOT. Moreover, the variations in aerosol vertical distributions have less impact on this parameter.

The Ångström coefficient values include information about proportion between the fine and coarse modes. The fine mode usually can be attributed to the continental/industrial aerosols while the coarse mode represents sea-salts or dust particles (if there is evidence that dust particles can be present). In view of the dependence of the aerosol optical properties on the size distribution and the chemical composition, and the chemical speciation as function of particle size, a relation is expected between the Ångström coefficient and the chemical composition. Kuśmierczyk-Michulec et al. (2002) demonstrated that empirical relations between aerosol mass concentrations and Ångström parameters can be derived. The authors showed that the relations apply to mass concentrations of sea salts, black carbon and organic carbon, expressed in terms of their ratio to the total particulate matter.

The high correlation coefficients between BC/PM₁₀ and the Ångström coefficients (Kuśmierczyk-Michulec et al., 2002; 2007) prove the usefulness of the latter parameter. Therefore it is recommended to use it as an additional parameter in air quality estimation.

6. Conclusions

The increasing number of AERONET stations and thus easy access to ground-based AOT data explains a growing interest in using optical measurements of aerosols in air quality estimation. Moreover, the continuous effort in making improvements of the aerosol retrieval from the satellite data indicates that optical measurements will be one of the standard future methods of estimation the level of pollution.

This chapter gives an overview of various efforts tending toward finding a relationship between AOT and PM₁₀. It discusses advantages and disadvantages of using optical measurements of atmospheric aerosols in estimation of the particulate matter. One of the aspects discussed is that the AOT-PM relationship depends on the chemical composition of the atmospheric aerosol mixture. Because of that reason, to avoid ambiguity in comparing various formulas proposed by different authors for different locations, it would be valuable to use the spectral measurements, and include the information about the Ångström coefficient.

Since the AOT-PM relationship is a simple parametric equation, having a very local character, we should accept that we will not obtain one general equation valid for all locations. However, it would be advantageous to use a similar methodology in obtaining such a relationship. It would make the comparisons between locations and formulas much easier.

7. References

- Alexandrov, M.D., Carlson, B.E., Laci, A.A. & Cairns, B. (2005). Separation of fine and coarse aerosol modes in MFRSR data sets. *Journal of Geophysical Research D: Atmospheres*, Vol. 110, D13204, doi:10.1029/2004JD005226, pp. 1-19.
- Allen, G., Sioutas, C., Koutrakis, P., Reiss, R., Lurmann, F.W. & Roberts, P.T. (1997). Evaluation of the TEOM method for measurement of ambient particulate mass in urban areas. *Journal of Air and Waste Management Association*, Vol. 47, p. 682-689.

- Ångström, A. (1929). On the atmospheric transmission of sun radiation and on dust in the air. *Geogr. Ann.*, 11, 156-166.
- Artaxo, P., Martins, J. V., Yamasoe, M. A., Procópio, A. S., Pauliquevis, T. M., Andreae, M. O., Guyon, P., Gatti, L.V. & Leal, A.M.C. (2002). Physical and chemical properties of aerosols in the wet and dry seasons in Rondônia, Amazonia. *Journal of Geophysical Research D: Atmospheres*, Vol. 107, D208081, doi:10.1029/2001JD000666, pp. 49-1-49-14.
- Barnaba, F., Putaud, J.P., Gruening, C., Dell'Acqua, A. & Dos Santos, S. (2010). Annual cycle in co-located in situ, total-column, and height-resolved aerosol observations in the Po Valley (Italy): Implications for ground-level particulate matter mass concentration estimation from remote sensing. *Journal of Geophysical Research D: Atmospheres*, Vol. 115, D19209, doi:10.1029/2009JD013002, pp. 1-22.
- Bäumer, D., Vogel, B., Versick, S., Rinke, R., Möhler, O. & Schnaiter, M. (2008). Relationship of visibility, aerosol optical thickness and aerosol size distribution in an ageing air mass over South-West Germany. *Atmospheric Environment*, Vol. 42, pp. 989-998.
- Bohren, C. F., & Huffman, D. R. (1983). *Absorption and Scattering of Light by Small Particles*, John Wiley, New York, pp. 550.
- Buringh, E., & Opperhuizen, A., (editors): *On health risks of ambient PM in the Netherlands*, RIVM report 650010032, pp. 380, 2002.
(<http://www.mnp.nl/bibliotheek/rapporten/650010032.pdf>)
- Chu, D.A., Kaufman, Y.J., Zibordi, G., Chern, J.D., Mao, J., Li, C. & Holben, B.N. (2003). Global monitoring of air pollution over land from the Earth Observing System-Terra Moderate Resolution Imaging Spectroradiometer (MODIS). *Journal of Geophysical Research*, Vol 108, 4661.
- De Meij, A., Krol, M., Dentener, F., Vignati, E., Cuvelier, C. & Thunis, P. (2006). The sensitivity of aerosol in Europe to two different emission inventories and temporal distribution of emissions. *Atmospheric Chemistry and Physics*, Vol.6, pp. 4287-4309.
- Dubovik, O. & King, M. D. (2000). A flexible inversion algorithm for retrieval of aerosol optical properties from Sun and sky radiance measurements, *Journal of Geophysical Research*, Vol. 105, pp. 20673 - 20696.
- Dubovik, O., Smirnov, A., Holben, B. N., King, M. D., Kaufman, Y. J., Eck, T. F. & Slutsker, I. (2000). Accuracy assessments of aerosol optical properties retrieved from AERONET sun and sky-radiance measurements, *Journal of Geophysical Research*, Vol. 105, pp. 9791-9806.
- Eck, T. F., Holben, B. N., Reid, J.S., Dubovik, O., Smirnov, A., O'Neill, N.T., Slutsker, I. & Kinne, S. (1999). Wavelength dependence of the optical depth of biomass burning, urban, and desert dust aerosol, *Journal of Geophysical Research*, Vol. 104, pp. 31333-31350.
- Engle-Cox, J. A., Holloman, C.H. & Coutant, B. W. (2004). Qualitative and quantitative evaluation of MODIS satellite sensor data for regional and urban scale air quality. *Atmospheric Environment*, 38, 2495-2509.
- Fischer, E.V., Hsu, N.C., Jaffe, D.A., Jeong, M.-J. & Gong, S.L. (2009). A decade of dust: Asian dust and springtime aerosol load in the U.S. Pacific Northwest. *Geophysical Research Letters*, Vol. 36, L03821, doi:10.1029/2008GL036467, pp.1-5.
- Gong, S. L., Barrie, L. A. & Blanchet, J.-P. (1997). Modeling sea-salt aerosols in the atmosphere 1. Model development, *Journal of Geophysical Research*, Vol. 102, pp. 3805-3818.

- Hansen, J. E. & Travis, L. D. (1974). Light scattering in planetary atmospheres. *Space Science Reviews*, Vol. 16, pp. 527-610.
- Hammingh, P. (editor). (2001). *Air Quality. Annual Survey 1998 and 1999* (in Dutch), National Institute of Public Health and the Environment, report 725301006, Bilthoven, the Netherlands.
- Harrison, L. & Michalsky, J. (1994). Objective algorithms for the retrieval of optical depths from ground-based measurements. *Applied Optics*, Vol. 33, pp. 5126-5132.
- Herman, J. R., P. K. Bhartia, O. Torres, C. Hsu, C. Seftor, and E. Celarier (1997), Global distributions of UV-absorbing aerosols from NIMBUS 7 TOMS data, *J. Geophys. Res.*, 102, 16,911– 16,922.
- Hess, M., P. Koepke, & I. Schult. (1998). Optical properties of aerosols and clouds: The software package OPAC. *Bull. Amer. Meteor. Soc.*, 79, 831-844.
- Hodzic, A., Madronich, S., Bohn, B., Massie, S., Menut, L. & Wiedinmyer, C. (2007). Wildfire particulate matter in Europe during summer 2003 : meso-scale modeling of smoke emissions, transport and radiative effects. *Atmospheric Chemistry and Physics*, Vol. 7, pp. 4043-4064.
- Holben, B.N., Eck, T.F., Slutsker, I., Tanre, D., Buis, J.P., Setzer, A., Vermote, E., Reagan, J. A., Kaufman, Y., Nakajima, T., Lavenu, F., Jankowiak, I. & Smirnov, A. (1998). AERONET- A federated instrument network and data archive for aerosol characterisation, *Remote Sens. Environ.*, Vol. 66, pp. 1-16.
- Holben, B.N., Tanre, D., Smirnov, A. et al. (2001). An emerging ground-based aerosol climatology: Aerosol optical depth from AERONET, *Journal of Geophysical Research*, Vol. 106, pp. 12067-12097.
- Holzer-Popp, T., Schroedter, M. & Gesell, G. (2002), Retrieving aerosol optical depth and type in the boundary layer over land and ocean from simultaneous GOME spectrometer and ATSR-2 radiometer measurements, 1, Method description, *J. Geophys. Res.*, Vol. 107, 4578, doi:10.1029/2001JD002013.
- IPCC, Climate change 2007: The physical science basis. Contribution of Working Group I to the Fourth Assessment Report of the International Panel on Climate Change (<http://www.ipcc.ch/ipccreports>)
- Jung, J., Lee, H., Kim, Y.J., Liu, X., Zhang, Y., Hu, M. & Sugimoto, N. (2009). Optical properties of atmospheric aerosols obtained by in situ and remote measurements during 2006 Campaign of Air Quality Research in Beijing (CAREBeijing-2006), *Journal of Geophysical Research D: Atmospheres*, Vol. 114, D00G02, doi:10.1029/2008JD010337, pp.1-18.
- Kanakidou, M., et al. (2005): Organic aerosol and global climate modelling: a review. *Atmos. Chem. Phys.*, 5, 1053-1123.
- Kaufman, Y. J., and D. Tanre' (1996), Strategy for direct and indirect methods for correcting the aerosol effect on remote sensing: From AVHRR to EOS-MODIS, *Remote Sens. Environ.*, 55, 65- 79.
- Koelemeijer, R.B.A., Homan, C.D. & Matthijsen, J. (2006). Comparison of spatial and temporal variations of aerosol optical thickness and particulate matter over Europe. *Atmospheric Environment*, Vol. 40, pp. 5304-5315.
- Koelemeijer, R. B. A., J. F. de Haan, & P. Stammes.(2003). A database of spectral surface reflectivity in the range 335- 772 nm derived from 5.5 years of GOME observations. *J. Geophys. Res.*, Vol.108, 4070, doi:10.1029/2002JD002429.

- Koschmieder, H. (1925). Theorie der horizontalen sichtweite II: Kontrast und sichtweite. *Beiträge zur Physik der Freien Atmosphäre*, 12, 171-181.
- Kuśmierczyk-Michulec, J. & Rozwadowska, A. (1999). Seasonal changes of the aerosol optical thickness for the atmosphere over the Baltic Sea-preliminary results. *Oceanologia* Vol. 41, pp. 127-145.
- Kuśmierczyk-Michulec, J., de Leeuw, G. & Robles Gonzalez, C. (2002). Empirical relationships between aerosol mass concentrations and Angstrom parameter. *Geophys., Res. Letters*, Vol. 29, pp. 491-494 .
- Kuśmierczyk-Michulec, J., De Leeuw, G. & Moerman, M. M. (2007). Physical and optical aerosol properties at the Dutch North Sea coast based on AERONET observations. *Atmospheric Chemistry and Physics*, Vol. 7, pp. 3481-3495.
- Kuśmierczyk-Michulec, J., van Eijk, A. M. J., Moerman, M. M., Cohen, L. H., de Jong, A. N. & P. Frits. (2008). Transmissometer versus sun photometer measurements of the aerosol optical properties. *Proc. SPIE 7090(0L)*, pp. 1-12, doi:10.1117/12.797837.
- Kuśmierczyk-Michulec, J. & van Eijk. (2007). Angstrom coefficient as a tracer of the continental aerosols. *Proc. SPIE 6708-25*, pp. 1-9.
- Kuśmierczyk-Michulec, J. (2009). Ångström coefficient as an indicator of the atmospheric aerosol type for a well- mixed atmospheric boundary layer: Part 1: Model development. *Oceanologia*, Vol. 51, p. 5-39 .
- Kuśmierczyk-Michulec, J. & G. de Leeuw. (2005). Aerosol optical thickness retrieval over land and water using GOME data. *J. Geophys. Res.*, Vol. 110, doi:10.1029/2004JD004780.
- Lasserre, F., Cautenet, G., Bouet, C., Dong, X., Kim, Y. J., Sugimoto, N., Matsui, I. & Shimizu, A. (2008). A model tool for assessing real-time mixing of mineral and anthropogenic pollutants in East Asia: a case study of April 2005. *Atmospheric Chemistry and Physics*, Vol. 8, pp. 3603-3622.
- Lee, K.H., Kim, Y.J. & Kim, M.J. (2006). Characteristics of aerosol observed during two severe haze events over Korea in June and October 2004. *Atmospheric Environment*, Vol. 40, pp. 5146-5155.
- Li, C.C., Mao, J.T., Lau, A.K., et al. (2005a). Application of MODIS aerosol product in the study of air pollution in Beijing. *Science in China-Series, D Earth Science*, Vol. 35, p. 177-186.
- Li, C.C., Lau, A.K., Mao, J.T., et al. (2005b). Retrieval, validation and application of the 1-km aerosol optical depth from MODIS measurement over Hong Kong. *IEEE Transactions on Geoscience and Remote Sensing*, Vol. 43, 2650-2658.
- Liu, Y., Sarnat, J.A., Kilaru, V., et al. (2005). Estimating ground-level PM_{2.5} in the eastern United States using satellite remote sensing. *Environmental Science and Technology*, Vol. 39, 3269-3278.
- McClatchey, R. A., Bolle, H. -J., Kondratyev, K. Y. , Joseph, J. H., McCormick, M. P., Raschke, E., Pollack, J. B., Spänkuch, D. & Mateer, C. (1984). A preliminary cloudless standard atmosphere for radiation computation, report, 53 pp., Intl. Radiat. Comm., Boulder, Colo.
- Mie, G. (1908). *Annales de Physic*, 25, 377-445
- Morel, A. (1988), Optical modeling of the upper ocean in relation to its biogenous matter content (case I waters), *J. Geophys. Res.*, 93, 10,749-10,768.

- Olszewski, J., Kuśmierczyk-Michulec, J. & Sokólski, M. (1995). The method of continuous measurement of the diffusivity of the natural light field. *Oceanologia*, Vol. 37, pp. 299-310.
- Orr, Jr., C., Hurd, F. K. & Corbett, W. J. (1958). Aerosol size and relative humidity, *J. Colloid Sci.*, Vol.13, 472-482.
- Péré, J.-C., Pont, V., Mallet, M. & Bessagnet, B. (2009). Mapping of PM10 surface concentrations derived from satellite observations of aerosol optical thickness over South-Eastern France. *Atmospheric Research*, Vol. 91, pp. 1-8.
- Pelletier, B., Santer, R. & Vidot, J. (2007). Retrieving of particulate matter from optical measurements: A semiparametric approach. *Journal of Geophysical Research D: Atmospheres*, Vol. 112, D06208, doi:10.1029/2005JD006737, pp. 1-18.
- Remer, L.A., Kaufman, Y.J., Tanre', D., Mattoo, S., Chu, D.A., Martins, J.V., Li, R. -R., Ichoku, C., Levy, R.C., Kleidman, R.G., Eck, T.F., Vermote, E. & Holben, B.N. (2005). The MODIS aerosol algorithm, products and validation. *Journal of the Atmospheric Science*, Vol. 62, 947-973.
- Retalis, A. & Sifakis, N. (2010). Urban aerosol mapping over Athens using the differential textural analysis (DTA) algorithm on MERIS-ENVISAT data. *ISPRS Journal of Photogrammetry and Remote Sensing*, Vol. 65, pp. 17-25.
- Rodriguez, S., Van Dingenen, R., Putaud, J.-P., Dell'Acqua, A., Pey, J., Querol, X., Alastuey, A., Chenery, S., Ho, K.-F., Harrison, R. M., Tardivo, R., Scarnato, B. & Gianelle, V. (2007). A study on the relationship between mass concentrations, chemistry and number size distribution of urban fine aerosols in Milan, Barcelona and London. *Atmospheric Chemistry and Physics Discussion*, Vol. 7, pp. 605-639.
- Seinfeld, J. H. & Pandis, S. N. (1998). *Atmospheric Chemistry and Physics; from Air Pollution to Climate Change*, John Wiley and Sons, pp. 1326, ISBN 0-471-17815-2, USA.
- Smirnov, A., Holben, B.N., Eck, T.F., Dubovik, O. & Slutsker, I. (2000). Cloud screening and quality control algorithms for the AERONET data base, *Remote Sens. Environ.*, Vol. 73, pp. 337-349.
- Tang, I., 1996, Chemical and size effects of hygroscopic aerosols on light scattering coefficients, *Journal of Geophysical Research*, Vol. 101, D14, pp. 19245-19250.
- Tang, I. N. (1976). Phase transformation and growth of aerosol particles composed of mixed salts, *Journal of Aerosol Science*, 7, 361-371.
- Tang, I.N., & Munkelwitz, H. R. (1994), Water activities, densities, and refractive indices of aqueous sulfates and sodium nitrate droplets of atmospheric importance, *Journal of Geophysical Research*, Vol. 99, D9, pp.18801-18808.
- Van de Kasstele, J., Koelemeijer, R. B. A., Dekkers, A. L. M., Schaap, M., Homan, C. D. & Stein, A. (2006). Statistical mapping of PM10 concentrations over Western Europe using secondary information from dispersion modeling and MODIS satellite observations. *Stochastic Environmental Research and Risk Assessment*, Vol. 21, pp. 183-194.
- Van Elzakker, B.G. (2000). Monitoring activities in the Dutch National Air Quality Monitoring Network in 2000, report 723101055, Rijksinstituut voor volksgezondheid en Milieu (RIVM), Bilthoven, The Netherlands, 2000.
- Vaughan, J. K., Claiborn, C. & Finn, D. (2001). April 1998 Asian dust event over the Columbia Plateau. *Journal of Geophysical Research D: Atmospheres*, Vol.106, D16, pp. 18381-18402.

- Vidot, J., Santer, R. & Ramon, D. (2007). Atmospheric particulate matter (PM) estimation from SeaWiFS imagery. *Remote Sensing Environment*, Vol. 111, p. 1-10.
- Wang, J. & Christopher, A. (2003). Inter-comparison between satellite-derived aerosol optical thickness and PM_{2.5} mass: Implications for air quality studies. *Geophysics Research Letters*, Vol. 30, 1-4.
- Wang, Z., Chen, L., Tao, J., Zhang, Y. & Su, L. (2010). Satellite-based estimation of regional particulate matter (PM) in Beijing using vertical-and-RH correcting method. *Remote Sensing of Environment*, Vol. 114, pp. 50-63.
- Xia, X.A., Chen, H.B., Wang, P.C., Zhang, W.X., Goloub, P., Chatenet, B., Eck, T.F. & Holben, B.N. (2006). Variation of column-integrated aerosol properties in a Chinese urban region. *Journal of Geophysical Research D: Atmospheres*, Vol. 111, D05204, doi: 10.1029/2005JD00623, pp. 1-10.
- Yttri, K.E., Aas, W., Bjerke, A., Cape, J. N., Cavalli, F., Ceburnis, D., Dye, C., Emblico, L., Facchini, M.C., Forster, C., Hanssen, J.E., Hansson, H.C., Jennings, S. G., Maenhaut, W., Putaud, J. P. & Tørseth, K. (2007). Elemental and organic carbon in PM₁₀ : a one year measurement campaign within the European Monitoring and Evaluation Programme EMEP. *Atmospheric Chemistry and Physics*, Vol. 7, pp. 5711-5725.

A Mobile Measuring Methodology to Determine Near Surface Carbon Dioxide within Urban Areas

Henninger, Sascha
Technical University of Kaiserslautern
Germany

1. Introduction

Atmospheric carbon dioxide is one of the infra-red active trace gases responsible for the anthropogenic global warming. Due to the increasing use of fossil fuels within the lower atmosphere, but also within the urban boundary layer of urban agglomerations, an increase of the CO₂ concentration must be expected. Less is known about the temporal and spatial behavior of this trace gas, especially in cities and their surrounding areas. Between 2002 and 2004 first investigations were made about the distribution of the CO₂ concentration within the urban canopy layer of the city of Essen, Germany (51°28'N, 7°0'E). These first measurements should develop and verify a mobile measuring methodology to determine the air quality indicators, first of all CO₂, but also CO, NO, SO₂, O₃, in dependence of the urban types of land use, the topographical circumstances and the meteorological conditions and how to transfer this methodology to other cities. For this implementation there were additional mobile measurements done in different cities within different climatic zones from 2006 till 2010.

The structure of emission within an urban area is mainly characterized by traffic and the private domestic heating (especially in winter). The proportion of power plant and industrial facilities is less, because of the plume height of the stacks. Most of this emission is blown away from the urban sites. On the basis of the predominantly low source heights and the invariable and variable factors, which determine the distribution of the trace substances and define their chemical transformation, the question was how the emission is dependent on the local urban types of land use and how these were affiliated with each other. Because of the different sources of emission the urban air quality is spatially as well as temporarily extremely volatile. Some reasons for this inhomogeneous field of emission are the transportation infrastructure, different heights of the emission sources and the limited exchange of the urban canopy layer within the street canyons. Therefore, it is hardly possible to use results of air quality measurements from fixed urban measuring stations. An adequate transferability of these could not be guaranteed for more than the immediate proximity of the station. One way of analyzing the fine structure of the different fields of emission is creating a numerical analysis model which enables a prediction of the traffic-related exposure. However, this modeling requires a corresponding number of input values and a suitable validation.

Another possibility detecting the inhomogeneous urban fields of emission is using mobile air quality measurements. The advantage of this type of methodology is the high density of measurements, which could be mapped spatially. Although especially in the applied urban climatology the methodology of mobile measurements to detect data of air temperature and air humidity has been practiced for a long time, mobile air quality measurements do not have quite a long tradition. Already in the 1920's mobile air temperature measurements were made (Schmidt, 1927; Pepler, 1929). The first ones were semi-mobile, but in the course of the time the technological development allowed to measure continuously from the beginning to the end of the transect. Due to the high quality demands on the measurement equipment the number of mobile air quality measurements is low, mainly with a bulk on the air pollutants CO, NO and O₃, also for particulate matters. Up to now, there is no adequate single methodology for mobile air quality measurements, which ultimately ensures a comparability of the results of different publications. Thus all publications vary on the subject of travelling speed, length of the measuring route, the sampling rate of the analyzers, the measuring time and period and the types of detected trace elements (e. g. Heussner, 1988; Luria et al., 1990; Shorter et al., 1998; Kuttler & Straßburger, 1999; Idso et al., 2001; Bukowiecki et al., 2002; Kuttler & Weber, 2006; Henninger, 2008a).

2. Urban carbon dioxide

Attention on the urban CO₂ concentration was already paid in the 19th century. Probably one of the oldest analysis of continuously measured carbon dioxide within an urban area was from 1877 till 1910 in the outskirts of Paris, France (Stanhill, 1982). During the measuring period the annual average of the carbon dioxide varied between 284 ppm and 325 ppm. After the mid-20th century investigations considering the urban CO₂ started in its entirety. One of the first was a two-year measurement campaign in Vienna (Austria). Already at this time Steinhauser et al. (1959) were able to point out that an increase of the CO₂ concentration is dependent on the wind direction, which blows gently from the urban sectors and that domestic fuel combustion caused a significant difference of trace gas concentration between summer and winter month.

Traffic, domestic fuel combustion, industrial facilities, and power stations are verifiably the most important sources of CO₂ emission within urban conurbations. But in the case of carbon dioxide, the urban vegetation must also be mentioned, in fact the plant respiration has an undeniable amount on the total urban CO₂ concentration. But of course urban green areas have the function of natural CO₂ sinks of the anthropogenic carbon dioxide (Nowak & Crane, 2001; Yang et al., 2005; Henninger, 2005a; 2008; Henninger & Kuttler, 2007; 2010). Down to the present day the available literature shows a continuously increasing number of publications dealing with the arise and allocation of urban carbon dioxide. A simple classification offers five types of detecting CO₂ within the urban boundary layer:

1. Investigations of the turbulent vertical flux of carbon dioxide, especially within urban street canyons (e. g. Nemitz et al., 2002; Grimmond et al., 2004; Moriwaki & Kanda, 2004; Salmond et al., 2005; Velasco et al., 2005; Vogt et al., 2005; Coutts et al., 2007).
2. Analyzing the stable carbon isotopes to determine CO₂ sources (e. g. Clarke-Thorne & Yapp, 2003; Pataki et al., 2003; Carmi et al., 2005; Pataki et al., 2006).
3. Stationary CO₂ measurements to determine the diurnal or seasonal course of the concentration within a given type of land-use (e. g. Ghauri et al., 1994; Derwent et al., 1995; Inoue & Matseuda, 2001; Manuel et al., 2002; Sikar & La Skala, 2004; Salmond et al., 2005).

4. Measuring the gradient of carbon dioxide between urban and rural locations (e. g. Berry & Colls, 1990a/b; Ziska et al., 2004; George et al., 2007).

All of these studies were carried out by stationary measurements. These investigations require a lot of time, work, and equipment to ensure the transferability from the measurement location to its nearby vicinity. Measuring vertical turbulent fluxes and long time-series of CO₂ present representative concentration and fluxes, which can be very heterogeneous over small spatial scales.

An opportunity to solve this problem made it necessary to create a measurement methodology, which is applicable for different types of land usage and of trace elements, but also representative, so that an ultimately statistical reproducibility of the results can be guaranteed. This enables to classify a fifth type to determine urban carbon dioxide:

5. Mobile measurements with the aid of mobile air quality laboratories (e. g. Idso et al., 1998; 2001; Henninger, 2005a; 2008; Henninger & Kuttler, 2007; 2010).

Although mobile measurements promise a high spatial and temporal density of area-covering information, still only few publications deal with mobile measurements of CO₂ within urban environments. Especially, there is a gap between considering various influencing factors within the urban canopy layer, which could affect the pattern of the CO₂ concentration permanently. Publications about mobile measurements were based on a definite measuring route to determine typical inhomogeneous fields of air pollutants within urban spaces (e. g. Luria et al., 1990; Shorter et al., 1998; Idso et al., 1998; 2001; Bukowiecki et al., 2002). All these exemplarily shown investigations were only made over short time periods of few days up to several weeks. Due to this it is impossible to consider different seasons and different times of the day, which affect the variability of the CO₂ concentration within the urban boundary layer. Accordingly it is also impossible to get representative and reliable statements about the atmospheric CO₂ concentration within the urban canopy layer. Particularly with regard to the current discussion about reducing the emission of CO₂, analyzing urban trace elements becomes a specific relevance because today's urban agglomerations must be considered as one of the major carbon dioxide sources with an increasing tendency in the future. An accurate impression of the exhaust of the greenhouse gas is only possible if multifarious patterns of the different urban land uses are considered because not every urban land use is coevally a CO₂ source. So this is one of the major uncertainties, precisely because it is very difficult to relate CO₂ concentration to a specific type of land use by 100 %. Advective processes may have more or less influence, which could not be completely eliminated. However, it is very important to differ between urban green areas, industrial, commercial and residential areas. Mobile measurements have the ability to assure this because all different types of land use could be achieved, so that there is not only a differentiation between the land use, but also a diverse structure within one land use. For example residential areas can be classified by the variation of the structure of housing (Henninger, 2008a).

Due to a heterogeneous structure of different types of land use within urban areas we must expect a great number of diverse fields of emission of different atmospheric trace gases. Therefore these could poorly be recorded by conventional stationary measurements. Stationary measurements are particularly suitable for long-range homogeneous areas, however, their temporally highly resolved results could hardly be transferred to other types of land use. Hence, there is the opportunity of mobile measurements to solve this problem within such a heterogeneous structure of an urban area. An important point of discussion regarding mobile air quality measurements is the temporal and spatial representation in contrast to standardized stationary measurements. With the aid of highly frequented spatial

air quality measurement trips it is possible to have numerous measuring points along the measuring route. Due to this highly frequented spatial detection of different trace substances a mobile measuring route is well suited for recording the non-homogeneous urban area with its diverse fields of emission based on their different types of urban land use. Generally, the urban field of emission is mainly dependent from the emissions of traffic and the domestic fuel combustion, less from the emission of power plants and industrial areas. Especially, because of the uneven distribution of these different types of emission sources, mobile measurements are inevitable and the only possibility of obtaining spatially high resolutions of the pattern of different air quality substances. In addition, a high quantity of mobile survey tests solves the disadvantage of a low temporal resolution (Henninger, 2005a; 2008; Henninger & Kuttler, 2007; 2010).

Due to the fact that it is not possible to fade out the weather conditions and other influencing factor it must be the aim to analyze the dependence of urban CO₂ concentration by temporal variable (e. g. air temperature, atmospheric stability) as well as invariable (e. g. surface configuration) influencing factors within the urban canopy layer. It should prove how the urban CO₂ concentration is influenced by spatial variations as well as diurnal and seasonal meteorological conditions (Henninger, 2005a; 2008).

3. Measurement methodology

3.1 Mobile measurements

Even though, there exist many different investigations of mobile air quality measurements, there are lots of significant differences in spite of the used methodology. So it was necessary to create a general measuring method, which has the ability to determine the urban air quality in a representative way so that an ultimate statistical demonstrable reproducibility of results can be guaranteed.

The mobile measurements were made by a mobile laboratory. The analytical equipment allowed, in addition to CO₂, a continuous determination of the air quality indicators carbon monoxide (CO), nitrogen monoxide (NO), nitrogen oxides (NO_x), ozone (O₃) and particulate matter (PM₁₀) during the measuring trips at a height of 1.50 m above ground level. The air sampling was done on the right-hand side of the mobile laboratory to reduce the influence of passing motor vehicles. In addition to the trace elements the meteorological values air temperature and air humidity were measured in the front of the mobile lab at 2 m above ground level, also barometric pressure, solar radiation and UV radiation at 3.50 m above ground level on the roof top of the vehicle.

In consequence that the different air quality indicators were based on diverse analytical methods the equipment had to be calibrated before every measuring trip. Due to the fact that carbon dioxide is not classified as a classical air pollutant there is no engaging guideline how CO₂ should be measured in ambient air. So the CO₂ analyzer was calibrated according to the official guideline of the German VDI (VDI guideline 3950, sheet 1, 1994). The analyzers of the other air pollutants were also verified according to the VDI guidelines 2459, sheet 6, 1980 (CO), 2453, sheet 2, 2002 (NO, NO_x) and 2468, sheet 6, 1979 (O₃). Carbon dioxide and carbon monoxide were analyzed using IR absorption, ozone by UV absorption. In contrast, the nitrogen oxides were determined by chemiluminescence. Air quality analyzers as well as the equipment for meteorology were calibrated with a measuring frequency of 1 Hz, which made temporal corrections of all data less complicated.

The maximum driving speed was 30 km h⁻¹ along streets (8 m s⁻¹) and 60 km h⁻¹ (about 16 m s⁻¹) on freeways. In spite of the known delay times of the analyzers (e. g. CO₂ = 13 sec.) and a measuring frequency of 1 Hz the spatial resolution of the measurement was 8 m and 16 m respectively. With regard to the delay times of the different instruments and the low driving speed of the mobile lab measurements could be made approximately in real time. At the end of each measuring trip the analyzers were still kept on running for another of 30 seconds. Due to this the delay times of all analyzers were considered. This subsequent temporal correction of the measured values for CO₂, CO, NO, NO_x, O₃ and PM₁₀, but also for the meteorological parameters enabled most accurate and representative results of the air quality and meteorology along the transect. In addition to the measured values also GPS coordinates (measurement frequency of 1 Hz) allowed to relate every recorded value of the air quality indicators to its GPS-point along the measuring route.

Looking for a representative and an almost unaffected measuring method for air quality indicators within streets canyons to determine the pollutants without a direct influence of diverse vehicles standing or waiting in front of the mobile laboratory or beside it, was a great afford. Due to traffic jams or red lights there could be a lot of interruptions of the analysis of the data. Such a situation causes an accumulation of the air borne pollutants and accordingly ensures an increase of the concentration. A similar problem for measuring more or less representative values could be the exhaust plume of the vehicles, which are driving directly in front of the mobile lab and thus leads to a distortion of the results. Every second logged data were marked manually using GPS to solve this problem. For that each traffic stop and traffic jam could be mapped along the transect and was filtered out before the analysis of the raw data. It is of great importance that the suction unit of the air quality indicators of the mobile laboratory is placed on the opposite side of the road traffic and thus is already protected against the direct impact of vehicle emissions. Additionally a safety distance of > 2 m from the directly vehicles in front of the mobile lab was adhered to reduce the influence of others. This safety distance is based on Clifford et al. (1997). They could prove by different simulations that the influence on the concentration of the exhaust plume of vehicles in front of another is significantly decreasing and is nearly negligible up to 1.50 m or more meters. Nevertheless, the raw data must be checked for plausibility despite marking the data. So individual values of the data set, which deviate significantly from the others, should be removed manually before the subsequent analysis.

However a comparison of the concentration CO₂ concentration pattern along the transect indicates that there are no significant differences between the carbon dioxide courses with and without filtering out the stops (n = 150, $\alpha > 0.5$). A correlation between the corrected and the uncorrected results for the diverse measuring routes offers a correlation coefficient $R^2 = 0.94$ (n = 150; $\alpha > 0.5$) for all measuring times, day and night. This correlation coefficient is shown exemplarily for the whole measuring period in figure 1. Divided into day and nighttime measurements, the nighttime survey test indicates a plainly higher $R^2 = 0.98$ (n = 60; $\alpha > 0.5$) in comparison to the measuring trips during the day ($R^2 = 0.90$; n = 90; $\alpha > 0.5$). Due to a lower probability of traffic-related interruptions and verifiable more stable atmospheric conditions overnight the effect of different sources of CO₂ emissions is vanishingly low. The atmospheric conditions are based on the calculation of the stability index of Pasquill (1961) and Polster (1969) by using the data of meteorological stations, which were installed along the measuring route. Anyhow it was not abandoned filtering out the obviously influenced data because ultimately, even if there is a correlation coefficient of $R^2 > 0.90$ for all measuring trips, the determined values were still influenced.

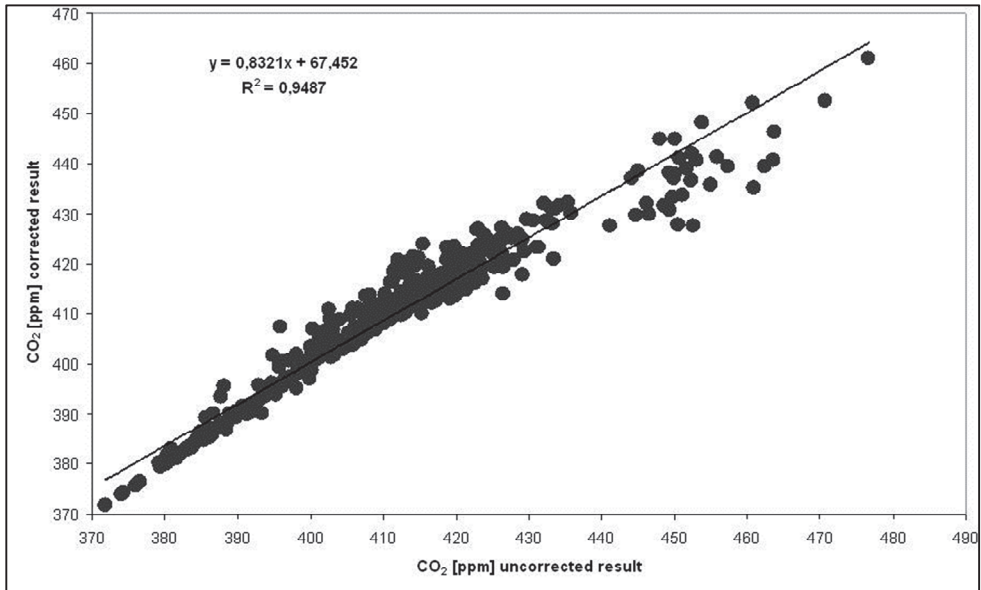


Fig. 1. Scattergram for the correlation between the uncorrected and corrected results of the CO₂ measurements made within different urban areas (n = 150)

Because of a relatively high spatial fluctuation of the trace gas concentration along the measuring route it was necessary to calculate the arithmetic mean values of the so-called homogeneous road sections (Kuttler & Wacker, 2001; Henninger, 2005a; 2008; Henninger & Kuttler, 2007; 2010). Spatial fluctuations could be caused by the change of the structure of housing along the streets, varying density of traffic or the change of land use and different climatopes. By this way, creating different route sections along the transect enables a direct comparison of single measuring trips with each other and a better interpretation for the data processing. Though every road section is characterized by a type of land usage, the length of a section could vary from time to time. So it is unavoidable that a continuous transition from one type of land usage to another could not always be guaranteed. Exemplarily, due to a length of 63 kilometers the measuring route could be subdivided into 61 road sections with a length of nearly 1000 meters each (Henninger, 2008a). In order to reduce the influence of the transition from one area to the neighboring road section it was ensured that these five seconds of travelling (~ 40 m) were not taken into account.

3.2 Measuring site

Generally all urban areas present a heterogeneous structure due to the different types of land use. As it is reflected in the local emission structure of the different trace elements within the urban site. For this reason, the measuring route has to take all urban types land of use into account in order to obtain a representative pattern of the appropriate carbon dioxide situation.

First measurements determined the near surface urban carbon dioxide by a mobile laboratory in the city of Essen, Germany (51°28'N, 7°0'E) between 2002 and 2004 to verify the theoretical deliberations. Due to its location and structure within the conurbation area

“Ruhrgebiet“, Essen should be representative for its structure of anthropogenic carbon dioxide emissions. Regarding its structure of emission within the urban canopy layer of Essen, the most important impacts within the investigation area are determined to be the low emission heights of traffic and domestic fuel. The measurement route had a total length 63 kilometers and led the transect from the south to the north of the urban area. It displayed a serpentine route to ensure that the measuring transect included all varieties of urban land use. Additional mobile measurements have been made between 2003 and 2010 within different urban areas with diverse sizes and in different climatic zones to investigate the transferability of the measuring method (Tab. 1):

Location	Measuring time	Trace elements	References
Essen, Germany (51°28'N, 7°0'E); 580,000 inhabitants; A = 210 km ²	2002 till 2004	CO ₂ , CO, NO, NO _x , O ₃	Henninger, 2005a/b; Henninger, 2008a; Henninger & Kuttler, 2007; Henninger & Kuttler, 2010
Krefeld, Germany (51 ° 20'N, 6° 35 'E); 238,000 inhabitants; A = 138 km ²	2003 till 2004	CO ₂ , CO, NO, NO _x , O ₃	Henninger, 2005b
Bad Ems, Germany (50°25'N, 7°45'E); 10,000 inhabitants; A = 16 km ²	2005	CO ₂ , CO, NO, NO _x , O ₃ , PM ₁₀	Henninger 2008b/c
Koblenz, Germany (50°21'N, 7°36'E); 106,500 inhabitants; A = 105 km ²	2006	CO ₂ , CO, NO, NO _x , O ₃ , PM ₁₀	
Kigali, Rwanda (1°57'S, 30°4'E); 1,000,000 inhabitants; A = 738 km ²	2008-2009	CO ₂ , CO, NO, NO _x , O ₃ , PM ₁₀	Henninger 2009a/b
Saarbrücken, Germany (49°14'N, 7°0'E); 176,000 inhabitants; A = 167 km ²	2010	CO ₂ , CO, NO, NO _x , O ₃ , PM ₁₀	

Table 1. Schedule of mobile CO₂ measurements with the same measuring methodology

Based on the described measuring method further investigations were made by Ptak (2009). Between 2005 and 2007 she performed in two German cities (Münster; 51°57'N, 7°37'E and Lüdenscheid; 51°13'N, 7°37'E) mobile carbon dioxide measurements, confirmed the method and the following described representative status of it.

Generally, for the choice of a measuring route in dependence of the location and its characteristic and typical urban types of land use the following factors should be considered:

- a big variety of different types of land use because all types of urban usage within the urban area should be taken into account,
- the route should be planned along roads with not much traffic, to ensure that increased CO₂ concentration within the investigation area does not necessarily be attributable only to urban traffic and

- a comparable and a similar type of land use respectively should be at the beginning and end of the measuring route.

3.3 Measuring times

A total of 150 mobile measurements was made between 2002 and 2010 on weekdays and weekends regarding different conditions. Most of the mobile measurements were made during clear and calm weather conditions ($v \leq 1.5 \text{ m s}^{-1}$) and at different times of the day. The low wind speed guaranteed more pronounced local differences of the near surface urban carbon dioxide in relation to the respective types of land use. Thus enables a representation of the urban CO₂ situation for a so-called "worst-case" with low exchange ratios and a negligible influence on a long-distance transport.

The measurement times were primarily based on the daily occurring rush hour. Due to the fact that during the daily rush hours only a short-term situation of the daily air pollution is rendered, the measurements were made in each case before (4 a.m. - 7 a.m. respectively 1 p.m. - 4 p.m.) and after the traffic peak hours (10 a.m. - 1 p.m. respectively 7 p.m. - 10 p.m.) to enable inter alia a uniform traffic flow along the measuring route, but of course also a homogeneous structure of trace elements, especially for CO₂, in order to show a representative carbon dioxide situation within the urban canopy layer.

The mobile measurements should be performed during both day- and nighttime hours. So the influence of e. g. urban green areas as potential sources of CO₂ (respiratory gas exchange at night) and CO₂ sinks (photosynthetic gas exchange during the day) can be considered. The natural diurnal variations in CO₂ concentration, aroused by the gas-exchange cycle of the biosphere could be represented. For this reason additional trips were taken between 11 p.m. and 2 a.m. to cover the transition time from the first to the second part of the night. This night-time measuring period ensures the determination of the second peak of natural CO₂ caused by the respiratory gas exchange around midnight (Allen, 1965). In addition it was also possible to have a look at the atmospheric boundary layer conditions in connection with the times of the day and its influence on the urban CO₂. Regardless, the dependence of the time of the day measurements should be placed on weekdays (Monday till Friday) as well as on weekends (Sunday) and holidays (Henninger, 2005a; 2008).

3.4 Classification of variable and invariable influencing factors

Trace elements within the urban area are highly volatile components of the air. As a result of the heterogeneous urban structure the pattern of the CO₂ concentration along a measuring route is affected by a number of different temporal variable as well as invariable influencing factors (Henninger, 2008a). Therefore it is not possible to evaluate the urban carbon dioxide along a transect considering only different measuring times and different weather conditions like e. g. Idso et al. (1998; 2001) did in Phoenix, Arizona, USA, giving a representative statement about the behavior of near surface urban carbon dioxide. Instead, the multidimensional dependence of CO₂ was determined first by a correlation analysis (*Pearson and Bravais*) and a partial/multiple correlation analysis (Schönwiese, 2006). The different influencing factors were analyzed separately to identify the dominant one. Hence, it was necessary to differentiate between the following temporal variable and invariable factors (Tab. 2; Henninger, 2008a):

Temporal variable factors	Temporal invariable factors
Atmospheric stability of the urban canopy layer	Sky view factor (ψ_s)
Air temperature	Surface configuration
Air humidity	Traffic density
Urban vegetation	

Table 2. Schedule of the different influencing factors which could manipulate the CO₂ pattern within the urban canopy layer

The decision to interpret traffic density as a temporal invariable factor is based on the calculation of traffic data from the council, which is being published at the end of each month. Thus, there is a fixed number of vehicles for each hour.

4. Statistical proofs

Using various statistical methods like cluster analysis, test of significance (*t-test*) and correlation analysis the reproducibility of the mobile measuring trips should be verified. A statement should be given for the situation of air quality within its urban investigation area and whether this determined pattern of carbon dioxide concentration is not only a snap-shot, but rather a recurring incident. The statistical analysis should show whether the measured CO₂ data is in both temporal and spatial behavior representative and reproducible for the route sections or whether it is the result of a random acquired CO₂ pattern.

Primarily, the single linkage cluster analysis with an Euclidean distance (in ppm) should give information about similarities of the behavior of CO₂ concentration along the transect between all completed measuring trips for a definite investigation area. Exemplarily, this is shown in figure 3. It offers five separate clusters, which are identical with the five different times of measuring. This result was checked by a comparison between two measuring trips, being connected in one cluster but also for measuring trips being placed in different clusters by a big distance. Figure 4 presents a uniform allocation of CO₂ along the transect for the measurements made at the same time of the day which creates one similar cluster. An additional test of significance (*t-test*) confirmed this validation. Measurements taken at the same time of the day, but on different days display no significant differences ($\alpha > 0.5$, Fig. 4). In contrast, trips driven at diverse times show significant differences ($\alpha < 0.05$) respectively a high significant difference ($\alpha < 0.01$) and no similarities in respect of the pattern along the transect (Fig. 5).

These results could be proven for all survey tests of the first initial measurements which were taken between 2002 and 2004 ($n = 44$) as well as for the all additional ones driven between 2003 till 2010 ($n = 150$) to validate the measuring methodology being devised by Henninger (2005a). The preliminary statistical analysis demonstrates that there is, in dependence on the time of the day, a recurrent CO₂ pattern along the transect. That is why a reproducibility of the behavior of CO₂ concentration can be verified and enables an allocation of the different classified variable and invariable influencing factors along the transect (Henninger, 2008a).

5. Reproducibility of the data

At this stage the statistical analysis of the mobile measurements of near surface carbon dioxide between 2002 and 2010 has shown that it is possible to resolve the CO₂ mixing ratio spatially as well as temporarily in dependence of the structure of the urban types of land use. It could be demonstrated that the methodology of measuring carbon dioxide near the ground was not only feasible for one urban area, but it rather works for every urban settlement. Notwithstanding of the general achievements mentioned before, the reproducibility of the data should be offered for one detailed example reconstructing the conclusion of this disquisition. As a consequence the results of a measuring period of at least two years within the city of Essen could explain the applicability of the method the best way. First of all, with the aid of a cluster analysis the CO₂ data for the whole measuring period ($n = 40$) were divided into meaningful sub-collectives and groups respectively. This calculation based on the comparison of the temporal courses of the CO₂ concentration patterns during each measuring trip. As it is shown in figure 2 three defined clusters were composed of the respective measuring trips for the seasons autumn, winter and spring. Therefore it could be assumed that the temporal behavior of the involved measurements offer extensive similarities within each season. A solitary exception indicated the summer months. The splitting of the summer measuring trips into two clusters could be explained by the significant concentration differences, which occur between the day- and night-time situation during this season. Indeed, there are also detectable night and day concentration gradients for carbon dioxide during the other three seasons, but plainly smaller and less noticeable.

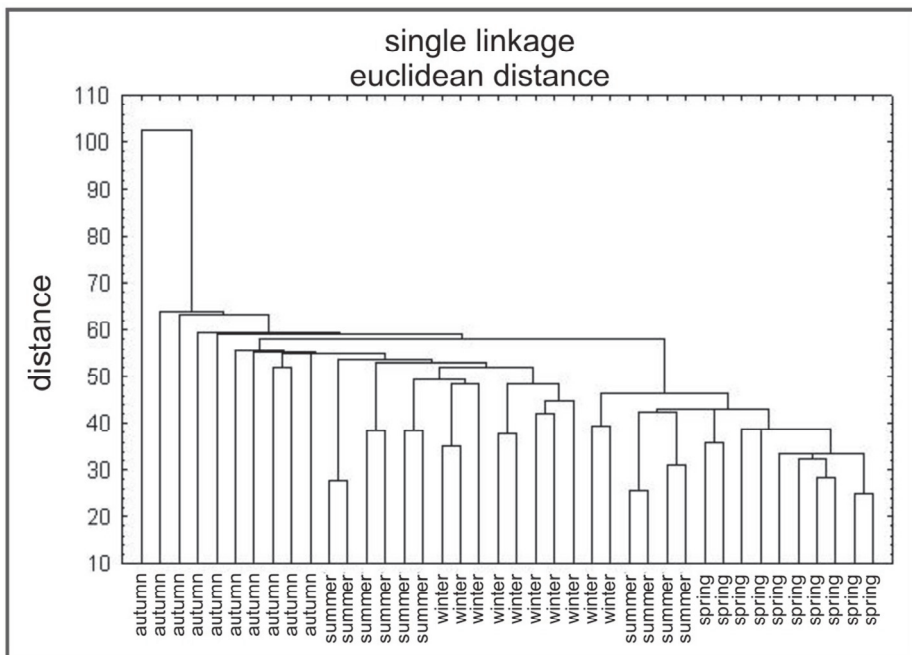


Fig. 2. Seasonal cluster analysis and cluster diagram of all CO₂ measuring trips taken in 2002 and 2003 within the urban area of Essen, Germany ($n = 40$)

This result was also analyzed by a test of significance (*t-test*), which showed that $\alpha < 0.05$ ($S_i = 95\%$) indicates, however, that there is no direct correlation between the measuring trips in spring, summer, autumn and winter. Finally, this *t-test* confirmed the results of the cluster analysis displayed in figure 2.

For the next step the data of each “seasonal cluster” were treated separately. A secondary cluster analysis revealed that in the individual assessment of the seasons the groups were clearly distinguished from each other again. Five different clusters could be established within the four “seasonal clusters”, each identical with the five different times of measuring. As an example of this result the “summer cluster” is shown in figure 3. This one was not only specifically chosen to point out the similarities of the measuring period from June to August because it could not only be shown how the five clusters represent the different measuring times, but also the well-known splitting within the season, which was mentioned in figure 2. The day time measurements were reflected in one cluster group (10 a.m. – 1 p.m.; 1 p.m. – 4 p.m.), also the night-time measuring trips (11 p.m. – 2 a.m.; 4 a.m. – 7 a.m.; Fig. 3). The measurements from 7 p.m. till 10 p.m. can also be assigned to the day time hours because throughout this part of the day there was no sundown at all during the measurements.

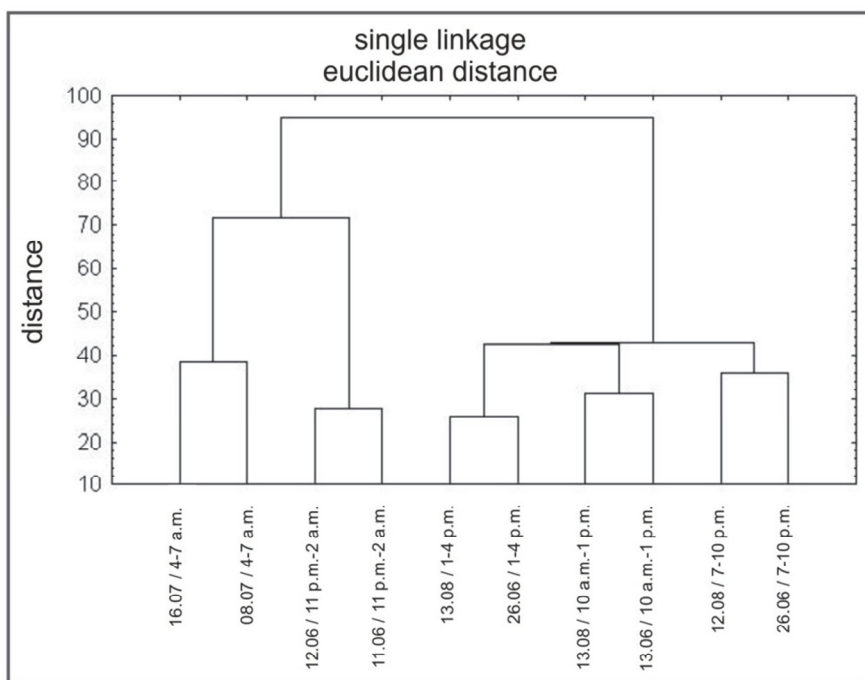


Fig. 3. Cluster diagram of the summer CO₂ measuring trips within the urban area of Essen, Germany (n = 10)

Nevertheless, there had to be similarities within the measurements at the same time to constitute a separate cluster for these trips. Therefore, measuring trips, which offered a common cluster (e. g. 16.06.03, 7 p.m. – 10 p.m. and 12.08.03, 7 p.m. – 10 p.m., Fig. 3), were

analyzed on their relationship between two characteristics (route sections and average values of the route sections) and ongoing calculating of the correlation coefficient after *Pearson* and *Bravais*. The result is, that the CO₂ patterns of the two measuring trips along the transect reveal a nearly identical profile (Fig. 4). This feature of figure 4 was confirmed by a high correlation coefficient of $R^2 = 0.91$. The variety in the concentration levels along the measuring route and the difference between the two curves respectively could be explained in virtue of wind speed (16.06.03 $v > 1.5 \text{ m s}^{-1}$ and 12.08.03 $v \leq 1.5 \text{ m s}^{-1}$) during the measurements. However, it is obvious that wind speed affects the height of the near surface urban CO₂ concentration, but not the spatial pattern and the occurrence of trace elements.

A comparison of two measuring trips, which were not related in a temporal cluster (e. g. 11.06.03, 11 p.m. – 2 a.m. and 08.07.03, 4 a.m. – 7 a.m., Fig. 5), confirmed the output of figure 3 as well as figure 4. There are almost no similarities shown in the CO₂ pattern of two survey tests ($R^2 = 0.17$), which had not been done at the same time of day. A crucial moment to this significant difference is the distinction of the atmospheric stability and the variation of the traffic density during these two times of measuring.

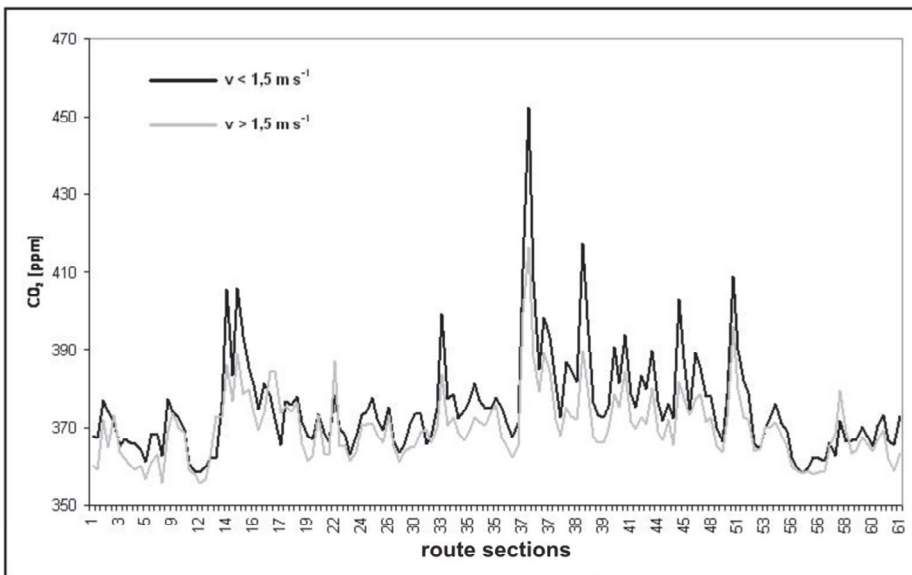


Fig. 4. CO₂ profiles ($R^2 = 0.91$) for two summer measuring trips with an identical measuring time (7 p.m. – 10 p.m.), but different measuring days within the urban area of Essen, Germany. Though both trips are part of one cluster (fig. 3) they showed up different wind speed, but no significant differences ($\alpha > 0.5$) for the carbon dioxide situation along the measuring route

An additionally implemented calculation of the product moment correlation coefficient by *Pearson* ratifies similarities to the results of the cluster analysis (Tab. 3). Thus the calculation showed high correlation coefficients for the same times of measuring, but only low positive to low negative correlations for the different times. Furthermore, using the *t-test*, it could be demonstrated that the measuring trips of the same season driven at the same measuring time, revealing a common cluster, offered no significant differences ($\alpha > 0.5$). Accordingly to this, it could be calculated that for measurements taken at different times of the day

indicated a significant ($\alpha < 0.05$) and a highly significant difference respectively from each other ($\alpha < 0.01$). These results could be illustrated for all seasons. That is why it could be postulated that in dependence of the time of day and the season a recurring pattern of near surface carbon dioxide along the measuring route is verifiable. So this could be regarded as an evidence for the conclusion that the reproducibility and thus the representativeness of the CO₂ data is given determined within the urban area.

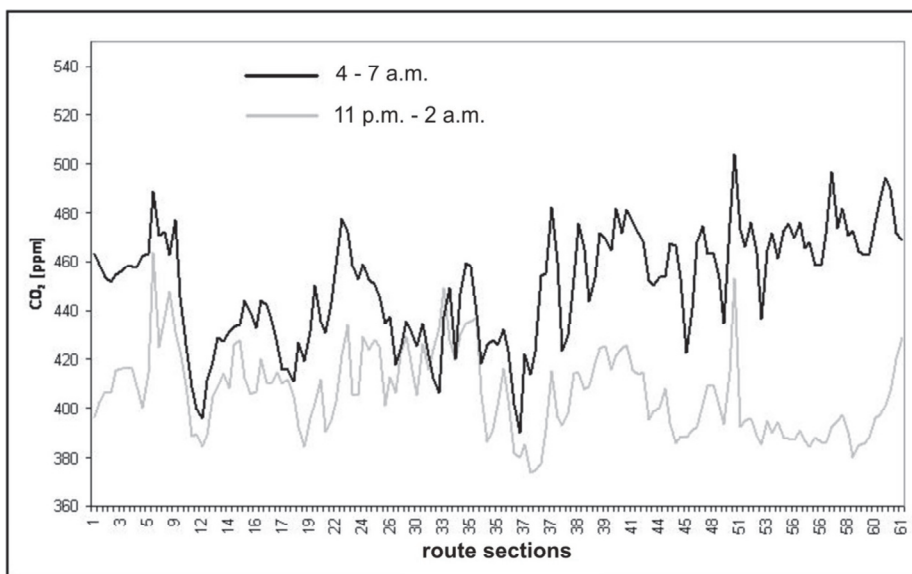


Fig. 5. CO₂ profiles ($R^2 = 0.17$) for two measuring trips with different measuring times (4 a.m. – 7 a.m. & 11 p.m. – 2 a.m.), but identical wind speed ($v < 1.5 \text{ m s}^{-1}$) within the urban area of Essen, Germany. Both trips are not part of the similar cluster (fig. 3), showing a significant difference of $\alpha < 0.05$ for the carbon dioxide situation along the measuring route

	Evening 1	Evening 2	Midnight 1	Midnight 2	Morning 1	Morning 2	Night 1	Night 2	Day 1	Day 2
Evening 1	1.00	0.89	0.26	0.38	0.06	0.31	-0.27	-0.44	0.12	-0.10
Evening 2	0.89	1.00	0.28	0.39	0.11	0.35	-0.25	-0.38	0.13	-0.05
Midnight 1	0.26	0.28	1.00	0.85	-0.12	-0.09	-0.21	-0.20	0.22	-0.02
Midnight 2	0.38	0.39	0.85	1.00	-0.09	-0.01	-0.34	-0.39	0.06	-0.16
Morning 1	0.06	0.11	-0.12	-0.09	1.00	0.76	0.07	0.06	0.02	0.08
Morning 2	0.31	0.35	-0.09	-0.01	0.76	1.00	0.12	0.01	0.27	0.36
Night 1	-0.27	-0.25	-0.21	-0.34	0.07	0.12	1.00	0.92	0.47	0.48
Night 2	-0.44	-0.38	-0.20	-0.39	0.06	0.01	0.92	1.00	0.42	0.47
Day 1	0.12	0.13	0.22	0.06	0.02	0.27	0.47	0.42	1.00	0.80
Day 2	-0.10	-0.05	-0.02	-0.16	0.08	0.36	0.48	0.47	0.80	1.00

Table 3. Product moment correlation coefficient exemplarily shown for CO₂ measuring trips in winter (evening = 7 p.m. - 10 p.m.; midnight = 11 p.m. - 2 a.m.; morning = 10 a.m. - 1 p.m.; night = 4 a.m. - 7 a.m.; day = 1 a.m. - 4 p.m.); evening 1 = 11.12.02, evening 2 = 05.02.03; midnight 1 = 06.01.03, midnight 2 = 19.02.03; morning 1 = 02.12.02, morning 2 = 12.02.03; night 1 = 19.12.02, night 2 = 12.02.03; day 1 = 05.02.03, day 2 = 18.02.02.

The statistical analysis of the CO₂ concentration in 2002 and 2003 was confirmed in the following years by comparing measurements along the same measuring route. Measuring trips throughout the different seasons of winter and summer 2004 as well as in spring 2005 have revealed that there is a roughly similar pattern of carbon dioxide near the ground ($R^2 > 0.78$; $\alpha > 0.5$). Exemplarily, this is shown with the aid of another cluster analysis (Fig. 6) and a CO₂ profile (Fig. 7) for measuring trips within Essen in summer 2004 compared to those from 2003.

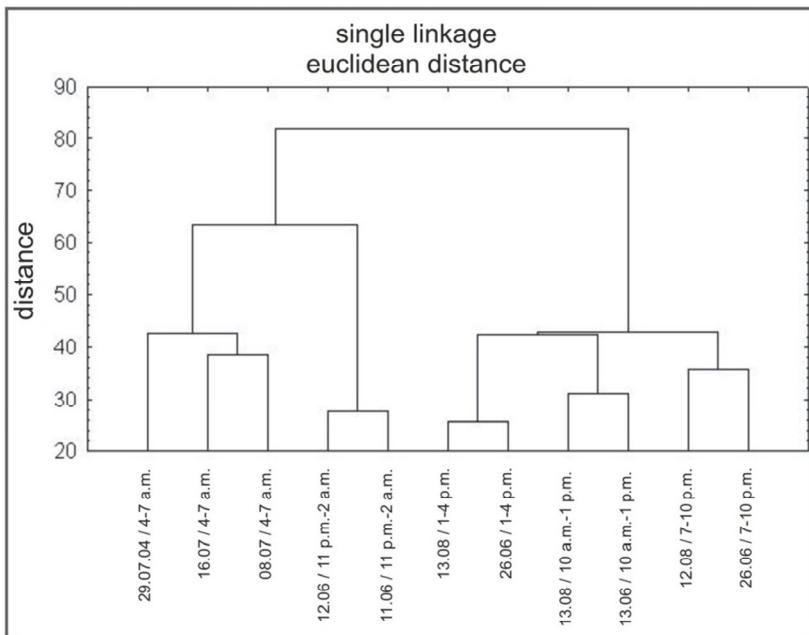


Fig. 6. Cluster diagram for CO₂ measuring trips within the urban area of Essen, Germany, for summer 2003 appended by an additional CO₂ measurement in summer 2004 at the same time of the day (4 a.m. - 7 a.m.), the same measuring route and comparable weather conditions

Figure 8 offers that the applied measuring methodology tested within the city of Essen is solely suitable for mobile measurements at this city structure. It could be proven that statistically representative, recurring patterns of CO₂ and other trace elements can also be determined within other urban areas, as it is shown for one route within the city of Krefeld. For day time as well as for the night-time measuring trips it is clearly obvious that there is no significant difference ($\alpha > 0.5$) between the CO₂ patterns along the transect. Particularly, the comparison of the night-time measurements of 17.02.04 and 20.02.04 showed a nearly congruent CO₂ profile ($R^2 = 0.98$; Fig. 7) due to a several days lasting clear and calm weather condition with $v \leq 1 \text{ m s}^{-1}$ and a negligible atmospheric exchange. Similar to the city of Essen a lower correlation coefficient ($R^2 = 0.70$), which is displayed in figure 6 for the day time measurements of 11.03.2004 and 13.03.2004, indicated a higher variability of potential CO₂ sources (primarily from motor vehicles).

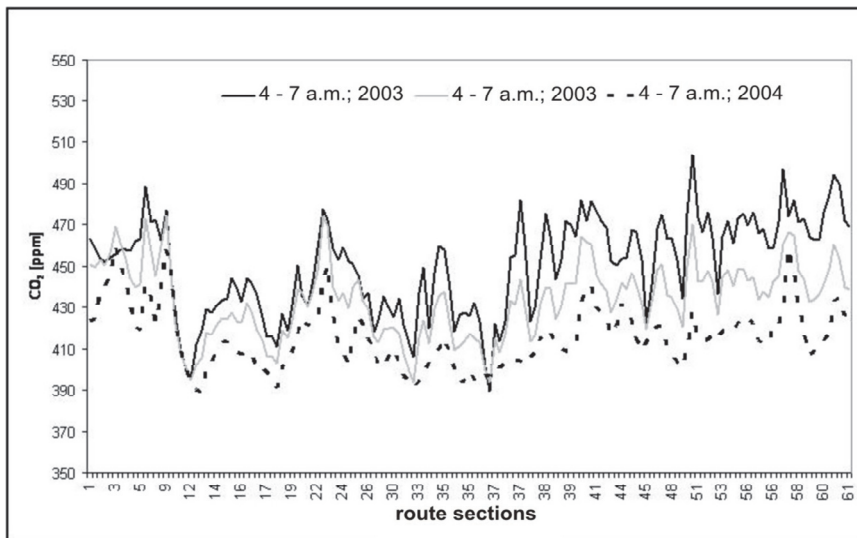


Fig. 7. CO₂ profiles ($R^2 = 0.79$) for three summer measuring trips with an identical measuring time (4 a.m. - 7 a.m.) within the urban area of Essen, Germany, different measuring days (black line = 2003; grey line = 2004), but comparable wind speed ($v < 1.5 \text{ m s}^{-1}$). The trips are part of one cluster (fig. 6) and showed up no significant differences ($\alpha > 0.5$) for the carbon dioxide situation along the measuring route

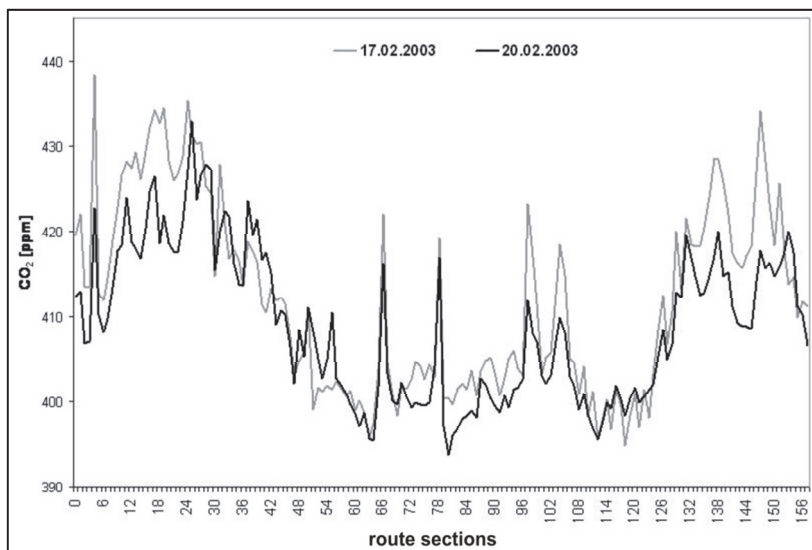


Fig. 8. CO₂ profiles ($R^2 = 0.90$) for two winter measuring trips with an identical measuring time (10.30 p.m. - 1.00 a.m.), but different measuring days within the urban area of Krefeld, Germany, $\alpha < 0.5$

The transferability of the measuring methodology was also checked for mobile measurements of near surface carbon dioxide and particulate matters (PM_{10}) in smaller towns, which do not have such an enormous emission of trace elements in comparison to urban agglomerations. Moreover, the method was used to determine different air quality indicators in the tropical city of Kigali, Rwanda. Exemplarily, based on figure 9 it is revealed for measuring trips within the city for Kigali, Rwanda, during the dry seasons of 2008 and 2009 for two different day time measuring periods.

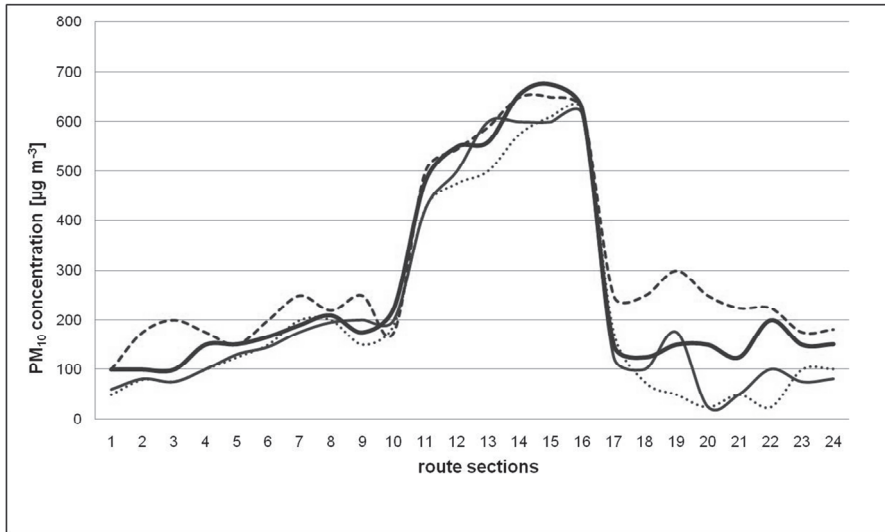


Fig. 9. PM_{10} profiles ($R^2 = 0.89$) for measuring trips during the dry seasons of 2008 and 2009 with identical measuring times (9 a.m. – 10 a.m. = solid lines & 4 p.m. – 5 p.m. = dotted lines) within the urban area of Kigali, Rwanda, and different measuring days, but comparable wind speed ($v < 1.5 \text{ m s}^{-1}$). The trips showed up no significant differences ($\alpha > 0.5$) for the particulate matter situation along the measuring route

6. Discussion and concluding remarks

Carbon dioxide is one greenhouse gas, which is responsible for the anthropogenic induced climate change. Above all, urban agglomerations are a potential CO_2 source due to its usage of fossil energy sources. Less is known about the temporal and spatial behavior of this trace gas, especially in cities and their surrounding areas. Most studies were carried out by stationary measurements. But these investigations could hardly ensure the transferability from the measurement location to its nearby vicinity. An opportunity to solve this problem is using mobile air quality measurements, which ensure a highly frequented spatial as well as temporal density of area-covering information within an urban environment. Unfortunately, there are less investigations using the methodology of mobile measurements

along exactly coordinated transects. Furthermore the problem of existing methods is the significant difference within the methodologies of mobile air quality measurements. Thus it was necessary to create a methodology, which is applicable for different types of trace elements, but it also has to be representative, so that a ultimately statistical reproducibility of the results can be guaranteed.

Momentarily valid is the statistical analysis of the collected mobile measurements of near surface carbon dioxide between 2002 and 2010 has shown the possibility to resolve the CO₂ pattern within the urban canopy layer spatially as well as temporally in a high frequency in dependence of the structure of urban types of land use. It could be demonstrated that the methodology of measurements was not only feasible for one urban area, but it rather works for every urban settlement, because the transfer to other urban settlements is possible. Also it was obviously necessary to have a measuring period of more than one year and an exact consideration of the specific types of land usage because otherwise seasonal and spatial variations of the urban CO₂ mixing ratio could not be reproduced satisfactorily. So this investigation could be considered as a supplemental step in measuring urban CO₂ apart from fixed measurement locations using statistical proofs (test of significance, correlation analysis, product-moment analysis) to demonstrate which factors most strongly influence CO₂ within the urban canopy layer.

Based on these solid results of the diverse investigations within different urban areas (different sizes of the urban areas as well as varying climatic zones) three findings could be accentuated, which should be considered in the context of planning mobile air quality measurements, which need a minimum of necessary mobile measuring trips along the transect to determine the spatial and temporal behavior of near surface urban carbon dioxide:

1. The comparison of different measurement times throughout the day indicated that there is only one significant difference between day- and night-time measuring trips ($\alpha < 0.05$, Fig. 3). Therefore it remains to be noted that two day- and night-time measurements at a predefined time, however, showed only a weakly significance ($\alpha > 0.1$). It may be sufficient to get a first look and compare the time of day CO₂ profile of an urban space. The most important requirement for a comparison of measuring trips with one another is not measuring within the same year, but at the same time of day.
2. Two more additionally trips should be made at exactly the same day- or night-time and at similar atmospheric conditions (clear and calm weather conditions; low wind speed $v \leq 1.5 \text{ m s}^{-1}$) to confirm the area-use-dependent CO₂ pattern for the comparative trips and to ensure an adequate comparability of the determined data of the first two measuring trips (one day, one night-time trip). Following the analysis of two equal measuring times with a distinct comparable CO₂ profile ($\alpha > 0.5$), it must be assumed, based on the results of all measurements from 2002 to 2010, that also a third and fourth measuring trip for analog conditions constitutes a similar result, which ultimately reveals that more than four runs (two day and two night-time measurements) seem to be superfluous. A necessity of a third or perhaps fourth measuring trip is only given, when the first differs significantly from the second one (whether it is a day- or night-time trip). Also it is negligible, if it is on weekdays and on weekends respectively. The differences between the CO₂ patterns along the measuring route are undersized and not significant, as it is displayed for the cluster analysis in figure 10 and the CO₂ profiles in figure 11.

3. Furthermore it could be demonstrated in the course of the measurements from 2002 till 2010, that there are significant differences between the seasons (Fig. 2). So consequently, all four seasons must be considered to get an adequate impression of the spatial as well as temporal near surface pattern of the urban CO_2 . At least it could be concluded that it is sufficient, being planned to measure urban carbon dioxide within the urban canopy layer over a minimum period of one year, calculating with at least sixteen mobile measurements (eight day- and eight night-time measurements), and assuming that the exit criteria mentioned in fact number 2 are fulfilled.

Based on the mentioned three-point plan Ptak (2009) used this handout for measuring carbon dioxide near the ground with the aid of a mobile laboratory within to urban areas. At least she planned a measuring period of one year. While it was great afford measuring CO_2 within the urban canopy layer of two cities which are far apart from each other, she calculated, as it was supposed, 16 measuring trips (four per season; two per night and day) for Münster as well as Lüdenscheid. Finally, she got a highly frequented spatial as well as temporal area-covering pattern of the CO_2 situation of both urban sites, which were also replicable and recurring for comparing trips one year later.

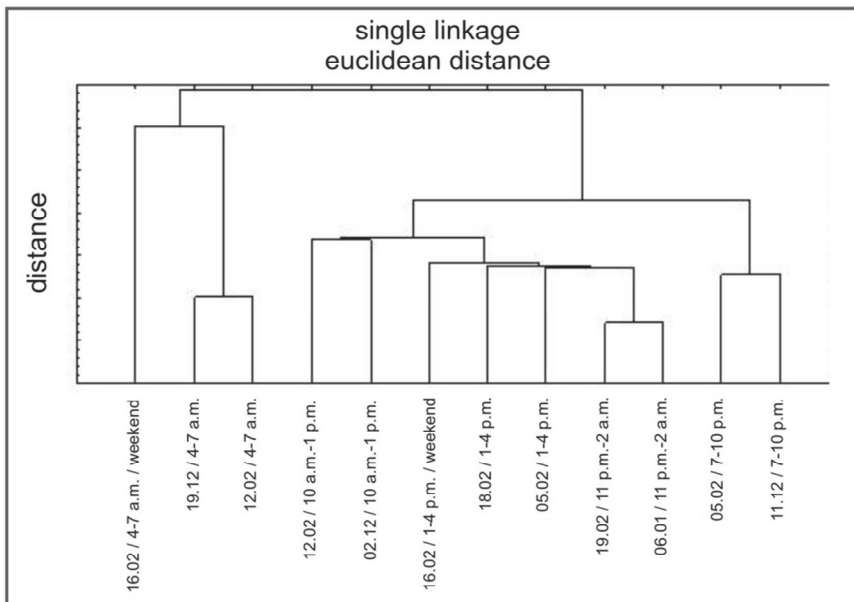


Fig. 10. Cluster diagram for CO_2 measuring trips within the urban area of Essen, Germany, for summer 2003 appended by an additional CO_2 measurement on a weekend at the same time of the day (4 a.m. - 7 a.m.), the same measuring route and comparable weather conditions

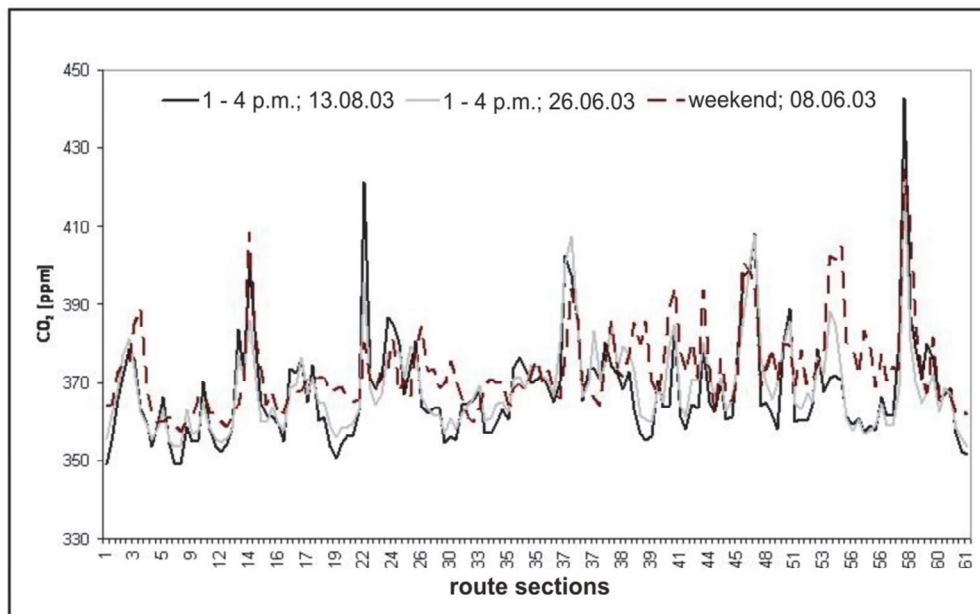


Fig. 11. CO₂ profiles ($R^2 = 0.89$) for three summer measuring trips with an identical measuring time (4 a.m. – 7 a.m.) within the urban area of Essen, Germany, and different measuring days (solid lines = weekdays; dotted line = weekend), but comparable wind speed ($v < 1.5 \text{ ms}^{-1}$). The trips are part of one cluster (fig. 10) and showed up no significant differences ($\alpha > 0.5$) for the carbon dioxide situation along the measuring route

7. References

- Allen, L.H. (1965): Variations of carbon dioxide concentration over an agricultural field. *Agriculture Meteorology*, Vol. 8, pp. 5-24, ISSN 0168-1923
- Berry, R.D & J.J. Colls (1990a): Atmospheric carbon dioxide and sulphur dioxide on an urban/rural transect-I. Continuous measurements at the transect ends. *Atmospheric Environment*, Vol. 24A, No. 10, pp. 2681-2688, ISSN 1352-2310
- Berry, R.D & J.J. Colls (1990b): Atmospheric carbon dioxide and sulphur dioxide on an urban/rural transect-II. Measurements along the transect. *Atmospheric Environment*, Vol. 24A, No. 10, pp. 2689-2694, ISSN 1352-2310
- Bukowiecki, N.; Dommen, J.; Prevot, A.S.H.; Richter, R.; Weingartner, U. & U. Baltensperger (2002): A mobile pollutant measurement laboratory-measuring gas phase and aerosol ambient concentrations with high spatial and temporal resolution. *Atmospheric Environment*, Vol. 36, pp. 5569-5579, ISSN 1352-2310
- Carmi, I.; Haklay, R.; Rozalis, S. & J. Kronfeld (2005): The concentration and $\delta^{13}\text{C}$ of CO₂ in the urban atmosphere of Tel-Aviv. *Geochrono*, Vol. 24, 59-61, ISSN 1733-8387
- Clarke-Thorne, S.T. & C.J. Yapp (2003): Stable carbon isotope constraints on mixing and mass balance of CO₂ in an urban atmosphere: Dallas metropolitan area, Texas, USA. *Applied Geochemistry*, Vol. 18, No. 1, pp. 75–95, ISSN 0883-2927
- Clifford, M.J.; Clarke, R. & S.B. Riffat (1997): Local aspects of vehicular pollution. *Atmospheric Environment*, Vol. 31, No. 2, pp. 271–276, ISSN 1352-2310

- Coutts, A.M.; Beringer, J. & N.J. Tapper (2007): Characteristics influencing the variability of urban CO₂ fluxes in Melbourne, Australia. *Atmospheric Environment*, Vol. 41, pp. 51-62, ISSN 1352-2310
- Derwent, R.G.; Middleton, D.R.; Field, R.A.; Goldstone, M.E.; Lester, J.N. & R. Perry (1995): Analysis and interpretation of air quality data from an urban roadside location in central London over the period from July 1991 to July 1992. *Atmospheric Environment*, Vol. 29, No. 8, pp. 923-946, ISSN 1352-2310
- George, K.; Ziska, L.H.; Bunce, L.A. & B. Quebedeaux (2007): Elevated atmospheric CO₂ concentration and temperature across an urban-rural transect. *Atmospheric Environment*, Vol. 41, pp. 7654-7665, ISSN 1352-2310
- Ghuri, B.; Salam, M. & M.I. Mirza (1994): An assessment of air quality in Karachi, Pakistan. *Environmental Monitoring and Assessment*, Vol. 32, pp. 37-45, ISSN 0167-6369
- Grimmond, C.S.B.; Salmond, J.A.; Oke, T.R.; Offerle, B. & A. Lemonsu (2004): Flux and turbulence measurements at a densely built-up site in Marseille: Heat, mass (water and carbon dioxide), and momentum. *Journal of Geophysical Research Letters*, Vol. 109, D 24101 online, ISSN 0094-8276
- Henninger, S. (2005a): Analyse der atmosphärischen CO₂-Konzentrationen am Beispiel der Stadt Essen (Analyzing the atmospheric CO₂ concentration within the city of Essen, Germany). *Essener Ökologische Schriften*, Vol. 23, ISBN 3-89432-109-1, Hohenwarsleben, Germany
- Henninger, S. 2005b: Urban CO₂ - Determination of urban air quality indicators. *Koblenzer Geographisches Kolloquium*, Vol. 27, pp. 55-74, ISSN 1616-4784
- Henninger, S. (2008a): Analysis of near surface CO₂ variability within the urban area of Essen, Germany. *Meteorologische Zeitschrift*, Vol. 17, No. 1, pp. 19-27, ISSN 0941-2948
- Henninger, S. (2008b): Analysis of PM₁₀ along a pedestrian precinct. *Urban Climate News*, Vol. 27, pp. 12-13
- Henninger, S. (2008c): Analysis of increasing particulate matter (PM₁₀) within a street canyon during a road closure. *Klimat i bioklimat miast, Wydawnictwo Uniwersytetu Łódzkiego*, pp. 525-535, ISBN 978-83-7525-243-9
- Henninger, S. (2009a): Urban climate and air pollution in Kigali, Rwanda. *Proceedings of ICUC '07*, pp. 1038-1041, Yokohama, Japan, June/July 29-03, 2009
- Henninger, S. (2009b): Urbane Luftverschmutzung am Beispiel einer afrikanischen Großstadt. *Umweltchemie und Ökotoxikologie*, Vol. 3, pp.58-60, ISSN 1618-3258
- Henninger, S. & W. Kuttler (2007): Methodology for mobile measurements of carbon dioxide within the urban canopy layer. *Climate Research*, Vol. 34, No. 2, pp. 161-167, ISSN 0936-577X
- Henninger, S. & W. Kuttler (2010): Near surface carbon dioxide within the urban area of Essen, Germany. *Physics and Chemistry of the Earth*, Vol. 35, No. 1-2, pp. 76-84, ISSN 1474-7065
- Heussner, S. (1988): Schadstoffe in der Luft. Eine Untersuchung zur Schadstoffverteilung in Stadtgebieten. ISBN 3-926952-15-6, Hamburg, Germany
- Idso, C.D.; Idso, S.B. & R.C. Balling (1998): The urban CO₂ dome of Phoenix, Arizona. *Physical Geography*, Vol. 19, No. 2, pp. 95-108, ISSN 0272-3646
- Idso, C.D., Idso, S.B. & R.C. Balling (2001): An intensive two-week study of an urban CO₂ dome in Phoenix, Arizona, USA. *Atmospheric Environment*, Vol. 35, pp. 995-1000, ISSN 1352-2310
- Inoue, H.Y. & H. Matseuda (2001): Measurements of atmospheric CO₂ from a meteorological tower in Tsukuba, Japan. *Tellus*, Vol. 53B, pp. 205-219, ISSN 0280-6509

- Kuttler, W. & A. Strassburger (1999): Air quality measurements in urban green areas – a case study. *Atmospheric Environment*, Vol. 33, pp. 4101-4108, ISSN 1352-2310
- Kuttler, W. & T. Wacker (2001): Analyse der urbanen Luftqualität mittels mobiler Messungen (Analyzing the urban air quality by mobile measurements). *Österreichische Beiträge zur Meteorologie und Geophysik*, Vol. 27, No. 399, pp. 1-16, ISSN 1016-6254
- Kuttler, W. & S. Weber (2006): Angewandte Stadtklimaforschung in deutschen Großstädten. *Geographische Rundschau*, Vol. 58, No. 7/8, pp. 42-50, ISSN 0016-7460
- Luria, M., Weisinger, R. & M. Peleg (1990): CO and NO_x levels at the center of city roads in Jerusalem. *Atmospheric Environment*, Vol. 24B, pp. 93-99, ISSN 1352-2310
- Manuel, J.A.; Gajghate, D.G.; Hasan, M.Z. & R.N. Singh (2002): Short term concentration of CO₂ in the ambient air of Nagpur City. *Indian Journal of Environment*, Vol. 44, pp. 225-230, ISSN 0367-827X
- Moriwaki, R. & M. Kanda (2004): Seasonal and diurnal fluxes of radiation, heat, water vapor, and carbon dioxide over a suburban area. *Journal of Applied Meteorology*, Vol. 43, pp. 1700–1709, ISSN 0894-8763
- Nemitz, E.; Hargreaves, K.J.; McDonald, A.; Dorsey, J.R. & D. Fowler (2002): Micrometeorological measurements of the urban heat budget and CO₂ emissions on a city scale. *Environmental Science and Technology*, Vol. 36, No. 14, pp. 3139-3146, ISSN 0013-936X
- Nowak, D.J. & D.E. Crane (2001): Carbon storage and sequestration by urban trees in the USA. *Environmental Pollution*, Vol. 116, 381-389, ISSN 0269-7491
- Pasquill, F. (1961): The estimation of the dispersion of windborne material. *Meteorological Magazine*, Vol. 90, pp. 33-49, ISSN 0026-1149
- Pataki, D.E.; Bowling, D.R. & J.R. Ehleringer (2003): Seasonal cycle of carbon dioxide and its isotopic composition in an urban atmosphere: anthropogenic and biogenic effects. *Journal of Geophysical Research Letters*, Vol. 108, No. D23, pp. 4375, ISSN 0094-8276
- Pataki, D.E.; Bowling, D.R.; Ehleringer, J. R. & J.M. Zobitz (2006): High resolution atmospheric monitoring of urban carbon dioxide sources. *Journal of Geophysical Research Letters*, Vol. 33, L03813, ISSN 0094-8276
- Peppler, A. (1929): Das Auto als Hilfsmittel der meteorologischen Forschung. *Wetter*, Vol. 46, pp. 305-308
- Ptak, D. (2009): Bodennahe CO₂-Konzentrationen in zwei Städten unterschiedlicher Topographie. *Essener Ökologische Schriften*, Vol. 28, ISBN 978-3-89432-121-5, Hohenwarsleben, Germany
- Polster, G. (1969): Erfahrungen mit Strahlungs-, Temperaturgradient- und Windmessungen als Bestimmungsgrößen der Diffusionskategorien. *Meteorologische Rundschau*, Vol. 22, pp. 170-175, ISSN 0026-1211
- Salmond, J.A.; Grimmond, C.S.B.; Roberts, S. & B. Offerle (2005): Venting of heat and carbon dioxide from urban canyons at night. *Journal of Applied Meteorology*, Vol. 44, pp. 1180-1194, ISSN 0894-8763
- Schmidt, W. (1927): Die Verteilung der Minimumtemperaturen in der Frostnacht des 12.05.1927 im Gemeindegebiet von Wien. *Fortschritte der Landwirtschaft*, Vol. 2, pp. 21
- Schönwiese, C.D. (2006): Praktische Statistik für Meteorologen und Geowissenschaftler (Practical statistics for meteorologists and geoscientists). ISBN 978-3443010577, Berlin, Stuttgart, Germany
- Shorter, J.H.; McManus, J.B.; Kolb, C.E.; Allwine, E.J.; O'Neill, J.M.; Lamb, B.K.; Scheuer, E.; Crill, P.M.; Talbot, R.W.; Ferreira, J. & G.J. McRae (1998): Recent measurements of

- urban metabolism and trace gas respiration. *Proceedings of 2nd Symposium on Urban Environment*, pp. 49-52, Albuquerque, Canada, June 2-6, 1998
- Sikar, E. & N. La Scala (2004): Methan and carbon dioxide seasonal cycle at urban brasilian inland sites. *Journal of Atmospheric Chemistry*, Vol. 47, pp. 101-106, ISSN 0167-7764
- Stanhil, G. (1982): The Montsouris series of carbon dioxide concentration measurements, 1877-1910. *Climate Change*, Vol. 4, pp. 221-237, ISSN 0165-0009.
- Steinhauser, F.; Eckel, O. & F. SAUBERER (1959): *Klima und Bioklima von Wien*, III Teil. ISBN, Vienna, Austria
- VDI guideline 2453, sheet 2 (2002): Messen gasförmiger Immissionen; Messen Stickstoffmonoxid- und Stickstoffdioxid-Konzentrationen; Kalibrierung von NO/NO_x-Chemolumineszenz-Messgeräten mit Hilfe der Gasphasentitration. *Kommission der Reinhaltung Luft (KRdL) im VDI und DIN Normenausschuss*, ISSN 13.040.20
- VDI guideline 2459, sheet. 6 (1980): Messen der Kohlenmonoxid-Konzentrationen; Verfahren der nichtdispersiven Infrarot-Absorption. *Kommission der Reinhaltung Luft (KRdL) im VDI und DIN Normenausschuss*, ISSN 543.422.4
- VDI guideline 2468, sheet 6 (1979): Messen gasförmiger Immissionen; Messen der Ozon-Konzentrationen; Direktes UV-photochemisches Verfahren (Basis-Verfahren). *Kommission der Reinhaltung Luft (KRdL) im VDI und DIN Normenausschuss*, ISSN 535.243.25
- VDI guideline 3950, sheet 1 (1994): Emissionen aus stationären Quellen – Qualitätssicherung für automatische Mess- und elektronische Auswerteeinrichtungen. *Kommission der Reinhaltung Luft (KRdL) im VDI und DIN Normenausschuss*, ISSN 13.040.10
- Velasco, E.; Pressley, S.; Allwine, E.; Westbug, H. & B. Lamb (2005): Measurements of CO₂ fluxes from Mexico City urban landscape. *Atmospheric Environment*, Vol. 39, pp. 7433-7446, ISSN 1352-2310.
- Vogt, R.; Christen, A.; Rotach, M.V.; Roth, M. & A.N.V. Sayanarayana (2006): Temporal dynamics of CO₂ fluxes and profiles over a central European city. *Theoretical and Applied Climatology*, Vol. 84, No. 1-3, pp. 117-126, ISSN 0177-798X.
- Yang, J.; McBride, J.; Zhou, J. & Z. Sun (2005): The urban forest in Beijing and its role in air pollution reduction. *Urban Forest, Urban Green*, Vol. 3, No. 2, pp. 65-78, ISSN 1618-8667.
- Ziska, L.H.; Bunce, J.A. & E.W. Goins (2004): Characterization of urban-rural CO₂/temperature gradient and associated changes in initial plant productivity during secondary succession. *Oecologica*, Vol. 139, pp. 454-458, ISSN 0029-8549.

Part 4

Urban Air Pollution: Case Studies

Impacts of Photoexcited NO₂ Chemistry and Heterogeneous Reactions on Concentrations of O₃ and NO_y in Beijing, Tianjin and Hebei Province of China

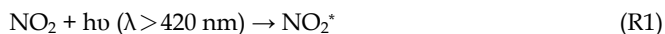
Junling An¹, Ying Li¹, Feng Wang¹ and Pinhua Xie²

¹*State Key Laboratory of Atmospheric Boundary Layer Physics and Atmospheric Chemistry (LAPC), Institute of Atmospheric Physics (IAP), Chinese Academy of Sciences, Beijing,*

²*Anhui Institute of Optics and Fine Mechanics, Chinese Academy of Sciences, China*

1. Introduction

Nitrous acid (HONO) plays a significant role in the photochemistry of the troposphere, especially in the polluted urban atmosphere, due to its photolysis by solar UV radiation into the hydroxyl radical (OH), which is one of the most important oxidant in the atmosphere (Alicke et al., 2002). Some previous observations showed unexpected high HONO concentrations up to several ppb at urban or rural sites during the daytime or nighttime (Qin et al., 2009; Su et al., 2008a, 2008b; Yu et al., 2009) but gas-phase chemical models usually underestimated HONO observations, particularly in the daytime. HONO sources are thought to be direct emissions, homogeneous gas reactions, and heterogeneous reactions on aerosol surfaces. Sarwar et al. (2008) incorporated gas-phase reactions, direct emissions, a heterogeneous reaction, and a surface photolysis reaction into the CMAQ model, and simulations still indicated HONO underestimation by comparison with measurements, especially in the daytime. Li et al. (2008) suggested a reaction of electronically excited nitrogen dioxide (NO₂^{*}) with water vapor as follows,



The reaction rate for Reaction R2 given by Li et al. (2008) is $1.7 \times 10^{-13} \text{ cm}^3 \text{ molecule}^{-1} \text{ s}^{-1}$, which is an order of magnitude larger than that found by Crowley and Carl (1997). Although further experiments to reduce uncertainty in the rate constant need to be conducted, the HONO increase due to Reaction R2 may be potentially significant in some industrialized regions with elevated emission levels of NO_x (= NO + NO₂) and volatile organic compounds (VOCs). Wennberg and Dabdub (2008) implemented the NO₂^{*} chemistry into an air quality

model and found that simulated ozone (O_3) were enhanced by as much as 55 ppb in the southern California for a summer episode in 1987. However, Sarwar et al. (2009) did similar work and illustrated that the simulated increases were considerably smaller than those reported by Wennberg and Dabdub (2008) due primarily to the current low emissions of NO_x and VOCs compared to the emission levels in 1987. Ensberg et al. (2010) then used the emissions in both 1987 and 2005 to assess impacts of the NO_2^* chemistry on air pollution in the south coast air basin of California showed that the NO_2^* chemistry increased the effectiveness in reducing O_3 through NO_x emissions reductions alone. Li et al. (2010) coupled the NO_2^* chemistry, four heterogeneous reactions on aerosol surfaces recommended by Jacob (2000), and secondary HONO formation from the NO_2 heterogeneous reaction with semivolatile organics suggested by Gutzwiller et al. (2002) into the WRF-CHEM model version 3.2, and found that the additional HONO sources significantly improved HONO simulations by comparison with differential optical absorption spectroscopy (DOAS) observations (Zhu et al., 2009), especially in the daytime.

The purpose of this study is to use the state-of-the-art WRF-CHEM model version 3.2 to assess effects of the photoexcited NO_2 chemistry and heterogeneous reactions on concentrations of O_3 and NO_y (total reactive N-containing compounds) in Beijing, Tianjin and Hebei Province of China (BTH region), where emissions of NO_x and particulate matter (PM) are high (Zhang et al., 2009).

2. Model description

2.1 WRF-CHEM model

Used in this research is the Weather Research and Forecasting/Chemistry (WRF-CHEM) model version 3.2 (Fast et al., 2006; Grell et al., 2005). The WRF-CHEM model contains two components: a meteorological module and a chemistry module. The two modules use the same mass and scalar preserving flux scheme, the same horizontal and vertical resolutions, the same physics schemes for subgrid-scale transport, and the same time step (Grell et al., 2005). A detailed description of the WRF-CHEM model can be found on the website <http://ruc.noaa.gov/wrf/WG11/> and <http://www.wrf-model.org>. In this study, the WRF-CHEM model employs the microphysics scheme of Lin et al. (1983), the Yonsei University (YSU) PBL scheme (Noh et al., 2001), the Noah land-surface model (Chen & Dudhia, 2001), the RRTM long wave radiation parameterization (Mlawer et al., 1997), and the Goddard short wave scheme (Chou & Suarez, 1994). For gas chemistry chosen is an updated lumped-structure photochemical mechanism CBM-Z (Zaveri & Peters, 1999). Photolysis rates are calculated by the TUV scheme (Madronich, 1987). The chosen aerosol module is MOSAIC (Fast et al., 2006; Zaveri et al., 2008) with an 8-size-bin representation and the biogenic module is based on the description of Guenther et al. (1993, 1994), Simpson et al. (1995), and Schoenemeyer et al. (1997).

Two nested domains shown in Fig. 1. are employed in the simulation. Domain 1, 2, and 3, consists of 83×65 , 58×55 and 55×55 horizontal grid cells with 81 km, 27 km and 9 km, primarily covering East Asia, North China, and the BTH region, respectively. The stretched vertical coordinate in the model that extends up to approximately 50 mb uses 28 vertical model layers with nonuniform thickness and a 28 m first layer above the ground. Meteorological initial and boundary conditions are from NCEP reanalysis data, which are also used for nudging every 6 h. The chemical initial and lateral boundary conditions are constrained by the output of a global chemical transport model MOZART-4 (Emmons et al., 2009) every 6 h. The detailed description of mapping species concentrations from the

MOZART to the WRF-CHEM can be found on the website <http://www.acd.ucar.edu/wrf-chem/>. Monthly anthropogenic emissions of SO₂, NO_x, CO, VOCs, PM₁₀, PM_{2.5}, BC, and OC in 2006/2007 were obtained from (Zhang et al., 2009) and those of NH₃ from Streets et al. (2003) and monthly emissions of other species were derived from Zhang et al. (2009). Model simulations were performed in August 1-31, 2007 with a spin-up period of 7 days (July 25-31).

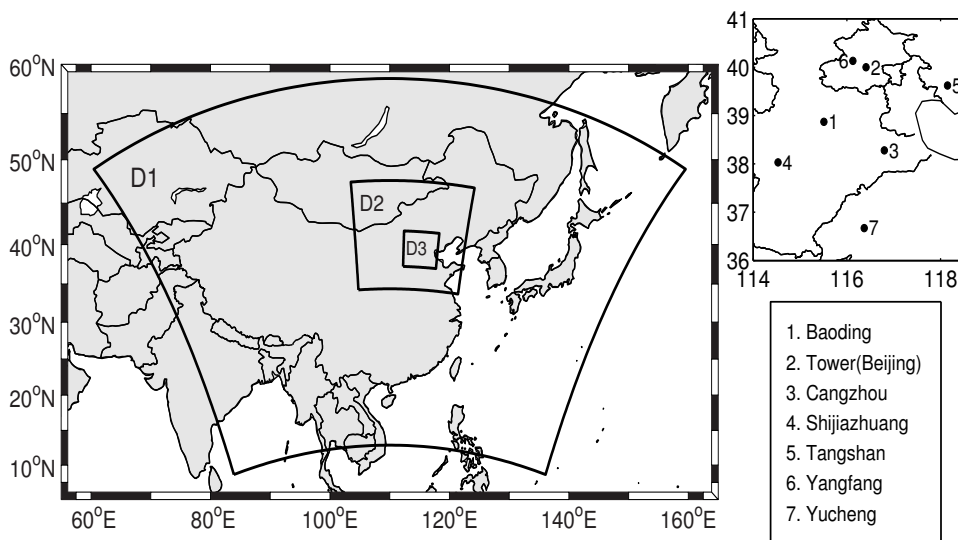


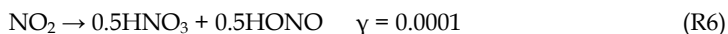
Fig. 1. Modeling domains used in this study and seven measurement sites in Beijing, Tianjin, and Hebei Province in Domain three.

Four different model simulations, i.e., Cases R, S, T and E, were conducted to assess impacts of the NO₂* chemistry and heterogeneous reactions on O₃ and NO_y in the BTH region. Case R is a reference, using the standard CBMZ mechanism and the MOSAIC module. Case S contains Case R with Reactions R1-R3. Case T is the same as Case S besides inclusion of 3.1% emissions of HONO/ NO_x (See Section 2.2). Case E includes Case T with Reactions R4-R7 (See Section 2.2).

2.2 Parameterization of HONO sources

The NO₂* chemistry (Reactions 1-3) (Li et al., 2008) is added to the CBM-Z mechanism. The rate of photoexcitation is simplified as 3.5 times the photolysis of NO₂ because the former is 3~4 times higher than the latter (Ensberg et al., 2010). The quenching rate constants for Reaction (R3) are 2.7×10^{-11} , 3.0×10^{-11} , and 1.7×10^{-10} cm³ molecule⁻¹ s⁻¹ for N₂, O₂, and H₂O, respectively (Li et al., 2008). The uncertainty in the rate constant for Reaction (R2) is $\pm 50\%$ (Li et al., 2008), so the rate constant (R2) is chosen as 9.1×10^{-14} cm³ molecule⁻¹ s⁻¹, which is the mean value of 1.7×10^{-13} cm³ molecule⁻¹ s⁻¹ from Li et al. (2008) and 1.2×10^{-14} cm³ molecule⁻¹ s⁻¹ from Crowley and Carl (1997).

For heterogeneous reactions on aerosol surfaces we follow Jacob (2000) recommendations as below,



The reactive uptake of HO_2 , NO_3 , NO_2 , and N_2O_5 by aerosols is depicted by using a simple reaction probability parameterization (Jacob, 2000),

$$k = \left(\frac{a}{D_g} + \frac{4}{v\gamma} \right)^{-1} A \quad (1)$$

where k is the first-order rate constant, a , the aerosol equivalent radius (m), D_g , the gas-phase molecular diffusion coefficient being $10^{-5} \text{ m}^2\text{s}^{-1}$ (Dentener & Crutzen, 1993), v , the mean molecular speed (ms^{-1}), A , the aerosol surface area per unit volume of air, and γ , the uptake coefficient of reactive species. Considered aerosols are sulfate, nitrate, organic carbon, and black carbon. Taken from Chin et al. (2002) are parameters for aerosol density, size distributions, and hygroscopic growth rates at ambient relative humidity. A fraction of 2.3% of the NO_x emitted in diesel exhaust is assumed to be heterogeneously converted to HONO (Gutzwiller et al., 2002). Additionally, direct HONO emissions are estimated by 0.8% emissions of NO_x (Kurtenbacha et al., 2001), which is also adopted in other studies (Aumont et al., 2003; Sarwar et al., 2008). Thus, 3.1% (= 2.3% + 0.8%) of NO_x emissions is used to reflect HONO direct emissions and secondary HONO formation from the NO_2 heterogeneous reaction with semivolatile organics in diesel exhaust.

3. Results and discussion

3.1 Impacts of the NO_2^* chemistry and heterogeneous reactions on O_3 and NO_y

Shown in Fig. 2. are the largest differences in simulated daily maximum 1-h O_3 concentrations between Cases S and R. Typically 10~20 ppb increases in daily maximum 1-h O_3 concentrations are found in suburban areas and 30~50 ppb enhancements in major cities, i.e., Beijing, Tianjin, Shijiazhuang, and Baoding, over the BTH region. The values are much higher than the results (1~13 ppb) given by Sarwar et al. (2009). This demonstrates that the NO_2^* chemistry can play a key role in some industrialized regions with elevated emissions of NO_x and VOCs. The conclusion is consistent with the suggestion of Sarwar et al. (2009). Monthly mean daily maximum 8-h O_3 concentrations near the surface are enhanced in the range of 8~18 ppb in most areas of the BTH region due to the NO_2^* chemistry and the largest increase is located close to Shijiazhuang (Fig. 3.). The enhanced concentration range in the BTH region is much higher than that of 1~6 ppb in some urban areas and in the vicinity of isolated large NO_x sources in the United States of America (Sarwar et al., 2009).

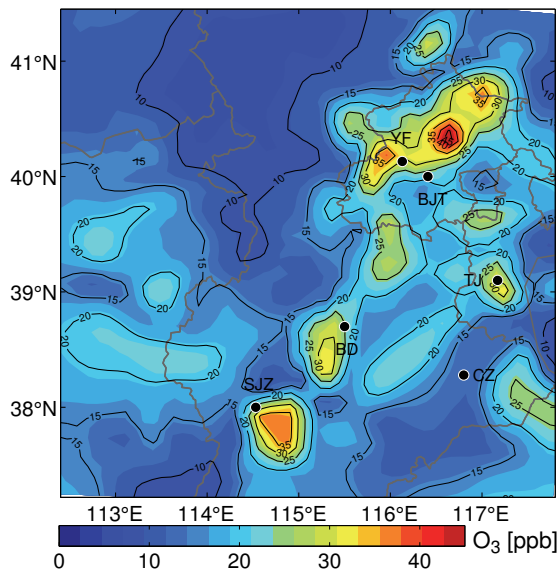


Fig. 2. Largest enhancements of daily maximum 1-h O_3 (ppb) in Beijing, Tianjin, and Hebei Province in August of 2007 due to the NO_2^* chemistry (Case S - Case R). YF, BJT, TJ, CZ, BD, and SJZ denotes Site Yangfang, Beijing Tower, Tianjin, Cangzhou, Baoding, and Shijiazhuang, respectively.

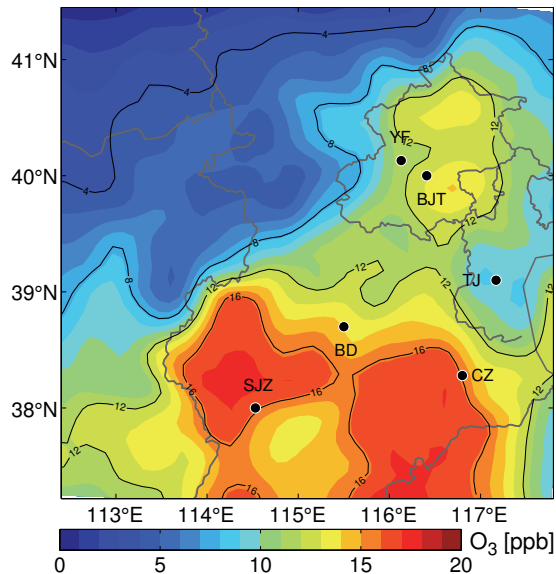


Fig. 3. Monthly mean enhancements of daily maximum 8-h O_3 (ppb) near the surface in August 2007 due to the NO_2^* chemistry (Case S - Case R). YF, BJT, TJ, CZ, BD, and SJZ are the same as mentioned in Fig. 2.

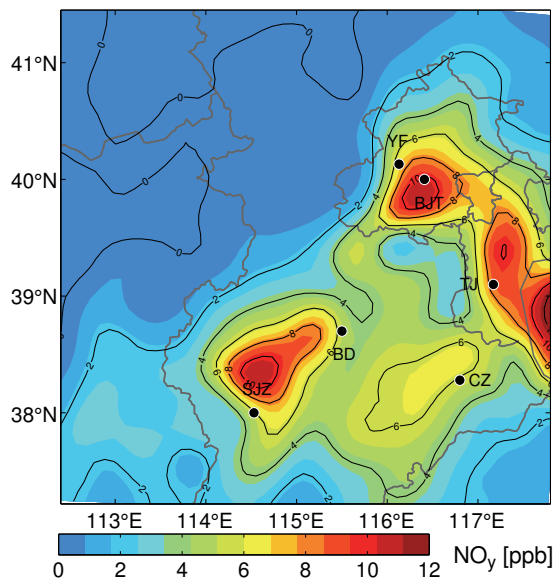


Fig. 4. Monthly mean daytime NO_y concentration differences (ppb) near the surface in August 2007 due to the NO_2^* chemistry (Case S - Case R). YF, BJT, TJ, CZ, BD, and SJZ are the same as mentioned in Fig. 2.

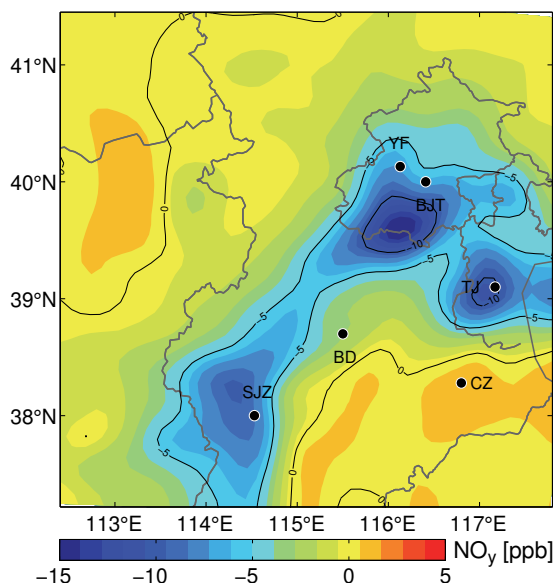


Fig. 5. Monthly mean daytime NO_y concentration differences (ppb) near the surface in August 2007 due to heterogeneous reactions on aerosol surfaces (Case E - Case T). YF, BJT, TJ, CZ, BD, and SJZ are the same as mentioned in Fig. 2.

For monthly mean daytime surface NO_y concentrations the NO₂* chemistry causes 4~15 ppb increases in the BTH region and the largest enhancement is found near the Bohai Bay (Fig. 4.) due to much lower heights of the planetary boundary layer (PBL) and much higher values of relative humidity around the Bohai Bay than those in the other areas of the BTH (Figures are not shown here). This agrees with the results of Sarwar et al. (2009).

Elevated PM concentrations in Beijing, Tianjin, and Shijiazhuang lead to 5~15 ppb decreases in monthly mean daytime NO_y concentrations near the surface when heterogeneous reactions on aerosol surfaces are considered (Fig. 5.). Comparatively, during the nighttime high relative humidity, low heights of the PBL, and stable atmospheric conditions are favorable for enhancements in PM concentrations and PM hygroscopic growth rates and finally result in 10~29 ppb decreases in the nighttime NO_y concentrations in Beijing, Tianjin, and Shijiazhuang cities and increases in areas with the reduced nighttime NO_y concentrations being larger than 10 ppb over the BTH region (Fig. 6.).

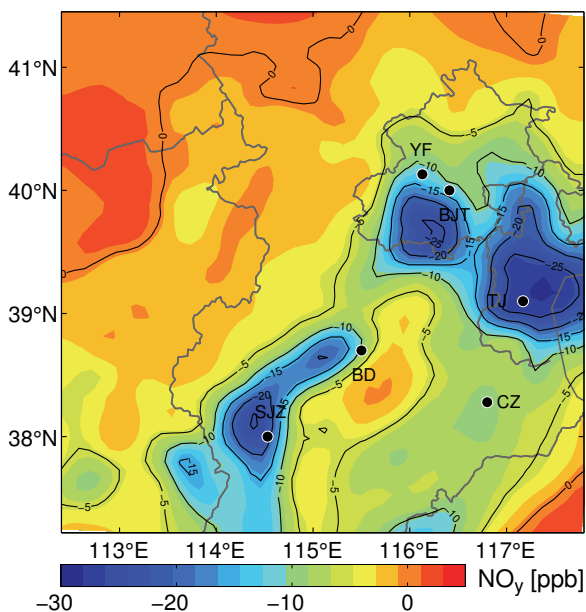


Fig. 6. Monthly mean nighttime NO_y concentration differences (ppb) near the surface in August 2007 due to heterogeneous reactions on aerosol surfaces (Case E - Case T). YF, BJT, TJ, CZ, BD, and SJZ are the same as mentioned in Fig. 2.

3.2 Comparison of simulations and observations

3.2.1 Observed data used for model comparison

HONO observations in Beijing in August 13-25 of 2007 were from Zhu et al. (2009). HONO concentrations were measured by the differential optical absorption spectroscopy (DOAS), which was described in detail by Zhu et al. (2009) and Qin et al. (2006). The specific detection limits are 0.41 ppb for HONO, 2.17 ppb for O₃, and 0.63 ppb for NO₂, respectively (Zhu et al., 2009). O₃ and NO_x were also simultaneously monitored at seven sites across

Beijing, Tianjin, and Hebei Province (BTH region), partially as the Beijing Atmospheric Environmental Monitoring Action conducted by Chinese Academy of Sciences. The detection limit of a Thermo Environmental Instrument (TEI) model 49 analyzer is 2 ppb for O_3 , and that of a conventional chemiluminescent gas analyzer (TEI Model 42C) is 0.05 ppb for NO_2 . Li et al. (2010) find that there is a nice agreement between O_3 and NO_2 measurements from DOAS and Chemiluminescence in Beijing. The correlation coefficient is 0.97 for O_3 and that is 0.83 for NO_2 . The intercept of 0.75 for NO_2 is much better than that of 12.0 given by An et al. (2009). This is due to inclusion of heavy emissions from the Badaling expressway for DOAS measurements, and also confirms the suggestions of An et al. (2009).

3.2.2 Comparison of simulated and observed HONO concentrations

For Case R simulated hourly HONO concentrations are always considerably underestimated by comparison with observations in the period of August 13-25, 2007 (Fig. 7a). Diurnal averages in 13 days (August 13-25, 2007) are approximately 25 times lower than observations (Fig. 7b). The mean bias (MB), the normal mean bias (NMB), the root mean square error (RMSE), the normal mean error (NME), and the correlation coefficient (RC) is -0.98 ppb, -97%, 1.10 ppb, 97%, -0.56, respectively. When the four HONO sources are included (Case E), the WRF-CHEM model well simulates observed HONO daily variations within the studied period (Fig. 7a) and simulated daytime HONO concentrations are also considerably improved (Fig. 7b). This leads to significant improvements in diurnal averaged HONO levels, and the corresponding MB, NMB, RMSE, NME, and RC is improved to -0.28 ppb, -28%, 0.37 ppb, 29%, 0.91, respectively.

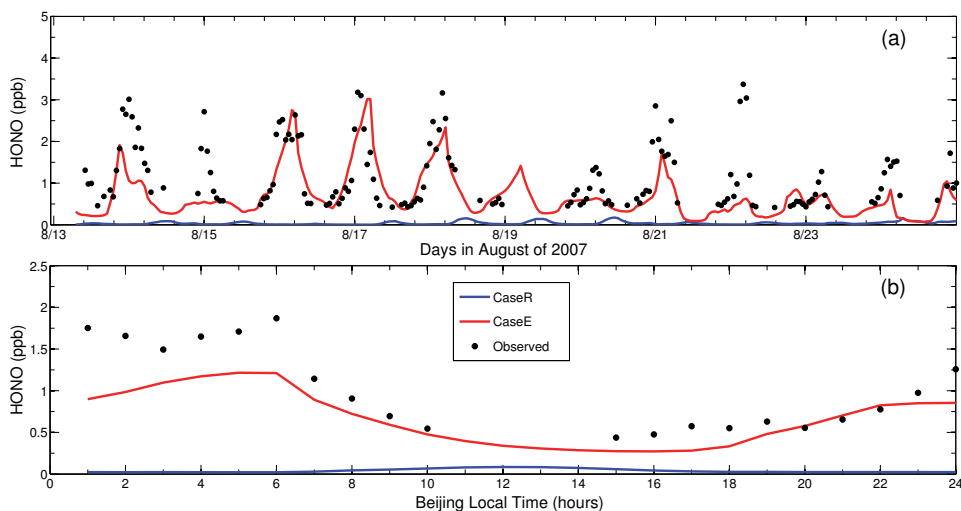


Fig. 7. Comparison of simulated hourly mean (a) and (b) diurnal-mean HONO concentrations (ppb) with observations from DOAS in August 13-25 of 2007.

3.2.3 Comparison of simulations and observations of O₃ and NO₂

Daily O₃ peaks are substantially improved in most cases when the four HONO sources are included (Case E) although Cases R and E show similar daily O₃ variations (Fig. 8.). This further indicates the importance of the NO₂^{*} chemistry, heterogeneous reactions on aerosol surfaces, secondary HONO formation from the NO₂ heterogeneous reaction with semivolatile organics, and direct emissions in the industrialized region with high emissions of NO_x, VOCs and PM. Daily NO_x simulations also demonstrate certain improvements at some sites, e.g., Sites Baoding and Shijiazhuang, in different days (Fig. 9.). For diurnal averages in 13 days (August 13-25, 2007) the O₃ peak is improved (Case E, Fig. 10a), with an increase of 25.5 ppb (= 64.2 - 38.7 ppb). NO variations are excellently reproduced both in the day and at night (Fig. 10c). NO₂ levels are well simulated in the nighttime whereas those are underestimated in the daytime (Fig. 10b).

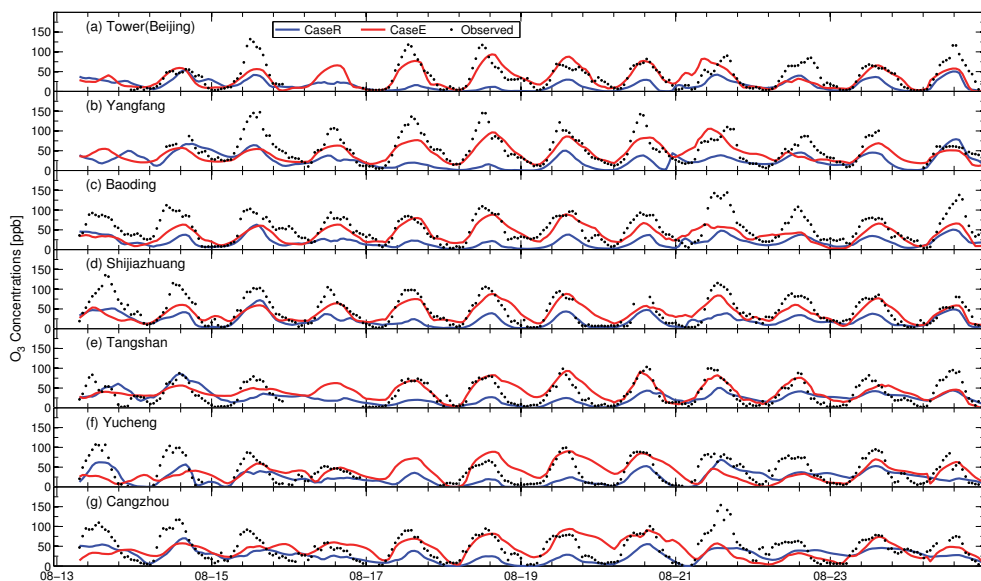


Fig. 8. Simulated and observed O₃ concentrations (ppb) at seven sites in Beijing, Tianjin, and Hebei Province in August 13-25 of 2007. O₃ measurements are from Chemiluminescence.

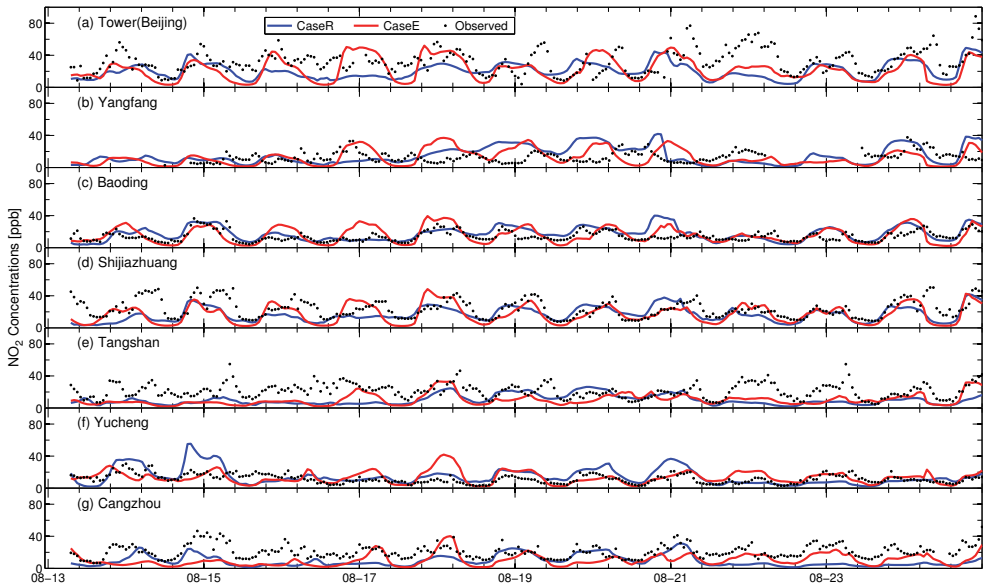


Fig. 9. Simulated and observed NO_2 concentrations (ppb) at seven sites in Beijing, Tianjin, and Hebei Province in August 13-25 of 2007. NO_2 measurements are from Chemiluminescence.

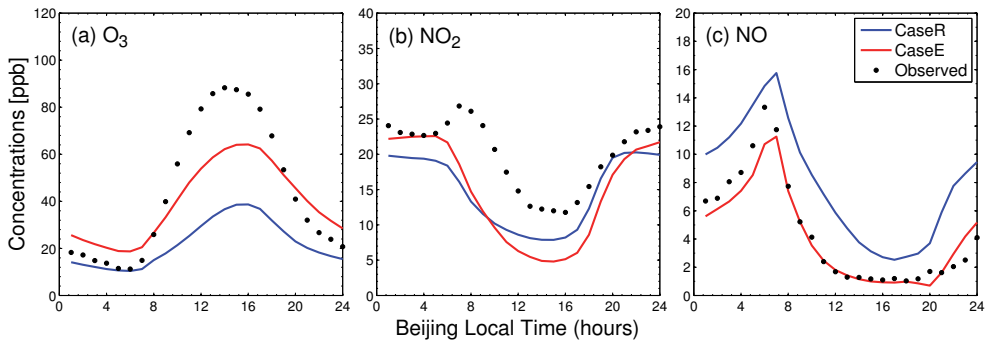


Fig. 10. Comparison of simulated diurnal-mean O_3 (a), NO_2 (b), and NO (c) concentrations with observations (ppb) averaged over all monitoring sites in August 13-25 of 2007.

4. Conclusions

Incorporated into the state-of-the-art WRF-CHEM model were four sources of HONO, i.e., photoexcited NO_2 (NO_2^*) chemistry, heterogeneous reactions on aerosol surfaces, secondary HONO formation from the NO_2 heterogeneous reaction with semivolatile organics, and direct emissions, and simulations were conducted in Beijing, Tianjin, and Hebei Province (BTH region) in August of 2007. Results indicate that the NO_2^* chemistry and heterogeneous

reactions on aerosol surfaces have considerable impacts on concentrations of O₃ and NO_y (total reactive N-containing compounds) in the BTH region. The NO₂* chemistry produces 30~50 ppb enhancements in daily maximum 1-h surface O₃ concentrations in major cities, 8~18 ppb enhancements in monthly mean daily maximum 8-h surface O₃ concentrations, and 4~15 ppb increases in monthly mean daytime surface NO_y concentrations over the BTH region. Heterogeneous reactions on aerosol surfaces lead to 5~15 ppb decreases in monthly mean daytime NO_y concentrations and further substantial decreases in monthly mean nighttime NO_y concentrations, with a maximum decrease of nearly 29 ppb in major cities over the BTH region. This suggests that inclusion of the four HONO sources could aggravate acid deposition in industrialized areas with high emissions of NO_x (NO + NO₂), volatile organic compounds, and particulate matter. Comparison with observations indicates that HONO simulations are significantly improved and O₃ concentrations are well simulated in most cases when the four sources of HONO are included in the WRF-CHEM model.

5. Acknowledgement

The research was partly supported by Knowledge Innovation Key Projects of Chinese Academy of Sciences (kzcx1-yw-06-04, KZCX2-YW-Q02-03, and kzcx1-yw-06-06) and the National Natural Science Foundation of China (Grant No. 40905055). Special thanks are given to Prof. Yuesi Wang from CERN, LAPC, Institute of Atmospheric Physics (IAP), Chinese Academy of Sciences for offering NO_x and O₃ observed data at seven sites of Hebei Province, and INTECH for providing the opportunity to publish the paper in time.

6. Reference

- Alicke, B.; Platt, U. & Stutz, J. (2002). Impact of nitrous acid photolysis on the total hydroxyl radical budget during the Limitation of Oxidant Production/Pianura Padana Produzione di Ozono study in Milan. *Journal of Geophysical Research*, Vol.107, No.D22, 8196, (November 2002), ISSN 0148-0227
- An, J.; Zhang, W. & Qu, Y. (2009). Impacts of a strong cold front on concentrations of HONO, HCHO, O₃, and NO₂ in the heavy traffic urban area of Beijing. *Atmospheric Environment*, Vol.43, No.22-23, (July 2009), pp. 3454-3459, ISSN 1352-2310
- Aumont, B.; Chervier, F. & Laval, S. (2003). Contribution of HONO sources to the NO_x/HO_x/O₃ chemistry in the polluted boundary layer. *Atmospheric Environment*, Vol.37, No.4, (February 2003), pp. 487-498, ISSN 1352-2310
- Chen, F. & Dudia, J. (2001). Coupling an advanced land-surface/hydrology model with the Penn State/NCAR MM5 modeling system. Part I: Model description and implementation. *Monthly Weather Review*, Vol.129, No.4, (April 2001), pp. 569-585, ISSN 0027-0644
- Chin, M.; Ginoux, P.; Kinne, S.; Torres, O.; Holben, B. N.; Duncan, B. N.; Martin, R. V.; Logan, J. A.; Higurashi, A. & Nakajima, T. (2002). Tropospheric aerosol optical thickness from the GOCART model and comparisons with satellite and sun photometer measurements. *Journal of the Atmospheric Science*, Vol.59, No.3, (February 2002), pp. 461-483, ISSN 0022-4928

- Chou, M. D. & Suarez, M. J. (1994). An efficient thermal infrared radiation parameterization for use in general circulation models. *NASA Technical Memorandum*, Vol.104606, No.3, pp. 85
- Crowley, J. N. & Carl, S. A. (1997). OH formation in the photoexcitation of NO₂ beyond the dissociation threshold in the presence of water vapor. *The Journal of Physical Chemistry A*, Vol.101, No.3, (June 1997), pp. 4178–4184, ISSN 1089-5639
- Dentener, F. J. & Crutzen, P. J. (1993). Reaction of N₂O₅ on Tropospheric Aerosols' Impact on the Global Distributions of NO_x, O₃, and OH. *Journal of Geophysical Research*, Vol.98, No.D4, (April 1993), pp. 7149-7163, ISSN 0148-0227
- Emmons, L. K.; Walters, S.; Hess, P. G.; Lamarque, J.-F.; Pfister, G. G.; Fillmore, D.; Granier, C.; Guenther, A.; Kinnison, D.; Laepple, T.; Orlando, J.; Tie, X.; Tyndall, G.; Wiedinmyer, C.; Baughcum, S. L. & Kloster, S. (2009). Description and evaluation of the Model for Ozone and Related chemical Tracers, version 4 (MOZART-4). *Geoscientific Model Development Discussion*, Vol.2, (August 2009), pp. 1157-1213, ISSN 1991-9611
- Ensberg, J. J.; Carreras-Sospedra, M. & Dabdub, D. (2010). Impacts of electronically photo-excited NO₂ on air pollution in the South Coast Air Basin of California. *Atmospheric Chemistry and Physics*, Vol.10, No.3, (February 2010), pp. 1171-1181, ISSN 1680-7316
- Fast, J. D. Jr.; W. I. G.; Easter, R. C.; Zaveri, R. A.; Barnard, J. C.; Chapman, E. G.; Grell, G. A. & Peckham, S. E. (2006). Evolution of ozone, particulates, and aerosol direct radiative forcing in the vicinity of Houston using a fully coupled meteorology-chemistry-aerosol model. *Journal of Geophysical Research*, Vol.111, No.D21305, (November 2006), ISSN 0148-0227
- Grell, G. A.; Peckham, S. E.; Schmitz, R.; McKeen, S. A.; Frost, G.; Skamarock, W. C. & Eder, B. (2005). Fully coupled "online" chemistry within the WRF model. *Atmospheric Environment*, Vol.39, No.37, (December 2005), pp. 6957-6975, ISSN 1352-2310
- Guenther, A.; Zimmerman, P.; Harley, P. C.; Monson, R. K. & Fall, R. (1993). Isoprene and monoterpene emission rate variability: model evaluations and sensitivity analyses. *Journal of Geophysical Research*, Vol.98, No.D7, pp. 12609-12617, ISSN 0148-0227
- Guenther, A.; Zimmerman, P. & Wildermuth, M. (1994). Natural volatile organic compound emission rate estimates for US woodland landscapes. *Atmospheric Environment*, Vol.28, No.6, (April 1994), pp. 1197-1210, ISSN 1352-2310
- Gutzwiller, L.; Arens, F.; Baltensperger, U.; Gaggeler, H. W. & Ammann, M. (2002). Significance of semivolatile diesel exhaust organics for secondary HONO formation. *Environmental Science and Technology*, Vol.36, No.4, (January 2002), pp. 677-682, ISSN 0013-936X
- Jacob, D. J. (2000). Heterogeneous chemistry and tropospheric ozone. *Atmospheric Environment*, Vol.34, No.12-24, pp. 2131-2159, ISSN 1352-2310
- Kurtenbacha, R.; Beckera, K. H.; Gomesa, J. A. G.; Kleffmanna, J.; Lorzera, J. C.; Spittler, M.; Wiesen, P.; Ackermann, R.; Geyer, A. & Platt, U. (2001). Investigations of emissions and heterogeneous formation of HONO in a road traffic tunnel. *Atmospheric Environment*, Vol.35, No.20, (July 2001), pp. 3385-3394, ISSN 1352-2310
- Li, S.; Matthews, J. & Sinha, A. (2008). Atmospheric hydroxyl radical production from electronically excited NO₂ and H₂O. *Science*, Vol.319, No.5870, (March 2008), pp. 1657-1660, ISSN 0036-8075

- Li, Y.; An, J.; Min, M.; Zhang, W.; Wang, F. & Xie, P. (2010). Impacts of HONO sources on the air quality in Beijing, Tianjin and Hebei Province of China. *Atmospheric Environment*, (in press)
- Lin, Y. L.; Farley, R. D. & Orville, H. D. (1983). Bulk parameterization of the snow field in a cloud model, *Journal of Applied Meteorology*, Vol.22, (June 1983), pp. 1065–1092, ISSN 0894-8763
- Madronich, S. (1987). Photodissociation in the atmosphere 1. actinic flux and the effects of ground reflections and clouds. *Journal of Geophysical Research*, Vol.92, No.D8, pp. 9740-9752, ISSN 0148-0227
- Mlawer, E. J.; Taubman, S. J.; Brown, P. D.; Iacono, M. J. & Clough, S. A. (1997). Radiative transfer for inhomogeneous atmosphere: RRTM, a validated correlated-k model for the long-wave. *Journal of Geophysical Research*, Vol.102, No.D14, (July 1997), pp. 16663–16682, ISSN 0148-0227
- Noh, Y.; Cheon, W. G. & Raasch, S. (2001). The improvement of the K-profile model for the PBL using LES. Preprints, *Int. Workshop of Next Generation NWP Models*, Seoul, South Korea, Laboratory for Atmospheric Modeling Research, pp. 65–66.
- Qin, M.; Xie, P. H.; Liu, W. Q.; Li, A.; Dou, K.; Fang, W.; Liu, H. G. & Zhang, W. J. (2006). Observation of atmospheric nitrous acid with DOAS in Beijing, China. *Journal of Environmental Sciences*, Vol.18, No.1, (July 2006), pp. 69–75, ISSN 1001-0742
- Qin, M.; Xie, P.; Su, H.; Gu, J.; Peng, F.; Li, S.; Zeng, L.; Liu, J.; Liu, W. & Zhang, Y. (2009). An observational study of the HONO–NO₂ coupling at an urban site in Guangzhou City, South China. *Atmospheric Environment*, Vol.43, No.36, (November 2009), pp. 5731-5742, ISSN 1352-2310
- Sarwar, G.; Roselle, S. J.; Mathur, R.; Appel, W.; Dennis, R. L. & Vogel, B. (2008). A comparison of CMAQ HONO predictions with observations from the Northeast Oxidant and Particle Study. *Atmospheric Environment*, Vol.42, No.23, (July 2008), pp. 5760-5770, ISSN 1352-2310
- Sarwar, G.; Robert W.; Appel, K.; Mathur, R. & Carlton, A. (2009). Examination of the impact of photoexcited NO₂ chemistry on regional air quality, *Atmospheric Environment*, Vol.43, No.40, (December 2009), pp. 6383-6387, ISSN 1352-2310
- Schoenemeyer, T.; Richter, K. & Smiatek, G., 1997. Vorstudie über ein raumlich und zeitlich aufgelöstes Kataster anthropogener und biogener Emissionen fuer Bayern mit Entwicklung eines Prototyps und Anwendung für Immissionsprognosen. Abschlussbericht an das Bayerische Landesamt für Umweltschutz. Fraunhofer-Institut fuer Atmosphärische Umweltforschung, Garmisch-Partenkirchen
- Simpson, D.; Guenther, A.; Hewitt, C. N. & Steinbrecher, R. (1995). Biogenic emissions in Europe 1. estimates and uncertainties. *Journal of Geophysical Research*, Vol.100, No.D11, pp. 22875-22890, ISSN 0148-0227
- Streets, D. G.; Bond, T. C.; Carmichael, G. R.; Fernandes, S. D.; Fu, Q.; He, D.; Klimont, Z.; Nelson, S. M.; Tsai, N. Y.; Wang, M. Q.; Woo, J.-H. & Yarber, K. F. (2003). An inventory of gaseous and primary aerosol emissions in Asia in the year 2000. *Journal of Geophysical Research*, Vol.108, No.D21, 8809, (November 2003), ISSN 0148-0227
- Su, H.; Cheng, Y. F.; Cheng, P.; Zhang, Y. H.; Dong, S. F.; Zeng, L. M.; Wang, X. S.; Slanina, J.; Shao, M. & Wiedensohler, A. (2008a). Observation of nighttime nitrous acid (HONO) formation at a non-urban site during PRIDE-PRD2004 in China.

- Atmospheric Environment*, Vol.42, No.25, (August 2008), pp. 6219-6232, ISSN 1352-2310
- Su, H.; Cheng, Y. F.; Shao, M.; Gao, D. F.; Yu, Z. Y.; Zeng, L. M.; Slanina, J.; Zhang, Y. H. & Wiedensohler, A. (2008b). Nitrous acid (HONO) and its daytime sources at a rural site during the 2004 PRIDE-PRD experiment in China. *Journal of Geophysical Research*, Vol.113, No.D14312, (July 2008), ISSN 0148-0227
- Wennberg, P. O. & Dabdub, D. (2008). Rethinking ozone production. *Science*, Vol.319, No.5870, (March 2008), pp. 1624-1625, ISSN 0036-8075
- Yu, Y.; Galle, B.; Panday, A.; Hodson, E.; Prinn, R. & Wang, S. (2009). Observations of high rates of NO₂-HONO conversion in the nocturnal atmospheric boundary layer in Kathmandu, Nepal. *Atmospheric Chemistry and Physics*, Vol.9, No.17, (September 2009), pp. 6401-6415, ISSN 1680-7316
- Zaveri, R. A. & Peters, L. K. (1999). A new lumped structure photochemical mechanism for large-scale applications. *Journal of Geophysical Research*, Vol.104, No.D23, (December 1999), pp. 30387-30415, ISSN 0148-0227
- Zaveri, R. A.; Easter, R. C.; Fast, J. D. & Peters, L. K. (2008) Model for Simulating Aerosol Interactions and Chemistry (MOSAIC), *Journal of Geophysical Research*, Vol.113, No.D13, (July 2008), ISSN 0148-0227
- Zhang, Q.; Streets, D. G.; Carmichael, G. R.; He, K. B.; Huo, H.; Kannari, A.; Klimont, Z.; Park, I. S.; Reddy, S.; Fu, J. S.; Chen, D.; Duan, L.; Lei, Y.; Wang, L. T. & Yao, Z. L. (2009). Asian emissions in 2006 for the NASA INTEX-B mission. *Atmospheric Chemistry and Physics*, Vol.9, No.14, (January 2009), pp. 5131-5153, ISSN 1680-7316
- Zhu, Y.; Liu, W.; Xie, P.; Dou, K.; Liu, S.; Si, F.; Li, S. & Qin, M. (2009). Observations of atmospheric HONO in summer of Beijing. *Environmental Science*, Vol.30, No.6, (June 2009), pp. 1567- 1573. ISSN 0250-3301 (in Chinese)

Analyzing Black Cloud Dynamics over Cairo, Nile Delta Region and Alexandria using Aerosols and Water Vapor Data

Hesham M. El-Askary^{1,2,3}, Anup K. Prasad^{1,2}, George Kallos⁴,
Mohamed El-Raey⁵ and Menas Kafatos^{1,2}

¹*School of Earth and Environmental Sciences,*

Schmid College of Science, Chapman University, Orange,

²*Center of Excellence in Earth Observing, Chapman University, Orange,*

³*Department of Environmental Sciences, Faculty of Science,*

Alexandria University, Moharem Bek, Alexandria,

⁴*Atmospheric Modeling and Weather Forecasting Group,*

School of Physics, University of Athens, Athens,

⁵*Institute of Graduate Studies and Research,*

Alexandria University, Alexandria,

^{1,2}USA

^{3,5}Egypt

⁴Greece

1. Introduction

Cairo is the largest city of Africa and one of the world's megacities, with a population of more than 20 million people and containing more than one third of the national industry. It is a rapidly expanding city which leads to many associated environmental problems. As a result, it is also one of the most air polluted megacities in the world (Molina and Molina, 2004). It suffers from high ambient concentrations of atmospheric pollutants including particulates (PM), carbon monoxide, nitrogen oxides, ozone and sulfur dioxide (Abu-Allaban et al., 2007, Abu-Allaban et al., 2002, El-Metwally et al., 2008). The pollution phenomenon locally known as "Black cloud" over Cairo has been attributed to many reasons among which are biomass burning, local emission and long range transport during the fall season. Several studies have been conducted to address and discuss the forth mentioned reasons for the increased pollution levels over Cairo and the greater Delta region using ground-based and satellite air quality data as compared to other megacities (Abu-Allaban et al., 2002, 2007, 2009; Alfaro and Wahab, 2006; El-Askary and Kafatos, 2008; El-Metwally et al., 2008; Favez et al., 2008; Kanakidou et al., 2011; Mahmoud et al., 2008; and Marey et al., 2010; Prasad et al., 2010 and Zakey et al., 2004). Marey et al. (2010) utilized a multi sensor approach using the Moderate Resolution Imaging Spectrometer (MODIS) and

the Multi-angle Imaging SpectroRadiometer (MISR) with meteorological data and trajectory analyses to determine the cause of these events and to examine reasons for the black cloud formation over Cairo. MODIS fire counts identify the aerosol source as the burning of agricultural waste after harvest season in the Nile Delta region. MISR data show that these fires create low altitude (<500 m) plumes of smoke that flow over Cairo in a few hours, as confirmed by Hybrid Single-Particle Lagrangian Integrated Trajectory (HYSPLIT) forward trajectory analyses. However, Prasad et al. (2010) suggest that the long range transport of dust at high altitude (2.5-6 km) from the Western Sahara and its deposition over the Nile Delta region is one of the major contributors to air pollution episodes during this season. Cairo experiences different seasonal climate systems impacted by the western desert through sand and dust storms, as well as local, increasing anthropogenic activities. As a result, it is characterized by a complicated meteorology, varying with the time of the year and resultant pollution which is worst during the black cloud episodes reported in this paper and in turn affecting the local climate (Zakey et al., 2004) During winter the climate is generally cold, humid and rainy; while during the summer season the predominant weather is hot and dry (Zakey et al., 2008). Hence, the city witnesses significant impacts on the public health (Hossny et al., 2001). On the other hand, Alexandria as a Mediterranean city has better climate conditions, yet being the largest industrial city, with ~55% of total Egyptian industry, suffers from pollution episodes, which are, however, still not as intense as the ones usually observed over Cairo. El-Metwally et al., (2008) and El-Askary et al., (2009) revealed that Cairo's and Alexandria's aerosol includes; "background pollution", "pollution-like", and "dust-like" components. Generally speaking, Egypt is influenced by the regional scale trade wind system that is enhanced during the warm period of the year resulting in winds over Egypt are from North supporting the sea-breezes along the Mediterranean coastline (Kallos et al., 1998, 2007; El-Askary et al. 2009). It has been thought that pollution episodes occur only over Cairo and are due to local emissions; however, we will show that there are large emissions from the surrounding cities that are likely contributing to Cairo pollution. On the other hand, it is noteworthy that the low topography of Cairo bounded by Giza (western highlands) and Mokattam (eastern highlands) contributes as well to the onset of these pollution events, compared to the surrounding region previously reported (El-Askary, 2006). During the autumn season, aerosols originating from the biomass burning from different cities within the Nile Delta, add to the region's anthropogenic aerosols, and hence contribute to bigger pollution events. Here, we propose a wider contribution from other anthropogenic sources in surrounding cities among the major contributors to this problem. Cairo, Alexandria, together with other cities within the greater Nile Delta region extending from ~ 29° to 31° N, are the sites of the present study. Five locations within the Delta together with Alexandria, a coastal city, have been selected for this analysis based on their locations with respect to Cairo and the reported polluting events. Cairo together with the other relevant cities is located in the Northern Delta Region, which is a heavily populated area. However, Alexandria is located along the Mediterranean Sea and is the only coastal city involved in this analysis (Figure 1).

This work presents an attempt to study the wide spatial distribution of pollution over Northern Egypt. (Table 1) shows the locations of the cities under investigation and their main sources of air pollution, namely heavy traffic / industrial / residential / commercial / mixed emissions or biomass burning.



Fig. 1. Base Map for cities under consideration

City	Latitude	Longitude	Activity or pollution source
Alexandria	31.213 N	29.944 E	Industrial/Residential and traffic sectors
Tanta	30.779 N	30.996 E	Burn harvest byproducts Industrial/Residential
Damanhur	31.040 N	30.469 E	Burn harvest byproducts/Residential
El Mahala	30.975 N	31.163 E	Industrial/Excessive emissions from brick factories
El Mansoura	31.039 N	31.379 E	Burn harvest byproducts Industrial/Residential
Cairo	30.064 N	31.249 E	Excessive pollution from industrial/Dump sites burning and traffic sectors

Table 1. Cities locations for AOD and WV analysis and their possible pollution source

2. Aerosol Optical Depth (AOD) and Water Vapor Column (WVC) data used

Over the last decade aerosols have been studied quantitatively regionally and globally using satellite remote sensing. Such studies are very useful in climate studies (Kaufman et al., 2002; King et al., 1999). The Mediterranean basin aerosols belong to a variety of sources, either being natural (sea salts, desert dust) or anthropogenic (local sources) due to the increasing urbanization and industrialization, as well as long range transport from Europe (Astitha et al., 2008; Kallos et al., 1998, 2007). As such, AOD obtained from the MODIS data was used to study urban air quality (Engel-Cox et al., 2004). Diversity in the aerosol origin influences to a great extent their optical properties (Pace et al., 2006). The data set used in this study involves six years of monthly average observations of AOD over the Delta region derived from MODIS level-2 AOT atmospheric daily products data at a 10 km resolution. The WVC data are obtained at the 1-km MODIS spatial resolution. The Level 2 data are generated at the 1-km spatial resolution level using the near-infrared algorithm during the

day and at 5×5 1-km pixel resolution for both day and night. The AOD parameter obtained from the MODIS data is used as an indicator for the black cloud impacts on the optical properties of the aerosols forming in the vertical column of the atmosphere. It is well known that Northern Egypt suffers from variability of atmospheric pollutant sources and hence the mixing processes scenario in the atmosphere is most likely a mixed aerosol type. Since we are studying the impact of anthropogenic pollutants on aerosol optical properties during the fall season, characterized by the well known black cloud pollution episodes, a seasonal component is expected to affect the AOD values. Therefore, AOD obtained from the MODIS sensor over the period February 2000 to August 2009 is detrended using climatological values to remove any seasonal contribution to observed main anomalies (Gautam et al., 2007). De-seasonalizing is performed for the time series at each grid location by calculating the deviations from the climatological mean annual cycle. Hence, the anomalies in the annual cycle can more easily be inferred.

The high AOD values over Cairo are a result of the unregulated continuous emissions, coupled with the stable meteorological conditions by weak wind currents as well as almost neutral stratification (El-Askary, and Kafatos, 2008). High AOD values associated with slowly moving air masses are generally accompanied by higher precipitable water vapor (Xia et al., 2007). We anticipate that high WVC will be observed regionally over locations where high AOD is also observed. The MODIS precipitable water product consisting of the water-vapor column is essential in understanding the aerosol properties, and aerosol-cloud interactions (Jin et al., 2005).

2.1 Aerosol data analysis

Monthly average Aerosol Optical Depth (AOD) and Water Vapor Clear Column (WVC) over Cairo, Alexandria and the Delta cities of Damanhur, Tanta, El Mahala and El Mansoura were analyzed for 2000-2009. High AOD values are observed during the September, October and November (SON) season, over all locations at different levels showing the regional extent of such pollution events. Figures 2a and 2b show monthly average values of AOD and monthly AOD anomaly during the period from February 2000 to August 2009 over the six cities.

Figure 2a shows a strong variability and similarity in the aerosol patterns over the entire region associated with the presence of a clear annual component for the locations under investigation. It also shows the presence of two main peaks corresponding to dust and anthropogenic episodes superimposed on the annual variability over the six locations within the entire time period (Figure 4) (El-Askary, and M. Kafatos, 2008). This result favours the idea of treating the overall pollution phenomenon as a regional one, rather than just being a local phenomenon over Cairo. However, for better visualizing the high AOD concentrations without the annual variability component, the climatology has been extracted out and only the anomaly is presented here (Figure 2b). Moreover, it is clear that the AOD variability over Cairo, El Mahala and Tanta are slightly higher than El Mansoura and definitely higher than those over Alexandria and Damanhur (Figure 2b).

This is attributed to the fact that Alexandria and Damanhur are located in the vicinity of the Mediterranean and are subject to a component of sea and land breeze as well as wet deposition which contribute to a speedy cleaning up of the atmosphere. Alexandria is the biggest industrial city of Egypt, since it accommodates >65 % of the petroleum related industries and >55 % of the entire industrial sector, yet as we said above, it doesn't suffer as intense pollution episodes as Cairo, raising a question about the overall sink of these pollutants.

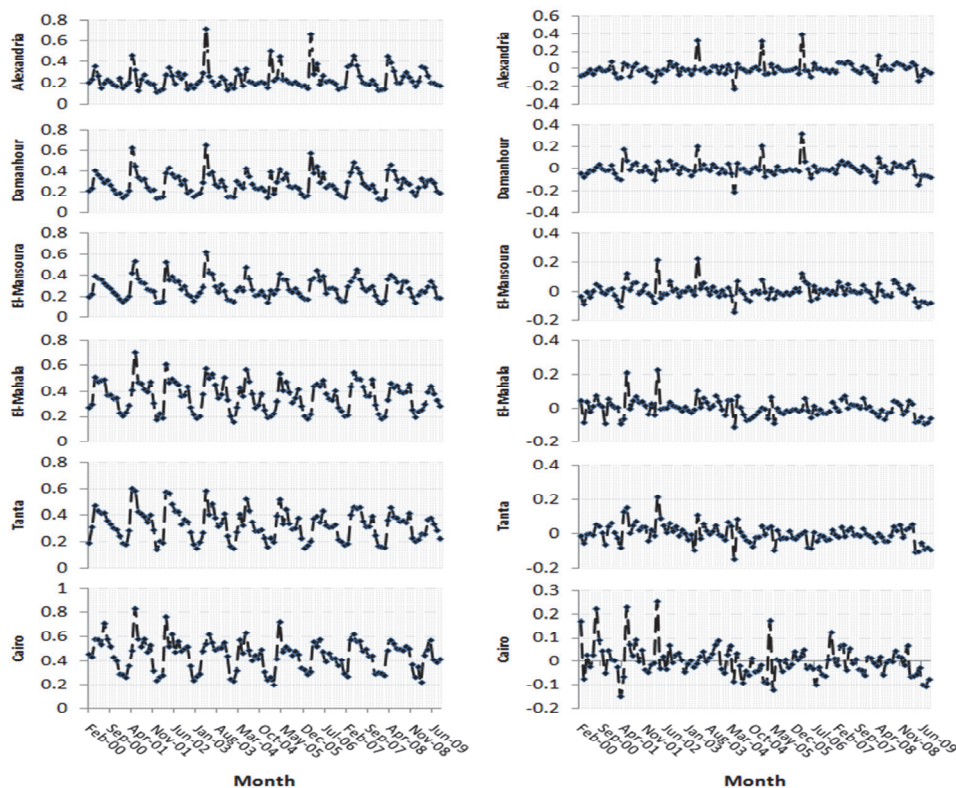


Fig. 2. Aerosol Optical Depth (unitless) Over Delta Region Cities from February 2000 to August 2009 a) Original data B) De-seasonalized data

As emphasized here, the aerosols over the Northern coast of Egypt and the Delta region can have origins other than just local ones. These seasonal aerosols may be either from natural causes, for instance desert dust particles directly transported from the Western desert regions; or anthropogenic aerosols from the industrialized areas, maritime particles produced over the Mediterranean and smoke particles from seasonal biomass fires (Barnaba and Gobbi, 2004). Luria et al. (1996), Millan et al. (1997), Kallos et al. (1998, 2007), Prasad et al. (2010) found that this geographical region is exposed to long range transport of anthropogenic pollutants as well as dust particles. According to their findings, long range transported (mainly from Europe) anthropogenic aerosol concentrations are very high during the warm period of the year due to the prevailing trade wind patterns, photochemical activity and absence of precipitation. During the transient seasons, and mainly spring, the desert dust transport is a major contributor. Sea-salt particles contribute to aerosol concentrations over the coastal areas, mainly during weather conditions with strong winds (synoptic scale component). It becomes more important during winter due to the passage of synoptic systems and during summer due to trade winds (from N) and the wave breaking activity along the coast. Here we also show long range transport of desert dust from Western Sahara that passes over the eastern Sahara during September-October (Figure 3).

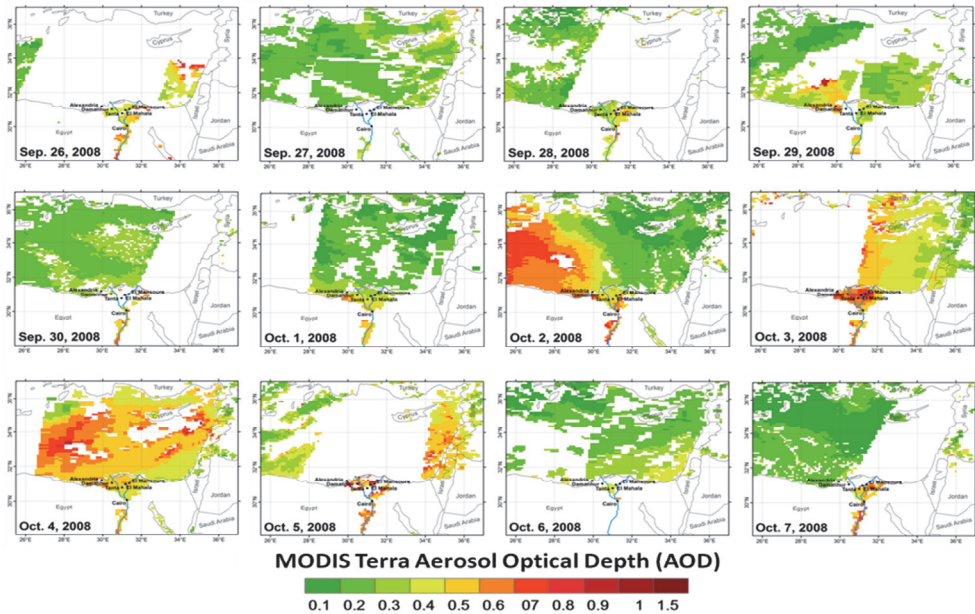


Fig. 3. The long range transport of pollution (aerosols) across the Mediterranean Sea (west to east) during Fall season.

The eastward movement of plume of desert dust (red color region, Figure 3) is visible over the Mediterranean using daily MODIS AOD during the month of October, 2008 (Figure 3). The high altitude desert dust gets deposited over the Nile Delta due to the presence of favourable wind field (subsidence) over the region. This phenomena not only causes large increase in the aerosol loading over the region but also increases the complexity of nature and source of aerosols (Prasad et al., 2010) (Figure 3). The mixing of anthropogenic pollution with the desert dust eventually increases the total pollution load and also affect the climatic conditions over the region. The variability in AOD follows this known pattern (Figure 4). Small error bars in the plot reflect a narrow region of uncertainty; in other words, the accuracy of the plotted data with varying AOD values over different months of the year is high. The primary peak is during the spring season in all cities and can be easily attributed to the contribution from desert dust (Figure 4). This is due to the well known intense dust storms over Sahara associated with the prevailing south western winds, called Khamasine, affecting the Greater Cairo region. Figure 2 also indicates a smaller increase in the aerosol levels during October of each year compared to April and May, with particularly high values over Cairo, El Mahalla and Tanta; while the data show slightly earlier increase during the month of September over Alexandria, Damanhur and El Mansoura, and continuing through November. Higher AOD values have been observed from the AOD seasonal mean plots over Cairo, El Mahala and Tanta during September and October of each year, yet lower values have been observed over El Mansoura, Damanhur and Alexandria. The highest AOD values are observed over Cairo owing to its low topography and the frequent appearance of an inversion layer during this time of the year (El-Askary, 2006). As it is well known, during autumn, the prevailing winds are from northern and west sectors

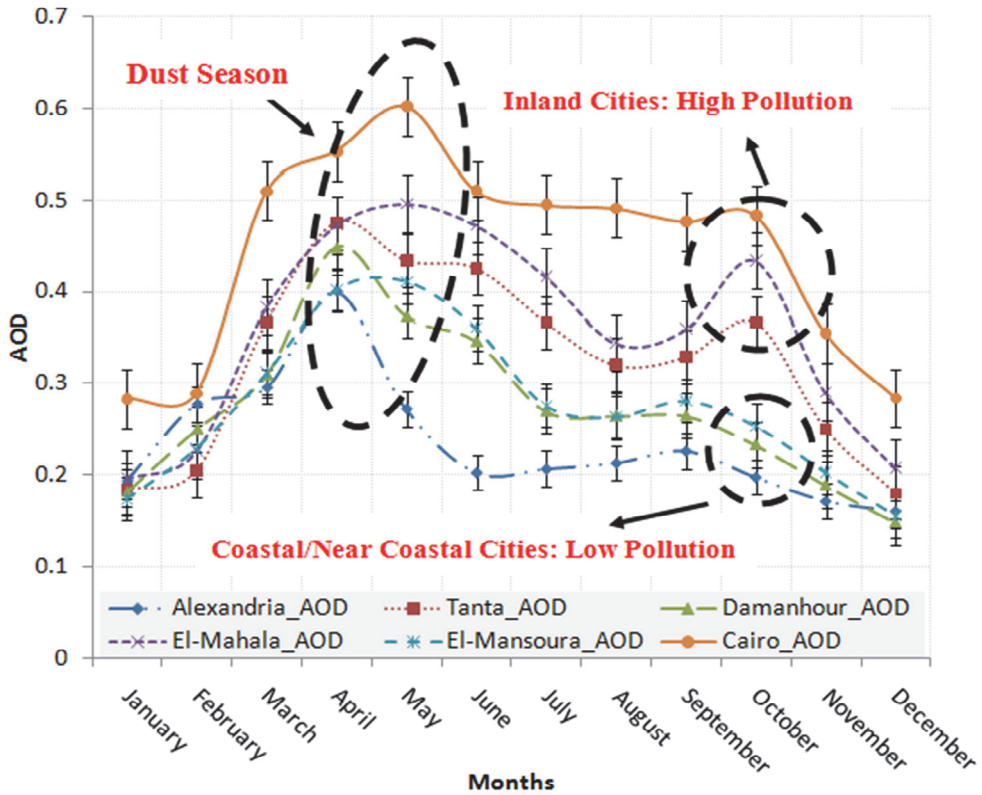


Fig. 4. Seasonal means of Aerosol Optical Depth (unitless) from February 2000 until August 2009 over the Delta region

with moderate to low speeds (>65%) (Favez et al., 2008). This is attributed mainly to the sea breeze formation that exhibits a daily variability. These sea breezes penetrate deep inside from the coast since they are supported by the regional circulation. Since Cairo is downwind from well known pollution sources (e.g. the industrial area of Alexandria, seasonal biomass burning in Nile Delta, and other major urban areas), the resultant air pollution concentrations in the vicinity of it must have a considerable contribution over regional scale.

2.2 Enhanced total column water vapor with dust storms and pollution aerosols

Our aerosol related results have been corroborated through studying the WVC during the same time frame over the same locations. The relationship between water vapor and aerosols of all kind is well known (Steyn and Kallos, 1992). Therefore, looking at the water content in the atmosphere over the area under consideration we will be able to derive useful correlations with the aerosol concentrations (or AOD) and better explain the seasonal variability. For this reason, time series of WVC were constructed for the same time period and locations as for AOD (Figure 5).

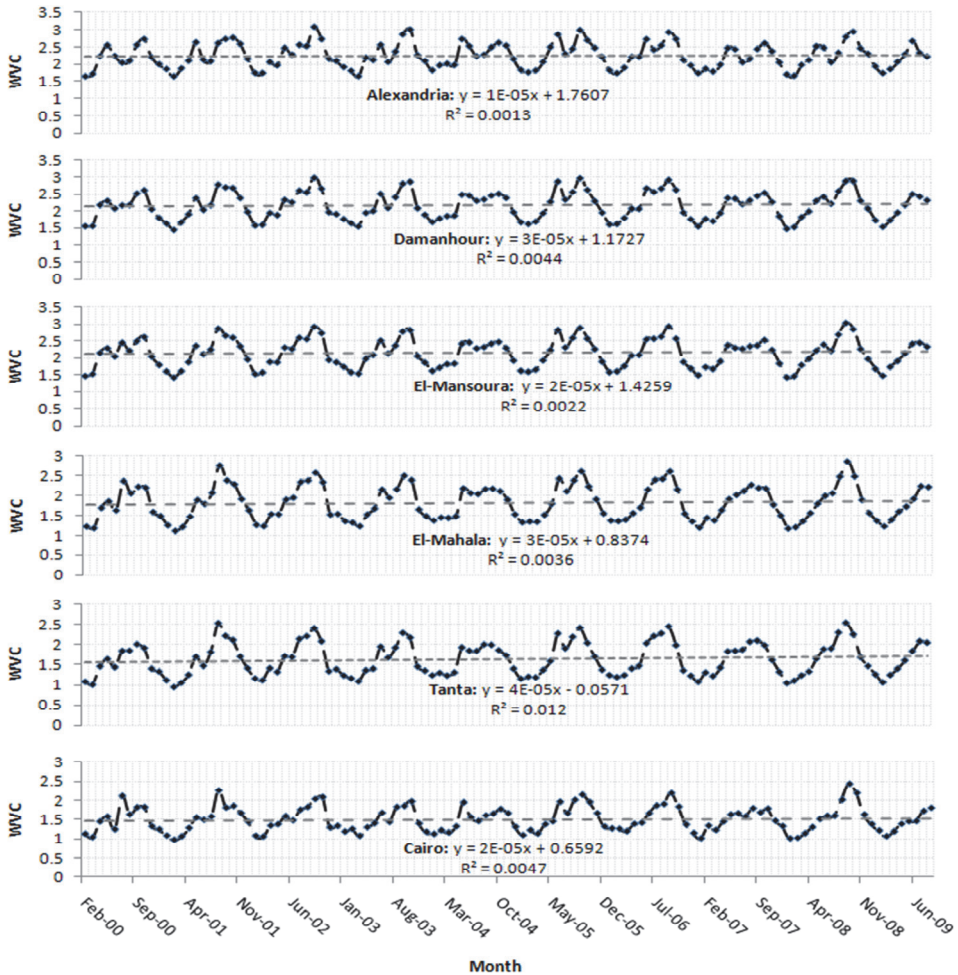


Fig. 5. Water Vapor Column (cm) over the Delta region cities and Alexandria from February 2000 until August 2009

Precipitable water vapor is a measure of the water vapor content of the air. It is one of the most important greenhouse gases of the atmosphere, participating in a major way in the energy cycle (latent heat). Moreover, it regulates the planetary temperatures through absorption and radiation emission, most significantly in the thermal infrared (the greenhouse effect). However, the indirect forcing involving the interactions between aerosols and clouds, impacting climate, has large uncertainties (Houghton et al., 2007).

Satellite data over the area under consideration show that there is an increasing trend in WVC off the coast of Egypt and over the Nile Delta region. The increase over Cairo and the Delta region is consistent with pollution patterns, implied by the AOD values, during 2000–2009. This is due to the existence of absorbing and non-absorbing aerosols emitted from the

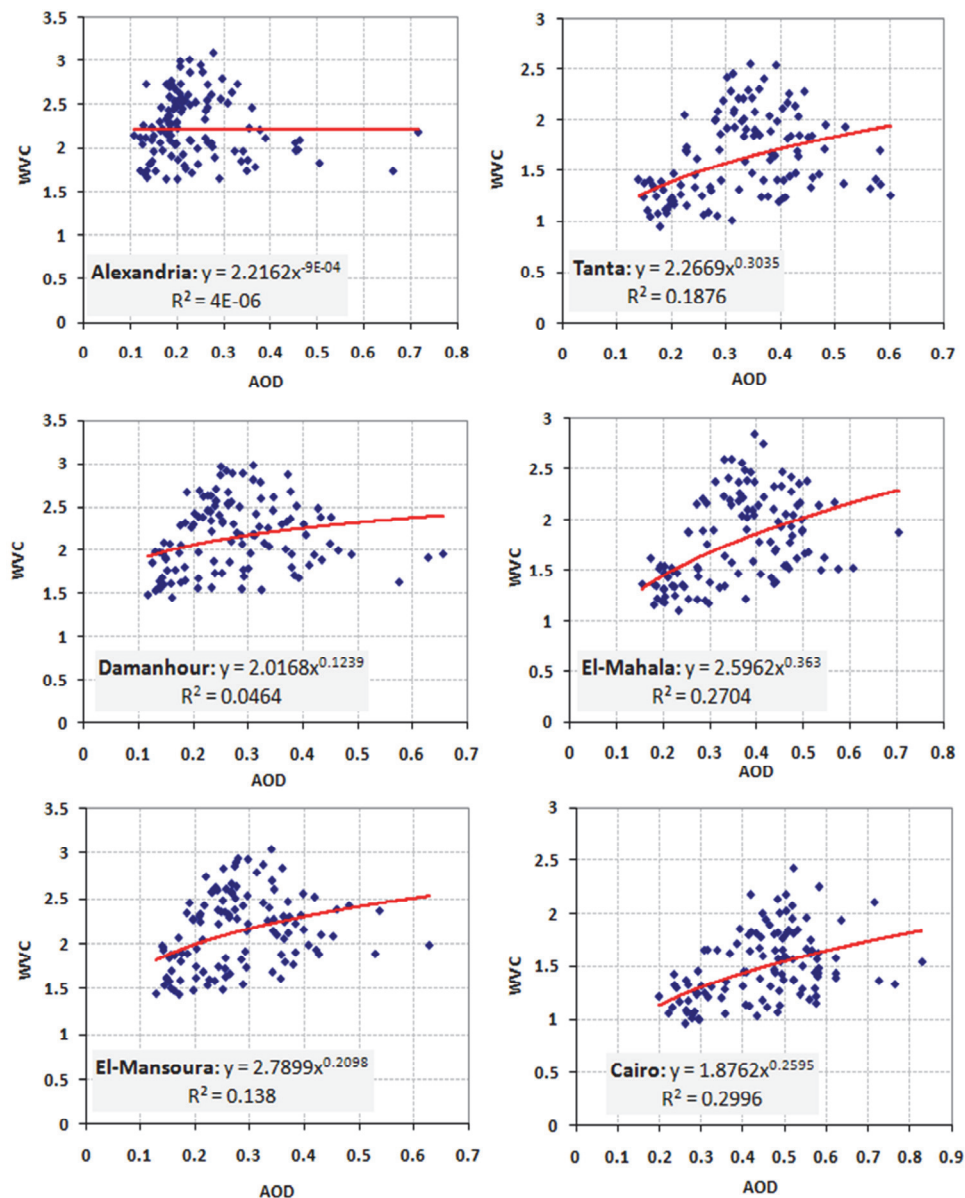


Fig. 6. Power correlation between MODIS AOD and MODIS water vapor (near infra-red, clear column) from February 2000 till May 2009 the six cities.

different cities (Prasad et al., 2006) (Figure 5). However a more increasing trend has been observed over Alexandria, Damanhur and Mansoura as compared to the increasing trend over Cairo, Tanta and El Mahala. This is likely due to the near coastal location of the first three cities compared to the inland location of the later ones. Their location contributes to a

higher degree in the presence of more WV particulates due to higher evaporation rates associated with the Mediterranean. The observed increasing trend of the WVC over the Delta region suggests the aerosol contribution in possible local climate changes. Figure 6 shows monthly MODIS derived AOD versus mean water vapor (near-infrared, clear column) variations.

Enhanced level of water vapor is found over the inland cities (Cairo, Mahala and Tanta) subjected to intense dust storms and anthropogenic pollution. We have studied total column aerosol loading and associated water vapor content during the whole time period. Inland cities clearly indicate an increase in power correlation between mean MODIS AOD and mean MODIS water vapor (near-infrared clear column) from 0.0004%, 4.6%, 13.8% (Over Alexandria, Damanhur, Mansoura) to 18.7%, 27%, 29.9% (Over Tanta, Mahala, Cairo) due to the influence of dust and pollution outbreaks evidenced from the absolute rise in AOD (Figure 4). Power correlation study of mean MODIS AOD with mean MODIS WVC is found to be more sensitive for such studies than the use of max MODIS AOD (Prasad et al., 2007).

2.3 AOD and WVC cross correlation analysis

A cross correlation analysis was carried out for the six cities twice, in order that any aerosol contribution from one location to another would be determined. The first analysis deals with the AOD observations while the second analysis is performed on the WVC values. For each parameter this analysis has been carried out six times having each city taken as a reference point, with lags ranging from the preceding to the following six days during the entire period of study.

(Table 2) shows only the significant correlation coefficients (CCs) for AOD with their corresponding lag values. The term rank is used here to indicate the order of the highest correlations between the ranked and the reference cities for lag 0.

High and significant CCs with confidence level 95% are observed between all the cities and their corresponding reference city at zero lag. High CC between cities indicates the regional scale of the phenomenon (i.e. subject to the same meteorology), hence are more dominant in cities within the Delta region that are more inland and away from the Mediterranean Sea. Delay in CC means local transport between cities, yet high and significant coefficients are still observed at a lag of one preceding or following days in most of the cases. This shows that pollution might not be local for some cities, in other words, some cities may be receiving most of the pollutants from the surrounding locations. Figure 7 shows high and significant CCs of AOD between Alexandria and Cairo for few days through different years at one day lag which provide the evidence of transported pollutants from Alexandria to Cairo.

The presented results strongly support the notion of contributing aerosols from surrounding cities to the pollution crisis over Cairo.

CCs and rank values in (Table 2) show that El Mahala and Tanta AOD values contribute to a great extent to the severe pollution episode experienced over Cairo. A CC of 0.995 and a rank of 1 are observed between Cairo and El Mahala in both cases when each of them is the reference city. Moreover a CC of 0.7558 is observed at lag -1 and lag 1 when El Mahala and Cairo are considered as the reference cities for each other, respectively. Since the reference city leads to positive lag values, it is clear that El Mahala is the site contributing to the Cairo pollution and not the other way around. This means that the ground based strong pollution from smokestacks of brick factories and other industrial activities located in El Mahala, are partially contributing to the black cloud events over Cairo and the Delta region.

a) Alexandria Reference*			b) Tanta Reference*			c) Damanhur Reference*		
City	CC	lag	City	CC	lag	City	CC	lag
	0.4959	-1		0.4707	-2		0.4037	-2
Tanta	0.7775	0	Alexandria	0.6890	-1	Alexandria	0.6398	-1
Rank (3)	0.6890	1	Rank (5)	0.7775	0	Rank (5)	0.8896	0
	0.4707	2		0.4959	1		0.5150	1
	0.5150	-1		0.4052	-2		0.6617	-1
Damanhur	0.8896	0	Damanhur	0.7558	-1	Tanta	0.9425	0
Rank (1)	0.6398	1	Rank (4)	0.9425	0	Rank (2)	0.7558	1
	0.4037	2		0.6617	1		0.4052	2
	0.4353	-1		0.7013	-1		0.6058	-1
El Mahala	0.7409	0	El Mahala	0.9867	0	El Mahala	0.9259	0
Rank (5)	0.7122	1	Rank (2)	0.7858	1	Rank (4)	0.7926	1
	0.4884	2		0.3982	2		0.4301	2
	0.4982	-1		0.3846	-2		0.6578	-1
El Mansoura	0.8249	0	El Mansoura	0.7412	-1	El Mansoura	0.9678	0
Rank (2)	0.6915	1	Rank (3)	0.9571	0	Rank (1)	0.7377	1
	0.4214	2		0.7064	1		0.3412	2
	0.4655	-1		0.7227	-1		0.6313	-1
Cairo	0.7519	0	Cairo	0.9902	0	Cairo	0.9276	0
Rank (4)	0.7186	1	Rank (1)	0.7874	1	Rank (3)	0.7911	1
	0.4933	2		0.4173	2		0.4416	2
d) El Mahala Reference*			e) El Mansoura Reference*			f) Cairo Reference*		
City	CC	lag	City	CC	lag	City	CC	lag
	0.4884	-2		0.4214	-2		0.4933	-2
Alexandria	0.7122	-1	Alexandria	0.6915	-1	Alexandria	0.7186	-1
Rank (5)	0.7409	0	Rank (5)	0.8249	0	Rank (5)	0.7519	0
	0.4353	1		0.4982	1		0.4655	1
	0.3982	-2		0.7064	-1		0.4173	-2
Tanta	0.7858	-1	Tanta	0.9571	0	Tanta	0.7874	-1
Rank (2)	0.9867	0	Rank (2)	0.7412	1	Rank (2)	0.9902	0
	0.7013	1		0.3846	2		0.7227	1
	0.4301	-2		0.3412	-2		0.4416	-2
Damanhur	0.7926	-1	Damanhur	0.7377	-1	Damanhur	0.7911	-1
Rank (4)	0.9259	0	Rank (1)	0.9678	0	Rank (4)	0.9276	0
	0.6058	1		0.6578	1		0.6313	1
	0.4026	-2		0.6546	-1		0.7365	-1
El Mansoura	0.7782	-1	El Mahala	0.9546	0	El Mahala	0.9950	0
Rank (3)	0.9546	0	Rank (3)	0.7782	1	Rank (1)	0.7558	1
	0.6546	1		0.4026	2		0.3527	2
	0.3527	-2		0.6750	-1		0.4180	-2
Cairo	0.7558	-1	Cairo	0.9529	0	El Mansoura	0.7725	-1
Rank (1)	0.9950	0	Rank (4)	0.7725	1	Rank (3)	0.9529	0
	0.7365	1		0.4180	2		0.6750	1

Table 2. Lag correlation analysis of daily AOD values from February 2000 until August 2009 over Alexandria and the five other cities within the Delta Region (* Reference station leads for positive lags)

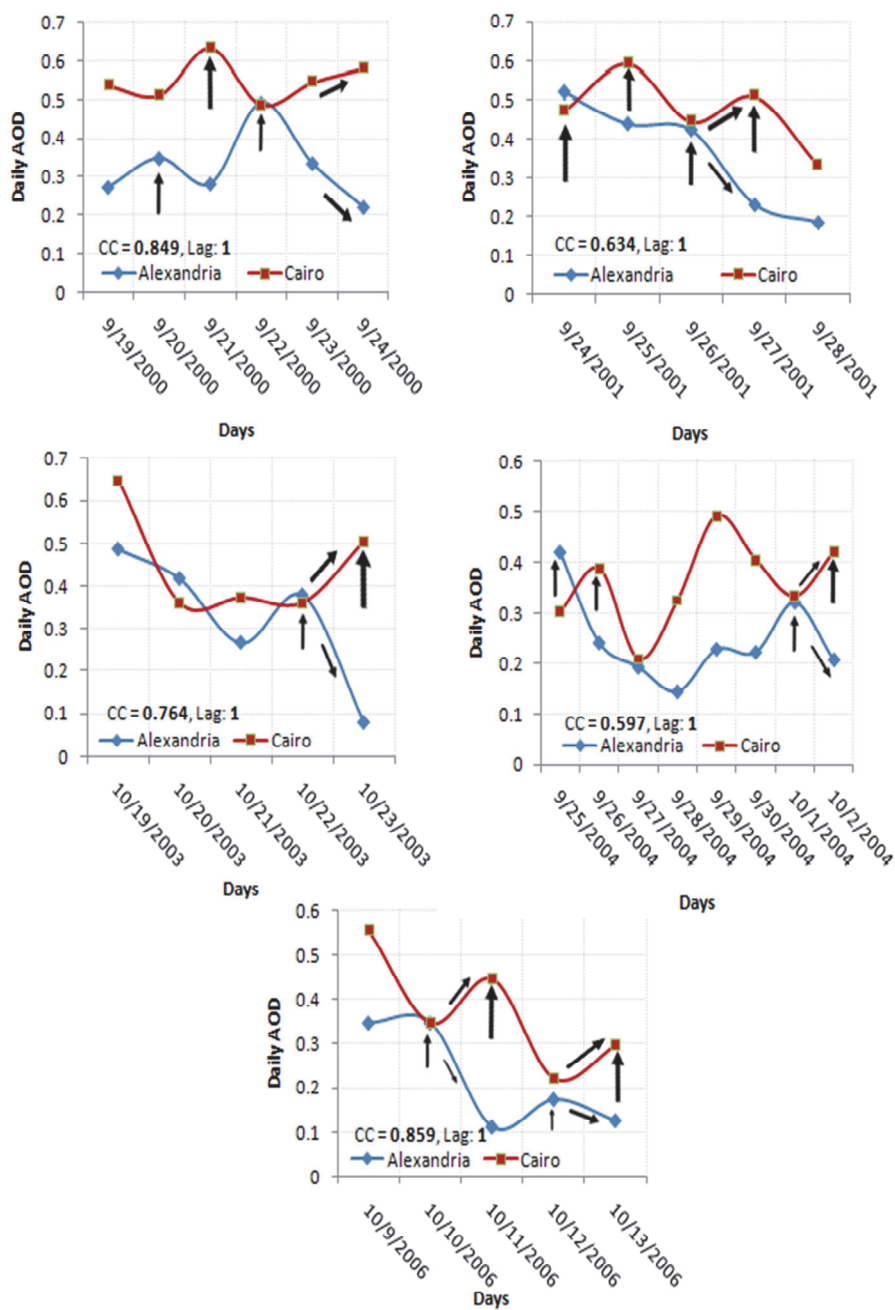


Fig. 7. Evidence of pollutants transportation from Alexandria to Cairo for selected days with high CCs at one day lag

High CC between two cities can be explained also as that the regional scale meteorology is responsible for the formation of air pollution episodes. It can be interpreted also as plume travelling times are small and after a while polluted air masses are merged forming uniform conditions.

The CC between Tanta and Cairo shows how the AOD over Tanta played a considerable role in the Cairo pollution episodes. Having Cairo as a reference city, Tanta came in the second position with a CC of 0.9902 after El Mahala; however taking Tanta as a reference city, Cairo occupied first rank with the highest CC of 0.9902. Meanwhile, high CC of 0.7874 is also observed at lags of -1 and 1 day when Cairo and Tanta are the reference cities, respectively. This means that Tanta is also contributing to the Cairo pollution event and, again not, the other way around. From the CCs observed at 0, 1 and -1 lags for El Mahala, Tanta and Cairo, it is clear that most of pollution forming activities is mainly observed during the months of September and October per the high AOD values observed.

The CCs and the ranks of El Mansoura, Damanhur and Alexandria indicate that these cities have fixed ranking all the time, namely rank 3, 4 and 5, respectively when taking El Mahala, Tanta and Cairo as reference cities. Therefore, the AOD analysis shows that these three cities contribute less to the black cloud events over Cairo. Similar cross correlation analysis of the WVC has been performed to understand the dynamics of cloud formation in association with the aerosol loadings in the atmosphere. Due to the high observed AOD levels over the 6 locations during the dust and pollution seasons, we conclude that the Delta region is a strong source of pollution airborne particles. These particles can travel long distances to other cities and neighboring Mediterranean countries and thus influence the aerosol radiative forcing at regional scales. Moreover, aerosols are likely to affect the water cycle by suppressing precipitation in a region of the world which is already very dry (Favez et al., 2008), (Rosenfeld, 2000, 2008). Favez et al. (2008) analyzed the chemical composition of bulk aerosols over 1.5–3 years at two urban sites in Cairo. Their analysis indicated very high levels of mineral dust (over 100 $\mu\text{g}/\text{m}^3$) in winter and spring; and more than 50 $\mu\text{g}/\text{m}^3$ in summer and autumn. There is an important effect, namely direct and indirect radiative forcing because of the aerosol relation with water vapor (Houghton et al., 2001; Tegen et al., 1996 and Hsu et al., 2003). The use of water vapor column as an indicator for dust storms and massive pollution events has been pointed out by (El-Askary and Kafatos, 2008; El-Askary et al., 2003), owing to cloud condensation nuclei formation as an indirect effect of such atmospheric phenomena.

(Table 3) shows high and significant CCs for WVC with confidence level 95% between all the cities and their corresponding reference city at zero lag as observed in the AOD case shown in (Table 2). In this analysis we have sub-categorized the six locations under investigation into two main categories, coastal (Alexandria) and near coastal/inland (El Mansoura and Damanhur) versus further inland (Cairo, Tanta and El Mahala). We have found that the ranking of the six locations based on the cross correlation analysis of the WVC taking each one of the three further inland cities as a reference, matches very well the ranking observed from the AOD correlation analysis. However, when considering the coastal, near coastal/inland cities as the reference stations, the rankings differ from the ones obtained when correlating the AOD values.

For instance, when having any of the coastal/near coastal/inland cities designated as the reference station, the other two cities of the same category achieve the first two ranks which was not the case obtained in the AOD case (Table 2). This is because coastal cities are highly exposed to the sea breeze that transfers water vapor from the sea, leading to the formation of higher WVC. Therefore, we can say that the WVC observed over these locations is primarily due to sea breeze. When examining the inland cities, a similar ranking observed

as the AOD one (Table 2), suggests higher water vapor content over the inland cities due to aerosol loading either from natural or anthropogenic origin (Figure 6).

a) Alexandria Reference*			b) Tanta Reference*			c) Damanhur Reference*		
City	CC	lag	City	CC	lag	City	CC	lag
Tanta	0.3478	-1	Alexandria	0.5876	0	Alexandria	0.5652	-1
Rank (5)	0.5876	0	Rank (5)	0.3478	1	Rank (2)	0.9620	0
							0.6190	1
							0.2570	2
Damanhur	0.2570	-2	Damanhur	0.3591	-1		0.4737	-1
Rank (1)	0.6190	-1	Rank (4)	0.7396	0	Tanta	0.7396	0
	0.9620	0		0.4737	1	Rank (5)	0.3591	1
	0.5652	1						
El Mahala	0.5128	-1	El Mahala	0.5583	-1		0.2832	-2
Rank (4)	0.7688	0	Rank (1)	0.9398	0	El Mahala	0.6107	-1
	0.3644	1		0.5881	1	Rank (3)	0.8975	0
							0.5128	1
							0.2696	-2
El Mansoura	0.5920	-1	El Mansoura	0.3732	-1		0.6314	-1
Rank (2)	0.9466	0	Rank (3)	0.7585	0	El Mansoura	0.9947	0
	0.5588	1		0.4805	1	Rank (1)	0.6410	1
							0.5618	-1
Cairo	0.4937	-1	Cairo	0.4979	-1	Cairo	0.8869	0
Rank (3)	0.7857	0	Rank (2)	0.9313	0	Rank (4)	0.4898	1
	0.3554	1		0.5668	1			
d) El Mahala Reference*			e) El Mansoura Reference*			f) Cairo Reference*		
City	CC	lag	City	CC	lag	City	CC	lag
Alexandria	0.3644	-1	Alexandria	0.5588	-1	Alexandria	0.3554	-1
Rank (5)	0.7688	0	Rank (2)	0.9466	0	Rank (5)	0.7857	0
	0.5128	1		0.5920	1		0.4937	1
	0.2433	-2		0.4805	-1		0.2617	-2
Tanta	0.5881	-1	Tanta	0.7585	0	Tanta	0.5668	-1
Rank (2)	0.9398	0	Rank (5)	0.3732	1	Rank (2)	0.9313	0
	0.5583	1					0.4979	1
	0.5128	-1		0.6410	-1		0.4898	-1
Damanhur	0.8975	0	Damanhur	0.9947	0	Damanhur	0.8869	0
Rank (4)	0.6107	1	Rank (1)	0.6314	1	Rank (4)	0.5618	1
	0.2832	2		0.2696	2			
	0.5164	-1		0.2745	-2		0.2693	-2
El Mansoura	0.9151	0	El Mahala	0.6119	-1	El Mahala	0.5886	-1
Rank (3)	0.6119	1	Rank (3)	0.9151	0	Rank (1)	0.9799	0
	0.2745	2		0.5164	1		0.5493	1
	0.5493	-1		0.5623	-1		0.4897	-1
Cairo	0.9799	0	Cairo	0.9035	0	El Mansoura	0.9035	0
Rank (1)	0.5886	1	Rank (4)	0.4897	1	Rank (3)	0.5623	1
	0.2693	2						

Table 3. Lag correlation analysis of daily WVC values from February 2000 until August 2009 over Alexandria and the five other cities within the Delta Region (* Reference station leads for positive lags)

Favez et al., (2008) observed very high chloride levels during the autumn season over Cairo. At most 50% or even less of this is attributed to sea salt particles. However, the high concentrations of non-sea-salt chloride are thought to be of industrial origin. This observation matches well with our conclusions not only over Cairo but also is more evident with our AOD and WVC analyses over the other five cities. The higher increasing trends of the WVC observed over the coastal and near coastal cities, as compared with lower still increasing trends over the inland cities, are now better understood. Although sea salt contributes to some extent in such trends, yet the anthropogenic component appears to be dominant.

3. Hysplit air mass back-trajectories showing possible sources of pollution outbreaks

The black cloud extent is believed to be of regional nature yet it is more dominant over Cairo. AOD, WVC and cross correlation analyses have demonstrated the contribution of other cities to Cairo pollution. For better understanding the climatology, we have used the NOAA Air Resources Laboratory (ARL) HYSPLIT_4 model (<http://www.arl.noaa.gov>) (Draxler and Hess, 1998; Draxler, 1997) for computing trajectories over Cairo and hence supporting our investigation of the different sources of the pollution episodes over Cairo. Gridded meteorological data, at regular time intervals, are used in calculation of air mass trajectories. For the back-trajectories, data are obtained from existing archives.

A complete description of input data, methodology, equations involved, and sources of error for calculation of air mass trajectory is presented by (Draxler and Hess, 1997). The back trajectories of the black cloud event of October 2006, showing its source and path followed before its arrival over Cairo, are studied using a one day back-trajectory (Figure 8). In this analysis we show air mass back-trajectory at four different sets of heights above the earth's surface to locate vertical extent of the different contributions in the pollution during the black cloud season over Cairo. These heights are panel a) 1100, 1200 and 1300 m, panel b) 800, 900 and 1000 m, panel c) 500, 600 and 700 m, and panel d) 200, 300 and 400m. The reason for selecting different heights is because we know that the Delta region and Cairo are subject to an inversion layer that has been described in (El-Askary and Kafatos, 2008). They concluded that anthropogenic pollutants during September, October, (mainly), and November are found at a very low altitudes, less than 1 km from the earth surface, as revealed from cloud top pressure values (> 920 mb). A disturbed temperature gradient leading to an inversion layer prevents pollutants from rising, occupying low elevation, hence, keeping the air from naturally being ventilated. Trapping aerosols and pollutants below the temperature inversion layer, results in an increase of their concentration, hence, creating a permanent haze that develops into a health hazardous situation (El-Askary and Kafatos, 2008).

The HYSPLIT back trajectory was initialized with a starting date of October 10, 2006 over Cairo, El Mahala and Alexandria at every hour interval up to the previous day over the above mentioned heights (Figure 8). Wind rose diagrams are also presented to show the dominant wind directions during the trajectory analysis at the corresponding altitudes as close as possible. These back-trajectories show that at the layer 800-1300, (panels a & b), the origin of the air masses is from the west along the coast. Since the land does not become too

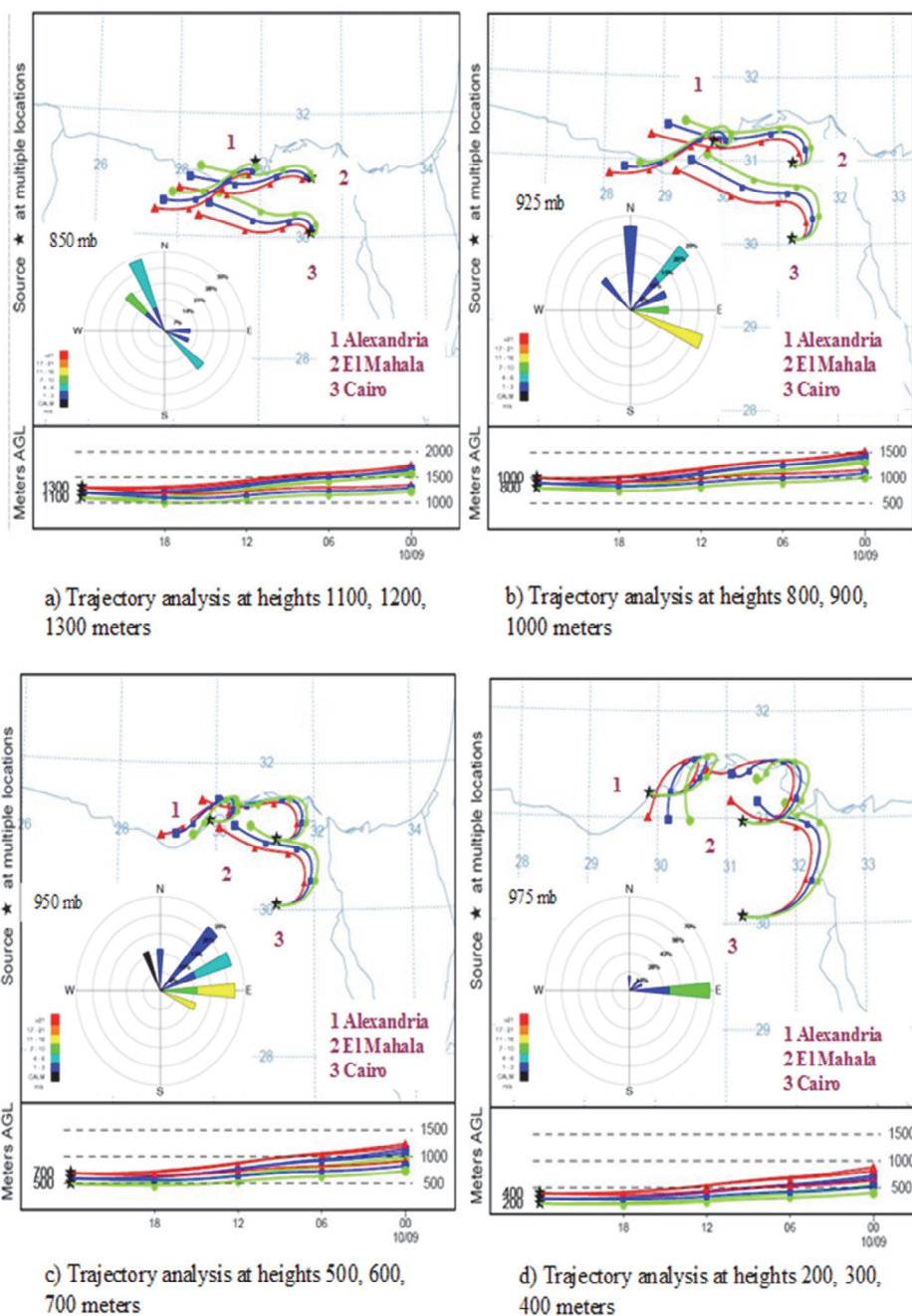


Fig. 8. OAA HYSPLIT MODEL Backward trajectories ending at 00 UTC 10 Oct 06 using CDC1 Meteorological Data over Cairo, El Mahala and Alexandria

hot during this period of the year, we assume that this layer (800-1300) is above the boundary layer especially at night hours. The layers below 800 m seem to have a daily variability that is shown as track changes. This is evident due to the sea breeze formation as well as the other non-classical mesoscale circulations, sea-land breeze type of circulations between the dry land and the wetlands at the Nile Delta, (Segal et al., 1989). This kind of atmospheric circulation with almost neutral stratification form poor dispersion and transport conditions that makes the polluted air masses remains long time over bigger areas of the cities under consideration. Therefore, it is clear that at lower altitudes, trajectories representing stationary patterns indicate the presence of polluted air masses for longer time periods over Cairo and the Delta region. This is attributed to the fact that in autumn times the local meteorology, i.e. lower wind speed and weaker convection, favour aerosols accumulation in a shallow boundary layer and thus promote Black Cloud formation. (Panel c) green curve represents the trajectory at 500 m above the surface which roughly corresponds to the middle of the boundary layer height (Favez et al., 2008). It is clear that at this level there is a great contribution from El Mahala local loadings to the pollutants observed over Cairo.

This observation matches well the CC shown in (Table 3) suggesting the great contribution of El Mahala pollutants to the black cloud outbreaks observed at Cairo.

Moreover, the red curve representing the trajectory at 700 m above the surface shows that there is a great contribution from Alexandria local loadings to the pollutants observed over Cairo. This in turn sheds light on the fact that ash burns from the rice harvest are not the only and direct reason for such pollution outbreaks. This output agrees well with the conclusion that the thermal inversion is a major player during this pollution episode as well as the varying aerosols condition over Alexandria (El-Askary, 2006; El-Askary and Kafatos, 2008; El-Askary et al., 2009). The back trajectory curves obtained in (panel d) show that a low elevated inversion is observed that keeps most of the aerosols hanging locally (Kandil et al., 2006).

The wind field over the northern part of Egypt exerts a clock wise daily rotation due to the local thermal circulations "sea breezes". Such rotation is well known in coastal areas with sea breeze formation (Kusuda and Alpert, 1986; Steyn and Kallos, 1992). It is worth noting that the sea breezes in the area penetrate deep inside Egypt because they are supported by the regional flow pattern directed from north to south "differential heating between land of Africa and Europe and the Mediterranean waters" during the warm period of the year (Astitha et al., 2008; Kallos et al., 1998, 2007). This pattern is always from north to North West, opposite the land breeze cells hence don't allow the development of land breeze circulation cell. Therefore most of the locally produced pollutants from Alexandria and other Delta cities migrate south towards Cairo and not towards the Mediterranean Sea (see Figure 1. in El-Askary and Kafatos, 2008).

4. Conclusions

This study clearly indicates the complicated pattern of aerosol production and transport over the Nile Delta and Cairo. Air masses exhibit mesoscale circulations and each city air quality is affected from other cities, mainly from North which is clearly shown over Cairo. AOD analysis clearly indicates large amounts of aerosols forming the black cloud events over various locations within the Delta region and Alexandria. We can now observe the wide spatial extent of such hazardous phenomena, not only over Cairo. Water vapor plots

show a gradual increase in the WVC in accordance with the excess aerosol loading (high AOD) during the black cloud season possibly attributed to urban pollution. Power correlation of mean AOD and WVC increases over cities with higher aerosol loadings. Cross correlations among time series variations of AOD and WVC are performed to investigate their dynamics and mutual relationships. The preformed cross correlation analysis showed a high correlation in the AOD values over the different locations, emphasizing the wide extent of the black cloud over other Delta cities and not only over Cairo. Taking Cairo as the reference location, our analysis indicates the heavy contribution of El Mahala and Tanta local emissions to the permanent haze over Cairo. This in turn highlights the importance of the transportation pattern contributing to such motion. Episodes of high aerosols loading from natural and anthropogenic nature are observed over study area in varying magnitudes concurrently during April and October of each year. Moreover, cross correlation analysis shows high dependence between aerosol patterns of Cairo with El Mahala and Tanta. Moreover, it shows a higher association of WVC with AOD for inland cities as compared with the coastal ones. The atmospheric pattern is also revealed from the backward trajectory analysis performed using the HYSPLIT model. The model runs emphasized the fact of the regional contribution from other locations to the excessive pollution episodes over Cairo. Different altitudes show different wind circulation patterns and hence different vertical levels of contribution, yet higher amounts are observed below the inversion layer. Hence, it is clear that the HYSPLIT backward trajectory analysis confirmed the origination of pollution episodes over Cairo from El Mahala and Alexandria at different pressure levels that still fall below the inversion layer reported previously. Wind rose diagrams at different altitudes show a significant agreement with the trajectory directions observed.

In conclusion, our approach used here in studying the aerosol components has enabled us to obtain useful information on relationships and dynamics of atmospheric aerosols and water vapor over Cairo and the Nile Delta region with the following summary:

1. Monthly variation of aerosol and water vapor in the atmosphere indicate a consistent and accountable variation over the whole region. It has also illustrated the origin and dynamics of the black cloud over Cairo and the Nile delta
2. Cross correlations indicate strong correspondence between aerosol conditions in Cairo and those of El Mahalla and Tanta indicating feedback of pollution.
3. Back trajectories of aerosol profile variations indicate different vertical levels of pollution contribution, consistent with the picture of the prevailing low elevation temperature inversion.
4. It is suggested that observations at higher time resolution may be capable of revealing more information on relationships among aerosol components over the Nile Delta cities.
5. It is also suggested that the same techniques could be carried out at other cities of Egypt such as Suez, Arish and Aswan.
Such analysis could have important implications for policy makers in Egypt and other highly polluted urban environments.

5. Acknowledgements

This work is funded by NSF grant 0922772 and the Science and Technology for Development Fund (STDF, <http://www.stdf.org.eg>) through the US-Egypt joint agreement. We also would like to acknowledge the support from CIRCE project (Climate Change and

Impact Research: the Mediterranean Environment) funded by the Commission of the European Union (Contract No 036961 GOCE) <http://www.circeproject.eu/>. The data used in this study were obtained from the NASA Goddard Distributed Active Archive Center (GES-DISC). We thankfully acknowledge the usage of the National Oceanic and Atmospheric Administration Air Resources Laboratory (NOAA ARL) HYSPLIT transport and dispersion model. The authors would also like to extend their appreciation to Prof. Ayman El-Dessouki, NARSS Director for his helpful comments and continuous support.

6. References

- Abu-Allaban, M.; Gertler, A.W. & Lowenthal, D.H. (2002). A preliminary apportionment of the sources of ambient PM₁₀, PM_{2.5} and VOCs in Cairo. *Atmospheric Environment*, Vol.36, No.35, (November 2002), pp. 5549- 5557, ISSN 1352-2310
- Abu-Allaban, M.; Lowenthal, D.H.; Gertler, A.W. & Labib, M. (2007). Sources of PM₁₀ and PM_{2.5} in Cairo's ambient air. *Environmental Monitoring and Assessment*, Vol.133, No.1-3, (October 2007), pp. 417-425, ISSN 1573-2959
- Abu-Allaban, M.; Lowenthal, D.H.; Gertler, A.W. & Labib, M. (2009). Sources of volatile organic compounds in Cairo's ambient air. *Environmental Monitoring and Assessment*, Vol.157, No.1-4, (October 2009), pp. 179-189, ISSN 0167-6369
- Alfaro, S.C. & AbdelWahab, M.M. (2006). Extreme variability of aerosol optical properties: The Cairo aerosol characterization experiment case study. *Proceedings of the NATO Advanced Research Workshop on Remote Sensing of the Atmosphere for Environmental Security*, pp. 285-299, ISBN: 978-1-4020-5089-3, Rabat, Morocco, 16-19 November, 2005
- Astitha, M.; Kallos, G. & Katsafados, P. (2008). Air pollution modeling in the Mediterranean Region: Analysis and forecasting of episodes. *Atmospheric Research*, Vol.89, No.4, (September 2008), pp. 358-364, ISSN 0169-8095
- Barnaba, F. & Gobbi, G.P. (2004). Aerosol seasonal variability over the Mediterranean region and relative impact of maritime, continental and Saharan dust particles over the basin from MODIS data in the year 2001. *Atmospheric Chemistry and Physics Discussions*, Vol.4, No.4, (August 2004), pp. 4285-4337, ISSN 16807367
- Draxler, R.R. & Hess, G.D. (1998). An overview of the HYSPLIT_4 modeling system for trajectories, dispersion and deposition. *Australian Meteorological Magazine*, Vol.47, No.4, (January 1998), pp. 295-308
- Draxler, R.R. & Hess, G.D. (1997). Description of the HYSPLIT_4 modeling system. *NOAA Technical Memorandum ERL ARL-224*, 24pp
- El-Askary, H.; Farouk, R.; Ichoku, C. & Kafatos, M. (2009). Transport of dust and anthropogenic aerosols across Alexandria, Egypt. *Annales Geophysicae*, Vol.27, No.7, (July 2009), pp. 2869-2879, ISSN 0992-7689
- El-Askary H. & Kafatos, M. (2008). Dust Storm and Black Cloud Influence on Aerosol Optical Properties over Cairo and the Greater Delta Region, Egypt. *International Journal of Remote Sensing*, Vol.29, No.24, (December 2008), pp. 7199 - 7211, ISSN 0143-1161
- El-Askary, H. (2006). Air pollution Impact on Aerosol Variability over mega cities using Remote Sensing Technology: Case study, Cairo, Egypt. *Egyptian Journal of Remote Sensing & Space Science*, Vol.9, (July 2006), pp. 31-40
- El-Askary, H.; Sarkar, S.; Kafatos, M. & El-Ghazawi, T. (2003). A multisensor approach to dust storm monitoring over the Nile Delta. *IEEE Transactions on Geoscience & Remote Sensing*, Vol.41, No.10, (October 2003), pp. 2386 - 2391, ISSN 0196-2892

- El-Metwally, M.; Alfaro, S.C.; Abdel Wahab, M.M. & Chatenet, B. (2008). Aerosol characteristics over urban Cairo: Seasonal variations as retrieved from Sun photometer measurements. *Journal Geophysical. Research*, Vol.113, No.D14219, (July 2008), pp. 1-13 ISSN 0148-0227
- Engel-Cox, J.A.; Holloman, C.H.; Coutant, B.W. & Hoff, R.M. (2004). Qualitative and quantitative evaluation of MODIS satellite sensor data for regional and urban scale air quality. *Atmospheric. Environment*, Vol.38, No.16, (May 2004), pp.2495-2509, ISSN 1352-2310
- Favez, O.; Cachier, H.; Sciare, J.; Alfaro, S.C.; El-Araby, T.M.; Harhash, M.A. & AbdelWahab, M.M. (2008). Seasonality of major aerosol species and their transformations in Cairo megacity. *Atmospheric. Environment*, Vol.42, No.7, (March 2008), pp. 1503-1516, ISSN 1352-2310
- Gautam, R.; Hsu, N.C.; Kafatos, M. & Tsay, S.-C. (2007). Influences of winter haze on fog/low cloud over the Indo-Gangetic plains. *Journal Geophysical Research*, Vol.112, No.D05207, (March 2007), pp. 1-11, ISSN 0148-0227
- Hossny, E.; Mokhtar, G.; El-Awady, M.; Ali, I.; Morsy, M. & Dawood, A. (2001). Environmental exposure of the pediatric age groups in Cairo city and its suburbs to cadmium pollution. *The Science of the Total Environment*, Vol.273, No.1-3, (June 2001), pp. 135-146, ISSN 0048-9697
- Houghton, J.T.; Ding, Y.; Griggs, D.J.; Noguer, M.; Van der Linden, P.J. & Xiaosu, D. (2001). Climate Change 2001: The Scientific Basis, Contribution of Working Group 1 to the Third Assessment Report of the Intergovernmental Panel on Climate Change. *Cambridge University Press*, (Ed.) 1-994, ISBN: 9780521014953, UK
- Hsu, N.C.; Herman, J.R. & Tsay, S.-C. (2003). Radiative impacts from biomass burning in the presence of clouds during boreal spring in Southeast Asia. *Geophysical Research Letters*, Vol.30, No.5, (March 2003), pp. 28.1-28.4, ISSN 0094-8276
- Jin, M.; Shepherd, J.M. & King, M.D. (2005). Urban aerosols and their variations with clouds and rainfall: A case study for New York and Houston. *Journal Geophysical Research*, Vol.110, No.D10S20, (April 2005), pp1-12, ISSN 0148-0227
- Kallos, G.; Astitha, M.; Katsafados, P. & Spyrou, C. (2007). Long-Range Transport of Anthropogenically and Naturally Produced Particulate Matter in the Mediterranean and North Atlantic: Current State of Knowledge. *Journal of Applied Meteorology and Climate*, Vol.46, No.8, (August 2007), pp. 1230-1251, ISSN 1558-8424
- Kallos, G.; Kotroni, V.; Lagouvardos, K. & Papadopoulos, A. (1998). On the Long-Range Transport of Air Pollutants from Europe to Africa. *Geophysical Research Letters*, Vol.25, No.5, (March 1998), pp. 619-622, ISSN 00948276
- Kanakidou, M.; Mihalopoulos, N.; Kindap, T.; Im, U.; Vrekoussis, M.; Gerasopoulos, E.; Dermizaki, E.; Unal, A.; Kocak, M.; Markakis, K.; Melas, D.; Kouvarakis, G.; Youssef, A.F.; Richter, A.; Hatzianastassiou, N.; Hilboll, A.; Ebojje, F.; Wittrock, F.; Savigny, C.V.; Burrows, J.P.; Ladstaetter-Weissenmayer, A.; Moubasher, H. (2011). Megacities as hot spots of air pollution in the East Mediterranean. *Atmospheric Environment*, Vol.45, No.6, (February 2011), pp. 1223-1235, ISSN 1352-2310
- Kandil, H.A.; Kader, M.A.; Moaty, A.; El-Hadidi, B. & Sherif, A.O. (2006). Simulation of atmospheric temperature inversions over greater Cairo using the MM5 meso-scale atmospheric model. *Egyptian Journal of Remote Sensing & Space Science*, Vol.9, (July 2006), pp. 15-30

- Kaufman, Y.J.; Tanrè, D. & Boucher, O.A. (2002). Satellite view of aerosols in the climate system. *Nature*, Vol.419, No.6903 (September 2002), pp. 215–223, ISSN 0028-0836
- King, M.D.; Kaufman, Y.J.; Tanrè, D. & Nakajima, T. (1999). Remote sensing of tropospheric aerosols from space: Past, present, and future. *Bulletin of American Meteorological Society*, Vol.80, No.11, (November 1999), pp. 2229–2260, ISSN 0003-0007
- Kusuda, M. & Alpert, P. (1983). Anticlockwise rotation of the wind hodograph. Part I: Theoretical study. *Journal of Atmospheric Sciences*, Vol.40, No.2, (February 1983), pp. 487-499
- Luria, M.; Peleg, M.; Sharf, G.; Tov-Alper, D.; Spitz, N.; Ben Ami, Y.; Gawii, Z.; Lifschitz, B.; Yitzchaki, A. & Seter, I. (1996). Atmospheric sulfur over the east Mediterranean region. *Journal Geophysical Research*, Vol.101, No.D20, (May 1996), pp.25917-25930, ISSN: 0148-0227
- Mahmoud, K.F.; Alfaro, S.C.; Favez, O. & AbdelWahab, M.M. (2008). Origin of black carbon concentration peaks in Cairo (Egypt). *Atmospheric Research*, Vol.89, No.1-2, (July 2008), pp. 161-169, ISSN: 0169-8095
- Marey, H.S.; Gille, J.C.; El-Askary, H.M.; Shalaby, E.A. & El-Raey, M.E. (2010). Study of the formation of the “black cloud” and its dynamics over Cairo, Egypt, using MODIS and MISR sensors. *Journal Geophysical Research*, Vol.115, No.D21206, (November 2010), pp. 1-10, ISSN 01480227
- Millan, M.M.; Salvador, R.; Mantilla, E. & Kallos, G. (1997). Photo oxidant dynamics in the Mediterranean basin in summer: results from European research projects. *Journal Geophysical Research*, Vol.102, No.7, (April 1997), pp. 8811-8823, ISSN 01480227
- Molina, M.J. & Molina, L.T. (2004). Critical Review: Megacities and atmospheric pollution. *Journal of Air and Waste Management Association*, Vol.54, No.6, (June 2004), pp. 644-680, ISSN 1096-2247
- Pace, G.; Di Sarra, A.; Meloni, D.; Piacentino, S. & Chamard, P. (2006). Aerosol optical properties at Lambduca (Central Mediterranean). 1. Influence of transport and identification of different aerosol types. *Atmospheric Chemistry and Physics*, Vol.6, No.3, (March 2006), pp. 697–713, ISSN 16807316
- Prasad A. K.; El-Askary, H.M. & Kafatos, M. (2010). Implications of high altitude desert dust transport from Western Sahara to Nile Delta during biomass burning season. *Environmental Pollution*, Vol.158, No.11, (November 2010), pp. 3385-3391, ISSN 0269-7491
- Prasad, A.K. & Singh, R.P. (2007) Changes in aerosol parameters during major dust storm events (2001–2005) over the Indo-Gangetic Plains using AERONET and MODIS data. *Journal Geophysical Research*, Vol.112, No.D09208, (May 2007), pp. 1-18, ISSN 0148-0227
- Prasad, A.K.; Singh, R.P. & Kafatos, M. (2006). Influence of coal based thermal power plants on aerosol optical properties in the Indo-Gangetic basin. *Geophysical Research Letters*, Vol. 33, No.L05805, (March 2006), pp. 1-4, ISSN 0094-8276
- Rosenfeld, D.; Lohmann, U.; Raga, G.B.; O'Dowd, C.D.; Kulmala, M.; Fuzzi, S.; Reissell, A. & Andreae, M.O. (2008). Flood or Drought: How Do Aerosols Affect Precipitation?. *Science*, Vol.321, No.5894, (September 2008), pp. 1309 - 1313, ISSN 0036-8075
- Rosenfeld, D. (2000). Suppression of rain and snow by urban and industrial air pollution. *Science*, Vol.287, No.5459, (March 2000), pp. 1793-1796, ISSN 0036-8075

- Segal, M.; Garratt, J.R.; Kallos, G. & Pielke, R.A. (1989). The Impact of Wet Soil and Canopy Temperatures on Daytime Boundary - Layer Growth. *Journal of Atmospheric Sciences*, Vol.46, No.24, (December 1989), pp.3673-3684, ISSN 0022-4928
- Steyn, D. & Kallos, G. (1992). A study of the dynamics of hodograph rotation in the sea breezes of Attica, Greece. *Boundary-Layer Meteorology*, Vol.58, No.3, (February 1992), pp. 215-228, ISSN 0006-8314
- Tegen, I.A.; Lacis, A.A. & Fung, I. (1996). The influence on climate forcing of mineral aerosols from distributed soils. *Nature*, Vol.380, (April 1996), pp. 419-422
- Xia, X.; Chen, H. & Zhang, W. (2007). Analysis of the dependence of column-integrated aerosol properties on long-range transport of air masses in Beijing. *Atmospheric Environment*, Vol.41, No.36, (November 2007), pp. 7739-7750, ISSN 1352-2310
- Zakey, A.S.; Abdelwahab, M.M. & Makar, P.A. (April 2004). Atmospheric turbidity over Egypt. *Atmospheric Environment*, Vol.38, No.11, (2004), pp. 1579-1591, ISSN 1352-2310
- Zakey, A.S.; Abdel-Wahab, M.M.; Pettersson, J.B.C.; Gatari, M.J. & Hallquist, M. (2008). Seasonal and spatial variation of atmospheric particulate matter in a developing megacity, the Greater Cairo, Egypt. *Atmosfera* Vol.21, No.2, (January 2008), pp. 171-189, ISSN 0187-6236

Spatial Variation, Sources and Emission Rates of Volatile Organic Compounds Over the Northeastern U.S.

Rachel S. Russo et al.,*
*Climate Change Research Center, Institute for the Study of Earth,
Oceans, and Space University of New Hampshire,
Durham, NH 03824
United States*

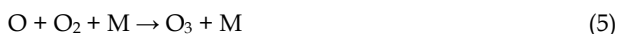
1. Introduction

New England is an ideal region for studying air quality because of its unique geographic location, diverse landscapes and ecosystems, and varying climatic conditions. New England is often referred to as the “tailpipe” of the United States because it is directly downwind of major urban and industrial pollution sources located throughout the Midwest, Ohio Valley, and Washington D.C.-New York City metropolitan corridor (Fig. 1a). Sources in these urban areas emit pollutants into air masses which are then transported to the northeastern U.S. by the prevailing circulation patterns over the U.S. (i.e., the jet stream). Consequently, the air quality of New England reflects a combination of local, regional, and distant anthropogenic and natural trace gas and aerosol sources.

In order to study the chemical and physical mechanisms influencing the atmospheric composition over New England, the University of New Hampshire’s (UNH) AIRMAP program has been conducting continuous measurements of important trace gas (e.g., ozone (O_3), carbon monoxide (CO), nitric oxide (NO), total reactive nitrogen (NO_y), sulfur dioxide (SO_2), carbon dioxide (CO_2), mercury) and meteorological parameters throughout the region for the past decade. Continuous measurements of volatile organic compounds (VOCs) have also been made at the UNH Atmospheric Observing Station at Thompson Farm (TF) (43.11 °N, 70.95 °W, elevation 24 m) in Durham, New Hampshire (NH) since 2002 (Fig. 1b). VOCs are ubiquitous components of the atmosphere, and this broad category consists of nonmethane hydrocarbons (NMHCs), halocarbons, oxygenated VOCs (OVOCs), organic nitrates, and reduced sulfur compounds. VOCs enter the atmosphere from numerous primary anthropogenic (i.e., vehicles, natural gas, industrial solvents, fossil fuel combustion) and natural (i.e., vegetation, ocean) sources, and may also serve as precursors to secondary pollutant (i.e., O_3 , OVOCs, secondary organic aerosol (SOA)) production (e.g., Fehsenfeld et al., 1992; Singh and Zimmerman, 1992). The oxidation of NMHCs (RH) in the presence of

* Marguerite L. White, Yong Zhou, Karl B. Haase, Jesse L. Ambrose, Leanna Conway, Elizabeth Mentis, Robert Talbot, and Barkley C. Sive

sufficient levels of nitrogen oxides ($\text{NO}_x = \text{NO} + \text{NO}_2$; $\text{NO}_2 =$ nitrogen dioxide) is the major production mechanism for O_3 in the lower troposphere (Equations 1-5) (e.g., Carter, 1994). Ozone and particulate matter are the major components of photochemical smog and thus impact visibility, potentially damage vegetation and crops, and serve as respiratory lung irritants (U.S. EPA, 2010). A minor branch in the NMHC- NO_x - O_3 reaction mechanism produces alkyl nitrates (RONO_2) (Equations 1-6) (e.g., Roberts, 1990; Flocke et al., 1998).



In addition, VOCs have a wide range of atmospheric lifetimes (seconds to years), and are removed from the atmosphere by oxidation (OH, O_3 , nitrate, halogens), photolysis, and/or deposition. Furthermore, several NMHCs (i.e., benzene, toluene, C_8 aromatics), OVOCs (i.e., formaldehyde, acetaldehyde), and halocarbons (i.e., tetrachloroethene) are classified as hazardous air pollutants by the U.S. Environmental Protection Agency because they are potential carcinogens and/or harmful to human health (U.S. EPA, 1998, 2008, 2010). Therefore, a complete, accurate, and quantitative description of the atmospheric VOC distribution is necessary for characterizing the air quality in a particular region, studying the oxidation capacity of the atmosphere, and evaluating air quality and climate change models. Prior research conducted at TF has found that the air quality of this semi-rural area of New England is influenced by a complex mixture of anthropogenic VOCs from local, regional and more distant source regions, as well as from substantial biogenic sources (forests, coastal seaweed/algae) (e.g., Russo et al., 2010a, 2010b; Sive et al., 2007; Talbot et al., 2005; White et al., 2008, 2009; Zhou et al., 2005, 2008). Unique spatial and diurnal VOC trends are exemplified by a study conducted at six different locations throughout the New Hampshire seacoast region in August 2003. During this one day study, several anthropogenic NMHCs exhibited large nighttime mixing ratio enhancements (White et al., 2008), the marine derived halocarbons exhibited a distinct spatial gradient from coastal to inland sites (Zhou et al., 2005), and the alkyl nitrates were uniformly distributed throughout the study area (Russo et al., 2010a). The distinct VOC trends observed in the continuous measurements at TF and from the August 2003 study led to a concerted effort to determine the sources and processes contributing to the VOC distribution over New England. We are aware of only one other detailed regional VOC measurement campaign conducted in the southwestern U. S. focused on examining the spatial variation of VOC mixing ratios and sources (Katzenstein et al., 2003). Similar types of studies are clearly needed. The objectives of this chapter are to discuss the sources and spatial and temporal trends of VOCs during four spatial surveys conducted throughout New England during 2006 and 2007 and to put the results in context with the overall atmospheric distribution of VOCs observed at the Thompson Farm field site in Durham, NH.

2. Methods

Spatial surveys were conducted on June 21, 2006, September 21-22, 2006, January 10-11, 2007, and May 22-23, 2007. Ambient air samples were collected in 2 liter canisters along four ~250-300 mile (~400-480 km) loops radiating out from UNH in Durham, NH and included portions of western Maine (ME), eastern Vermont (VT), northern and eastern Massachusetts (MA), extreme northeastern Connecticut (CT), and northern Rhode Island (RI) (Fig. 1b). During each survey, four pairs of researchers collected samples every 10-15 miles (16-24 km) for a total of 24 samples on each route. The time of sample collection and the geospatial coordinates were recorded at each sampling location using a global positioning sensor (GPS). The sampling sites were generally open areas (i.e., fields, public parks) upwind of major sources and were chosen during the first sampling trip (June 21, 2006) which was conducted during the daytime (~09:00-19:00 EDT). The three subsequent surveys were conducted at night (~19:00-05:00 EDT) when winds were predicted to be low (<5 m s⁻¹) to minimize the influence of photochemistry and to capture local nighttime emissions. The four sampling routes covered a wide geographic area that spanned considerable variation in altitude, land use, and population density. Moreover, the four surveys provide information on the seasonal variation of VOC sources.

In order to characterize the diurnal variation of VOCs throughout the region, hourly ambient canister samples were collected over 24 hour periods on September 8-9, 2006 in Waterford, ME, September 12-13, 2006 in Hinesburg, VT, September 27-28, 2006 at Pack Monadnock, NH and at six locations on January 13-14, 2007 and May 29-30, 2007 (Fig. 1b). These diurnal sampling sites were selected to cover a range of local housing and population densities and included public parks and private property where permission was granted from local authorities and landowners.

Prior to sampling, the 2-liter electropolished stainless steel canisters (University of California, Irvine, CA) were prepared by flushing with UHP helium that had passed through an activated charcoal/molecular sieve (13X) trap immersed in liquid nitrogen. The canisters were then evacuated to 10⁻² torr. After each sampling campaign, the canisters were analyzed at UNH on a three gas chromatograph (GC) system equipped with two flame ionization detectors (FID), two electron capture detectors (ECD), and a mass spectrometer (MS) for C₂-C₁₀ NMHCs, C₁-C₂ halocarbons, C₁-C₅ alkyl nitrates, OVOCs, and select reduced sulfur compounds (Sive et al., 2005; Zhou et al., 2005, 2008). The compounds discussed in this work are C₂-C₇ alkanes, C₂-C₃ alkenes, isoprene, ethyne, C₆-C₈ aromatics, monoterpenes (α -pinene, β -pinene), trichloroethene (C₂HCl₃), tetrachloroethene (C₂Cl₄), methyl iodide (CH₃I), dibromomethane (CH₂Br₂), bromoform (CHBr₃), methyl nitrate (MeONO₂), ethyl nitrate (EtONO₂), 2-propyl nitrate (2-PrONO₂), and 2-butyl nitrate (2-BuONO₂). A 1500 cc aliquot from one of two working standards was assayed every ninth analysis. The measurement precision for the whole air standards (i.e., relative standard deviation (RSD) = (standard deviation of peak areas/average of peak areas) was <1-4% for the C₂-C₁₀ NMHCs and 5-10% for the halocarbons and alkyl nitrates.

Hourly measurements from the automated in situ GC system at TF (Sive et al., 2005; Zhou et al., 2005, 2008) corresponding to the same time periods as the regional sampling surveys are also used to describe the diurnal variation of NMHCs and to calculate emission rates. Details of the custom designed four channel (2 FIDs, 2 ECDs) GC system, sample preconcentrator, sample trapping and splitting, calibrations, and instrument control are given in Sive et al. (2005) and Russo et al. (2010b). A 1500 cc aliquot from one of two

working standards was assayed every tenth analysis. The precision (i.e., RSD) for each of the hydrocarbons discussed in this work ranged from 3-10%. Additionally, measurements of O_3 , CO_2 , wind speed, and wind direction (e.g., Mao and Talbot, 2004a, 2004b; Talbot et al., 2005) at TF are included to further characterize the air mass composition and atmospheric dynamics during each survey.

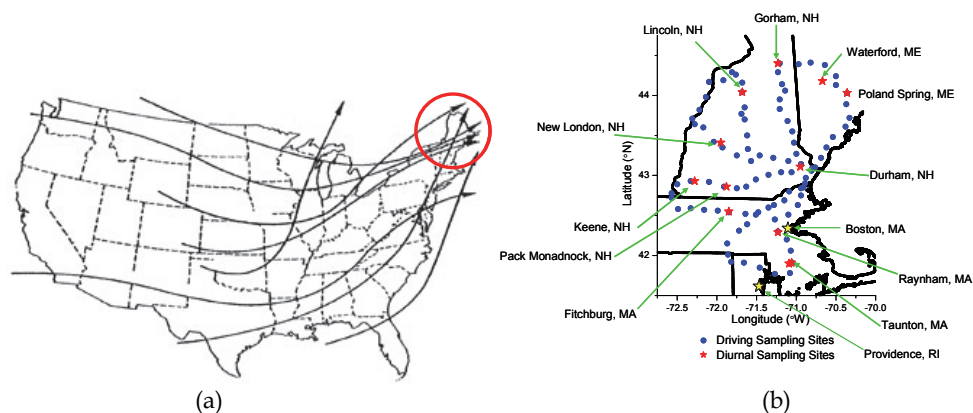


Fig. 1. (a) Location of New England (enclosed in circle) in the United States. (b) Sampling sites during the four regional spatial surveys (blue dots) and diurnal studies (red stars) conducted throughout Maine, New Hampshire, Vermont, Massachusetts, northeastern Connecticut, and northern Rhode Island.

3. Atmospheric distribution of VOCs throughout New England

3.1 Seasonal variation and general distributions

The general seasonal variation of C_2 - C_8 NMHCs, C_2HCl_3 , C_2Cl_4 , and C_1 - C_5 alkyl nitrates at TF during 2004-2008 is presented in detail in Russo et al. (2010a,b), but a brief discussion is given here. The dominant removal mechanism of NMHCs, C_2HCl_3 , and C_2Cl_4 from the atmosphere is reaction with the hydroxyl radical (OH) which is produced following the photolysis of O_3 . Hence, atmospheric OH concentrations in the Northern Hemisphere are highest during the summer and are lowest during winter (e.g., Logan et al., 1981; Spivakovsky et al., 2000). Furthermore, the rate of reaction between NMHCs and OH generally increases with increasing carbon number (e.g., Atkinson et al., 2006). Overall, the highest monthly mean C_2 - C_8 NMHC, alkyl nitrate, and halocarbon mixing ratios were observed in winter (December, January, February) and decreased throughout the spring at TF (Russo et al., 2010b). The lowest mixing ratios were observed during middle to late spring through the summer corresponding to the time period when NMHC removal processes are fastest. Ethane is the longest lived NMHC in the atmosphere and was generally the most abundant. More specifically, ethane peaked in January-February (~2400 pptv; pptv = parts per trillion by volume) and was minimum in late summer (~900 pptv, August-September). The C_3 - C_4 alkane mixing ratios decreased from December-January peak levels (propane ~1500 pptv, i-butane ~270 pptv, n-butane ~500 pptv) to minimum mixing ratios in May-September (propane ~400-600 pptv, i-butane ~50-75 pptv, n-butane ~100-120

pptv). The minimum monthly mean mixing ratios of the short-lived VOCs (C_5 - C_6 alkanes, propene, toluene and C_2HCl_3) occurred in April-May and were factors of 2-4 lower than in winter. Their monthly mean mixing ratios increased in early summer and remained at similar levels through late summer (September). Benzene, ethyne, and ethene exhibited minimum monthly mean mixing ratios from late spring through summer. The monthly mean C_2Cl_4 mixing ratios were fairly uniform all year (~ 10 -15 pptv). The total alkyl nitrate ($\Sigma RONO_2$ = sum of C_1 - C_5 alkyl nitrates) mixing ratio was highest in late winter (February-March) and lowest in late summer. Methyl nitrate was relatively uniform (monthly mean ~ 3 pptv) all year. Ethyl nitrate was slightly lower in summer (mean ~ 2.2 pptv) than in winter (~ 2.7 pptv). 2-propyl and 2-butyl nitrate were the most abundant alkyl nitrates and exhibited the largest seasonal variation (monthly mean mixing ratios were factors of 1.5-3 higher in winter) (Russo et al., 2010a).

The spatial distributions of NMHC, halocarbon, and alkyl nitrate mixing ratios during the four driving sampling campaigns are shown in Fig. 2, and the statistics for each survey are given in Table 1. Most hydrocarbon mixing ratios were lower during June 2006 than during the overnight September 2006, January 2007, and May 2007 sampling campaigns reflecting more active photochemistry during the summer and the daytime (Table 1). The minimum NMHC, halocarbon, $MeONO_2$, and $2-PrONO_2$ mixing ratios observed during each survey were highest in January and follow the general seasonal trend in background mixing ratios discussed in the preceding paragraph. In addition, the mean and median mixing ratios of *i*-butane, *n*-butane, ethyne, and benzene were higher during January than during the other three surveys (Table 1, Fig. 2). However, the distribution of VOCs throughout the atmosphere over New England during the four intensive spatial surveys exemplifies the influence of short-term pollution events and local emissions on the general VOC pattern.

Ethane was the most abundant compound measured throughout the region in June (mean \pm standard deviation $\sim 990 \pm 150$ pptv), January (mean $\sim 1970 \pm 170$ pptv), and May ($\sim 1440 \pm 3650$ pptv) (Fig. 2a, Table 1). Daytime propane levels during June were lower (390 ± 370 pptv), with a few local hot spots above 1000 pptv. The highest mean and median mixing ratios of propane (mean 2150 ± 2600 pptv), ethene (mean 580 ± 480 pptv), propene (mean 175 ± 150 pptv), and ethylbenzene (mean 60 ± 50 pptv) were observed during the September 2006 survey (Table 1). During September 2006, propane was the most abundant NMHC followed by ethane (mean 1300 ± 1300 pptv). The major source of propane in New England is liquefied petroleum gas (LPG), while ethene and propene are minor components of LPG (Blake and Rowland, 1995; Chen et al., 2001; Jobson et al., 2004). These results suggest that LPG emissions had a significant influence on New England air quality on the night of September 21-22, 2006. Despite the high mean and median levels in September, the maximum propane, ethene, propene, and ethylbenzene mixing ratios, as well as ethane, ethyne, *n*-heptane, benzene, toluene, *m*+*p*-xylene, and *o*-xylene, were observed during May.

Furthermore, the C_5 - C_7 alkanes exhibited comparable mean and median mixing ratios during September and May (mean *i*-pentane ~ 260 pptv, *n*-pentane ~ 120 pptv, *n*-hexane ~ 60 pptv, *n*-heptane ~ 40 pptv) (Table 1). Their mean and medians were slightly higher in May likely reflecting strong evaporative emissions. Moreover, the average toluene and xylene mixing ratios were highest in May. Overall, these results indicate that local emissions had a strong influence on alkane, alkene, and aromatic mixing ratios throughout New England

during the nighttime September and May sampling surveys. Interestingly, the highest maximum i-butane, n-butane, i-pentane, n-pentane, and n-hexane mixing ratios were observed during the daytime June trip at a site off of a major traffic route in Northern, MA. This likely reflects strong local fuel evaporation emissions.

		June 21, 2006	Sept. 21-22, 2006	Jan. 10-11, 2007	May 22-23, 2007
Ethane	Mean (SD)	989 (149)	1313 (1299)	1966 (113)	2384 (3657)
	Median (Range)	934 (889-1758)	933 (418-11545)	1951 (1739-2554)	1443 (1271-28634)
Propane	Mean (SD)	388 (367)	2145 (2619)	1075 (381)	1991 (3126)
	Median (Range)	266 (116-2690)	1196 (198-13782)	1025 (800-4486)	1134 (268-27537)
i-Butane	Mean (SD)	81 (332)	167 (242)	189 (27)	190 (383)
	Median (Range)	33 (12-3200)	99 (22-1664)	185 (144-371)	98 (23-2643)
n-Butane	Mean (SD)	155 (735)	212 (374)	334 (33)	267 (489)
	Median (Range)	49 (19-7048)	110 (35-3456)	332 (268-420)	171 (59-4618)
i-Pentane	Mean (SD)	185 (635)	257 (305)	133 (19)	264 (415)
	Median (Range)	66 (18-5867)	159 (23-2404)	127 (106-203)	168 (42-3861)
n-Pentane	Mean (SD)	79 (243)	120 (133)	81 (10)	126 (174)
	Median (Range)	33 (12-2306)	73 (7-1028)	80 (58-114)	80 (19-1194)
n-Hexane	Mean (SD)	24 (58)	64 (74)	26 (5)	62 (69)
	Median (Range)	11 (3-543)	39 (5-483)	25 (15-43)	43 (6-537)
n-Heptane	Mean (SD)	16 (14)	37 (38)	16 (4)	40 (46)
	Median (Range)	11 (3-72)	22 (4-215)	16 (7-30)	28 (8-377)
Ethyne	Mean (SD)	181 (113)	441 (529)	532 (123)	432 (432)
	Median (Range)	138 (101-805)	287 (103-3825)	503 (438-1510)	341 (192-4184)
Ethene	Mean (SD)	166 (144)	579 (488)	277 (132)	469 (770)
	Median (Range)	119 (42-819)	423 (42-2264)	241 (135-975)	299 (81-7035)
Propene	Mean (SD)	52 (42)	176 (150)	49 (26)	128 (235)
	Median (Range)	36 (13-218)	130 (13-691)	43 (20-201)	82 (28-2022)
Benzene	Mean (SD)	37 (28)	99 (90)	116 (19)	103 (230)
	Median (Range)	26 (4-129)	71 (11-620)	110 (96-230)	67 (29-2252)
Toluene	Mean (SD)	112 (121)	262 (256)	77 (26)	300 (452)
	Median (Range)	67 (16-746)	153 (21-1142)	69 (47-200)	191 (43-3872)

		June 21, 2006	Sept. 21-22, 2006	Jan. 10-11, 2007	May 22-23, 2007
Ethylbenzene	Mean (SD)	16 (22)	57 (47)	11 (4)	46 (82)
	Median (Range)	9 (3-159)	43 (3-262)	10 (5-27)	26 (8-561)
m+p-Xylene	Mean (SD)	47 (78)	121 (112)	25 (14)	156 (298)
	Median (Range)	22 (6-580)	79 (9-541)	22 (7-86)	90 (17-2190)
o-Xylene	Mean (SD)	17 (28)	45 (46)	12 (6)	63 (127)
	Median (Range)	9 (2-209)	29 (4-230)	10 (5-25)	31 (6-827)
Isoprene	Mean (SD)	791 (585)	68 (55)	-	33 (30)
	Median (Range)	623 (127-3468)	42 (5-229)	-	27 (5-200)
α -Pinene	Mean (SD)	116 (83)	344 (362)	16 (6)	377 (619)
	Median (Range)	91 (20-424)	263 (24-2598)	15 (6-32)	241 (21-5641)
β -Pinene	Mean (SD)	50 (54)	166 (157)	6 (2)	222 (317)
	Median (Range)	34 (2-300)	118 (18-921)	6 (5-8)	151 (4-2565)
C ₂ Cl ₄	Mean (SD)	11 (13)	18 (26)	8 (2)	17 (11)
	Median (Range)	7 (5-115)	9 (2-205)	8 (6-22)	14 (5-65)
C ₂ HCl ₃	Mean (SD)	2.3 (2.7)	4.5 (7.4)	2.5 (0.7)	7.4 (18)
	Median (Range)	1.3 (0.2-21)	1.2 (0.2-35)	2.3 (1.2-5.2)	1.9 (0.2-125)
CH ₃ I	Mean (SD)	1.5 (1.6)	0.93 (0.72)	0.97 (0.28)	0.94 (0.65)
	Median (Range)	0.76 (0.4-8.5)	0.76 (0.3-5.9)	0.91 (0.7-2.8)	0.71 (0.2-3.6)
CH ₂ Br ₂	Mean (SD)	0.92 (0.2)	0.98 (0.1)	1.1 (0.1)	0.99 (0.3)
	Median (Range)	0.87 (0.7-1.7)	0.99 (0.6-1.5)	1.1 (0.9-1.7)	0.93 (0.7-2.6)
CHBr ₃	Mean (SD)	1.8 (2.3)	3.4 (1.4)	3.7 (1.3)	2.7 (2.2)
	Median (Range)	0.95 (0.5-13.9)	3.0 (0.7-9.9)	3.5 (2.0-8.4)	2.1 (0.5-14.5)
MeONO ₂	Mean (SD)	2.4 (0.4)	2.1 (0.4)	3.3 (0.2)	2.7 (0.5)
	Median (Range)	2.3 (2.0-3.5)	2.1 (1.2-3.3)	3.3 (2.9-3.6)	2.6 (1.8-4.2)
EtONO ₂	Mean (SD)	1.9 (0.5)	1.4 (0.3)	2.7 (0.1)	4.3 (1.2)
	Median (Range)	1.6 (1.4-3.5)	1.4 (0.6-2.3)	2.7 (2.4-2.9)	3.8 (2.6-7.3)
2-PrONO ₂	Mean (SD)	3.1 (1.5)	2.6 (1.5)	5.8 (0.3)	5.5 (2.2)
	Median (Range)	2.4 (1.7-7.9)	2.4 (0.9-3.4)	5.8 (4.2-6.5)	4.3 (3.2-11.3)
2-BuONO ₂	Mean (SD)	2.1 (1.5)	2.2 (0.6)	7.8 (1.2)	5.1 (2.7)
	Median (Range)	1.4 (0.8-8.5)	2.0 (0.7-3.3)	8.1 (1.9-9.8)	4.0 (2.5-13.6)

Table 1. VOC statistics during the four regional surveys. Mixing ratios are in parts per trillion by volume (pptv). SD is the standard deviation.

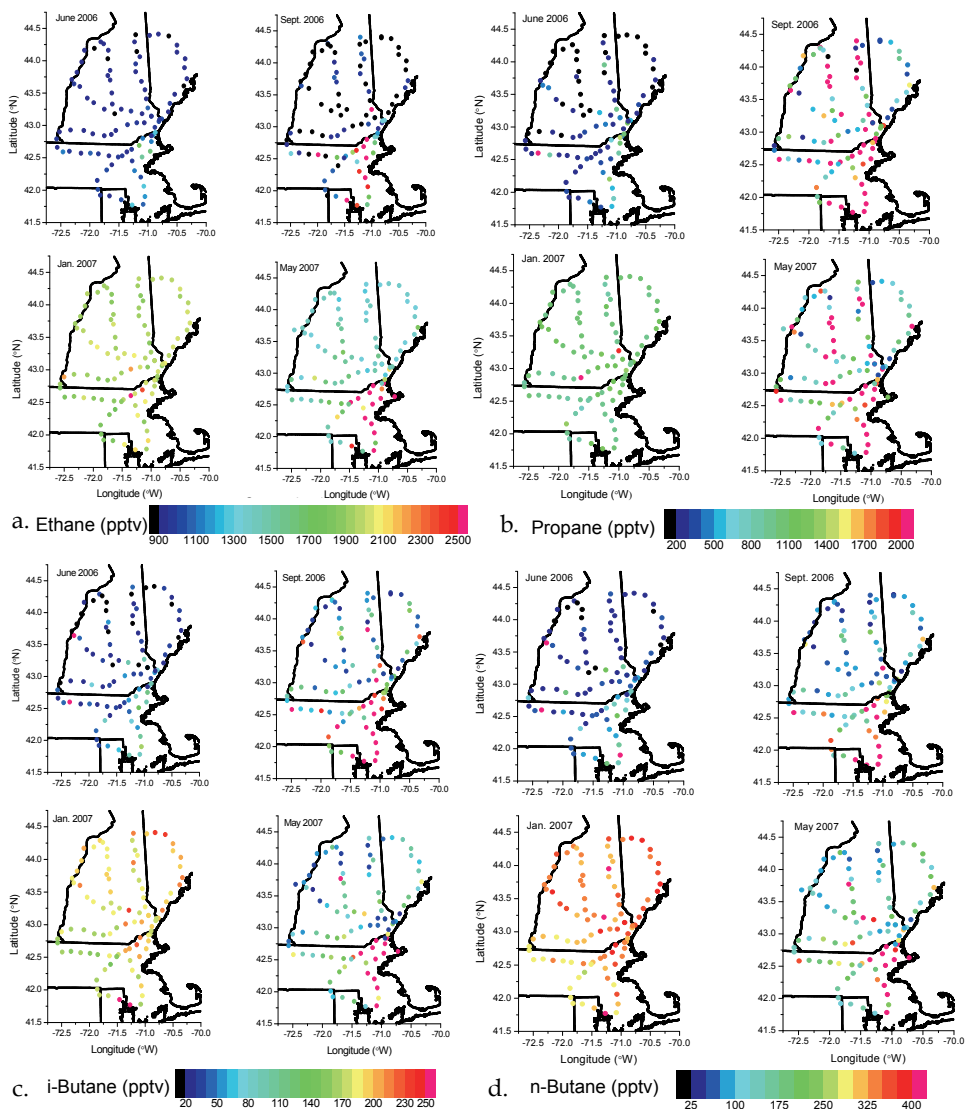


Fig. 2. Spatial variation of VOC mixing ratios (pptv) during the four regional sampling surveys conducted throughout New England. The four panels for each compound represent the four surveys: upper left panel-June 21, 2006; upper right panel-September 21-22, 2006; bottom left panel-January 10-11, 2007; bottom right panel-May 22-23, 2007. (a) ethane, (b) propane, (c) i-butane, (d) n-butane, (e) i-pentane, (f) n-pentane, (g) ethene, (h) propene, (i) ethyne, (j) benzene, (k) toluene, (l) α -pinene, (m) isoprene (not observed during January), (n) CH_3I , (o) C_2Cl_4 , (p) C_2HCl_3 , (q) CH_2Br_2 , (r) CHBr_3 , (s) MeONO_2 , (t) EtONO_2 , (u) 2-PrONO_2 , (v) 2-BuONO_2 .

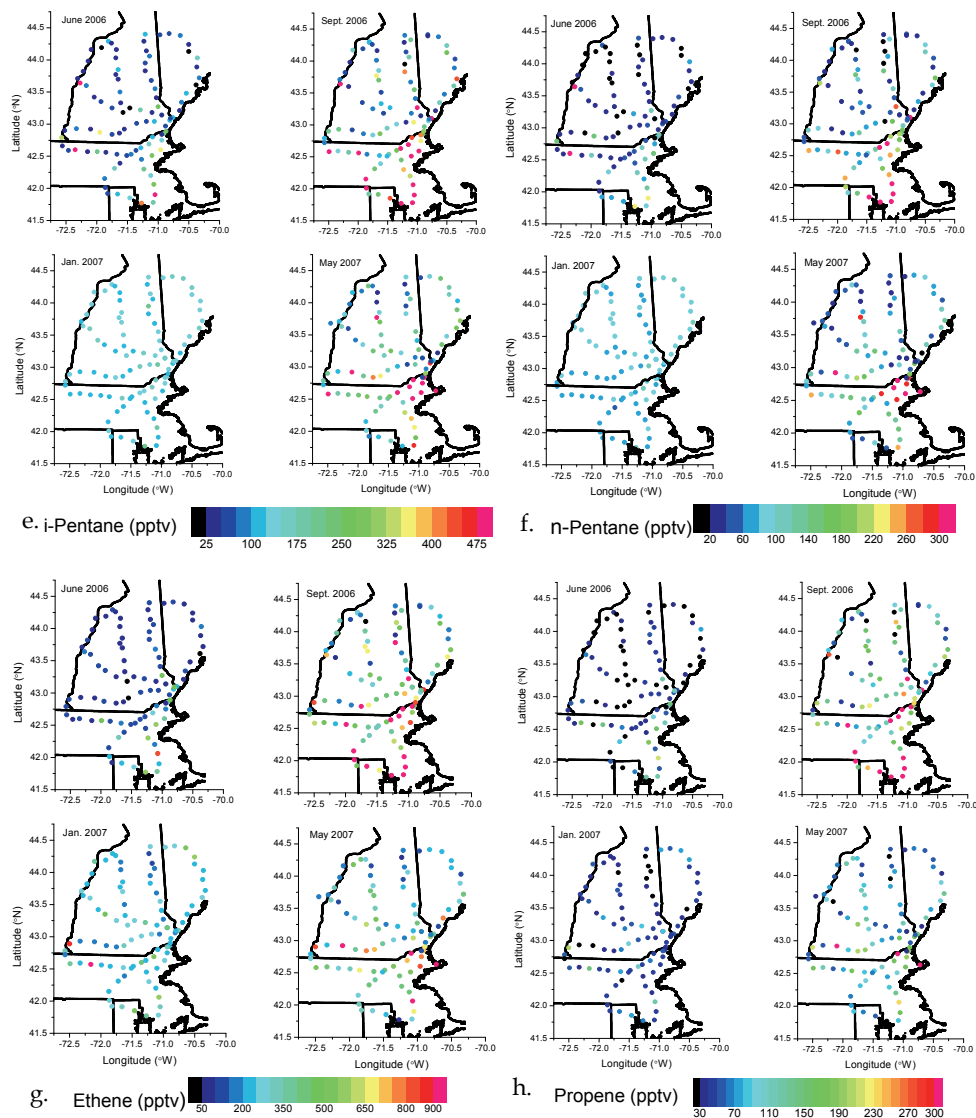


Fig. 2 continued

The biogenic NMHCs included in this analysis are isoprene and the monoterpenes, α -pinene and β -pinene. Isoprene and monoterpene emissions are dependent on both light and temperature (Guenther et al., 1995; Fehsenfeld et al., 1992). Isoprene is primarily emitted from deciduous vegetation and is detected in significant amounts when leaves are present (Guenther et al., 1995), specifically June-September at the TF site (Russo et al., 2010b). Thus, isoprene mixing ratios were highest during summer (Table 1). The mean isoprene mixing ratio was $\sim 800 \pm 585$ pptv, and isoprene was the second most abundant NMHC observed

following ethane in June. In contrast to isoprene, the monoterpenes were observed during all seasons. Alpha- and beta-pinene were lowest during January and were at comparable levels during September 2006 and May 2007 (mean and median ~120-380 pptv). Monoterpene mixing ratios were presumably lower in June compared to September and May because sampling was conducted during the day when removal rates were highest.

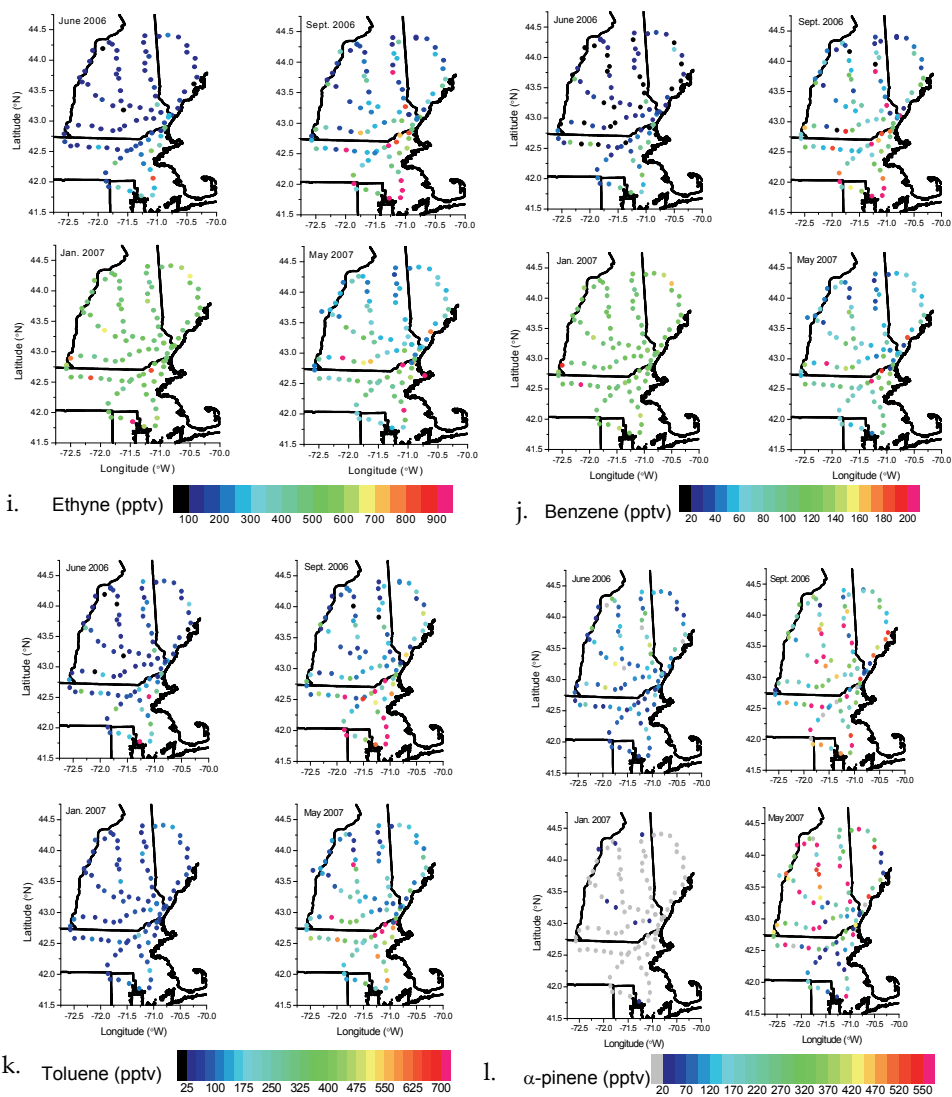


Fig. 2 continued

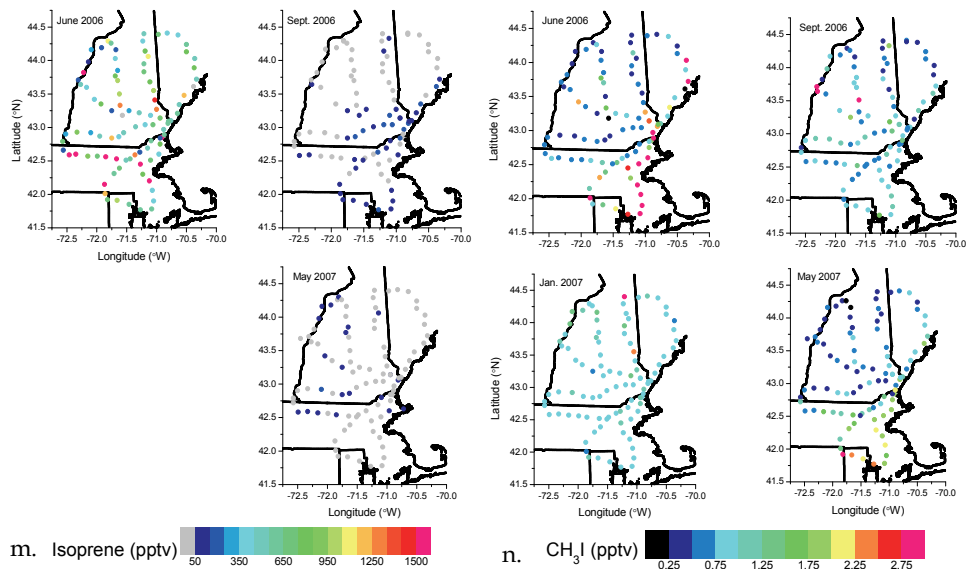


Fig. 2. continued

Methyl iodide (photolysis lifetime of several days to ~ 1 week) is the dominant organic iodine compound in the atmosphere and is primarily emitted from oceanic sources (e.g., Bell et al., 2002). A recent study conducted in the eastern U.S. identified a significant terrestrial source of CH₃I as well (Sive et al., 2007). In addition to isoprene, CH₃I was the only compound with highest mean ($\sim 1.5 \pm 1.6$ pptv) and maximum (8.5 pptv) mixing ratios during June (Table 1). At the TF monitoring site, CH₃I had a similar seasonal variation as isoprene (Sive et al., 2007). Overall, the range of CH₃I mixing ratios (~ 0.2 -6 pptv) was comparable throughout New England during September, January, and May.

The anthropogenic halocarbons, C₂HCl₃ and C₂Cl₄, are primarily emitted from industrial sources (dry cleaning solvents, degreasing agents) (e.g., McCulloch and Midgley, 1996; Wang et al., 1995), and thus are excellent tracers of industrial emissions. The atmospheric distributions and budgets of C₂HCl₃ and C₂Cl₄ are of interest because they are (1) toxic air pollutants, (2) precursors to toxic oxidation products (phosgene, trichloroacetic acid) (e.g., Kindler et al., 1995), and (3) a potential source of chlorine atoms in the troposphere and stratosphere (Schauffler et al., 2003; Thompson et al., 2004). Similar to the pentanes and aromatics, the highest mean (7 ± 18 pptv) and maximum (125 pptv) C₂HCl₃ was observed during May suggesting the influence of evaporative emissions (Table 1). This is consistent with results from the long-term measurements at TF which suggested that evaporative emissions from industrial sources contributed to the seasonal trend in ambient C₂HCl₃ (Russo et al., 2010b). Median C₂Cl₄ mixing ratios (14 pptv) were also highest in May, while mean (18 ± 25 pptv) and maximum (205 pptv) C₂Cl₄ mixing ratios were observed in September (Table 1).

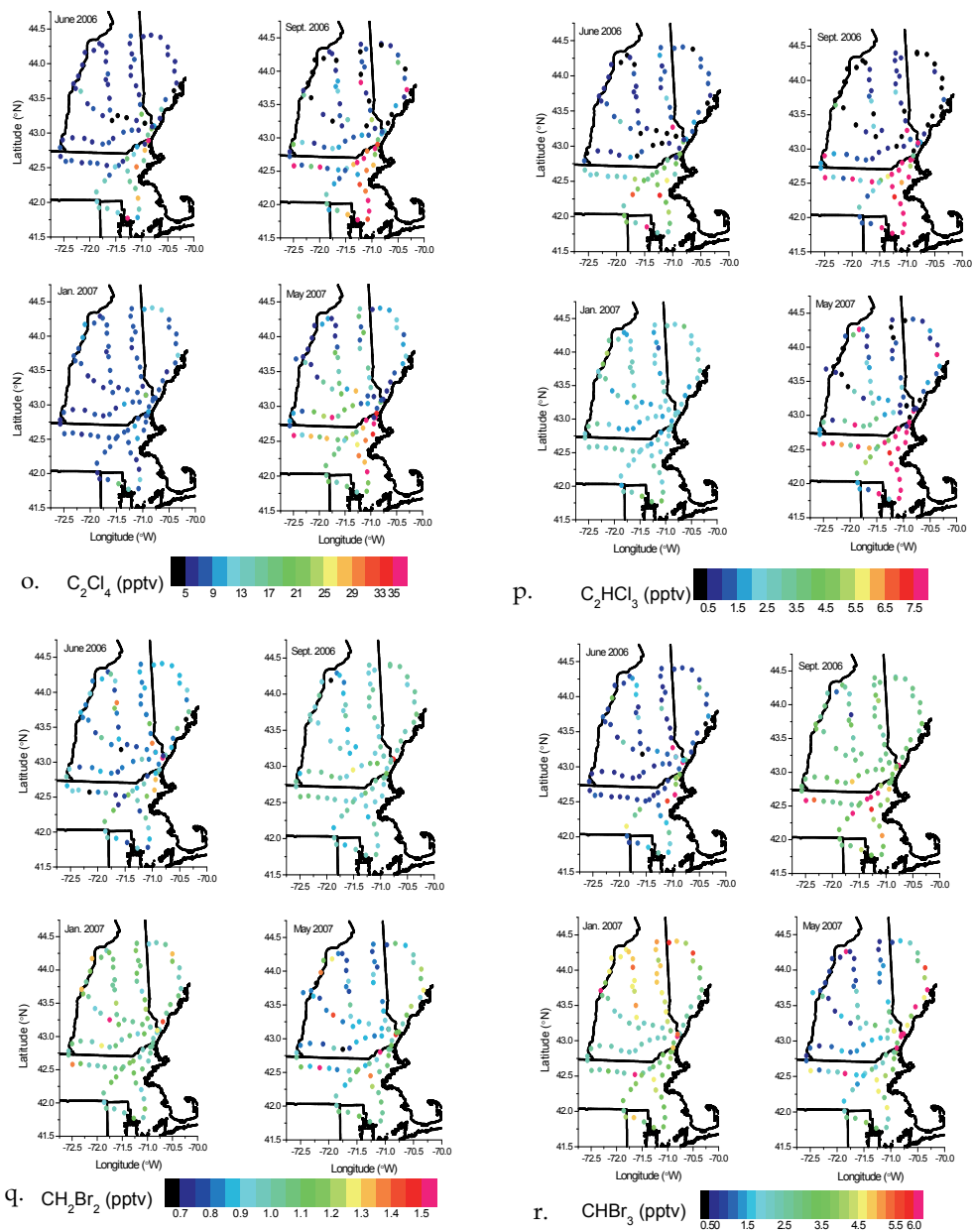


Fig. 2. continued

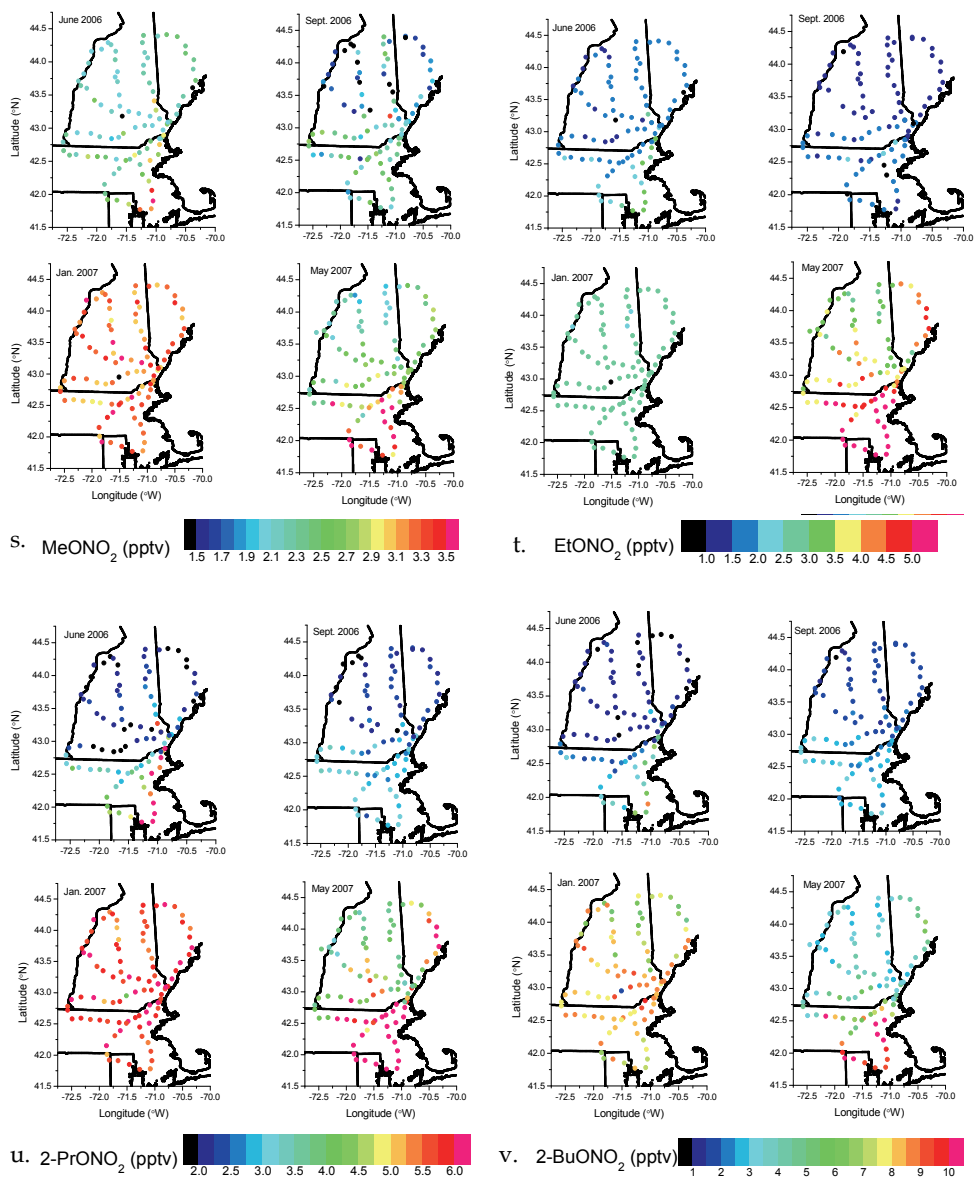


Fig. 2 continued

Short-lived brominated organic gases, such as bromoform (CHBr₃) (atmospheric lifetime 2-4 weeks) and dibromomethane (CH₂Br₂) (atmospheric lifetime several months), are the largest source of organic bromine to the atmosphere and are a potential source of bromine to the upper troposphere and stratosphere (e.g., Butler et al., 2007; Liang et al., 2010; Quack and Wallace, 2003). Consequently, the Br atoms and BrO radicals produced following the

photodissociation of organobromine compounds can impact catalytic O_3 destruction in the stratosphere (e.g., Schauffler et al., 1999). Organobromine compounds primarily originate from macroalgal and planktonic sources in surface seawater and enter the atmosphere through air-sea exchange processes. Anthropogenic sources (such as coastal power plants, chlorination of waste water and seawater, desalination) are minor (Quack and Wallace, 2003; Zhou et al., 2005). Coastal seawater and estuarine regions have been identified as a significant source of $CHBr_3$ and CH_2Br_2 to the atmosphere over New England (Zhou et al., 2005, 2008). Thus, $CHBr_3$ and CH_2Br_2 are useful tracers of marine emissions on New England air quality. Overall, the mean and median CH_2Br_2 mixing ratios were similar during the four surveys (~ 1 pptv) (Table 1). The median and mean $CHBr_3$ mixing ratios were comparable in September and January (~ 3.0 - 3.7 pptv) and higher than in June and May. However, both CH_2Br_2 and $CHBr_3$ had their highest peak mixing ratio in May. Furthermore, the highest $CHBr_3$ maximum mixing ratios and standard deviations were observed in June and May suggesting larger mixing ratio variability during the warmer months. This is consistent with the long-term TF data and may reflect variability in emission rates and/or the more rapid removal during summer (e.g., Zhou et al., 2005).

Alkyl nitrates are secondary compounds produced following the oxidation of their parent alkanes (i.e., methane, ethane, propane, n-butane) (Equations 1-6). The highest mean and median $MeONO_2$, $2-PrONO_2$, and $2-BuONO_2$ mixing ratios were observed in January, whereas $EtONO_2$ was highest in May (Table 1). The general distribution of the alkyl nitrates during the four spatial surveys was consistent with their long-term trends (Russo et al., 2010a). More specifically, $2-PrONO_2$ (mean ~ 2.6 - 6 pptv) was the most abundant alkyl nitrate in June, September, and May while $2-BuONO_2$ (~ 8 pptv) was dominant in winter.

3.2 Spatial variation and sources of VOCs

Specific NMHCs are primarily emitted by certain sources and thus can be used as tracers of those sources. The following source signature information is used to interpret and identify the various VOC sources in this work. The major sources of ethyne, benzene, and alkenes are incomplete combustion of fossil fuels, biomass burning, and vehicle exhaust emissions (e.g., Choi and Ehrman, 2004; Harley et al., 1992; 2001; McLaren et al., 1996). C_2 - C_4 alkanes are emitted from natural gas, incomplete combustion, and unburned gasoline. Fuel evaporation emissions (caused by ambient temperature changes or residual engine heat during vehicle operation, resting, or refueling) are a dominant source of C_4 - C_5 alkanes because of their high vapor pressures (Choi and Ehrman, 2004; Harley et al., 2001). The leakage of unburned liquefied petroleum gas (LPG) (during storage, distribution, or refilling) is a significant source of propane, i-butane, and n-butane and a minor source of alkenes (Blake and Rowland, 1995; Chen et al., 2001; Jobson et al., 2004). Aromatics are a major component of liquid gasoline and are often observed in vehicle exhaust because of incomplete combustion or leakage of unburned fuel (e.g., Harley et al., 2000, 2001; Kirchstetter et al., 1999). Toluene, ethylbenzene, m+p-xylene, and o-xylene are also emitted from fuel evaporation and industrial processes (i.e., painting, architectural coating, manufacturing, printing, degreasing solvents) (e.g., Monod et al., 2001). Furthermore, as mentioned in the preceding section, C_2Cl_4 and C_2HCl_3 are tracers of industrial/solvent emissions, CH_3I , CH_2Br_2 , and $CHBr_3$ reflect the influence of marine emission sources, and alkyl nitrates are indicators of photochemical processing.

Typical summer daytime NMHC mixing ratios were prevalent throughout the majority of the study area during the June 2006 sampling campaign (with the exception of a few isolated sites with high propane, butane, and pentane mixing ratios). Furthermore, most VOCs exhibited a relatively uniform range of mixing ratios throughout ME, NH, eastern VT, and northern MA (Fig. 2). During the daytime, the atmosphere is well mixed which may have contributed to the low variability in mixing ratios throughout New England. A region of higher NMHC, C_2Cl_4 , and C_2HCl_3 mixing ratios was observed in eastern MA and northern RI which was likely associated with increased urban activity near Boston, MA and Providence, RI (Fig. 2). This coincided with enhanced CH_3I (~3-8 pptv), $MeONO_2$ (2.5-3.5 pptv), and 2- $PrONO_2$ (4-8 pptv) mixing ratios which extended into southeast NH. In addition, in June, the highest $CHBr_3$ and CH_2Br_2 mixing ratios were observed in the seacoast region of NH and northeast MA, which likely reflects the influence of emissions from coastal algae (Fig. 2q, r).

Biogenic NMHCs had a persistent influence throughout New England during June, September, and May reflecting the highly forested nature of the region. Isoprene mixing ratios ranged from 130-3500 pptv during the daytime June survey (Fig. 2m). A corridor of elevated isoprene (>100 pptv) was located in southeastern NH during September. Sites with elevated α -pinene (range <50-5600 pptv) and β -pinene (range <50-2560 pptv) mixing ratios were distributed throughout New England overnight during September and May (Fig. 2l, Table 1).

An important feature of the VOC spatial distributions (Fig. 2) is the region of enhanced NMHC, C_2Cl_4 , and C_2HCl_3 mixing ratios in eastern and northeastern MA particularly during September and May. This reflects strong anthropogenic emissions from the Boston, MA area, southeast NH, and the I-95 corridor which extends northeastward into Maine. The fact that VOCs which are tracers of different sources were all elevated in this region indicates that a complex mixture of emissions from natural gas, LPG, fuel evaporation, unburned gasoline, combustion, and industrial sources contributed to the air quality of the region.

Another notable observation is the region of enhanced propane mixing ratios (~2000-14000 pptv) in northern NH during both the September and May surveys indicating strong local emissions from LPG leakage (Fig. 2b). The absence of elevated ethane, ethyne, and i-pentane corresponding to the areas of high propane suggests that natural gas, combustion, and fuel evaporation sources were not important contributors to the high propane mixing ratios. Moreover, the high propane levels are noteworthy because they occurred during the warmer time of year (spring-fall) and thus are not likely associated with residential heating. Furthermore, in September, enhanced ethene (>500 pptv) and propene (>150 pptv) mixing ratios were collocated with sites exhibiting high propane providing additional evidence of an impact from LPG leakage (Fig. 2g, h).

A unique feature of the May regional survey is the corridor of enhanced $CHBr_3$ mixing ratios (~3-7 pptv) extending from southeast NH to the northeast along the Maine coast; CH_2Br_2 exhibited a similar, but less pronounced, trend with mixing ratios of ~1-1.2 (Fig. 2q,r). The elevated organobromine compound mixing ratios along the NH and ME coasts likely reflects the influence of marine emissions. Methyl iodide did not exhibit higher coastal mixing ratios illustrating the different marine sources or production mechanisms of brominated and iodinated halocarbons (e.g., Butler et al., 2007). Interestingly, high $EtONO_2$, 2- $PrONO_2$, and to a lesser extent $MeONO_2$ mixing ratios were collocated with several of the sites with enhanced $CHBr_3$ in southwest ME (Fig. 2). This is suggestive of a marine contribution to the alkyl nitrates (e.g., Atlas et al., 1993; Chuck et al., 2002) or the presence of an air mass containing a mixture of marine and photochemically processed emissions.

A significant feature of the January survey results is the uniform spatial distribution of VOC mixing ratios throughout the entire study area (Fig. 2). The low variability is illustrated by

the similar mean and median mixing ratios and the low standard deviations (Table 1). During the January 2007 sampling survey, the mean and median alkane, alkene, ethyne, benzene, toluene, ethylbenzene, C_2Cl_4 , and C_2HCl_3 mixing ratios were lower than average (Russo et al., 2010b) indicating the presence of a clean air mass over New England. At TF, the wind direction was from the NW indicating the transport of clean, Canadian air to New England. The xylenes and alkyl nitrates were near typical January levels.

An interesting observation during the January survey is the elevated $CHBr_3$ (~4-6 pptv) and lower 2-BuONO₂ (~4-7 pptv) mixing ratios in northern NH and western ME compared to the rest of the region (Figure 2r, v). In contrast, throughout Massachusetts and southern NH, $CHBr_3$ and 2-BuONO₂ mixing ratios ranged from ~2-4 pptv and 6-10 pptv, respectively. It is unlikely that the elevated $CHBr_3$ in northern NH reflected marine emissions because the other marine tracers, CH_2Br_2 and CH_3I , do not exhibit a similar trend. This observation may reflect a local winter $CHBr_3$ source or a unique chemical signature from a source to the NW of New England and requires additional study.

3.3 Ambient ratios

In order to further characterize and identify the sources of VOCs in New England, ambient ratios were compared with emission ratios from the literature and from source samples collected near LPG refueling stations and gasoline storage containers throughout New Hampshire during summer 2004 and during the regional sampling trips. For example, typical ambient *i*-butane/*n*-butane ratios are ~0.2-0.3 for urban, fuel evaporation, and vehicle exhaust emissions, 0.46 for LPG emissions, and ~0.6 to >1 for natural gas (e.g., Barletta et al., 2002; Choi and Ehrman, 2004; Fujita, 2001; Goldan et al., 2000; Jobson et al., 1998, 2004; Lawrimore & Aneja, 1997; Mukerjee et al., 2004; Scheff and Wadden, 1993; B. Sive, unpublished data; Velasco et al., 2007; Watson et al., 2001). During the June and January surveys, the *i*-butane/*n*-butane ratio ranged from ~0.4-1.1 suggesting that a mix of vehicular, evaporative, LPG, and natural gas emissions influenced New England air quality (Fig. 3a). Higher *i*-butane/*n*-butane ratios were observed during September (range 0.4-2.9) and May (range 0.4-6) illustrating the influence of widespread liquefied petroleum and natural gas emissions. The highest mean (0.80) and median (0.72) *i*-butane/*n*-butane ratios were observed in September further supporting the presence of strong LPG emissions demonstrated by the high mean and median propane, ethene, and propene mixing ratios discussed in section 3.1.

The *i*-pentane/*n*-pentane emission ratios for several sources are fairly uniform with ranges of ~2.2-3.8 for vehicle exhaust, ~1.5-3 for liquid gasoline, and ~1.8-4.6 for fuel evaporation (e.g., Conner et al., 1995; Harley et al., 2001; Jobson et al., 2004; Lough et al., 2005; McGaughey et al., 2004; Mukund et al., 1996; Watson et al., 2001; Velasco et al., 2007). The mean and median *i*-pentane/*n*-pentane ratios during June, September, and May were similar at ~2.1 (range ~0.5-6.6) indicating the influence of emissions from exhaust, gasoline, and evaporative sources (Fig. 3b). The *i*-pentane/*n*-pentane ratio exhibits a seasonal variation at the TF site likely associated with enhanced fuel evaporation emissions of *i*-pentane in the summer (e.g., Rubin et al., 2006). Based on data from TF throughout 2004-2008, the *i*-pentane/*n*-pentane ratio is ~1.6 during the colder months (October-May) and increases to ~2.2 during the warmer months (June-September) (Russo et al., 2010b). The mean *i*-pentane/*n*-pentane ratio during the January regional survey was 1.6 ± 0.1 which is consistent with the long-term measurements.

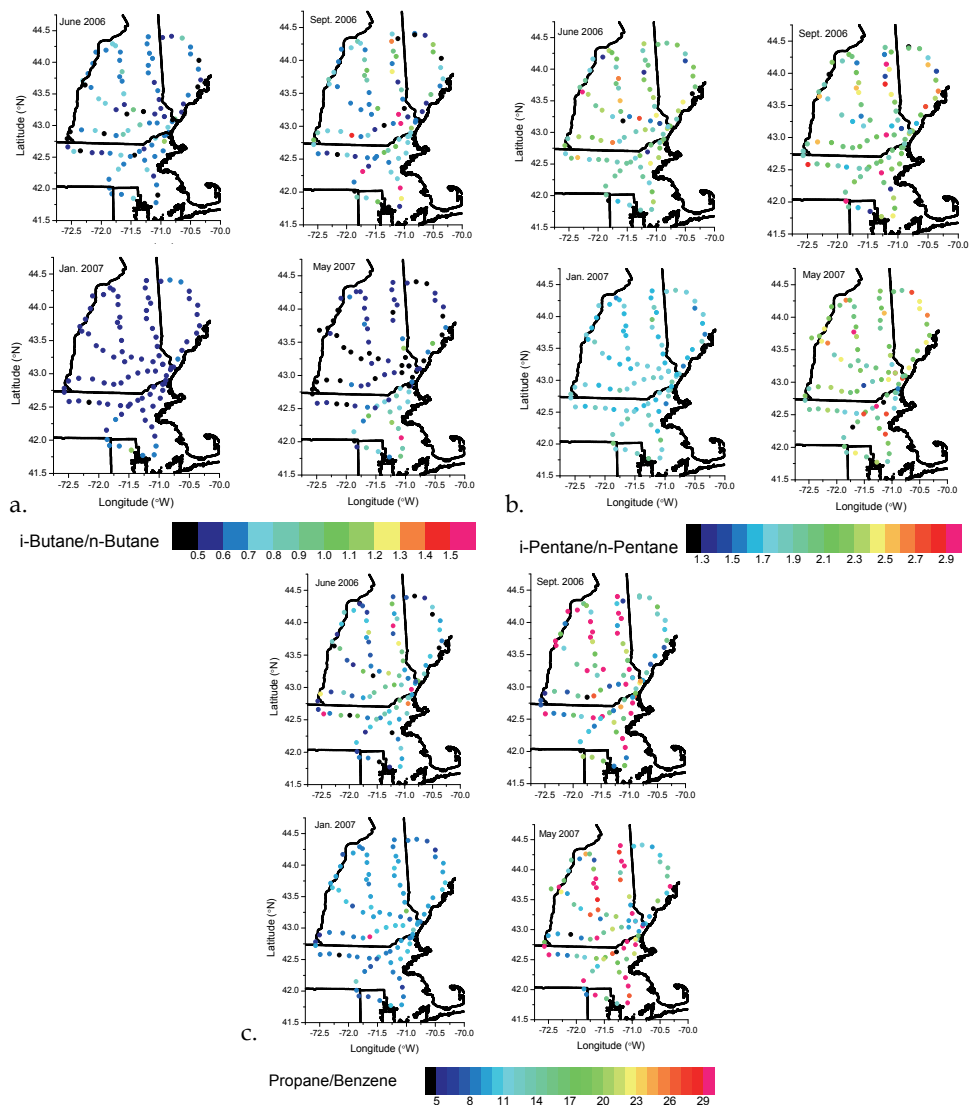


Fig. 3. Ambient NMHC ratios during the four regional surveys. The format is the same as in Figure 2. (a) i-butane/n-butane, (b) i-pentane/n-pentane, (c) propane/benzene.

A useful technique to characterize sources is to compare the ratio of two compounds with different sources but similar photochemical lifetimes. The ratio should remain relatively constant because neither compound will be removed preferentially during transport; thus the ratio can be assumed to equal the emission ratio (e.g., Parrish et al., 1998). An excellent

example is to compare ratios between propane, benzene, and ethyne because their rate constants for reaction with OH are similar to within $\leq 30\%$ of each other (e.g., Atkinson et al., 2006). Propane is a tracer of liquefied petroleum gas while benzene and ethyne are tracers for vehicle exhaust and incomplete combustion. During the four regional surveys, the propane/benzene ratio ranged from 2-145 (with the exception of one site with a ratio of 0.3). The mean (~ 24) and median (~ 16) propane/benzene ratios were similar in September and May and higher than in June and January (mean ~ 9 and 13, respectively) (Fig. 3c). Similarly, the average propane/ethyne ratios were higher in September (5.6 ± 6.1) and May (4.8 ± 5.0) compared to June (2.2 ± 2.2) and January (2.1 ± 0.8). These results are additional evidence of the widespread influence from LPG leakage and refilling during all seasons throughout New England and indicate a stronger relative impact from LPG, natural gas, or evaporative emissions relative to combustion.

3.4 Regional emission rates

Ambient emission rates of speciated VOCs are required for developing regional budgets, implementing effective control strategies, and evaluating emission inventories and air quality models. However, emission rate estimates based on ambient data are limited and are primarily reported on global scales (e.g., Boissard et al., 1996; Gupta et al., 1998) or in urban areas during specific campaigns (e.g., Blake and Rowland, 1995; Chen et al., 2001, Velasco et al., 2005). Additionally, emission rates are usually lumped into specific classes (i.e., alkane, alkene, aromatic, biogenic). A major reason for the lack of regional VOC emission rate estimates is the difficulty associated with differentiating between local, regional, and distant sources. In order to reduce this complication, we focused on measurements obtained when it was determined that air mass mixing was minimal.

In order to estimate speciated emission rates, we followed a simple box model approach which has been effectively used in previous studies to calculate emission and removal rates of trace gases in New England using measurements from the TF field site (i.e., Russo et al., 2010b; Sive et al., 2007; Talbot et al., 2005; White et al., 2008; Zhou et al., 2005). This method uses measurements made on nights with low wind speeds and when a stable inversion layer has developed because under these conditions, the exchange of air between the nocturnal boundary layer (NBL) and the residual layer above is limited (e.g., Gusten et al., 1998; Hastie et al., 1993; Talbot et al., 2005). Therefore, advection and vertical mixing of air masses can be neglected. Under these conditions, we can assume that a change in NMHC mixing ratios reflects local sources or sinks. Two criteria were used for identifying nights when a stable inversion layer developed: (1) wind speeds $< 1 \text{ m s}^{-1}$ and (2) $\text{O}_3 < 10 \text{ ppbv}$. On both the nights of September 21-22, 2006 and May 29-30, 2007 at TF, O_3 decreased to less than 10 ppbv and the wind speed was stable at $\sim 0.2 \text{ m s}^{-1}$ demonstrating that a stable NBL developed (Figs. 4a and 5a). Another indication of a stable NBL is the significant increase in CO_2 mixing ratios. On both nights, CO_2 increased from background levels ($\sim 375 \text{ ppmv}$ (parts per million by volume)) to near 440 ppmv reflecting local emissions from vegetation respiration or anthropogenic sources. Furthermore, the NMHC mixing ratios increased substantially compared to before the development of the NBL. For example, on September 21-22, propane mixing ratios were a factor of 6 higher and the butanes, pentanes, ethyne, and benzene were factors of 2-4 higher under the NBL compared to the 3 hours prior to sunset ($\sim 18:00 \text{ EDT}$) (Fig. 4b). Similarly, on May 29-30 at TF, propane, butanes, pentanes,

ethyne, and aromatic mixing ratios increased by factors of ~ 1.5 -6 while α -pinene and β -pinene were factors of 13 and 20, respectively, higher under the NBL (Figs. 5b,c). Moreover, as demonstrated in Figure 5, the propane and α -pinene mixing ratios at TF are within the range observed at the five additional sampling sites indicating that the emission rates calculated using measurements at TF are representative of the region.

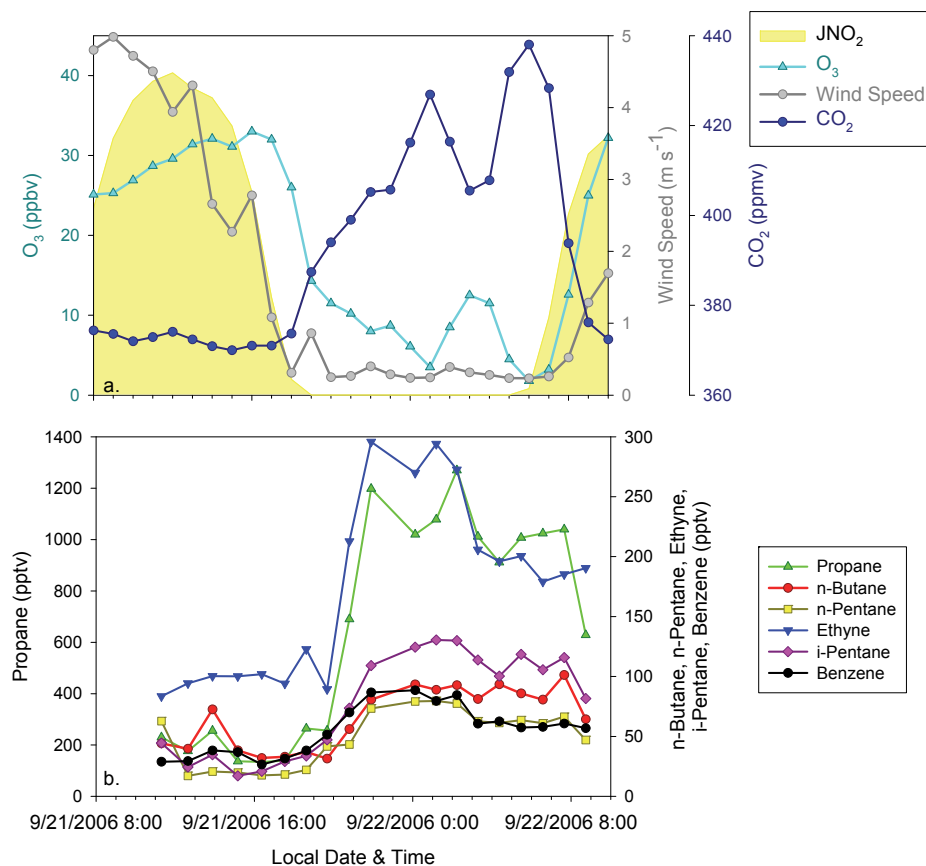


Fig. 4. Trace gas, wind speed, and nitrogen dioxide photolysis rate (J_{NO_2} , indicator of when sunlight is available) between 08:00 September 21 to 08:00 September 22, 2006 (EDT) at the Thompson Farm field site in Durham, NH. (a) hourly average O_3 (ppbv), CO_2 (ppmv), and wind speed ($m s^{-1}$) and (b) propane (left axis), ethyne, n-butane, i-pentane, n-pentane, and benzene (right axis) (pptv).

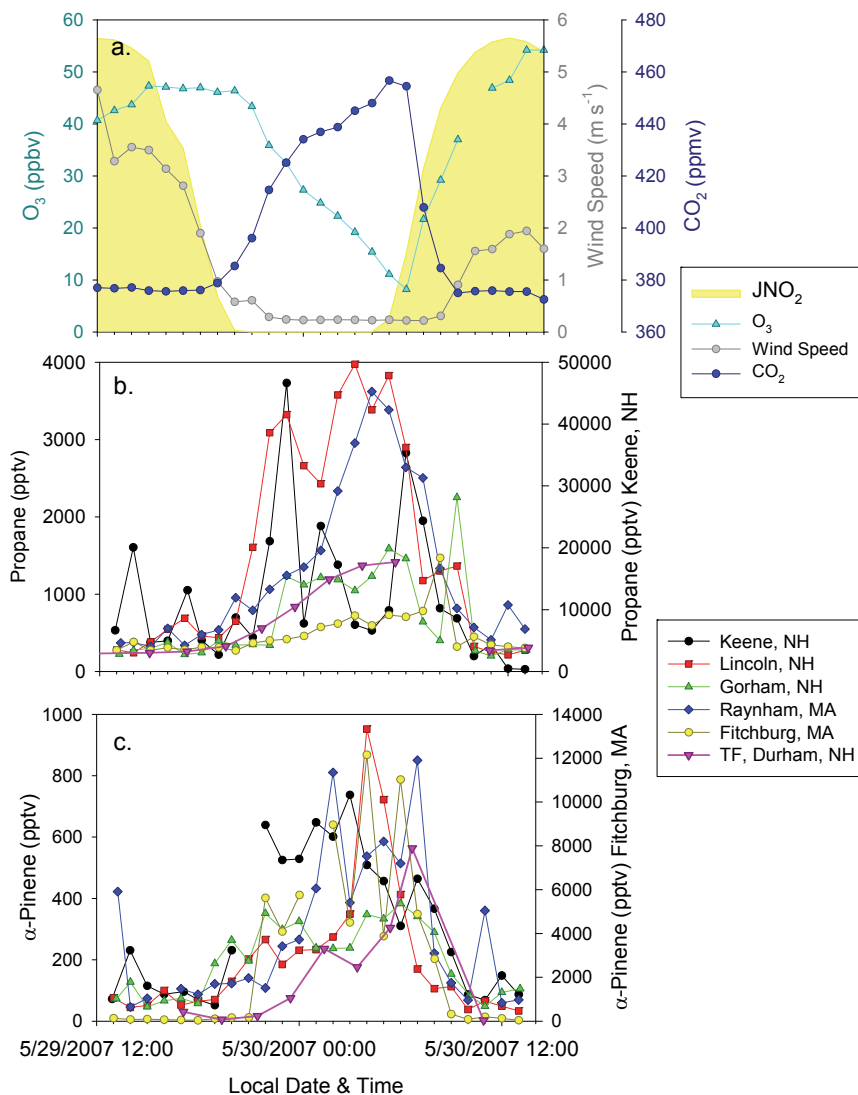


Fig. 5. (a) Hourly average O_3 (ppbv), CO_2 (ppmv), wind speed ($m s^{-1}$), and JNO_2 at Thompson Farm 12:00 May 29 to 13:00 May 30, 2007 (EDT). (b) Propane mixing ratio (pptv) at six diurnal sampling sites throughout New Hampshire and Massachusetts. The right axis shows the propane mixing ratio at the Keene, NH site. (c) same as (b) but for α -pinene. The right axis shows the α -pinene mixing ratio in Fitchburg, MA.

Emission rates (ER) were calculated by multiplying the slope of the linear regression between the change in hourly average concentrations (dC in molecules cm^{-3}) per unit time ($dt = 5$ hours) by the boundary layer height:

$$ER = \left[\frac{dC}{dt} \right] \times H \quad (1)$$

As shown by Eq. 1, the emission rate estimates are directly proportional to the nocturnal boundary layer height. Stable nocturnal boundary layer heights typically range from ~50-200 m at midlatitude continental locations and vary with meteorological conditions, time of day, and season (e.g., Gusten et al., 1998; Hastie et al., 1993; McKendry and Lundgren, 2000; Talbot et al., 2005; White et al., 2003); thus we chose 125 m as a representative value for the TF site (e.g., Mao et al., 2008; Sive et al., 2007; Talbot et al., 2005; White et al., 2008; Zhou et al., 2005). If $H = 50$ m or 200 m is used in Eq. 1, the emission rate estimates vary by $\pm 60\%$.

The emission rates of several NMHCs are shown in Table 2. During both September 2006 and May 2007, the propane emission rate ($\sim 18 \times 10^9$ molec. $\text{cm}^{-2} \text{s}^{-1}$) at TF was an order of magnitude larger than the other NMHCs ($(\sim 0.5-6) \times 10^9$ molec. $\text{cm}^{-2} \text{s}^{-1}$) on these calm nights reflecting local emissions rather than boundary layer dynamics or transport from a distant source. In fact, the propane emission rate may be larger than estimated here. For example, at the rural Lincoln, NH site in northwest NH, propane increased by ~ 1220 pptv/hour (from ~ 650 to 4000 pptv) whereas propane only increased by ~ 300 pptv/hour at TF (Fig. 5b). Furthermore, these results indicate that high propane emission rates from northern New England occur during each season. These large propane emission rates are significant, particularly because of the rural nature of this region. LPG use as a heating and cooking fuel is widespread throughout northern New England (e.g., EIA, 2005). Assuming the emission rate calculated for TF is applicable to all of New Hampshire, potentially over 20 tons of propane are emitted on a daily basis (Table 2); $\sim 1-10$ tons of $\text{C}_4\text{-C}_5$ alkanes, benzene, and toluene may be emitted per day. Because propane is relatively long-lived compared to other NMHCs, large inputs to air masses transported off of the continent and across the Atlantic Ocean could significantly impact tropospheric O_3 production, particularly in downwind locations, such as Europe.

Emission rates estimated using the same method during summers 2003 and 2004 (White et al., 2008) and winter 2006 (Russo et al., 2010b) are also included for comparison (Table 2). The emission rates calculated in this work are consistent with the summer and winter emission rates presented in White et al. (2008) and Russo et al. (2010b). Both the summer 2003 and 2004 ($(3-20) \times 10^9$ molecules $\text{cm}^{-2} \text{s}^{-1}$) and May 2007 ($\sim 5 \times 10^9$ molecules $\text{cm}^{-2} \text{s}^{-1}$) emission rates illustrate the potential for significant monoterpene emissions from New England. Monoterpenes are extremely reactive in the atmosphere during spring and summer (lifetime of hours) and thus can contribute to O_3 production. Furthermore, the oxidation of monoterpenes produces low volatility products which can subsequently nucleate or condense onto preexisting aerosol particles and produce SOA (e.g., Atkinson and Arey, 2003; Hoffman et al, 1997).

The emission rates for a specific NMHC, which represent different seasons and years, agree within the given stated uncertainty (Table 2). This is an important result because it suggests that the emission rate of NMHCs from New Hampshire, and possibly all of New England, does not vary significantly with season or year. Thus, these emission rates may be useful for regional air quality modeling studies.

	Emission Rate (molecules cm ⁻² s ⁻¹) × 10 ⁹				New Hampshire Emission Rate (Mg/day)		
	Summers 2003 & 2004 ^a	Winter 2006 ^b	Sept. 21-22, 2006 ^c	May 29-30, 2007 ^d	Winter 2006 ^b	Sept. 2006 ^c	May 2007 ^d
Propane	9-23	42±25	17±12	19±12	61±37	25±18	28±17
i-Butane	0.2-1	3.2±2.0	0.9±0.6	2.2±1.7	6.1±3.8	1.7±1.1	4.3±3.2
n-Butane	0.2-1.4	3.6±2.3	1.3±0.8	5.4±3.4	6.9±4.4	2.5±1.6	10.4±6.6
i-Pentane	2	2.4±1.5	1.9±1.2	2.3±1.5	5.8±3.6	4.5±2.8	5.5±3.6
n-Pentane		1.4±0.8	1.0±0.6	1.5±1.0	3.3±2.0	2.3±1.5	3.6±2.4
Ethyne		7.4±4.9	4.0±2.8		6.4±4.2	2.4±2.4	
Benzene		1.6±1.1	0.6±0.5	0.2±0.2	4.3±2.8	0.5±0.5	0.5±0.5
Toluene		2.7±1.7		1.8±1.2	8.2±5.3		5.6±3.7
m+p-Xylene		1.3±0.8		0.6±0.5	4.4±2.9		2.2±1.8
o-Xylene		0.5±0.3		0.2±0.2	1.8±1.1		0.8±0.6
α-Pinene	20			5.8±3.8			20.4±17
β-Pinene	3			5.3±3.5			18.6±16

^aWhite et al. (2008), ^bRusso et al. (2010b), ^{c,d}This work

Table 2. Emission rates (molecules cm⁻² s⁻¹) of C₃-C₁₀ NMHCs calculated using data from the Thompson Farm field site on the nights of September 21-22, 2006 and May 29-30, 2007. The uncertainty was calculated by propagating the standard error of the linear regression between the change in NMHC concentration per unit time and the assumed variation in nocturnal boundary layer height (125 m±75 m). Emission rates for summers 2003 and 2004 and winter 2006 were estimated in previous works and are included for comparison. Assuming the estimated emissions are representative of the region, the rates were extrapolated to the state of New Hampshire (Mg/day) using a land area of 2.3 × 10¹⁰ m².

4. Summary

The objective of this analysis was to present an overview of the VOC distribution (C₂-C₁₀ nonmethane hydrocarbons, tetrachloroethene, trichloroethene, methyl iodide, dibromomethane, bromoform, methyl nitrate, ethyl nitrate, 2-propyl nitrate, 2-butyl nitrate) in the atmosphere over New England during four regional surveys (June 21, 2006, September 21-22, 2006, January 10-11, 2007, May 22-23, 2007). The seasonal and spatial variation of VOCs during the four surveys was discussed and put in context with the general seasonal trends of VOCs at the Thompson Farm field site in Durham, NH. Additionally, VOCs sources were identified and emission rates of several NMHCs were estimated. Future and ongoing research will include detailed analysis of the meteorological conditions on the days when regional surveys were conducted to determine the source regions more precisely and the influence of atmospheric dynamics on the VOC behavior, examination of additional trace gas (O₃, CO, NO, NO_y, SO₂) data from TF, estimation of

emission rates from diurnal sampling sites located throughout ME, NH, and MA, and in depth comparisons with emission ratios and the long-term continuous VOC data from TF.

5. Acknowledgements

We would like to thank several individuals who assisted with collecting canister samples—Su Youn Kim, Pallavi Mittal, Huiting Mao, Theresa Belanger, Rich Luciano, Salena Reynolds, and AIRMAP staff for maintenance of the monitoring sites and management of the database. Financial support for this work was provided through the Office of Oceanic and Atmospheric Research at the National Oceanic and Atmospheric Administration.

6. References

- Atkinson, R., & Arey, J. (2003). Atmospheric degradation of volatile organic compounds, *Chem. Rev.*, Vol. 103, pp. 4605-4638.
- Atkinson, R., Baulch, D. L., Cox, R. A., Crowley, J. N., Hampson, R. F., Hynes, R. G., Jenkin, M. E., Rossi, M. J., & Troe, J. (2006). Evaluated kinetic and photochemical data for atmospheric chemistry: Volume II - gas phase reactions of organic species, *Atmos. Chem. Phys.*, Vol. 6, pp. 3625-4055.
- Atlas, E., Pollock, W., Greenberg, J., Heidt, L., & Thompson, A. M. (1993). Alkyl nitrates, nonmethane hydrocarbons, and halocarbon gases over the equatorial Pacific ocean during SAGA-3, *J. Geophys. Res.*, Vol. 98, pp. 16933-16947.
- Barletta, B., Meinardi, S., Simpson, I. J., Khwaja, H. A., Blake, D. R., & Rowland, F. S. (2002). Mixing ratios of volatile organic compounds (VOCs) in the atmosphere of Karachi, Pakistan, *Atmos. Environ.*, Vol. 36, pp. 3429-3443.
- Bell, N., Hsu, L., Jacob, D. J., Schultz, M. G., Blake, D. R., Butler, J. H., King, D. B., Lobert, J. M., & Maier-Reimer. (2002). Methyl iodide: Atmospheric budget and use as a tracer of marine convection in global models. *J. Geophys. Res.*, Vol. 107, No. D17, 4340, doi:10.1029/2001JD001151.
- Blake, D. R., & Rowland, F. S. (1995). Urban leakage of liquefied petroleum gas and its impact on Mexico City air quality, *Science*, Vol. 269, pp. 953-956.
- Boissard, C., Bonsang, B., Kanakidou, M., & Lambert, G. (1996). TROPOZ II: Global distributions and budgets of methane and light hydrocarbons, *J. Atmos. Chem.*, Vol. 25, pp. 115-148.
- Butler, J. H., King, D. B., Lobert, J. M., Montzka, S. A., Yvon-Lewis, S. A., Hall, B. D., Warwick, N. J., Mondeel, D. J., Aydin, M., & Elkins, J. W. (2007). Oceanic distributions and emissions of short-lived halocarbons, *Global Biogeochem. Cycles*, Vol. 21, GB1023, doi:10.1029/2006GB002732.
- Carter, W. P. L. (1994). Development of ozone reactivity scales for volatile organic compounds, *J. Air & Waste Manage. Assoc.*, Vol. 44, pp. 881-899.
- Chen, T. Y., Simpson, I. J., Blake, D. R., & Rowland, F. S. (2001). Impact of the leakage of liquefied petroleum gas (LPG) on Santiago air quality, *Geophys. Res. Lett.*, Vol. 28, pp. 2193-2196.
- Choi, Y.-J., & Ehrman, S. H. (2004). Investigation of sources of volatile organic carbon in the Baltimore area using highly time-resolved measurements, *Atmos. Environ.*, Vol. 38, pp. 775-791, 10.1016/j.atmosenv.2003.10.004, 2004.

- Chuck, A. L., Turner, S. M., & Liss, P. S. (2002). Direct evidence for a marine source of C₁ and C₂ alkyl nitrates, *Science*, Vol. 297, pp. 1151-1154.
- Conner, T. L., Lonneman, W. A., & Seila, R. L. (1995). Transportation related volatile hydrocarbon source profiles measured in Atlanta, *J. Air & Waste Manage. Assoc.*, Vol. 45, pp. 383-394.
- Energy Information Administration. (2005). Liquefied petroleum gases consumption, price, and expenditure estimates by sector, U.S. Department of Energy, Washington, D. C., <http://www.edi.doe.gov>,
- Fehsenfeld, F., Calvert, J., Fall, R., Goldan, P., Guenther, A. B., Hewitt, C. N., Lamb, B., Liu, S., Trainer, M., Westberg, H., & Zimmerman, P. (1992). Emissions of volatile organic compounds from vegetation and the implications for atmospheric chemistry, *Global Biogeochem. Cycles*, Vol. 6, pp. 389-430.
- Flocke, F., Volz-Thomas, A., Buers, H. J., Patz, W., Garthe, H. J., & Kley, D. (1998). Long-term measurements of alkyl nitrates in southern Germany 1. General behavior and seasonal and diurnal variation, *J. Geophys. Res.*, 103, pp. 5729-5746.
- Fujita, E. M. (2001). Hydrocarbon source apportionment for the 1996 Paso del Norte Ozone Study, *Sci. Total Environ.*, Vol. 276, pp. 171-184.
- Goldan, P. D., Parrish, D. D., Kuster, W. C., Trainer, M., McKeen, S. A., Holloway, J., Jobson, B. T., Sueper, D. T., & Fehsenfeld, F. C. (2000). Airborne measurements of isoprene, CO, and anthropogenic hydrocarbons and their implications, *J. Geophys. Res.*, Vol. 105, pp. 9091-9105.
- Guenther, A., Hewitt, C. N., Erickson, D., Fall, R., Geron, C., Graedel, T., Harley, P., Klinger, L., Lerdau, M., McKay, W. A., Pierce, T., Scholes, B., Steinbrecher, R., Tallamraju, R., Taylor, J., & Zimmerman, P. (1995). A global model of natural volatile organic compound emissions, *J. Geophys. Res.*, Vol. 100, No. D5, pp. 8873-8892.
- Gupta, M. L., Cicerone, R. J., Blake, D. R., Rowland, F. S., & Isaksen, I. S. A. (1998). Global atmospheric distributions and source strengths of light hydrocarbons and tetrachloroethene, *J. Geophys. Res.*, Vol. 103, pp. 28219-28235.
- Gusten, H., Heinrich, G., & Sprung, D. (1998). Nocturnal depletion of ozone in the Upper Rhine Valley, *Atmos. Environ.*, Vol. 32, pp. 1195-1202.
- Harley, R. A., Hannigan, M. P., & Cass, G. R. (1992). Respeciation of organic gas emissions and the detection of excess unburned gasoline in the atmosphere, *Environ. Sci. Technol.*, Vol. 26, pp. 2395-2408.
- Harley, R. A., Coulter-Burke, S. C. & Yeung, T. S. (2000). Relating liquid fuel and headspace vapor composition for California reformulated gasoline samples containing ethanol, *Environ. Sci. Technol.*, Vol. 34, pp. 4088-4094.
- Harley, R. A., McKeen, S. A., Pearson, J., Rodgers, M. O., & Lonneman, W. A. (2001). Analysis of motor vehicle emissions during the Nashville/Middle Tennessee Ozone Study, *J. Geophys. Res.*, Vol. 106, pp. 3559-3567.
- Hastie, D. R., Shepson, P. B., Sharma, S., & Schiff, H. I. (1993). The influence of the nocturnal boundary layer on secondary trace species in the atmosphere at Dorset, Ontario, *Atmos. Environ. A-Gen.*, Vol. 27, pp. 533-541.
- Hoffmann, T., Odum, J. R., Bowman, F., Collins, D., Klockow, D., Flagan, R. C., & Seinfeld, J. H. (1997). Formation of organic aerosols from the oxidation of biogenic hydrocarbons, *J. Atmos. Chem.*, Vol. 26, pp. 189-222.

- Jobson, B. T., Parrish, D. D., Goldan, P., Kuster, W., Fehsenfeld, F. C., Blake, D. R., Blake, N. J., & Niki, H. (1998). Spatial and temporal variability of nonmethane hydrocarbon mixing ratios and their relation to photochemical lifetime, *J. Geophys. Res.*, Vol. 103, pp. 13557-13567.
- Jobson, B. T., Berkowitz, C. M., Kuster, W. C., Goldan, P. D., Williams, E. J., Fehsenfeld, F. C., Apel, E. C., Karl, T., Lonneman, W. A., & Riemer, D. (2004). Hydrocarbon source signatures in Houston, Texas: Influence of the petrochemical industry, *J. Geophys. Res.*, Vol. 109, D24305, doi:10.1029/2004jd004887.
- Katzenstein, A. S., Doezema, L. A., Simpson, I. J., Blake, D. R. & Rowland, F. S. (2003). Extensive regional atmospheric hydrocarbon pollution in the southwestern United States, *P. Natl. Acad. Sci.*, Vol. 100, No. 21, pp. 11975-11979.
- Kindler, T. P., Chameides, W. L., Wine, P. H., Cunnold, D. M., Alyea, F. N. & Franklin, J. A. (1995). The fate of atmospheric phosgene and the stratospheric chlorine loadings of its parent compounds: CCl_4 , C_2Cl_4 , C_2HCl_3 , CH_3CCl_3 , and CHCl_3 , *J. Geophys. Res.*, Vol. 100, No. D1, pp. 1235-1251.
- Kirchstetter, T. W., Singer, B. C., Harley, R. A., Kendall, G. R. & Hesson, J. M. (1999). Impact of California reformulated gasoline on motor vehicle emissions. 2. Volatile organic compound speciation and reactivity, *Environ. Sci. Technol.*, Vol. 33, pp. 329-336.
- Lawrimore, J. H., & Aneja, V. P. (1997). A chemical mass balance analysis of nonmethane hydrocarbon emissions in North Carolina, *Chemosphere*, Vol. 35, pp. 2751-2765.
- Liang, Q., Stolarski, R. S., Kawa, S. R., Nielsen, J. E., Douglass, A. R., Rodriguez, J. M., Blake, D. R., Atlas, E. L. & Ott, L. E. (2010). Finding the missing stratospheric Br_y: a global modeling study of CHBr_3 and CH_2Br_2 , *Atmos. Chem. Phys.*, Vol. 10, pp. 2269-2286.
- Logan, J. A., Prather, M. J., Wofsy, S. C. & McElroy, M. B. (1981). Tropospheric Chemistry: A global perspective, *J. Geophys. Res.*, Vol. 86, No. C8, pp. 7210-7254.
- Lough, G. C., Schauer, J. J., Lonneman, W. A., & Allen, M. K. (2005). Summer and winter nonmethane hydrocarbon emissions from on-road motor vehicles in the Midwestern United States, *J. Air & Waste Manage. Assoc.*, Vol. 55, pp. 629-646.
- Mao, H., & Talbot, R. (2004a). O₃ and CO in New England: Temporal variations and relationships, *J. Geophys. Res.*, Vol. 109, D21304, 10.1029/2004jd004913.
- Mao, H., & Talbot, R. (2004b). Role of meteorological processes in two New England ozone episodes during summer 2001, *J. Geophys. Res.*, Vol. 109, D20305, doi:10.1029/2004jd004850.
- Mao, H., Talbot, R. W., Sigler, J. M., Sive, B. C. & Hegarty, J. D. (2008). Seasonal and diurnal variations of Hg⁰ over New England, *Atmos. Chem. Phys.*, Vol. 8, pp. 1403-1421.
- McCulloch, A., & Midgley, P. M. (1996). The production and global distribution of emissions of trichloroethene, tetrachloroethene and dichloromethane over the period 1988-1992, *Atmos. Environ.*, Vol. 30, pp. 601-608.
- McGaughey, G. R., Desai, N. R., Allen, D. T., Seila, R. L., Lonneman, W. A., Fraser, M. P., Harley, R. A., Pollack, A. K., Ivy, J. M., & Price, J. H. (2004). Analysis of motor vehicle emissions in a Houston tunnel during the Texas Air Quality Study 2000, *Atmos. Environ.*, Vol. 38, 3363-3372, 10.1016/j.atmosenv.2004.03.006.
- McKendry, I. G., & Lundgren, J. (2000). Tropospheric layering of ozone in regions of urbanized complex and/or coastal terrain: a review, *Prog. Phys. Geog.*, Vol. 24, pp. 329-354.

- McLaren, R., Singleton, D. L., Lai, J. Y. K., Khouw, B., Singer, E., Wu, Z., & Niki, H. (1996). Analysis of motor vehicle sources and their contribution to ambient hydrocarbon distributions at urban sites in Toronto during the Southern Ontario Oxidants Study, *Atmos. Environ.*, Vol. 30, pp. 2219-2232.
- Monod, A., Sive, B. C., Avino, P., Chen, T., Blake, D. R., & Rowland, F. S. (2001). Monoaromatic compounds in ambient air of various cities: a focus on correlations between the xylenes and ethylbenzene, *Atmos. Environ.*, Vol. 35, pp. 135-149.
- Mukerjee, S., Norris, G. A., Smith, L. A., Noble, C. A., Neas, L. M., Ozkaynak, A. H., & Gonzales, M. (2004). Receptor model comparisons and wind direction analyses of volatile organic compounds and submicrometer particles in an arid, binational, urban air shed, *Environ. Sci. Technol.*, Vol. 38, pp. 2317-2327.
- Mukund, R., Kelly, T. J., & Spicer, C. W. (1996). Source attribution of ambient air toxic and other VOCs in Columbus, Ohio, *Atmos. Environ.*, Vol. 30, pp. 3457-3470.
- Parrish, D. D., Trainer, M., Young, V., Goldan, P. D., Kuster, W. C., Jobson, B. T., Fehsenfeld, F. C., Lonneman, W. A., Zika, R. D., Farmer, C. T., Riemer, D. D., & Rodgers, M. O. (1998). Internal consistency tests for evaluation of measurements of anthropogenic hydrocarbons in the troposphere, *J. Geophys. Res.*, Vol. 103, pp. 22339-22359.
- Quack, B. & Wallace, D. W. R. (2003). Air-sea flux of bromoform: Controls, rates, and implications, *Global Biogeochem. Cycles*, Vol. 17, No. 1, 1023, doi:10.1029/2002GB001890.
- Roberts, J. M. (1990). The atmospheric chemistry of organic nitrates, *Atmos. Environ. A-Gen*, Vol. 24, pp. 243-287.
- Rubin, J. I., Kean, A. J., Harley, R. A., Millet, D. B., & Goldstein, A. H. (2006). Temperature dependence of volatile organic compound evaporative emissions from motor vehicles, *J. Geophys. Res.*, Vol. 111, D03305, doi:10.1029/2005JD006458.
- Russo, R. S., Zhou, Y., Haase, K. B., Wingenter, O. W., Frinak, E. K., Mao, H., Talbot, R., & Sive, B. C. (2010a). Temporal variability, sources, and sinks of C₁-C₅ alkyl nitrates in coastal New England, *Atmos. Chem. Phys.*, Vol. 10, pp. 1865-1883.
- Russo, R. S., Zhou, Y., White, M. L., Mao, H., Talbot, R., & Sive, B. C. (2010b). Multi-year (2004-2008) record of nonmethane hydrocarbons and halocarbons in New England: Seasonal variations and regional sources, *Atmos. Chem. Phys.*, Vol. 10, pp. 4909-4929.
- Schauffler, S. M., Atlas, E. L., Blake, D. R., Flocke, F., Lueb, A., Lee-Taylor, J. M., Stroud, V. & Travnicek. (1999). Distributions of brominated organic compounds in the troposphere and lower stratosphere, *J. Geophys. Res.*, Vol. 104, No. D17, pp. 21513-21535.
- Schauffler, S. M., Atlas, E. L., Donnelly, S. G., Andrews, A., Montzka, S. A., Elkins, J. W., Hurst, D. F., Romashkin, P. A., Dutton, G. S. & Stroud, V. (2003). Chlorine budget and partitioning during the Stratospheric Aerosol and Gas Experiment (SAGE) III Ozone Loss and Validation Experiment (SOLVE), *J. Geophys. Res.*, Vol. 108, No. D5, 4173, doi:10.1029/2001JD002040.
- Scheff, P. A., & Wadden, R. A. (1993). Receptor modeling of volatile organic compounds. 1. Emission inventory and validation, *Environ. Sci. Technol.*, Vol. 27, pp. 617-625.
- Singh H. B., & Zimmermann, P. B. (1992). Atmospheric distribution and sources of nonmethane hydrocarbons, ed. J. O. Nriagu, *Gaseous Pollutants: Characterization and cycling*, John Wiley & Sons Inc., pp. 177-235.

- Sive, B. C., Zhou, Y., Troop, D., Wang, Y. L., Little, W. C., Wingenter, O. W., Russo, R. S., Varner, R. K., & Talbot, R. (2005). Development of a cryogen-free concentration system for measurements of volatile organic compounds, *Anal. Chem.*, Vol. 77, pp. 6989-6998, doi:10.1021/ac0506231.
- Sive, B. C., Varner, R. K., Mao, H., Blake, D. R., Wingenter, O. W., & Talbot, R. (2007). A large terrestrial source of methyl iodide, *Geophys. Res. Lett.*, Vol. 34, L17808, doi:10.1029/2007gl030528.
- Spivakovsky, C. M., Logan, J. A., Montzka, S. A., Balkanski, Y. J., Foreman-Fowler, M., Jones, D. B. A., Horowitz, L. W., Fusco, A. C., Brenninkmeijer, C. A. M., Prather, M. J., Wofsy, S. C., & McElroy, M. B. (2000). Three-dimensional climatological distribution of tropospheric OH: Update and evaluation, *J. Geophys. Res.*, Vol. 105, 8931-8980.
- Talbot, R., Mao, H. T., & Sive, B. (2005). Diurnal characteristics of surface level O₃ and other important trace gases in New England, *J. Geophys. Res.*, Vol. 110, D09307, doi:10.1029/2004jd005449.
- Thompson, T. M., Butler, J. G., Daube, B. C., Dutton, G. S., Elkins, J. W., Hall, B. D., Hurst, D. F., King, D. B., Kline, E. S., Lafleur, B. G., Lind, J., Lovitz, S., Mondeel, D. J., Montzka, S. A., Moore, F. L., Nance, J. D., Neu, J. L., Romashkin, P. A., Scheffer, A., & Snible, W. J. (2004). Halocarbons and other atmospheric trace species, CMDL Summary Report #27, 115-135, <http://www.esrl.noaa.gov/gmd/publications/annrpt27>.
- U.S. Environmental Protection Agency. (1998). Carcinogenic Effects of Benzene: An Update (Final). U.S. Environmental Protection Agency, Office of Research and Development, National Center for Environmental Assessment, Washington Office, Washington, DC, EPA/600/P-97/001F.
- U.S. Environmental Protection Agency. (2008). National Air Quality and Emissions Trends Report, EPA 454/R-03-005.
- U.S. Environmental Protection Agency. (2010). Our Nation's Air: Status and trends through 2008, EPA-454/R-09/002.
- Velasco, E., Lamb, B., Pressley, S., Allwine, E., Westberg, H., Jobson, B. T., Alexander, M., Prazeller, P., Molina, L., & Molina, M. (2005). Flux measurements of volatile organic compounds from an urban landscape, *Geophys. Res. Lett.*, Vol. 32, L20802, doi:10.1029/2005GL023356.
- Velasco, E., Lamb, B., Westberg, H., Allwine, E., Sosa, G., Arriaga-Colina, J. L., Jobson, B. T., Alexander, M. L., Prazeller, P., Knighton, W. B., Rogers, T. M., Grutter, M., Herndon, S. C., Kolb, C. E., Zavala, M., de Foy, B., Volkamer, R., Molina, L. T., & Molina, M. J. (2007). Distribution, magnitudes, reactivities, ratios and diurnal patterns of volatile organic compounds in the Valley of Mexico during the MCMA 2002 & 2003 field campaigns, *Atmos. Chem. Phys.*, Vol. 7, pp. 329-353, 2007.
- Wang, C. J. L., Blake, D. R., & Rowland, F. S. (1995). Seasonal variations in the atmospheric distribution of a reactive chlorine compound, tetrachloroethene (CCl₂=CCl₂), *Geophys. Res. Lett.*, Vol. 22, 1097-1100.
- Watson, J. G., Chow, J. C., & Fujita, E. M. (2001). Review of volatile organic compound source apportionment by chemical mass balance, *Atmos. Environ.*, Vol. 35, pp. 1567-1584.

- White, A. B., Templeman, B. D., Angevine, W. M., Zamora, R. J., King, C. W., Russell, C. A., Banta, R. M., Brewer, W. A., & Olszyna, K. J. (2003). Regional contrast in morning transitions observed during the 1999 Southern Oxidants Study Nashville/Middle Tennessee Intensive, *J. Geophys. Res.*, Vol. 107, 4726, doi:10.1029/2001JD002036.
- White, M. L., Russo, R. S., Zhou, Y., Mao, H., Varner, R. K., Ambrose, J., Veres, P., Wingenter, O. W., Haase, K., Stutz, J., Talbot, R., & Sive, B. C. (2008). Volatile organic compounds in northern New England marine and continental environments during the ICARTT 2004 campaign, *J. Geophys. Res.*, Vol. 113, D08S90, doi:10.1029/2007jd009161.
- White, M. L., Russo, R. S., Zhou, Y., Ambrose, J. L., Haase, K., Frinak, E. K., Varner, R. K., Wingenter, O. W., Mao, H., Talbot, R., & Sive, B. C. (2009). Are biogenic emissions a significant source of summertime atmospheric toluene in the rural Northeastern United States?, *Atmos. Chem. Phys.*, Vol. 9, pp. 81-92.
- Zhou, Y., Varner, R. K., Russo, R. S., Wingenter, O. W., Haase, K. B., Talbot, R., & Sive, B. C. (2005). Coastal water source of short-lived halocarbons in New England, *J. Geophys. Res.*, Vol. 110, D21302, doi:10.1029/2004jd005603.
- Zhou, Y., Mao, H., Russo, R. S., Blake, D. R., Wingenter, O. W., Haase, K. B., Ambrose, J., Varner, R. K., Talbot, R. & Sive, B. C. (2008). Bromoform and dibromomethane measurements in the seacoast region of New Hampshire, 2002-2004, *J. Geophys. Res.*, Vol. 113, D08305, doi:10.1029/2007jd009103.

Evaluation of an Emission Inventory and Air Pollution in the Metropolitan Area of Buenos Aires

Laura E. Venegas, Nicolás A. Mazzeo and Andrea L. Pineda Rojas
National Scientific and Technological Research Council (CONICET)
National Technological University
Argentina

1. Introduction

Air is a vital resource, so its quality must fall within a tightly bound range. This quality is the level needed to protect public health. In addition, the quality must be able to support other life, notably diverse and sustainable ecosystems. The atmosphere is an extremely complex system in which numerous physical and chemical processes occur simultaneously. Ambient measurements give us only a snapshot of atmospheric conditions at a particular time and location. Such measurements are often difficult to interpret without a clear conceptual model of atmospheric processes. Moreover, measurements alone cannot be used directly by policymakers to establish an effective strategy for solving air quality problems. An understanding of individual atmospheric processes (chemistry, transport, removal, etc.) does not imply an understanding of the system as a whole. Mathematical models provide the necessary framework for integration of our understanding of individual atmospheric processes and study of their interactions. A combination of state-of-the-science measurements with state-of-the-science models is the best approach for making real progress toward understanding the atmospheric environment. Over the past four decades, there has been a significant increase in the number of locations where air quality data have been obtained. Also, there has been a substantial improvement in the technique for modelling the different physical and chemical processes occurring in the atmosphere. Despite this progress, currently available observations are still spatially and temporally sparse and the predictions of current generation of air quality models are still uncertain. Consequently, observations and model outputs should be combined to create high-resolution spatial-temporal maps of air quality. However, at present air quality observations and model results are generally used separately.

Urban air pollution is still on rise at many cities worldwide, or has experienced only small improvements. Some causes of urban air pollution problems are the amount and density of air pollutant sources, particularly vehicles, residences and industries. Because of the complexity of urban systems, air quality management in these areas is still a serious problem.

Emission inventories are important tools to describe the emission situation and eventually to manage air quality. An emission inventory is a list of the amount of pollutants from

different sources entering the air in a given time period and a particular geographical area. It usually includes information on the amount of the pollutants released from major industrial sources, and averages figures for the emissions from smaller sources throughout the area. The information included in an emission inventory helps to identify the sources and in the development of abatement strategies. Ball & Radcliffe (1979) have identified several applications for urban air pollution emission inventories. Their information is useful to elaborate a map showing the geographic distribution of emissions. This map can be an important aid in land use planning by identifying parts of the region that are likely to be subject to high levels of pollution, and the location of pollution sources in relation to sensitive areas. Emission inventories can point out the major sources whose control can lead to a considerable reduction of pollution in the area. They can be used in conjunction with an atmospheric dispersion model, to estimate air pollutant concentrations at ground level and/or assess trends in air quality. They can also help in the design of air quality monitoring networks, by indicating, for example, where the highest concentrations of pollution are likely to be found, or which areas are the most representative.

The method used to develop an emission inventory does have some elements of error, but other two alternatives are expensive and subject to their own errors. The first alternative would be to monitor continually every major source in the area. The second alternative would be to monitor continually the pollutants in ambient air at many points and apply appropriate dispersion equations to calculate the emissions. In practice, the most informative system would be a combination of all three, knowledgeably applied. Air pollution emission inventories have been developed for several urban areas (Andrade et al., 2010; Ariztegui et al., 2004; Beaton et al., 1992; Borrego et al., 2003; Butler et al., 2008; D'Avignon et al., 2010; Gurjar et al., 2008; Kim, 1996; Miller et al. 2006; Mohan et al., 2007; Nishikawa & Kannari, 2010; Saija & Romano, 2002; Sallés et al., 1996; Seika et al., 1996; Sturm et al., 1999; Tsilingiridis et al., 2002; Wang et al., 2010; Zárate et al., 2007). Particularly, a few years ago, the first versions of an urban emission inventory (year 2000) for the city of Buenos Aires (Mazzeo & Venegas, 2003) and for area sources located in the Metropolitan Area of Buenos Aires (year 2005) (Pineda Rojas et al., 2007) have been prepared.

An emission inventory is an essential tool in the management of local air quality, particularly when its information is used in conjunction with atmospheric dispersion models.

A model is a simplified representation of real conditions. It contains assumptions and sometimes also some experimentally derived constants. Operational decisions based on predictions of a model should be made therefore when the underlying assumptions are met and when the model is being applied within the range of values for which the model has been tested. Atmospheric dispersion models provide a link between the source emissions and ambient concentrations. The heart of the matter is to estimate the concentration of a pollutant at a particular receptor point by calculating from basic information about the source of the pollutant, the meteorological conditions and the surface characteristics. Atmospheric dispersion models help us to understand the way air pollutants behave in the environment and are a useful tool in the urban air quality management system. There are many reasons for using atmospheric dispersion models, such as working out which sources are responsible for what proportion of concentration at any receptor; estimating population exposure on a higher spatial or temporal resolution than is practicable by measurement; targeting emission reductions on the highest contributors; and predicting concentration changes over time. Urban atmospheric dispersion models range from simple empirical

models to complex three-dimensional urban air-shed models. Sometimes, available input data make application of complex numerical tools not possible, and simple urban background pollution models become an acceptable alternative giving as good results as computations with more sophisticated models (Berkowicz, 2000; Hanna et al., 2002). Some examples of urban scale dispersion modelling systems developed during last decades are the UAM model (Morris & Myers, 1990), the DAUMOD model (Mazzeo & Venegas, 1991; 2010); the Danish OML model (Olesen, 1995), the UK-ADMS Urban model (Carruthers et al., 1994; CERC, 2003; McHugh et al., 1997) and the UDM-FMI (Karppinen et al., 2000) model. Dispersion models for the urban scale estimate urban background concentrations.

This chapter presents a summary of the development and results of a high spatial and temporal resolution version of the emission inventory of carbon monoxide (CO) and nitrogen oxides (NO_x) for the Metropolitan Area of Buenos Aires (MABA), including area source emissions (motor vehicles, aircrafts, residential heating systems, commercial combustion and small industries). The spatial distributions of CO and NO_x annual emission rates from area sources within the Metropolitan Area of Buenos Aires are shown with a spatial resolution of 1 x 1 km. The urban atmospheric dispersion model DAUMOD is applied to evaluate the air quality in the MABA due to the contribution of area source emissions in the urban area. Estimations of horizontal distributions of CO and nitrogen dioxide (NO₂) background concentrations in the MABA are presented.

2. Description of the Metropolitan Area of Buenos Aires

The Metropolitan Area of Buenos Aires (MABA) is considered the third megacity in Latin America, following Mexico City (Mexico) and Sao Paulo (Brazil). It is integrated by the city of Buenos Aires (CBA) and the Greater Buenos Aires (GBA). The city of Buenos Aires (Lat. 34°35'S – Long. 58°26'W), capital of Argentina, is located on the west coast of de la Plata River. The city has an extension of 203km² and 2891082 inhabitants (Instituto Nacional de Estadística y Censos [INDEC], 2010). The city of Buenos Aires is surrounded by the Greater Buenos Aires. This area is compound by 24 districts. It has an extension of 3627km² and 9910282 inhabitants (INDEC, 2010). The area of the MABA is 0.14% of the territory of Argentina and its population is approximately 32% of the population of the country. Fig. 1 shows the different districts of the Metropolitan Area of Buenos Aires and the grid net considered in calculations.

The terrain is flat with height differences lesser than 30 m. The de la Plata River is a shallow estuary, which covers 35000 km² approximately. The estuary is 320 km long, and its width varies between 38 km and 230 km in the upper and lower regions, respectively. In front of the CBA, the width of the river is about 42 km. The mean water temperature in the river varies from 12°C in winter to 24°C in summer.

The de la Plata River plain has a temperate climate. In summer (December to February), the city of Buenos Aires is warm and moist, with a mean temperature of 24°C. During autumn and spring atmospheric conditions are variable, with fluctuating temperatures. The winter months (June to August) are temperate and moist, with a mean temperature of 12°C. The annual mean temperature in the city is 18°C, and between 15-16°C in its surroundings. In the MABA, frosts occur between June and August, and snowfalls are very rare. The annual precipitation varies between 900 mm and 1600 mm, influenced by winds that advect humidity from the Atlantic Ocean. Rains are heavier on March. Winds are generally of low intensity. Strong winds are more frequent between September and March, when the greatest

storm frequency is observed. The annual frequency of winds blowing clean air from the river towards the urban area is 58%, and that of calm conditions is 3%. Cases of wind direction persistence may last more than 6 hours at any wind direction sector (Mazzeo & Venegas, 2004).

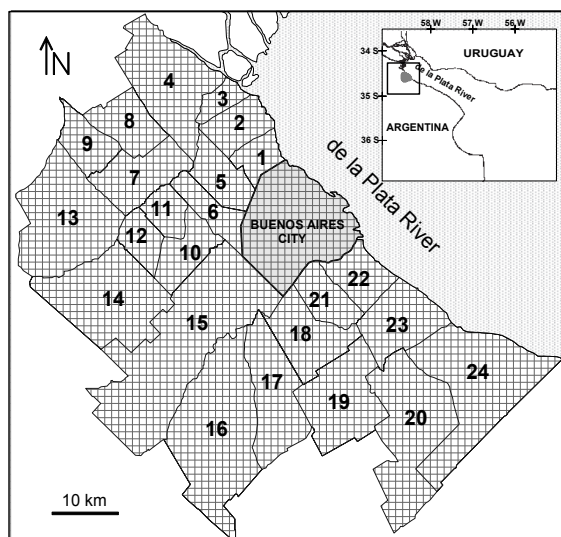


Fig. 1. Map of the Metropolitan Area of Buenos Aires, including the city of Buenos Aires and the Greater Buenos Aires. Districts of the Greater Buenos Aires (*inhabitants*): 1: Vicente López (270929); 2: San Isidro (291608); 3: San Fernando (163462); 4: Tigre (380709); 5: Gral. San Martín (422830); 6: Tres de Febrero (343774); 7: San Miguel (281120); 8: Malvinas Argentinas (321833); 9: José C. Paz (263094); 10: Morón (319934); 11: Hurlingham (176505); 12: Ituzaingó (168419); 13: Moreno (462242); 14: Merlo (524207); 15: La Matanza (1772130); 16: Ezeiza (160219); 17: Esteban Echeverría (298814); 18: Lomas de Zamora (613192); 19: Almirante Brown (555731); 20: Florencio Varela (423992); 21: Lanús (453500); 22: Avellaneda (340985); 23: Quilmes (580829); 24: Berazategui (320224). Grid cell side: 1km.

Mazzeo & Venegas (2008, 2010) and Venegas & Mazzeo (2006a, 2010a) proposed and applied methodologies to design different air quality monitoring networks for the city of Buenos Aires. At present, air pollutant concentrations are registered at the first three air quality monitoring stations of the network in the city (Venegas & Mazzeo, 2010b). The air quality in the city of Buenos Aires has been the subject of several studies carried out during the last years using different methodologies: analysis of data obtained from some measurement surveys of pollutants in urban air (Arkouli et al., 2010; Bocca et al., 2006; Bogó et al., 1999, 2001, 2003; Mazzeo & Venegas, 2002, 2004; Mazzeo et al., 2005; Venegas & Mazzeo, 2000, 2003; Vogt et al., 2007) and application of atmospheric dispersion models (Mazzeo & Venegas, 2010; Mazzeo et al., 2010; Venegas & Mazzeo, 2005, 2006b, 2010a). In the Greater Buenos Aires, very few air quality measurements have been made (Fagundez et al., 2001; Japan International Cooperation Agency-Secretaría de Desarrollo Sustentable y Política Ambiental [JICA-SAyDS], 2002).

3. Brief description of pollutants considered in this chapter

The pollutants considered in this chapter are carbon monoxide (CO) and nitrogen oxides (NO_x). Carbon monoxide is generated primarily by incomplete combustion of carbonaceous fuels in automobile engines and is a colourless and odourless gas. It is a very stable compound having a lifetime of two to four months in the atmosphere. There are studies (e.g. Harte et al., 1991), which show that high concentrations of CO can cause physiological and pathological changes and ultimately death of human. Carbon monoxide is a poisonous inhalant that deprives the body tissues of necessary oxygen. It is toxic because haemoglobin absorbs CO more readily than oxygen. With the bloodstream carrying less oxygen, brain functions is affected and heart rate increases in an attempt to offset the oxygen deficit. In very high doses it is fatal due to cerebral and cardiac hypoxia.

The stable gaseous oxides of nitrogen include nitrous oxide (N₂O), nitric oxide (NO), nitrogen trioxides (N₂O₃), nitrogen dioxide (NO₂) and nitrogen pentoxide (N₂O₅). An unstable NO₃, also exist. The nitrogen oxides present in the atmosphere in any significant amount are N₂O, NO and NO₂. N₂O is an inert gas with anaesthetic characteristics. Its atmospheric concentrations are considerably below the threshold concentration for biological effects, but it may be a significant contributor to global warming. NO is a colourless gas and at its air concentrations its biological toxicity in terms of human health is insignificant. However, NO is a precursor to the formation of NO₂ and is an active compound in photochemical smog formation as well. NO₂ is a reddish brown gas and is quite visible in sufficient amounts. The toxicological and epidemiological effects of NO₂ on human being are not completely known (WHO, 2006a). NO₂ may penetrate to the pulmonary region increasing susceptibility to respiratory pathogens.

4. The emission inventory for the MABA

4.1 Inventory technique

To develop an emission inventory for an area, one must: a) determine the type of air pollutants of concern, such as CO and NO_x; b) list the types of sources for the area, such as motor vehicles, aircrafts, residential, commercial and industrial combustions; c) examine the literature to find valid emission factors for each pollutant of concern; d) through an actual count, or means of some estimating technique, determine the number and size of specific sources in the area; and e) multiply the corresponding numbers from c) and d) to obtain the total emissions for each activity and then sum the similar emissions to obtain the total for the area. Valid emission factors for each source of pollution are the key to an emission inventory. Emission factors are then applied to the activity data in order to estimate the likely emissions:

$$\text{Emission} = \text{Activity level} \times \text{Emission factor} \quad (1)$$

This chapter focuses on area source emissions of CO and NO_x in the Metropolitan Area of Buenos Aires. The following source categories are considered:

- Mobile sources: road traffic and aircrafts
- Fixed sources: residential, commercial and small industries activities.

Point source emissions could not be included because, at present, there is not available sufficient data on the large industries located in the MABA. Information on the actual point source emissions is only available in a limited number of cases. There is also a lack of

homogeneity among the amount and quality of basic information available for each district of the MABA. The existence of multiple local Administrations in the region is the main reason for such heterogeneity. Furthermore, it should be noted that the city of Buenos Aires is a city-state and the 24 districts of the Greater Buenos Aires are part of the Province of Buenos Aires. CBA and GBA have different Governments.

4.2 Emissions from mobile sources

Main mobile sources in the Metropolitan Area of Buenos Aires have been divided into the following groups:

- Road traffic: passenger cars (including taxis), buses (including coaches) and heavy-duty vehicles.
- Air traffic: aircraft's landing-take-off (LTO) cycles at the domestic airport located in the city of Buenos Aires and at the international airport located in the Greater Buenos Aires.

4.2.1 Road traffic emissions

There are usually about three million vehicles circulating in the MABA during working days. The city of Buenos Aires and its surroundings concentrate approximately 43% of private cars, 60% of taxis, 50% of urban and interurban buses and 29% of cargo transportation of Argentina. As mentioned above, the methodological approach to estimate the emission rates from road traffic is based on the multiplication of activity data by emission factors. The first step involves the determination of an estimate of vehicle activity. Five traffic parameters are considered: volume, composition, vehicle velocity, vehicle age and travel distance in each grid cell. All traffic data have been obtained from the National Secretary of Transportation, the Buenos Aires City Government and the Secretary of Transportation of the Province of Buenos Aires. Available information includes mean daily traffic flow at several locations as well as traffic flow and composition measured at different hours of the day on different streets, routes, avenues and highways in the MABA. Most private cars are petrol-driven and taxis burn natural gas. All the buses and heavy duty vehicles are considered to run on diesel. The approximately age of the vehicle fleet is illustrated in Fig.2.

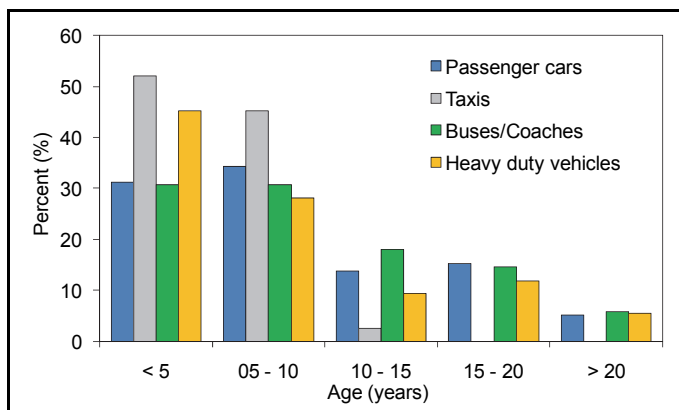


Fig. 2. Distribution of the age of each vehicle category.

The road network of the Metropolitan Area of Buenos Aires is assumed to be integrated by: highways, routes, avenues, main streets and streets. These specifications are quite useful since they generally correspond to particular traffic density levels and fleet compositions. Statistical shapes for traffic rates and average speed on these road types are then applicable to the CBA and the GBA. Based on measurements at several sites, the following vehicle fleet compositions are considered for the entire domain: a) highways: 89.7% (passenger cars) and 10.3% (buses and heavy duty vehicles); b) routes, avenues and main streets: 95.0% (passenger cars) and 5.0% (buses and heavy duty vehicles); and c) streets: 99.0% (passenger cars) and 1.0% (buses and heavy duty vehicles). As it is difficult to define a law to estimate a spatial vehicle speed evolution along a road, an average vehicle speed has been set for each road type (highways, routes, avenues, main streets, streets). The second step involves selecting emission factors. The emission factors used for mobile sources are based on measurements of in-service emissions in Buenos Aires (Rideout et al. 2005) and on the European Environment Agency’s Atmospheric Emission inventory Guidebook (COPERT method) (European Environment Agency, 2001). Results for the city of Buenos Aires and for the Greater Buenos Aires are described below.

In the city of Buenos Aires passenger cars employ the following fuels: 78.9% gasoline; 16.0% diesel and 5.1% compressed natural gas (CNG). Traffic flow data in the city are available at different sites located in highways, avenues and streets (Gobierno de la Ciudad de Buenos Aires, [GCBA], 2006). In the interest of completeness, where there are no traffic flow data available for a particular road street, a local mean flow is assigned according to the traffic map elaborated by the Secretary of Transport for the city of Buenos Aires (see detail in Fig. 3). Using this information, population density distribution and representative traffic flow measured at different points of the city, the vehicle kilometres travelled in each grid cell are estimated.

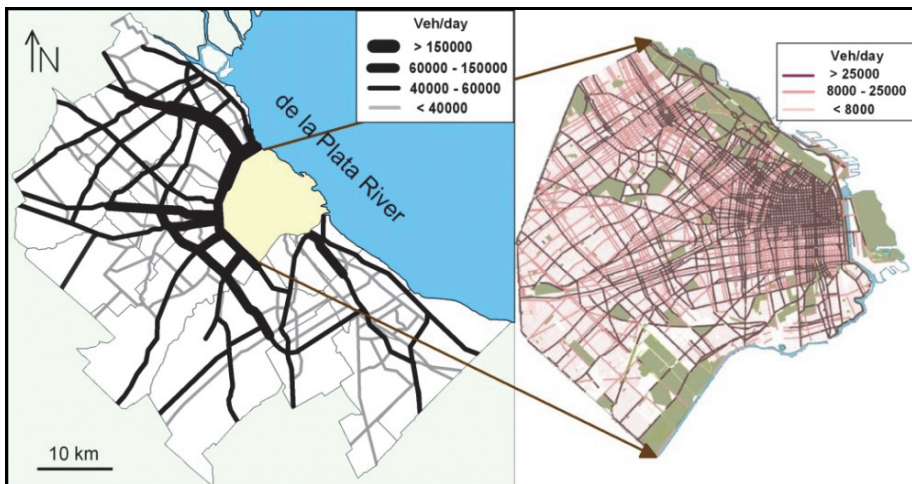


Fig. 3. Traffic flow map in the MABA and the city of Buenos Aires (detail).

Examples of traffic profile registered at different locations within the CBA are shown in Fig. 4 (left). The average vehicle speed considered for the different roads within the city of

Buenos Aires is: 80km/h (highways); 35km/h (avenues); and 15km/h (streets). The representative emission factors for CO and NO_x considered for the vehicles in the CBA are included in Table 1.

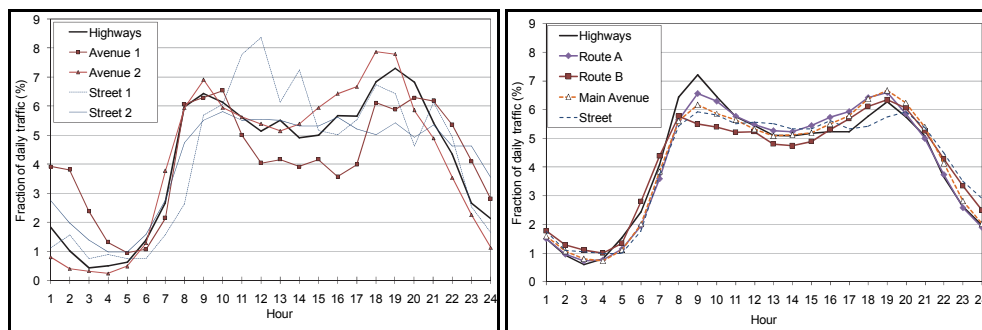


Fig. 4. Hourly traffic profiles at different sites registered within the CBA (left) and the GBA (right).

City of Buenos Aires							
Vehicle type	Fuel	Highways		Avenues		Streets	
		F (CO)	F (NO _x)	F (CO)	F (NO _x)	F (CO)	F (NO _x)
Passenger cars	Gasoline	12.0	2.8	18.7	1.8	38.0	1.5
	Diesel	0.5	0.8	0.6	1.0	1.0	1.1
	CNG	8.0	2.6	2.0	2.1	7.0	2.0
Buses	Diesel	2.2	3.0	5.5	5.0	8.0	14.7
Heavy Duty Vehicles	Diesel	1.8	3.6	2.5	6.1	6.0	10.0
Greater Buenos Aires							
Vehicle type	Fuel	Highways		Routes and Avenues		Streets	
		F (CO)	F (NO _x)	F (CO)	F (NO _x)	F (CO)	F (NO _x)
Passenger cars	Gasoline	10.0	3.4	16.7	1.9	38.0	1.5
	Diesel	0.4	0.8	0.5	0.9	1.0	1.1
	CNG	8.0	2.8	2.0	2.2	7.0	2.0
Buses	Diesel	2.0	5.6	5.0	6.7	8.0	14.7
Heavy Duty Vehicles	Diesel	1.5	4.0	2.0	6.0	6.0	10.0

Table 1. Emission factors (F) (g veh⁻¹ km⁻¹) for CO and NO_x.

In the Greater Buenos Aires, passenger cars employ the following fuels: 66.1% gasoline; 15.6% diesel and 18.3% CNG. Traffic flow data in the GBA are available at different sites in highways, routes and avenues. Even when data are given for a specific road, they are usually measured within a particular duration of time and in discrete locations. Since information is not available everywhere along a given road, both spatial and temporal assumptions have been made in order to obtain the characteristics for the whole road and so

finally to describe emissions over the entire region in a daily evolution. In order to elaborate a map of the traffic flow in the main roads of the GBA, vehicle rates (R) are extrapolated anywhere along every main road. These estimations are based mostly on empirical assumptions. In the GBA, highways and most major roads are roughly either radial or semi-circular. This feature facilitates the direct setting of roads on a polar reference frame. From available data, it may be assumed that radial road traffic rates decrease with distance (x) to the border of the city of Buenos Aires. An empirical exponential law is used to describe this typical star-form network behaviour (Sallés et al, 1996). The traffic rate ($R(x)$) at a given distance from the border of the city of Buenos Aires is estimated by:

$$R(x) = R(0) \exp [-\alpha x] \tag{2}$$

where $R(0)$ is a reference value (traffic rate at the border of the CBA) and α is an empirical coefficient. The values of α have been obtained by fitting to traffic flow measurements registered at several points in highways and routes. Fig. 5 shows the values of $R(0)$ and α for each sector considered in calculations.

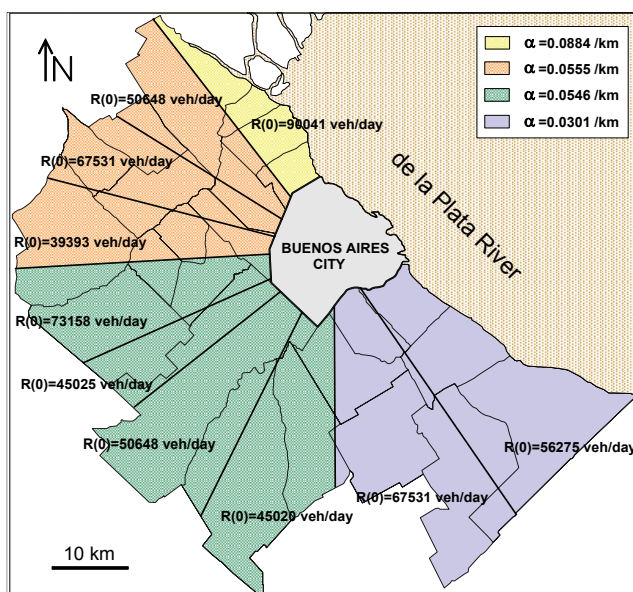


Fig. 5. Values of $R(0)$ and α for each sector, considered in Equation (2) to estimate the traffic flow along the highways and main roads in the GBA.

Available data suggest that semi-circular road traffic rates remain constant along the main roads, within each sector. The traffic map for the Greater Buenos Aires showing the obtained mean daily traffic flow in highways, routes, avenues and main streets is included in Fig. 3. These vehicle flux data are further used to account for vehicle distribution in the streets of the urban area in the GBA. The extrapolation assumption includes both the traffic in the main roadways and the spread traffic in streets and is based on a flux balance criterion between ingoing and outgoing vehicles in each grid cell. Hourly variation of traffic

rate is obtained applying hourly typical traffic rate profiles. Representative traffic profiles at different roadways within the GBA are shown in Fig. 4. The average vehicle speed considered for the different roads within the Greater Buenos Aires is: 100km/h (highways); 40km/h (routes and avenues); and 15km/h (streets). The representative emission factors for CO and NO_x considered for the vehicles in the GBA are presented in Table 1.

CO and NO_x emissions from buses in the MABA are obtained from the emission factors, the total distance travelled by each bus within each grid cell, the bus service frequency and the mean speed of the vehicles in each grid cell. Finally, CO and NO_x emissions from road traffic are estimated for each grid cell over the entire region in a daily evolution.

4.2.2 Air traffic emissions

Aircraft emissions have been estimated using the “alternative simple methodology” proposed by Romano et al. (1999). The aircraft operations of interest that may affect ground level pollutant concentrations are defined as the landing and takeoff (LTO) cycle. The cycle begins when the aircraft approaches the airport on its descent from the cruising altitude, lands and taxis to the gate. It continues as the aircraft taxis back out to the runway for subsequent takeoff and climb-out as it heads back to the cruising altitude. For all forms of commercial aircrafts, the time spent in each of the LTO modes is reckoned at 19 min for idling and taxiing out, 42 sec for take-off, 2.2 min for climb-out and; at the other end of the cycle, 4 min for approach to landing and 7 min for taxiing and idling (Romano et al. 1999). Fuel consumption and CO and NO_x emission factors for each operation mode depend on engine type (European Environment Agency, 2001; Romano et al., 1999; US.EPA, 1995). Emissions from aircrafts are calculated considering the modes related to the departure and arrival parts of the LTO cycle separately. For example, the total emission for an aircraft type during its departure is calculated multiplying the emission rates by the amount of time in each mode of the departure part of the LTO cycle, and then summing results from the considered modes. The aircraft type that operates at the domestic airport is mainly Boeing B-737, as it is used in domestic and regional flights. At the international airport the airlines operate the following aircraft types: Boeing B-737, B-747, B-757, B-767, B-777 and Airbus A319, A320, A321, A340. Fig. 6 shows the hourly distribution of the mean daily frequency of departures and arrivals at each airport, respectively. The daily evolution of aircraft emissions is added to the area source emissions estimated for the grid cells where each airport is located.

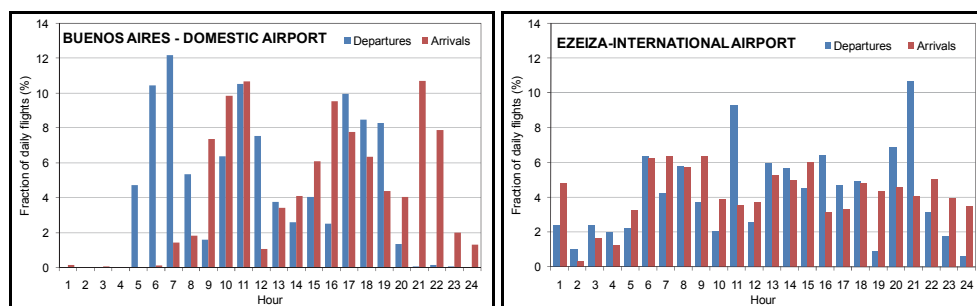


Fig. 6. Hourly distribution of the fraction (%) of mean daily departures and arrivals at the domestic and the international airports.

4.3 Emissions from fixed sources

The small size fixed sources (residential, commercial and small industries combustion activities) are considered as area sources. These sources consume natural gas for heating, cooking and other activities. The monthly natural gas consumed by residential houses was spatially distributed considering population density. Then, using the CO and NO_x emission factors for natural gas combustion for domestic heating units given in US.EPA (1995) residential emission rates at each grid cell are estimated. Considering monthly natural gas consumed by commercial activity, its spatial distribution in the MABA and the emission factors (US.EPA, 1995), CO and NO_x emission rates for this activity are computed for each grid cell. Finally, considering the monthly natural gas consumed by small industries, their spatial distribution in the MABA and the emission factors (US.EPA, 1995), CO and NO_x emission rates of this activity were estimated for each grid cell. Natural gas consumption and a typical diurnal variation of the consumption for each activity have been provided by the National Gas Administration (ENARGAS).

4.4 Carbon monoxide and nitrogen oxides emissions in the Metropolitan Area of Buenos Aires.

Annual area source emission rates estimated for the city of Buenos Aires (CBA) are 324.7 Gg-CO yr⁻¹ and 22.9 Gg-NO_x yr⁻¹ and for the Greater Buenos Aires (GBA) are 294.6 Gg-CO yr⁻¹ and 43.9 Gg-NO_x yr⁻¹. Therefore, for the Metropolitan Area of Buenos Aires (MABA) annual area source emissions result 619.3 Gg-CO yr⁻¹ and 66.8 Gg-NO_x yr⁻¹. Fig. 7 shows the percentage distribution of the annual emission of carbon monoxide and nitrogen oxides by source category in the MABA. Road traffic accounts for 99.4% of CO and 80.6% of NO_x annual area source emissions in the MABA.

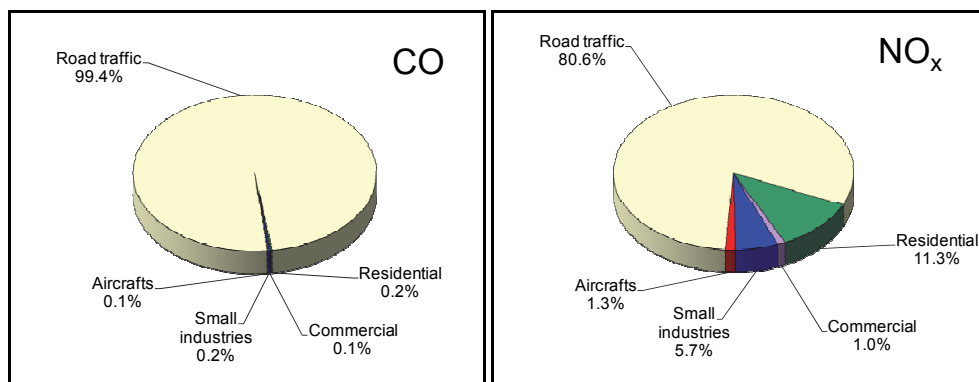


Fig. 7. Estimated annual area source emission of CO and NO_x by source category in the MABA.

The spatial distributions of CO and NO_x annual emission rates (in ton km⁻² yr⁻¹) from area sources within the MABA are shown in Fig. 8. The intensity of emissions varies considerably across the urban area. There is a wide range in CO and NO_x emissions between different grid cells depending on the density of road transportation sources in each grid cell. It is clear that high emission rates per unit area can be found in downtown of the city of Buenos Aires.

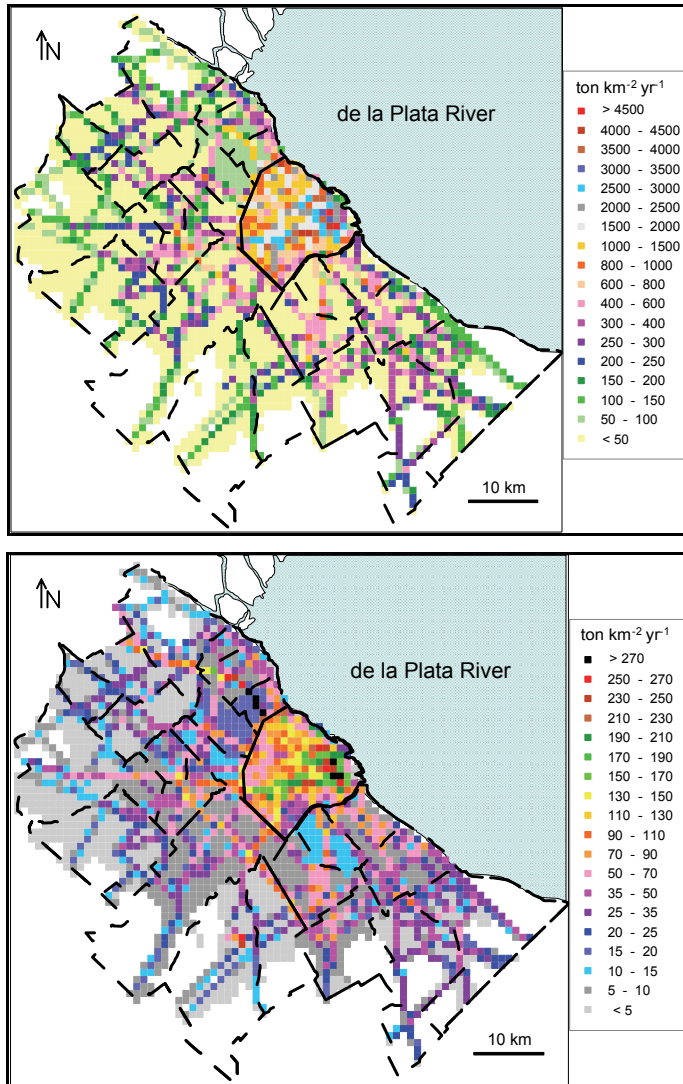


Fig. 8. Annual emission rates (ton km⁻² yr⁻¹) of CO (top) and NO_x (bottom) from area sources in the MABA. Grid resolution is 1 x 1 km.

4.5 Uncertainty assessment

Uncertainty is a statistical term that is used to represent the degree of accuracy and precision of data. It often expresses the range of possible values of a parameter or a measurement around a preferred value. Various approaches for representing uncertainty in the context of different domains are widely described (Azondèkon & Martel, 1999; Draper, 1995).

Emission inventories are based on assumptions that are needed to be made and statistical data. Real measurements are available for a few emission sources and/or for certain time

periods only. Therefore, uncertainty estimations are of importance and should always be foreseen (Sturm, 2003). However, it is not easy to assess uncertainty at the level of aggregated datasets. Information related to emissions and their uncertainties that originates from a few measurements has to be applied for a large number of sources. As the latter may differ strongly, even within the same category, the uncertainty increases as the emission inventory becomes more detailed. On a more aggregated level, averaging helps to improve the uncertainty situation (Sturm, 2003). There are different studies (Frey & Li, 2003; Frey & Zheng, 2002; Regan et al., 2003; Romano et al, 2004) done in differentiating and quantifying the contributions from uncertainty and natural variability to emission data. The reliability of the information provided by emission inventories is strongly biased by a wide range of causes. Particularly, when the emissions are estimated through emission factors the following points have to be taken into account: a) uncertainty related to the choice of the indicators, b) uncertainty related to the quantitative value of the indicators, c) uncertainty related to emission factors and d) uncertainty related to the structure of emission estimate models. In the MABA, the use of traffic flow values registered at several sites on different days to compute the average vehicle fleet in each road type, results in a mean error of approximately 20-30%. The uncertainty estimation of the average vehicle speed for different road types is found to be near 20%. These uncertainties may introduce an error in the selection of emission factors of about 20%. Other uncertainties may come from the spatial grid resolution. The estimation of travel distance along each road type in each grid cell has an error of 10-15%. The uncertainty of the spatial distribution of population density, commercial activity and small industries in each grid cell of the urban area is about 40%. In general, the error in the estimation of the emissions of carbon monoxide and nitrogen oxides in the MABA are expected to be around 40%.

5. Air pollutant concentration estimations

5.1 Brief description of the urban atmospheric dispersion model used

Urban background concentrations of CO and NO₂ in the Metropolitan Area of Buenos Aires have been estimated applying the urban atmospheric dispersion model DAUMOD(v.2) to the area sources described above. This model has been developed and introduced in former papers (Mazzeo & Venegas, 1991, 2010; Venegas & Mazzeo, 2002; 2006b). However, a brief description of its main considerations and assumptions is included below.

The DAUMOD model (Mazzeo & Venegas, 1991) is an urban atmospheric dispersion model valid for steady-state conditions. It is assumed that effluents are emitted continuously from the surface. The x-axis is in the direction of the mean wind and the z-axis is vertical. At a given distance, the vertical extension of the plume of contaminants is given by $h(x)$. Concentration at $h(x)$ is negligible and there is no transport of mass through the upper limit of the plume. The variation of $h(x)$ is parameterised in the model by potential functions given by (Mazzeo & Venegas, 1991),

$$\frac{h}{z_0} = a \left(\frac{x}{z_0} \right)^b \quad (3)$$

where z_0 is the surface roughness length and coefficients a and b depend on atmospheric stability (Mazzeo & Venegas, 2010). Other basic assumption included in the model is that

background air pollutant concentration $[C(x,z)]$ can be expressed by the following polynomial form:

$$C(x,z) = C(x,0) \sum_{j=0}^6 A_j \left(\frac{z}{h}\right)^j \quad (4)$$

Coefficients A_j ($j=0,\dots,6$) depend on surface roughness and atmospheric stability (Mazzeo & Venegas, 2010) and have been computed by fitting Equation (4) to the results given by the following expression (Pasquill & Smith, 1983):

$$C(x,z) = C(x,0) \exp\left[-4.605 \left(\frac{z}{z_m}\right)^s\right] \quad (5)$$

where s is a shape factor which depends on atmospheric stability and surface roughness (Gryning et al., 1987) and z_m is the height at which concentration is $0.01C(x,0)$. The height z_m is usually considered to be the upper limit of the plume, so it is assumed $h = z_m$. Considering different atmospheric stability conditions, the coefficients (A_0, A_1, \dots, A_6) of the polynomial of grade 6 are obtained for each fitting. There are excellent fittings of polynomial forms (given by Equation (4)) to values obtained from Equation (5), with coefficients of determination of ≈ 1.0 (the reader can find details of these results in Mazzeo & Venegas, 1991).

In an urban area, a horizontal distribution of area sources with strength varying according to a typical square grid pattern may be assumed. Each grid square has a uniform source strength Q_i ($i = 0, 1, 2, \dots, N$) expressed as mass per unit area per unit time. According to the DAUMOD model $C(x,z)$ can be estimated by:

$$C(x,z) = \frac{a \left[Q_0 x^b + \sum_{i=1}^N (Q_i - Q_{i-1})(x - x_i)^b \right]}{\left(|A_1| k_v z_0^b u_* \right)} \sum_{j=0}^6 A_j \left(\frac{z}{h}\right)^j \quad (6)$$

where k_v is the von Kármán's constant and u_* is the friction velocity.

A constant wind direction is required for application of Equations (6). It has been noted from the applications of Equation (6) that estimated concentration at any receptor is mainly originated from the emission in the grid square in which the receptor is located. This is because area source distributions in a city are generally quite smooth and, the contribution of upstream grid squares (from Equation (6)) rapidly reduces with distance to the receptor. The simplification of assuming that the uniform area source strength Q_i only varies with x (in the wind direction), suppose to consider a "narrow plume" hypothesis. This assumption has also been included in other simple urban dispersion models (Arya, 1999; Gifford, 1970; Gifford & Hanna, 1973). The spatial resolution of the model calculations is given by the resolution of the area source emission inventory.

The performance of DAUMOD model in estimating concentrations has been evaluated comparing estimated and observed concentration data from several cities. Results for Bremen (Germany), Frankfurt (Germany) and Nashville (USA) have been reported in

Mazzeo & Venegas (1991) and for Copenhagen (Denmark) can be found in Venegas & Mazzeo (2002). The comparison of DAUMOD estimations of background air pollutant concentrations with observations in the city of Buenos Aires can be found in Venegas & Mazzeo (2006b). Results show that the performance of the model in estimating short-term concentrations (hourly and daily) is good and it improves when estimating long averaging time values (monthly and annual). Several applications of different versions of DAUMOD to Buenos Aires have been reported in former papers (Mazzeo & Venegas, 2004, 2008, 2010; Mazzeo et al., 2010; Pineda Rojas & Venegas, 2008, 2009, 2010; Venegas & Mazzeo, 2005, 2006a; 2006b).

At present, photochemical transformations involving NO, NO₂ and O₃ are not included in DAUMOD model. However, DAUMOD(v.2) estimates concentrations of NO₂ on the basis of an empirical relationship between NO₂ and NO_x (Derwent & Middleton, 1996; Dixon et al., 2001; Middleton et al., 2008). The concentration of NO₂ is calculated using the polynomial expression (CERC, 2003; Derwent & Middleton, 1996):

$$[\text{NO}_2] = 2.166 - [\text{NO}_x] (1.236 - 3.348 B + 1.933 B^2 - 0.326 B^3)$$

where $B = \log_{10}([\text{NO}_x])$ and $[\text{NO}_x]$ is hourly-averaged concentration in ppb.

An application of DAUMOD(v.2) to estimate the influence of NO_x emitted from area sources in the Metropolitan Area of Buenos Aires on the air quality of the city of Buenos Aires have been reported in Venegas & Mazzeo (2007).

5.2 Application of DAUMOD model to area source emissions in the Metropolitan Area of Buenos Aires

The DAUMOD(v.2) model is applied to area source emissions in the MABA, to estimate hourly ground level background concentrations of CO and NO₂ in the area. Calculations are performed considering three years of hourly meteorological information registered at the weather stations of the Argentine Meteorological Office located at the domestic airport (in the city of Buenos Aires) and at the international airport (in the Greater Buenos Aires, 30 km southwest the city of Buenos Aires). The spatial resolution used in calculations is 1x1 km.

One consideration to take into account is that this modelling approach does not produce 3-dimensional wind fields, so land-sea breezes are not modelled. Breeze circulations over the wide estuary of the river could bring pollutants back to the receptor area. However, the frequency of atmospheric recirculation events over the city is small: 8% in summer, 7% in autumn, 5% in winter and 7% in spring (Venegas & Mazzeo 1999). In this way, it is expected that this modelling limitation will not significantly affect the results.

5.2.1 Concentrations of CO in the MABA

Three years of hourly and running 8-h average ground level CO concentrations are estimated for the entire MABA. As expected, estimated CO concentration values are higher in the city of Buenos Aires than in the Greater Buenos Aires.

Hourly CO concentrations are all below the air quality standard value of 35ppm (Res. 198/06 city of Buenos Aires and Res. 242/97 Province of Buenos Aires). The highest hourly concentration value resulted 25.7ppm and appeared at downtown of the city of Buenos Aires. In order to illustrate the spatial distribution of CO concentration in the MABA, Fig. 9 shows the computed hourly CO concentrations at rush hour in the evening (20:00), averaged over the three years.

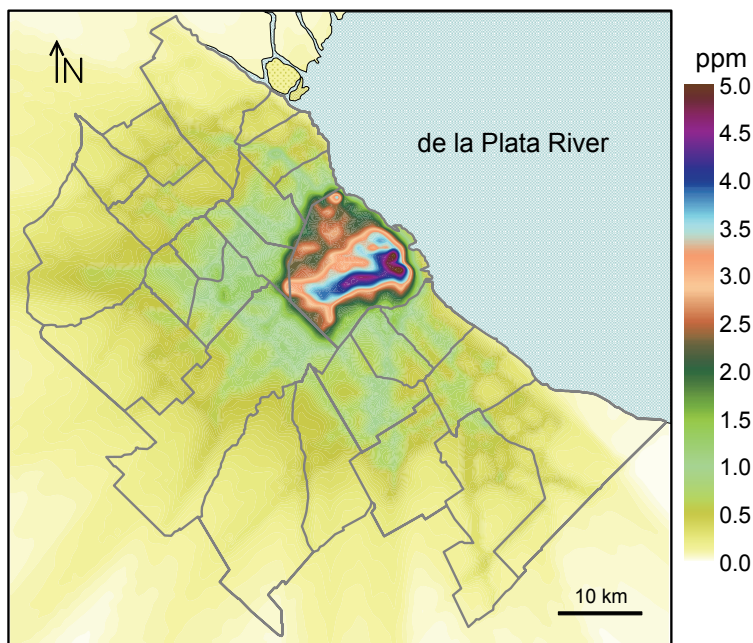


Fig. 9. Mean hourly ground level CO concentrations for rush hour in the evening (20:00)

Also, as an example, the spatial distribution of mean (three years average) running 8-h average ground level CO concentrations in the MABA for the period 08:00-16:00 is shown in Fig. 10. The highest running 8-h average CO concentration (C_{8h}) estimated for the three years is 16.1ppm. This value is greater than the air quality standard value (9ppm) established for the MABA. However, as can be seen in Fig. 11, the highest mean annual frequency of $C_{8h} > 9\text{ppm}$ at one grid cell reaches 118 cases and appears in the downtown area of the CBA. This value represents the 1.3% of the annual cases of running 8-h average concentrations. Therefore, the air quality regulation for the CBA (Res. 198/06) is accomplished as it requires that 98th percentile of annual cases (considering three years) should be below 9ppm. The analysis of the situations with $C_{8h} > 9\text{ppm}$ reveals that 41% of these cases affect areas of 1km² (Fig.12). Only in 10% of the cases the extension of the affected areas is between 16-35 km².

Fig. 13 shows the frequency distribution of the running 8-h average CO concentrations greater than 9ppm obtained during the three years according to the end hour of the 8-h period. Most exceedances are associated to high emission values during the evening (when most people returns home) and nocturnal atmospheric conditions (low wind speed, neutral or stable atmospheric stability). Monthly distribution of the estimated running 8-h average CO concentrations greater than 9ppm is included in Fig.14. These situations are more frequent between May and August, during late autumn and winter.

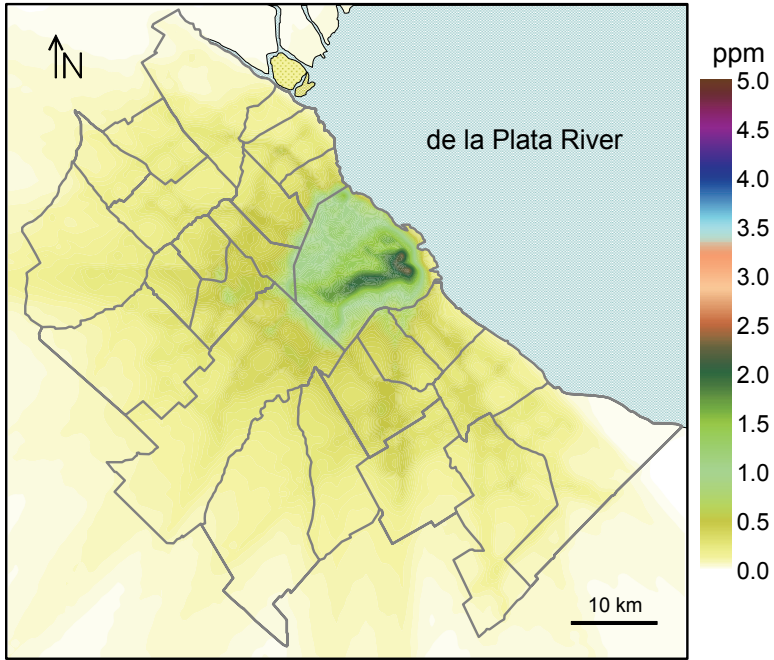


Fig. 10. Estimated mean running 8-h average ground level CO concentrations (period: 08:00-16:00)

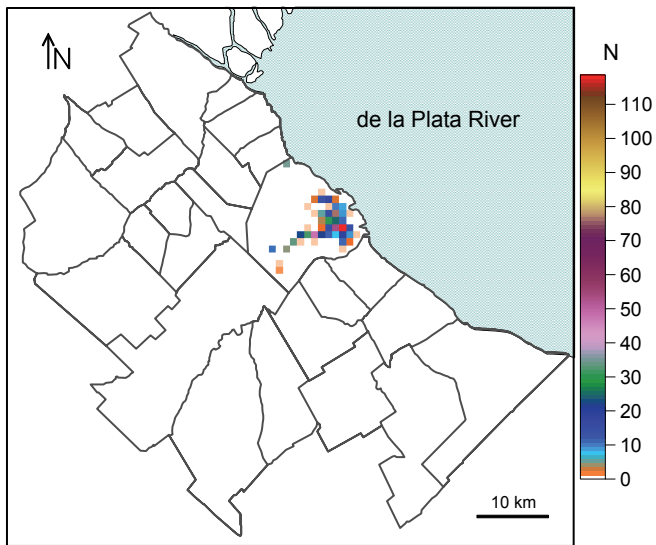


Fig. 11. Annual mean number of cases with running 8-h average CO concentration greater than 9ppm.

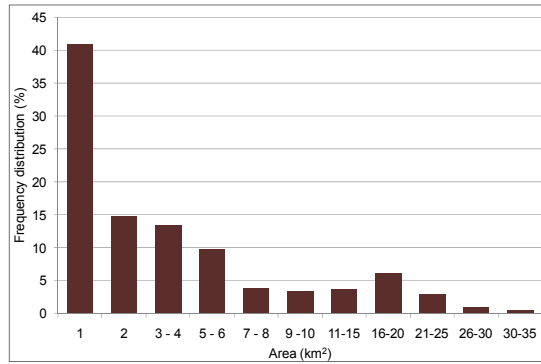


Fig. 12. Frequency distribution of the affected area (km²) of the situations with running 8-h average CO concentration greater than 9ppm.

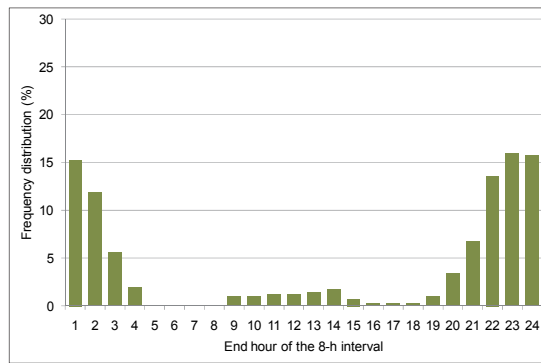


Fig. 13. Daily distribution of estimated running 8-h average CO concentrations greater than 9ppm.

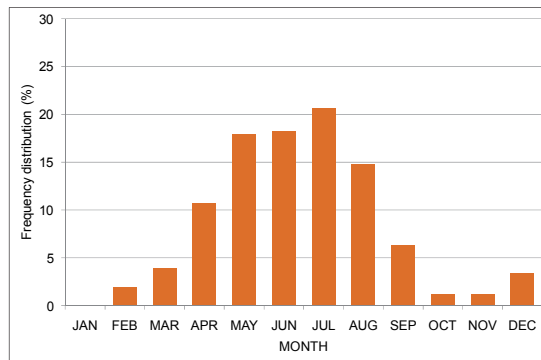


Fig. 14. Monthly distribution of estimated running 8-h average CO concentrations greater than 9ppm.

5.2.2 Concentrations of NO₂ in the MABA

Three years of hourly NO₂ ground level concentrations are estimated for the whole MABA. The higher NO₂ concentration values are obtained at downtown of the city of Buenos Aires and along the highways of the Metropolitan Area of Buenos Aires. The highest hourly NO₂ concentration estimated in the three years period is 184ppb, at downtown. Hourly concentrations are below the air quality standard (200ppb) for the city of Buenos Aires (Res. 198/06, city of Buenos Aires) and for the Greater Buenos Aires (Res.242/97, Province of Buenos Aires). The spatial distribution of the mean hourly NO₂ concentrations for the rush hour in the evening is shown in Fig. 15. These results are the hourly values obtained for 20:00 averaged over the three years.

The spatial distribution of annual mean NO₂ concentrations in the MABA is included in Fig. 16. The concentration distribution pattern shows a large spatial variability across the urban area. Different areas with high concentration values can be identified, as highways, areas with dense traffic and close to the airports. NO₂ annual concentration may reach 28ppb downtown. All values are below the air quality standard (53ppb) for the CBA (Res. 198/06, city of Buenos Aires) and for the GBA (Res. 242/97, Province of Buenos Aires).

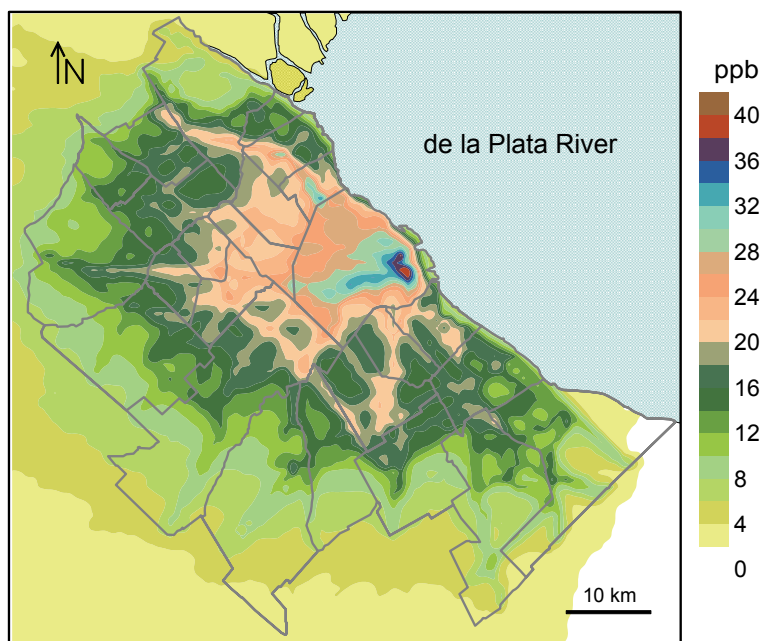


Fig. 15. Mean hourly ground level NO₂ concentrations for rush hour in the evening (20:00)

As mentioned above, model results indicate that NO₂ hourly background concentrations may exceed the air quality guideline proposed by the World Health Organisation (100ppb) (WHO, 2006b) at some places in the MABA. The mean annual number of hourly NO₂ concentrations that exceed 100ppb at each grid cell is shown in Fig. 17. Most exceedances occur in the city of Buenos Aires, where they may reach a maximum of 50 cases per year at one grid cell located downtown. In the Greater Buenos Aires, hourly NO₂ concentrations

greater than 100ppb have been obtained in the Northern and Southern highways. These highways constitute two main entrances to the CBA. Also, exceedances are obtained close to the international airport located in the GBA, approximately 30km southwest the CBA.

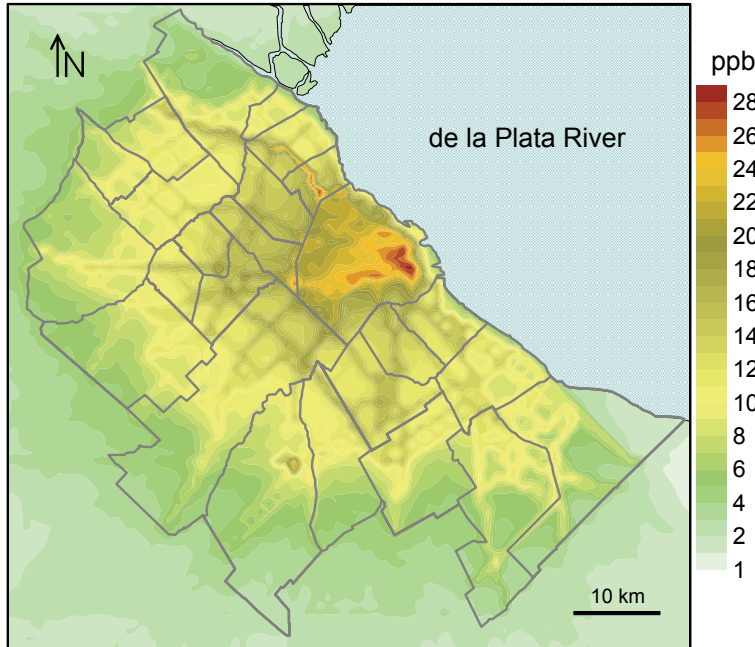


Fig. 16. Annual mean ground level NO₂ concentrations.

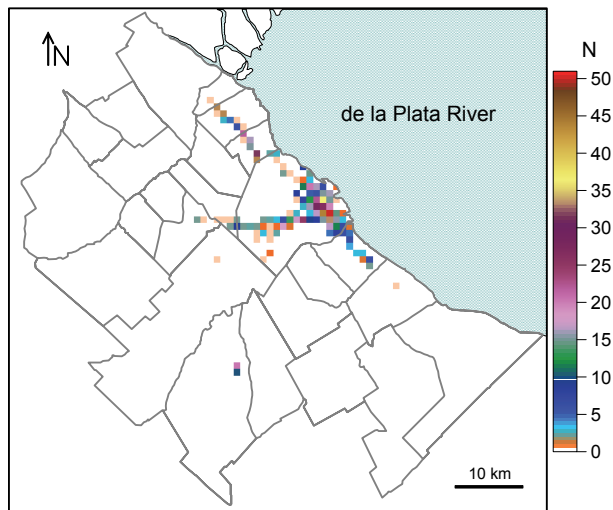


Fig. 17. Annual mean number of hourly NO₂ concentrations greater than 100ppb.

The analysis of the situations with hourly NO₂ concentrations greater than 100ppb obtained in the three years, reveals that the extension of the affected area is 1km² in 29% of the cases but it may reach a maximum of 43km² (1%) (Fig. 18). As shown in Fig. 19, high values of hourly NO₂ concentrations are obtained mainly during rush hours in the morning (07:00 to 09:00) and the evening (18:00 to 22:00). The frequency of values greater than 100ppb is higher in the evening/night than in the morning. High vehicle emissions and reduced atmospheric dispersion conditions are responsible for this result. Situations with hourly NO₂ concentrations greater than 100ppb in the MABA are more frequent from May to August (Fig. 20).

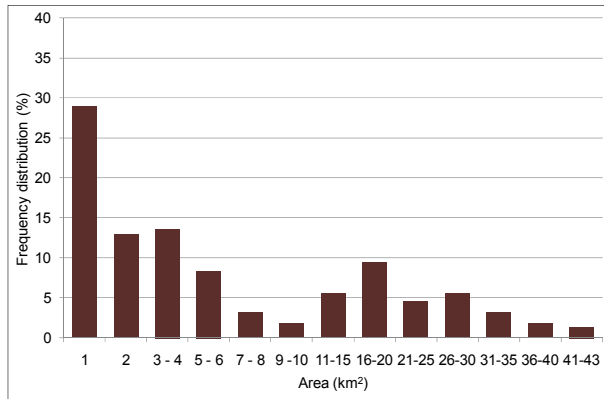


Fig. 18. Frequency distribution of affected areas (km²) with hourly NO₂ concentrations greater than 100ppb.

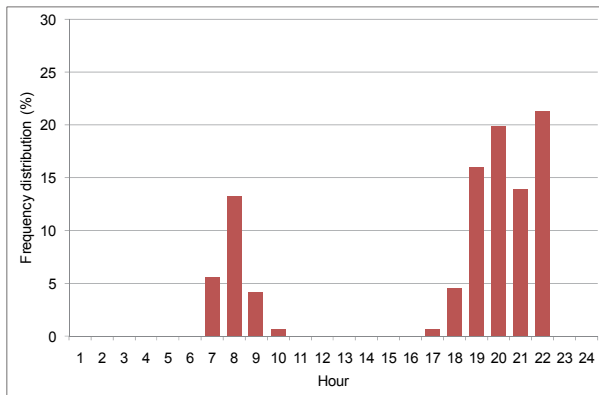


Fig. 19. Daily distribution of hourly NO₂ concentrations greater than 100ppb.

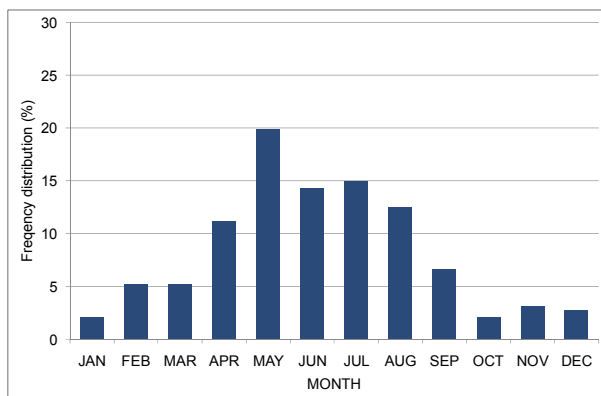


Fig. 20. Monthly distribution of hourly NO_2 concentrations greater than 100ppb.

6. Summary

This chapter presents the results of a high spatial and temporal resolution version of the area source emission inventory of carbon monoxide (CO) and nitrogen oxides (NO_x), and the evaluation of the air quality in the Metropolitan Area of Buenos Aires (MABA). The inventory includes mobile sources (passenger cars/taxis, buses and aircrafts) and fixed sources (emissions arising from residential, commercial and industrial buildings). Its main originality is that it deals as much as possible with distinctive on-road traffic features in order to describe more accurately the emission distribution at a scale comparable to that of the air quality models. The emission inventory for the Metropolitan Area of Buenos Aires can be characterised by the presence of an important contribution of CO and NO_x emitted from mobile sources. Mobile sources contribute with 99.4% of CO and 80.6% of NO_x annual emissions of area sources in the MABA. Annual area source emission rates estimated for the city of Buenos Aires are 324.7 Gg-CO yr^{-1} and 22.9 Gg- NO_x yr^{-1} and for the Greater Buenos Aires are 294.6 Gg-CO yr^{-1} and 43.9 Gg- NO_x yr^{-1} . Therefore, for the MABA annual area source emissions result 619.3 Gg-CO yr^{-1} and 66.8 Gg- NO_x yr^{-1} . Spatial distributions of carbon monoxide and nitrogen oxides emissions show an appreciable variation across the MABA. The urban atmospheric dispersion model DAUMOD is applied to evaluate the air quality in the MABA due to the contribution of area source emissions in the urban area. Estimations of horizontal distributions of CO and nitrogen dioxide (NO_2) background concentrations in the MABA are presented. Air quality regulations established for CO and NO_x in the MABA are accomplished. The analysis of running 8-h average CO concentrations greater than 9ppm reveals that 41% of these cases affect areas of 1km². Only in 10% of these cases the affected areas show extensions between 16-35 km². Model results indicate that NO_2 hourly background concentrations may exceed the air quality guideline proposed by the World Health Organisation at some places in the MABA. Most exceedances occur in the city of Buenos Aires, where they may reach a maximum of 50 cases per year at one grid cell located downtown. In the Greater Buenos Aires, hourly NO_2 concentrations greater than the air quality guideline have been obtained in the Northern and Southern highways. The analysis of the situations with hourly NO_2 concentrations greater than the air quality guideline reveals that the extension of the affected area is 1km² in 29% of the cases but it may reach a maximum of 43km² (1%).

7. Acknowledgements

The authors kindly acknowledge the support given by ENARGAS, the National Secretary of Transportation, the Buenos Aires city Government and the Secretary of Transportation of the Province of Buenos Aires on providing valuable information on fuel and gas consumptions and traffic flow patterns. The support from the National Scientific and Technological Research Council of Argentina (CONICET) is also acknowledged

8. References

- Andrade, M.F.; Miranda, R.M.; Fornaro, A.; Kerr, A.; Oyama, B.; Andre, P.A. & Saldiva, P. (2010). Vehicle emissions and PM_{2.5} mass concentrations in six Brazilian cities. *Air Quality Atmosphere & Health*. DOI 10.1007/s11869-010-0104-5.
- Ariztegui, J.; Casanova, J. & Valdes, M. (2004). A structured methodology to calculate traffic emissions inventories for city centres. *The Science of the Total Environment*, Vol. 334-335, pp. 101-109.
- Arkouli, M.; Ulke, A.G.; Endlicher, W.; Baumbach, G.; Schultz, E.; Vogt, U.; Müller, M., Dawidowski, L.; Faggi, A.; Wolf-Benning, U. & Scheffknecht, G. (2010). Distribution and temporal behaviour of particulate matter over the urban area of Buenos Aires, *Atmospheric Pollution Research*, Vol. 1, pp.1-8.
- Arya, S. P. (1999). *Air Pollution Meteorology*. Oxford University Press. New York.
- Azondèkon, S.H. & Martel, J.M. (1999). "Value" of additional information in multi-criterion analysis under uncertainty. *European Journal of Operational Research*, Vol. 117, pp.45-62.
- Ball, D.J. & Radcliffe, S.W. (1979). *An inventory of sulfur dioxide emissions to London's air*. Research Report 23. Greater London Council, London.
- Beaton, S.P.; Bishop, G.A. & Stedman, D.H. (1992). Emission characteristics of Mexico City vehicles. *Journal Air & Waste Management Association*, Vol. 42, pp.1424-1429.
- Berkowicz, R. (2000). A simple model for urban background pollution. *Environmental Monitoring and Assessment*, Vol. 65, pp.259-267.
- Bocca, B.; Caimi, S.; Smichowski, P.; Gómez, D. & Cairoli, S. (2006) Monitoring Pt and Rh in urban aerosols from Buenos Aires, Argentina. *The Science of the Total Environment*, Vol. 358, pp. 255-264.
- Bogo, H.; Negri, R.M. & San Román, E. (1999). Continuous measurement of gaseous pollutants in Buenos Aires City. *Atmospheric Environment*, Vol. 33, pp.2587-2598.
- Bogo, H.; Gómez, D. R.; Reich, S. L.; Negri, R. M. & San Román, E. (2001). Traffic pollution in downtown of Buenos Aires City. *Atmospheric Environment*, Vol. 35, pp.1717-1727.
- Bogo, H.; Otero, M.; Castro, P.; Ozafrán, M. J.; Kreiner, A.; Calvo, E. J. & Negri, R. M. (2003). Study of atmospheric particulate matter in Buenos Aires city. *Atmospheric Environment*, Vol. 37, pp.1135-1147.
- Borrego, C.; Tchepel, O.; Costa, A.M.; Amorim, J.H. & Miranda, A.I. (2003). Emission and dispersion modelling of Lisbon air quality at local scale. *Atmospheric Environment*, Vol. 37, pp. 5197-5205.
- Butler, T.M.; Lawrence, M.G.; Gurjar, B.R.; van Aardenne, J.; Schultz, M. & Lelieveld, J. (2008). The representation of emissions from megacities in global emission inventories. *Atmospheric Environment*, Vol. 42, pp.703-719.

- Carruthers, D.J.; Holroyd, R.J.; Hunt, J.C.R.; Weng, W.S.; Robins, A.G.; Ashley, D.D.; Thompson, D.J. & Smith, F.B. (1994). UK-ADMS: a new approach to modelling dispersion in the earth's boundary layer. *Journal of Wind Engineering*, Vol. 52, pp. 139-153.
- CERC (2003). *ADMS-Urban. An Urban Air Quality Management System. User Guide. Version 2.0*. Cambridge Environmental Research Consultants Ltd., Cambridge.
- D'Avignon, A.; Carloni, F.A.; Rovere, E.L.L. & Dubeux, C.B.S. (2010). Emission inventory: An urban public policy instrument and benchmark. *Energy Policy*, Vol. 38, pp.4838-4847.
- Derwent, R.G. & Middleton, D.R. (1996). An empirical function for the ratio $\text{NO}_2:\text{NO}_x$. *Clean Air*, Vol. 26, pp. 57-62.
- Dixon, J.; Middleton, D.R. & Derwent, R.G. (2001). Sensitivity of nitrogen dioxide concentrations to oxides of nitrogen controls in the United Kingdom. *Atmospheric Environment*, Vol. 35, pp. 3715-3728.
- Draper, D. (1995). Assessment and propagation of model uncertainty. *Journal of Royal Statistical Society*, Vol. 57, pp.45-97.
- European Environment Agency. (2001). *Joint EMEP/CORINAIR Atmospheric Emission Inventory Guidebook*, Third Edition, Copenhagen.
- Fagundez, L.A.; Fernández V.L.; Marino T.H.; Martín I.; Persano D.A.; Rivarola y Benítez M.; Sadañowski I.V.; Codnia J. & Zalts A. (2001). Preliminary air pollution monitoring in San Miguel, Buenos Aires. *Environmental Monitoring and Assessment*, Vol. 71, pp. 61-70.
- Frey, H.C. & Zheng, J. (2002). Quantification of variability and uncertainty in utility NO_x emission inventories. *Journal Air & Waste Management Association*, Vol. 52, pp.1083-1095.
- Frey, H.C. & Li, S. (2003). Methods for quantifying variability and uncertainty in AP-42 emission factors: case studies for natural gas-fueled engines. *Journal of Air & Waste Management Association*, Vol. 53, pp. 1436-1447.
- GCBA (2006) *Informes sobre Índice de Tránsito*. (Período 2004-2006). Gobierno de la Ciudad de Buenos Aires. Buenos Aires. (in Spanish).
- Gifford, F.A. (1970). *Atmospheric Diffusion in an Urban Area*, NOAA Research Lab. N° 33. Oak Ridge, N. C.
- Gifford, F.A. & Hanna, S.R. (1973). Modelling urban air pollution. *Atmospheric Environment*, Vol. 7, pp. 131-136.
- Gryning, S.E.; Fookslog, A.A.M.; Irwin, J.S. & Sivertsen, B. (1987). Applied dispersion modelling based on meteorological scaling parameters. *Atmospheric Environment*, Vol. 21, pp. 79-89.
- Gurjar, B.R.; Butler, T.M.; Lawrence, M.G. & Lelieveld, J. (2008). Evaluation of emissions and air quality in megacities. *Atmospheric Environment*, Vol. 42, pp. 1593-1606.
- Hanna, S.; Britter, R. & Franzese, P. (2002). Simple screening models for urban dispersion. *Proceedings of the 8th International Conference on Harmonisation within Atmospheric Dispersion Modelling for Regulatory Purposes*, Sofia, Bulgaria, October 2002.
- Harte, J.; Holdren, C.; Schneider, R. & Shirley C. (1991). *Toxics A to Z. A guide to everyday pollution hazards*. The Regents of the University of California. USA.

- INDEC. (2010). *Censo Nacional de Población, Hogares y Viviendas 2010: total del país, resultados provisionales*. 1a edición. Buenos Aires. Instituto Nacional de Estadística y Censos. (in Spanish).
- JICA-SAYDS, (2002). *Estudio o línea de base de concentración de gases contaminantes en atmósfera en el área de Dock Sud en Argentina*. Agencia de Cooperación Internacional del Japón en Argentina-Sec. de Desarrollo Sustentable y Política Ambiental. Informe Final. (in Spanish).
- Karppinen, A.; Kukkonen, J.; Elolähde, T.; Konttinen, M.; Koskentalo, T. & Rantakrans, E. (2000). A modelling system for predicting urban air pollution: model description and applications in the Helsinki metropolitan area. *Atmospheric Environment*, Vol. 34, pp. 3723-3733
- Kim, Y.J. (1996). Preparation of Emissions Inventories and Establishment of the National Emission Inventory System of Air Pollutants in Korea. *Proceedings of the Conference on the Emissions Inventory: Programs & Progress*, Research Triangle Park, NC, Pittsburg, June 1996, pp. 683-686.
- Mazzeo, N.A. & Venegas, L.E. (1991). Air pollution model for an urban area. *Atmospheric Research*, Vol. 26, pp. 165-179.
- Mazzeo, N.A. & Venegas, L.E. (2002). Estimation of cumulative frequency distribution for carbon monoxide concentration from wind-speed data in Buenos Aires (Argentina). *Water, Air and Soil Pollution, Focus*, Vol. 2, pp. 419-432.
- Mazzeo, N.A. & Venegas, L.E. (2003). Carbon monoxide and nitrogen oxides emission inventory for Buenos Aires City (Argentina). *Proceedings of the 4th International Conference on Urban Air Quality – Measurement, Modelling and Management*, Prague, Czech Republic, March 2003. pp. 159-162.
- Mazzeo, N.A. & Venegas, L.E. (2004). Some aspects of air pollution in Buenos Aires City (Argentina). *International Journal of Environment and Pollution*, Vol. 22, pp. 365-378.
- Mazzeo, N.A. & Venegas, L.E. (2008). Design of an air quality surveillance system for Buenos Aires city integrated by a NO_x monitoring network and atmospheric dispersion models. *Environmental Modelling & Assessment*, Vol. 13, pp. 349-356.
- Mazzeo, N.A. & Venegas, L.E. (2010). Chapter 2: Development and application of a methodology for designing a multi-objective and multi-pollutant air quality monitoring network for urban areas. In: *Air Quality*, A. Kumar (Ed.), pp. 23-47, Sciyo, Rijeka, Croatia. www.sciyo.com
- Mazzeo, N.A.; Venegas, L.E. & Choren, H. (2005). Analysis of NO, NO₂, O₃ and NO_x concentrations measured at a green area of Buenos Aires City during wintertime, *Atmospheric Environment*, Vol. 39, pp. 3055-3068.
- Mazzeo, N.A.; Pineda Rojas, A.L. & Venegas, L.E. (2010). Carbon monoxide emitted from the city of Buenos Aires and transported to neighbouring districts, *International Journal of Latin American Applied Research*, Vol.40, pp. 267-273.
- McHugh, C.A.; Carruthers, D.J. & Edmunds, H.A. (1997). ADMS-Urban: An air quality management system for traffic, domestic and industrial pollution. *International Journal of Environment & Pollution*, Vol. 8, pp.437-440.
- Middleton, D.R.; Jones, A.R.; Redington, A.L.; Thomson, D.J.; Sokhi, R.S.; Luhana, L. & Fisher, B.E.A. (2008). Lagrangian modelling of plume chemistry for secondary pollutants in large industrial plumes. *Atmospheric Environment*, Vol. 42, pp. 415-427.

- Miller, C.A.; Hidy, G.; Hales, J.; Kolb, C.E.; Werner, A.S., Haneke, B.; Parrish, D.; Frey H.C.; Rojas-Bracho, L.; Deslauriers, M.; Pennell, B. & Mobley, J.D. (2006). Air emission inventories in North America: a critical Assessment. *Journal Air & Waste Management Association*. Vol. 56, pp.1115-1129.
- Mohan, M; Dagar, L. & Gurjar, B.R. (2007). Preparation and Validation of Gridded Emission Inventory of Criteria Air Pollutants and Identification of Emission Hotspots for Megacity Delhi. *Environmental Monitoring & Assessment*, Vol. 130, pp. 323-339.
- Morris, R.E. & Myers, T.C. (1990). *User's Guide to the Urban Airshed Model*, Vol. I-V. U.S. Environmental Protection Agency, Research Triangle Park, NC.
- Nishikawa, Y. & Kannari, A. (2010). Atmospheric concentration of ammonia, nitrogen dioxide, nitric acid and sulphur dioxide by passive method within Osaka Prefecture and their emission inventory. *Water, Air & Soil Pollution*. Vol. 215, pp. 229-237.
- Olesen, H.R. (1995). Regulatory dispersion modelling in Denmark. *International Journal of Environment and Pollution*, Vol. 5, pp.412-417.
- Pasquill, F. & Smith, F.B. (1983). *Atmospheric Diffusion*, John Wiley & Sons, New York.
- Pineda Rojas, A.L.; Venegas, L.E. & Mazzeo, N.A. (2007). Emission inventory of carbon monoxide and nitrogen oxides for area sources at Buenos Aires Metropolitan Area (Argentina). *Proceedings of the 6th International Conference on Urban Air Quality*, Limassol, Cyprus, March 2007.
- Pineda Rojas, A.L. & Venegas, L.E. (2008). Dry and wet deposition of nitrogen emitted in Buenos Aires city to waters of de la Plata river. *Water, Air and Soil Pollution*, Vol. 193, pp. 175-188.
- Pineda Rojas, A.L. & Venegas, L.E. (2009). Atmospheric deposition of nitrogen emitted in the Metropolitan Area of Buenos Aires to coastal waters of de La Plata River, *Atmospheric Environment*, Vol. 43, pp. 1339-1348.
- Pineda Rojas, A.L. & Venegas, L.E. (2010). Interannual variability of estimated monthly nitrogen deposition to coastal waters due to variations of atmospheric variables model input, *Atmospheric Research*, Vol. 96, pp. 88-102.
- Regan, H.M.; Akcakaya, H.R.; Ferson, S.; Root, K.V.; Carroll, S. & Ginzburg, L.R. (2003). Treatments of uncertainty and variability in ecological risk assessment of single-species populations. *Human and Ecological Risk Assessment*, Vol. 9, pp. 4-12.
- Rideout, G.; Gourley, D. & Walker, J. (2005). *Measurement of in-service vehicle emissions in Sao Paulo, Santiago and Buenos Aires*. ARPEL Environmental Report #25. Ottawa. ESAA. Canada.
- Romano, D.; Gaudioso, D. & De Lauretis, R. (1999). Aircraft emissions: a comparison of methodologies based on different data availability. *Environmental Monitoring & Assessment*, Vol. 56, pp. 51-74.
- Romano, D.; Bernetti, A. & De Lauretis, R. (2004). Different methodologies to quantify uncertainties of air emissions. *Environmental International*, Vol. 30, pp. 1099-1107.
- Saija, S. & Romano, D. (2002). A methodology for estimation of road transport air emissions in urban areas of Italy. *Atmospheric Environment*, Vol. 36, pp. 5377-5383.
- Sallés, J.; Janischewski, J.; Jaecker-Voirol, A. & Martin, B. (1996). Mobile source emission inventory model. Application to Paris area. *Atmospheric Environment*, Vol. 30, pp. 1965-1975.

- Seika, M.; Metz, N. & Harrison, R.M. (1996). Characteristics of urban and state emissions inventories- a comparison of examples from Europe and the United States. *The Science of the Total Environment*, Vol. 189/190, pp.221-234.
- Sturm, P.J.; Sudy, Ch.; Almbauer R. A. & Meinhart, J. (1999). Updated urban emission inventory with a high resolution in time and space for the city of Graz. *The Science of the Total Environment*, Vol. 235, pp.111-118.
- Sturm, P.J. (2003). Air Pollutants Emissions in Cities. In Moussiopoulos N. (Ed). *Air Quality in Cities*. Saturn. EUROTRAC-2. Subproject Final Report. Springer.
- Tsilingiridis, G.; Zachariadis, T. & Samaras, Z. (2002). Spatial and temporal characteristics of air pollutant emissions in Thessaloniki, Greece: investigation of emission abatement measures. *The Science of the Total Environment*, Vol. 300, pp. 99-113.
- US.EPA. (1995). *Compilation of Air Pollution Emission Factors*, AP-42, 5th ed., United States Environmental Protection Agency, Office of Air Quality Planning and Standards, Research Triangle Park, NC.
- Venegas, L.E. & Mazzeo, N.A. (1999). Atmospheric stagnation, recirculation and ventilation potential of several sites in Argentine, *Atmospheric Research*, Vol. 52, pp. 43-57.
- Venegas, L.E. & Mazzeo, N.A. (2000). Carbon monoxide concentrations in a street canyon at Buenos Aires City (Argentina). *Environmental Monitoring & Assessment*, Vol. 65, pp. 417-424.
- Venegas, L.E. & Mazzeo, L.E. (2002). An Evaluation of DAUMOD Model in Estimating Urban Background Concentrations. *Water, Air and Soil Pollution: Focus*, Vol. 2, 5-6, pp. 433-443
- Venegas, L.E. & Mazzeo, N.A. (2003). Air quality in an area of Buenos Aires City (Argentina), *Proceedings of the III Congresso Interamericano de Qualidade do Ar, Canoas, Brasil, July 2003*. (in Spanish).
- Venegas, L.E. & Mazzeo, N.A. (2005). Application of atmospheric dispersion models to evaluate population exposure to NO₂ concentration in Buenos Aires. *International Journal of Environment and Pollution*, Vol. 25, pp. 224-238.
- Venegas, L.E. & Mazzeo, N.A. (2006a). Air Quality Monitoring Network Design to Control PM₁₀ in Buenos Aires. *International Journal of Latin American Applied Research*, Vol. 36, pp. 241-247.
- Venegas, L. E. & Mazzeo, N. A. (2006b). Modelling of urban background pollution in Buenos Aires city (Argentina). *Environmental Modelling & Software*, Vol. 21, pp. 577-586.
- Venegas, L.E. & Mazzeo, N.A. (2007). Influence of surrounding areas and wind on air quality of Buenos Aires City. *Proceedings of the 11th International Conference on Harmonisation within Atmospheric Dispersion Modelling for Regulatory Purposes*, Vol. 2, Cambridge, UK, July 2007, pp. 327-331.
- Venegas, L.E. & Mazzeo, N.A. (2010a). An ambient air quality monitoring network for Buenos Aires city. *International Journal of Environment and Pollution*, Vol.40, pp. 184-194.
- Venegas, L.E. & Mazzeo, N.A. (2010b). Air quality at different sites in the city of Buenos Aires. *Proceedings of the A&WMA International Specialty Conference. Leapfrogging Opportunities for Air Quality Improvement*, Xi'an, China, May 2010, pp.175-180.
- Vogt, U.; Endlicher, W.; Baumbach, G.; Schultz, E.; Dawidowski, L.; Arkouli, M.; Müller, M.; Wolf-Benning, U. & Ulke, G. (2007). Air quality and urban climate investigations in

- the megacity of Buenos Aires. *Proceedings of the 6th International Conference on Urban Air Quality, Emissions Measurements and Modelling*, Limassol, Cyprus, March 2007.
- Wang, H.; Fu, L.; Zhou, Y.; Du X. & Ge, W. (2010). Trends in vehicular emissions in China's mega cities from 1995 to 2005. *Environmental Pollution*, Vol. 158, pp. 394-400.
- WHO. (2006a). *Air quality guidelines. Global update 2005*. World Health Organization.
- WHO. (2006b). *WHO Air quality guidelines for particulate matter, ozone, nitrogen dioxide and sulfur dioxide. Global update 2005*. World Health Organization. WHO/SDE/PHE/OEH/06.02. Geneva. 20pp
- Zárate, E.; Belalcázar, L.C.; Clappier, A.; Manzi, V. & Van den Bergh, H. (2007). Air quality modelling over Bogota, Colombia: Combined techniques to estimate and evaluate emission inventories. *Atmospheric Environment*, Vol. 41, pp. 6302-6318.

Variation of Greenhouse Gases in Urban Areas-Case Study: CO₂, CO and CH₄ in Three Romanian Cities

Iovanca Haiduc and Mihail Simion Beldean-Galea
*Babeş-Bolyai University, Faculty of Environmental Science,
 Cluj-Napoca,
 Romania*

1. Introduction

The natural equilibrium of atmospheric gases has been maintained for millions of years, but with the beginning of the industrial age, it became more fragile due to human activity. In the Intergovernmental Panel on Climate Change Report (IPCC) named "Climate Change 2007" (IPCC-AR4, 2007) it is specified that *"the keep going emissions of the greenhouse gases (GHG) at/over current rate, will cause in the future global warming and will induce more global climate changes in the 21st century than those of 20th century"*. More than , in the coming IPCC Report named "Carbon cycle including ocean acidification (CCT)" (IPCC-AR5, 2010) is stipulated that ocean acidification will be a further critical and direct consequence of increasing atmospheric GHG concentrations.

In 1886, the chemist Svante Arrhenius (Nobel prize for Chemistry in 1903) calculated for the first time the CO₂ contribution (from fossil fuel combustion) to climatic changes and used for the first time the term of "greenhouse effect". Almost 100 years were necessary for the confirmation of Arrhenius predictions about the evolution of global climatic factors, and the fact that CO₂ is the main greenhouse gas, with a contribution of 55% to Global Warming Effect. The first IPCC Report (IPCC-FAR, 1990) draws the conclusion about the possible existence of a global warming phenomenon. The second IPCC Report (IPCC-SAR, 1995) shows the contribution of humans to global warming and predicts a major warming in the 21st century. The third IPCC Report (IPCC-TAR, 2001) affirms a very probable (60% - 90%) warming for the next century. In the IPCC-AR4 Report (IPCC-AR4, 2007) adds for the understanding of the impact of climate changes over the vulnerability and the adaptation of the environment, the most relevant scientific, technical and socio-economical information from more than 1500 scientific papers. This report accepts with a probability of over 90% that the emission of greenhouse gases and not the environmental conditions gives the global warming effect.

The IPCC Guide from 2006 makes an inventory of gases from atmosphere and distinguishes between:

- a. gases with GWP (Global Warming Potential) listed in IPCC 2001: CO₂, CH₄, N₂O, hydro fluorocarbons, per fluorocarbons, SF₆, NF₃, SF₅CF₃, halogenated ether, C₄F₉OC₂H₅, CHF₂OCF₂OC₂F₄OCHF₂, CHF₂OCF₂OCHF₂ and other halocarbons CF₃I, CH₂Br₂, CHCl₃, CH₃Cl, CH₂Cl₂.

b. gases without GWP: $C_3F_7C(O)C_2F_5$, C_7F_{16} , C_4F_6 , C_5F_8 and C_4F_8O .

As a follow-up of these reports, the scientific community had started a cycle of research programs having as scientific goal the complex study (emission sources, consumption sources, the balance of changes between the components of environment etc.) of these gases and the effect produced by them (Projects CARBOEUROPE, AEROCARD, CHIOTTO, Global Carbon Project, IGOS, NACP etc).

The CO_2 it is an important green-house gas and its level in the atmosphere has significantly increased from 280 ppm in the pre-industrial era to current 380 ppm. The first increase of 50 ppm occurred during a period of ca. 200 years, starting with the beginning of the industrial revolution until 1973. Between 1973 and 2006 the concentration of CO_2 increased with another 50 ppm.

The Global Warming Potential (GWP) for CO_2 is conventionally choose as 1, i.e. the atmospheric residence time between 50 and 200 years, and its contribution to the greenhouse effect is ca. 52 %.

According to IPCC Report (IPCC-AR4, 2007), the contribution of anthropic CO_2 is predominant, and the main anthropic sources are:

- the energetic sector 30 %
- industrial processes 20 %
- fuels used in transportation 20 %
- burning of biomass 9.1 %
- processing and distribution of fossil fuels 8.4 %
- other sources 12.5%

According to IPCC estimations, the increase of CO_2 concentration in the atmosphere leads to climate changes and will produce a global warming of the planet through the greenhouse effect.

The monitoring of the global levels of CO_2 is the concern of American government since about 30 years. The National Oceanic & Atmospheric Administration - Earth System Research Laboratory (NOAA-ESRL) performs measurements for main greenhouse gases in about 68 locations spread all over the world. According to NOAA data, the concentration of CO_2 has an ascending trend. Figure 1 shows the CO_2 variations in Mauna Loa for the period of 2003-2008 according to NOAA-ESRL source.

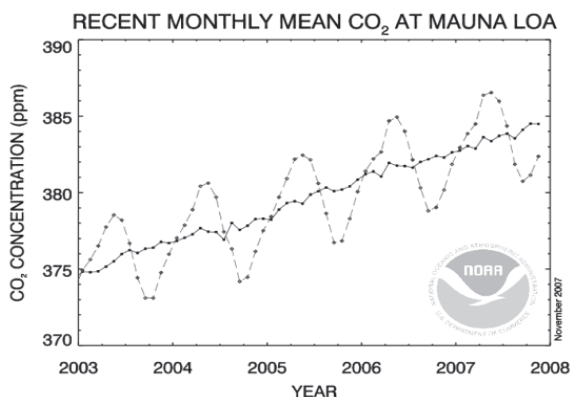


Fig. 1. Variation of the monthly average of CO_2 in Mauna Loa

At the European level, the Carboeurope-Clusters Program (CarboEurope) carries out measurements of atmospheric CO₂ concentrations in 61 locations in 17 countries. This program contains eight different projects working together to contribute to the understanding of the carbon cycle at the European level. The projects involved in this program are: AEROCARB, CAMELS, CARBOAGE, CARBODATA, CARBOEUROFLUX, CARBOEUROPE GHG; CARBOINVENT, CHIOTTO, CARBODATA, TACOS, EUROSIBERIAN CARBONFLUX, FORCAST, GREENGRASS, RECAP, TACOS-INFRASTRUCTURE, and TCOS SIBERIA. Two other projects, CARBOMONT and SILVISTRAT are associated to this program.

In 1998 Idso and co-workers (Idso et al., 2001) introduced the term “urban DOME” for the persistence of CO₂ over the urban cities as a result of anthropogenic contribution to CO₂ budget. After that, several individual studies regarding to CO₂ variation in urban areas have been reported (Day et al., 2002; Idso et al., 2002). These studies showed that the concentration of CO₂ in urban area is higher than the CO₂ concentration in rural area and this fact is a consequence of human activities. A literature review about these results is presented in this chapter.

Methane (CH₄) is another important greenhouse gas, with GWP = 25 and a residence time of more than 100 years. It is produced both naturally and through human activities. The global mixing ratios of CH₄ in the atmosphere have more than doubled since the pre-industrial period, rising from around 750 ppb (parts per billion) in 1800 (Simpson et al., 2002; Dlugokencky et al., 2003) to the current level of around 1770 ppb (NOAA-ESRL). The global trend of the methane concentration in the air is ascending, with a rate of increase of 5–10 ppb/year, and for the period 1984–2004 this tendency is shown in Figure 2.

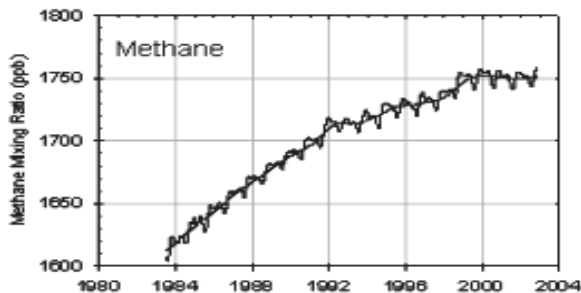


Fig. 2. The variation of the global average concentration of CH₄. (source NOAA-ESRL)

The main natural source of methane are dominated by wetlands. The primary way for CH₄ transformation is its destruction in the atmosphere by hydroxyl radicals (Prinn et al., 1995, 2001). Some CH₄ is also oxidized by microorganisms (called methanotrophs), which use CH₄ as a source of carbon and energy. Tropospheric CH₄ is eventually oxidized to carbon dioxide; its atmospheric lifetime is estimated to be 8–12 years (NOAA-ESRL; Cunnold et al., 2002; IPCC-AR4, 2007).

It is estimated that the contribution of methane to the greenhouse effect is 18%, and the most important sources are:

- Residual agricultural products 40%
- Processing and distribution of fossil fuels 29.6%

- Storage and processing of domestic waste 18.1%
- Burning of biomass and grazing 6.6%
- Other sources 4.8%

In the IPCC Report (IPCC-TAR, 2001) is suggested that the natural sources account for ca. 40% of total methane sources. Aikawa (Aikawa, 2006) indicates that the transportation contributes 1.1% of CH₄ emissions in Japan and suggests that there is a small influence of methane emissions from mobile sources on the concentrations in ambient air. The possible evolution of anthropogenic methane emissions at global level has been discussed by Cofala (Cofala et al., 2007) who predicts an increase of CH₄ emissions from 250 Tg/year in 1990 to 420 Tg/year in 2030.

Carbon monoxide (CO) is the most significant pollutant. It has a short life time in the atmosphere due to its reaction with other atmospheric components, such as hydroxyl radicals. It has an indirect radiative effect by increasing the concentration of methane and tropospheric ozone. In urban areas, CO reacts photochemically with aldehydes, to produce peroxy radicals. These radicals react with nitrogen oxide, to form nitrogen dioxide, which is the main responsible for the formation of the fotochemical smog.

Through natural processes, the CO can be oxidized to CO₂, thus contributing to the increase of the later in the atmosphere. Thus, through resulting products the anthropogenic CO can indirectly contribute to the greenhouse effect and to the global warming.

Anyway, even if CO₂ and CH₄ are the main greenhouse gases, with a contribution of more than 70% (CO₂ 55%, CH₄ 15%) on global warming (IPCC-AR4, 2007), for a good estimation of these two gases to the Global Warming Potential (GWP) in urban areas it is necessary to take into account the indirect contribution of CO which is not a greenhouse gas but changes the atmospheric chemistry and the abundance of other greenhouse gases. CO is a key air pollutant which can be utilized like tracer in the separation of CO₂ and CH₄ from biogenic and anthropogenic sources (Daniel & Solomon, 1998).

Different studies (Daniel & Solomon, 1998; Fuglesvedt et al., 1996; Prather, 1996 cited in IPCC-TAR, Chapter 4, 2001) estimate the indirect GWP of the CO due to O₃ production and to feedbacks on the CH₄. This approach was made using a box model and estimate the indirect GWP of CO for time horizons of 20, 100, and 500 years. The indirect GWP value due to CO is gave in table 1.

Authors/Models	Indirect Global Warming Potentials of CO, Time horizon		
	20 years	100 years	500 years
Daniel and Solomon (1998): box model considering CH ₄ feedbacks only	2.8	1.0	0.3
Fuglestvedt et al. (1996): two-dimensional model including CH ₄ feedbacks and tropospheric O ₃ production by CO itself	10	3.0	1.0
Johnson and Derwent (1996): two-dimensional model including CH ₄ feedbacks and tropospheric O ₃ production by CO itself	-	2.1	-

Table 1. Estimated Indirect Global Warming Potentials of CO for time horizons of 20, 100, and 500 years, (source IPCC-TAR, 2001)

Regarding to long time measurement of CO₂ concentration in urban area as well as the variation of meteorological parameters allow to understanding the rule of the ecosystem functioning and meteorological parameters over inter-annual variation in carbon fluxes. The inter-annual variation of CO₂ fluxes has been typically studied either by modeling approaches (Higuchi et al., 2005; Ito et al., 2005; Bergeron & Strachan, 2011) or by correlation coefficient analyses together with meteorological parameters (Aubinet et al., 2002; Aurela et al., 2004; Wohlfahrt et al., 2008). These studies showed that, the CO₂ flux is strongly influenced by biological vegetation cycle and the variation of meteorological parameters. Thus the maximum value of CO₂ is registered during the cold season while the minimum value of CO₂ was registered during the summer. Another study (Sottocornola & Kiely, 2010), show that the wet conditions favored the CO₂ uptake by the ecosystem in autumn and in winter, while the warmer and dryer weather reduce the sequestration of CO₂ in the ecosystem. A study performed in urban and sub-urban area of Montreal (Bergeron & Strachan, 2011) showed that the CO₂ flux is also influenced by the anthropic activity. According to this study, *“Lower emissions at the suburban site are attributed to the large biological uptake in summer and to its relatively low population density inducing low anthropogenic emissions. Higher emissions at the urban site are partly associated with its greater population and building density, promoting higher emissions from vehicular traffic and heating fuel combustion. Vehicular traffic CO₂ emissions influenced the diurnal cycle of CO₂ fluxes throughout the year at the urban site. At the suburban site, summer CO₂ fluxes were dominated by vegetation sources and sinks as daytime CO₂ uptake occurred and CO₂ fluxes responded to incoming light levels and air temperature in a fashion similar to natural ecosystems. To a lesser extent, the vegetation component also helped offset CO₂ emissions from other sources in summer at the urban site.”*

This chapter will present the results of a case study of CO₂, CH₄ and CO variations during one year in three selected cities from Romania with different anthropic activity. In order to identify the influence of biogenic and anthropogenic sources to the budget of mentioned greenhouse gases the ¹³CO₂ and ¹³CH₄ isotopic composition have been determinate. Experimental results were finally correlated with meteorological parameters.

2. CO₂ in urban area

2.1 Trends of CO₂ variation in urban areas. A literature review

The problem of urban carbon dioxide came into the attention of scientists in the year 1998, with the discovery and characterization of the urban CO₂ dome of Phoenix, Arizona, USA by Idso and col. (Idso et al., 2001). Early work found that under certain meteorological conditions, urban CO₂ concentrations could be as high as 550-600 ppm (some 200 ppm higher than the surrounding countryside) (Idso et al., 2002). Soegaard and Moller-Jensen (Soegaard & Moller-Jensen, 2003) studied the urban CO₂ dome of Copenhagen and indicated that "traffic is the largest single CO₂ source in the city," and demonstrate that "emission rates range from less than 0.8 g CO₂ m⁻² h⁻¹ in the residential areas up to a maximum of 16 g CO₂ m⁻² h⁻¹ along the major entrance roads in the city center."

Following these studies, research regarding the urban CO₂ domes has been performed in many other parts of the world (Table 2). The results obtained from studies conducted in several cities from all over the world, show several commonalities. Thus, anthropogenic CO₂ emissions are the primary source of the urban CO₂ dome; the dome is generally stronger in city centers, in winter, on weekdays, at night, under conditions of heavy traffic, close to the ground, with little to no wind, and in the presence of strong temperature inversions. These

conclusions are in agreement with the data provided by Commonwealth Scientific and Industrial Research Organisation (CSIRO) which indicate that typical concentrations of CO₂ in urban areas is situated between 350 and 600 ppm and depend on meteorological parameters and urban agglomeration.

Authors	Place of measurements	Period of measurement	CO ₂ range concentrations
Coutts A. M.	Melbourne, Australia	February - July, 2004	355 - 380 ppm (daily mean concentration).
Day T. A. et al.	Phoenix, USA	March - April, 2000	377 - 396 ppm (daily mean concentration)
George K. et al.	Baltimore, USA	2007	488 in urban area, 442 in sub-urban area, 422 in rural area
Ghauri B.	Six cities, Pakistan	2003 - 2004	270 - 325 ppm in Islamabad, 289 - 389 ppm in Quetta, 316.5 - 360 ppm in Karachi, 324.1 - 380 ppm in Lahore 295.2 - 356 ppm in Rawalpindi, 312 - 382 ppm in Peshawar.
Gratani L. et al.	Rome, Italy	1995 - 2004	367 ± 29 ppm in 1995 (monthly mean variation) 477 ± 30 ppm in 2004 (monthly mean variation) 414 ± 25 ppm green zone 505 ± 28 centrale zone
Grimmond et al.	Chicago, USA	July 11- August 14, 1995	338 - 370 ppm (diurnal variation) 405 - 441 ppm (nightly variation)
Idso S. B. et al.	Phoenix, USA	2000	390.2 ± 0.2 ppm (minimum daily concentration) 424.3 - 490.6 ppm (maximum daily concentration) 619.3 ppm (maximum daily concentration in cold season)
Kuc T. et al.	Kasprowy Wierch and Krakow, Poland	2000	370 ppm (monthly mean variation in Kasprowy Wierch) 370 - 430 ppm (monthly mean variation in Krakow)
Moriwaki R. et al.	Tokyo, Japan	October-Nov., 2005	380 - 580 ppm (daily mean concentration).
Nasrallah H.A. et al.	Kuwait City, Kuwait	1996 - 2001	368 - 371 ppm (daily mean concentration at 7 metter high).
Velasco E. et al.	Mexico city, USA	June 11- August 14, 1995	398 - 444 ppm (daily variation) 421 ppm (daily mean)

Table 2. Overview of urban CO₂ measurements

Taking in to account the concentration of CO₂ from the cities, some of researches were focused on the impact of local CO₂ emissions over local temperature. Thus, Balling et al. running the CO₂ concentration through a radiation model calculated that local CO₂ emissions modify the local temperature with more than one-tenth of one degree Celsius. In fact, Balling

et al. suggest that this increasing of temperature is insignificant by comparing it to the overall urban heat island in Phoenix which typically adds 5 to 10 degrees C. (Balling, Jr., et al., 2001). Recently, Jacobson (Jacobson, 2010) found that domes form above cities more than a decade ago, cause local temperature increases that in turn increase the amounts of local air pollutants, raising concentrations of health-damaging ground-level ozone, as well as particles in urban air. Also, this study has shown that "CO₂ dome" that develops over urban areas is a local problem, which creates much more health problems than in rural areas. The conclusions of Jacobson about the human health effects of CO₂ created many controversies; therefore, more research is necessary on the measurement of CO₂ variation over the urban areas.

2.2 CO₂ variation in three Romanian cities. Case study

The available literature contains no information about the variation of CO₂ concentrations in Romania in urban areas. However, the American system of global monitoring of CO₂ (NOAA-ESRL) has a station of continuous measurement of the main parameters of air quality placed in Constanta, which also measures CO₂ concentrations.

According to NOAA-ESRL data, the variation of CO₂ concentrations at the Constanța measurement station has an ascending trend; the yearly average values are between 365 ppm in 1995 and 395 ppm in 2007. According to the same source the concentration of CO₂ has a seasonal variation with maxima in the cold season and minima in the warm season.

In order to study the influence of anthropic activity upon the CO₂ level the study was performed in three different Romanian cities from Cluj County, as follows:

- a. Cluj-Napoca city, 400 000 inhabitants,
- b. Turda city, 59 600 inhabitants
- c. Huedin town, 10 000 inhabitants

The case study has been carried out during one year (four seasons) from July 2008 to June 2009.

The measurements were performed monthly (during 8 hours from 8.30 am to 15.30 pm) in all the three selected locations using a NDIR CO₂ analyzer model EMG-4. The measurements of CO₂ levels were performed in a portable meteorological shelter.

For the estimation of the anthropogenic contribution over the CO₂ budget in all three studied areas a reference point situated outside of the cities has been chosen (Roba et al, 2009).

For the Cluj-Napoca city, three measurement points have been selected: one situated in a zone with intense traffic (Piața Mărăști), one with moderate traffic (Cartier Grigorescu) and a reference point located in a periphery location (meteorological station in Cartier Gruia).

The results of the measurements recorded in the three locations in the city of Cluj-Napoca show that during the year the CO₂ level is strongly influenced by the amplitude of the anthropic activities. The highest levels were recorded in the location with intense anthropic activity (Piata Marasti) and the lowest levels in the reference point located outside of the city. The recorded values are comprised between 380 and 530 ppm (Mărăști), 376-456 (Grigorescu) and 373-444 (reference point).

It was also found that the highest values were recorded during the months of October and November (during the final period of the biological cycle of plants) and during the winter. It was also found that starting with the months of March; the CO₂ concentrations decrease and become comparable with the summer values (Figure 3).

For the Turda city two measurement points have been selected: one in the city (Potaisa School) and another one located outside of the city (Meteo Station).

The results of the measurements in the two locations indicate a concentration difference between 15 and 20 ppm, depending of the period of measurements. The largest values of CO₂ concentration were obtained in the months of October and November, at the end of the biological cycle of plants and in the winter. The concentrations measured are in the range 380-502 ppm at Potaisa site and 371-450 ppm at the reference point.

In the town of Huedin the measurements were carried out simultaneously in two locations: one in the interior of the city (Liceul Octavian Goga) and a reference point in the peripheral area (Meteo Station). The results show a slight difference between the two locations. It was also observed again that the largest values are recorded in the months of October and November, i.e. at the end of the biological cycle of plants, and during the winter.

Starting with the month of March, the CO₂ concentrations decrease to normal values, comparable to those of the summer. The values recorded are in the range 355- 433 ppm (Octavian Goga site) and 350-411 ppm (reference point).

A comparison of the measured values carried out in different locations shows that the CO₂ concentrations depend on the size of the town, the highest values being recorded in Cluj-Napoca city, followed by Turda and Huedin (Figure 3).

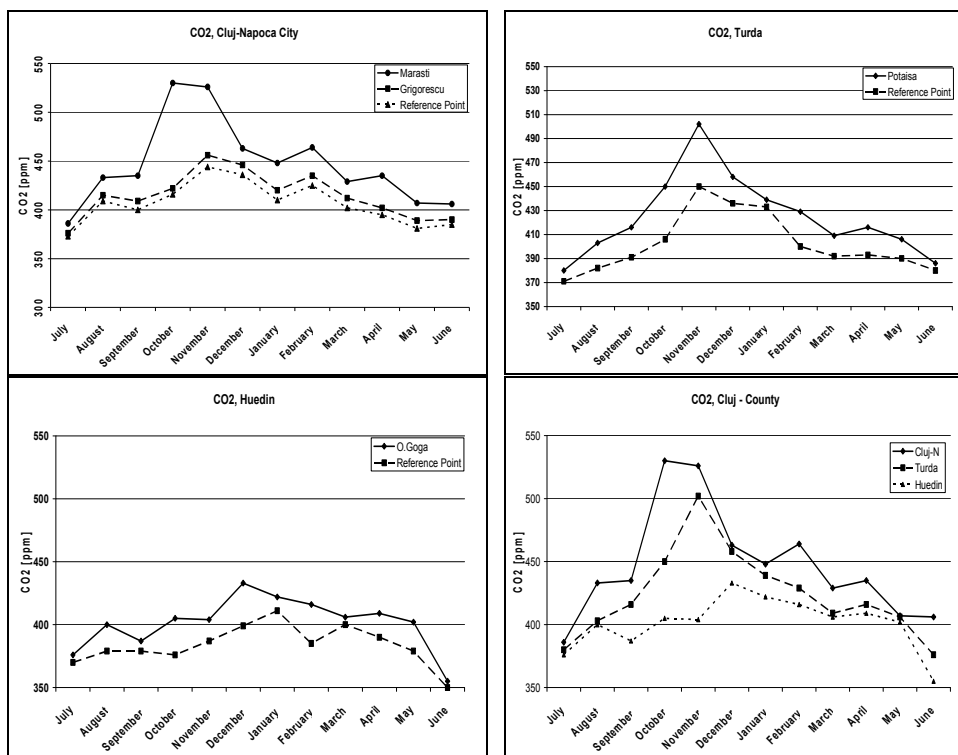


Fig. 3. Annual variation of CO₂ in urban studied areas

Diurnal variations were also observed; the highest values were measured in the morning and the lowest values at the astronomic midday, both in summer and in winter seasons (Figure 4).

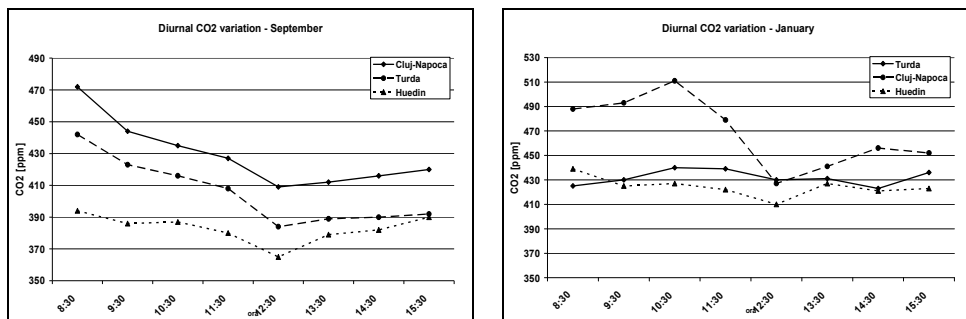


Fig. 4. Diurnal variation of CO₂ in urban studied areas

Taking into account the results of this case study we can conclude that the variation of CO₂ in studied urban areas is in agreement with other results reported in the scientific literature, which report that in urban areas the CO₂ levels are situated between 350 and 600 ppm, depending on meteorological parameters and urban agglomeration, with the observation that in the absence of rainfall the CO₂ level increases both in urban areas and outside.

3. CH₄ in urban area

3.1 Trends of CH₄ variation in urban areas. A literature review

Regarding to CH₄ variation in urban areas there are only a few studies about the level of methane in urban atmosphere, and these results are reported starting after the year 1980. For Romania such data are available only after 1995.

According to data from CSIRO the common concentrations of CH₄ in urban areas have values between 1700-2500 ppb and are influenced by meteorological parameters and urban agglomeration. Kuc and co-workers (Kuc et al., 2003) show that, the CH₄ level in urban areas is comprised between the natural level (1650 ppb) and 4200 ppb. Ito and co-workers (Ito et al. 2000) compared the atmospheric CH₄ concentrations recorded in Nagoya with the values measured at Mauna Loa Observatory in Hawaii (USA) and estimated that the excess concentration of CH₄ in the urban atmosphere of Nagoya was 170 ppb in 1988 and 150 ppb in 1997. A selective bibliography on the subject is presented in Table 3.

3.2 CH₄ variation in three Romanian cities. Case study

In Romania, the available literature provides no information about the variation of methane concentrations in urban areas and no such studies are reported. However, the American System of Global Monitoring of Air Quality (NOAA-ESRL), has a station of continuous measurements of atmospheric methane concentrations at Constanța. According to NOAA data, the concentration of CH₄ has an ascending trend, with average values comprised between 1880 ppb in 1995 and 1980 ppb in 2006. According to the same source, the methane concentration shows a seasonal variation, with maxima in the summer months and minima in the autumn and spring.

Authors	Place of measurements	Period of measurement	CH ₄ range concentrations
Aikawa M. et al.	Urban, Sub-urban, Nagoya, Japan	2004	1.80 - 1.84 ppm -urban area 1.78 - 1.80 ppm-suburban area
Derwent R.G. et al.	Island	1990 - 2003	1.75 - 2.00 ppm
Ghauri B. et al.	Pakistan	2003 - 2004	0.5 - 1.7 ppm
Hsu Y.K. et al.	California, USA	April 2007 - Feb. 2008	1.75 - 2.16 ppm
Ito A. et al.	Nagoya, Japan	1983 - 1997	1.85 ppm in 1998, 1.91 ppm in 1995, 1.90 ppm in 1997. 1983 - 1997 increase 13 ppb/year
Kuc T. et al	Kasprowy Wierch Krakow, Poland	2000	1650 ppb Kasprowy Wierch (monthly mean concentration) 2000 - 2800 ppb Krakow (monthly mean concentration)
Sikar E. & La Scala N.	Urban area, Brasil	1998 - 1999	1.80 ppm
Smith F.A. et al.	Mexico City	March, 1993	1.8 ppm during the night 7.971 ppm in the morning 2.001 - 2.999 middle of the day
Thi Nguyen H et al.	Seul, Korea	1996 - 2006	2.24 ± 0.42 ppm urban road-side 2.06 ± 0.31 ppm urban background
Veenhuysen D. et al	Amsterdam, Netherlands	1994	1.75 - 3.00 ppm
Wang J.L. et al.	Sub-urban area, Taiwan	1-27 April, 2000	1.9 - 3.7 ppm

Table 3. Overview of urban CH₄ measurements

Our case study has been focused on the measurement of the CH₄ variation in three urban areas from Cluj county as described in sub-chapter 2. The study was carried out during one year (four seasons) from July 2008 to June 2009. The measurements were performed monthly in all selected areas at the astronomic midday (in Romania at 12.30 h). In all three areas a measurement point located in the city and a reference point located outside has been selected. The samples were collected in Cluj-Napoca, in Marasti location in the city and as reference point at Gruia location. In Turda the measurements in the city were made at Liceul Potaisa, and the reference point at the Meteo station. In Huedin the measurements were made at Liceul Octavian Goga in the town and the reference point was the meteo station. For atmospheric CH₄ measurements, the air samples where collected by the flask sampling method and analysed by gas chromatography technique (GC) coupled with a flame ionisation detector (FID) (Cristea et al., 2009).

The results show a significant variation of atmospheric methane, depending on the season and the urban agglomeration degree. Thus, the highest values were recorded in the city of Cluj-Napoca (11.5 ppm in April 2009) and the lowest values were recorded in the month of August 2008 (2.5 ppm).

In Turda the concentrations of atmospheric methane were comprised between 2.2 and 8.6 ppm, with the lowest values measured in August 2008 (2.2 ppm) and the highest values recorded in April 2009 (8.6 ppm).

In Huedin the concentrations of methane were measured between 1.4 and 7 ppm, with the lowest values recorded in July 2008 (1.4 ppm) and the highest ones in April 2009 (7 ppm).

Significant differences are also observed between the methane concentrations in the interior of the cities and the reference points located outside. These differences were recorded throughout the experiments, which leads to the conclusion that the anthropic activities, the automobile traffic in particular, are an important source of methane in the urban atmosphere. The analysis of the methane concentrations in the three areas investigated indicates a similar profile for the measurements in the interior of the cities, with minima in the summer months and maxima during the spring. This may be attributed to the absence of rains in the spring (March-April). In May 2009, when the precipitations started, the concentration of atmospheric methane became closer to the values measured at the reference points.

For the reference points, the values of the atmospheric methane concentrations are in the range 2.1-4.2 ppm in Cluj-Napoca, 1.7-3.5 in Turda and 1.4-2.9 ppm in Huedin. As for the measurements in the city, a slight increase of the concentrations were observed in the spring period of 2009, due to the lack of precipitations.

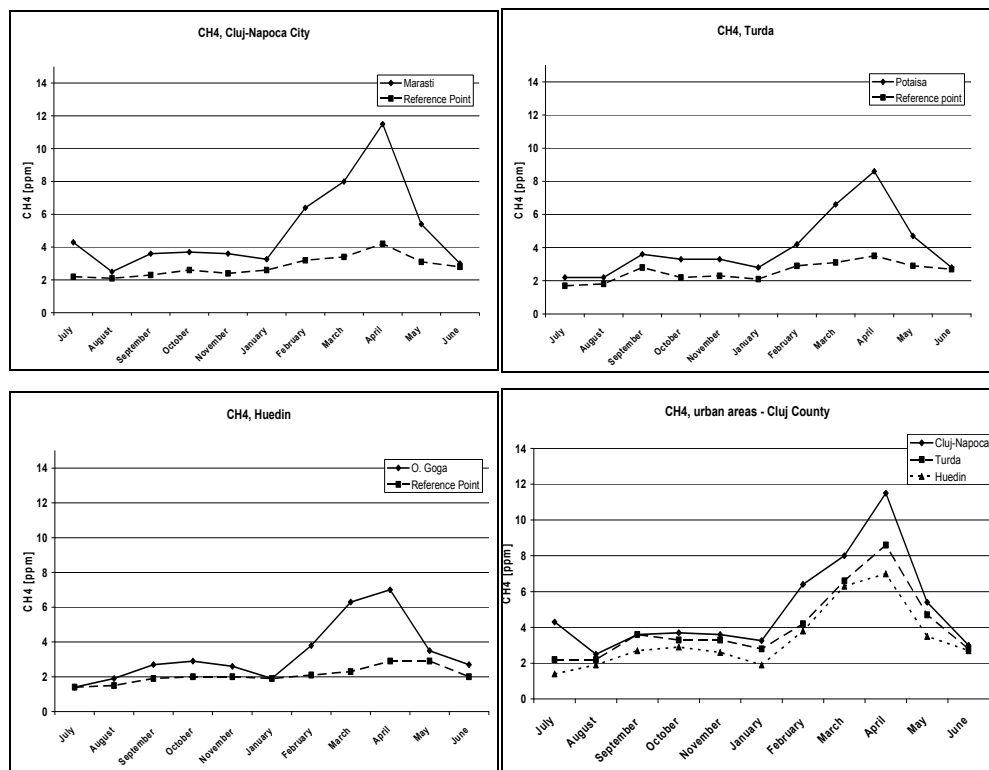


Fig. 5. The variation of methane concentration in the urban areas of Cluj county locations.

The results of our measurements indicate that the atmospheric CH₄ level in urban areas is strongly influenced by the size of the urban agglomeration as well as by the meteorological parameters. These results are in agreement with other results from scientific literatures.

4. CO in urban areas

4.1 Trends of CO variation in urban areas. A literature review

According to World Health Organization data (WHO, 2000), in the main European cities the average atmospheric CO concentration is situated under 2 mg/m³ air, with a maximum concentration lower than 6.0 mg/m³ air. At global level, the concentration of CO is composed between 0.05 and 0.12 ppm in the air. This concentration is an average between the values measured in urban and rural areas. In rural areas the CO concentration is due mainly to natural processes, but in urban areas it is strongly influenced by anthropic activities.

The CO concentration in the air of urban zones depends upon the density of combustion sources, the topography of the measurements location, the meteorological conditions and from the distance between the measurement point and the auto traffic routes.

The monitoring of CO in USA is carried out since 1980; currently, there are 243 measurement stations distributed all over the USA territory. According to EPA Reports (EPA, 2009), the concentration of CO decreased in the period 1980-2006 from 14 ppm to 3 ppm.

In Europe, the monitoring of CO in urban areas is 20 years old. Several European projects were in action, to evaluate the exposure of the population to CO, and the measurements were carried out both with fixed and mobile stations. According to WHO data (WHO, 2000) in large European cities the CO concentrations (during 8 hours measurements) are situated below 20 mg/m³ in the air, and the maxima are not higher than 10 mg/m³ in the air.

The first network for the measurement of pollutants resulted from anthropic activities was created in France in 1979 under the name AIRPARIF and measures the daily, monthly and annual concentrations of NO_x, SO₂, O₃, PM, CO and of some organic compounds. According to this source, the CO concentration in the Paris region decreased from 4000 µg/m³ air in 1994 to 1200 µg/m³ air in 2006. In 2004 started measuring background measurements. The variation of annual average decreased from 500 µg/m³ air in 2003 to 400 µg/m³ air in 2006.

In Great Britain, the measurement of the concentrations of atmospheric pollutants dates from 1973; currently, there are more than 100 stations in urban zones for continuous monitoring of the air quality parameters. In London, the quality of air is monitored by as many as 30 stations. The network was created in 1993 under the name London Air Quality Network (LAQN), and since 1997 this network also measures the evolution of daily CO concentrations.

At the European level functions the European Environment Agency (EEA) with 32 members: all the 27 EU member countries, also Island, Liechtenstein, Norway, Switzerland and Turkey. Under the coordination of EEA was created the European Environment Information and Observation Network (EIONET), with the role of processing and validating the data from the stations of the member countries connected to this network. The information is available as Reports to interested users. Among the workstations connected to EIONET, 163 measure the concentrations of CO. According to EEA data, the concentration of CO at the European level decreased from 1 mg/m³ air in 1995 to 0.5 mg/m³ air in 2005.

In addition to the data from the monitoring stations there are numerous studies about the determination of CO concentrations in urban zones all over the world. A synthesis of these results is given in Table 4.

Authors	Place of measurements	Period measurement	CO range concentrations [ppm]
Chatterton T. et al.	Norwich, UK	1997 - 1998	0.4 - 10.9
Chelani A.B. et al.	Delhi, India	2000 - 2003	1.66 - 8.4
Cheng C. S. et al.	Canada	1974 - 2000	Montreal: 0.5 - 2.1, Toronto: 0.7 - 3.7
Corti A. et al.	Salerno, Italy	Not specified	0.55 - 0.85
DEQ-Oregon	Portland-SUA	1980 - 1998	13.0 - 4.7
Emmerson K. et al.	Birmingham, UK	1999 - 2000	0.17 - 0.66
EPA	USA	1990 - 2006	Washington (decrease from 9 to 2), New-York (8.6 - 1.8), Los Angeles (14 - 4) ,
Ghauri B. et al.	Pakistan	2003 - 2004	Islamabad : 6 - 13; Quetta: 1.9 - 14 , Karachi: 1.6 - 8.0; Lahore: 1.3 - 12; Rawalpindi: 1.6 - 8
Ghose M. K. et al.	Calcutta, India	2003	2.6 - 5.1
Jones S. G. et al.	Paris, France	1997	0.38 - 1.45
Kim S.Y. et al.	Seoul , Korea	2002	0.8 - 44.0
Kukkonen J. et al.	Helsinki, Sweden	1997	0.1 - 4.5
Lijteroff R. et al.	San Luis, Argentina	1994 - 1995	3.43 - 9.17
Linden J. et al.	Burkina Faso, Africa	2004 - 2005	Background: 1 - 9, Traffic: 6.5 - 6.0
Makra L. et al.	Szeged, Hungary	1997 - 2001	0.24 - 0.93
Manning A.J. et al.	Leek, UK	1997	0.25 - 4.0
Martín M.L. et al.	Bay of Algeciras	1999 - 2001	0.5 - 2.9
Milton R. et al.	Londra, UK	2004 - 2005	0.9 - 14.9
Muttamara S. et al.	Bangkok	1997	8.23 - 26.89
Ni-Bin Chang et al.	Kaohsiung, Taiwan	1995	0.1 - 2.0
Park S. S. et al.	Seoul, Korea	1998 - 1999	1.74 - 2.81
Reich S. et al.	Buenos Aires	2001	0.60 - 2.44
Rubio M. A. et al.	Santiago City, Chile	2005 - 2006	0.31 - 3.06
Sanchez-Coyllo O. et al.	Sao-Paulo, Brazilia	1999	1.20 - 4.00
Sathitkunarath S. et al.	Chiang Mai, China	2002	0.9 - 1.5
Shiva Nagendra S.M.	Delhi, India	1997 - 1999	0.1 - 18
Turias I.J. et al.	Campo de Gibraltar	1999 - 2001	0.4 - 4.5
Venegas L.E. et al.	Buenos Aires	1994 - 1996	Autumn:10,0, Winter: 9.80, Spring :10,7

Table 4. Overview of urban CO measurements

4.2 Case study Cluj-Napoca city

In Romania, the monitoring of air quality is done by the Agencies for Environment Protection and follows the concentrations of nitrogen oxides, sulfur dioxide, ozone, BTEX, material particles, etc. Of these, 53 monitoring stations are connected to the European EIONET System and 12 stations also measure the concentrations of CO in urban zones.

In the city of Cluj-Napoca, there are four stations for continuous monitoring of air quality, and beginning with August 2005 the Agency measures the CO concentrations in two locations in the city of Cluj-Napoca and one in the city of Dej. The measurements in Cluj county show that the concentration of CO in the atmosphere is much below the admitted level (10 mg/m^3) and varies between 0.09 and 0.4 mg/m^3 air.

In this case study the measurements were performed daily in Cluj-Napoca at the astronomic midday (in Romania at 12.30 h) using a NDIR CO analyzer Horiba model APMA-360. The results showed that the CO level in Cluj-Napoca is less than 1 mg/m^3 with a tendency of accumulation during the winter season. It is also observed a trend of accumulation during the spring months, due to the lack of precipitations. Beginning with the end of May, when the rain regime becomes normal, the values of CO concentrations are around 0.1 mg/m^3 air (Figure 6).

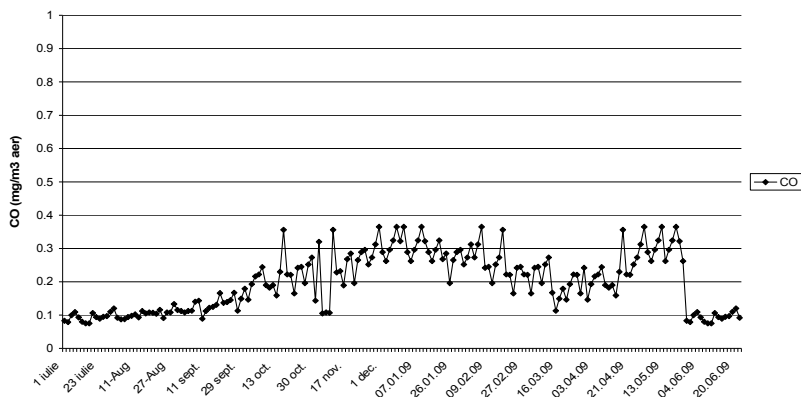


Fig. 6. Variation of CO concentrations in Cluj-Napoca in the period July 2008-June 2009

5. Anthropogenic contribution in CO_2 and CH_4 budgets

5.1 Isotopic ^{13}C measurements

Knowledge of the terrestrial CO_2 cycle will help to understand the climate change phenomena and to predicting the future atmospheric CO_2 concentrations and global temperatures. By estimating the terrestrial CO_2 cycle, including such factors as emissions, storages and fluxes and combining this with the isotope compositions of atmospheric CO_2 will help to identify the contribution of different factors to the atmospheric CO_2 budget. More than the observation of the CO_2 isotopic composition provides important information about sources such as fossil fuel combustion and biogenic respiration. The determination of isotopic concentrations of ^{13}C enforces the analyze of different species of atmospheric CO_2 and CH_4 collected in situ in glass recipients of different measures (flask sampling) by mass spectrometry. Thus, Takahashi et al. (2001, 2002) using CO_2 isotope compositions method

for investigating the sources of atmospheric CO₂ observed carbon isotope compositions of Δ¹⁴C and δ¹³C in atmospheric CO₂ and estimated the contributions of fossil fuels and biogenic respiration, while Pataki (Pataki et al., 2003, 2006a,b) observing δ¹³C and δ¹⁸O isotope compositions in atmospheric CO₂ has reported the contribution of natural gas combustion, gasoline combustion and biogenic respiration over the total atmospheric CO₂ budget.

To identify sources of carbon and to quantify these sources it is used the Keeling plot (Pataki et al., 2003). The equation used in the Keeling plot is derived from the basic assumption that the atmospheric concentration of a substance (CO₂, CH₄) in air reflects the combination of some background amount of the substance that is already present in the atmosphere and some amount of substance that is added or removed by sources or sinks:

$$C_T = C_A + C_S \quad (1)$$

where C_T, C_A, and C_S are the concentrations of the substance in air, in the background of atmosphere, and that contributed by sources, respectively. Isotope ratios of these different components can be expressed by a simple mass balance equation:

$$C_T \delta_T = C_A \delta_A + C_S \delta_S \quad (2)$$

where δ_T, δ_A, and δ_S represent the isotopic composition of the substance in the atmosphere, in the background, and of the sources, respectively. By combine Eqs. 1 and 2 it is obtained equation 3:

$$\delta_T = C_A (\delta_A - \delta_S) / (C_T) + \delta_S \quad (3)$$

This is a linear relationship with a slope of C_A (δ_A - δ_S) and an intercept at the δ_S value of the net sources/sinks in the atmosphere.

According to Pataki (Pataki et al., 2006) the mixing ratios originating from local sources (C_S) is composed from the CO₂ mixing of natural gas combustion (C_N) and CO₂ mixing of gasoline combustion (C_G):

$$C_T = C_A + C_N + C_G \quad (4)$$

Using the values of measured concentrations of CO₂ (C_T) in the same time and in the same air as the measurements of δ_T, and know the δ_N, δ_G and C_N it is possible to estimate C_G. The isotopic mass balance equation in this case is:

$$\delta_T C_T = \delta_B C_B + \delta_N C_N + \delta_G C_G \quad (5)$$

where δ_T and δ_G represent the isotopic composition of the CO₂ results from natural gas combustion and δ_G is the isotopic composition of the CO₂ results from gasoline combustion. In order to study the effects of the emission and diffusion of CO₂ from fossil fuel combustion most of the recent studies have focused on urban areas where CO₂ is mainly the product of power plants and transportation. The results of these measurements were correlated with variations in carbon isotopic composition and its show that while the natural level of δ¹³C value is -8.02‰, in urban areas the δ¹³C values is down to -12‰ for atmospheric CO₂. This difference is given by the increasing input of CO₂ derived from fossil fuel (Clark- Thorne and Yapp, 2003, Lichtfouse et al., 2003; Widory and Javoy, 2003, Newman S et al. 2008, Wada et al 2010).

5.2 Isotopic ^{13}C measurements

The carbon isotopic composition (^{12}C , ^{13}C and ^{14}C) of atmospheric methane is used to estimate the local CH_4 sources contribution over the CH_4 budget in a local areas (Moriizumi et al., 1998)

According to (Miller et al., 2003 cited by Cuna et al. 2008) the methane mixing ratio in air, $[\text{CH}_4]$, and its isotopic ratio, $\delta^{13}\text{C}_{\text{CH}_4}$, may be derived from three main sources: methane produced by microbial, $[\text{CH}_4]_{\text{micr}}$, fossil methane, $[\text{CH}_4]_{\text{ff}}$, and methane produced from biomass burning, $[\text{CH}_4]_{\text{bmb}}$

$$[\text{CH}_4]_{\text{T}} = [\text{CH}_4]_{\text{micr}} + [\text{CH}_4]_{\text{ff}} + [\text{CH}_4]_{\text{bmb}} + [\text{CH}_4]_{\text{bg}} \quad (1)$$

In equation (1) $[\text{CH}_4]_{\text{bg}}$ is defined as the smoothed marine boundary layer (MBL) at the latitude of interest (Dlugokencky et al., 1994 cited by Cuna et al. 2008).

Each of these emissions has a more-or-less distinct isotopic signature with bacterial methane $\delta^{13}\text{C}_{\text{micr}} \approx 60\%$, thermogenic methane $\delta^{13}\text{C}_{\text{ff}} \approx 40\%$, and biomass burning methane $\delta^{13}\text{C}_{\text{bmb}} \approx 25\%$ (Quay et al., 1999 cited by Cuna et al. 2008).

$$\delta^{13}\text{C}[\text{CH}_4]_{\text{T}} = \delta^{13}\text{C}[\text{CH}_4]_{\text{micr}} + \delta^{13}\text{C}[\text{CH}_4]_{\text{ff}} + \delta^{13}\text{C}[\text{CH}_4]_{\text{bmb}} + \delta^{13}\text{C}[\text{CH}_4]_{\text{bg}} \quad (2)$$

Separating CH_4 sources using isotopic signatures is complicated by enrichment during uptake processes such as bacterial CH_4 oxidation, or methanotrophy (Chanton et al., 2005 cited by Cuna et al. 2008). Thus, the methane mixing ratio changes over time according to Eq. (3), where $[\text{CH}_4]_{\text{S}}$ is the sum of all sources and τ is the lifetime of methane with respect to its destruction by OH and addition from other processes (Montzka et al., 2000; Hein et al., 1997 cited by Cuna et al. 2008):

$$d[\text{CH}_4] / dt = [\text{CH}_4]_{\text{S}} - ([\text{CH}_4] / \tau) \quad (3)$$

The $\delta^{13}\text{C}$ of methane measured in an air sample results from several different sources, such that

$$\delta^{13}\text{C}_{\text{S}} = \delta^{13}\text{C}_{\text{bg}} + \varepsilon \quad (4)$$

In Eq. (4) $\delta^{13}\text{C}_{\text{S}}$ is the flux-weighted isotopic ratio of all sources expressed in δ notation, $\delta^{13}\text{C}_{\text{bg}}$ is the atmospheric background isotopic ratio and ε is the average isotopic fractionation associated with these processes (Cantrell et al., 1990 cited by Cuna et al. 2008). Using the values of measured concentrations of methane $[\text{CH}_4]_{\text{T}}$ in the same time and in the same air as the measurements of $\delta^{13}\text{C}$, it is possible to estimate the contribution of all sources at the atmospheric methane budget. Thus, Moriizumi (Moriizumi et al., 1998) analyzing the CH_4 in Nagoya, Japan found that “the contribution of fossil CH_4 to local CH_4 released from the urban area was calculated to be $102 \pm 8\%$, and its $\delta^{13}\text{C}$ was $-40.8 \pm 3.0\%$. In a suburban area of Nagoya fossil, CH_4 contributed to less than 10% of local release and the calculated value of $\delta^{13}\text{C}$ for non-fossil CH_4 was approximately -65% , which is within the range of reported values of $\delta^{13}\text{C}$ for CH_4 derived from bacterial CH_4 sources such as irrigated rice paddies”. Kuc (Kuc et al. 2003), measuring the CH_4 in Krakow found that “The linear regression of $\delta^{13}\text{C}$ values of methane plotted versus reciprocal concentration yields the average $\delta^{13}\text{C}$ signature of the local source of methane as being equal to -54.2% . This value agrees very well with the measured isotope signature of natural gas being used in Krakow ($-54.4 \pm 0.6\%$) and points to leakages in the distribution network of this gas as the main anthropogenic source of CH_4 in the local atmosphere”. Nakagawa (Nakagawa et al., 2005), using the stable carbon and hydrogen isotopic compositions ($\delta^{13}\text{C}$

and δD) of methane quantified the contribution of automobile exhaust to local CH₄ budget. The authors estimated that for local sources, automobile exhaust in Nagoya, Japan, contribute significant amounts (up to 30%) of CH₄ to the troposphere in the studied area. Studies performed in wetlands showed that the isotopic signature $\delta^{13}C$ of methane is situated between -67.4 and -53.3‰ with lower values in the summer and higher values in the winter (Cuna et al., 2008; Tarasova et. al., 2006). These values confirm that in the wetlands, the biogenic CH₄ is the main source of atmospheric CH₄.

5.3 Isotopic ¹³CO₂ measurements in Cluj county. Case study

In order to study the role of CO₂ resulted from anthropic activities in the urban atmosphere of Cluj county, the variation of CO₂ concentrations and the corresponding $\delta^{13}C$ values, in samples collected in the three areas (Cluj-Napoca, Turda, Huedin) were measured (by flask sampling) during a whole year (July 2008-June 2009). For each area two points of measurements were selected, one in the city and one reference outside of the city. The determination of CO₂ concentrations was done with an infrared gas analyzer, and the isotopic ratios were measured with a DELTA V Advantage, Thermo Finnigan mass spectrometer. A graphic representation of the isotopic ratios as a function of 1/ [CO₂] gives a Keeling plot and the value of the intercept of Keeling slope provide information about the isotopic signature of the source. Depending on the climatic conditions and the size of the urban agglomeration, correlations between $\delta^{13}C$ values and corresponding CO₂ concentrations were between -11 ‰ for Cluj-Napoca, -10.0‰ for Turda and -9.0‰ for Huedin (Tables 5-7). If we consider $\delta^{13}C = -8‰$ the isotopic composition of natural CO₂, the anthropogenic contribution for CO₂ budget is higher for Cluj-Napoca and near the natural level for small town Huedin. As the data in tables show, for the locations in the interior of the cities, the isotopic values are displaced from the average values by 0.5-1.5 ‰ compared with the reference points, which suggests that the CO₂ source in the urban location is composed from the zone with $\delta^{13}C = -8‰$, with clean air, and an anthropic source which can be CO₂ resulted from burning fossil fuels (mainly gasoline and methane) plus a biogenic source of CO₂ resulted from the respiration of the local vegetation. The largest difference occurred in the municipality of Cluj-Napoca (1.376), where the average values of $\delta^{13}C = -$

Measurement month	Time	City Point (Mărăști)		Reference Point	
		CO ₂ (ppm)	$\delta^{13}C$ (‰)	CO ₂ (ppm)	$\delta^{13}C$ (‰)
July 2008	12.30	386	-8.773	373	-8.670
August 2008	12.30	433	-10.529	409	-8.928
September 2008	12.30	435	-10.683	400	-8.901
October 2008	12.30	530	-10.926	416	-8.936
November 2008	12.30	526	-10.836	444	-8.940
January 2009	12.30	538	-10.200	450	-8.949
February 2009	12.30	773	-11.012	438	-8.939
March 2009	12.30	665	-10.543	455	-8.943
April 2009	12.30	682	-10.657	428	-8.921
May 2009	12.30	458	-9.542	420	-8.901
June 2009	12.30	425	-9.230	395	-8.763

Table 5. Values of CO₂ (ppm) and $\delta^{13}C_{PDB}$ (‰) in Cluj-Napoca city

Measurement month	Time	City Point (Potaisa)		Reference Point	
		CO ₂ (ppm)	δ ¹³ C (‰)	CO ₂ (ppm)	δ ¹³ C (‰)
July 2008	12.30	380	-8.797	371	-8.720
August 2008	12.30	403	-8.826	382	-8.762
September 2008	12.30	416	-8.802	391	-8.851
October 2008	12.30	450	-8.973	406	-8.878
November 2008	12.30	502	-10.620	450	-8.953
January 2009	12.30	463	-9.274	425	-8.900
February 2009	12.30	483	-9.560	450	-8.940
March 2009	12.30	450	-9.200	420	-8.760
April 2009	12.30	490	-10.146	435	-9.120
May 2009	12.30	399	-8.870	371	-8.832
June 2009	12.30	425	-9.132	355	-8.900

Table 6. Values of CO₂ (ppm) and δ¹³C_{PDB} (‰) in Turda city

Measurement month	Time	City Point (O.Goga)		Reference Point	
		CO ₂ (ppm)	δ ¹³ C (‰)	CO ₂ (ppm)	δ ¹³ C (‰)
July 2008	12.30	376	-8.180	370	-8.168
August 2008	12.30	408	-8.438	379	-8.187
September 2008	12.30	387	-8.175	379	-8.141
October 2008	12.30	405	-8.382	376	-8.138
November 2008	12.30	404	-8.390	387	-8.221
January 2009	12.30	422	-9.455	411	-8.324
February 2009	12.30	416	-9.342	385	-8.122
March 2009	12.30	406	-9.142	400	-8.786
April 2009	12.30	409	-10.620	390	-9.200
May 2009	12.30	402	-8.761	379	-8.100
June 2009	12.30	355	-8.956	350	-8.212

Table 7. Values of CO₂ (ppm) and δ¹³C_{PDB} (‰) in Huedin town

10.266‰ were obtained in the city center, compared with the δ¹³C = -8.890‰ for the reference point. For the other locations studied (Turda and Huedin) the isotopic concentrations are close to the atmospheric background, namely -9,291‰ for Turda and -8,895‰ for Huedin, comparable with the average values for the reference points (-8.874‰ for Turda and -8.327‰ and Huedin) suggesting that anthropic CO₂ is not contributing to the pollution.

5.4 Isotopic ¹³CH₄ measurements in Cluj county. Case study

For the evaluation of the role of CH₄ resulted from anthropic activities in the urban atmosphere in the Cluj county, the variation of CH₄ concentrations and the corresponding δ¹³C values were measured in air samples collected in three areas: Cluj-Napoca (Piața

Mărăști), Turda (Potaisa School) and Huedin (O. Goga High School) during the period between January-June 2009, using the flask sampling. Again, the $\delta^{13}\text{C}$ values were measured with a ThermoFinnigan Delta V Advantage mass spectrometer. The methane concentrations in the same samples were measured with a gas chromatograph equipped with a FID detector. The observed variation of methane concentrations (Table 8) is rather large, between 4.7 and 11.5 ppm. The values measured are above the atmospheric background, which suggests that there is an anthropic source of CH₄ in all investigated areas. The average value of $\delta^{13}\text{C} = -40\text{‰}$ suggests that the source of methane in the atmosphere is the gas fuel network of the urbane zone investigated.

Measurement month	Cluj-Napoca		Turda		Huedin	
	CH ₄ (ppm)	$\delta^{13}\text{C}$ (‰)	CH ₄ (ppm)	$\delta^{13}\text{C}$ (‰)	CH ₄ (ppm)	$\delta^{13}\text{C}$ (‰)
January 2009	11.5	-39.21	10.4	-39.45	10.6	-39.78
March 2009	8.0	-37.90	6.3	-38.75	5.5	-38.97
April 2009	11.5	-39.80	11.0	-38.92	10.5	-38.98
May 2009	8.4	-38.02	7.4	-38.80	4.7	-38.85

Table 8. Simultaneous value of CH₄ (ppm) and $\delta^{13}\text{C}$ (‰) in the Cluj district.

6. Correlation between CO₂ trend variation in urban area and variation of meteorological parameters

6.1 Case study Cluj-Napoca city

For this study a daily measurements of the CO₂ concentration and the main meteorological parameters (temperature, relative humidity and wind velocity) were recorded for a whole calendar year, beginning with July 2008 until June 2009. The measurements were carried out in the centre of Cluj-Napoca city, the time of midday (12.30), at the selected latitude. The results of measurements revealed a daily variation of CO₂ concentrations correlated with the meteorological factors and biological cycles of plants. Thus, the largest values of CO₂ were recorded in the fall and winter in the absence of vegetation, and the lowest values in the summer months, when the biologic cycle of plants is at the maximum.

The graphic representation of the CO₂ values as a function of meteorological parameters indicates a direct correlation with temperature and an inverse correlation with the wind velocity and relative humidity.

A computation of linear regression slopes of CO₂ versus air temperature for two months from winter (January and February) and two months from summer (July and August) gives positive slopes for both seasons with a highest correlation factor (0.666) in winter in the absence of photosynthesis (figure 7).

The same representation for CO₂ and for relative humidity shows a negative slope in summer and a positive slope in the winter. The computation of linear regression slopes for CO₂ versus wind velocity show a negative slopes both in summer and in winter (figure 7).

The results of this case study show that in urban area it is difficult to estimate by correlation coefficient analyses the influence of meteorological parameters over the CO₂ variation. In order to correlate the variation of CO₂ concentrations with the variation of meteorological parameters a statistic analysis of data is necessary. For the statistical approach the regression analysis and principal component analysis (PCA) has been used.

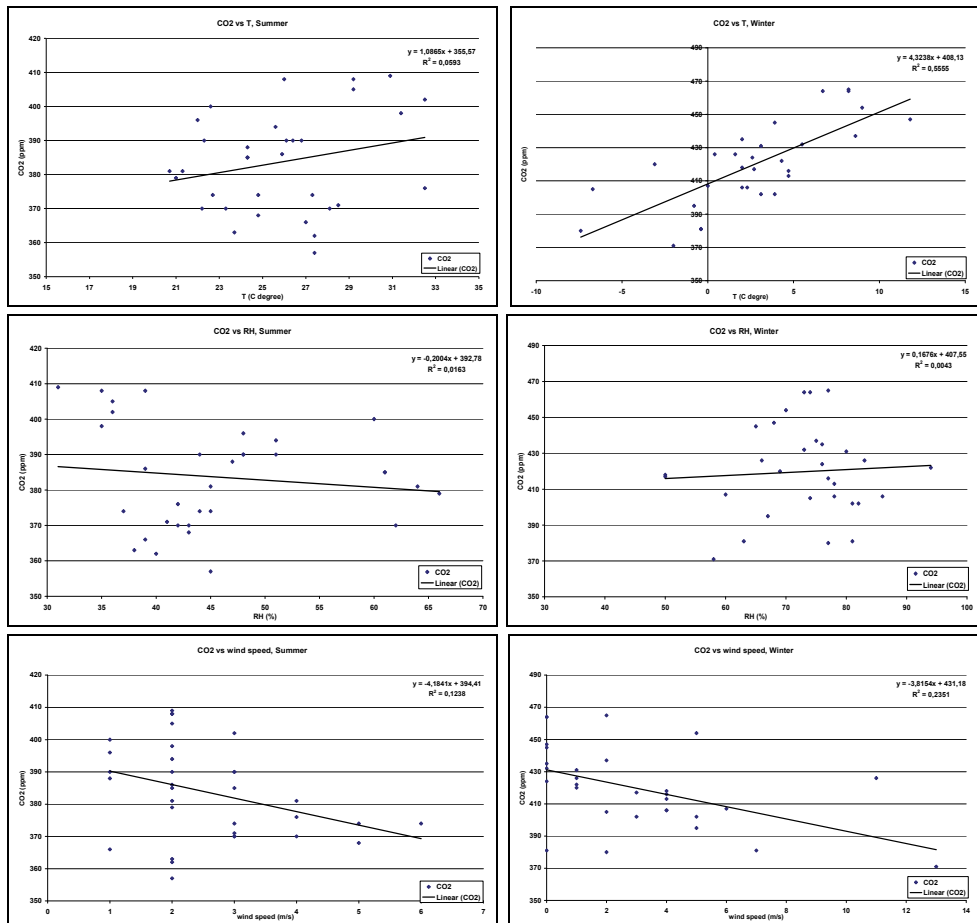


Fig. 7. Correlation between CO₂ variation and meteorological parameters in two seasons

6.1.1 The regression analysis

The regression analysis was performed with the aid of Curve estimation model of SPSS statistics program and the regression coefficients were calculated, having the CO₂ concentration as independent variable and the meteorological parameters as dependent variables. For analysis the squares of regression coefficients and the regression curves were used. The regression coefficients R² were computed for the most frequently used types of regression, namely linear, logarithmic, polynomial and exponential (Table 8).

The analysis of regression coefficients leads to some important conclusions.

The only meteorological parameter which correlated with the CO₂ concentration over the 0.6 threshold is the air temperature. Both the air humidity and the wind velocity have very low regression coefficients, suggesting that there is a low probability that the variation of the CO₂ is influenced by these meteorological factors. However, there are singular situations, when the correlation coefficients are close to the 0.6 threshold. Thus, for the relative

Month	Rt	Ta °C	RH %	V m/s
I (January)	Li	.842	.042	.014
	Lo	.843	.040	.013
	Po	.	.040	.
	Ex	.	.041	.
II (February)	Li	.802	.000	.426
	Lo	.789	.000	.430
	Po	.	.001	.
	Ex	.	.000	.
III (March)	Li	.461	.011	.166
	Lo	.456	.011	.168
	Po	.550	.003	.090
	Ex	.549	.003	.087
IV (April)	Li	.392	.034	.064
	Lo	.392	.033	.064
	Po	.368	.037	.012
	Ex	.368	.039	.012
V (May)	Li	.750	.462	.546
	Lo	.741	.462	.544
	Po	.865	.454	.380
	Ex	.869	.455	.381
VI (June)	Li	.632	.485	.000
	Lo	.632	.489	.000
	Po	.673	.520	.020
	Ex	.673	.516	.019
VII (July)	Li	.117	.158	.003
	Lo	.121	.159	.004
	Po	.116	.161	.019
	Ex	.113	.160	.018
VIII (August)	Li	.028	.271	.088
	Lo	.026	.278	.082
	Po	.025	.166	.120
	Ex	.027	.160	.126
IX (September)	Li	.368	.033	.337
	Lo	.376	.035	.342
	Po	.481	.004	.287
	Ex	.471	.003	.283

X (October)	Li	.121	.045	.088
	Lo	.123	.047	.092
	Po	.206	.	.065
	Ex	.202	.	.061
XI (November)	Li	.270	.189	.143
	Lo	.269	.180	.144
	Po	.	.152	.
	Ex	.	.160	.
XII (December)	Li	.571	.172	.028
	Lo	.581	.176	.027
	Po	.667	.196	.024
	Ex	.656	.193	.023

Table 9. The Estimation of regression coefficients (R^2). Note: The types of regression R are: Li - linear, Lo - logarithmic, Po - polynomial, Ex - exponential

humidity the highest regression coefficient was 0.52, for the type polynomial in June 2009. For the wind velocity the largest coefficient was 0.56 in May 2009, for the linear regression. The regression between CO_2 concentration and temperature reveals two interesting aspects. The 0.6 threshold of the correlation coefficient was overfull filed in the three months of winter, at the end of spring and beginning of the summer, in May and June. The lowest value of the correlation coefficient was observed in August when the measurements were made at high temperatures over 30 Celsius degree. Large values, above 0.8 were observed in January and May. To illustrate the correlations we present in table 9 all the situations when the correlation coefficient was higher than 0.6.

6.1.2 The analysis of main components (PCA)

This type of analysis was necessary, because we wanted to see, which is the weight of meteorological parameters and CO_2 concentrations in the explanation of total variations. The PCA (Principal Component Analysis) method without factor rotation was used and the results are shown in Table 10.

Component	Initial Eigenvalues			Extraction Sums of Squared Loadings		
	Total	% of Variance	Cumulative %	Total	% of Variance	Cumulative %
1	1.760	44.002	44.002	1.760	44.002	44.002
2	1.066	26.646	70.648	1.066	26.646	70.648
3	.900	22.491	93.139	.900	22.491	93.139
4	.274	6.861	100.000			

Table 10. Explanation of total variations. Extraction Method: Principal Component Analysis

After the value of 0.5 was selected for the Eigenvalue, three components were extracted which together explain 93.139% of the total variation. The first component explains 44.002 %

of the variation, the second 26.649 and the third 22.5 %. The difference to 100 % is due to a fourth component, which was eliminated because it had an Eigenvalue of only 0.274. The matrix of components (Table 11) allows the identification of each factor. Thus, the first factor is very well correlated with the air temperature (inverse correlation) and with the air humidity (direct correlation). The second component is very well correlated with the wind velocity. The concentration of CO₂ is very well correlated with the third component.

	Component		
	1	2	3
CO ₂	.480	-.283	.824
Ta	-.897	-.245	.045
V	-.045	.961	.234
RH	.850	-.048	-.406

Table 11. Matrix of components

7. Conclusions

The monitoring of the CO₂ levels in urban area could estimate the contribution of anthropic activities over the global CO₂ level. This contribution is essential in order to establish the presence of CO₂ dome over the cities. The results of presented case study confirm the presence of a CO₂ dome over the urban studied area. More than that, it confirms that the anthropogenic CO₂ emissions are the primary source of the urban CO₂. Taking into account the obtained results it can be observed that the level of CO₂ in urban areas is influenced by the size of the city and by the amplitude of anthropic activities. Thus the highest values of CO₂ were obtained in the biggest city Cluj-Napoca (between 380 and 530 ppm at Mărăști Square, 376-456 at Grigorescu and 373-444 at reference point) followed by Turda (380-502 ppm at Potaisa School and 371-450 ppm at the reference point) and Huedin (355- 433 ppm at O. Goga High School and 350-411 ppm at the reference point. It is also observed that the concentration of urban CO₂ has an annual variation with the lower value in the summer and the highest value in the autumn and spring. Regarding the daily CO₂ variation it also observed that it is dominated by the photosynthesis.

The results of the atmospheric methane measurements show a significant variation depending on the season and the urban agglomeration degree. Thus, the methane concentrations in the three investigated areas indicate a similar profile for the measurements carried out in the cities, with minima in the summer months and maxima during the spring. The highest values were recorded in the city of Cluj-Napoca (11.5 ppm in April 2009) and the lowest values were recorded in the month of August 2008 (2.5 ppm). In Turda the concentrations of atmospheric methane were comprised between 2.2 and 8.6 ppm, with the lowest values measured in August 2008 (2.2 ppm) and the highest values recorded in April 2009 (8.6 ppm) while in Huedin the concentrations of methane varied between 1.4 and 7 ppm, with the lowest values recorded in July 2008 (1.4 ppm) and the highest ones in April 2009 (7 ppm). Significant differences are also observed between the methane concentrations in the interior of the cities and the reference points located outside. These differences prove that the anthropic activities, in particular the automobile traffic, are an important source of methane in the urban atmosphere.

The carbon isotopic composition measurement of CO₂ and CH₄ is the best way to establish the biogenic and anthropic contribution at CO₂ and CH₄ budget in urban areas. Regarding the case study performed in three Romanian cities the results of ¹³C_{CO₂ show that the value of δ¹³C is depending on the size of the urban agglomeration. Thus, the lower value -11 ‰ were obtained for Cluj-Napoca, followed by Turda (-10.0‰) and Huedin (-9.0‰). If we consider δ¹³C = -8‰ the isotopic composition of natural CO₂, the anthropogenic contribution for CO₂ budget is higher for Cluj-Napoca and near the natural level for small town Huedin. More than, the recorded data show a difference of 0.5-1.5 ‰ between the measurements city points and reference points which suggests that the CO₂ source in the urban location is composed from the zone with δ¹³C = -8‰, with clean air, and an anthropic source which can be CO₂ resulted from burning fossil fuels (mainly gasoline and methane) plus a biogenic source of CO₂ resulted from the respiration of the local vegetation. The largest difference occurred in the municipality of Cluj-Napoca (1.376), where the average values of δ¹³C = -10.266‰ were obtained in the city center, compared with the δ¹³C = -8.890‰ for the reference point. For the other locations studied (Turda and Huedin) the isotopic concentrations are close to the atmospheric background, namely -9.291‰ for Turda and -8.895‰ for Huedin, comparable with the average values for the reference points (-8.874 for Turda and -8.327 and Huedin).}

Regarding the ¹³CH₄ measurements the results obtained in the case study are above -40 ‰ which suggests that there is an anthropic source of CH₄ in all investigated areas. We think that these values are a consequence of methane resulted from gas fuel network of the urbane investigated areas.

Regarding the correlation between CO₂ variation in urban area and variation of meteorological parameters the results of the case study indicate a direct correlation of CO₂ level with temperature and an inverse correlation with the wind velocity and relative humidity. Although, these correlations are poor and the analysis of regression coefficients showed that only the air temperature is correlated with the CO₂ concentration over the 0.6 threshold. The 0.6 threshold of the correlation coefficient was overfull filed in the three months of winter, at the end of spring and beginning of the summer, in May and June. The lowest value of the correlation coefficient was observed in August when the measurements were made at high temperatures, over 30 degrees Celsius. Large values, above 0.8 were observed in January and May. The air humidity and the wind velocity have very low regression coefficients, suggesting that in the urban areas studied, there is a low probability that the variation of the CO₂ is influenced by these meteorological factors. Thus, for the relative humidity the highest regression coefficient was 0.52, for the type polynomial in June 2009 while for the wind velocity the largest coefficient was 0.56 in May 2009, for the linear regression.

Taking into account the results obtained, the present case study shows that the variation of CO₂ in urban area is in agreement with other results reported in the scientific literature. Thus, according to the carbon isotopic composition measurements of CO₂ the anthropogenic CO₂ emissions are the primary source of the urban CO₂ dome; the dome is generally stronger in city centers, in winter, under conditions of heavy traffic, with little or no wind, and in the presence of strong temperature inversions.

8. Acknowledgements

The case study has been supported by the Romanian National Authority for Scientific Research, Project no. 213-1/2007

9. References

- Aikawa, M.; Hiraki, T. & Eiho, J. (2006). Vertical atmospheric structure estimated by heat island intensity and temporal variations of methane concentrations in ambient air in an urban area in Japan. *Atmospheric Environment*, Vol. 40, Iss. 23, pp. 4308-4315.
- AIRPARIF: Available from: <http://www.airparif.asso.fr/index.php?setlang=en>
- Aubinet, M.; Heinesch, B. & Longdoz, B. 2002. Estimation of the carbon sequestration by a heterogeneous forest: night flux corrections, heterogeneity of the site and inter-annual variability. *Global Change Biology*, Vol. 8, pp. 1053-1071.
- Balling Jr.; R.C., Cervený, R.S. & Idso, C. D. (2001). Does the urban CO₂ dome of Phoenix, Arizona contribute to its heat island? *Geophysical Research Letters*, Vol. 28, pp. 4599-4601.
- Bergeron, O. & Strachan I.B. (2011). CO₂ sources and sinks in urban and suburban areas of a northern mid-latitude city. *Atmospheric Environment*, Vol. 45, pp. 1564-1573.
- CarboEurope, Available from: <http://carboeurope.org/>
- Chang, N.-B. & Tseng, C.C. (1999). Optimal design of a multi-pollutant air quality monitoring network in a metropolitan region using Kaohsiung, Taiwan as an example. *Environmental Monitoring and Assessment*, Vol. 57, pp. 121-148.
- Chantterton, T.; Dorling, S.; Lovett, A. & Stephenson, (2000). Air quality in Norwich, UK, Multi-scale modeling to assess the significance of city, county and regional pollution sources. *Environmental Monitoring and Assessment*, Vol. 65, pp. 425-433.
- Chelani, A.B. & Devotta, S. (2007). Air Quality Assessment in Delhi: Before and After CNG as fuel. *Environmental Monitoring and Assessment*, Vol. 125, pp. 257-263.
- Cheng, C.S.; Campbell, M.; Li, Q.; Li, G.; Auld, H.; Day, N.; Pengelly, D.; Gingrich, S. & Yap, D. (2007). A Synoptic Climatological Approach to Assess Climatic Impact on Air Quality in South-central Canada. Part I: Historical Analysis. *Water Air Soil Pollution*, Vol. 182, pp. 131-148.
- Clark-Thorne, S.T. & Yapp, J.C. (2003). Stable carbon isotope constraints on mixing and mass balance of CO₂ in an urban atmosphere: Dallas metropolitan area, Texas, USA. *Applied Geochemistry*, Vol. 18, pp. 75-95.
- Cofala, J.; Amann, M.; Klimont, Z.; Kupiainen, K. & Isaksson L.H. (2007). Scenarios of global anthropogenic emissions of air pollutants and methane until 2030. *Atmospheric Environment*, Vol. 41, Iss.38, pp. 8486-8499.
- Corti, A. & Senatore A. (2000). Project of an Air Quality Monitoring Network for Industrial Site in Italy. *Environmental Monitoring and Assessment*, Vol. 65, pp. 10-9117.
- Coutts A.M.; Beringer, J. & Tapper, N.J. (2007). Characteristics influencing the variability of urban CO₂ fluxes in Melbourne, Australia. *Atmospheric Environment*, Vol. 41, No.1, pp. 51-62.
- Cristea, G.; Haiduc, Iv.; Beldean-Galea, M.S. & Cuna, S. (2009). The variation of CH₄ in the urban areas from Cluj county. *Studia Universitatis Babeş-Bolyai, series Geographia*, Iss. 3, pp. 91-94
- CSIRO, Available from: <http://www.csiro.au/science/Climate-Change.html>
- Cuna, S.; Pendall, E.; Miller, J.B.; Tans, P.P.; Dlugokencky, E. & White, J.W.C. (2008). Separating contributions from natural and anthropogenic sources in atmospheric methane from the Black Sea region, Romania. *Applied Geochemistry*, Vol. 23, pp. 2871-2879.

- Daniel J.S. & Solomon S. (1998). On the climate forcing of carbon monoxide. *Journal of Geophysical Research-Atmospheres*, Vol. 103, pp. 13249-13260.
- Daniel, J.S. & Solomon, S. (1998). On the climate forcing of carbon monoxide. *Journal of Geophysical Research*, Vol. 103, No.D11, pp13249-13260: in IPCC-TAR, 2001, Chapter 4.
- Day, T.A.; Gober, P.; Xiong, F.S., & Wentz E.A. (2002). Temporal patterns in near-surface CO₂ concentration over contrasting vegetation types in the Phoenix metropolitan area. *Agricultural and Forest Meteorology*, Vol. 110, Nr. 3, pp. 229-245.
- DEQ-Oregon, 2007: Available from: <http://www.deq.state.or.us/aq/toxics/index.htm>
- Derwent, R.G.; Simmonds, P.G.; O'Doherty, S.; Stevenson, D.S.; Collins, W.J.; Sanderson, M.G.; Johnson, C.E.; Dentener, F.; Cofala, J.; Mechler, R. & Amann, M. (2006). External influences on Europe's air quality: Baseline methane, carbon monoxide and ozone from 1990 to 2030 at Mace Head, Ireland. *Atmospheric Environment*, Vol. 40, pp. 844-855.
- EEA: Available from: <http://www.eea.europa.eu>
- EIONET: Available from: <http://www.eionet.europa.eu>
- Emmerson, K.M.; Carslaw, N.; Carpenter, L.J.; Heard, D.E.; Lee, J.D. & Pilling, M. J.(2005) Urban Atmospheric Chemistry During the PUMA Campaign 1: Comparison of Modelled OH and HO₂ Concentrations with Measurements. *Journal of Atmospheric Chemistry*, Vol. 52, pp. 143-164.
- EPA, 2009: Available from: <http://www.epa.gov/oar/airtrends/carbon.html>
- Fuglestvedt, J.S.; Isaksen, I.S.A. & Wang, W.-C. (1996). Estimates of indirect global warming potentials for CH₄, CO, and NO_x. *Climate Change*, Vol. 34, pp. 405-437: in IPCC-TAR, 2001, Chapter 4.
- George, K.; Ziska, L.H.; Bunce, J.A. & Quebedeaux, B. (2007). Elevated atmospheric CO₂ concentration and temperature across an urban-rural transect. *Atmospheric Environment*, Vol. 41, No.35, pp.7654-7665.
- Ghauri, B.; Lodhi, A. & Mansha, M. (2007). Development of baseline (air quality) data in Pakistan. *Environmental Monitoring Assessment*, Vol. 127, pp. 237-252.
- Ghose, M.K.; Paul, R. & Banerjee, R. K. (2005). Assessment of the status of urban air pollution and its impact of human health in the city of Kolkata. *Environmental Monitoring and Assessment*, Vol. 108, pp. 151-167.
- Gratani, L. & Varone L. (2005). Daily and seasonal variation of CO₂ in the city of Rome in relationship with the traffic volume. *Atmospheric Environment*, Vol. 39, No.14, pp. 2619-2624.
- Grimmond, C.S.B.; King, T.S.; Cropley, F.D.; Nowakb, D.J., & Souch, C. (2002). Local-scale fluxes of carbon dioxide in urban environments: methodological challenges and results from Chicago, *Environmental Pollution*, Vol. 116, No.1, pp. S243-S254.
- Higuchi, K.; Shashkov, A.; Chan, D.; Saigusa, N.; Murayama, S.; Yamamoto, S.; Kondo, H.; Chen, J.; Liu, J. & Chen B. (2005). Simulations of seasonal and inter-annual variability of gross primary productivity at Takayama with BEPS ecosystem model. *Agricultural and Forest Meteorology*, Vol. 134, Iss.1-4, Pp. 143-150.
- Hsu, Y.K.; VanCuren, T.; Park, S.; Jakober, C.; Herner, J.; FitzGibbon, M.; Blake, D.R. & Parrish, D.D. (2010). Methane emissions inventory verification in southern California. *Atmospheric Environment*, Vol. 44, pp. 1-7.

- Idso, C.D.; Idso, S.B. & Balling, R.C. (2001). An intensive two-week study of an urban CO₂ dome. *Atmospheric Environment*, Vol. 35, Iss.6, pp. 995-1000.
- Idso, S.B.; Idso, C.D. & Balling, R.C. (2002). Seasonal and diurnal variations of near-surface atmospheric CO₂ concentrations within a residential sector of the urban CO₂ dome of Phoenix, AZ, USA. *Atmospheric Environment*, Vol. 36, pp. 1655-1660.
- IPCC-AR1 , 1992, Available from: http://www.ipcc.ch/ipccreports/far/IPCC_1990_and_1992_Assessments/English/ipcc-90-92-assessments-overview.pdf
- IPCC-AR4 , 2007, Available from: http://www.ipcc.ch/pdf/assessment-report/ar4/syr/ar4_syr.pdf
- IPCC-AR5 , 2010, Available from: <http://www.ipcc-wg2.gov/AR5/ar5.html>
- IPCC-SAR, 1995, Available from: <http://www.ipcc.ch/pdf/climate-changes-1995/ipcc-2nd-assessment/2nd-assessment-en.pdf>
- IPCC-TAR, 2001, Available from: http://www.grida.no/publications/other/ipcc_tar/
- Ito, A.; Takahashi, I.; Nagata, Y.; Chiba, K. & Haraguchi, H. (2000). The long-term evolutions and the regional characteristics of atmospheric methane concentrations in Nagoya, 1983-1997. *Science of the Total Environment*, vol. 263, pp. 37-45.
- Ito, A.; Saigusa, N.; Murayama, S.; Yamamoto, S. (2005). Modeling of gross and net carbon dioxide exchange over a cool-temperate deciduous broad-leaved forest in Japan: Analysis of seasonal and interannual change. *Agricultural and Forest Meteorology*, Vol. 134, Iss.1-4, pp. 122-134.
- Jacobson, M. Z. (2010). Enhancement of local air pollution by urban CO₂ domes. *Environmental Science and Technology*, Vol. 44, pp. 2497-2502.
- Johnson, C.E.; Collins, W.J.; Stevenson, D.S. & Derwent, R.G. (1999). The relative roles of climate and emissions changes on future oxidant concentrations. *Journal of Geophysical Research*, Vol 104, pp. 18631-18645: in IPCC-TAR, 2001, Chapter 4.
- Jones, S.G.; Fisher, B.E.A; Gonzales-Flesca, N. & Sokhi, R. (2000). The use of measurement programmes and models to assess concentrations next to major roads in urban areas. *Environmental Monitoring and Assessment*, Vol. 64, pp. 531-547.
- Kèlomé, N.C.; Lévêque, J.; Andreux, F.; Milloux, M.-J. & Oyédé, L.-M. (2006). C4 plant isotopic composition ($\delta^{13}\text{C}$) evidence for urban CO₂ pollution in the city of Cotonou, Benin (West Africa). *Science of the Total Environment*, Vol. 366, pp. 439-447.
- Kim, S.-Y.; O'Neill, M.S.; Lee, J.-T.; Cho, Y.; Kim, J. & Kim, H. (2007). Totlul. *Intetnational Archives Occupational Environmental Health*, Vol. 80, pp. 701-710.
- Kuc, T.; Rozanski, K.; Zimnoch, M.; Necki, J. M. & Korus A. (2003). Anthropogenic emissions of CO₂ and CH₄ in an urban environment. *Applied Energy*, Vol. 75, Iss. 3-4, pp. 193-203.
- Kukkonen, J.; Valkonen, E.; Walden, J.; Koskentalo, T.; Karppinen, A.; Berkowicz, R. & Kartastenpaa, R. (2000). Measurements and modeling of air pollution in a street canyon in Helsinki. *Environmental Monitoring and Assessment*, Vol. 65, pp. 371-379.
- LAQN: Available from: <http://www.londonair.org.uk>
- Lichtfouse, E.; Lichtfouse, M. & Jaffrezic, A. (2003). $\delta^{13}\text{C}$ values of grasses as a novel indicator of pollution by fossil-fuel-derived greenhouse gas CO₂ in urban area. *Environmental Science and Technology*, Vol. 37, pp. 87-90.
- Lijteroff, R.; Cortinez, V. & Raba, J. (1999). Urban development and air quality in San Luis City, Argentina. *Environmental Monitoring and Assessment*, Vol. 57, pp. 169-182.

- Lindén, J.; Thorsson, S. & Eliasson, I. (2007). Carbon Monoxide in Ouagadougou, Burkina Faso - A Comparison between Urban Background, Roadside and In-traffic Measurements. *Water Air Soil Pollution*, DOI 10.1007/s11270-007-9538-2.
- Makra, L.; Mika, J.; Bartzokas, A.; Beczi, R.; Borsos, E. & Sumeghy, Z. (2006). An objective classification system of air mass types for Szeged, Hungary, with special interest in air pollution levels. *Meteorological Atmosphere Physics*, Vol. 92, pp. 115-137.
- Manning, A.J.; Nicholson, K.J.; Middleton, D.R. & Rafferty, S. C. (2000). Field study of wind and traffic to test a street canyon pollution model. *Environmental Monitoring and Assessment*, Vol. 60, pp. 283-313.
- Martín, M.L.; Turias, I.J.; González, F.J.; Galindo, P.L.; Trujillo, F.J.; Puntonet, C.G. & Gorriç, J.M. (2008). Prediction of CO maximum ground level concentrations in the Bay of Algeciras, Spain using artificial neural networks. *Chemosphere*, Vol. 70, Iss.7, pp. 1190-1195.
- Milton, R. & Steed, A. (2007). Mapping carbon monoxide using GPS tracked sensors. *Environmental Monitoring and Assessment*, Vol. 124, pp. 1-19.
- Moriwaki, R.; Kanda, M. & Nitta H. (2006). Carbon dioxide build-up within a suburban canopy layer in winter night. *Atmospheric Environment*, Vol. 40, No.8, pp.1394-1407.
- Muttamara, S.; Leong, S.T. (2000). Titlul. *Environmental Monitoring and Assessment*, Vol. 60, pp. 163-180.
- Nakagawa, F.; Tsunogai, U.; Komatsu, D.D.; Yamada, K.; Yoshida, N.; Moriizumi, J.; Nagamine, K.; Iida, T. & Ikebe, Y. (2005). Automobile exhaust as a source of ¹³C- and D-enriched atmospheric methane in urban areas. *Organic Geochemistry*, Vol. 36, pp. 727-738.
- Nasrallah, H.A.; Balling Jr. R.C.; Madi, S.M. & Al-Ansari L. (2003). Temporal variations in atmospheric CO₂ concentrations in Kuwait City, Kuwait with comparisons to Phoenix, Arizona, USA. *Environmental Pollution*, Vol. 121, No.2, pp. 301-305.
- Newman, S.; Xu, X.; Affek, H.P.; Stolper, E. & Epstein, S. (2008). Change in mixing ratio and isotopic composition of CO₂ in urban air from the Los Angeles basin, California, between 1972 and 2003. *Journal of Geophysical Research*, vol. 113, pp. D23304.
- NOAA-ESRL, Available from: <http://www.esrl.noaa.gov/>
- Park, S.S. & Kim, Y.J. (2007). Titlul. *Environmental Monitoring and Assessment*, Vol. 128, pp.231-240.
- Pataki, D.E.; Alig, R.J.; Fung, A.S.; Golubiewski, N.E.; Kennedy, C.A.; Mcpherson, E.G.; Nowak, D.J.; Pouyat, R.V. & Romero-Lankao, P. (2006a). Urban ecosystems and the North American carbon cycle. *Global Change Biology*, Vol. 12, pp. 2092-2102.
- Pataki, D.E.; Bowling, D.R. & Ehleringer, J.R., (2003). Seasonal cycle of carbon dioxide and its isotopic composition in an urban atmosphere: anthropogenic and biogenic effects. *Journal of Geophysical Research*, Vol. 108, NO.D23, pp. 4735.
- Pataki, D.E.; Bowling, D.R.; Ehleringer, J.R. & Zobitz, J.M. (2006b). High resolution atmospheric monitoring of urban carbon dioxide sources. *Geophysical Research Letters*, Vol. 33, pp. L03813.
- Reich, S.; Magallanes, J.; Dawidowski, L.; Gomez, D.; Groselj, N & Zupan, J. (2006). An analysis of secondary pollutants in Buenos Aires city. *Environmental Monitoring and Assessment*, Vol. 119, pp. 441-457.

- Roba, C., Haiduc, Iv. & Beldean-Galea, M.S.(2009). Diurnal and seasonal variation of CO₂ in urban areas from Cluj county. *Studia Universitatis Babeş-Bolyai, seria Geographia*, Iss, 3, pp. 49-55
- Rubio, M.A.; Lissi, E.; Jorquera, H.; Salinas, E.; Castro, J. & Cádiz, M. (2007). Carbon monoxide concentrations in Santiago City at street levels and their vertical gradient. *Environmental Monitoring and Assessment*, DOI 10.1007/s10661-007-9857-1.
- Sanchez-Ccoyllo, O.R.; Silva Dias, P.L.; de Fatima Andrade, M. & Freitas, S. R. (2006). Determination of O₃, CO- and PM10-transport metropolitan area of São Paulo, Brazil synoptic-scale analysis of back trajectories. *Meteorology and Atmospheric Physics*, Vol. 92, pp. 83-93.
- Sathikunarat, S.; Wongwises, P.; Pan-Aram, R. & Zhang M. (2006). Titlul. *Advances. in Atmospheric Sciences*, Vol. 26, No.6, pp. 901-908.
- Shiva Nagendra, S. M. & Khare, M. (2005). Modelling urban air quality using artificial neural network. *Clean Technology and Environment Policy*, Vol. 7, pp.116-126.
- Sikar, E. & La Scala, N. (2004). Methane and Carbon Dioxide Seasonal Cycles at Urban Brazilian Inland Sites. *Journal of Atmospheric Chemistry* , Vol. 47, No. 2, pp. 101-106.
- Smith, F.A.; Elliott, S.; Blake, D.R. & Sherwood Rowland, F. (2002). Spatiotemporal variation of methane and other trace hydrocarbon concentrations in the Valley of Mexico. *Environmental Science & Policy*, Vol. 249, pp. 1-13.
- Soegaard, H.& Moller-Jensen, L. (2003). Towards a spatial CO₂ budget of a metropolitan region based on textural image classification and flux measurements. *Remote Sensing of Environment*, vol. 87, pp. 283-294.
- Sottocornola, H. & Kiely G. (2010).Hydro-meteorological controls on the CO₂ exchange variation in an Irish blanket bog. *Agricultural and Forest Meteorology*, Vol. 150, pp. 287-297.
- Takahashi, H.; Hiyama, T.; Konohira, E.; Takahashi, A.; Yoshida, N. & Nakamura, T. (2001). Balance and behavior of carbon dioxide at an urban forest inferred from the isotopic and meteorological approaches. *Radiocarbon*, Vol. 43, pp. 659-669.
- Takahashi, H.A.; Konohira, E.; Hiyama, T.; Minami, M.; Nakamura, T. & Yoshida, N. (2002). Diurnal variation of CO₂ concentration, D¹⁴C and d¹³C in an urban forest: estimate of the anthropogenic and biogenic CO₂ contributions. *Tellus*, Vol. 54B, pp. 97-109.
- Thi Nguyen, H.; Kim, K.H.; Ma, C.J.; Cho, S.J. & Ryeul Sohn, (2010). A dramatic shift in CO and CH₄ levels at urban locations in Korea after the implementation of the Natural Gas Vehicle Supply (NGVS) program. *Journal of Environmental Research*, Vol. 110, No.4, pp. 396-409.
- Turias, I.J.; González, F.J.; Martin, M.L. & Galindo, P.L. (2006). A competitive neural network approach for meteorological situation clustering. *Atmospheric Environment*, Vol. 40, Iss. 3, pp. 532-541.
- Veenhuysen, A.; Vermeulen, T.; Hofschreuder P. & Van Den Bulk W.C.M. (1998). Methane emission of the Amsterdam urban area. *Water, Air, and Soil Pollution* , Vol. 107, pp. 321-333.
- Velasco, E.; Pressley, S.; Allwine, E.; Westberg H. & Lamb, B. (2005). Measurements of CO₂ fluxes from the Mexico City urban landscape. *Atmospheric Environment*, Vol. 39, No.38, pp. 7433-7446.

- Venegas, L.E. & Mazzeo, N.A. (2000). Carbon monoxide concentration in a street canyon of Buenos Aires City (Argentina). *Environmental Monitoring and Assessment*, Vol. 65, pp. 417-424.
- Wada, R.; Pearce, J.K.; Nakayama, T.; Matsumi, Y.; Hiyama, T.; Inoue, G. & Shibata, T. (2010). Observation of carbon and oxygen isotopic compositions of CO₂ at an urban site in Nagoya using Mid-IR laser absorption spectroscopy. *Atmospheric Environment*, pp.1-7.
- Wang, J.L.; Kuo, S.R.; Maa, S. & Chen, T.Y. (2001). Construction of a low-cost automated chromatographic system for the measurement of ambient methane. *Analytica Chimica Acta*, Vol. 448, pp. 187-193.
- WHO, 2000: Available from:
http://www.euro.who.int/__data/assets/pdf_file/0005/74732/E71922.pdf
- Widory, D. & Javoy, M. (2003). The carbon isotopic composition of atmospheric CO₂ in Paris. *Earth Planet Science Letter*, Vol. 215, pp. 289-298.
- Wohlfahrt, G.; Hammerle, A.; Haslwanter, A.; Bahn, M.; Tappeiner, U. & Cernusca, A., (2008). Seasonal and inter-annual variability of the net ecosystem CO₂ exchange of a temperate mountain grassland: effects of weather and management. *Journal of Geophysical Research*, Vol. 113, pp. D08110.
- Yamada, K.; Ozaki, Y.; Nakagawa, F.; Tanaka, M. & Yoshida, N. (2003) An improved method for measurement of the hydrogen isotope ratio of atmospheric methane and its application to a Japanese urban atmosphere, *Atmospheric Environment*, Vol. 37, Iss.14, pp. 1975-1982.

Part 5

Urban Air Pollution: Health Effects

Assessment of Environmental Exposure to Benzene: Traditional and New Biomarkers of Internal Dose

Piero Lovreglio¹ et. al.*

*¹Dipartimento di Medicina Interna e Medicina Pubblica,
Sezione di Medicina del Lavoro "E.C. Vigliani"
University of Bari, Bari,
Italy*

1. Introduction

In view of the widespread ubiquity of benzene in the environment and of its carcinogenic effects on man, this toxicant poses a public health problem that has prompted nations to undertake active measures to contain environmental concentrations below the limit judged to be an acceptable risk threshold for the general population (World Health Organization [WHO], 2000).

In the occupational field, until the 1950s benzene was the solvent most commonly employed in some industrial processes, and especially in rubber, printing and shoemaking industries, because of its chemico-physical properties and low cost. This caused exposure of these workers to high benzene concentrations that induced toxic effects and acute non lymphocytic leukemia (Agency for Toxic Substances and Disease Registry [ATSDR], 2007; WHO, 1993). Due to these adverse effects, its use in industrial processes was then abandoned, replacing benzene firstly by hexane, but this proved to provoke peripheral neuropathies, and then by less toxic solvents such as heptane. In Italy the use of benzene as a solvent is banned by Law 245/1963, although traces below 2% are permitted in solvents of a different chemical nature (Italian Parliament, 1963).

Benzene is still used as a raw material or intermediate product in the chemical industry, mainly to synthesize ethylbenzene, cumene and cyclohexane, and to a limited extent as a

* Maria Nicolà D'Errico¹, Silvia Fustinoni², Ignazio Drago¹, Anna Barbieri³, Laura Sabatini³, Mariella Carrieri⁴, Pietro Apostoli⁵, Leonardo Soleo¹

*1 Dipartimento di Medicina Interna e Medicina Pubblica, Sezione di Medicina del Lavoro "E.C. Vigliani".
University of Bari, Bari, Italy*

2 Dipartimento di Medicina del Lavoro, University of Milan and Fondazione IRCCS Ca' Granda Ospedale Maggiore Policlinico, Milano, Italy.

*3 Dipartimento di Medicina Interna, dell'Invecchiamento e Malattie Nefrologiche,
Unità Operativa di Medicina del Lavoro, University of Bologna, Bologna, Italy*

4 Dipartimento di Medicina Ambientale e Sanità Pubblica, University of Padova, Padova, Italy

*5 Dipartimento di Medicina Sperimentale ed Applicata, Sezione di Medicina del Lavoro ed Igiene Industriale,
University of Brescia, Brescia, Italy*

chemical reagent in the laboratory. It is contained in crude oil, that is its main source of production nowadays, and is formed as a result of the incomplete combustion of fossil fuels such as coal and, to a lesser extent, wood.

Moreover, fuels derived from crude oil contain benzene not only because it is already present in the raw material but also because it is formed during the refining process (Brief et al. 1980; Holmberg & Lundberg 1985). For this reason, occupational exposure to benzene, albeit at concentrations of 2-3 orders of magnitude below the occupational limit values, such as the threshold limit value-time weighted average (TLV-TWA) of 1600 $\mu\text{g}/\text{m}^3$ proposed by the American Conference of Governmental Industrial Hygienists (ACGIH), and the European limit value of 3250 $\mu\text{g}/\text{m}^3$ issued by the European Directive 1999/38/CE, is still present in oil refining and petrochemical industries, as well as in fuel tanker drivers and filling station attendants, workers in cokeries and in chemical laboratories (ACGIH, 2010; European Parliament, 1999).

The natural sources of emission into the atmosphere, originally volcanoes and fires, play a negligible role while human activities are the main source of benzene released in the environment (ATSDR, 2007). Among human activities one of the principal forms of emissions of benzene in the environment is in automobile exhaust. Evidence in literature reports higher concentrations of this toxicant in urban and dense traffic areas than in less busy traffic and rural areas.

Another source of environmental pollution by benzene is evaporation during filling operations at gasoline stations or during loading and unloading of fuel tanker lorries, even if the use of aspiration systems to retrieve the vapors during such operations has significantly reduced these emissions, by up to 75% (Duarte-Davidson et al., 2001). In addition, higher concentrations of benzene than the background outdoor levels are present inside vehicles, including buses and private cars, due not only to the penetration inside the body of the vehicle of exhaust fumes from other vehicles, but also to leaks from gasoline tanks and gasoline leads and circuits (Geiss et al., 2009; Li et al., 2009). The levels of benzene emitted by vehicles depend on the type and age of the vehicle, the type of traffic and the ventilation within the body of the car (Duarte-Davidson et al., 2001). Finally, in some geographic areas, apart from road traffic, other sources of benzene emission into the atmosphere, such as factories, hazardous waste dumps and domestic wood fires, can play a significant role in causing outdoor pollution (Barrefors & Petersson, 1995; Edgerton & Shah, 1992).

In western nations, the pollution of urban areas by benzene has gradually declined in recent years, thanks to the legislation introduced to reduce the content of benzene in fuels, currently limited in Italy to concentrations below 1% in volume (law n. 413/97), and to the application in the EU of the norms targeting an annual average exposure for benzene of 5 $\mu\text{g}/\text{m}^3$ as from 2010 (European Commission, 2000; Italian Parliament, 1997). Airborne benzene concentrations are proportionally lower than the true quantity of emissions thanks to the rapid chemical degradation of this toxicant, largely as a reaction to hydroxyl radicals. This limits the persistence of volatile benzene in the atmosphere to a few days or hours.

Active cigarette smoking is another important source of exposure to benzene in the general population, as mainstream smoke contains quantities of 28.0-105.9 $\mu\text{g}/\text{cigarette}$, and sidestream smoke no less than 70.7-134.3 $\mu\text{g}/\text{cigarette}$ (International Agency for Research on Cancer [IARC], 2004). Wallace (1989) estimated a benzene intake of 1.8 mg/day with an average consumption of 32 cigarettes/day, equal to at least 10-fold the intake of a non-smoker, while Duarte-Davidson et al. (2001) estimated a dose of 400 $\mu\text{g}/\text{day}$ of benzene

retained within the organism by a smoker of 20 cigarettes/day. Thus, cigarette smoking can induce a similar or higher benzene intake than that occurring in most occupationally exposed workers in western nations, and certainly higher than the intake caused by environmental exposure to airborne benzene levels near the upper limits for air quality. Moreover, the role of smoking as a source of benzene has become progressively more important as urban pollution levels have declined (Duarte-Davidson et al. 2001; Hattemer-Frey et al. 1990). In fact, in the period 1989-1997 Fruin et al. (2001) observed a marked reduction in the benzene quota derived from the environment (12%) and thus a proportional increase in the quota due to cigarette smoking (78%). Passive smoking can also induce significant exposure to benzene, equal to about 10% of the total intake in non smokers, and higher than the quota contributed by the entire set of US industrial emissions in the atmosphere (Duarte-Davidson et al., 2001; Wallace, 1995). Confirming this, higher benzene concentrations have been reported in homes with one or more smokers among the inhabitants (median $10.6 \mu\text{g}/\text{m}^3$) than in non smoker homes ($7.0 \mu\text{g}/\text{m}^3$) (Wallace 1989).

In man, benzene has myelotoxic and carcinogenic effects. As regards the former environmental exposure to benzene is unlikely to cause the myelosuppression effects previously observed in occupational contexts, since a NOAEL of $1790 \mu\text{g}/\text{m}^3$ has been individuated for these effects, that will probably never again be reached in the human living environment (Collins et al., 1997). The carcinogenic effect manifests in the form of a greater prevalence of acute non lymphocytic leukemia, as stated above. Benzene has been classified carcinogenic to humans by the IARC, ever since the first classification published in the 1980s (IARC, 1982). A review conducted in 2009 confirmed benzene in the same group, associated with acute non lymphocytic leukemia. Instead, there is still only limited evidence of a causal relationship with the onset of acute lymphocytic leukemia, chronic lymphocytic leukemia, multiple myeloma and non-Hodgkin lymphoma (Baan et al., 2009).

Exposure to benzene is considered to induce the onset of leukemias because benzene acts through a genotoxic carcinogenic mechanism, whereby a dose-response relationship of a linear type has been proposed, with no threshold. Although this hypothesis has recently been cast in doubt, the level of exposure that can be considered "safe" has not been identified, but only a LOAEL of $32000\text{-}80000 \mu\text{g}/\text{m}^3$ (Bolt et al., 2008; Duarte-Davidson et al., 2001). As to the carcinogenic risk posed by environmental exposure, the concentration of this toxicant judged to pose an acceptable risk in the general population, exposed over a lifetime, has been estimated on the basis of epidemiological studies of workers occupationally exposed to medium-high concentrations of benzene. The WHO estimate, in particular, predicts an excess risk of $6 \text{ cases} \times 10^{-6}$ for chronic exposure to $1 \mu\text{g}/\text{m}^3$ throughout life (WHO, 2000).

Absorption of benzene in the general population occurs virtually exclusively by inhalation, that accounts for more than 99% of the daily intake of this toxicant, whereas oral intake plays only a minor role, since the quantities of benzene present in water, foods and consumer products are minimal and skin intake is negligible (Hattemer-Frey et al., 1990). After being absorbed, benzene is partly eliminated as is in exhaled air, accounting for 16.8% of the quota absorbed, and in urine, albeit only for 0.1% of the absorbed quota (Ghittori et al., 1993; Nomiyama & Nomiyama, 1974). The remainder is rapidly distributed throughout the organism and undergoes a biotransformation process, prevalently in the liver. This occurs very similar in man and experimental animals, and involves the initial formation of benzene oxide catalyzed by microsomal cytochrome P450 and especially isoenzyme 2E1

(Snyder & Heidli, 1996). After the formation of this reactive intermediate, many different metabolites are then formed in succession through different metabolic pathways, namely phenol, catechol and hydroquinone by oxidation, again catalyzed by cytochrome P450, S-phenylmercapturic acid (SPMA) through the action of the glutathione transferase system, 1,2-benzene dihydrodiol through the action of epoxide hydrolase and the subsequent oxidation to catechol and *t,t*-muconic acid (*t,t*-MA) through the opening of the benzene ring (Snyder et al., 1993). All these metabolites are then excreted in the urine in the form of sulfate or glucuronate derivatives.

For the progressive reduction of the benzene workplace concentrations to which workers are exposed, ever more sensitive and specific biomarkers have needed to be identified, that maintain their validity even in conditions of low or extremely low benzene concentrations. This is why urinary phenol is no longer used in routine practice, because it has poor validity for exposure to less than 16250 $\mu\text{g}/\text{m}^3$, a value that is still one order of magnitude greater than the TLV-TWA of the ACGIH (Boogard & van Sitter, 1995; Ong et al., 1995). The biological markers currently recommended by the ACGIH are *t,t*-MA and SPMA, that reveal an increased urinary excretion already at levels of exposure to airborne benzene concentrations of 65 $\mu\text{g}/\text{m}^3$, while the relation becomes unambiguous at concentrations of more than 650 $\mu\text{g}/\text{m}^3$ (Kim et al., 2006). A new marker of internal dose is now under study, namely the determination of benzene as is in the urine (urinary benzene) that may prove particularly useful to monitor exposure to very low concentrations of airborne benzene, since a correlation has been shown with benzene concentrations ranging from 6 to 478 $\mu\text{g}/\text{m}^3$ (Fustinoni et al., 2005).

Despite the ample volume of studies in the occupational field, the behavior and significance of the above-described biomarkers of internal dose are still little known when used to monitor environmental exposure to airborne benzene concentrations near the upper limit of 5 $\mu\text{g}/\text{m}^3$ for air quality. In particular, the validity of these markers needs to be confirmed as a means of excluding environmental exposure beyond this limit, and hence the presence of a carcinogenic risk above what is considered acceptable. The behavior of these biomarkers of internal dose also needs to be assessed in relation to the relative contributions made to the overall intake of benzene by cigarette smoking and urban pollution, the main sources of environmental exposure to the toxicant.

Aim of the present study was to assess the significance and limits of *t,t*-MA, SPMA and urinary benzene for biological monitoring of subjects with non occupational exposure to very low concentrations of benzene as those found in the general environment, as well as to study the influence of the different sources of environmental exposure on these biomarkers.

2. Materials and methods

2.1 Subjects

The study sample included 123 adult males resident in the cities and hinterland of Bari and Foggia (Apulia - Italy), all in good health and with no occupational exposure to benzene. In the geographic area where this study has been conducted there are no major industries or waste incinerators that could produce benzene emissions. All participants filled out a questionnaire posing questions about personal data, job at the time of the study, smoking habit with particular reference to the number of cigarettes smoked during the environmental sampling, alcohol consumption, personal medical history, time spent in

urban traffic during the environmental sampling, and hobbies. All subjects gave prior written consent to take part in the study.

2.2 Air sampling

Exposure to airborne environmental benzene was monitored in all subjects by passive personal sampling, using radial diffusion samplers (Radiello®) containing an active carbon cartridge, worn in the respiratory zone for 8 hours, typically from 8:30 a.m. to 4:30 p.m. After the sampling, the Radiello® vials were preserved at +4°C until the time of analysis.

Analysis of the vials was then performed by gas chromatography - flame ionization detector after desorption of the benzene from the active carbon with a carbon disulfide low benzene content according to the method reported by the manufacturer (Supelco, 2010). The detection limit of the procedure for benzene was 2 µg/m³. All analyses were performed blinded.

2.3 Urine biomonitoring

Immediately after the environmental sampling, a urine sample was collected from all participants for assays of *t,t*-MA, SPMA and urinary benzene. Each urine sample was subdivided into two aliquots: 30 ml of urine were set aside to determine *t,t*-MA, SPMA and urinary creatinine, preserved in sterile containers, without the addition of preservatives or stabilizers, at -20°C until the time of analysis. The second aliquot, 10 ml of urine used to determine urinary benzene, was immediately transferred to a presealed 20 ml vial containing 4 g of NaCl and preserved at +4°C until the time of analysis. All analyses were conducted blinded.

Urinary *t,t*-MA analysis was carried out with the HPLC-UV method at 264 nm, after solid phase extraction (SPE) (SAX column-Varian) by an analytical method described elsewhere (Aprea et al., 2008). The limit of detection (LOD) of the procedure was 20 µg/L.

The analytical determination of urinary SPMA was performed following the application described in Sabatini et al. (2008). Briefly, after SPE and LC separation, samples were analyzed by a liquid chromatography/electrospray tandem mass spectrometry method (HPLC-ESI-MS/MS), operated in negative ion mode, using isotope-labeled analogs as internal standards. The LOD of the method was 0.03 µg/L.

The analytical determination of benzene in urine was performed by headspace analysis with automated solid phase micro-extraction (SPME), following a previously reported method (Barbieri et al., 2008). A gas chromatograph equipped with a split-splitless injector and coupled to a mass selective detector (GC/MS) was used for analysis. An autosampler (CTC Combi PAL system) was interfaced to GC/MS system for the SPME process. The LOD of the method was 0.02 µg/L.

Analyses of urinary creatinine were performed using the DCA 2000®+ analyzer. The creatinine assay is based on the Benedict/Behre test, and was performed on the same urine samples used for all the other analyses, collected at the end of the environmental sampling (Benedict & Behere, 1936).

All the laboratories conducting the analytical measurements conform to quality assurance procedures and participate in quality control programs.

2.4 Statistical analysis

Statistical analyses were done with the SPSS program (14.0 version, Chicago, IL, USA). A value corresponding to one-half of the LOD was assigned to measurements below the

analytical detection limit. A normal distribution of all the variables was checked with the Kolmogorov-Smirnov test. Non normally distributed variables were analyzed by parametric tests after logarithmic transformation or by non parametric tests. Correlation analyses were done with Spearman's test. Multiple linear regression models were applied to assess a dependency relation of the different biomarkers on the independent variables. The level of significance was set at $p < 0.05$.

3. Results

Of the 123 subjects, 55 were smokers and 68 non smokers, and the population sample featured a wide age (21-62 years) and BMI (19.4-44.4 Kg/m²) range (Table 1).

For all the biomarkers determined, the percentage of cases in the entire sample exceeding the LOD was significantly higher in smokers than non smokers. When the whole sample was subdivided according to exposure to urban traffic or not during the environmental sampling, a higher percentage of results above the LOD was found only for airborne benzene and urinary benzene (Table 2).

	N.	Mean±SD	Median	Range
Age (years)	123	41.5±11.8	44.0	21-62
Body mass index (Kg/m ²)	123	26.8±4.8	25.8	19.4-44.4
Residence				
- urban	79	64.2%		
- rural	44	35.8%		
Alcohol consumption				
- Teetotal	20	16.2%		
- <10 g/day	51	41.5%		
- >10 g/day	52	42.3%		
Smoking habit				
- Smokers	55	44.7%		
- Non smokers	68	55.3%		
N. cigarettes/day*	55	15.8±8.6	15.0	5-40
N. cigarettes smoked during environmental sampling*	55	6.6±4.1	6.0	0-20
Time between last cigarette and urine collection (minutes)*	53	54.3±69.0	30.0	2-360
Exposure to urban traffic during environmental sampling				
- Yes	27	21.9%		
- No	96	78.1%		

*In smokers

Table 1. Personal data of the 123 subjects examined.

	Smoking habit				Exposure to urban traffic			
	Yes		No		Yes		No	
	N _{>LOD} /N	N _{>LOD} /N%	N _{>LOD} /N	N _{>LOD} /N%	N _{>LOD} /N	N _{>LOD} /N%	N _{>LOD} /N	N _{>LOD} /N%
Airborne benzene	14/55	25.5%	20/68	29.4%	18/27	66.7% ^c	16/96	16.7%
<i>t,t</i> -MA	55/55	100.0% ^a	62/68	91.2%	27/27	100.0%	90/96	93.7%
SPMA	44/53	83.0% ^b	2/66	3.0%	12/27	44.4%	34/92	37.0%
Urinary benzene	53/54	98.1% ^b	22/65	33.8%	25/27	92.6% ^c	50/92	54.3%

Smokers vs non smokers: ^ap<0.05; ^bp≤0.001; Exposed vs not exposed to urban traffic: ^cp<0.001

Table 2. Percentage of determinations of airborne benzene, *t,t*-MA, SPMA and urinary benzene above the LOD in the sample, subdivided by smoking habit and exposure to urban traffic during sampling.

To assess a simultaneous influence of smoking habit and exposure to urban traffic on the levels of airborne benzene and the urinary biomarkers, two-way analysis of variance was done, including in the model only the environmental and urinary values exceeding the LOD (Table 3). The results demonstrated an evident association between airborne benzene or *t,t*-MA or urinary benzene and cigarette smoking, whereas it was not possible to perform the analysis for SPMA because only 2 determinations were above the LOD in non smokers. In any case, there was no significant difference in the urinary concentrations of SPMA in smokers between subjects with or without exposure to urban traffic.

	Exposure to urban traffic	Smokers				Non smokers				ANOVA
		N _{>LOD}	Mean±SD	Median	Range	N _{>LOD}	Mean±SD	Median	Range	
Airborne benzene (µg/m ³)	Yes	10	7.4±3.7	7.3	3.9-16.3	8	4.7±1.0	4.5	3.3-6.2	Model: F=8.3 ^a Smoke: F=8.4 ^a Traffic: F=4.0
	No	4	6.2±3.9	5.7	2.0-11.5	12	3.4±1.1	3.0	2.0-5.7	
<i>t,t</i> -MA (µg/g creat)	Yes	14	80.4±52.9	73.5	13.0-196.0	13	51.0±16.5	46.0	30.0-90.0	Model: F=13.0 ^b Smoke: F=14.1 ^b Traffic: F=0.0
	No	41	102.8±58.6	89.7	19.0-307.0	49	55.7±105.0	35.6	9.6-734.0	
SPMA (µg/g creat)	Yes	11	1.47±1.30	0.99	0.38-4.48	1	-	-	-	-
	No	33	1.54±1.19	1.28	0.29-5.22	1	-	-	-	
Urinary benzene (µg/L)	Yes	14	2.24±3.62	0.41	0.04-11.40	11	0.07±0.02	0.06	0.04-0.10	Model: F=21.2 ^b Smoke: F=58.7 ^b Traffic: F=0.0
	No	39	0.97±1.00	0.60	0.06-4.27	11	0.07±0.03	0.06	0.04-0.12	

^ap<0.01; ^bp<0.001

Table 3. Concentrations of airborne benzene, *t,t*-MA, SPMA and urinary benzene in the determinations above the LOD in the sample, subdivided by smoking habit and exposure to urban traffic.

In non smokers, a possible association between exposure to passive smoke during the environmental sampling and higher airborne benzene levels or urinary excretion of its metabolites was studied. No association was found in non smokers exposed or not exposed to passive smoke and airborne benzene and its urinary metabolites (data not shown).

Analysis of correlations between the general lifestyle of the participants, variables linked to smoking habit and exposure to urban traffic, the airborne benzene concentrations and the biomarkers studied was done on the entire sample and then subdivided into smokers and non smokers (Table 4). Airborne benzene was found to be correlated to the time spent in urban traffic during the sampling, both in the entire sample and when analyzing smokers and non smokers separately, whereas there was no correlation between airborne benzene and the number of cigarettes smoked per day or during the sampling time (Table 4). Among the biomarkers studied, airborne benzene was correlated only with urinary benzene, and only in the non smoker group. When analyzing the entire sample together, all the biological markers studied were found to be significantly correlated to the number of cigarettes smoked per day or during the sampling time. In smokers this correlation was significant only for SPMA. Moreover, *t,t*-MA and urinary benzene were correlated in non smokers with the time spent in urban traffic; when taking the group as a whole, this correlation was confirmed for urinary benzene only, albeit with a low rho value. Finally, the three biological markers were all mutually correlated in the entire sample taken as a whole (Table 4).

		Age (years)	BMI	N. cig. /day	N. cig./ sampling	Time since last cig.	Alcohol	Urban traffic (minutes)	Airborne benzene	<i>t,t</i> -MA	SPMA
BMI (Kg/m ²)	Total	0.35 ^c	-	-	-	-	-	-	-	-	-
	Smokers	0.36 ^b	-	-	-	-	-	-	-	-	-
	Non smokers	0.32 ^b	-	-	-	-	-	-	-	-	-
N. cig. /day	Total	-0.22 ^a	-0.05	-	-	-	-	-	-	-	-
	Smokers	-0.08	0.11	-	-	-	-	-	-	-	-
	Non smokers	-	-	-	-	-	-	-	-	-	-
N. cig. / sampling	Total	-0.21 ^a	-0.04	0.94 ^c	-	-	-	-	-	-	-
	Smokers	-0.02	0.08	0.55 ^c	-	-	-	-	-	-	-
	Non smokers	-	-	-	-	-	-	-	-	-	-
Time since last cigarette	Total	-	-	-	-	-	-	-	-	-	-
	Smokers	0.23	0.08	-0.48 ^c	-0.22	-	-	-	-	-	-
	Non smokers	-	-	-	-	-	-	-	-	-	-
Alcohol	Total	0.37 ^c	0.25 ^b	0.005	0.01	-	-	-	-	-	-
	Smokers	0.35 ^b	0.14	0.02	0.11	0.12	-	-	-	-	-
	Non smokers	0.38 ^c	0.37 ^b	-	-	-	-	-	-	-	-
Urban traffic	Total	0.14	0.07	0.04	0.04	-	0.11	-	-	-	-
	Smokers	0.46 ^c	0.31 ^a	-0.13	-0.04	0.21	0.25	-	-	-	-
	Non smokers	-0.17	-0.14	-	-	-	-0.03	-	-	-	-
Airborne benzene	Total	0.17	0.09	0.001	0.03	-	0.11	0.51 ^c	-	-	-
	Smokers	0.33 ^a	0.26	-0.03	0.17	-0.01	0.13	0.61 ^c	-	-	-
	Non smokers	-0.01	-0.06	-	-	-	0.10	0.40 ^c	-	-	-
<i>t,t</i> -MA	Total	-0.15	-0.03	0.57 ^c	0.55 ^c	-	-0.02	0.04	0.04	-	-
	Smokers	0.03	0.10	0.23	0.07	-0.11	0.01	-0.22	-0.13	-	-
	Non smokers	-0.12	-0.12	-	-	-	-0.08	0.29 ^a	0.22	-	-
SPMA	Total	0.05	-0.01	0.76 ^c	0.76 ^c	-	0.11	0.003	0.02	0.56 ^c	-
	Smokers	0.32 ^a	0.08	0.42 ^c	0.43 ^c	-0.17	0.26	-0.13	0.04	0.28 ^a	-
	Non smokers	0.33 ^b	0.04	-	-	-	0.09	0.02	-0.05	0.19	-
Urinary benzene	Total	-0.30 ^c	-0.06	0.77 ^c	0.74 ^c	-	-0.13	0.19 ^a	0.16	0.44 ^c	0.56 ^c
	Smokers	-0.12	0.10	0.23	0.17	-0.18	-0.38 ^b	0.01	0.20	0.14	0.23
	Non smokers	-0.19	-0.08	-	-	-	0.07	0.50 ^c	0.31 ^a	0.06	-0.19

^ap<0.05; ^bp<0.01; ^cp≤0.001

Table 4. Spearman correlations among personal data, lifestyle, airborne benzene and biomarkers in the whole sample and subdivided by smoking habit.

The dependency of *t,t*-MA, SPMA and urinary benzene on the variables age, BMI, number of cigarettes/day, urban traffic and airborne benzene was studied in the sample as a whole,

applying different multiple linear regression models. The results demonstrated a dependency of the urinary concentrations of *t,t*-MA and SPMA on the number of cigarettes smoked per day, and of urinary benzene both on the number of cigarettes/day and on the time spent in urban traffic (Table 5).

To verify the influence of cigarette smoking on the biotransformation of benzene, the urinary benzene/*t,t*-MA ratio was studied in smokers and non smokers, and showed significantly higher levels in smokers (median 0.0071 vs 0.0008; $p \leq 0.001$).

	<i>t,t</i> -MA		SPMA		Urinary benzene	
	t	p	t	p	t	p
Age (years)	NS		NS		NS	
BMI (Kg/m ²)	NS		NS		NS	
N. cigarettes/day	5.8	<0.001	11.9	<0.001	12.5	<0.001
Urban traffic (minutes)	NS		NS		2.1	0.034
Airborne benzene (µg/m ³)	NS		NS		NS	
Model	F	p	R ²	F	p	R ²
	34.2	<0.001	0.22	141.0	<0.001	0.55
					F	p
					80.6	<0.001
						R ²
						0.59

NS= non significant

Table 5. Multiple linear regression analysis of the whole sample, taken as a single group, for the dependent variables *t,t*-MA, SPMA and urinary benzene.

4. Discussion

This research analyzed the contribution of both traditional and new biological markers of internal dose, namely *t,t*-MA and urinary SPMA as compared to urinary benzene, to the monitoring of environmental exposure to very low concentrations of benzene. A particular attention was paid to how much a smoking habit and exposure to urban traffic, the main non occupational sources of this toxicant, could condition the urinary excretion of the various biomarkers.

Environmental monitoring demonstrated that overall, the general population studied was exposed to only very low concentrations of benzene, with 72.4% of the air samples showing values of less than 2 µg/m³, a much higher percentage than in a recent study of a population with no occupational exposure resident in a large Northern Italian city with very dense road traffic, Milan. In that study, the 5th percentile of environmental benzene distribution was equal to 1.5 µg/m³ and the 25th percentile to 3.0 µg/m³ (Fustinoni et al., 2010). Thus, our results suggest that our study sample, resident in small-medium cities with a population of less than 500 thousand inhabitants, is exposed to generally similar or lower levels of environmental pollution by benzene than inhabitants of other industrial, urban and suburban/residential/rural areas in Italy and worldwide (Table 6). Apart from the lesser traffic volume, this difference is also due to climatic conditions, in particular the strong winds that commonly blow in this area and tend to prevent the stagnation of pollutants. Nevertheless, exposure to road traffic was in any case the main factor determining environmental benzene concentrations exceeding the LOD, even if no significantly higher benzene concentrations could be determined in the traffic-exposed group as compared to the non-exposed group when analyzing only the values obtained in excess of the LOD, possibly due to small sample sizes.

Although the airborne benzene levels measured were generally low, concentrations above the threshold limit for air quality of $5 \mu\text{g}/\text{m}^3$ were observed in 13 cases, highlighting the fact that exposure to excess benzene levels in the daily environment is still possible in western nations even nowadays. In fact, the threshold of $5 \mu\text{g}/\text{m}^3$ represents the mean annual exposure posing a carcinogenic risk considered to lie within acceptable limits for the general population with exposure over a lifetime. No definitive level of exposure below which the genotoxic carcinogenic effect of benzene is completely revoked has yet been identified, while adopting a threshold of 0, the only value that could guarantee the absence of risk, seems practically impossible bearing in mind the widespread ubiquity of benzene sources. It is now common practice to use the threshold value for air quality when interpreting the results of personal sampling for carcinogenic environmental agents in both occupational and non-occupational settings. All the same, it must be taken into account that the threshold value represents a mean value referred to annual measurements, and is thus less affected in the long term by the inevitably wide variability of benzene concentrations occurring over such a long period, whereas environmental samplings conducted as in our study refer to a short period, in our case 8 hours, and can therefore be affected by occasional peaks of exposure. Therefore, the finding of values in excess of the $5 \mu\text{g}/\text{m}^3$ threshold during sampling lasting 8 hours does not necessarily indicate a raised health risk.

As regards the influence of a smoking habit, previous studies have demonstrated that the benzene concentrations measured with personal samplers do not reflect the true level of exposure to benzene induced by cigarette smoke (Fustinoni et al., 2005; Lovreglio et al., 2010). The results of the present study partly confirm reports in literature, since a smoking habit did not affect the percentage of benzene determinations exceeding the LOD, and no correlation was observed between airborne benzene and the number of cigarettes smoked during the sampling period. However, higher concentrations of airborne benzene were observed in smokers when only the values exceeding the LOD were analyzed, even after stratification for exposure to urban traffic.

OCCUPATIONAL EXPOSURE						
Occupational settings	Sampling	Year	Exposure levels ($\mu\text{g}/\text{m}^3$)			References
			Mean \pm SD	Median	Range	
Chemicals manufacture Heavy truck drivers Crude petroleum extraction	Personal (8 h) ^{NA}	1996-2007	357.5 \pm 1300.0 357.5 \pm 195.0 97.5 \pm 260.0	- - -	6.5-1300.0 81.2-487.5 3.25-975.0	Scarselli et al., (2011)
Fuel tanker drivers Filling station attendants	Personal (8 h) [*]	2006	306.7 \pm 266.7 23.5 \pm 17.4	246.6 20.9	7.4-1017.1 4.5-66.3	Lovreglio et al., (2010)
Petrochemical factories Gasoline service stations	Ambient (8 h) ^{**}	-	214.6 \pm 78.8 209.9 \pm 57.0	34.6 114.3	5.3-1766.2 5.6-773.6	Navasumrit et al., (2005)
Refinery blue collars	Personal (8h) ^{****}	-		190	60-2310	Fustinoni et al., (2011)
Sewage workplace	Personal (4 d) [*]	2008-2009	19.1 \pm 2.9			Al Zabadi et al.(2011)
Urban policemen	Personal (6 h) ^{***}	2004		9.6	5.4-22.5	Campo et al., (2011)

ENVIRONMENTAL EXPOSURE						
City	Sampling	Year	Exposure levels ($\mu\text{g}/\text{m}^3$)			References
INDUSTRIAL AREA						
URBAN AREA						
Lin-Yuan TWN Ping-Tung TWN	Ambient Outdoor (1-2 h) ^{****}	2003-2004	25.8±34.7 5.9±3.4	8.4 5.0	3.7-120.6 ND-13.7	Hsieh et al., (2006)
La Plata ARG	Ambient Indoor (4 w) ^{**} Ambient Outdoor (4 w) ^{**}	2000-2002	19.1 16.1	18.0 13.4	max 59.5 max 37.2	Massolo et al., (2009)
Yokohama JPN	Ambient Outdoor ^{****}	2007-2008	6.8±8.7			Tiwari et al., (2010)
Dunkerque FRA	Ambient Outdoor [*]	2007	1.9±2.1		0.8-6.7	Roukos et al., (2009)
INDUSTRIAL AREA						
URBAN AREA						
Bangkok THA	Ambient Outdoor Roadside ^{**} Ambient Outdoor School ^{**}	-	109.2±22.4 26.7±2.5	91.8 27.9	50.2-212.9 22.5-28.7	Navasumrit et al., (2005)
Naples ITA	Ambient Outdoor (24h) [*]	2006	9.8±4.4		4.4-17.2	Iovino et al., (2009)
Milano ITA	Personal (72 h) [*] Ambient Indoor work (1 w) [*] Ambient Outdoor work (1 w) [*]	2003	8.5±3.0		Bruinen de Bruin et al., (2008)	
Catania ITA	Personal (72 h) [*] Ambient Indoor work (1 w) [*] Ambient Outdoor work (1 w) [*]		3.0±1.5 1.9±1.4			
	Personal (72 h) [*] Ambient Indoor work (1 w) [*] Ambient Outdoor work (1 w) [*]		5.2±1.6 5.0±3.4 4.2±1.8			
Brussels BEL	Personal (72 h) [*] Ambient Indoor home (1 w) [*] Ambient Indoor work (1 w) [*] Ambient Outdoor work (1 w) [*]		2.0±0.9 1.7±1.0 1.0±0.3 1.0±0.2			
	Personal (72 h) [*] Ambient Indoor home (1 w) [*] Ambient Outdoor work (1 w) [*] Ambient Indoor work (1 w) [*]		3.2±1.4 2.7±1.2 2.1±0.2 1.9±0.6			
Helsinki FIN	Personal (72 h) [*] Ambient Indoor home (1 w) [*] Ambient Outdoor work (1 w) [*] Ambient Indoor work (1 w) [*]	2.0±0.9 1.7±1.0 1.0±0.3 1.0±0.2				
Bucharest ROM Madrid ESP Lisbon PRT Brussels BEL Ljubljana SVN Dublin IRL	Ambient Outdoor (1 d) [*]	2003 2003 2002 2002 2003 2004	7.1 4.5 3.8 2.5 3.1 1.1		max 18.2 max 15.0 max 7.9 max 6.2 max 5.4 max 2.9	Perez Ballesta et al., (2005)
Bari ITA	Personal (8 h) [*]	2006	4.6±2.6	4.3	<3.0-11.5	Lovreglio et al., (2010)
Milan ITA	Personal (5h) [*]	-	4.0		1.5-16.1	Fustinoni et al., (2011)
Beijing CHN	Ambient Outdoor (13 h) ^{****}	2008	3.7±3.0			Liu et al., (2009)
LaPlata ARG	Indoor (4 w) ^{**} Outdoor (4 w) ^{**}	2000-2002	3.6 3.1	3.2 3.1	max 12.7 max 5.6	Massolo et al., (2009)
Bari ITA	Ambient Indoor (24h) [*]	2005	(weekly average) 1.3-14.8			Bruno et al., (2008)
Bari ITA	Ambient Outdoor (1 w) [*]	2008 Autumn 2008 Spring			1.3-9.0 0.8-2.7	Caselli et al., (2010)
Antwerp BEL	Ambient Outdoor (5 d) [*] Ambient Indoor (5 d) [*]	2002-2003	1.9 1.5		0.7-4.4 0.3-3.1	Stranger et al., (2008)

ENVIRONMENTAL EXPOSURE							
City	Sampling	Year	Exposure levels ($\mu\text{g}/\text{m}^3$)			References	
			Mean \pm SD	Median	Range		
URBAN AREA							
Spain	Ambient Outdoor home (1 w)*	2004-2008	1.6 \pm 0.9			Estarlich et al.,(2011)	
Toulouse FRA	Ambient Outdoor *	2001	1.1 \pm 0.3	2.0-0.7		Simon et al., (2004)	
SUBURBAN/ RESIDENTIAL/ RURAL AREA							
Naples ITA	Ambient Outdoor (24h)*	2006	5.7 \pm 3.2	2.3-12.8		Iovino et al., (2009)	
LaPlata ARG	Indoor (4w)**	2000-2002	4.7	3.1	max 13.2	Massolo et al., (2009)	
	Outdoor (4w)**		1.6	1.7	max 1.8		
Spain	Ambient Outdoor home (1 w)*	2004-2008	1.5 \pm 0.7			Estarlich et al., (2011)	
Yokohama JPN	Ambient Outdoor ****	2007-2008	1.3 \pm 1.0			Tiwari et al., (2010)	
Antwerp BEL	Ambient Indoor (5 d) *	2002-2003	0.4			0.1-0.7	Stranger et al., (2008)
	Ambient Outdoor (5 d) *						
Auvergne FRA	Ambient Indoor (1w) *	-	0.8			0.3-9.8	Hulin et al., (2010)

* passive sampling by Radiello; ** passive sampling by 3M OVM 3500; *** passive sampling by Carbopack B; **** active sampling; ^{NA} not available; (sampling period): h= hour; d= day; w= week.

Table 6. Levels of occupational and environmental exposure to benzene observed in the last 10 years.

Thanks to progressive improvements in the analytical techniques used to assay biomarkers since the 1970s, it has become possible to measure ever lower concentrations of chemical substances or their metabolites in human biological fluids after exposure to toxicants in the daily environment. For this reason, from being a tool used exclusively to assess occupational risks, biological monitoring has now become a valuable means of evaluating the risk of exposure to toxicants in the daily environment that integrates, but does not replace, environmental monitoring results. It thus could play a central role in public health and environmental medicine policies, helping to identify population groups at higher risk of exposure and/or effects, contributing to measure the internal dose and thus providing helpful information that can direct subsequent corrective measures (Angerer et al., 2007).

The results of biological monitoring in the general public are generally interpreted by comparison with reference values. These are obtained by statistical processing of the results of assays of the concentrations of a toxicant or its metabolites in biological fluids collected from a population or reference group with no occupational exposure to the substance (Apostoli & Minoia, 1999). It must be remembered, however, when assessing the risk of exposure to benzene, that unlike the threshold for air quality that derives from an estimate, albeit indirect, of the carcinogenic risk of exposure to benzene judged acceptable for the general population, the reference values do not bear any relation to the carcinogenic effect of benzene. Although the use of reference values does not therefore allow us to exclude a public health risk, it is important as a means of individuating specific population groups with higher levels of exposure to a toxicant than those of the reference population, due to residence in a highly polluted area, for instance, thus addressing one of the main objectives of biological monitoring in the non occupational field.

Many biological monitoring studies have been conducted to assess occupational exposure to benzene, but only few studies of the living environment. Moreover, these experiences have been gained largely in workers such as traffic wardens or public transport drivers who have occupational exposure to road traffic and so to generally higher concentrations of benzene than those affecting the general population (Barbieri et al., 2008; Campo et al., 2011; Fustinoni et al., 2005; Manini et al., 2008).

In this work the three main biological markers of internal dose currently in use, or under study for validation in biological monitoring of exposure to benzene, namely *t,t*-MA, SPMA and urinary benzene, were studied. Urinary *t,t*-MA is the only one of the three that is not entirely specific for benzene, since it can also derive from the metabolism of sorbic acid, an anti-mycotic preservative present in many foods, and so commonly absorbed in the diet, and in cosmetics. Although only a small percentage of the sorbic acid ingested is biotransformed to *t,t*-MA, the contribution of the diet can induce comparable concentrations of this metabolite to those observed in workers with occupational exposure to benzene levels equal to the TLV-TWA of ACGIH. Indeed, this phenomenon is growing proportionally as environmental exposure to benzene declines (Pezzagno et al., 1999). In 8 urine samples observed in the present population the concentrations of *t,t*-MA were above the upper limit of the reference range for the Italian population, equal to 15.2-163.1 µg/g creatinine (5th-95th percentile), recently defined in a multicentric national study (Aprea et al., 2010). However, the concentrations observed seem to be in line with the reference values for male subjects subdivided by smoking habit, since only 1 smoker and 3 non smokers had values exceeding the 95th percentile established for the relative group (274.7 µg/g creatinine and 117.8 µg/g creatinine, respectively).

The concentrations of *t,t*-MA, unlike those of the other markers of internal dose studied, were nearly always above the LOD, even in the non smokers. Moreover, the highest concentration, 734.0 µg/g creatinine, that is, in fact, higher than the BEI of 500 µg/g creatinine recommended by the ACGIH to control occupational exposure, was observed in a non smoker without exposure to urban traffic. This result could be attributed to the intake of sorbic acid in the diet. However, assessment of the contribution of sorbic acid to the *t,t*-MA levels excreted in the population studied was not possible because no data were available on the population's diet in the days before the study. Despite the reduced specificity of *t,t*-MA, cigarette smoke can condition urinary excretion of this marker, that shows a dependency relation on the number of cigarettes/day characterized by a R² of 0.22. This finding is in agreement with those by Pezzagno et al. (1999), who estimated that only 25% of urinary *t,t*-MA can be attributed to the biotransformation of benzene.

This dependency of urinary *t,t*-MA on the dietary intake of sorbic acid and the quantity of benzene absorbed in cigarette smoke explains the absence of a relation between *t,t*-MA and the concentrations of airborne benzene, and hence the poor validity of this marker as a means of monitoring exposure to very low concentrations of benzene like those observed in this study. Nevertheless, a significant correlation was found, when considering only the non smokers, between urinary *t,t*-MA and the time spent in urban traffic, in agreement with the report by Bergamaschi et al. (1999).

Unlike *t,t*-MA, SPMA is a highly specific metabolite of benzene, and in the occupational field it has been shown to be a valid biomarker of exposure to even low concentrations of this toxicant (Hoet et al., 2009). All the SPMA assays made in our sample, both adjusted and non adjusted for creatinine, were below the top limit of the reference values for the Italian population of 0.1-10 µg/L (5th-95th percentile) (Biolind, 2011), even if in 15 smokers and 2

non smokers the concentrations were higher than the 95th percentile of the values recently observed in a population with no occupational exposure resident in a northern Italian city (Milan) (Fustinoni et al., 2011). Cigarette smoke seems to be the only environmental factor causing such a high absorption of benzene as to condition the urinary excretion of SPMA, that was higher than the LOD practically only in smokers, yielding comparable results to those previously observed in a study of a population with no occupational exposure to benzene (Lovreglio et al., 2010). Unlike what was observed in subjects with occupational and non occupational exposure to higher concentrations of benzene, ranging from <3.0 to 66.5 $\mu\text{g}/\text{m}^3$, in which SPMA was found to be dependent not only on the number of cigarettes smoked per day but also on the levels of airborne benzene, in subjects exposed to concentrations of less than 16.3 $\mu\text{g}/\text{m}^3$, as in this study, SPMA was found to be conditioned only by a smoking habit (Lovreglio et al., 2011). Thus, urinary SPMA can be considered a very valid biomarker of internal dose when assessing exposure to low concentrations of benzene or excluding occupational exposure to benzene, but less useful for monitoring exposure to very low concentrations of benzene like those present in the living environment. Instead, thanks to its specificity and high sensitivity, urinary benzene has been proposed as a valid biomarker of even very low concentrations of benzene (Fustinoni et al. 2011). There are still some limits to the use of reference values to interpret the results of urinary benzene because the method for the pre-analytical phase of sample collection has not yet been standardized. This could explain why the top limit of the reference values for the Italian population of 0.05-1.45 $\mu\text{g}/\text{L}$ (5th-95th percentile) was exceeded in 14 determinations (Biolind, 2011), all in smoker subjects, whereas comparison with other recent data on a non occupationally exposed population showed values exceeding the 95th percentile only in 7 determinations, again all smokers (Fustinoni et al., 2011). In agreement with the data in literature, cigarette smoking is confirmed to be the main factor conditioning urinary benzene concentrations. In addition, unlike SPMA, it was dosable in 1/3 of the non smokers and showed a higher percentage of determinations above the LOD in subjects exposed to urban traffic than in those with no such exposure. Therefore, urinary benzene seems to be able to reflect even exposure to benzene due to pollution in urban areas, in agreement with what was previously observed in a population with exposure to higher concentrations of benzene attributable to the pollution of urban areas (Fustinoni et al., 2010). Moreover, urinary benzene was found to be the only biomarker correlated to the concentrations of airborne benzene after excluding the contribution of cigarette smoking, in agreement with the reports by Fustinoni et al. (2010) and Campo et al. (2011). The concentrations of airborne benzene in the latter two studies were higher than those in our study (median values 4.0 and 9.6 $\mu\text{g}/\text{m}^3$ vs. <2.0 $\mu\text{g}/\text{m}^3$). The different trend of airborne benzene-urinary benzene correlations in smokers versus non smokers seems to confirm a confounding effect of the relation between exposure to airborne benzene and the biomarkers of internal dose due to a compounding effect of the benzene absorbed with cigarette smoke. This aspect was already emphasized in our previous experience as an important point to be taken into account when interpreting the results of biological monitoring to assess non occupational exposure to benzene.

5. Conclusion

Overall, our results seem to highlight that even when assessing the risk of non occupational exposure to benzene to exclude the possibility that a given population is exposed to higher

concentrations of benzene than the reference population, biological monitoring with different biomarkers of internal dose can usefully integrate environmental monitoring results. In this sense, the use of reference values can have a great importance, especially if smokers and non smokers are considered separately. In fact, in agreement with the findings in previous studies, cigarette smoking was shown to be the main non occupational source of benzene in smokers, that conditions the urinary excretion of all the biomarkers studied. Moreover, our results seem to confirm that even in conditions of exposure to very low benzene concentrations there is a competitive inhibitory effect of cigarette smoking on the metabolism of this toxicant, that induces proportionally higher concentrations of urinary benzene in smokers than of the metabolites such as *t,t*-MA. This can be explained by the presence of high quantities of chemical substances in cigarette smoke, that are partly metabolized through the same biotransformation pathways as benzene, especially via the oxidation of CYP2E1 (van Vleet et al., 2001).

Among the biomarkers analyzed in this study, urinary benzene seems to be the most sensitive and so the only one with a dependency relation not only on cigarette smoking but also on the time spent in urban traffic, as well as being the only one found to be correlated with the concentrations of airborne benzene, after excluding the effect of cigarette smoking. Thus, urinary benzene can be considered the biomarker of choice for assessing exposure to benzene in the daily environment, especially in terms of the contribution of urban traffic, but it is essential to take a smoking habit into account when interpreting the results of such studies.

6. References

- Agency for Toxic Substances and Disease Registry. (2007). *Toxicological profile for benzene*. ATSDR, US Department of Health and Human Services, Public Health Service, Atlanta, GA, US
- Al Zabadi, H., Ferrari, L., Sari-Minodier, I., Kerautret, M.A., Tiberghent, A., Paris, C., Zmirou-Navier, D. (2011). Integrated exposure assessment of sewage workers to genotoxicants: an urinary biomarker approach and oxidative stress evaluation. *Environmental Health*, 10, pp.23
- American Conference of Governmental Industrial Hygienists. (2010). *Threshold limit values and biological exposure indices*. ACGIH, ISBN 978-1-607260-19-6, Cincinnati, OH, US
- Angerer, J., Ewers, U. & Willhelm, M. (2007). Human biomonitoring: state of the art. *International Journal of Hygiene and Environmental Health*, 210 (3-4), pp. 201-228
- Apostoli, P. & Minoia, C. (1999). I valori di riferimento in medicina occupazionale ed ambientale. *Giornale Italiano di Medicina del Lavoro ed Ergonomia*, 21(1), pp.25-39
- Aprea, C., Sciarra, G., Bozzi, N., Pagliantini, M., Perico, A., Bavazzano, P., Leandri, A., Carrieri, M., Scapellato, M.L., Bettinelli, M. & Bartolucci, G.B. (2008). Reference Values of Urinary *Trans,trans*-muconic Acid: Italian Multicentric Study. *Archives of Environmental Contamination and Toxicology*, 55(2), pp.329-340
- Baan, R., Grosse, Y., Straif, K., Secretan, B., El Ghissassi, F., Bouvard, V., Benbrahim-Tallaa, L., Guha, N., Freeman, C., Galichet & L., Coglianò, V. on behalf of WHO International Agency for Research on Cancer Monograph Working Group. (2009). A review of human carcinogens-part F: Chemical agents and related occupations. *Lancet Oncology*, 10, pp.1143-1144

- Barbieri, A., Violante, F.S., Graziosi, F., Sabatini, L. & Mattioli, S. (2008). Urinary biomarkers and low-level environmental benzene concentration: assessing occupational and general exposure. *Chemosphere*, 74(1), pp.64-69
- Barrefors, G. & Petersson, G. (1995). Assessment by gas chromatography and gas chromatography-mass spectrometry of volatile hydrocarbons from biomass burning. *Journal of Chromatography A*, 710, pp.71-77
- Benedict, S.R. & Behre, J.A. (1936). Some application of a new color reaction for creatinine. *The Journal of Biology Chemistry*, 114, pp.515-532
- Bergamschi, E., Brustolin, A., De Palma, G., Manini, P., Mozzoni, P., Andreoli, R., Cavazzini, S. & Mutti, A. (1999). Biomarkers of dose and susceptibility in cyclists exposed to monoaromatic hydrocarbons. *Toxicology Letters*, 108(2-3), pp.241-247
- BIOLIND. (2011). In: *BIOLIND.NET*, Lista Valori di Riferimento SIVR 2005, last accessed 22.03.11, Available from <http://www.biolind.net/default.asp?nc=3346&id=161>
- Bolt, H.M. & Huici-Montagud, A. (2008). Strategy of the scientific committee on occupational exposure limits (SCOEL) in the derivation of occupational exposure limits for carcinogens and mutagens. *Archives of Toxicology*, 82(1), pp.61-64
- Boogaard, P.J. & van Sittert, N.J. (1995). Biological monitoring of exposure to benzene: a comparison between S-phenylmercapturic acid, trans, trans-muconic acid, and phenol. *Occupational and Environmental Medicine*, 52(9), pp.611-620
- Brief, R.S., Lynch, J., Bernath, T. & Scala, R.A. (1980). Benzene in the workplace. *American Industrial Hygiene Association Journal*, 41(9), pp.616-623
- Bruinen de Bruin, Y., Koistinen, K., Kephelopoulos, S., Geiss, O., Tirendi, S., Kotzias, D. (2008). *Environmental Science and Pollution Research International*, 15(5), pp.417-430
- Bruno, P., Caselli, M., De Gennaro, G., Iacobellis, S., Tutino, M. (2008). Monitoring of volatile organic compounds in non-residential indoor environments. *Indoor Air*, 18(3), pp.250-256
- Campo, L., Cattaneo, A., Consonni, D., Scibetta, L., Costamagna, P., Cavallo, D.M., Bertazzi, P.A. & Fustinoni, S. (2011). Urinary methyl tert-butyl ether and benzene as biomarkers of exposure to urban traffic. *Environment International*, 37(2), pp.404-411
- Caselli, M., De Gennaro, G., Marzocca, A., Trizio, L., Tutino, M. (2010). Assessment of the impact of the vehicular traffic on BTEX concentration in ring roads in urban areas of Bari (Italy). *Chemosphere*, 81(3), pp.306-311
- Collins, J.J., Ireland, B.K., Easterday, P.A., Nair, R.S., Braun, J. (1997). Evaluation of lymphopenia among workers with low-level benzene exposure and the utility of routine data collection. *Journal of Occupational and Environmental Medicine*, 39(3), pp.232-237
- Duarte-Davidson, R., Courage, C., Rushton, L. & Levy, L. (2001). Benzene in the environment: an assessment of the potential risks to the health of the population. *Occupational and Environmental Medicine*, 58(1), pp.2-13
- Edgerton, S.A. & Shah, J.J. (1992). Assessing total exposures to gasoline vapor using the source exposure model. *Journal of Exposure Analysis and Environmental Epidemiology*, 2(1), pp.109-115
- Estarlich, M., Ballester, F., Aguilera, I., Fernandez-Somoano, A., Lertxundi, A., Llop, S., Freire, C., Tardon, A., Basterrechea, M., Sunyer, J., Inguez, C. (2011). Residential Exposure to Outdoor Air Pollution during Pregnancy and Anthropometric

- Measures at Birth in a Multicenter Cohort in Spain. *Environmental Health Perspectives*, doi:10.1289/ehp.1002918
- European Commission. (2000). Directive 2000/69/EC of the European Parliament and of the Council of 16 November relating to limit values for benzene and carbon monoxide in ambient air. *Official Journal of the European Communities*, L313/12 of 13/12/2000
- European Parliament. (1999). Council Directive 1999/38/EC of 29 April 1999 amending for the second time Directive 90/394/EEC on the protection of workers from the risks related to exposure to carcinogens at work and extending it to mutagens. *Official Journal of the European Communities*, L138/66 of 01/06/1999
- Fruin, S.A., St. Denis, M., Winer, A.M., Colome, S.D. & Lurmann, F.W. (2001). Reductions in human benzene exposure in the California South Coast Air Basin. *Atmospheric Environment*, 35(6), pp.1069-1077
- Fustinoni, S., Consonni, D., Campo, L., Buratti, M., Colombi, A., Pesatori, A.C., Bonzini, M., Bertazzi, P.A., Foà, V., Garte, S., Farmer, P.B., Levy, L.S., Pala, M., Valerio, F., Fontana, V., Desideri, A. & Merlo, D.F. (2005). Monitoring low benzene exposure: comparative evaluation of urinary biomarkers, influence of cigarette smoking, and genetic polymorphisms. *Cancer Epidemiology, Biomarkers & Prevention*, 14(9), pp.2237-2244
- Fustinoni, S., Rossella, F., Campo, L., Mercadante, R. & Bertazzi, P.A. (2010). Urinary BTEX, MTBE and naphthalene as biomarkers to gain environmental exposure profiles of the general population. *Science of the Total Environment*, 408(14), pp.2840-2849
- Fustinoni, S., Campo, L., Mercadante, R., Consonni, D., Miekzynska, D. & Bertazzi, P.A. (2011). A quantitative approach to evaluate urinary benzene and S-phenylmercapturic acid as biomarkers of low benzene exposure. *Biomarkers*, DOI: 10.3109/1354750X.2011.561499
- Geiss, O., Tirendi, S., Barrero-Moreno, J. & Kotzias, D. (2009). Investigation of volatile organic compounds and phthalates present in the cabin air of used private cars. *Environment International*, 35(8), pp.1188-1195
- Ghittori, S., Fiorentino, M.L., Maestri, L., Cordioli, G. & Imbriani, M. (1993). Urinary excretion of unmetabolized benzene as an indicator of benzene exposure. *Journal of Toxicology and Environmental Health*, 38(3), pp.233-243
- Hattemer-Frey, H.A., Travis, C.C. & Land, M.L. (1990). Benzene: Environmental partitioning and human exposure. *Environmental Research*, 53(2), pp.221-232
- Hoet, P., De Smedt, E., Ferrari, M., Imbriani, M., Maestri, L., Negri, S., De Wilde, P., Lison, D. & Haufroid, V. (2009). Evaluation of urinary biomarkers of exposure to benzene: correlation with blood benzene and influence of confounding factors. *International Archives of Occupational and Environmental Health*, 82(8), pp.985-995.
- Holmberg, B. & Lundberg, P. (1985). Benzene: Standards, occurrence, and exposure. *American Journal of Industrial Medicine*, 7(5-6), pp.375-383
- Hsieh, L.T., Yang, H.H., Chen, H.W. (2006). Ambient BTEX and MTBE in the neighborhoods of different industrial parks in Southern Taiwan. *Journal of Hazardous Materials*, 128(2-3), pp. 106-115
- Hulin, M., Caillaud, D., Annesi-Maesano, I. (2010). Indoor air pollution and childhood asthma: variations between urban and rural areas. *Indoor Air*, 20(6), pp.502-514

- International Agency for Research on Cancer. (1982). Benzene, In: *Monographs on the Evaluation of the Carcinogenic Risk of Chemicals to Humans. Vol. 29. Some industrial chemicals and dyestuffs*. pp. 93, IARC, Lyon (France)
- International Agency for Research on Cancer. (2004). *Monographs on the Evaluation of Carcinogenic Risks to Humans. Vol. 83. Tobacco Smoke and Involuntary Smoking*, IARC, ISBN 92 832 1283 5, Lyon (France)
- Iovino, P., Polverino, R., Salvestrini, S., Capasso, S. (2009). Temporal and spatial distribution of BTEX pollutants in the atmosphere of metropolitan areas and neighbouring towns. *Environmental Monitoring and Assessment*, 150(1-4), pp.437-444
- Italian Parliament. Law n. 245 of 5.03.1963. Limitazione dell'impiego del benzolo nelle attività lavorative. *Official Journal of the Italian Republic*, n. 77 of 21.03.1963, Ordinary Supplement n. 108. Istituto Poligrafico Zecca dello Stato, Rome
- Italian Parliament. Law n. 413 of 4.11.1997. Misure urgenti per la prevenzione dell'inquinamento atmosferico da benzene. *Official Journal of the Italian Republic*, n. 282 of 3.12.1997. Istituto Poligrafico Zecca dello Stato, Rome
- Kim, S., Vermeulen, R., Waidyanatha, S., Johnson, B.A., Lan, Q., Smith, M.T., Zhang, L., Li, G., Shen, M., Yin, S., Rothman, N. & Rappaport, S.M. (2006). Modeling human metabolism of benzene following occupational and environmental exposures. *Cancer epidemiology, Biomarkers & Prevention*, 15(11), pp.2246-2252
- Li, S., Chen, S., Zhu, L., Chen, X., Yao, C. & Shen, X. (2009). Concentrations and risk assessment of selected monoaromatic hydrocarbons in buses and bus stations of Hangzhou, China. *Science of the Total Environment*, 407(6), pp.2004-2011
- Liu, J., Mu, Y., Zhang, Y., Zhang, Z., Wang, X., Liu, Y, Sun, Z. (2009). Atmospheric levels of BTEX compounds during the 2008 Olympic Games in the urban area of Beijing. *Science of the Total Environment*, 408(1), pp.109-116
- Lovreglio, P., Barbieri, A., Carrieri, M., Sabatini, L., Fracasso, M.E., Doria, D., Drago, I., Basso, A., D'Errico, M.N., Bartolucci, G.B., Violante, F.S. & Soleo L. (2010). Validity of new biomarkers of internal dose for use in the biological monitoring of occupational and environmental exposure to low concentrations of benzene and toluene. *International Archives of Occupational and Environmental Health*, 83(3), pp.341-356
- Lovreglio, P., Cancanelli, G., Barbieri, A., Sabatini, L., D'Errico, M.N., Scicolone, L., Ghitti, R., Violante, F.S., Apostoli, P. & Soleo, L. (2010). Ruolo dei fattori non occupazionali nel condizionare i livelli di indicatori di dose interna utilizzati per monitorare l'esposizione occupazionale a concentrazioni molto molto basse di benzene. *Giornale Italiano di Medicina del Lavoro ed Ergonomia*, 32(1), pp.49-58
- Lovreglio, P., Carrieri, M., Barbieri, A., Sabatini, L., Fracasso, M.E., Doria, D., Iavicoli, S., Drago, I., D'Errico, M.N., Imbriani, M., Violante, F.S., Bartolucci, G.B. & Soleo, L. (2011). Applicability of urinary benzene to biological monitoring of occupational and environmental exposure to very low benzene concentrations. *Giornale Italiano di Medicina del Lavoro ed Ergonomia*, 33(1), pp.41-46
- Manini, P., De Palma, G., Andreoli, R., Poli, D., Petyx, M., Corradi, M., Mutti, A. & Apostoli, P. (2008). Biological monitoring of low benzene exposure in Italian traffic policeman. *Toxicology Letters*, 181(1), pp.25-30
- Massolo, L., Rehwagen, M., Porta, A., Ronco, A., Herbarth, O., Mueller, A. (2010). Indoor-outdoor distribution and risk assessment of volatile organic compounds in the

- atmosphere of industrial and urban areas. *Environmental Toxicology*, 25(4), pp.339-349
- Navasmrit, P., Chanvaivit, S., Intarasunanont, P., Arayasiri, M., Lauhareungpanya, N., Parnlob, V., Settachan, D., Ruchirawat, M. (2005). Environmental and occupational exposure to benzene in Thailand. *Chemico-biological Interactions*, 153-154, pp. 75-83
- Nomiyama, K. & Nomiyama, H. (1974). Respiratory elimination of organic solvents in man. Benzene, toluene, n-hexane, trichloroethylene, acetone, ethyl acetate and ethyl alcohol. *Internationales Archiv für Arbeitsmedizin*, 32(1), pp.85-91
- Ong, C.N., Kok, P.W., Lee, B.L., Shi, C.Y., Ong, H.Y., Chia, K.S., Lee, C.S. & Luo, X.W. (1995). Evaluation of biomarkers for occupational exposure to benzene. *Occupational and Environmental Medicine*, 52(8), pp.528-533
- Perez Ballesta, P., Field, R.A., Connolly, R., Cao, N., Baeza Caracena, A., De Saeger E. (2006). Population exposure to benzene: One day cross-sections in six European cities. *Atmospheric Environment*, 40, pp.3355-3366
- Pezzagno, G., Maestri, L. & Fiorentino, M.L. (1999). Trans,trans-muconic acid, a biological indicator to low levels of environmental benzene: some aspects of its specificity. *American Journal of Industrial Medicine*, 35(5), pp.511-518
- Roukos, J., Riffault, V., Locoge, N., Plaisance, H. (2009). VOC in an urban and industrial harbor on the French North Sea coast during two contrasted meteorological situations. *Environmental Pollution*, 157(11), pp.3001-3009
- Sabatini, L., Barbieri, A., Indiveri, P., Mattioli, S. & Violante, F.S. (2008). Validation of an HPLC-MS/MS method for the simultaneous determination of phenylmercapturic acid, benzylmercapturic acid and o-methylbenzylmercapturic acid in urine as biomarkers of exposure to benzene, toluene and xylenes. *Journal of Chromatography B*, 863(1), pp.115-122
- Scarselli, A., Binazzi, A., Di Marzio, D. (2011). Occupational exposure levels to benzene in Italy: findings from a national database. *International Archives of Occupational and Environmental Health*, DOI 10.1007/s00420-011-0616-9
- Simon, V., Baer, M., Torres, L., Olivier, S., Meybeck, M., Della Massa, J.P. (2004). The impact of reduction in the benzene limit value in gasoline on airborne benzene, toluene and xylenes levels. *Science of the Total Environment*, 334-335, pp.177-183
- Snyder, R., Witz, G. & Gildstein, B.D. (1993). The toxicology of benzene. *Environmental Health Perspectives*, 100, pp.293-306
- Snyder, R. & Hedli, C.C. (1996). An overview of benzene metabolism. *Environmental Health Perspectives*, 10 (supp 6), pp.1165-1171
- Stranger, M., Potgieter-Vermaak, S.S., Van Grieken, R. (2008). Characterization of indoor air quality in primary schools in Antwerp, Belgium. *Indoor Air*, 18(6), pp.454-463
- Supelco. (2011). Volatile organic compounds (VOCs) chemically desorbed with CS₂. In: *Application Note Radiello*, 22.03.2011, Available from http://www.sigmaaldrich.com/etc/medialib/docs/Supelco/Application_Notes/radiello_d1_d6.Par.0001.File.tmp/radiello_d1_d6.pdf.
- Tiwari, V., Hanai, Y., Masunaga, S. (2010). Ambient levels of volatile organic compounds in the vicinity of petrochemical industrial area of Yokohama, Japan. *Air Quality, Atmosphere, & Health*, 3(2), pp.65-75

- Van Vleet, T.R., Bombick, D.W. & Coulombe, R.A. Jr. (2001). Inhibition of human cytochrome P450 2E1 by nicotine, cotinine, and aqueous cigarette tar extract in vitro. *Toxicological Sciences*, 64(2), pp.185-191
- Wallace, L.A. (1989). Major sources of benzene exposure. *Environmental Health Perspectives*, 82, pp.165-169
- Wallace, L.A. (1995). Human exposure to environmental pollutants: A decade of experience. *Clinical and Experimental Allergy*, 25(1), pp.4-9
- World Health Organization. (1993). *Environmental Health Criteria 155. Benzene*. WHO, Geneva (Switzerland).
- World Health Organization. (2000). Benzene, In: *Air quality guidelines for Europe. Second Edition*. WHO, pp. 1-18, Copenhagen (Denmark), Available from http://www.euro.who.int/__data/assets/pdf_file/0017/123056/AQG2ndEd_5_2_benzene.pdf

The Influence of Air Pollutants on the Acute Respiratory Diseases in Children in the Urban Area of Guadalajara

Ramírez-Sánchez HU, Meulenert-Peña AR, García-Guadalupe ME,
García-Concepción FO, Alcalá-Gutiérrez J and Ulloa-Godínez HH
*Astronomy and Meteorology Institute, University of Guadalajara
México*

1. Introduction

Today environmental pollution problems are well known, particularly air pollution, which gives rise to health risks and impacts the well being of the population. Many of the pollutants emitted into the atmosphere generate problems in the short and long term (i.e. global warming, climate change); also at local and regional levels, they generate public health problems such as respiratory and cardiovascular diseases (Ramírez-Sánchez et al., 2006; Romieu, 1991, 1995; Segala, 1999; World Health Organization/United Nations Environmental Programme [WHO/UNEP], 1995; Departamento del Distrito Federal/Gobierno del Estado de México/ Secretaría del Medio Ambiente, Recursos Naturales y Pesca/Secretaría de Salud [DDF/GEM/SEMARNAP/SS], 1990).

Both in the clinical and public health fields, air pollution is a phenomenon known and studied for a long time; however, it gained importance because of a series of episodes that occurred during the first half of the 20th century. The events of Meuse Valley, Belgium in 1930 (Firket, 1936), Donora, Pennsylvania, USA in 1948 (Shrenk, 1949) and London in December 1952 (Ministry of Health, United Kingdom [MHUK], 1954), would perhaps be the most notable and characteristic. These exceptional circumstances resulted in an increase in the mortality and morbidity rate, which left no doubt that high levels of air pollution are causally associated with an increase in early deaths (Schwartz & Marcus, 1990). In the London episode, dense fog covered the city from December 5th through the 8th of 1952, accompanied by an increase in mortality. The number of deaths attributed to this episode was between 3,500 and 4,000. This evidence led to the adoption of air pollution reduction control policies in Western Europe and in the United States.

Children are particularly vulnerable to environmental risks. Over 40% of global morbidity is attributed to environmental conditions affecting children under 5 years of age, a risk about four times greater than in the general population (Smith et al., 1999; Pan American Health Organization [PAHO], 2004b).

According to data from PAHO/WHO, there is little information on incidence and prevalence of respiratory diseases belonging to the group of Acute Respiratory Infections (ARI). However, in Latin American countries, all agree that the ARI represents the main cause of pediatric outpatient cases. Some studies have shown that between 40 and 60

percent of consultations are from ARI. It is common that children receive medical attention four to six times a year, with seasonal variation, which implies a high demand for healthcare. Only a small portion of the large volume of inquiries is for serious cases such as pneumonia or bronchiolitis in young children. In general these are viral infections of the upper respiratory tract and are usually self-limited and resolve spontaneously with home care. According to estimates from the late eighties and early nineties, in the Region of the Americas, ARI accounted for more than 100,000 annual deaths among children less than 1 year of age. About 90% of these deaths are due to pneumonia (PAHO, 1994).

Globally, high child mortality rates from ARI were recorded, with marked differences between developed and developing countries (PAHO, 1980). In some Latin American countries, the risk of dying from this cause in the first year of life can be up to 30 times higher than in the USA (Pio et al., 1984a). It is estimated that in developed countries, 2 percent of children die from pneumonia, while in countries with limited resources, the mortality rate ranges from 10 to 20 percent. In a study conducted by PAHO on the infant mortality rate from influenza and pneumonia in Latin America in children under 5 years, when comparing the deaths in the sixties with those of the seventies (Pio et al., 1984a), a decline in mortality is seen between one decade and another, but persists in 1977 with rates of 1,419 (per 100,000) in Guatemala and 1,718 in Peru. At the same time in Uruguay, the mortality rate for similar cases in children under one year was 241 per 100,000 live births and under 5 years, 67.8. However, the infant mortality rate in some countries is low as a result of relating them to the general population, which dilutes these figures. Analyzing the information reveals special risk groups where infant deaths are concentrated. In Mexico, mortality decreased but remains a risk to the children population as demonstrated in Table 1.

Year	< 1 year		1 - 4 years	
	Deaths	Rate ¹	Deaths	Rate ²
1990	10122	370.0	2785	32.7
1991	8594	311.8	1651	19.4
1992	8127	290.5	1470	17.2
1993	6996	246.4	1614	18.9
1994	7687	264.7	1669	18.8
1995	6955	252.9	1694	19.8
1996	6647	245.5	1498	16.9
1997	6218	281.2	1259	14.2
*Includes pneumonia and influenza				
¹ Rate per 100 000 live births registered (NVR)				
² Rate per 100 000 inhabitants in the age group				
Source, Department of Statistics and Informatics. S.S.A.				

Table 1. Mortality rates due to ARI* in children by age group under five years (Mexico 1990-1997).

Air pollution has multiple manifestations in communities, with children and older adults being the most vulnerable populations, with a high incidence of morbidity and mortality from acute respiratory and cardiovascular diseases. This forces clinical physicians,

toxicologists, environmentalists and epidemiologists to assess the adverse effects of atmospheric pollutants. Clinical physicians evaluated the health of exposed individuals, toxicologists defined the damage caused by the pollutants, environmentalists quantified the degree of pollution to which society is exposed and epidemiologists studied the effects on exposed groups.

Currently, there are concerns about the social costs of air pollution in terms of morbidity, disability and mortality, which have become a key task of governments and of international agencies responsible for the establishment of environmental policies. Special attention has been placed on the impact of air quality on the health of the most susceptible population: children, without forgetting that all inhabitants of the planet are exposed to different degrees.

The health effects attributable to air pollution exposure include excessive mortality from respiratory causes, such as: exacerbation of asthma, reduced lung function and immunological alterations. The epidemiological evidence comes from clinical, epidemiology, human exposure, clinical exposure and animal toxicology studies. However, some effects observed mechanisms and specific pollutants are not sufficiently well defined. The valuation of the costs of these diseases represents an estimate of the individual, social and institutional cost. However it is necessary to evaluate the consequences that chronic simultaneous exposure to high concentrations of air pollutants may have on health. The synergistic effects of pollutants have not been assessed; however, these can be short, medium or long term causing acute and chronic diseases.

There is epidemiological evidence showing that exposure to atmospheric contaminants, even at levels below the normal limits, is associated with an increase in the incidence and severity of asthma and lung function impairment, as well as with other respiratory diseases in children of less than five years of age.

This chapter aims to demonstrate how air pollutants affect human health, taking as an example a study case, which is intended to establish the influence of air pollutants in acute respiratory diseases in children of less than five years of age in the Urban Area of Guadalajara, Mexico.

2. Study area

The Urban Area of Guadalajara (UAG) is located at the center of the state of Jalisco, Mexico with coordinates limits 20°46'00" and 20°32'08" North latitude and 103°12'30" and 103°29'00" West longitude (Fig. 1), at an altitude of 1,540 meters (above mean sea level). The UAG is situated in the Rio Grande de Santiago Valley, Atemajac Valley and Tonalá plain, between the mountains of the Sierra Madre Occidental and the Transmexican volcanic belt, which constitutes a natural barrier to the circulation of the wind, limiting the release of polluted air outside of the UAG. Typical local meteorological conditions are thermal inversions that cause the deadlock of the pollutants. The frequency of thermal inversions is 283 days per year, and in the periods of January-June and November-December, they are present every day. The thickness of the thermal inversion is typically tens to hundreds of meters, being greater in the dry season and breaking at a layer where the atmospheric temperature is around 13 °C during the colder months of the year (January and February).

The dominant wind comes from the West 15.5% of the time, while winds from the East are present 7.5% of the time. In both cases, the typical speeds are between 5 to 20 km/h and sometimes reach 21 to 35 km/h. Calm conditions (absence of wind and/or very weak winds less than 4 km/h), are present 44.3% of the time, with great potential for accumulation of pollutants due to lack of ventilation in the UAG (Secretaría del medio ambiente, recursos

naturales y pesca - Secretaría de Salud - Gobierno del Estado de Jalisco [SEMARNAP/SS/GE]], 1997).

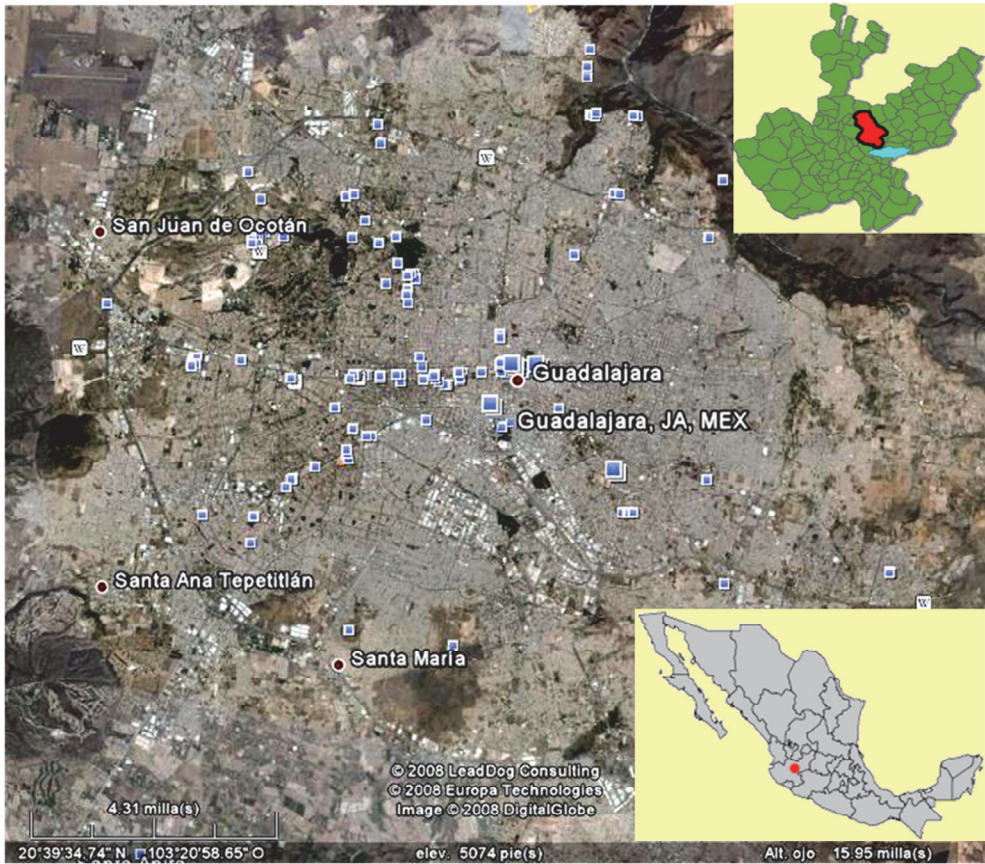


Fig. 1. Geographical location of the UAG. Courtesy of Google Earth.

3. Methods

The measurements of concentrations of air pollutants provided by the Automatic Atmospheric Monitoring Network (RAMA) of the Secretary of Environment for Sustainable Development (SEMADES) of the Jalisco State Government were revised, debugged and validated. From the databases of per month and per pollutant from 2000 to 2005, we obtained monthly averages, monthly modes and monthly maximums for concentrations of the atmospheric contaminants: CO, SO₂, NO₂, PM₁₀ and O₃, at the RAMA stations.

The consultations for acute respiratory diseases (ARD) in children of less than five years in health centers, clinics and hospitals of the IMSS (Instituto Mexicano del Seguro Social), ISSSTE (Instituto de Seguridad Social al Servicio de los Trabajadores del Estado) and SSJ (Secretaria de Salud Jalisco), in the study area of the UAG were provided by the Jalisco Health Ministry (SSJ).

The digital orthophotos and digital topographic maps, F13D65 Guadalajara West, F13D66 Guadalajara East, scale 1: 50,000 were used to perform the cartography of the UAG.

3.1 Information processing

3.1.1 Atmospheric contaminants

The databases with information on monthly averages, monthly modes and monthly maximums for each of the pollutants and for each year were obtained with the aim that concentration information can be entered and processed in the geographic information system (GIS) IDRISI.

3.1.2 Topographic maps and orthophotos, F13D65 and F13D66 scale 1:50,000

The study area was delimited, based on the area of influence of each monitoring station (2 kilometers radius around the station), which was carried out in a digital format on the orthophotos contained in the files of the Guadalajara topographic map. A georeferenced UAG map was built showing the main roads and municipal boundaries, the study area displaying the health centers, clinics and hospitals of the IMSS, ISSSTE and SSJ, and monitoring stations all located in the b, c, e and f F13D65 Guadalajara West orthophotos map and F13D66 Guadalajara East orthophotos map to scale 1:50,000 in the GIS IDRISI. The locations of medical care units and monitoring stations were corroborated in the field by using GPS in coordinates Universal Transverse Mercator (UTM).

3.1.3 Acute respiratory diseases

The ARD information was captured from the health centers, clinics and hospitals of the IMSS, ISSSTE and SSJ. Tables and graphs were prepared to observe trends and establish correlations. Once the information and databases designed for use in IDRISI were prepared, the interpolation technique for the production of concentrations maps of contaminants was applied using the IDRISI software. This process provided the isoconcentration maps and a list of values of the concentrations of the pollutants for each of the health centers, clinics and hospitals of the IMSS, ISSSTE and SSJ. With the databases (listed by month and pollutant), tables and graphs were produced to observe the trends in the pollutants over the years studied. The spatial analysis of pollutants was performed using the maps obtained, in order to observe trends.

3.1.4 Correlation between air pollutants and ARD

With the database of the monthly averages, monthly modes and monthly maximums in the concentrations of air pollutants in the health centers, clinics and hospitals (resulting from interpolation) and with the cases of ARD, we established single correlation, multiple correlation, variance analysis (ANOVA) and the t-student test between the six pollutants and the number of consultations per ARD for the years 2000 to 2005, using Excel and SPSS software. Finally, a spatial analysis of the trends of atmospheric pollutants and ARD consultations was made.

4. Results

4.1 Behavior of the air pollutants (CO, NO₂, O₃, SO₂, PM₁₀) in the UAG, from 2000 to 2005.

The results of the temporal distribution showed that the behavior of air pollutants is highly variable throughout the year and over the years analyzed. However, it was clear that the

more concentrated contaminants are those with particles smaller than 10 microns (PM_{10}), followed by the ozone (O_3), nitrogen dioxide (NO_2), carbon monoxide (CO) and sulfur dioxide (SO_2). The spatial distribution showed that the most affected areas are the south and southeast portions of the UAG, which have the highest levels for maximums, arithmetic means and modes; also they contain the sites with most high events during the period studied. The annual results showed that a significant percentage of days exceeded the Mexican standards of pollutant emission. The analysis of maximums showed that during 21 days in 2000, 5 in 2001, 7 in 2002, 11 in 2003, 8 in 2004 and 3 in 2005, the standard was exceeded for CO (11 ppm). In the case of NO_2 (0.21 ppm), the days above standard were: 18 in 2000, 21 in 2001, 26 in 2002, 5 in 2003, 6 in 2004, and 13 in 2005. For O_3 (0.11 ppm) the days above standard were: 65 days in 2000, 36 in 2001, 75 in 2002, 71 in 2003, 49 in 2004 and 66 in 2005. The PM_{10} (150 mg/m^3) is the pollutant that has the maximum number of days exceeding the standard, 199 days in 2000, 180 in 2001, 183 in 2002, 115 in 2003, 94 in 2004 and 93 in 2005. Finally, the SO_2 (0.13 ppm) is the one with a minimum number of days in which the standard was exceeded with 9 days in the year 2002 (Table 2 y Figure 2). April, May and June presented high concentrations of O_3 and CO while December, January, February and March reflected intense concentrations of PM_{10} , NO_2 , CO and SO_2 , as a result of the presence of low temperatures which prolonged the duration of the thermal inversions and low humidity in the environment, not permitting their dispersion. Table 3 presents the statistical results (averages, modes and monthly maximums).

Air pollutant	Limit values.	Acute exposure	2000	2001	2002	2003	2004	2005
			Ozone (O_3)	0.11 ppm (1 Hour) ¹	1 time per year	65	36	75
Nitrogen Dioxide (NO_2)	0.21 ppm (1 Hour) ²	1 time per year	18	21	26	5	6	13
Carbon Monoxide (CO)	11 ppm (8 Hours) ³	1 time every 3 years	21	5	7	11	8	3
Sulfur Dioxide (SO_2)	0.13 ppm (24 Hours) ⁴	1 time per year	0	0	9	0	0	0
Particles less than 10 microns (PM_{10})	150 mg/m^3 (24 Hours) ⁵	1 time per year	199	180	183	115	94	93

¹NOM - 020 - SSAI - 1993, ²NOM - 023 - SSAI - 1993, ³NOM - 021 - SSAI - 1993, ⁴NOM - 022 - SSAI - 1993, ⁵NOM - 025 - SSAI - 1993.

Table 2. Number of days exceeding the standard for each of the pollutants found in the UAG.

	Means				Modes				Maximums			
	X	S	Max	Min	X	S	Max	Min	X	S	Max	Min
CO	1.942	0.647	4.883	0.000	1.129	0.502	4.400	0.000	9.166	6.021	53.600	0.000
NO_2	0.034	0.011	0.089	0.000	0.025	0.012	0.136	0.000	0.114	0.071	0.526	0.000
O_3	0.023	0.008	0.053	0.000	0.009	0.006	0.047	0.000	0.110	0.044	0.650	0.000
PM_{10}	50.915	20.218	156.006	0.000	35.488	33.397	499.900	0.000	265.415	108.633	499.900	0.000
SO_2	0.009	0.005	0.068	0.000	0.007	0.003	0.052	0.000	0.049	0.056	0.534	0.000

X= Arithmetic Mean, S= Standard Deviation

Table 3. Statistical results of the means, modes and maximums monthly concentrations of air pollutants CO_2 , NO_2 , SO_2 , PM_{10} and O_3 in the UAG from 2000-2005.

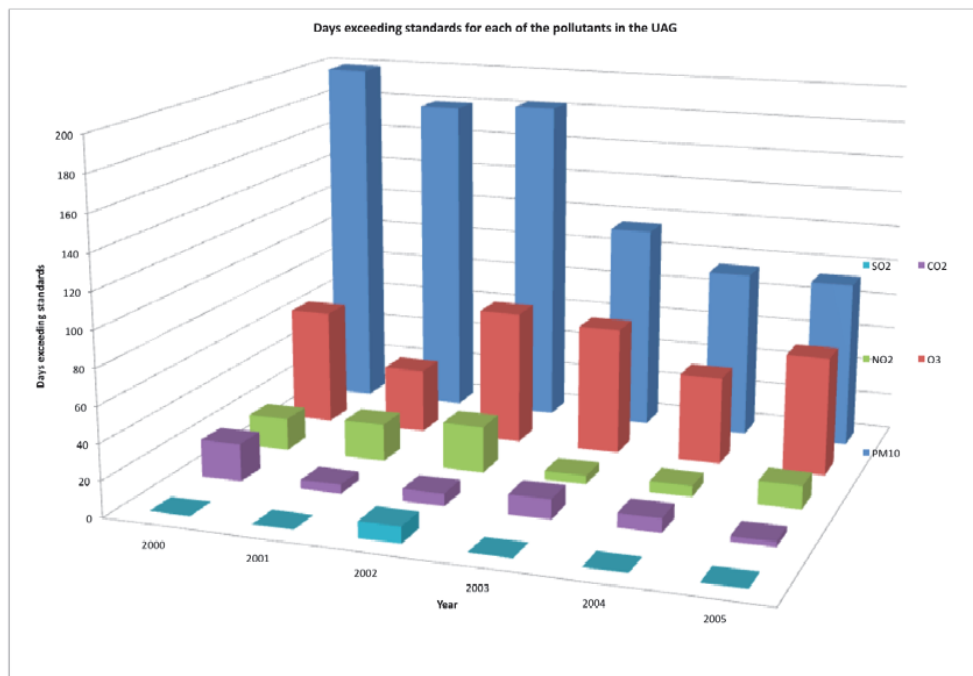


Fig. 2. Days exceeding standards for each of the pollutants in the UAG 2000-2005.

4.1.1 Carbon monoxide (CO)

The behavior of the average monthly concentrations has with seasonal variations, a tendency to maintain constant concentrations during the study period, with values below the norms of the United States Environmental Protection Agency USEPA (9 ppm) and the Mexican Official Norm NOM (11 ppm). The mean of the monthly averages was 1.942 ± 0.647 ppm. The range of the monthly average is between 0.000-4.883 ppm (Fig. 3).

The monthly mode of the concentration presented seasonal variations with a tendency to maintain constant concentrations during the study period, with values lower than EPA and NOM regulations. The average of the monthly modes was 1.129 ± 0.502 ppm. The range of the monthly modes is between 0.000-4.400 ppm (Fig. 4).

In turn, the monthly maximum concentrations showed values above the norm in the majority of the period analyzed (Fig. 5); however, there were major peaks reaching values close to 55.000 ppm, which represents five times the NOM and nine times the EPA regulations, so that these lapses were risk factors for the population. These events are registered in the driest period of the year (March, April, May, June), just before the period of precipitation. The average of the monthly maximums was 9.166 ± 6.021 ppm. The range of monthly maximums is between 0.000-53.600 ppm (Fig. 5).

The spatial distribution showed that the zones most affected were the central and southeast portions of the UAG (Figs. 18-20), however, the pollution generated by the CO in the UAG is considered significant only at times of the peak maximums.

4.1.2 Nitrogen dioxide (NO₂)

Most of the average monthly concentrations present values below the EPA (0.05 ppm) and NOM (0.21 ppm) limits; however, they show irregularities and in some cases values above the EPA limit (0.05-0.10 ppm). The mean of the monthly averages was 0.034 ± 0.011 ppm. The range of the monthly averages varied between 0.000-0.089 ppm (Fig. 6).

The monthly modes presented seasonal variations with a tendency to maintain constant concentrations during the study period, with values below the EPA and NOM limits. The average of the monthly mode was 0.025 ± 0.012 ppm. The range of values of monthly modes is larger than that of averages, with values between 0.000-0.136 ppm (Fig. 7).

In turn, the monthly maximums (Fig. 8) have very important variations with values from 0.000 to 0.526 ppm. The peaks of maximum concentration can occur in the winter or summer, not showing a cyclical behavior. The UAG shows very high maximums of NO₂ in the period of study. The average value of the monthly maximums was 0.114 ± 0.071 ppm. The range of the monthly maximum is between 0.000-0.526 ppm.

In this case, the spatial distribution showed that the zones most affected are the southwest, west and northwest of UAG where the maximum values occur; it is a problem of the whole UAG (Figs. 18-20). The contamination by NO₂ is serious in the UAG.

4.1.3 Ozone (O₃)

The average monthly concentrations showed seasonal variations with tendency to remain constant during the study period, with values below the NOM-020-SSA1-1993 (0.11 ppm). The mean of monthly averages was 0.023 ± 0.008 ppm. The range of the monthly averages oscillated between 0.000-0.053 ppm (Fig. 9).

The monthly modes presented seasonal variations with a tendency to maintain constant concentrations during the study period, with values below the limits. The average monthly mode was 0.009 ± 0.006 ppm. The range of the monthly mode values was between 0.000-0.047 ppm (Fig. 10).

The monthly maximums in most of the reporting period were above the limits and with a slight tendency to rise during recent years. There are very significant variations with values from 0.000 to 0.650 ppm; the highest concentration peaks occur in times of drought and summer when there is more sunshine and transformation of primary pollutants into O₃. The average value of the monthly maximums was 0.110 ± 0.044 ppm (Fig. 11).

The spatial distribution showed that the most affected zones of the UAG are the central, north and southeast (Figs. 18-20); however, the pollution generated by O₃ in the UAG is considered moderate, which represents a risk factor for people's health, especially when maximums occur.

4.1.4 Particles smaller than 10 microns (PM₁₀)

The average monthly concentrations present values between 0 and $156 \mu\text{g}/\text{m}^3$; the majority of the records are located between the limits of EPA ($50 \mu\text{g}/\text{m}^3$) and NOM ($150 \mu\text{g}/\text{m}^3$), and these levels are maintained without showing a reduction, making the PM₁₀ the most important contaminant in the UAG. The mean monthly average was $50.92 \pm 20.22 \mu\text{g}/\text{m}^3$ (Fig. 12).

The monthly modes presented seasonal variations with a tendency to maintain constant concentrations during the dry period from September to May; the majority of the values were below the EPA and NOM limits, with the exception of temporary droughts in

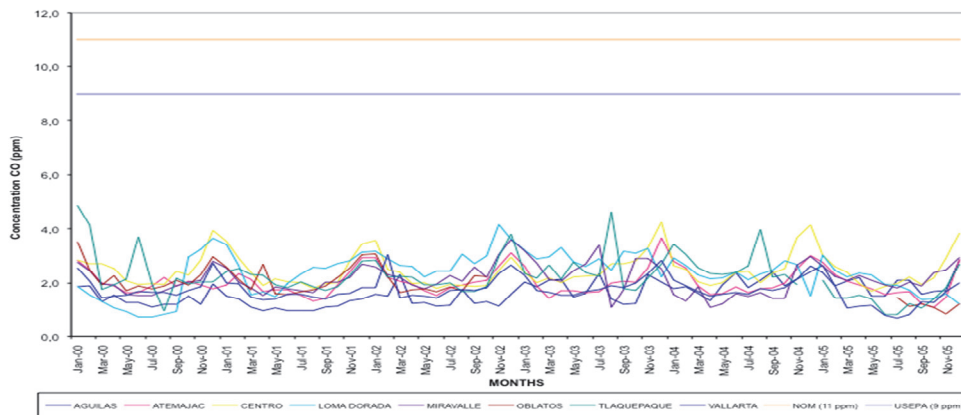


Fig. 3. Time series of monthly averages of CO in the UAG (2000-2005).

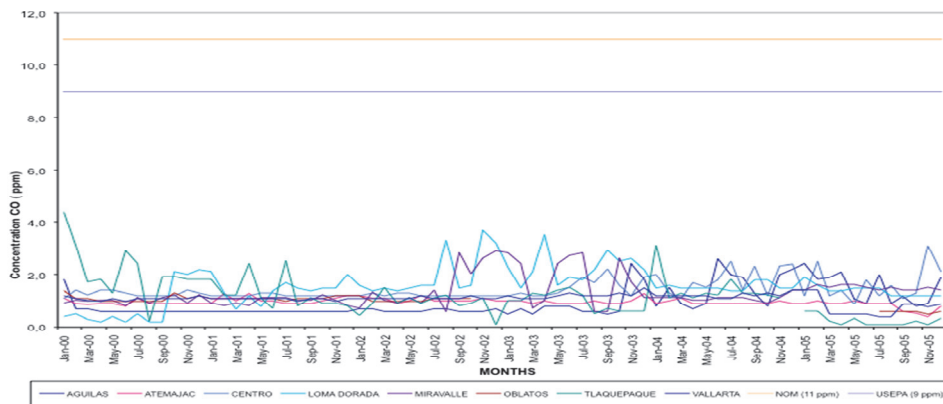


Fig. 4. Time series of monthly modes of CO in the UAG (2000-2005).

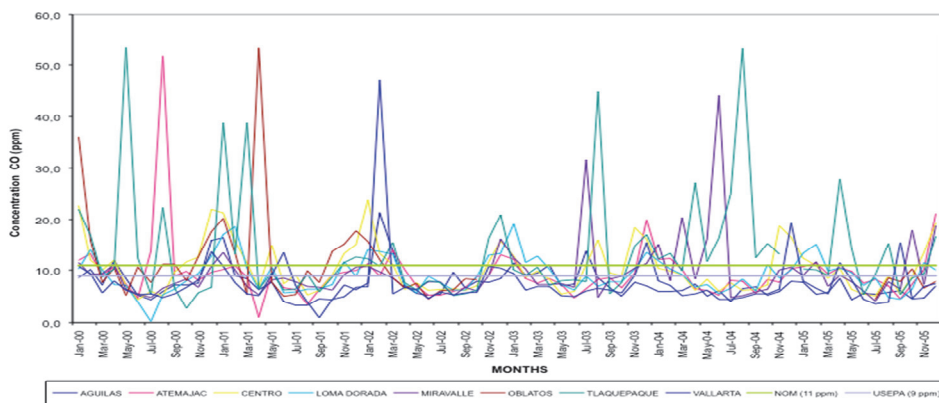


Fig. 5. Time series of monthly maximums of CO in the UAG (2000-2005).

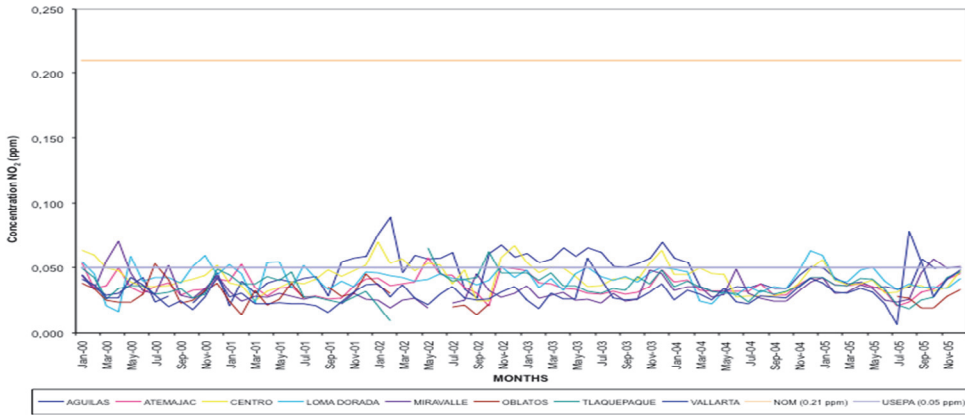


Fig. 6. Time series of monthly averages of NO₂ in the UAG (2000-2005).

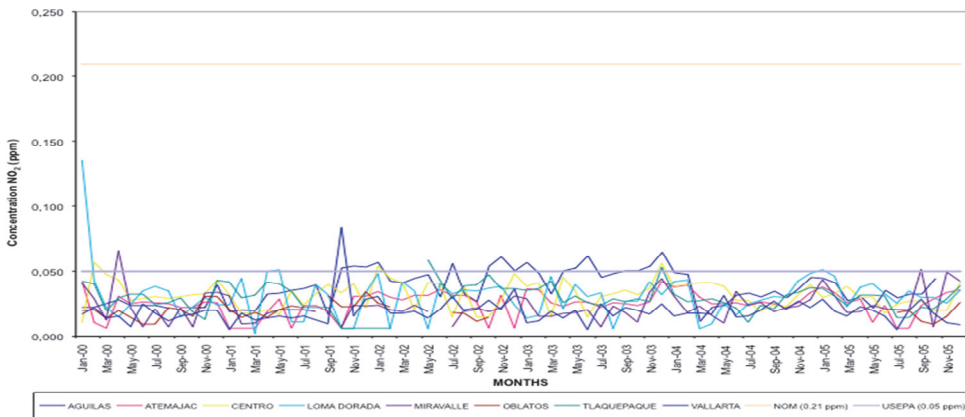


Fig. 7. Time series of monthly modes of NO₂ in the UAG (2000-2005).

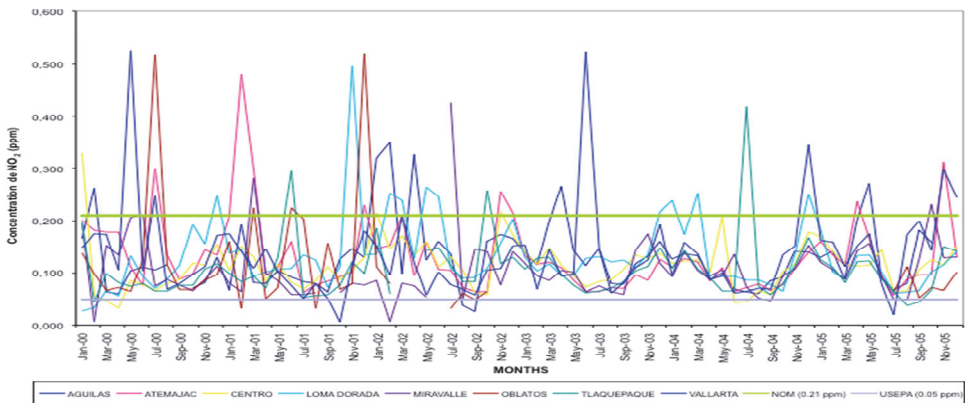


Fig. 8. Time series of monthly maximums of NO₂ in the UAG (2000-2005).

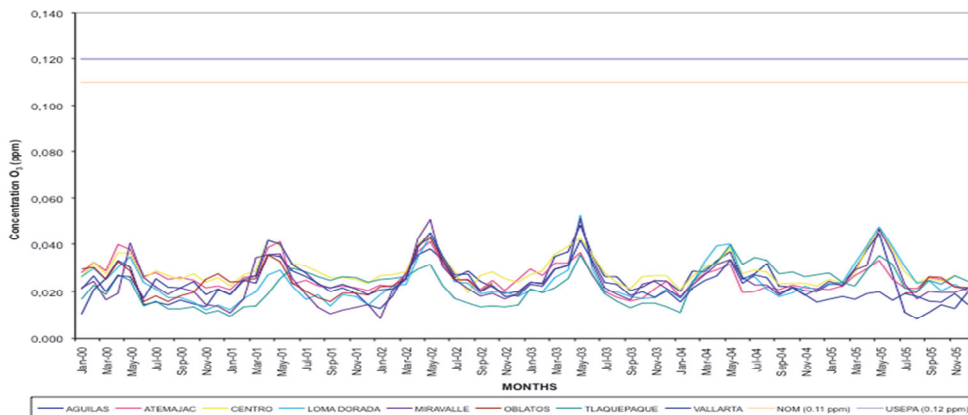


Fig. 9. Time series of monthly averages of O₃ in the UAG (2000-2005).

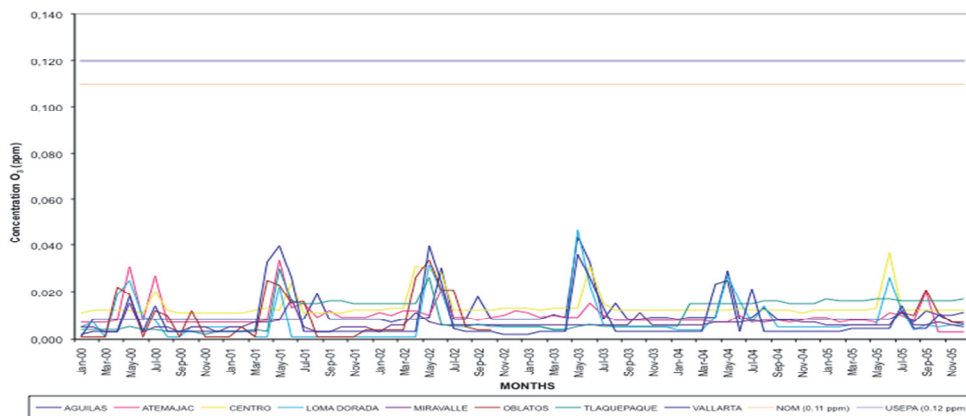


Fig. 10. Time series of monthly modes of O₃ in the UAG (2000-2005).

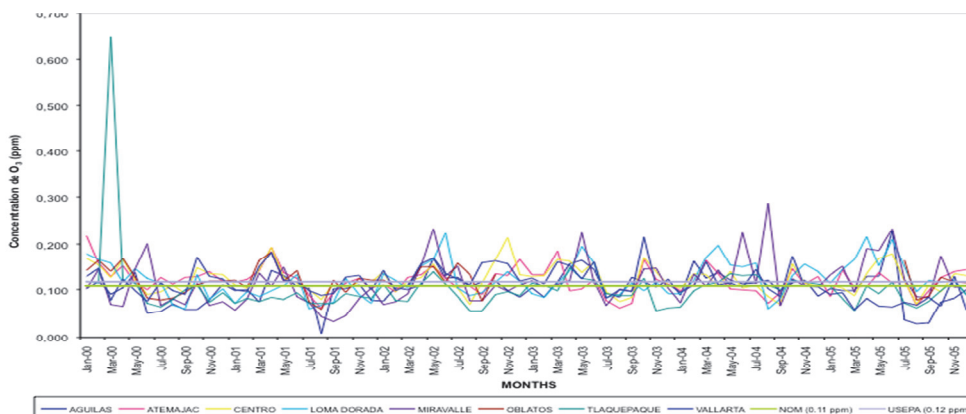


Fig. 11. Time series of monthly maximums of O₃ in the UAG (2000-2005).

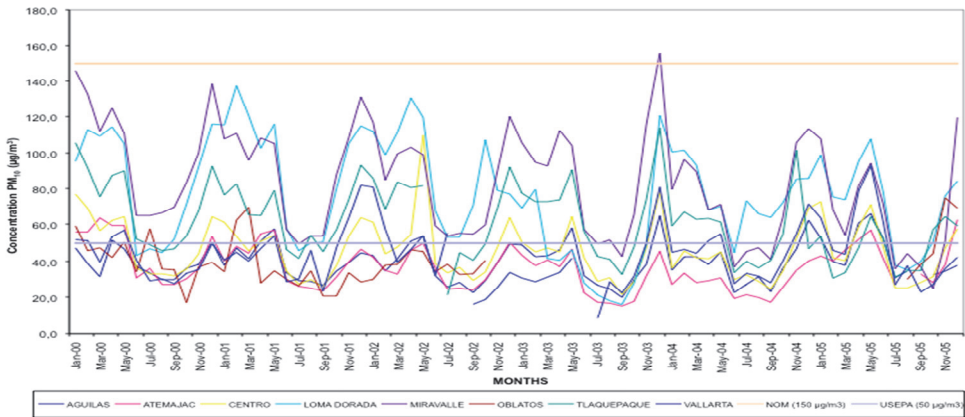


Fig. 12. Time series of monthly averages of PM₁₀ in the UAG (2000-2005).

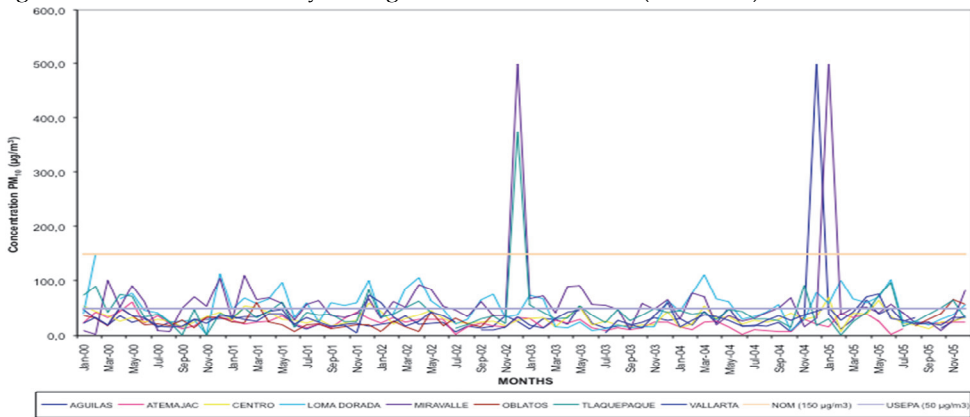


Fig. 13. Time series of monthly modes of PM₁₀ in the UAG (2000-2005).

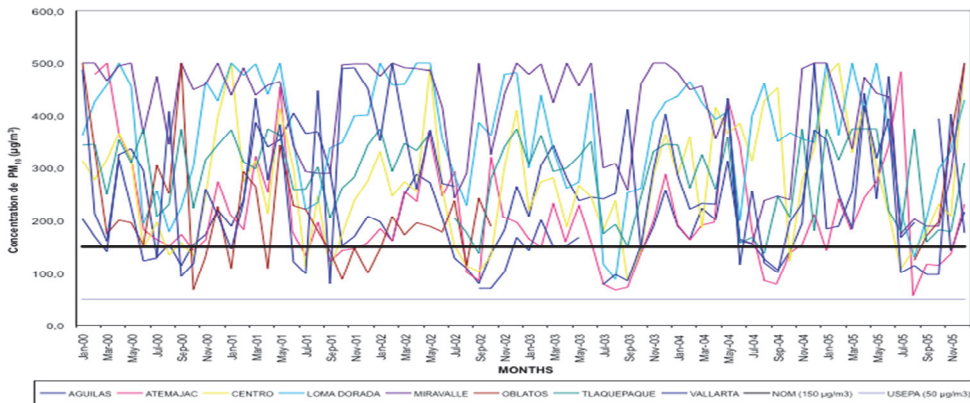


Fig. 14. Time series of monthly maximums of PM₁₀ in the UAG (2000-2005).

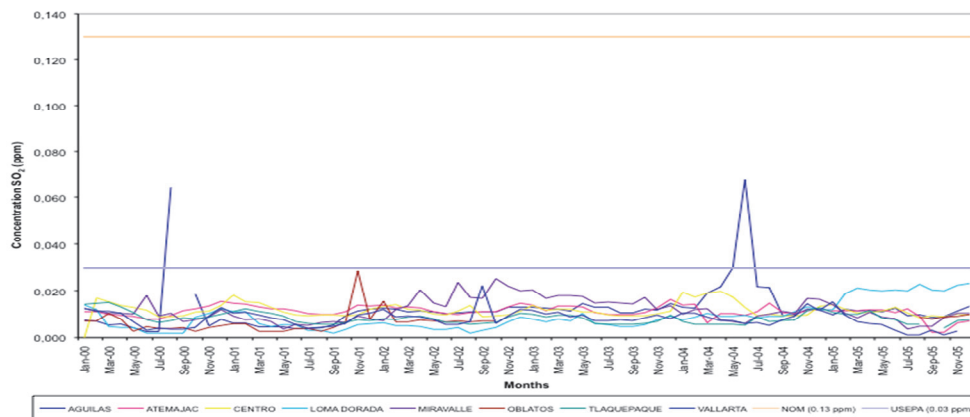


Fig. 15. Time series of monthly averages of SO₂ in the UAG (2000-2005).

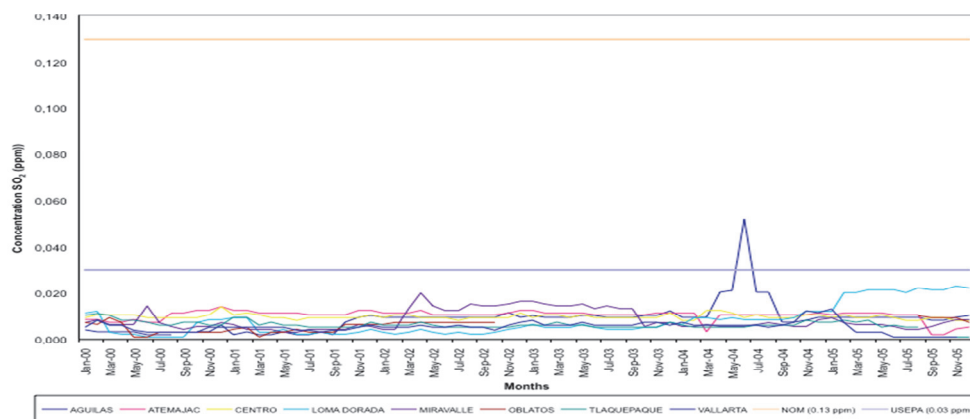


Fig. 16. Time series of monthly modes of SO₂ in the UAG (2000-2005).

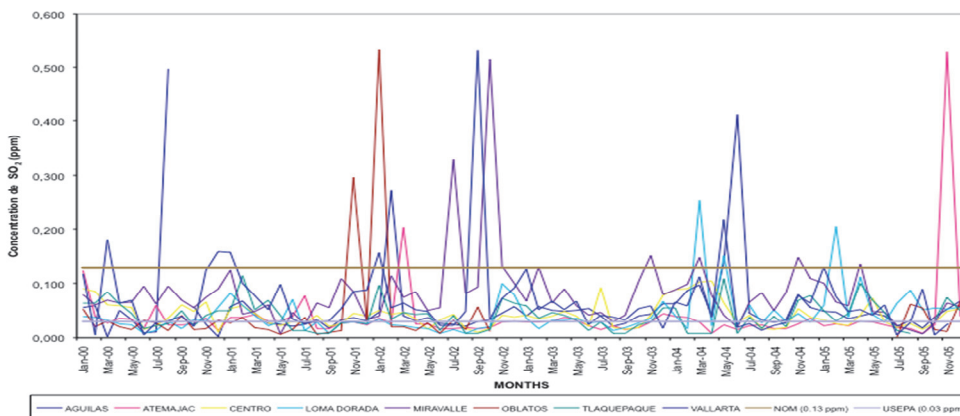


Fig. 17. Time series of monthly maximums of SO₂ in the UAG (2000-2005).

2003-2004 and 2004-2005 in the South and Southeast of the UAG. The mean of the monthly modes was $35.49 \pm 33.40 \mu\text{g}/\text{m}^3$, while the range of values was between 0-499.90 $\mu\text{g}/\text{m}^3$ (Fig. 13).

The monthly maximums are all above limits with a range of 0-500 $\mu\text{g}/\text{m}^3$; the concentrations vary with constant behavior. The measured values are above the limits, so they are the main air pollutants in the UAG. The average of the monthly maximums was $265.12 \pm 108.63 \mu\text{g}/\text{m}^3$ (Fig. 14). The concentrations of PM_{10} represent the main atmospheric contaminant in the UAG, and consequently an environmental contamination problem and risk factor to people's health. However, the spatial distribution showed that the extreme events were located in the south, southeast, east and northeast during the whole year (Figs. 18-20).

4.1.5 Sulfur dioxide (SO_2)

The average monthly concentrations varied between 0.000 and 0.068 ppm. Practically the values never exceeded the EPA (0.03 ppm) and NOM (0.13 ppm) limits. The values remained constant without tendency. The SO_2 is a contaminant of little influence on people's health in the UAG. The mean monthly averages were 0.009 ± 0.005 ppm (Fig. 15).

The monthly modes presented seasonal variations with a tendency to maintain constant concentrations during the period of study, with values below the EPA and NOM limits. The average of the monthly modes was 0.007 ± 0.003 ppm. The range of monthly modes presented values between 0.000-0.052 ppm. Only one extreme event in the summer of 2004 was recorded (Fig. 16).

The majority of the monthly maximums during the period presented values above the EPA limit, but below the NOM limit (Fig. 17). The events that exceeded the NOM limit occurred in the summer of 2000, winter 2001, all of 2002, spring 2004 and winter 2005. Thus, the monthly maximums presented very important variations between 0.000 and 0.534 ppm. The average of monthly maximums was 0.049 ± 0.056 ppm. The spatial distribution showed that the zones most affected were the central, north and southeastern of UAG (Figs. 18-20); however, the concentrations of SO_2 mean that it does not represent a risk to the health of the population in the UAG.

4.2 Results of acute respiratory diseases in children under 5 years from the UAG from 2000 to 2005.

The results obtained during the period from 2000 to 2005 showed that in the six years studied there were 1 664 811 consultations for ARD in children under 5 years in public health institutions distributed as follows: 294 251 in the year 2000, 316 899 in 2001, 336 855 in 2002, 258 068 in 2003, 242 225 in 2004 and 216 513 in 2005 (Table 4 and Figure 21). The annual arithmetic mean was $277\,469 \pm 46\,254$ consultations per year. The diseases with the highest percentage corresponded to Acute Respiratory Infections: acute rhinopharyngitis, acute sinusitis, acute pharyngitis, acute laryngitis, acute traquitis, acute upper airway multiple or unspecified sites, acute bronchitis and acute bronchiolitis with the 98.0% of consultations, followed by pneumonia and bronchopneumonia with 1.1%, asthma and asthmaticus status with 0.5% and streptococcal pharyngitis and streptococcal tonsillitis with 0.4% (Fig. 22).

The months with the greatest number of consultations by ARD were from October to March, with percentages between 8-12 on the annual total (Fig. 23). The most affected zone is the southeast of the UAG.

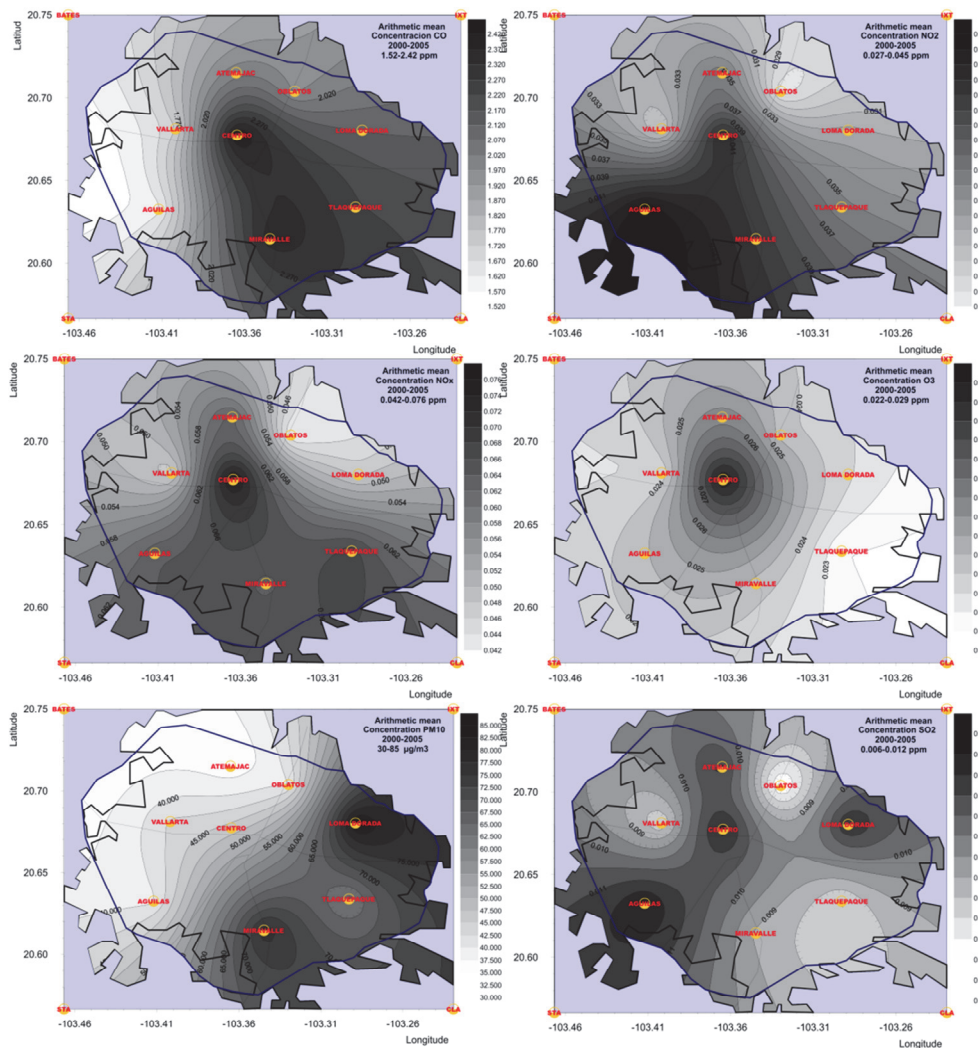


Fig. 18. The spatial-temporal distribution of the atmospheric polluting agents (arithmetic means) in the UAG (2000-2005).

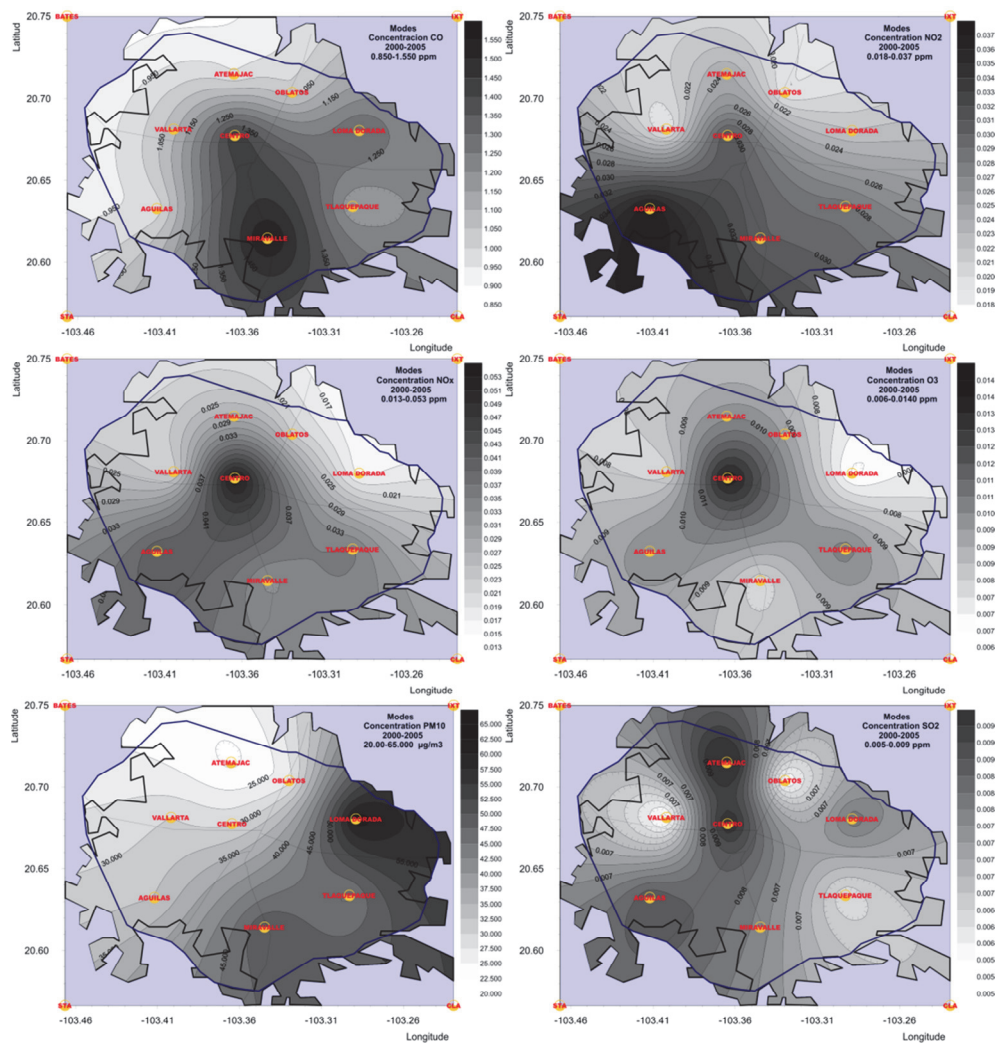


Fig. 19. The spatial-temporal distribution of the atmospheric polluting agents (modes) in the UAG (2000-2005).

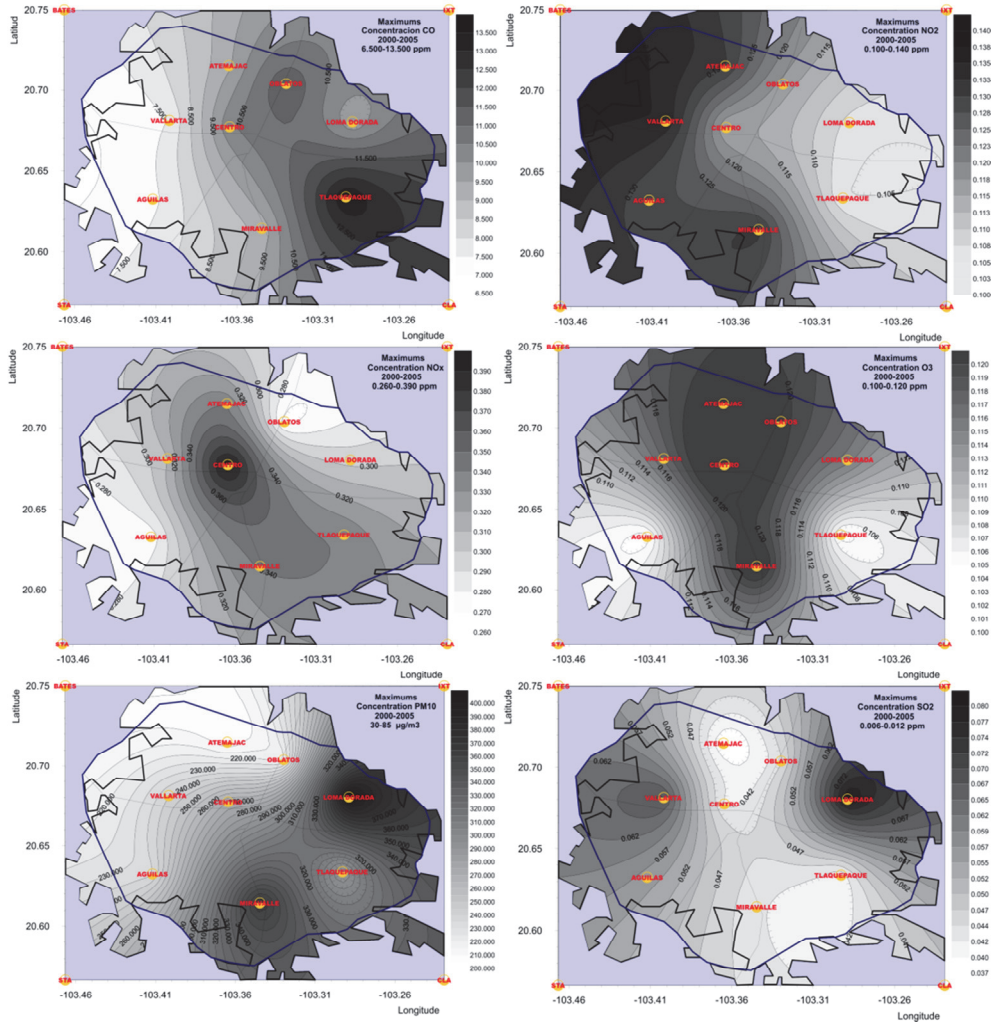


Fig. 20. The spatial-temporal distribution of the atmospheric polluting agents (maximums) in the UAG (2000-2005).

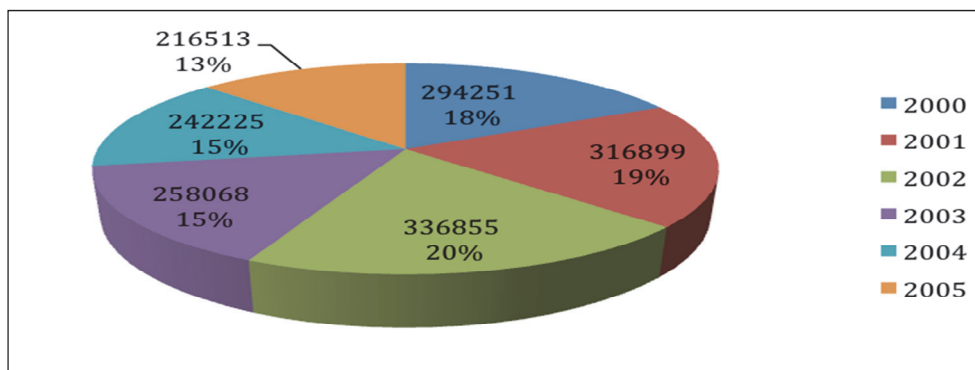


Fig. 21. Number of consultations and percentages of ARD from 2000 to 2005.

Year	Number of consultations
2000	294 251
2001	316 899
2002	336 855
2003	258 068
2004	242 225
2005	216 513
TOTAL	166 4811
Arithmetic mean = 277 469	Standard deviation = 46 254

Table 4. Number of consultations for ARD in children under 5 years of age in the AUG (2000-2005).

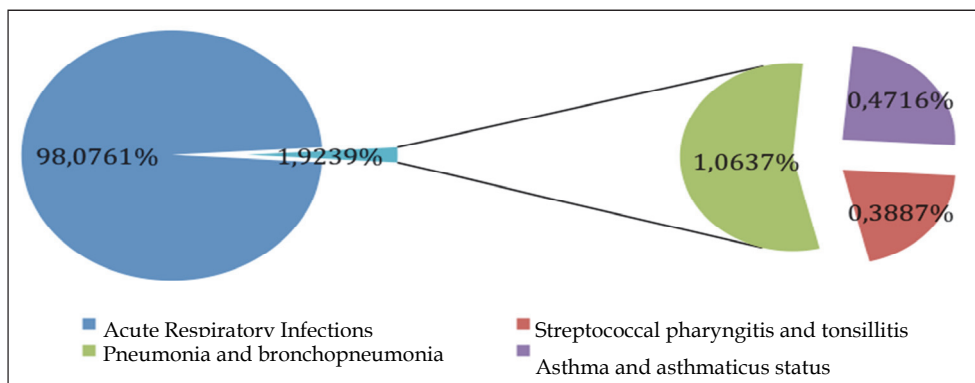


Fig. 22. Distribution of consultations for different ARD in the UAG from 2000 to 2005.

The percentage of consultations per month shows that November (11.97%), February (10.95%) and March (10.79%) are the months with the highest percentage of respiratory diseases (Fig. 24).

4.3 Correlations between air pollutants and acute respiratory diseases in the UAG.

The results of the correlations between air pollutants and acute respiratory infections in the UAG during the 2000-2005 period, showed the following results:

Analysis of the single and multiple correlations, variance analysis (ANOVA) and t-student test in the Acute Respiratory Diseases with monthly average, monthly modes and monthly maximums of CO, SO₂, NO₂, PM₁₀, and O₃, between 2000-2005 showed the highest significances for monthly averages, followed by maximums and with little significance for modes (Significance was analyzed with a confidence of 95% in all cases).

The analysis of correlations between the monthly average concentrations of air pollutants and ARD showed the following results: for NO₂ significance in 5 years, PM₁₀ significance in 4 years, CO significance in 3 years, SO₂ significance in two years and O₃ showed no correlation with the ARD (Table 5).

	2000							2001						
	ARD	CO	NO ₂	NO _x	O ₃	PM ₁₀	SO ₂	ARD	CO	NO ₂	NO _x	O ₃	PM ₁₀	SO ₂
ARD	1.0000	0.1216	0.0714	0.1211	-0.0281	0.0742	0.0659	1.0000	0.0667	0.0719	0.1019	-0.0350	0.0965	0.0736
CO	0.1216	1.0000	0.5166	0.7776	-0.0101	0.3823	0.2801	0.0667	1.0000	0.3278	0.6587	-0.3979	0.3955	0.4763
NO ₂	0.0714	0.5166	1.0000	0.8202	0.1038	0.5310	0.2453	0.0719	0.3278	1.0000	0.7746	-0.0885	0.1961	0.2872
NO _x	0.1211	0.7776	0.8202	1.0000	0.0044	0.4760	0.3424	0.1019	0.6587	0.7746	1.0000	-0.3736	0.2802	0.4939
O ₃	-0.0281	-0.0101	0.1038	0.0044	1.0000	0.1141	0.0143	-0.0350	-0.3979	-0.0885	-0.3736	1.0000	-0.1297	-0.1120
PM ₁₀	0.0742	0.3823	0.5310	0.4760	0.1141	1.0000	0.2114	0.0965	0.3955	0.1961	0.2802	-0.1297	1.0000	0.1093
SO ₂	0.0659	0.2801	0.2453	0.3424	0.0143	0.2114	1.0000	0.0736	0.4763	0.2872	0.4939	-0.1120	0.1093	1.0000
	2002							2003						
	ARD	CO	NO ₂	NO _x	O ₃	PM ₁₀	SO ₂	ARD	CO	NO ₂	NO _x	O ₃	PM ₁₀	SO ₂
ARD	1.0000	0.0881	0.0498	0.0788	-0.0694	0.0955	0.0113	1.0000	0.0094	0.1010	0.0832	0.0041	0.1013	0.0633
CO	0.0881	1.0000	0.1109	0.6090	-0.4863	0.4533	0.2187	0.0094	1.0000	0.3127	0.5628	-0.2507	0.3547	0.0414
NO ₂	0.0498	0.1109	1.0000	0.7497	0.1363	0.1488	0.0610	0.1010	0.3127	1.0000	0.8117	0.0475	0.3958	0.2276
NO _x	0.0788	0.6090	0.7497	1.0000	-0.1832	0.2714	0.1870	0.0832	0.5628	0.8117	1.0000	-0.2799	0.5014	0.2453
O ₃	-0.0694	-0.4863	0.1363	-0.1832	1.0000	0.1776	-0.1051	0.0041	-0.2507	0.0475	-0.2799	1.0000	0.2159	0.3320
PM ₁₀	0.0955	0.4533	0.1488	0.2714	0.1776	1.0000	0.0425	0.1013	0.3547	0.3958	0.5014	0.2159	1.0000	0.5234
SO ₂	0.0113	0.2187	0.0610	0.1870	-0.1051	0.0425	1.0000	0.0633	0.0414	0.2276	0.2453	0.3320	0.5234	1.0000
	2004							2005						
	ARD	CO	NO ₂	NO _x	O ₃	PM ₁₀	SO ₂	ARD	CO	NO ₂	NO _x	O ₃	PM ₁₀	SO ₂
ARD	1.0000	0.0436	0.0819	0.0951	0.0383	0.0340	0.0973	1.0000	0.1218	0.1130	0.1244	-0.0339	0.0519	0.0345
CO	0.0436	1.0000	0.4343	0.4591	-0.2231	0.1385	-0.0506	0.1218	1.0000	0.7013	0.7842	-0.1248	0.4258	0.3664
NO ₂	0.0819	0.4343	1.0000	0.7285	-0.0970	0.2799	0.1923	0.1130	0.7013	1.0000	0.7454	0.0088	0.4372	0.2256
NO _x	0.0951	0.4591	0.7285	1.0000	-0.0208	0.3277	0.1988	0.1244	0.7842	0.7454	1.0000	-0.2559	0.4232	0.2755
O ₃	0.0383	-0.2231	-0.0970	-0.0208	1.0000	-0.1640	0.1424	-0.0339	-0.1248	0.0088	-0.2559	1.0000	0.5528	0.3044
PM ₁₀	0.0340	0.1385	0.2799	0.3277	-0.1640	1.0000	0.3892	0.0519	0.4258	0.4372	0.4232	0.5528	1.0000	0.5105
SO ₂	0.0973	-0.0506	0.1923	0.1988	0.1424	0.3892	1.0000	0.0345	0.3664	0.2256	0.2755	0.3044	0.5105	1.0000

Correlations significant at $p < 0.0500$

Table 5. Correlation matrix between ARD cases in children younger than 5 years of age and pollutants from 2000 to 2006.

On the other hand, the presence of a pollutant in the atmosphere is related to the presence of other agents that may increase or counteract their effects (synergy effect); CO shows significant correlation with NO₂, O₃, SO₂ and PM₁₀. NO₂ shows significant correlation with NO_x, O₃, PM₁₀ and SO₂. SO₂ presented significant correlation with NO_x, O₃ and PM₁₀.

5. Discussion

The evolution of contaminants shows that the UAG presents similar environmental risks to Mexico City. During the last years, the UAG has experienced significant environmental contingencies due to the conjunction of factors such as heavy thermal inversions (hundreds of meters) and duration (breaking at 14:00-15:00 hours), atmospheric stability (calm winds) and large quantities of emissions that cannot be dispersed efficiently by climatic factors. Likewise, the vehicular traffic has grown by 20% and a significant portion of the vehicles has been in use for more than 10 years and lacks the proper maintenance. In the case of monthly averages (the most significant indicator of the three evaluated), it was noted that all atmospheric contaminants influenced the health of children under five years in the UAG in the following order: NO_x , NO_2 , PM_{10} , CO and SO_2 . It is paradoxical that O_3 , as one of the main air pollutants in the UAG, does not present correlation with the ARD.

Ruszkiewicz (1997) demonstrated cases of death by CO poisoning within vehicles and inside structures. Also, during the Gulf War, wells and oil refineries were burnt, Kuwait was exposed to this toxic gas and a substantial increase in consultations due to respiratory irritation was noted. Ocaña et al. (1991) noted a relation in the increase of hospital admissions due to respiratory illnesses attributed to CO. Quezada et al. (1997) demonstrated that second hand smoke results in an increase in the concentration of CO. The result of this work ratifies the results of these investigations.

The NO_2 has been linked significantly with asthma attacks and with the number of consultations for respiratory infections. The results of this study corroborate the link between acute respiratory infections and oxides and nitrogen dioxide. Indeed, the oxides of nitrogen (NO_x), have been studied slightly in relation to acute infections of the respiratory tract, the scant literature about the theme does not indicate a significant correlation. However, the results from this research describe a significant correlation between acute respiratory infections and NO_x .

The correlation between contaminants O_3 and SO_2 and acute respiratory infections were significant but not in all the analyzed years. Some other studies corroborate this correlation. The result of this research raises our awareness that pollutants NO_x , NO_2 , PM_{10} , CO, SO_2 affect the health of the population. With the use of the isoconcentration maps, we can infer the distribution of the highest concentrations of atmospheric contaminants and define areas and populations exposed to risk in the UAG (Central, South and Southeast of the UAG).

It is clear that there is still a lot to do, such as periodical inventories of the major emitting sources of atmospheric pollutants, specifically in areas with high concentrations. Also studies of the population exposed to the highest levels of concentration of pollutants. It is necessary to implement programs and concrete actions that lead us to reduce concentrations of air pollutants and reduce the risk factors for acute respiratory diseases in children and older adults.

The results of the analysis showed that the maximums of all the contaminants exceed the limit and that the average and modal concentrations are maintained below national limits (NOM), but above the international limits (USEPA), which represents potential risk factors for health.

The contamination by CO is considered significant only when the maximum peaks are presented (9.16-53.60 ppm). The parameter proposed by the World Health Organization (WHO) for CO is 10 ppm for 8 hours. The effects of exposure are frequently revealed in the organ systems most sensitive to the absence of oxygen, in particular, the circulatory and central nervous system. High levels of exposure can cause acute poisoning, coma and collapse. The classic symptoms of poisoning for CO are headaches, sickness, severe

headache and cardiovascular symptoms as well as the risk of comma and death (Bascom et al., 1996; Romieu, 1999).

The concentration of NO₂ is important when the maximum peaks are presented (0.11-0.52 ppm). The accumulation of NO₂ in the human body constitutes a risk for the airways, being more frequent in cases of chronic bronchitis. An increased dose results in a sequence of effects: problems with olfactory perception, respiratory inconveniences, acute respiratory pains, pulmonary edema and finally death (SEMARNAP/SS/GEJ, 1997; Romieu, 1999).

The concentration of O₃ is moderate (0.11- 0.65 ppm); however, the exposure to high concentrations during prolonged periods represents a risk to human health. The O₃ provokes injuries in the airways, pulmonary inflammation, depression of the immune system, systemic effects in the liver, decreased aspiratory capacity, bronchi constriction, and decreased pulmonary function, asthma and annoyance of the eyes, nose and gullet (SEMARNAP/SS/GEJ, 1997).

The concentrations of PM₁₀ present the highest maximum averages (265-499 $\mu\text{g}/\text{m}^3$) and is the main atmospheric contaminant in the UAG. This represents a significant problem of environmental pollution and risks to the health of the population. The exhibition to PM₁₀ reduces the pulmonary functions, increases the frequency of respiratory illnesses, cardiovascular and lung cancers, increases asthma attacks, pneumonia, bronchitis and chronic cough (Dockery et al., 1989; Dockery & Pope, 1996).

The concentration of SO₂ (0.05 ppm) remained below the limits (0.13 ppm), which does not represent a risk to human health. The spatial distribution (Figs. 18-20) shows that the most affected zones are the Center, South and Southeast of the UAG and eventually we expect extreme values in the rest of the UAG.

6. Conclusion

The statistical analysis of simple and multiple correlations showed that all air pollutants are influencing the presence and frequency of ARD in children under 5 years of age in the UAG. The results suggest that concentrations of PM₁₀, NO₂, CO, NO_x affect the health of children younger than five years old in the UAG, while concentrations of SO₂ and O₃, although they do influence, are not considered as highly significant.

7. References

- Bascom, R.; Bromberg P.; Costa D.; Devlin R.; Dockery D.; Frampton W.; Lambert W.; Samet J.; Speizer F. & Utell M. (1996). State of the art: Health effects of outdoor air pollution part 2. *Am J Respir Crit Care Med*, Vol. 153, No. 2, (Febrero 1996), pp. 477-498, ISSN 1073-449X
- Departamento del Distrito Federal/Gobierno del Estado de México/ Secretaría del Medio Ambiente, Recursos Naturales y Pesca/Secretaría de Salud (1990). Programa Integral Contra la Contaminación Atmosférica de la Zona Metropolitana de la Ciudad de México. México, D.F.
- Dockery, D; Speizer F.; Stram D.; Ware J.; Spengler J. & Ferris B. (1989). Effects of inhalable particles on respiratory health of children. *Am Rev Respir Dis.*, Vol. 139 No. 3, (Marzo 1989), pp. 587-594, ISSN 0003-0805

- Dockery, D. & Pope, A. (1996). Epidemiology of acute health effects: summary of time-series studies", In *Particles in our air. Concentration and health effects*. Wilson R. & Spengler J. (eds.), pp 123-148, Harvard University Press/Harvard School of Public Health.
- Firket J. (1936). *Fog along the Mesue Valley*. Trans Faraday Soc. Vol. 32 (Marzo 1936), pp. 1192-1197.
- Ministry of Health, United Kingdom (1954). Mortality and morbidity during the London fog of December 1952. Reports on Public Health and Medical Subjects No 95. London:London Ministry of Health.
- Pan American Health Organization (1980). Infecciones Respiratorias en las Américas. Bol. Epidemiol. Vol 1, No. 5 (Mayo 1980), pp 1-4.
- Pan American Health Organization/World Health Organization (1994). Las condiciones de salud en las Américas. Publicación Científica No., Organización Panamericana de la Salud/Organización Mundial de la Salud. Washington, D.C.
- Pan American Health Organization (2004). De la teoría a la práctica: Indicadores de salud ambiental infantil. Implementación de una iniciativa lanzada en la Cumbre Mundial sobre el Desarrollo Sostenible. Panamerican Health Organization.
- PIO, A; LEOWAKI, J; LUELMO, F. (1984a). Importancia epidemiológica del problema de las Infecciones respiratorias agudas de la infancia en países en desarrollo en Bases para el Control de las Infecciones Respiratorias Agudas en Niños. Guatemala: PAHO/WHO, pp. 1-21.
- PIO, A; LEOWAKI, J; LUELMO, F. (1984b). Programa de la Organización Mundial de la Salud de infecciones respiratorias en la infancia. Bol. Of. Sanit. Panam., Vol. 96, pp. 283.
- Ramírez-Sánchez H.; Andrade-García M.; González-Castañeda M. & Celis-De la Rosa A. (2006). Contaminantes atmosféricos y su correlación con infecciones agudas de las vías respiratorias en niños de Guadalajara, Jalisco. *Salud Publica Mex* Vol. 48, (septiembre-octubre 2006), pp. 385-394, ISSN 0036-3634.
- Romieu I, Weitzenfeld H. & Finkelman J. (1991). Urban air pollution in Latin America and the Caribbean. *J Air Waste Manage Assoc*. Vol. 41, No.9, pp. 1166-1170, ISSN 1047-3289
- Romieu I. (1995). Estudios epidemiológicos sobre los efectos en la salud por la contaminación del aire de origen vehicular. In: *Contaminación atmosférica causada por vehículos automotores*. Mage DT, Zali O, eds. Organización Mundial de la Salud, Ginebra.
- Romieu, I. (1999). Epidemiology studies of health effects arising from motor vehicle air pollution. In: *Urban traffic pollution*. D. Schwela, y O. Zali (eds.), Londres: E & Fn Spon, pp. 9-69.
- Schwartz J, Marcus A. (1990). Mortality and air pollution in London. A time series analysis. *Am J Epidemiol*. Vol. 131, (enero 1991), pp. 185-194, ISSN 0002-9262.
- Segala C. (1999). Health effects of urban outdoor air pollution in children. Current epidemiological data. *Pediatr Pulmonol* Vol. 18, (octubre de 1999), pp. 6-8, ISSN: 1099-0496
- SEMARNAP/SS/GEJ. (1997). Secretaría del medio ambiente, recursos naturales y pesca - Secretaría de Salud - Gobierno del Estado de Jalisco. Programa para el mejoramiento de la calidad del aire en la ZMG, 1997-2001, Guadalajara, Jalisco, México.

- Shrenk H.; Heimann H. & Clayton GD. (1949). Air pollution in Donora, Pa; epidemiology of the unusual smog episode of October 1948. Preliminary report.: US Public Health Service (Public Health Bulletin 306), Washington, D.C.
- Smith K.; Corvalan C.; Kjellstrom, T. (1999). How much global ill health is attributable to environmental factors. *Epidemiology*, Vol. 10, No 5, (septiembre 1999), pp. 573-584
- World Health Organization/United Nations Environmental Programme (1992). *Urban air pollution in megacities of the world*. Blackwell, Oxford.